Oil & Natural Gas Technology

DOE Award No.: DE-FC26-03NT15424

FINAL REPORT

THE MISSISSIPPIAN LEADVILLE LIMESTONE EXPLORATION PLAY, UTAH AND COLORADO – EXPLORATION TECHNIQUES AND STUDIES FOR INDEPENDENTS

Submitted by:
Utah Geological Survey
1594 West North Temple, Suite 3110
P.O. Box 146100
Salt Lake City, Utah 84114-6100
Ph.: (801) 537-3300/Fax: (801) 537-3400

Prepared for:
United States Department of Energy
National Energy Technology Laboratory

January 2009

Office of Fossil Energy

DISCLAIMER

This report was prepared as an account of work sponsored by an agency of the United States Government. Neither the United States Government nor any agency thereof, nor any of their employees, makes any warranty, express or implied, or assumes any legal liability or responsibility for the accuracy, completeness, or usefulness of any information, apparatus, product, or process disclosed, or represents that its use would not infringe privately owned rights. Reference herein to any specific commercial product, process, or service by trade name, trademark, manufacturer, or otherwise does not necessarily constitute or imply its endorsement, recommendation, or favoring by the United States Government or any agency thereof. The views and opinions of authors expressed herein do not necessarily state or reflect those of the United States Government or any agency thereof.

Although this product represents the work of professional scientists, the Utah Department of Natural Resources, Utah Geological Survey, makes no warranty, expressed or implied, regarding its suitability for a particular use. The Utah Department of Natural Resources, Utah Geological Survey, shall not be liable under any circumstances for any direct, indirect, special, incidental, or consequential damages with respect to claims by users of this product.

THE MISSISSIPPIAN LEADVILLE LIMESTONE EXPLORATION PLAY, UTAH AND COLORADO – EXPLORATION TECHNIQUES AND STUDIES FOR INDEPENDENTS

FINAL REPORT

Thomas C. Chidsey, Jr., Compiler and Editor

Date of Report: January 2009

Work Performed Under Contract No. DE-FC26-03NT15424

Prepared for
U.S. Department of Energy
Assistant Secretary for Fossil Energy

Virginia Weyland, Project/Contract Manager
National Energy Technology Laboratory
Williams Center Tower One
1 West 3rd Street
Tulsa, OK 74103-3532

Submitting Organization: **Utah Geological Survey**
1594 West North Temple, Suite 3110
P.O. Box 146100
Salt Lake City, Utah 84114-6100
(801) 537-3300

ABSTRACT

The Mississippian (late Kinderhookian to early Meramecian) Leadville Limestone is a shallow, open-marine, carbonate-shelf deposit. The Leadville has produced over 53 million barrels (8.4 million m^3) of oil/condensate from seven fields in the Paradox fold and fault belt of the Paradox Basin, Utah and Colorado. The environmentally sensitive, 7500-square-mile (19,400 km^2) area that makes up the fold and fault belt is relatively unexplored. Only independent producers operate and continue to hunt for Leadville oil targets in the region. The overall goal of this study is to assist these independents by (1) developing and demonstrating techniques and exploration methods never tried on the Leadville Limestone, (2) targeting areas for exploration, (3) increasing deliverability from new and old Leadville fields through detailed reservoir characterization, (4) reducing exploration costs and risk especially in environmentally sensitive areas, and (5) adding new oil discoveries and reserves. The final results will hopefully reduce exploration costs and risks, especially in environmentally sensitive areas, and add new oil discoveries and reserves.

The study consists of three sections: (1) description of lithofacies and diagenetic history of the Leadville at Lisbon field, San Juan County, Utah, (2) methodology and results of a surface geochemical survey conducted over the Lisbon and Lightning Draw Southeast fields (and areas in between) and identification of oil-prone areas using epifluorescence in well cuttings from regional wells, and (3) determination of regional lithofacies, description of modern and outcrop depositional analogs, and estimation of potential oil migration directions (evaluating the middle Paleozoic hydrodynamic pressure regime and water chemistry).

Leadville lithofacies at Libon field include open marine (crinoidal banks or shoals and Waulsortian-type buildups), oolitic and peloid shoals, and middle shelf. Rock units with open-marine and restricted-marine facies constitute a significant reservoir potential, having both effective porosity and permeability when dissolution of skeletal grains, followed by dolomitization, has occurred.

Two major types of diagenetic dolomite are observed in the Leadville Limestone at Lisbon field: (1) tight "early" dolomite consisting of very fine grained (<5 μm), interlocking crystals that faithfully preserve depositional fabrics; and (2) porous, coarser (>100-250 μm), rhombic and saddle crystals that discordantly replace limestone and earlier very fine grained dolomite. Predating or concomitant with late dolomite formation are pervasive leaching episodes that produced vugs and extensive microporosity. Most reservoir rocks within Lisbon field appear to be associated with the second, late type of dolomitization and associated leaching events. Other diagenetic products include pyrobitumen, syntaxial cement, sulfide minerals, anhydrite cement and replacement, and late macrocalcite. Fracturing (solution enlarged) and brecciation (autobrecciation) caused by hydrofracturing are widespread within Lisbon field. Sediment-filled cavities, related to karstification of the exposed Leadville, are present in the upper third of the formation. Pyrobitumen and sulfide minerals appear to coat most crystal faces of the rhombic and saddle dolomites. The fluid inclusion and mineral relationships suggest the following sequence of events: (1) dolomite precipitation, (2) anhydrite deposition, (3) anhydrite dissolution and quartz precipitation, (4) dolomite dissolution and late calcite precipitation, (5) trapping of a mobile oil phase, and (6) formation of bitumen. Fluid inclusions in calcite and

dolomite display variable liquid to vapor ratios suggesting reequilibration at elevated temperatures (50°C). Fluid salinities exceed 10 weight percent NaCl equivalent. Low ice-melting temperatures of quartz- and calcite-hosted inclusions suggest chemically complex Ca-Mg-bearing brines associated with evaporite deposits were responsible for mineral deposition. The overall conclusion from these analyses indicates late dolomitization, saddle dolomite, and dolomite cement precipitation, as well as sulfides and brecciation, may have developed from hydrothermal events that can greatly improve reservoir quality. The result can be the formation of large, diagenetic-type, hydrocarbon traps. The reservoir characteristics, particularly diagenetic overprinting and history, can be applied regionally to other fields and exploration trends in the Paradox Basin.

Stable carbon and oxygen isotope data indicate that all Lisbon field Leadville dolomites were likely associated with brines whose composition was enriched in ^{18}O compared with Late Mississippian seawater. The Leadville replacement dolomite's temperatures of precipitation ranged from about 140 to 194°F (~ 60 to 90°C). Saddle dolomite cements were precipitated at temperatures greater than 194°F (>90°C). High strontium isotopic ratios for Leadville late burial, diagenetic mineral phases indicate contributions by waters enriched in ^{87}Sr that were derived from either Precambrian granitic rocks or the Devonian McCracken Sandstone along basement-involved, high-angle normal faults. Brines from evaporites in the Pennsylvanian Paradox Formation may also have entered the Leadville along the large fault bounding the northeast flank of the field.

Burial history and temperature profiles for the Leadville Limestone at Lisbon field provide some guidance as to when the important diagenetic events occurred. Porous replacement dolomites probably formed during the early and middle portions of the burial history. Inferred elevated temperature spikes during maximum burial, late Laramide faulting/uplift, and Oligocene igneous intrusive activity may account for the high temperatures responsible for quartz precipitation, sulfide mineralization, pyrobitumen formation, late dissolution of carbonates, and late saddle dolomite cements. We propose a model with thermal convection cells bounded by basement-rooted faults to transfer heat and fluids from possible granitic basement, Pennsylvanian evaporites, and Oligocene igneous complexes.

Surface geochemical surveys have helped identify areas of poorly drained or by-passed oil in other basins. This study was therefore initiated to evaluate the effectiveness of low-cost, innovative, non-invasive, surface geochemical methods for predicting the presence of underlying Mississippian Leadville hydrocarbon reservoirs. Lisbon field was chosen for testing because it is the largest Leadville oil and gas producer in the Paradox Basin, sample sites are relatively easily accessible, and the surface geology is similar to the structure of the field. Also selected for comparison was a nearby, recently discovered Leadville field (Lightning Draw Southeast) which has similar geology to Lisbon field in terms of Leadville reservoir lithology, structure, and gas composition, but in comparison has nearly virgin reservoir pressure.

The geochemical survey consisted of collecting shallow soil samples over and around the fields covering the gas cap, oil leg (present only at Lisbon field), and background "barren" areas to map the spatial distribution of potential surface hydrocarbon anomalies. In addition, samples were collected near oil, gas, and dry wells for analogue matching purposes and to refine the discriminant model for the fields. Free-gas samples were also collected over Lightning Draw Southeast field and known non-productive areas off the structure. Finally, joints in the Jurassic Navajo and Entrada Sandstones may provide pathways for hydrocarbon microseepage to the surface. Therefore, soil, sand, bryophytes, and lichen samples were collected along joints for

geochemical analyses. Samples were analyzed for 40 hydrocarbon compounds in the C_1 to C_{12} range, 53 major and trace elements, seven anion species, and synchronous scanned fluorescence. Free-gas samples were analyzed for fixed gases and hydrocarbons.

The main conclusion of the study is that certain surface geochemical methods can discriminate between productive and non-productive Leadville reservoirs. Variables in surface soils and outcrop fracture-fill lichen and soils that best distinguish productive and non-productive areas are light (C_1 to C_6) alkane and heavy (C_{24} to C_{36}) aromatic hydrocarbons. The volatile and liquid hydrocarbons presumably ascend to the surface along faults within and at the margins of the fields. Mercury and lead are indirect indicators of hydrocarbon microseepage and they could be derived from the oil itself. Helium and carbon dioxide anomalies in free-soil gas at the margins of Leadville reservoirs could be the most diagnostic indicators of underlying Leadville reservoirs. These gases are enriched in Leadville reservoirs as compared with overlying productive intervals in the Ismay zone of the Pennsylvanian Paradox Formation. Anomalous hydrocarbons, carbon dioxide, and hydrogen in free gas over Lightning Draw Southeast field may be derived from productive intervals within the Paradox, Leadville, or a combination of reservoirs in both formations.

Cost-effective regional exploration for Leadville reservoirs would first involve the collection and analysis of surface soils and/or outcrop fracture-fill soil and lichen for thermally desorbed and solvent-extractable hydrocarbons. Anomalous areas could then be followed up with the collection of deep free-gas samples at short (<300 feet [100 m]) intervals and analysis of the gas for diagnostic indicators of Leadville reservoirs (that is, helium and carbon dioxide). Areas with anomalous helium and carbon dioxide in free gas could then by further explored with 3D seismic to define drillable structures.

Epifluorescence petrography makes it possible to clearly identify hydrocarbon shows in Leadville cuttings from regional exploration wells selected for study. It is a non-destructive procedure using a petrographic microscope equipped with reflected light capabilities, a mercury-vapor light, and appropriate filtering. Sample preparation is inexpensive and rapid. Cuttings from productive and dry exploratory wells penetrating the Leadville Limestone in the Utah part of the Paradox fold and fault belt were examined under a binocular microscope and selected for epifluorescence evaluation. Epifluorescence allows one to observe the presence or absence of any soluble hydrocarbons, especially in high porosity dolomite. The highest maximum and highest average epifluorescence readings from each well, based on a qualitative visual rating scale, were plotted and mapped. A regional southeast-northwest trend of relatively high epifluorescence for Leadville cuttings parallels the southwestern part of the Paradox fold and fault belt. The northeastern part of the fold and fault belt shows a regional trend of low epifluorescence. As expected, productive Leadville wells have cuttings distinguished by generally higher epifluorescence readings. Hydrocarbon migration and dolomitization were associated with regional northwest-trending faults and fracture zones, which created potential oil-prone areas along the southwest trend. Hydrocarbons may have migrated from organic-rich shales in the Pennsylvanian Paradox Formation where they are in contact with the Leadville Limestone along faults. Hydrothermal alteration associated with these faults and related fracture zones may have generated late, porous dolomite and thus produced diagenetic traps. Hydrocarbons flushed out to the southwest by hydrodynamic processes may also account for the lack of significant epifluorescence in the northeast trend. In addition, these epifluorescence trends could be related to facies or karst development in the Leadville. Exploration efforts

should be concentrated in suggested oil-prone areas along the southwest part of the Paradox fold and fault belt.

In the Paradox Basin, regional Leadville facies include open marine (crinoidal banks or oolitic shoals and Waulsortian-type buildups), middle shelf, and restricted marine (peloidal muds). Brecciation and sediment-filled cavities, related to karstification of the previously exposed Leadville, are relatively common throughout the upper third of the formation. The Leadville is more than 700 feet (200 m) to less than 200 feet (60 m) thick, thinning due to both depositional onlap and erosional wedging. It is bounded above and below by unconformities within the Paradox Basin. The Leadville is mostly pure limestone with some reflux dolomitization implying arid conditions on a shallow shelf. Subaerial erosion resulted in lateritic regolith over most of the Leadville in the Paradox Basin. Regionally, an intraformational unconformity divides the Leadville Limestone into informal upper and lower members. Early movement on northwest-trending faults may have also affected the depositional characteristics of the Leadville Limestone. Hydrocarbon production and shows in the Leadville Limestone are primarily along the northwest-trending faults in the Paradox fold and fault belt. Stratigraphic traps developed by the erosional regolith and Waulsortian mounds, or other carbonate buildups, may exist in the Leadville southwest of the fold and fault belt. Diagenetic traps resulting from dolomitization, both early and late (hydrothermal), represent untapped but difficult to identify drilling targets in the fold and fault belt.

Utah is fortunate that representative outcrop analogs (depositional or diagenetic) for the Leadville Limestone play are present near the Paradox Basin. The Mississippian Madison Limestone exposed along the south flank of the Uinta Mountains has the same characteristics as the Leadville. The Madison was deposited in a shallow, warm-water, relatively high energy, epeiric sea that extensively covered a large part of the craton. Madison depositional environments exposed include tidal flat mud, shallow subtidal bay, beach/foreshore, oolitic and crinoid shoals, and muddy intershoal. All of these Madison depositional environments are also observed in Leadville cores from Lisbon field.

The Madison Limestone contains local zones of breccia due to either collapse or natural hydrofracturing. Collapse features are related to paleokarstification of the Madison when exposed during Late Mississippian time. Brecciation caused by explosive natural hydrofracturing created the same shattered-looking, pulverized rock identified in Lisbon cores. Possible breccia pipes may be related to past hydrothermal activity. The basal Cambrian Tintic Quartzite and Lodore Formation served as aquifers supplying hot water from below the hydrothermal system. No hydrothermal breccia zones or pipes are located where the Tintic and Lodore are missing in the section. This suggests that targeting Leadville Limestone areas for potential hydrothermal dolomite and enhanced reservoir quality due to hydrofracturing may require an aquifer below as a necessary ingredient.

Environments of the Leadville Limestone have modern analogs in southern Florida-Bahamas region, a warm-water carbonate factory. This region represents a time horizon from which one can observe carbonate deposition, the conditions (physical, biological, and chemical) which create various carbonate sediments, and the processes by which the deposits change. Although the organisms in warm-water carbonate settings today are different from those of the past due to organic evolution, the roles of sediment producer and modifier have remained largely unchanged through time. Warm marine water is also often supersaturated with respect to calcium carbonate which can be precipitated to form carbonate grains such as ooids, peloids, grapestone, and carbonate mud.

Southern Florida is an attached, rimmed carbonate platform. From northwest to southeast, the platform consists of mangrove swamps and supratidal flats (Everglades), an inner shelf (Florida Bay), inner and outer shelf margins, and a shallow slope into the Straits of Florida. Florida Bay is triangular shaped due to barriers that restrict circulation. A variety of sedimentary environments are represented in Florida Bay as part of a transgressive record: (1) fresh-water pond, (2) coastal mangrove swamp, (3) broad, shallow bay basins ("lake"), (4) mud mounds, and (5) island. The rimmed platform margin is formed by the arcuate reef track that includes the forereef, discontinuous outer barrier reef, back reef, and lagoon (containing patch reefs and sand shoals). Shallow bay basins, mud mounds, patch reefs, and sand shoals are modern Leadville Limestone analogs.

The Great Bahama Bank is an unattached, isolated rimmed carbonate platform. From east to west, the Great Bahama Bank consists of Earth's third longest barrier reef, a narrow lagoon, Andros Island with carbonate tidal flats on the western side, the shelf lagoon, and oolitic shoals. Ooid shoals and shelf lagoonal sedimentation are modern Leadville Limestone analogs. Recognizing the modern characteristics of carbonate tidal flats in the Leadville Limestone, proven producers in other carbonate reservoirs, may provide additional target areas for drilling.

Through the Paradox Basin, there is a systematic change in the chemistry of both the Mississippian/Devonian- and Pennsylvanian-brine systems from north to south. The Pennsylvanian-system brines are more saline than the Mississippian/Devonian-system brines. Bicarbonate is very low in both brine systems. This suggests the direction of ground-water movement in the Mississippian/Devonian and Pennsylvanian systems is generally southwestward. Further research refined the regional hydrodynamic trends in the Mississippian of the Paradox Basin, Utah and Colorado, and how they affected hydrocarbon migration. Shut-in drill-stem test (DST) pressure data from petroleum exploration and development wells in the Paradox Basin established the major hydrodynamic trends, especially within the Mississippian. With the exception of the eastern edge of the basin, there is one pressure regime for the Mississippian with a composite pressure gradient of 0.47 pounds per square inch/foot (10.6 kPa/m) over an elevation range of +4000 to -10,000 feet (1200 to -3000 m) above sea level (ft asl [m asl]). This remarkably uniform pressure regime over an area of at least 100 by 100 miles (260 by 260 km) indicates relatively high permeability within the Mississippian. The gradient is about 10% above hydrostatic for fresh water, but consistent with the density of the brines. The head is between 3800 and 4000 ft asl (1160 and 1220 m asl), and coincides with the elevation of the lower Green River and Cataract Canyon section of the Colorado River where they traverse the basin. It appears that the Mississippian and older reservoirs across most of the Paradox Basin are in good hydrological communication with the Colorado River system. This large-scale hydrological connection between the surface and the Mississippian may be a geologically recent occurrence. Consideration of the rate of incision by the Colorado River system suggests that the Mississippian could have been hydrologically isolated and fully saturated several million years ago, and could have held significantly greater quantities of oil and gas.

CONTENTS

LISBON FIELD, SAN JUAN COUNTY, UTAH: A CASE STUDY OF LEADVILLE LIMESTONE LITHOFACIES AND DIAGENETIC HISTORY

EXPLORATION TECHNIQUES FOR THE MISSISSIPPIAN LEADVILLE LIMESTONE PLAY

REGIONAL STUDIES OF THE MISSISSIPPIAN LEADVILLE LIMESTONE

FIGURES

TABLES

ACKNOWLEDGMENTS

Project Financial Support

Funding for this research was provided as part of the Advanced and Key Oilfield Technologies for Independents (Area 2 – Exploration) Program of the U.S. Department of Energy, National Energy Technology Laboratory, Tulsa, Oklahoma, contract number DE-FC26-03NT15424. The Contracting Officer's Representative is Virginia Weyland. Support was also provided by the Utah Geological Survey, Salt Lake City, Utah; Eby Petrography & Consulting, Inc., Denver, Colorado; Direct Geochemical/Vista Geoscience Resources, Golden, Colorado; ST Oil Company, Denver, Colorado; and the Utah School and Institutional Trust Lands Administration, Salt Lake City, Utah.

Project Contributors

State Geologist and Director of the Utah Geological Survey

Richard G. Allis

Principal Investigator/Program Manager

Thomas C. Chidsey, Jr., Utah Geological Survey, Salt Lake City, Utah

Financial Officers

John Kingsley, Dan Kelly (now with the U.S. Department of Defense), Kathi Galusha, Utah Geological Survey, Salt Lake City, Utah

Task Contributing Scientists and Organizations

Richard G. Allis, Roger L. Bon, Thomas C. Chidsey, Jr., J. Wallace Gwynn, Sonja Heuscher, Kevin McClure (now with Castle Inspection Services), Ammon McDonald, Craig D. Morgan, and Michael D. Vanden Berg, Utah Geological Survey, Salt Lake City, Utah

David E. Eby, Eby Petrography & Consulting, Inc., Denver, Colorado

John D. Humphrey, Colorado School of Mines, Golden, Colorado

Joseph N. Moore, Energy & Geoscience Institute, Salt Lake City, Utah

Louis H. Taylor, Standard Geological Services, Inc., Littleton, Colorado

David M. Seneshen, Direct Geochemical/Vista Geoscience Resources, Golden, Colorado

Cores and petrophysical data from Lisbon field were provided by Tom Brown, Inc. (now

Encana Corp.), Denver, Colorado. Additional Leadville cores from the Paradox Basin were donated by the Oklahoma Geological Survey (Gene Kuhlman, Curator, Oklahoma Petroleum Information Center), Norman, Oklahoma. Gas analyses and oil samples as well as surface access in Lisbon field were provided by Encana Corp., Denver, Colorado We thank Dr. Larry St. Clair, Curator of Lichens and Bryophytes and Director of the Monte L. Bean Life Science Museum, Brigham Young University, Provo, Utah, for identifying bryophytes and lichens.

The author was graciously invited to attend the Brigham Young University (BYU) Department of Geological Sciences field course "Carbonate Geology of Southern Florida and the Bahamas," April 25-May 4, 2008, instructed by Drs. Scott Ritter and Thomas Morris. Most of the chapter on modern carbonate analogs was generated from observations made during the field course, lecture notes, and materials provided generously by Drs. Ritter and Morris. Their assistance was invaluable.

The project Web page was managed by Christine Wilkerson (Utah Geological Survey). Vicky Clarke, Stevie Emerson, Cheryl Gustin, Sharon Hamre, Kevin McClure, James Parker, and Liz Paton (Utah Geological Survey), drafted figures, assisted with data compilation, designed displays, and assembled reports. Thomas Dempster, Carolyn Olsen, Michael D. Laine, Brad Wolverton, and Ammon McDonald of the Utah Geological Survey photographed core, compiled and prepared maps, and collected well cuttings from the Utah Core Research Center. Geographic Information Systems support was provided by Sharon Wakefield and Sonja Heuscher of the Utah Geological Survey. Desktop publishing was by Cheryl Gustin, Utah Geological Survey. Additional photographs and figures were provided by the Scott Ritter, BYU Department of Geological Sciences.

This report, or portions of it, was reviewed by David E. Tabet, Michael Hylland, Robert Ressetar, Bryce T. Tripp, Kimm Harty, and Richard G. Allis, Utah Geological Survey; and Virginia Weyland, National Energy Technology Laboratory, U.S. Department of Energy, Tulsa, Oklahoma. Additional technical reviews of the surface geochemical survey and analysis were provided by Neil Fishman, U.S. Geological Survey, Denver, Colorado, and Jason Blake, Titan Energy, Park City, Utah.

EXECUTIVE SUMMARY

The Mississippian (late Kinderhookian to early Meramecian) Leadville Limestone is a shallow, open-marine, carbonate-shelf deposit. The Leadville has produced over 53 million barrels (8.4 million m^3) of oil/condensate from seven fields in the Paradox fold and fault belt of the Paradox Basin, Utah and Colorado. Most Leadville oil and gas production is from basement-involved structural traps. All of these fields are currently operated by independent producers. This environmentally sensitive, 7500-square-mile (19,400 km^2) area is relatively unexplored with only about 100 exploratory wells that penetrated the Leadville (less than one well per township), and thus the potential for new discoveries remains great. There have been no significant new oil discoveries since the early 1960s, and only independent producers continue to explore for Leadville oil targets in the region, 85% of which is under the stewardship of the federal government.

The overall goals of this report are to assist these independents by (1) developing and demonstrating techniques and exploration methods never tried on the Leadville Limestone, (2) targeting areas for exploration, (3) increasing deliverability from new and old Leadville fields through detailed reservoir characterization, (4) reducing exploration costs and risk especially in environmentally sensitive areas, and (5) adding new oil discoveries and reserves. The final results, summarized below, will hopefully reduce exploration costs and risk, especially in environmentally sensitive areas of the Paradox Basin, and add new oil discoveries and reserves.
The first objective of the project was to conduct a case study of the Leadville reservoir at Lisbon field, San Juan County, Utah, in order to understand the reservoir characteristics and lithofacies that can be applied regionally. The second objective was to conduct low-cost demonstrations of new exploration technologies to identify surface geochemical anomalies and potential oil-prone areas, especially in environmentally sensitive areas. The third objective was to determine regional facies (evaluating cores, geophysical well logs, outcrop, and modern analogs) and potential Leadville oil migration directions to target areas for Leadville exploration. These objectives were designed to assist the independent producers and explorers who have limited financial and personnel resources.

To achieve the goal, objectives, and carry out the Leadville Limestone study, the Utah Geological Survey (UGS) and Eby Petrography & Consulting, Inc., entered into a cooperative agreement with the U.S. Department of Energy (DOE), National Energy Technology Laboratory, Tulsa, Oklahoma. The research was funded as part of the DOE Advanced and Key Oilfield Technologies for Independents (Area 2 – Exploration) Program. This report covers research and results of this five-year project (October 1, 2003, through September 30, 2008).

Lisbon Field, San Juan County, Utah: A Case Study of Leadville Limestone Lithofacies and Diagenetic History

Prior to this study, reservoir characterization of the Leadville Limestone was not complete and little pertinent information (core descriptions, permeability data, and diagenetic analysis) had been published. Lisbon field accounts for most of the Leadville oil production in the Paradox Basin. Its reservoir characteristics, particularly diagenetic overprinting and history, and Leadville lithofacies can be applied regionally to other fields and exploration trends in the basin. The UGS had a wealth of undescribed core and other raw data at the Survey's Core Research Center. Initial investigations indicated the possible presence of hydrothermal dolomite,

a key component in the development of diagenetic hydrocarbon traps, which would imply a new potential for the Leadville in the Paradox Basin. Therefore, Lisbon was selected as the case-study field for this Leadville Limestone project. The following sections summarize the lithofacies, diagenesis (including scanning electron microscopy, epifluorescence, cathodoluminescence), fluid inclusion, isotopic, and burial history studies of Lisbon field, and provide conclusions and recommendations for companies exploring for Leadville targets.

Lithofacies

Leadville lithofacies include open marine (crinoidal banks or shoals and Waulsortian-type buildups), oolitic and peloid shoals, and middle shelf. Rock units with open-marine and restricted-marine lithofacies constitute a significant reservoir potential, having both effective porosity and permeability when dissolution of skeletal grains followed by dolomitization has occurred.

Diagenetic History

Leadville reservoir quality at Lisbon is greatly enhanced by dolomitization and dissolution of shallow water limestone. There are two basic types of dolomite: (1) very fine, early dolomite, and (2) coarse, late dolomite. Early dolomitization preserves depositional fabrics and has limited porosity development, except for limited dissolution of fossils, and has very low permeabilities. Late dolomitization has two morphologies: rhombic dolomites and saddle dolomites. Most reservoir rocks within Lisbon field appear to be associated with the second, late type of dolomitization and associated leaching events.

Pyrobitumen coats most intercrystalline dolomite as well as dissolution pores associated with the second type of dolomite. Fracturing and brecciation caused by hydrofracturing are widespread within Lisbon field. Sediment-filled cavities, related to karstification of the exposed Leadville, are relatively common throughout the upper third of the formation in the field. Other diagenetic products include syntaxial cement, sulfide minerals, anhydrite cement and replacement, and late macrocalcite. Late dolomitization, saddle dolomite, and dolomite cement precipitation, as well as sulfides and brecciation, may have developed from hydrothermal events that can greatly improve reservoir quality. The result can be the formation of large, diagenetic-type hydrocarbon traps.

Scanning electron microscopy (SEM): Scanning electron microscopy demonstrates how Leadville reservoir quality at Lisbon is greatly enhanced by dolomitization and dissolution of shallow water limestone. Pyrobitumen coats most intercrystalline dolomite in the Leadville as well as dissolution pores associated with the second type of dolomite. Fractures enhance the permeability in several intervals. Minor euhedral quartz is present in several samples. Anhydrite and sulfide mineral(s) are also present in moderate abundance. The general diagenetic sequence for these samples, based on SEM analysis, is (1) dolomitization, (2) dissolution, (3) dolomite cementation, (4) fracturing, (5) quartz cementation, (6) calcite cementation, (7) clay precipitation, (8) anhydrite cementation, (9) pyrobitumen emplacement, and (10) sulfide precipitation.

Epifluorescence (EF): Epifluorescence petrography makes it possible to clearly identify grain types and shapes, within both limestone and dolomite reservoir intervals in Leadville thin sections from cores examined in this study. In particular, peloids, skeletal grain types, and coated grains are easy to identify in rocks where these grains have been poorly preserved, partially leached, or completely dolomitized. Depositional textures that are frequently occult or poorly preserved can often be clearly distinguished using blue-light EF microscopy. In many limestones and finely crystalline dolomites of the Leadville reservoir at Lisbon field, the differences between muddy and calcarenitic fabrics can only be clearly appreciated with fluorescence lighting. Epifluorescence petrography clearly and rapidly images pore spaces that cannot otherwise be seen in standard viewing under transmitted polarized lighting. In addition, the cross-sectional size and shape of pores are easy to determine.

Much of the Leadville porosity is very heterogeneous and poorly connected as viewed under EF. In particular, intercrystalline porosity within some of the reservoir in Lisbon field can be resolved much more clearly with EF than with transmitted polarized lighting. The EF examination helps in seeing the origin of most types of porosity. Transmitted polarized lighting does not image intercrystalline porosity in carbonate samples very well, even though blue-dyed epoxy can be impregnated into even very small pores. In addition, opaque bitumen linings prevent light from passing through some of the pores to the observer. Without the aid of the EF view, the amount of visible open pore space would be underestimated in the plane-light image.

Where dolomitization has occurred, EF petrography often shows the crystal size, shape, and zonation far better than transmitted plane or polarized lighting. This information is often very useful when considering the origin and timing of dolomitization as well as evaluating the quality of the pore system within the dolomite. Permeability differences within these dolomite and limestone samples are also easy to image with EF because of the differential oil saturations between the tighter areas and the more permeable lithologies. Low-permeability carbonates from this study area show bright yellow fluorescence due to trapped live oil that is retained within tighter parts of the reservoir system. More permeable rocks show red fluorescence due to the epoxy fluorescence where oil has almost completely drained from the better quality portions of the reservoir.

Cathodoluminescence (CL): Cathodoluminescence imaging of samples nicely complements the types of information derived from EF of carbonate thin sections. Cathodoluminescence also displays original depositional textures and the outlines of original carbonate grains and distinctly images pore spaces. This information is often very useful when considering the origin and timing of dolomitization as well as evaluating the quality of the pore system within the dolomite. Finally, CL imaging also shows that the contact between the transported material related to karstification and the limestone country rock can be sharp, irregular, and corroded.

Cathodoluminescence shows a wide range of Leadville crystal size and growth habits within the dull red luminescing, matrix-replacing dolomite. The vast majority of the dolomite within areas of fabric-selective dolomitization is a deep or intense red color. Between many of the grains, there is a lighter red luminescence where early cements have been dolomitized. Some of the coarser dolomite crystals appear to have an overgrowth of brighter red luminescent material. The amount of open porosity under CL is considerably greater than that visible under plane-light microscopy. Between other grains, there are interparticle pores that are still open. In

a few areas, these early pores have been solution-enlarged and lined with a later generation of coarse, rhombic dolomite.

Examination of saddle dolomites in the Leadville can provide more information about these late, elevated temperature (often hydrothermal) mineral phases. For instance, saddle dolomites show nice growth banding. These saddle dolomites display dull, red luminescence in their core areas and slightly bright, orange-red luminescence toward their rim areas. In addition, CL makes it possible to see the growth bands in these coarse dolomite crystals due to slight luminescent differences between each growth zone.

Fluid inclusions: The fluid inclusion and mineral relationships suggest the following sequence of events: (1) dolomite precipitation, (2) anhydrite deposition, (3) anhydrite dissolution and quartz precipitation, (4) dolomite dissolution and late calcite precipitation, (5) trapping of a mobile oil phase, and (6) formation of bitumen. Aqueous fluid inclusions in early calcite, which typically forms coarse-grained crystals, display a range of liquid-to-vapor ratios suggesting they have necked. Oil inclusions yielded homogenization temperatures ranging from 48 to 70^{o}C (118-158^{o}F). These temperatures represent the minimum temperature of oil formation, not of calcite deposition. The oil was generated in place by maturation of organic material. Both the oil inclusions and the common presence of two-phase, necked aqueous inclusions imply trapping at elevated temperatures. It is suggested trapping occurred when the original calcite recrystallized during burial. Fluid inclusions in dolomite have re-equilibrated (stretched, necked, refilled) since trapping. The common presence of single-phase aqueous inclusions suggests that the fine-grained dolomite and cores of saddle dolomite were deposited at temperatures less than about 50^{o}C (<~122 ^{o}F). Low ice-melting temperatures of quartz- and calcite-hosted inclusions suggest chemically complex Ca-Mg-bearing brines associated with evaporite deposits were responsible for mineral deposition. Oil deposited in healed fractures within late, pore-filling calcite has similar fluorescence to the primary inclusions, but lower homogenization temperatures of about 40^{o}C (~104 ^{o}F). The lower temperatures of the secondary oil inclusions allow the possibility that the temperatures were decreasing, perhaps due to unroofing, prior to bitumen formation. It is possible live oil was preserved in the calcite and dolomite, but not in the main fractures, which now contain bitumen because the oil was not degassed.

Isotopic analysis: Stable carbon and oxygen isotope data indicate that all Lisbon Leadville dolomites were likely associated with brines whose composition was enriched in ^{18}O compared with Late Mississippian seawater (several per mil heavier than normal seawater). Stable oxygen isotope analyses of the Leadville replacement dolomites indicate that temperatures of precipitation ranged from about 60 to 90^{o}C (~140-194 ^{o}F). Saddle dolomite cements were precipitated at temperatures greater that 90^{o}C (>194 ^{o}F). High Sr isotopic ratios for late burial diagenetic mineral phases at Lisbon field indicate contributions by waters enriched in ^{87}Sr that were derived from either granitic Precambrian basement rocks or the Devonian McCracken Sandstone.

Burial history and possible heat sources: We propose a model with thermal convection cells bounded by basement-rooted faults to transfer heat and fluids from possible crystalline basement, Pennsylvanian evaporites, and Oligocene igneous complexes. We recommend that any future evaluation of a Leadville Limestone prospect include stable carbon and oxygen isotope analysis of diagenetic components, strontium isotope analysis for tracing the origin of fluids responsible

for different diagenetic events, and production of burial history and temperature profiles to help determine when the diagenetic events occurred.

Early Tertiary reactivation of basement-involved, high-angle normal faults associated with Precambrian tectonics may have allowed hot, deep-seated fluids from the granitic basement or the McCracken Sandstone to communicate upwards with the Leadville carbonate section. Brines from evaporites in the Pennsylvanian Paradox Formation may have also entered the Leadville along the large fault bounding the northeast flank of the field.

Burial history and temperature profiles for the Leadville at Lisbon field provide some guidance as to when important diagenetic and porosity-forming events occurred. Porous replacement dolomites probably formed during the early and middle portions of the burial history at Lisbon field. Inferred elevated temperature spikes during maximum burial, late Laramide faulting/uplift, and Oligocene igneous activity may account for the high temperatures responsible for quartz precipitation, sulfide mineralization, pyrobitumen formation, late dissolution of carbonates, and late saddle dolomite cements.

Exploration Techniques for the Mississippian Leadville Limestone Play

Exploring the Leadville Limestone has been high risk, with less than a 10% chance of success based on the drilling history of the region. New prospect definition often requires expensive, 3D seismic acquisition, at times in environmentally sensitive areas. These facts make exploring difficult for independents that have limited funds available to try new, unproven techniques that might increase the chance of successfully discovering oil. Using surface geochemical surveys and regional oil-show data to identify potential oil-prone areas first, will reduce the risk taken by an independent producer in looking for Leadville oil. These techniques will help independents to recognize or eliminate areas and exploration targets prior to spending significant financial resources on seismic data acquisition and potential environmental litigation, and therefore increase the chance of successfully finding new economic accumulations of Leadville oil.

Surface Geochemical Surveys in the Lisbon and Lightning Draw Southeast Field Areas

Surface geochemical surveys have helped identify areas of poorly drained or by-passed oil in other basins. This study was therefore initiated to evaluate the effectiveness of low-cost, innovative, non-invasive, surface geochemical methods for predicting the presence of underlying Mississippian Leadville hydrocarbon reservoirs. Lisbon field was chosen for testing because it is the largest Leadville oil and gas producer in the Paradox Basin, sample sites are relatively easily accessible, and the surface geology is similar to the structure of the field. Also selected for comparison was a nearby, recently discovered Leadville field (Lightning Draw Southeast) which has similar geology to Lisbon field in terms of Leadville reservoir lithology, structure, and gas composition, but in comparison has nearly virgin reservoir pressure.

The geochemical survey consisted of collecting shallow soil samples at 1500-foot (500 m) intervals on a 16-square-mile (42 km^2) rectangular grid over and around the Lisbon field to map the spatial distribution of surface hydrocarbon anomalies. The sampling grid extends beyond the proven limits of Lisbon field to establish background readings. The area chosen sufficiently covers the oil leg, gas cap, and water leg/background barren areas. In addition, samples were collected over gas, oil, and dry wells for analogue matching purposes and to refine

the discriminant model for Lisbon field. Samples were collected Lightning Draw Southeast field along northwest-southeast and northeast-southwest grid lines and around both the producing wells and barren dry wells. Free-gas samples were also collected over Lightning Draw Southeast field and known non-productive areas off the structure. Finally, joints in the Jurassic Navajo and Entrada Sandstones may provide pathways for hydrocarbon microseepage to the surface. Therefore, soil, sand, bryophytes, and lichen samples were collected along joints for geochemical analyses.

The soil, sand, bryophytes, and lichen samples were placed and stored in airtight, Teflon-sealed glass soil jars to prevent hydrocarbon contamination during transport. Samples were dried and sieved, and aliquots weighed out for geochemical analyses for 40 hydrocarbon compounds in the C_1 to C_{12} range, 53 major and trace elements, seven anion species, and for synchronous scanned fluorescence analyses. Free-gas samples were stored in 1-liter Tedlar bags for hydrocarbon and fixed gas analyses and/or in lead-lined CO_2 cartridges for helium analysis.

The main conclusion of the study is that certain surface geochemical methods can discriminate between productive and non-productive Leadville reservoirs. Variables in surface soils and outcrop fracture-fill lichen and soils that best distinguish productive and non-productive areas are light (C_1 to C_6) alkane and heavy (C_{24} to C_{36}) aromatic hydrocarbons. The volatile and liquid hydrocarbons presumably ascend to the surface along faults within and at the margins of the fields. Mercury and lead are indirect indicators of hydrocarbon microseepage and they could be derived from the oil itself. Other heavy metals such as cadmium, uranium, and molybdenum may be derived from mechanical and chemical dispersion of exposed mineralization and abandoned mine workings in the area. Fluoride, which is preferentially anomalous over and around Lightning Draw Southeast field, could reflect the ascent of brines to the surface in conjunction with oil seeps. Helium and carbon dioxide anomalies in free-soil gas at the margins of Leadville reservoirs could be the most diagnostic indicators of underlying Leadville reservoirs. These gases are enriched in Leadville reservoirs as compared with overlying productive intervals in the Ismay zone of the Pennsylvanian Paradox Formation. Anomalous hydrocarbons, carbon dioxide, and hydrogen in free gas over Lightning Draw Southeast field may be derived from productive intervals within the Ismay zone, Leadville Limestone, or a combination of both reservoirs.

Cost-effective regional exploration for Leadville reservoirs would first involve the collection and analysis of surface soils and/or outcrop fracture-fill soil and lichen for thermally desorbed and solvent-extractable hydrocarbons. Anomalous areas could then be followed up with the collection of deep free-gas samples at short (<300 feet [100 m]) intervals and analysis of the gas for diagnostic indicators of Leadville reservoirs (that is, helium and carbon dioxide). Areas with anomalous helium and carbon dioxide in free gas could then by further explored with 3D seismic to define drillable structures.

Potential Oil-Prone Areas in the Paradox Fold and Fault Belt Based on Shows in Drill Cuttings Using Epifluorescence Microscopy Techniques

Epifluorescence petrography makes it possible to clearly identify hydrocarbon shows in Leadville cuttings selected for study. It is a non-destructive procedure that can be done using a petrographic microscope equipped with reflected light capabilities, mercury-vapor light, and appropriate filtering. Sample preparation is inexpensive and rapid. Cuttings from 32 productive or dry exploratory wells penetrating the Leadville Limestone in the Utah part of the Paradox fold

and fault belt were examined under a binocular microscope. Over 900 samples of porous dolomite and some limestone were selected from various zones over the Leadville section for EF evaluation.

Epifluorescence allows one to observe the presence or absence of any soluble hydrocarbons, especially in high porosity dolomite. Samples displaying fluorescence represent areas where hydrocarbons may have migrated or accumulated. If no fluorescence is observed in porous dolomites, the samples are also good representatives of areas where hydrocarbons have not migrated or accumulated.

A qualitative visual "rating" scale (a range and average) based on EF evaluation was applied to the group of cuttings from each depth in each well. The highest maximum and highest average EF reading from each well were plotted and mapped. The maps show a regional southeast-northwest trend of relatively high EF for Leadville cuttings parallels the southwestern part of the Paradox fold and fault belt from Lisbon field northwest to west of the town of Green River. The northeastern part of the fold and fault belt shows a regional trend of low EF including a large area of essentially no EF centered around the town of Moab. As expected, productive Leadville wells have cuttings distinguished by generally higher EF ratings.

Hydrocarbon migration and alteration dolomitization were associated with regional northwest-trending faults and fracture zones, which created potential oil-prone areas along the southwest trend. Hydrocarbons may have migrated from organic-rich shales in the Pennsylvanian Paradox Formation where they are in contact with the Leadville Limestone along faults. Fluid inclusions indicate some oil may have formed in place. Hydrothermal alteration associated with these faults and related fracture zones may have generated late, porous dolomite and thus produced diagenetic traps. Hydrocarbons flushed out to the southwest by hydrodynamic processes may also account for the lack of significant EF in the northeast trend. In addition, these EF trends could be related to facies or karst development in the Leadville. Exploration efforts should be concentrated in suggested oil-prone areas along the southwest part of the Paradox fold and fault belt.

Regional Studies of the Mississippian Leadville Limestone

Regional facies were determined by evaluating cores and correlating geophysical well logs throughout the Paradox Basin to target areas for Leadville exploration. These facies were compared to both outcrop and modern analogs. The regional brine chemistries and hydrodynamic pressure regimes for the Paleozoic formations of the Paradox Basin provide clues as to potential Leadville oil migration directions; very little had been published previously on these topics for the Paradox Basin. These studies will further assist independent producers and explorers who have limited financial and personnel resources to conduct such studies on their own.

Regional Correlation and Facies of the Leadville Limestone in the Paradox Basin and Neighboring Area

Leadville facies include open marine (crinoidal banks or oolitic shoals and Waulsortian-type buildups), middle shelf, and restricted marine (peloidal muds). Brecciation and sediment-filled cavities, related to karstification of the exposed Leadville, are relatively common throughout the upper third of the formation. The Leadville Limestone is more than 700 feet (200

m) to less than 200 feet (60 m) thick, and thins to the southeast across the Paradox Basin due to both depositional onlap and erosional wedging. It is bounded above and below by unconformities within the basin. The Leadville is mostly pure limestone with some reflux dolomitization implying arid conditions on a shallow shelf. Subaerial erosion resulted in lateritic regolith formed over most of the Leadville Limestone in the Paradox Basin. Regionally, an intraformational disconformity divides the Leadville Limestone into informal upper and lower members. Early movement on northwest-trending faults may have affected deposition of the Leadville Limestone.

Hydrocarbon production and shows are primarily along the northwest-trending faults in the Paradox fold and fault belt. Stratigraphic traps developed by the erosional regolith and Waulsortian mounds, or other carbonate buildups, may exist in the Leadville southwest of the fold and fault belt. Diagenetic traps resulting primarily from late (hydrothermal) dolomitization, represent untapped but difficult to identify drilling targets in the fold and fault belt.

Outcrop Reservoir Analogs for the Mississippian Leadville Limestone: South Flank of the Uinta Mountains, Utah

Utah is fortunate that representative outcrop analogs (depositional or diagenetic) for the Leadville Limestone play are present near the Paradox Basin. Production-scale analogs provide an excellent view, often in 3D, of reservoir-facies characteristics, geometry, distribution, diagenetic characteristics, and nature of boundaries, all of which contribute to the overall heterogeneity of reservoir rocks. Although not exposed in southeastern Utah, Mississippian rocks equivalent to the Leadville Limestone crop out in the northern and western parts of the state. These units include the Madison, Gardison, Deseret, and Humbug Formations, and have generally the same characteristics as the Leadville.

The Madison and equivalent formations were deposited in a shallow, warm-water, relatively high energy, epeiric sea that extensively covered a large part of a craton. Madison depositional environments include tidal-flat mud; deeper, subtidal, burrowed, pellet muds; shallow, subtidal bay; beach/foreshore; oolitic shoal; storm-dominated, outer shelf, crinoid shoals; low-energy, open-marine, muddy intershoal; low-energy, open-marine, outer shelf above storm wave base. All of these Madison Limestone depositional environments are also observed in Leadville cores from Lisbon field.

The Madison Limestone contains local zones of breccia due to either collapse or natural hydrofracturing. Breccia associated with sediment-filled, collapsed cavities is relatively common. These cavities are related to paleokarstification of the Madison when exposed during Late Mississippian time. Brecciation caused by explosive natural hydrofracturing created the same shattered-looking, pulverized rock identified in Lisbon cores. Possible breccia pipes may be related to past hydrothermal activity. The basal Cambrian Tintic Quartzite and Lodore Formation are important contributors to the hydrothermal story. They served as aquifers supplying hot water from below the hydrothermal system. Through the central part of the south flank of the Uinta Mountains, the Cambrian is missing and the Mississippian lies unconformably on middle Neoproterozoic Red Pine Shale. No hydrothermal breccia zones or pipes are located in the central part of the south flank, leading credence to the concept that aquifers in the Tintic and Lodore are a required condition for hydrothermal activity to have occurred in the Madison. This suggests that target Leadville Limestone areas for potential hydrothermal dolomite and

enhanced reservoir quality due to hydrofracturing may require an aquifer below as a necessary ingredient.

Modern Reservoir Analogs for the Mississippian Leadville Limestone: Southern Florida and the Bahamas

Environments of the Leadville Limestone have modern analogs in southern Florida-Bahamas region – a world class natural laboratory to study "tropical" carbonate depositional systems. This region represents a time horizon from which one can observe carbonate deposition, the conditions (physical, biological, and chemical) which create various carbonate sediments, and the processes by which the deposits change.

The southern Florida and Bahamas region is a warm-water carbonate factory. The Leadville Limestone was most likely deposited in a warm-water carbonate factory during Mississippian time on an epeiric attached platform, that is, an extensive cratonic area covered by a shallow sea. Although the organisms in warm-water carbonate settings today are different from those of the past due to organic evolution, the roles of sediment producer and modifier have remained largely unchanged through time. Warm marine water is also often supersaturated with respect to calcium carbonate which can be precipitated to form carbonate grains such as ooids, peloids, grapestone, and carbonate mud.

Southern Florida is an attached, rimmed carbonate platform. From northwest to southeast, the platform consists of mangrove swamps and supratidal flats (Everglades), an inner shelf (Florida Bay), inner and outer shelf margins, and a shallow slope into the Straits of Florida. Florida Bay is triangular shaped due to barriers that restrict circulation. A variety of sedimentary environments are represented in Florida Bay as part of a transgressive record: (1) fresh-water pond, (2) coastal mangrove swamp, (3) broad, shallow bay basins ("lake"), (4) mud mounds, and (5) island. From our work on the Leadville Limestone, we recognize the shallow bay basins and mud mounds as modern analogs. The southern Florida platform has a rimmed margin formed by the arcuate reef track band. Sedimentary environments include the seaward forereef, discontinuous outer barrier reef, and back reef consisting of a sand apron and lagoon (containing patch reefs and sand shoals). There are no barrier reefs known in the Leadville Limestone. However, from our work, we recognize the marine mud mounds, patch reefs, and sand shoals in the reef tract as modern analogs.

The Great Bahama Bank is an unattached, isolated rimmed carbonate platform. From east to west, the Great Bahama Bank consists of Earth's third longest barrier reef, a narrow lagoon, Andros Island (exposed Pleistocene limestone) with modern carbonate tidal flats on the western side, the shelf lagoon, and oolitic shoals. The carbonate tidal flats are laterally extensive along strike and represent part of a shallowing upward cycle. From our work on the Leadville Limestone, we recognize the ooid shoals and shelf lagoonal sedimentation as modern analogs. Carbonate tidal flats are productive in Williston Basin fields and other carbonate reservoirs. Recognizing the modern characteristics of carbonate tidal flats in the Leadville Limestone may provide additional target areas for drilling.

Mississippian/Devonian and Pennsylvanian Brine Chemistry and Trends within the Paradox Basin, Utah

There is a systematic change in the chemistry of both the Mississippian/Devonian and Pennsylvanian brine systems from north to south through the Paradox Basin, and the associated counties. The Pennsylvanian-system brines are more saline than the Mississippian/Devonian-system brines. Piper and Stiff diagrams show that the brines from both systems are predominantly sodium-rich in nature, with some samples containing greater percentages of calcium and to a lesser extent magnesium. The Piper and Stiff diagrams also show that both brine systems are high in chloride with some samples being high in sulfate content. Bicarbonate is very low in both brine systems. Based on brine chemistry the direction of ground-water movement in the Mississippian/Devonian and Pennsylvanian systems is generally southwestward toward the topographically low outcrop areas along the Colorado River in Arizona.

Regional Middle Paleozoic Hydrodynamic Pressure Regime of the Paradox Basin, Utah and Colorado

Shut-in drill-stem test (DST) pressure data from petroleum exploration and development wells in the Paradox Basin were reviewed to establish the major hydrodynamic trends, especially within the Mississippian. Although about 5000 DST results have been reported, the dataset is very noisy and screening criteria were needed to upgrade it. This resulted in 1529 potentially useable DSTs for the basin, of which 395 DSTs are for the Mississippian and older formations. With the exception of the eastern edge of the basin (western flanks of the San Juan Mountains), there is a single pressure regime for the Mississippian, having a composite pressure gradient of 0.47 pounds per square inch/foot (10.6 kPa/m) over an elevation range of +4000 to -10,000 feet (1200 to -3000 m) above sea level (ft asl [m asl]). This remarkably uniform pressure regime over an area of at least 100 by 100 miles (260 by 260 km) indicates relatively high permeability within the Mississippian. The gradient is about 10% above hydrostatic for fresh water, but is consistent with the density of relatively saline water with a total dissolved solids concentration of 100,000 to 150,000 mg/kg. The head is between 3800 and 4000 ft asl (1160 and 1220 m asl), and coincides with the elevation of the lower Green River and Cataract Canyon section of the Colorado River where they traverse the basin. It appears that the Mississippian and older reservoirs across most of the Paradox Basin are in good hydrological communication with the Colorado River system, perhaps because they are within about 1000 feet (300 m) of the surface beneath Cataract Canyon. This large-scale hydrological connection between the surface and the Mississippian may be a geologically recent occurrence. Consideration of the rate of incision by the Colorado River system suggests that the Mississippian could have been hydrologically isolated and fully saturated several million years ago, and could have held significantly greater quantities of oil and gas.

CHAPTER 1
INTRODUCTION

Thomas C. Chidsey, Jr., Utah Geological Survey

Project Overview

The Mississippian (late Kinderhookian to early Meramecian) Leadville Limestone has produced over 53 million barrels (bbls) (8.4 million m^3) of oil/condensate as of September 1, 2008, from seven fields in the northern Paradox Basin region (Colorado Oil and Gas Conservation Commission, 2008; Utah Division of Oil, Gas and Mining, 2008), referred to as the Paradox fold and fault belt, of Utah and Colorado (figure 1-1). All of these fields are currently operated by independent producers. There have been no significant new oil discoveries since the early 1960s, and only independent producers continue to explore for Leadville oil targets in the region, 85% of which is under the stewardship of the federal government. This environmentally sensitive, 7500-square-mile (19,400 km^2) area is relatively unexplored with only about 100 exploratory wells that penetrated the Leadville (less than one well per township), and thus the potential for new discoveries remains great.

The overall goals of this study were to (1) develop and demonstrate techniques and exploration methods never tried on the Leadville Limestone, (2) target areas for exploration, (3) increase deliverability from new and old Leadville fields through detailed reservoir characterization, (4) reduce exploration costs and risk especially in environmentally sensitive areas, and (5) add new oil discoveries and reserves.

To achieve the goals and objectives, and to carry out the Leadville Limestone study, the Utah Geological Survey (UGS) and Eby Petrography & Consulting, Inc. entered into a cooperative agreement with the U.S. Department of Energy (DOE) as part of its Advanced and Key Oilfield Technologies for Independents (Area 2 – Exploration) Program. The project was conducted in two phases, each with specific objectives and separated by a continue-stop decision point based on results as of the end of Phase I (Budget Period I). The objective of Phase I was to conduct a case study of the Leadville reservoir at Lisbon field (the largest Leadville oil producer in the Paradox Basin), San Juan County, Utah, in order to understand the reservoir characteristics and lithofacies that can be applied regionally. The first objective of Phase II was to conduct low-cost demonstrations of new exploration technologies to identify surface geochemical anomalies, identify potential oil-prone areas, and potential Leadville oil migration directions, especially in environmentally sensitive areas. The second objective was to determine regional lithofacies (evaluating cores, geophysical well logs, outcrop, and modern analogs) to target areas for future Leadville exploration. These objectives are designed to assist the independent producers and explorers who have limited financial and personnel resources.

This report covers research and results of the five-year Leadville Limestone exploration play project (October 1, 2003, through September 30, 2008). The report is divided into three sections: (1) a case study of lithofacies and diagenetic history of the Leadville at Lisbon field, San Juan County, Utah, (2) exploration techniques and results of a surface geochemical survey conducted over the Lisbon and Lightning Draw Southeast fields (and areas in between) and identification of oil-prone areas using epifluorescence in well cuttings from regional wells, and (3) regional studies of Leadville lithofacies, a comparison of modern and outcrop depositional

analogs, and an estimation of potential oil migration directions by evaluating the hydrodynamic pressure regime and water chemistry of the middle Paleozoic strata of the Paradox Basin.

The results of this project have been provided to industry and other researchers through Technical Advisory and Stake Holders Boards, an industry outreach program, digital project databases, and a project Web page. The Technical Advisory Board was composed of industry representatives operating in the Paradox Basin and a Stake Holders Board composed of representatives of state and federal government agencies, and groups with a financial interest within the study area. Project results were also disseminated via core workshops, displays and technical presentations at national and regional professional conventions, non-technical presentations at public meetings and forums, and papers in various technical or trade journals, and UGS publications. All project maps, studies, and results are, or will be, publicly available in digital (interactive, menu-driven products on compact disc) or hard-copy format. Refer to Appendix A for a complete listing of technology transfer activities and publications.

Project Benefits and Potential Application

Exploring the Leadville Limestone is high risk, with less than a 10% chance of success based on the drilling history of the region. Prospect definition often requires expensive, three-dimensional (3D) seismic acquisition, at times in environmentally sensitive areas. These facts make exploring difficult for independents that have limited funds available to try new, unproven techniques that might increase the chance of successfully discovering oil. We believe that one or more of the project results will reduce the risk taken by an independent producer in looking for Leadville oil, not only in exploring but in using a new technique. For example, an independent would not likely attempt surface geochemical surveys without first knowing they have been proven successful in the region. Our project demonstrates geochemical surveys are an effective technique in environmentally sensitive areas, thus saving independents both time and money exploring for Leadville oil.

Another problem in exploring for oil in the Leadville Limestone is the lack of published or publicly available geologic and reservoir information, such as regional lithofacies maps, complete reservoir characterization studies, surface geochemical surveys, regional hydrodynamic pressure regime maps, and oil show data and migration interpretations. This project provides this information to save independents cash and manpower resources which they simply do not possess or normally have available only for drilling. The technology, maps, and studies generated from this project will help independents to identify or eliminate areas and exploration targets prior to spending significant financial resources on seismic data acquisition and potential environmental litigation, and therefore increase the chance of successfully finding new economic accumulations of Leadville oil.

These benefits may also apply to other high-risk, sparsely drilled basins or regions where there are potential shallow-marine carbonate reservoirs equivalent to the Mississippian Leadville Limestone. These areas include the Utah-Wyoming-Montana thrust belt (Madison Limestone), the Kaiparowits Basin in southern Utah (Redwall Limestone), the Basin and Range Province of Nevada and western Utah (various Mississippian and other Paleozoic units), and the Eagle Basin of Colorado (various Mississippian and other Paleozoic units).

Many mature basins have productive carbonate reservoirs of shallow-marine shelf origin. These mature basins include the Eastern Shelf of the Midland Basin, West Texas (Pennsylvanian-age reservoirs in the Strawn, Canyon, and Cisco Formations); the Permian Basin,

West Texas and southeast New Mexico (Permian-age Abo and other formations along the northwest shelf of the Permian Basin); and the Illinois Basin (various Silurian units). A successful demonstration in the Paradox Basin makes it very likely that the same techniques could be applied in other basins as well. In general, the average field size in these other mature basins is larger than fields in the Paradox Basin. Even though there are differences in depositional lithofacies and structural styles between the Paradox Basin and other basins, the fundamental use of this project's techniques and methods is a critical commonality.

General Geology of the Paradox Basin

The Paradox Basin is located mainly in southeastern Utah and southwestern Colorado, with small portions in northeastern Arizona and the northwestern corner of New Mexico (figure 1-1). The Paradox Basin is an elongate, northwest-southeast-trending, evaporitic basin that predominately developed during the Pennsylvanian, about 330 to 310 million years ago (Ma). The basin can generally be divided into three areas: the Paradox fold and fault belt in the north, the Blanding sub-basin in the south-southwest, and the Aneth platform in southeasternmost Utah (figure 1-1). The Mississippian Leadville Limestone is one of two major oil and gas reservoirs in the Paradox Basin, the other being the Pennsylvanian Paradox Formation (figure 1-2); minor amounts of oil are produced from the Devonian McCracken Sandstone at Lisbon field. Most Leadville production is from the Paradox fold and fault belt (figure 1-3).

The most obvious structural features in the basin are the spectacular anticlines that extend for miles in the northwesterly trending fold and fault belt. The events that caused these and many other structural features to form began in the Proterozoic, when movement initiated on high-angle basement faults around 1700 to 1600 Ma (Stevenson and Baars, 1986, 1987). During Cambrian through Mississippian time, this region, as well as most of eastern Utah, was the site of typical thin, shallow-shelf marine carbonate deposition on the craton while thick deposits accumulated in the miogeocline to the west (Hintze, 1993). However, major changes began in the Pennsylvanian when a pattern of basins and fault-bounded uplifts developed from Utah to Oklahoma as a consequence of the collision of South America, Africa, and southeastern North America (Kluth and Coney, 1981; Kluth, 1986), or from a smaller-scale collision of a microcontinent with south-central North America (Harry and Mickus, 1998). One result of this tectonic event was the uplift of the Ancestral Rockies in the western United States. The Uncompahgre Highlands (uplift) in eastern Utah and western Colorado initially formed as the westernmost range of the Ancestral Rockies during this ancient mountain-building period.

The Uncompahgre Highlands are bounded along their southwestern flank by a large, basement-involved, high-angle reverse fault identified from seismic surveys and exploration drilling (Frahme and Vaughn, 1983). As the highlands rose, an accompanying depression, or foreland basin, formed to the southwest — the Paradox Basin. Rapid subsidence, particularly during the Pennsylvanian and continuing into the Permian, accommodated large volumes of evaporitic and marine sediments that intertongue with non-marine arkosic material shed from the highland area to the northeast (Hintze, 1993).

The present Paradox Basin includes or is surrounded by other uplifts that formed during the Late Cretaceous-early Tertiary Laramide orogeny, such as the Monument upwarp in the west-southwest, and the Uncompahgre uplift, corresponding to the earlier Uncompahgre Highlands, forming the northeast boundary (figure 1-1). Oligocene laccolithic intrusions form the La Sal and Abajo Mountains in the north and central parts of the basin in Utah while the

Carrizo Mountains in Arizona, and the Ute, La Plata, and San Miguel Mountains in Colorado were intruded along the southeastern boundary of the basin (figure 1-1).

The area now occupied by the Paradox fold and fault belt was also the site of greatest Pennsylvanian/Permian subsidence and salt deposition. Folding in the Paradox fold and fault belt began as early as the Late Pennsylvanian as sediments were laid down thinly over areas of rising salt and thickly in areas between rising salt (Doelling, 2000). The Paradox fold and fault belt formed during the Late Cretaceous through Quaternary by a combination of (1) reactivation of basement normal faults, (2) additional salt flowage followed by dissolution and collapse, and (3) regional uplift (Doelling, 2000). Outcrops ranging in age from Pennsylvanian through Cretaceous, with surficial Quaternary deposits, are found within the Paradox Basin.

Most oil and gas produced from the Leadville Limestone is found in basement-involved, northwest-trending structural traps with closure on both anticlines and faults (figure 1-4). Lisbon, Big Indian, Little Valley, Lightning Draw Southeast, and Lisbon Southeast fields (figure 1-3) are sharply folded anticlines that close against the Lisbon fault zone. Salt Wash and Big Flat fields (figure 1-3), northwest of the Lisbon area, are east-west- and north-south-trending anticlines, respectively.

Outcrops ranging in age from Pennsylvanian through Cretaceous, with surficial Quaternary deposits, are found within the Paradox Basin, as illustrated in figure 1-5. The Appendix contains three stratigraphic sections representing the following areas: (1) the Moab-Arches-La Sal area, (2) the Canyonlands National Park area, and (3) the Monticello-Bluff-Aneth area. In the Moab-Arches-La Sal area, the Jurassic Navajo Sandstone is exposed at the surface; in the Canyonlands National Park area, the Permian Cedar Mesa Sandstone is exposed at the surface; and in the Monticello-Bluff-Aneth area, the Cretaceous Dakota Sandstone/Burro Canyon Formation units are exposed at the surface.

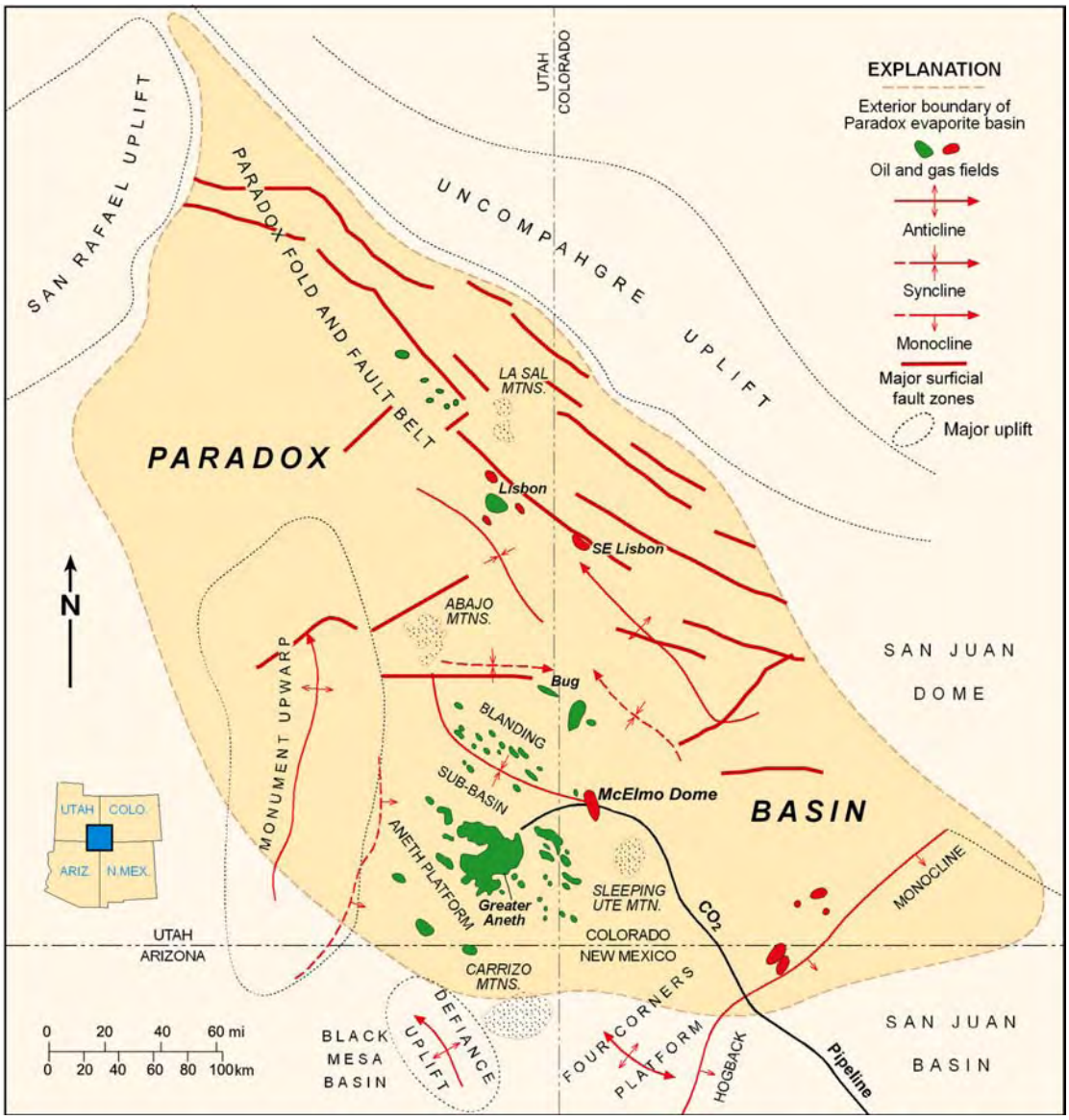

Figure 1-1. Regional setting and oil (green) and gas (red) fields in the Paradox Basin of Utah, Colorado, Arizona, and New Mexico (modified from Kitcho, 1981; Harr, 1996).

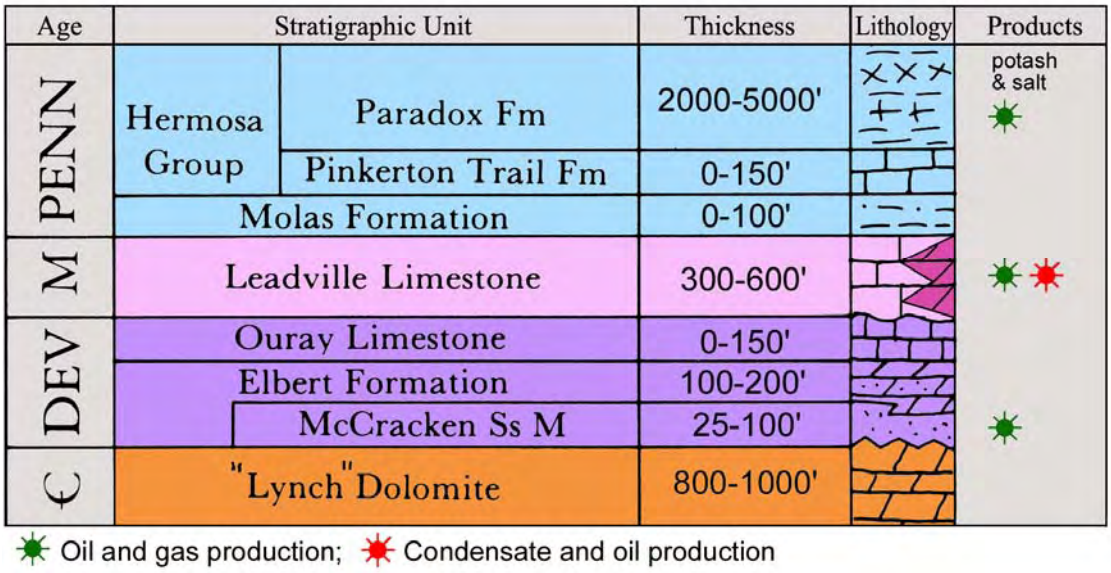

Figure 1-2. Paleozoic stratigraphic section for the central Paradox Basin near Monticello, Utah (after Hintze, 1993).

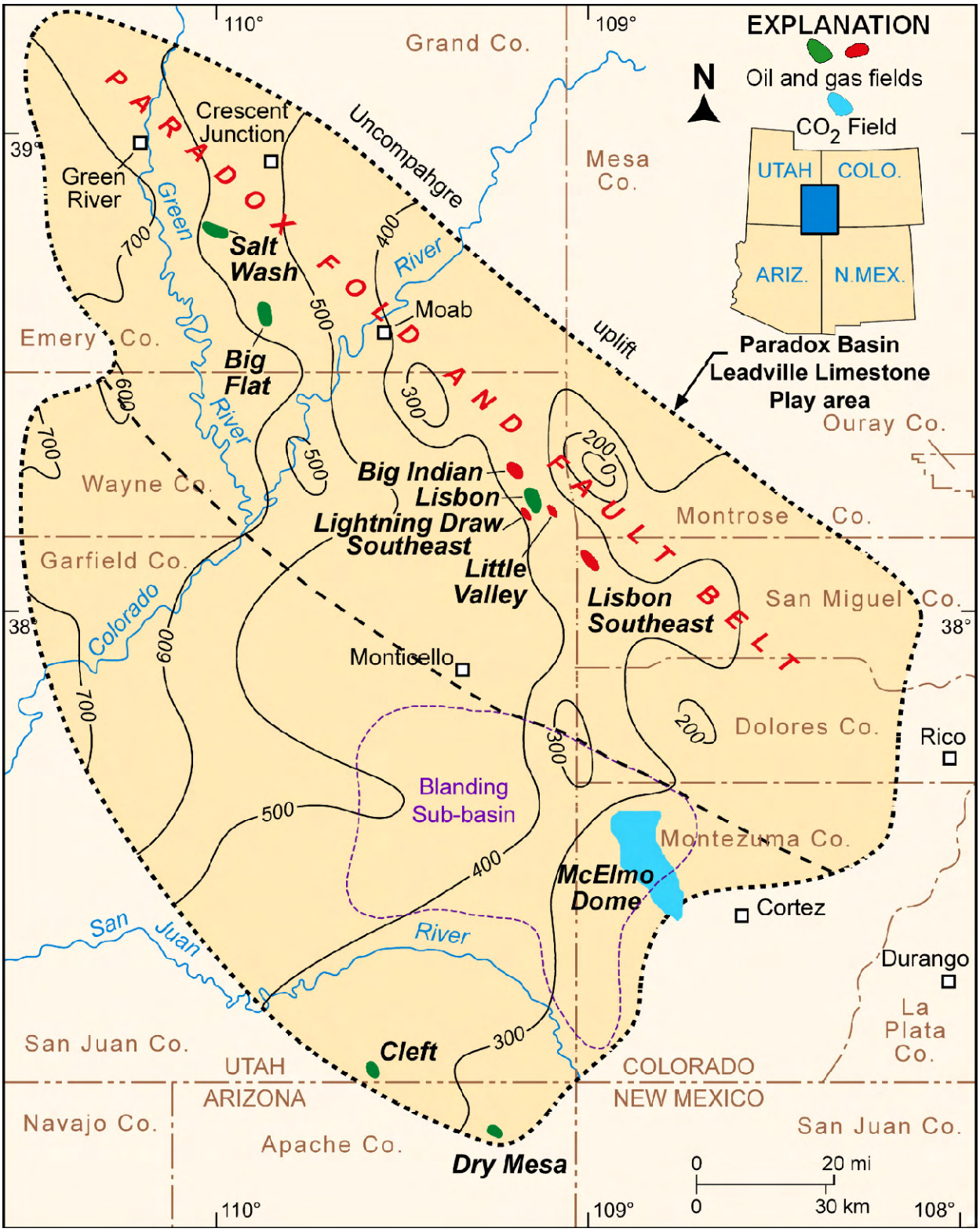

Figure 1-3. Regional setting of the Paradox Basin, showing oil and gas fields that produce from the Mississippian Leadville Limestone, and thickness of the Leadville (contour interval is 100 feet). Modified from Parker and Roberts (1963).

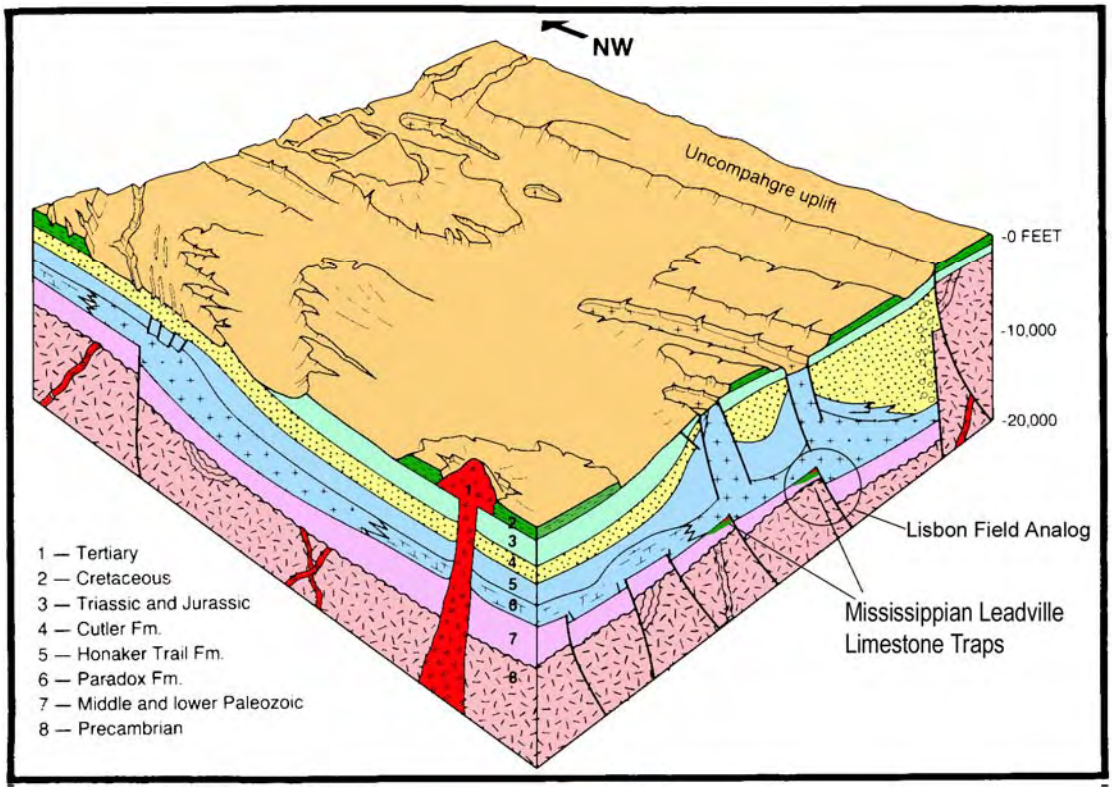

Figure 1-4. Schematic block diagram of the Paradox Basin displaying basement-involved structural trapping mechanisms for the Leadville Limestone fields (modified from Petroleum Information, 1984; original drawing by J.A. Fallin).

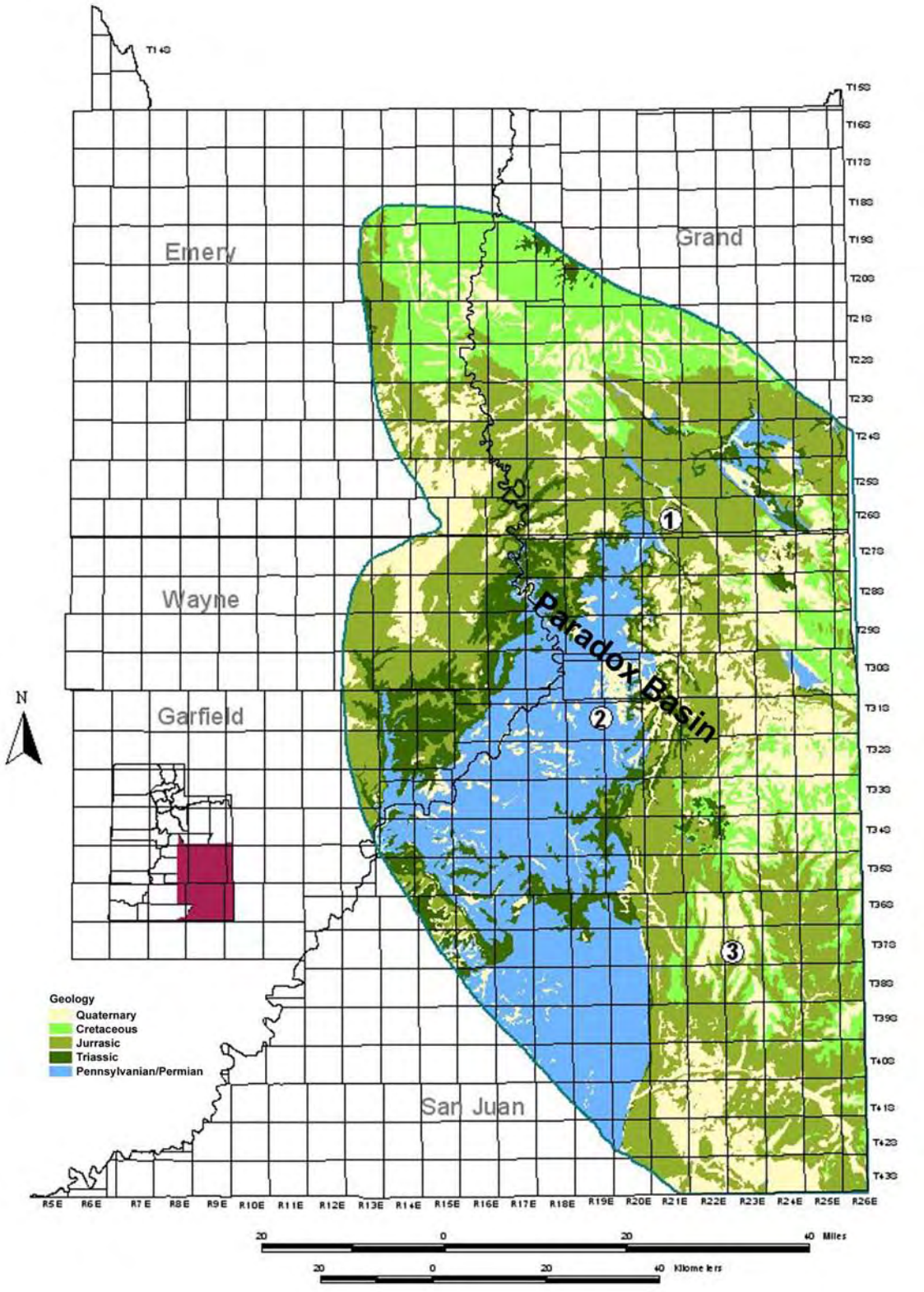

Figure 1-5. General geology of the Paradox Basin, and the locations (1 through 3) of the stratigraphic sections shown in Appendix B. Modified from Hintze and others (2000).

LISBON FIELD, SAN JUAN COUNTY, UTAH: A CASE STUDY OF LEADVILLE LIMESTONE LITHOFACIES AND DIAGENETIC HISTORY

CHAPTER 2
LISBON CASE-STUDY FIELD, SAN JUAN COUNTY, UTAH: GENERAL FIELD CHARACTERISTICS AND RESERVOIR MAPPING

Thomas C. Chidsey, Jr., Craig D. Morgan, and Kevin McClure,
Utah Geological Survey
and
David E. Eby, Eby Petrography & Consulting, Inc.

Introduction and Field Synopsis

Lisbon field, San Juan County, Utah (figure 1-3), accounts for most of the Leadville oil production in the Paradox Basin. A wealth of Lisbon core, petrographic, and other data is available to the UGS. The reservoir characteristics, particularly diagenetic overprinting and history, and Leadville lithofacies can be applied regionally to other fields and exploration trends in the Paradox Basin. Therefore, we selected Lisbon as the major case-study field for the Leadville Limestone project. This evaluation included data collection, and construction of various maps (top of structure, thickness, porosity, and so forth) and cross sections as summarized in this report.

The Lisbon trap is an elongate, asymmetric, northwest-trending anticline, with nearly 2000 feet (600 m) of structural closure and bounded on the northeast flank by a major, basement-involved normal fault with over 2500 feet (760 m) of displacement (Smith and Prather, 1981) (figures 2-1 and 2-2). Several minor, northeast-trending normal faults divide the Lisbon Leadville reservoir into compartments.

Producing units in Lisbon field contain dolomitized crinoidal/skeletal grainstone, packstone, and wackestone fabrics. Diagenesis includes fracturing, autobrecciation, karst development, hydrothermal dolomite, and bitumen plugging (described in detail in Chapter 4). The net reservoir thickness is 225 feet (69 m) over a 5120-acre (2100 ha) area (Clark, 1978; Smouse, 1993). Reservoir quality is greatly improved by natural fracture systems associated with the Paradox fold and fault belt. Porosity averages 6% in intercrystalline and moldic networks enhanced by fractures; permeability averages 22 millidarcies (mD). The drive mechanism is an expanding gas cap and gravity drainage; original water saturation was 39% (Clark, 1978; Smouse, 1993). The bottom-hole temperature ranges from 133 to 189ºF (56-87ºC). The oil and gas characteristics are summarized on table 2-1.

Lisbon field was discovered in 1960 with the completion of the Pure Oil Company No. 1 NW Lisbon USA well, NE1/4NW1/4 section 10, T. 30 S., R. 24 E., Salt Lake Baseline and Meridian (SLBL&M) (figure 2-1), with an initial flowing potential (IFP) of 179 bbls of oil per day (BOPD) (28 m^3) and 4376 thousand cubic feet of gas per day (124 MCMPD). The original reservoir field pressure was 2982 pounds per square inch (psi [20,560 kPa]) (Clark, 1978). Currently, 20 producing (or shut-in) wells, 11 abandoned producers, five injection wells (four gas injection wells and one water/gas injection well), and four dry holes are in the field. Cumulative production as of August 1, 2008, was 51,167,239 bbls of oil (8,135,591 m^3), 796.7 billion cubic feet of gas (BCFG) (22.6 BCMG) (cycled gas), and 50,470,353 bbls of water (8,024,786 m^3) (Utah Division of Oil, Gas and Mining, 2008). Hydrocarbon gas that was re-injected into the crest of the structure to control pressure decline is now being produced; acid gas is still re-injected.

Three factors create reservoir heterogeneity within productive zones: (1) variations in carbonate fabrics and facies, (2) diagenesis (including karstification), and (3) fracturing. The extent of these factors and how they are combined affect the degree to which they create barriers to fluid flow.

Log-Based Correlation Scheme

The typical vertical sequence or cycle of depositional lithofacies from Lisbon field, as determined from conventional core, was tied to the corresponding gamma-ray and neutron-density curves from geophysical well logs (figure 2-3). The correlation scheme enabled us to identify the major zone contacts, seals or barriers, baffles, producing or potential reservoirs, and depositional lithofacies. These contacts were used to produce field cross sections (figure 2-2 and plates 1 and 2 in **Deliverable 1-4 – Field Maps and Cross Sections: Lisbon Field, San Juan County, Utah**) and a variety of structure and isochore maps (figures 2-1, 2-4 through 2-11).

Seals or barriers include thick shales of the Molas Formation, which overlies the Leadville Limestone. Baffles are those rock units that restrict fluid flow in some parts of the field but may develop enough porosity and permeability in other parts, through diagenetic processes or lithofacies changes, to provide a conduit for fluid flow or even oil storage. Baffles are found throughout the Leadville stratigraphic section. The four reservoir zones defined in this study (1 through 4, from top to bottom) are those units containing 8% or more porosity based on the average of the neutron and density porosity values (figure 2-3).

Depositionally, rock units are divided into crinoid banks/shoals, Waulsortian-type carbonate buildups (mounds) (bafflestone, bindstone, grainstone, and packstone), and inter-bank/shoal and inter-mound seals or barriers (mudstone and shale). Associated with Waulsortian carbonate-buildup rock units are flank/off buildups (floatstone, rudstone, wackestone, and mudstone). Porosity units, and reservoir or potential reservoir layers, are identified within the crinoid banks/shoals and carbonate-buildup and flank/off-buildup intervals. The crinoid banks/shoals and carbonate-buildup units, and some of the flank/off-buildup units contain all productive reservoir lithofacies.

The correlation scheme was used for (1) predicting changes in reservoir and non-reservoir rocks across the field, (2) comparing field to non-field areas, (3) estimating the reservoir properties and identifying lithofacies in wells which were not cored, and (4) determining potential units suitable for horizontal drilling projects. It can be applied to other fields in the Paradox Basin, both those with cores and without.

Reservoir Mapping

We constructed isochore maps of reservoir zones 1 through 4 in the Leadville Limestone for Lisbon field (figures 2-4 through 2-7). These field maps incorporate zone tops and thickness from all geophysical well logs in the area. We generated the net feet of porosity isochore maps for reservoir zones 1 through 4 (figures 2-8 through 2-11) of the Leadville for those parts of the reservoir units containing 10% or more porosity based on the average of the neutron and density porosity values. While 8% or more porosity defines the reservoir zones, we used 10% or more porosity for greater definition of the zones mapped. The maps display well names, Leadville completions, and interval thickness for each well.

We plotted the bottom-hole temperature for most wells in Lisbon field (figure 2-12). The maps also include faulting. Contoured temperatures identify possible patterns in temperature data. All wells with available core show evidence of hydrothermal dolomitization. The presence of hydrothermal dolomite and its relationship to reservoir temperature and faulting are critical in identifying diagenetic trends.

We conducted production analysis for Lisbon field by compiling data through two principal tasks: (1) review of existing well-completion data, and (2) determination of production history from monthly production reports available through the Utah Division of Oil, Gas and Mining. We merged this information with geological characterization data and incorporated into the interpretation of reservoir diagenesis (described in Chapter 4).

Well-test data can provide key insights into the nature of reservoir heterogeneities, and also provide "large-scale" quantitative data on actual reservoir properties and lithofacies from the Lisbon case-study reservoir. Although a number of well tests have been conducted in all of the target reservoirs, only the IFP well tests provide quantitative reservoir property information. We plotted IFP well tests for each well (figure 2-13). Oil production from Lisbon field has shown a steady decline since peaking in the 1970s. We plotted cumulative production for each well (figure 2-14). These plots are used to determine possible production “sweet spots” and their relationship to faulting and reservoir diagenesis.

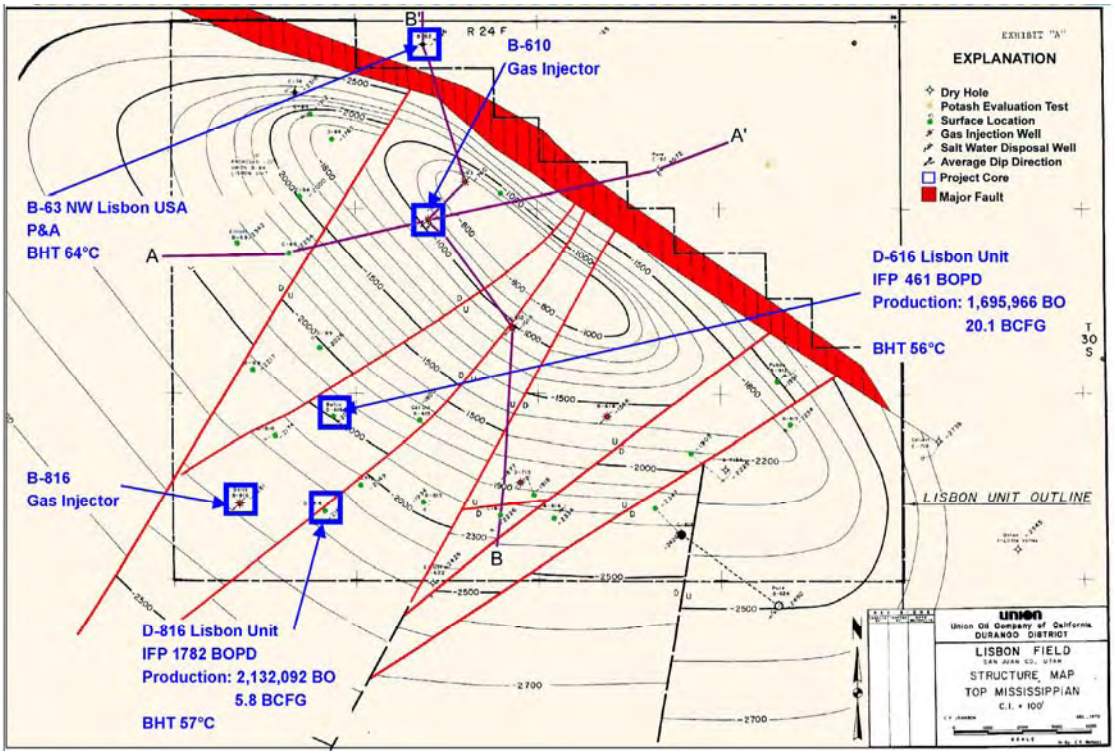

Figure 2-1. Top of structure of the Leadville Limestone, Lisbon field, San Juan County, Utah (modified from C.F. Johnson, Union Oil Company of California files, 1970; courtesy of Tom Brown, Inc.). Cross section A-A' shown on figure 2-2. Also displayed are wells from which cores were described in this study.

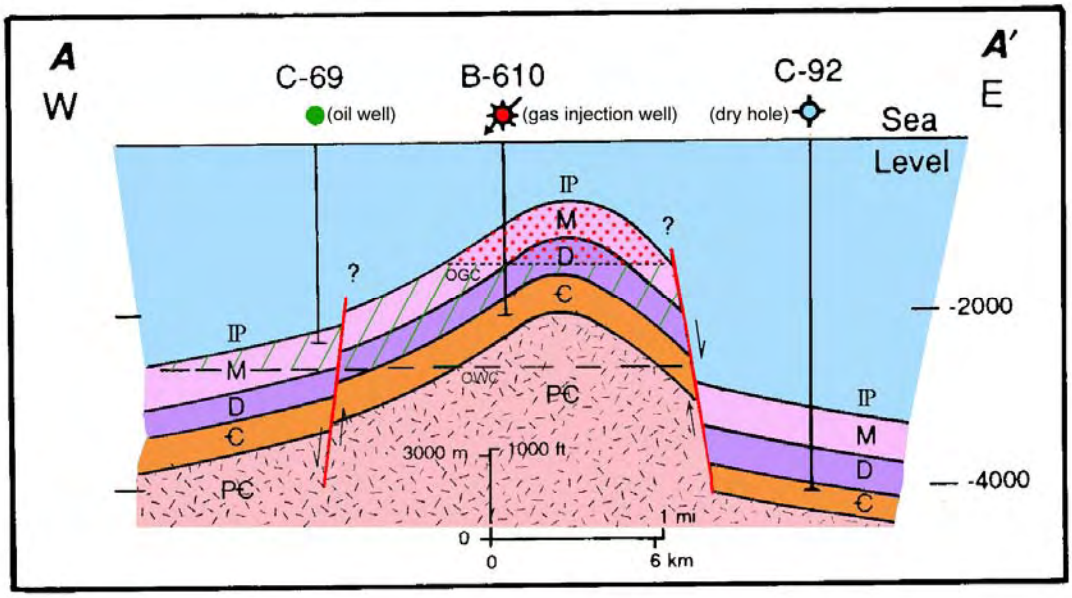

Figure 2-2. Schematic east-west structural cross section, Lisbon field. Line of section shown on figure 2-1. Note the juxtaposition of the Mississippian (M) section against the Pennsylvanian (IP) section which includes evaporites (salt) and organic-rich shale. OGC = oil-gas contact, OWC = oil-water contact. Modified from Clark, 1978.

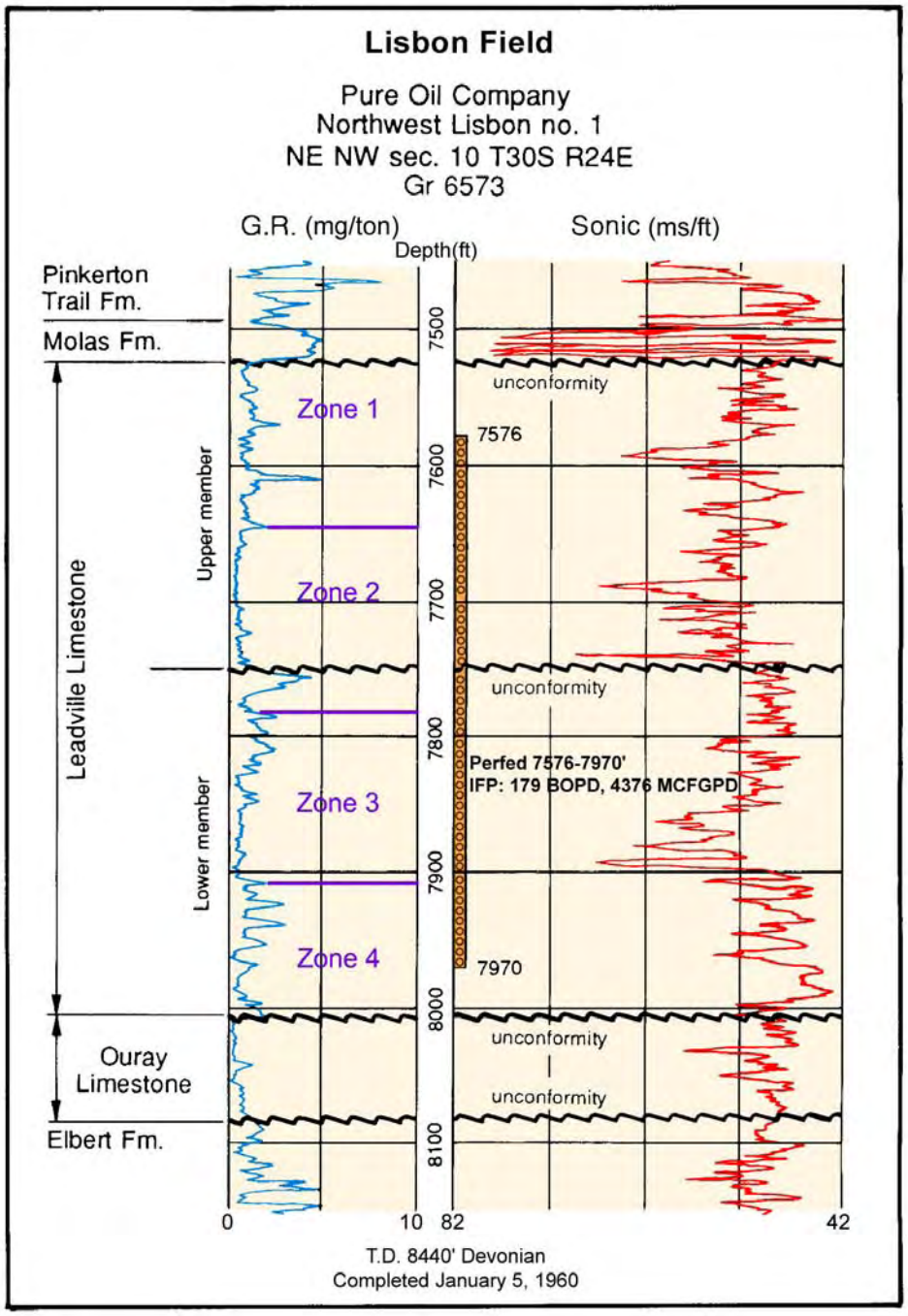

Figure 2-3. Typical gamma ray–sonic log of the Leadville Limestone showing the four reservoir zones defined in this study; Lisbon field discovery well, San Juan County, Utah. See figure 2-1 for well location.

Figure 2-4. Isochore of zone 1, Leadville Limestone, Lisbon field.

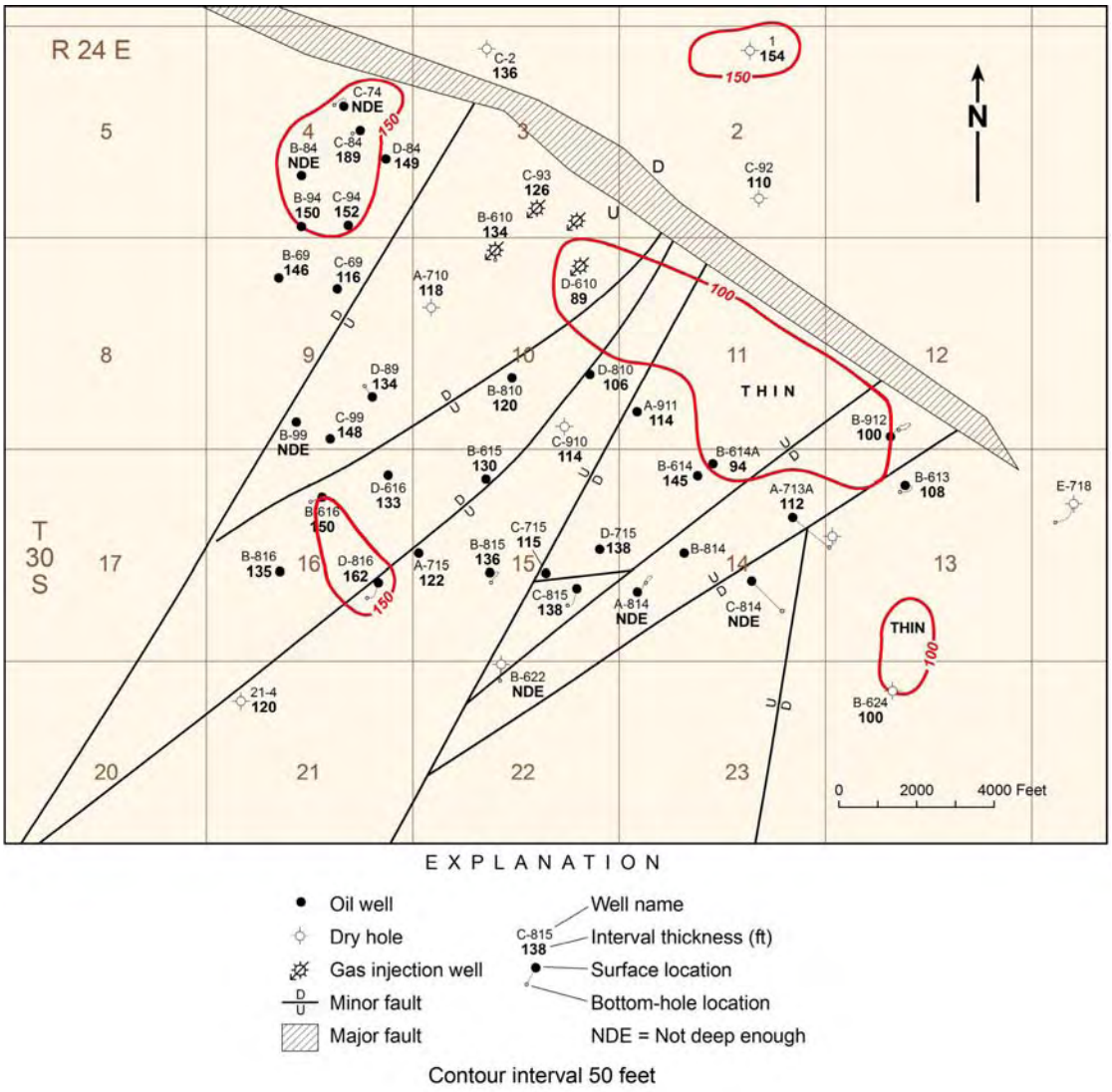

Figure 2-5. Isochore of zone 2, Leadville Limestone, Lisbon field.

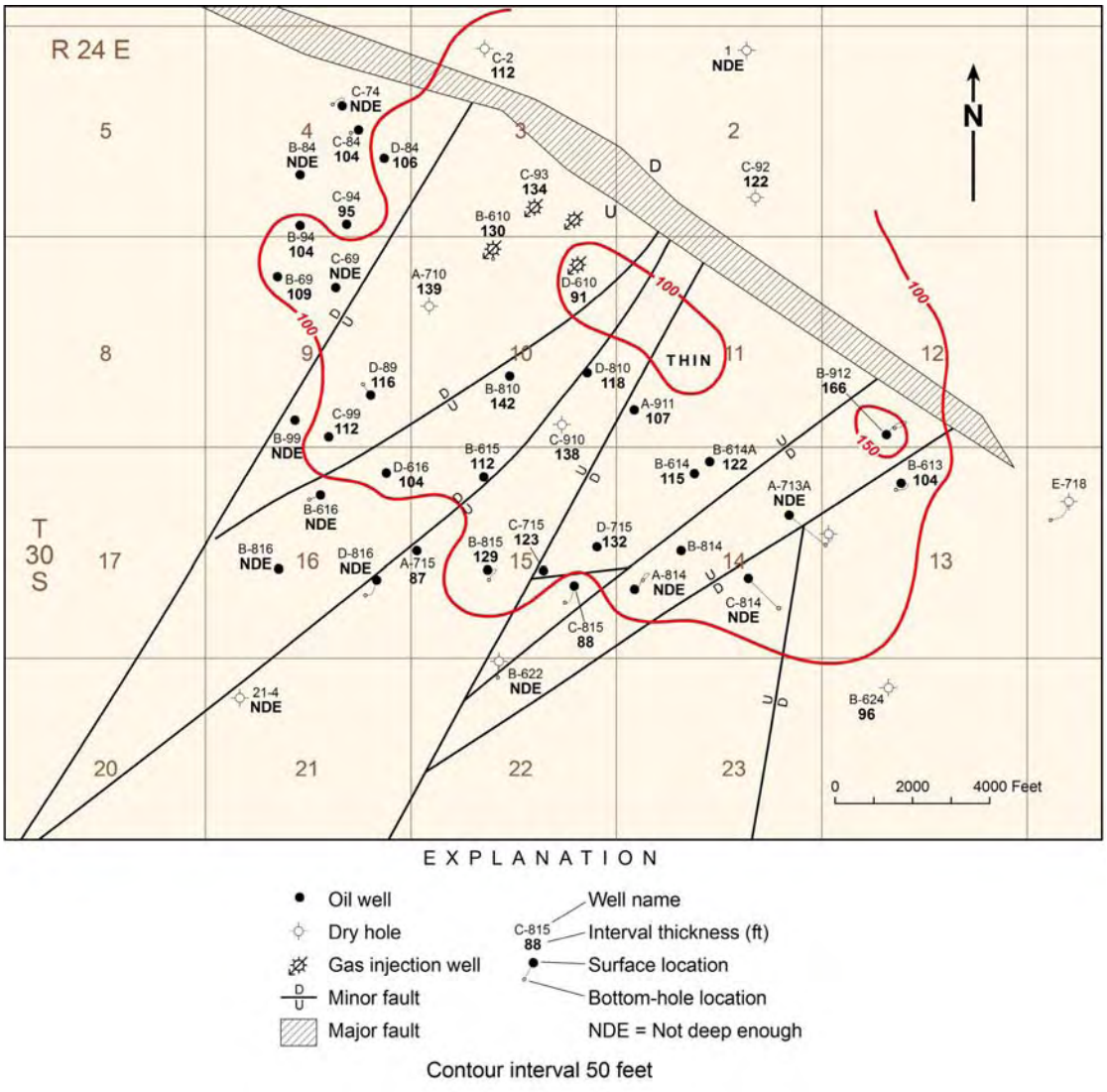

Figure 2-6. Isochore of zone 3, Leadville Limestone, Lisbon field.

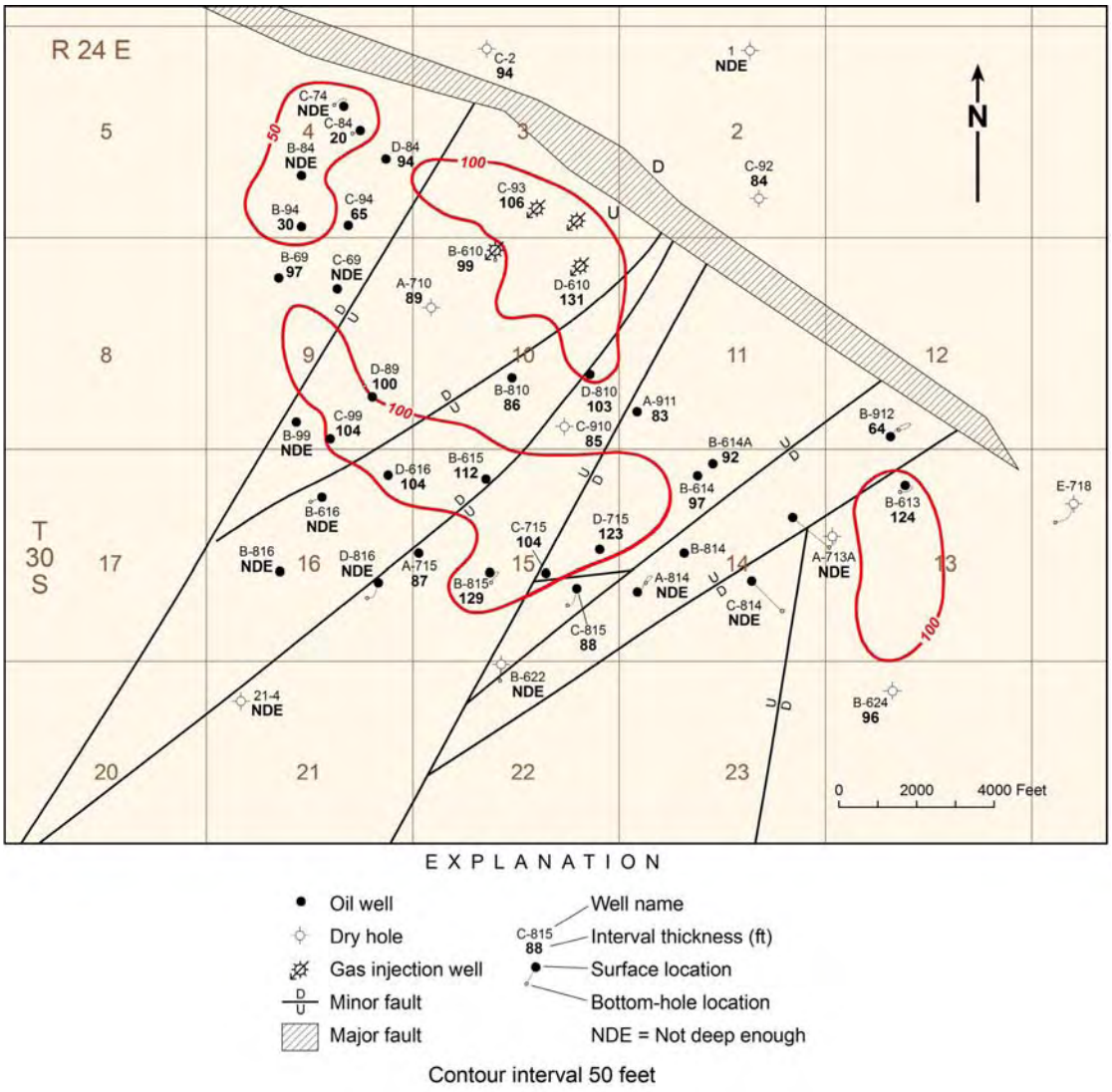

Figure 2-7. Isochore of zone 4, Leadville Limestone, Lisbon field.

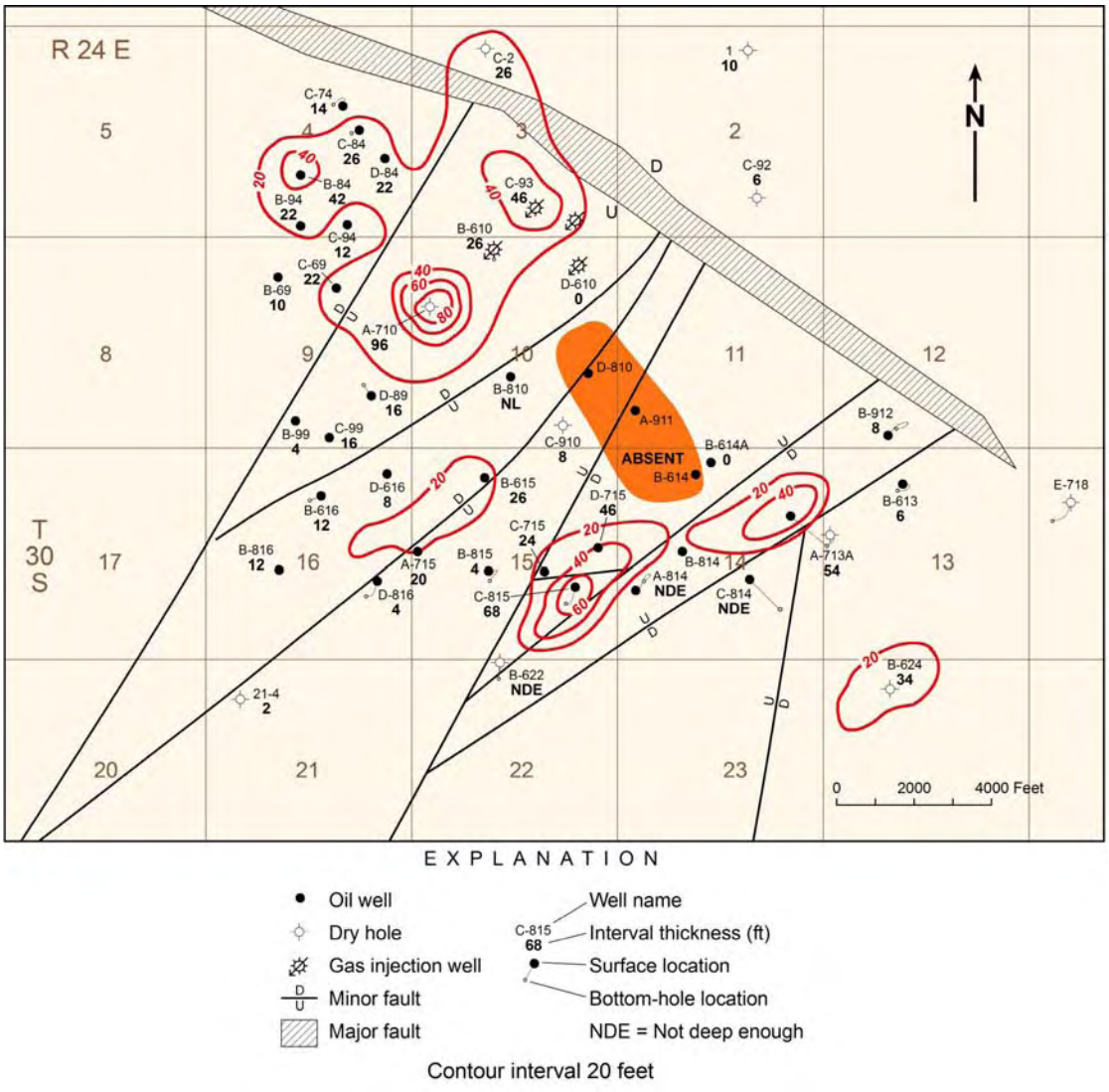

Figure 2-8. Net feet of porosity isochore for reservoir zone 1, Leadville Limestone, Lisbon field.

Figure 2-9. Net feet of porosity isochore for reservoir zone 2, Leadville Limestone, Lisbon field.

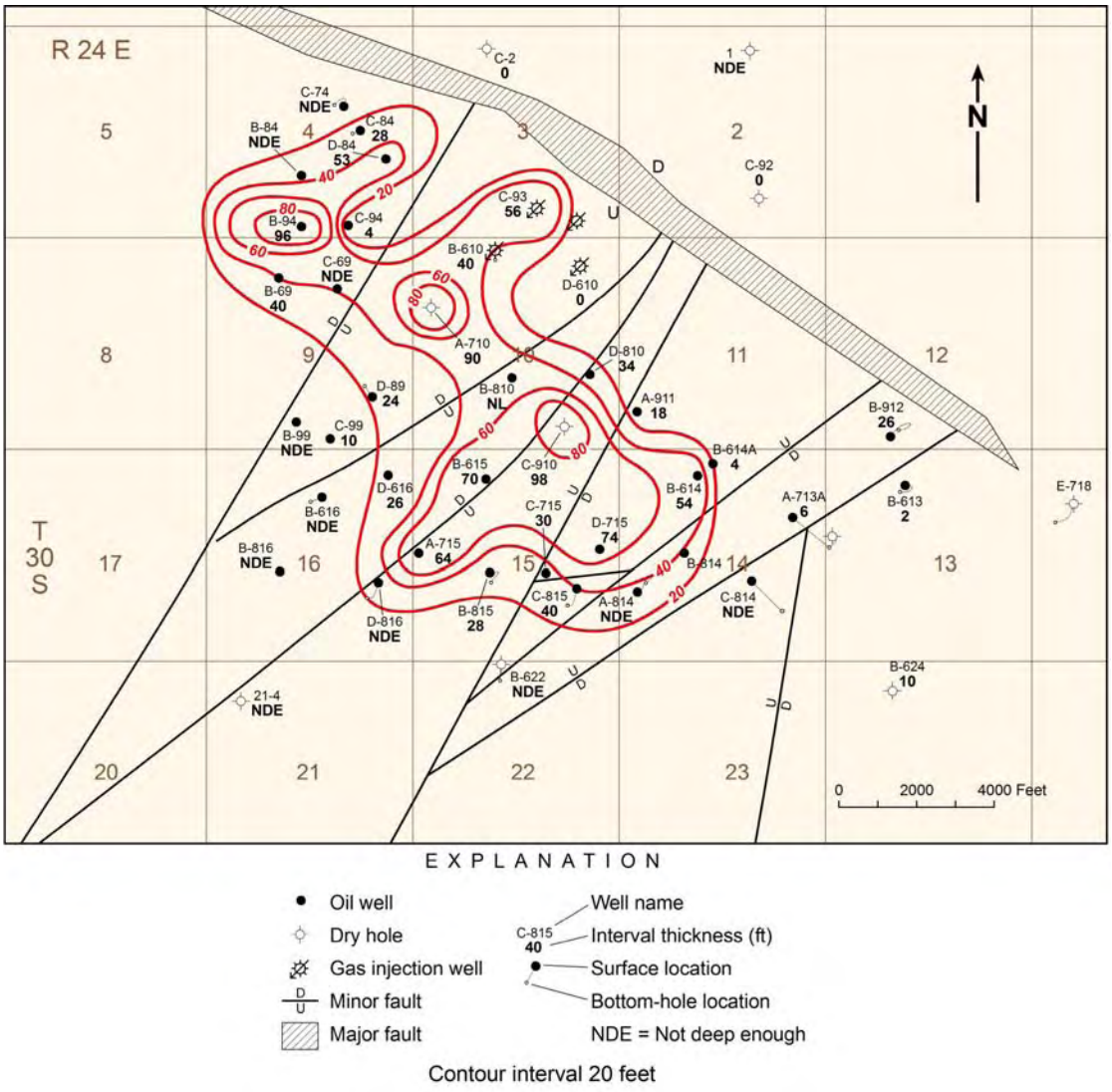

Figure 2-10. Net feet of porosity isochore for reservoir zone 3, Leadville Limestone, Lisbon field.

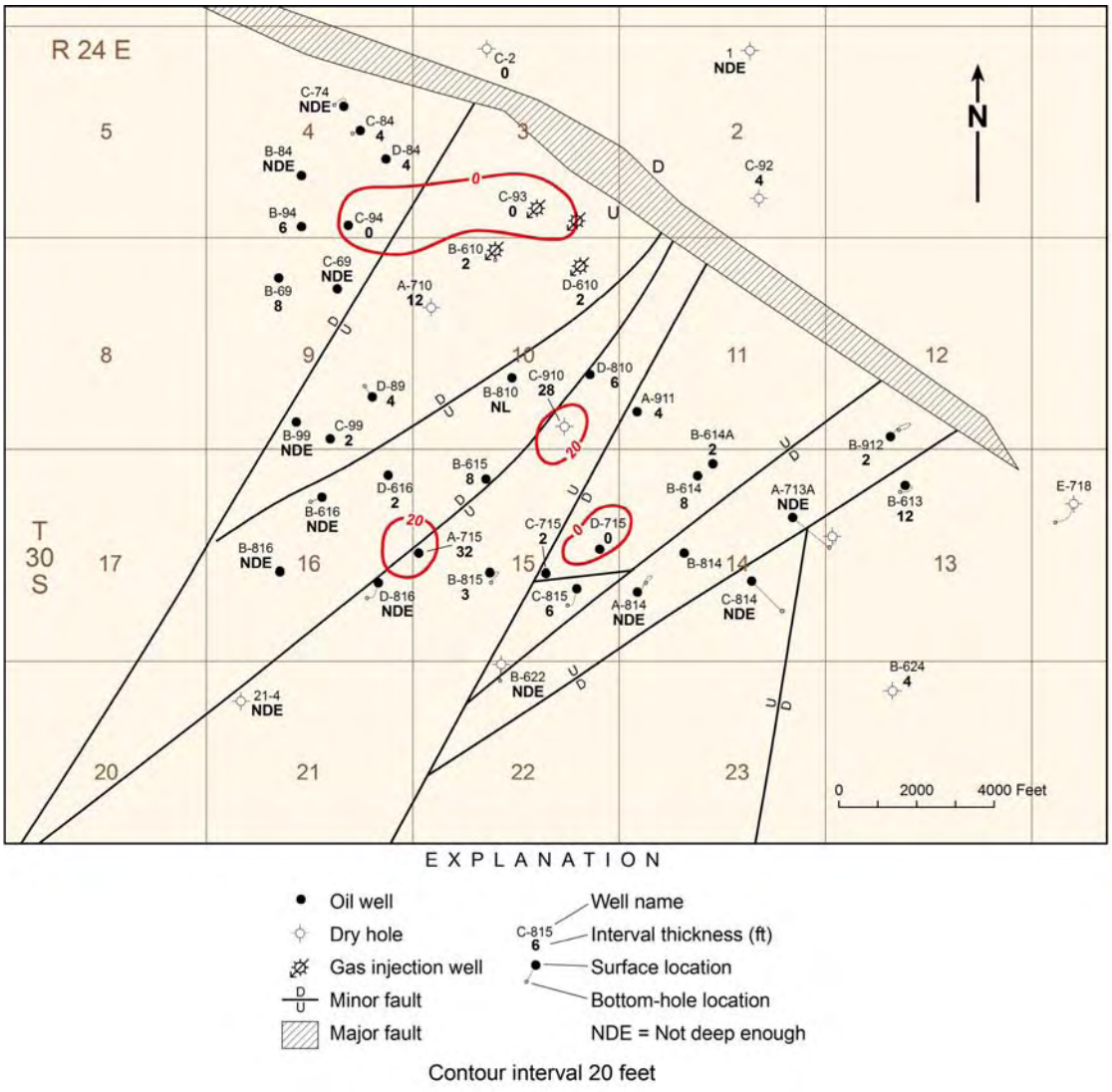

Figure 2-11. Net feet of porosity isochore for reservoir zone 4, Leadville Limestone, Lisbon field.

Figure 2-12. Bottom-hole temperature map, Leadville Limestone, Lisbon field.

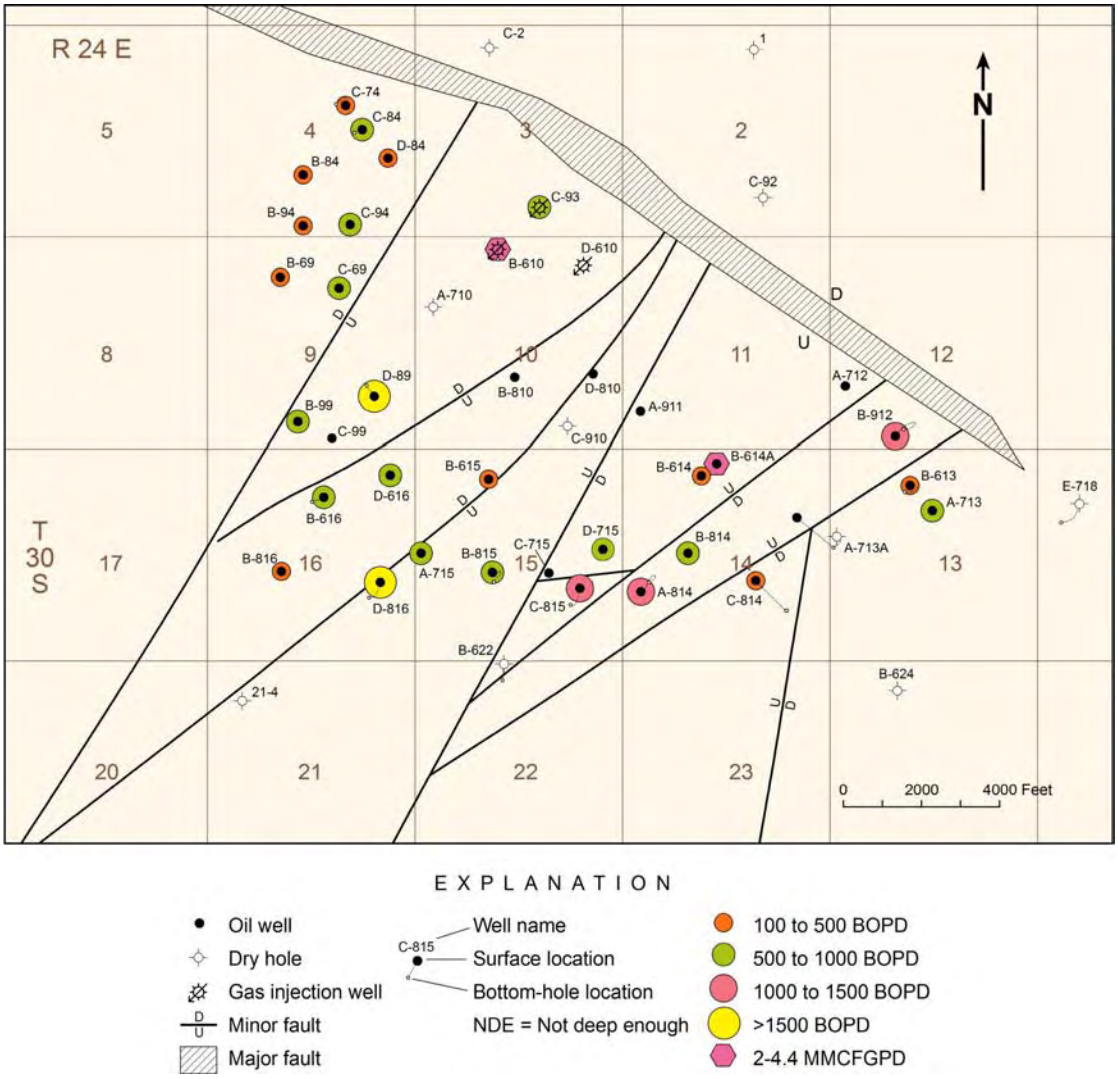

Figure 2-13. Initial flowing potential, Leadville Limestone, Lisbon field.

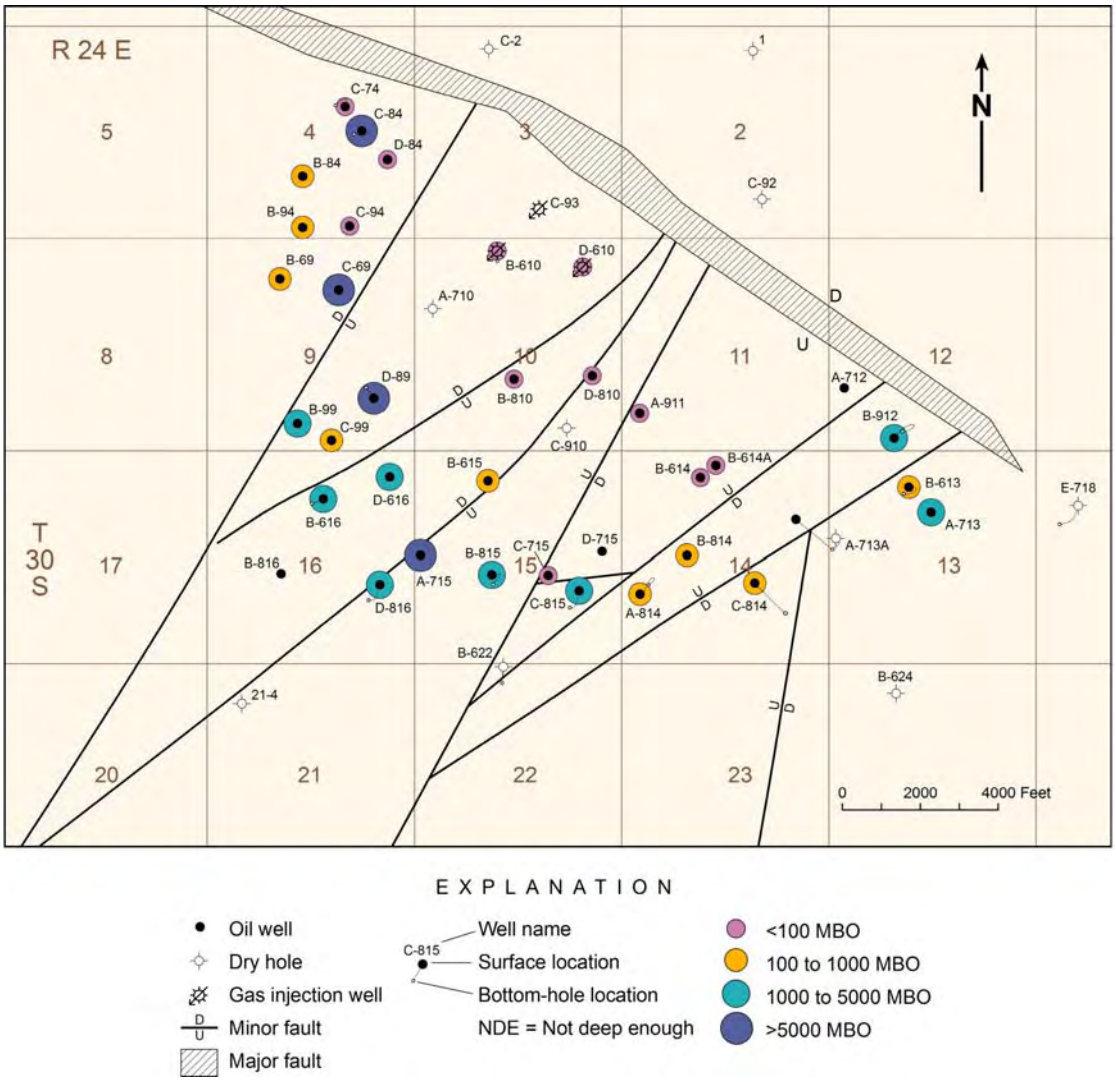

Figure 2-14. Cumulative oil production, Leadville Limestone, Lisbon field.

Table 2-1. General characteristics of the oil and gas produced from the Leadville Limestone at Lisbon field, San Juan County, Utah (Stowe, 1972; Morgan, 1993; UGS oil sample bank database).

Oil		Gas	
Gravity	54-62.6° API	Methane	48%
Specific Gravity	0.765	Higher Fractions	13%
Color	Yellow to Red	Nitrogen	24%
Pour Point	-35°F	Carbon Dioxide	14%
Viscosity (cst)*	1.03 @ 104°F	Hydrogen Sulfide	1.2%
Viscosity (sus)†	29.2 @ 104°F	Helium	trace-1.1%
Sulfur	0.2%	Specific Gravity	0.89
Nitrogen	0.002%	Heating Value	685 BTU/ft^3

* centistokes
† Saybolt Universal Seconds

CHAPTER 3
LITHOFACIES IN THE LEADVILLE LIMESTONE, LISBON CASE-STUDY FIELD

Thomas C. Chidsey, Jr., and Kevin McClure, Utah Geological Survey
and
David E. Eby, Eby Petrography & Consulting, Inc.

Regional Setting of the Leadville Limestone

The Mississippian (late Kinderhookian through Osagean to early Meramecian time) Leadville Limestone is a shallow, open marine, carbonate-shelf deposit (figure 3-1). The western part of the Paradox fold and fault belt includes a regional, reflux-dolomitized, interior bank lithofacies containing Waulsortian mounds (Welsh and Bissell, 1979). During Late Mississippian time, the entire carbonate platform in southeastern Utah and southwestern Colorado was subjected to subaerial erosion resulting in formation of a lateritic regolith (Welsh and Bissell, 1979). This regolith and associated carbonate dissolution is an important factor in Leadville reservoir potential (figure 3-2). Solution breccia and karstified surfaces are common, including possible local development of cavernous zones (Fouret, 1982, 1996).

The Leadville Limestone thins from more than 700 feet (230 m) in the northwest corner of the Paradox Basin to less than 200 feet (70 m) in the southeast corner (Morgan, 1993) (figure 1-3). Thinning is a result of both depositional onlap onto the Mississippian cratonic shelf and erosion. The Leadville is overlain by the Pennsylvanian Molas Formation and underlain by the Devonian Ouray Limestone (figure 1-2).

Periodic movement along northwest-trending faults affected deposition of the Leadville Limestone. Crinoid banks or mounds, the primary reservoir lithofacies (figure 3-1), accumulated in shallow-water environments on upthrown fault blocks or other paleotopographic highs. In areas of greatest paleorelief, the Leadville is completely missing as a result of non-deposition or subsequent erosion (Baars, 1966).

The Leadville Limestone is divided into two members (see figure 2-3) separated by an intraformational disconformity. The dolomitic lower member is composed of mudstone, wackestone, packstone, and grainstone deposited in shallow-marine, subtidal, supratidal, and intertidal environments (Fouret, 1982, 1996). Fossils include crinoids, fenestrate bryozoans, and brachiopods. Locally, mud-supported boundstone creates buildups or mud mounds (Waulsortian facies), involving growth of "algae" (Wilson, 1975; Fouret, 1982, 1996; Ahr, 1989). The upper member is composed of mudstone, packstone, grainstones (limestone and dolomite), and terrigenous clastics also deposited in subtidal, supratidal, and intertidal environments (Fouret, 1982, 1996). Fossils include crinoids and rugose coral. Reservoir rocks are crinoid-bearing packstone (Baars, 1966).

Data Collection and Compilation

Geophysical well logs, cores and cuttings, reservoir data, various reservoir maps, and other information from regional exploratory and field development wells were collected by the UGS. Well locations, formation tops, production data, completion tests, basic core analysis,

porosity and permeability data, and other data were compiled and entered in a database developed by the UGS. This database, INTEGRAL, is a geologic-information database that links a diverse set of geologic data to records using MS Access™. The database is designed so that geological information, such as lithology, petrophysical analyses, or depositional environment, can be exported to software programs to produce cross sections, strip logs, lithofacies maps, various graphs, and other types of presentations.

Core Descriptions

All available conventional cores from Lisbon field (figure 2-1, table 3-1) were photographed and described (**Deliverable 1-1 – Core Descriptions, Core Photographs, and Core Analysis: Lisbon Field, San Juan County, Utah and Deliverable 1-2 – Geophysical Well Logs Tied to Core Descriptions: Lisbon Field, San Juan County, Utah**). Special emphasis was placed on identifying a flow unit's bounding surfaces and depositional environments. The core descriptions follow the guidelines of Bebout and Loucks (1984), which include (1) basic porosity types, (2) mineral composition in percentage, (3) nature of contacts, (4) carbonate structures, (5) carbonate textures in percentage, (6) carbonate fabrics, (7) grain size (dolomite), (8) fractures, (9) color, (10) fossils, (11) cement, and (12) depositional environment. Carbonate fabrics were determined according to Dunham's (1962) and Embry and Klovan's (1971) classification schemes.

Geological characterization on a local scale focused on reservoir heterogeneity, quality, and lateral continuity, as well as possible compartmentalization within Lisbon field. This utilized representative core and modern geophysical well logs to characterize and initially grade various untested intervals in the field for possible additional completion attempts.

The typical vertical sequence or cycle of lithofacies from Lisbon field, as determined from conventional core, was tied to its corresponding log response (figure 3-3). These sequences graphically include (1) carbonate fabric, pore type, physical structures, texture, framework grain, and facies described from core; (2) plotted porosity and permeability analysis from core plugs; and (3) gamma-ray and neutron-density curves from geophysical well logs. The graphs can be used for identifying reservoir and non-reservoir rock, determining potential untested units suitable for completion or possible horizontal drilling projects, and comparing field to non-field areas.

Lisbon Field Lithofacies

Three depositional lithofacies have been identified from Leadville Limestone cores we described from the Lisbon case-study field (figure 3-1). Recognizing and mapping of these lithofacies regionally will delineate prospective reservoir trends containing porous and productive buildups or zones. Leadville lithofacies include open marine, oolitic and peloid shoals, and middle shelf.

Open Marine

Open-marine lithofacies are represented by crinoidal banks or shoals and Waulsortian-type buildups (figure 3-1). Crinoidal banks and shoals are common throughout Leadville deposition, often located on paleotopographic highs developed along the upthrown side of older

basement-involved fault blocks. This lithofacies represents a high-energy environment with well-circulated, normal-marine salinity water in a subtidal setting, although they can also be present in restricted marine, middle shelf settings. Wave action was strong (leaving broken crinoid columns and winnowing out mud) to moderate (leaving articulated crinoid columnals and some muddy matrix). Low to medium cross-bedding is common. Crinoid columnals were not transported far from the thickets where they grew. Rugose corals were also abundant in this environment. According to Wilson (1975), crinoid columnals or segments were covered with organic matter which allowed them to float until accumulating on nearby shoals and banks. Water depths ranged from 5 feet to 45 feet (1.5-14 m). The depositional fabrics of crinoidal banks and shoals include grainstone and packstone (figure 3-4). Rocks representing crinoidal banks and shoals typically contain the following diagnostic constituents: dominantly crinoids and rugose corals, and lesser amounts of broken fenestrate bryozoans, brachiopods, ostracods, and endothyroid forams as skeletal debris. Rock units having this lithofacies constitute a significant reservoir potential, having both effective porosity and permeability when dissolution of skeletal grains, followed by dolomitization, has occurred.

Waulsortian buildups or mud mounds developed exclusively during the Mississippian in many parts of the world (Wilson, 1975) and Waulsortian-type buildups were first described in Lisbon field by Fouret (1982). They are steep-sloped tabular, knoll, or sheet forms composed of several generations of mud deposited in a subtidal setting (Lees and Miller, 1995; Fouret, 1982, 1996) (figure 3-1). The lime mud was precipitated by bacteria and fungal/cyanobacterial filaments (Lees and Miller, 1995). Cyanobacteria were a likely precursor to the green algae *Ivanovia* responsible for Pennsylvanian buildups in the Paradox Basin (Fouret, 1982, 1996). Crinoids and sheet-like fenestrate byrozoans, in the form of thickets, are associated with the deeper parts of the mud mounds and are indicative of well-circulated, normal-marine salinity. Water depths ranged from 60 to 90 feet (20-30 m). The thickets surrounded and helped to stabilize the mound. Burrowing organisms added a pelletal component to the mud, and burrowing often destroyed laminations or made them discontinuous. Individual mounds range from a few feet to tens of feet thick, and cover hundreds of feet in area with distinctive flank deposits. They form thick, extensive aggregates often located on paleotopographic highs associated with basement-involved faults (figure 3-1). This lithofacies represents a low- to moderate-energy environment. The depositional fabrics of the Waulsortian-type buildups include mud-supported boundstone, packstone, and wackestone (figure 3-5). Rocks representing Waulsortian-type buildups typically contain the following diagnostic constituents: peloids, crinoids, bryozoans, and associated skeletal debris, and *stromatactis*. Rock units having this facies constitute a significant reservoir potential, having both effective porosity and permeability, especially after dolomitization. Waulsortian-type buildups are recognized in several additional cores described by Fouret (1982, 1996).

Shoal-flank lithofacies are associated with both crinoid bank/shoal and Waulsortian-type buildup facies (figure 3-1). This lithofacies represents a moderate-energy environment, again with well-circulated, normal-marine salinity water in a subtidal setting. Water depths ranged from 60 to 90 feet (20-30 m). In the shallower areas, wave action was strong to moderate, eroding the flanks of the shoals and mud mounds into a breccia. Bedding is generally absent in cores. The depositional fabrics of the shoal-flank lithofacies include peloidal/skeletal packstone and wackestone (figure 3-6). Rocks representing this lithofacies typically contain the following diagnostic constituents: peloids, crinoids, bryozoans, brachiopods, and associated skeletal debris, and talus, depositional breccia, and conglomerate (Fouret, 1982, 1996). Rock units having shoal-

flank lithofacies constitute a limited reservoir potential, having little effective porosity and permeability.

Oolitic and Peloid Shoals

Oolitic and "hard" peloid shoals developed as a result of regularly agitated, shallow-marine processes on the open-marine or bordering restricted-marine middle shelf (figure 3-1). Like crinoidal banks and Waulsortian-type buildups, hard peloid and oolitic shoals are common throughout Leadville deposition, especially on paleotopographic highs. This lithofacies represents a moderate- to high-energy environment, with moderately well-circulated water in an intertidal setting. The water probably had slightly elevated salinity compared to the other lithofacies. Sediment deposition and modification probably occurred in water depths ranging from near sea level to 20 feet (6 m) below sea level. Wave action winnowed out mud leaving various well-sorted grains. Characteristic features of this lithofacies include medium-scale cross-bedding and bar-type carbonate sand-body morphologies that formed not only shoals, but beaches and tidal bars (Fouret, 1982). Well-developed ooids were produced from movement of particles over algal or cyanobacterial mats by intertidal currents and continuous wave action (Mitchell, 1961; Fouret, 1982).

The depositional fabrics of the oolitic and peloid shoal lithofacies include grainstone and packstone (figure 3-7). Rocks representing this lithofacies typically contain the following diagnostic constituents: ooids, coated grains, and hard pelloids. Fossils are relatively rare.

Rock units having oolitic and peloid shoal lithofacies constitute good reservoir potential. Remnants of visible interparticle and moldic porosity may be present in this lithofacies. Dolomitization significantly increases the reservoir quality of this lithofacies.

Middle Shelf

Middle-shelf lithofacies covered extensive areas across the shallow shelf. This lithofacies represents a low-energy, often restricted-marine environment (figure 3-1). Mud and some sand were deposited in subtidal (burrowed), inter-buildup/shoal setting. Water depths ranged from 60 to 90 feet (20-30 m).

The depositional fabrics of the middle-shelf lithofacies include wackestone and mudstone (figure 3-8). The most common is bioturbated lime to dolomitic mudstone with sub-horizontal feeding burrows. Rocks representing this lithofacies typically contain the following diagnostic constituents: soft pellet muds, "soft" peloids, grain aggregates, crinoids and associated skeletal debris, and fusulinids.

Rock units having middle-shelf lithofacies act as barriers and baffles to fluid flow, having very little effective porosity and permeability. There are few megafossils and little visible matrix porosity, with the exception of an occasional moldic pore. However, recognizing this lithofacies is important because low-energy carbonates of the middle shelf form the substrate for the development of the higher energy crinoid banks, oolitic/hard peloid shoals, and Waulsortian-type buildups (figure 3-1). The middle-shelf lithofacies can contain reservoir-quality rocks if dolomitized.

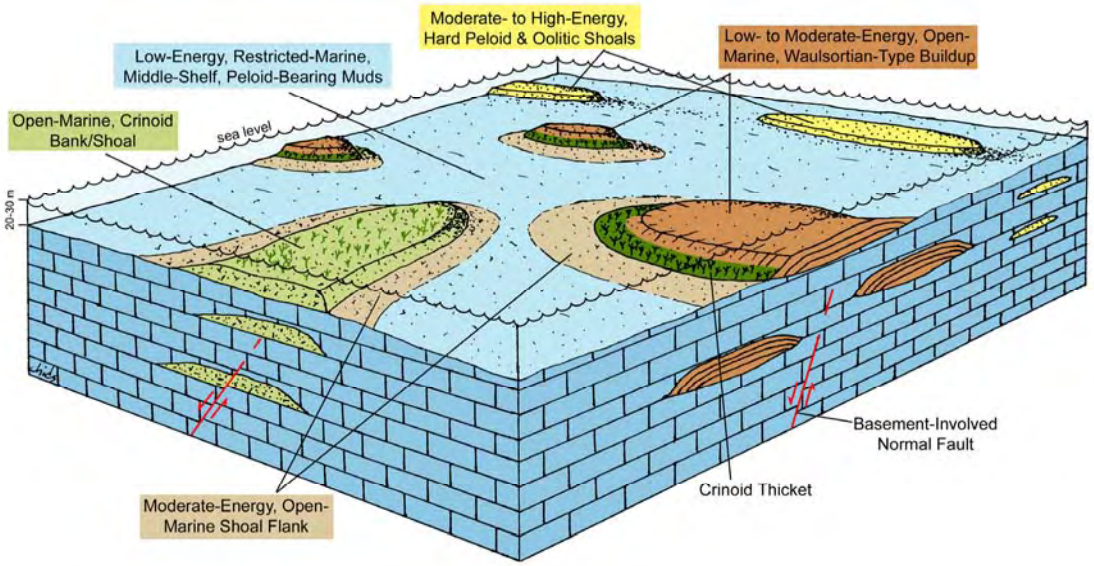

Figure 3-1. Block diagram displaying major depositional facies, as determined from core, for the Leadville Limestone, Lisbon field, San Juan County, Utah.

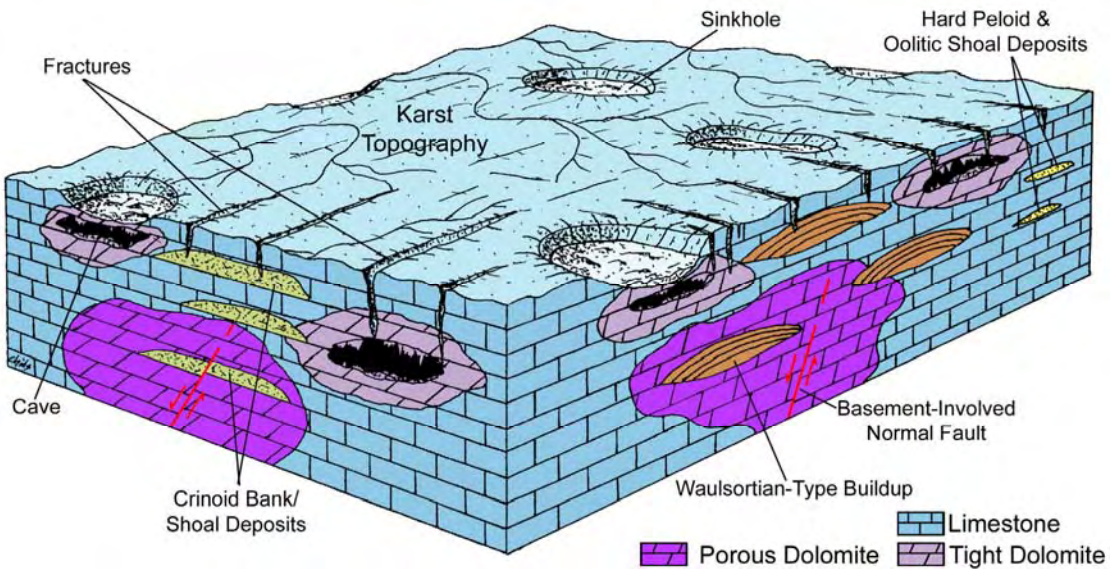

Figure 3-2. Block diagram displaying post-Leadville karst and fracture overprint.

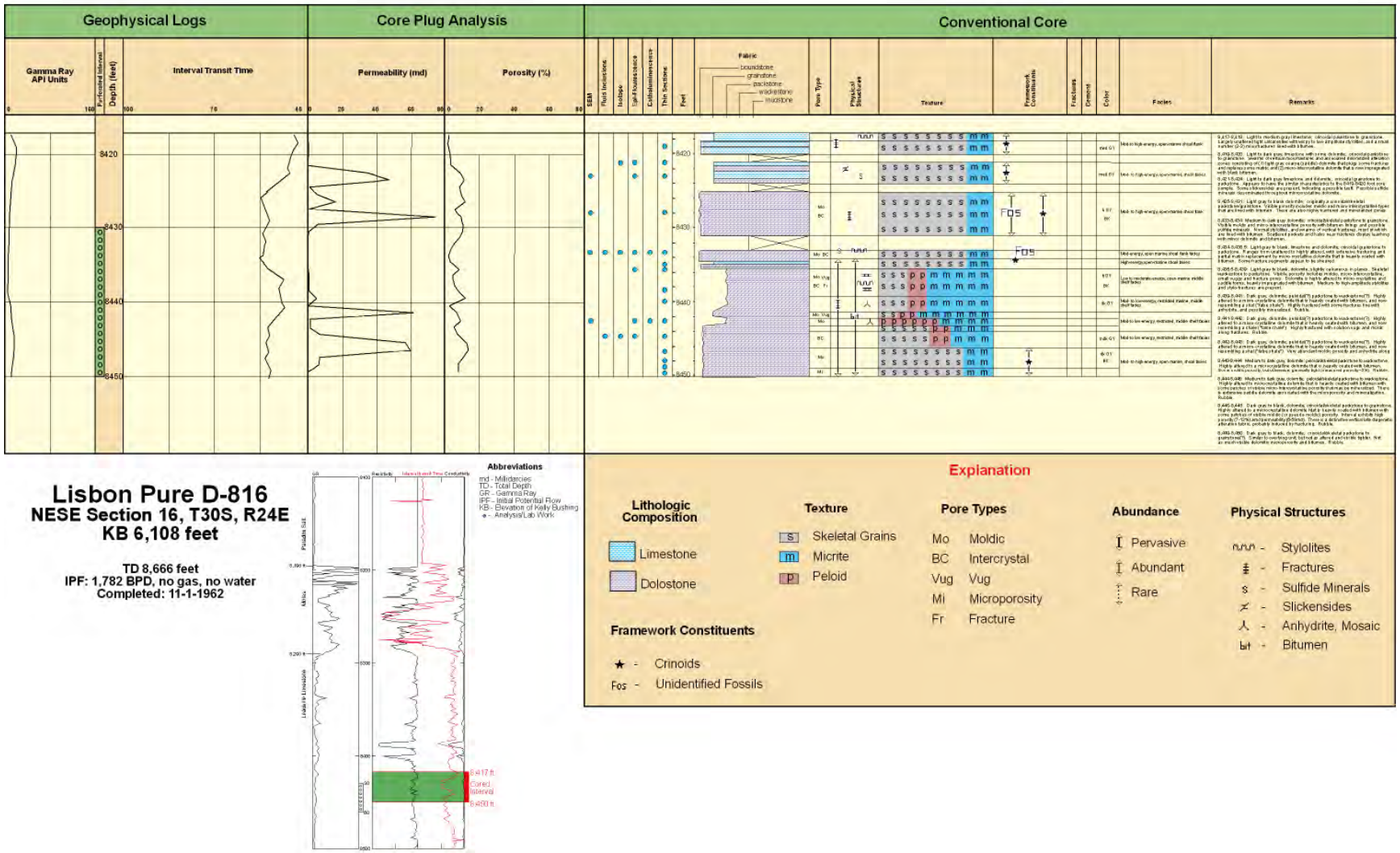

Figure 3-3. Typical Leadville vertical sequence from Lisbon field, including geophysical well logs, porosity/permeability plots, and core description, of the Lisbon Pure No. D-816 well (figure 2-1), San Juan County, Utah.

Figure 3-4. Typical crinoidal/skeletal grainstone/packstones representing high-energy, open-marine shoal lithofacies, Lisbon No. B-816 (NE1/4SW1/4 section 16, T. 30 S., R. 24 E., SLBL&M [figure 2-1]). (A) Slabbed core from 8506.5 feet. Note the large rugose coral. (B) Slabbed core from 8547 feet.

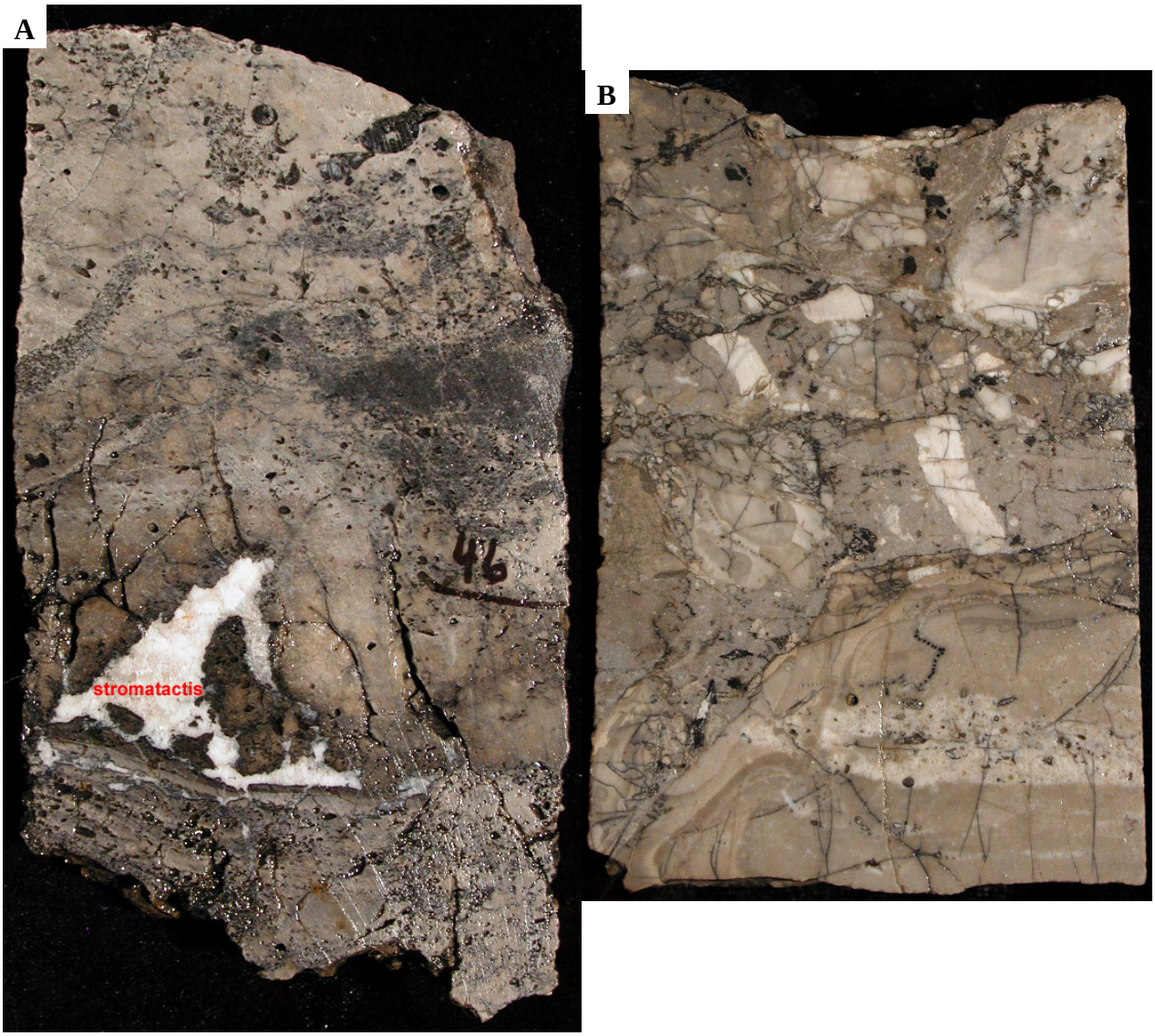

Figure 3-5. Typical peloidal/skeletal packstone/wackestones representing moderate- to low-energy, open-marine (and occasionally middle shelf), Waulsortian-type buildup lithofacies. (A) Lisbon No. B-816 (NE1/4SW1/4 section 16, T. 30 S., R. 24 E., SLBL&M [figure 2-1]); slabbed core from 8646 feet. (B) Lisbon No. D-616 (NE1/4NE1/4 section 16, T. 30 S., R. 24 E., SLBL&M); slabbed core from 8514 feet.

Figure 3-6. Typical peloidal/skeletal packstone/wackestone representing moderate-energy, open-marine, shoal-flank lithofacies. Lisbon No. B-816 (NE1/4SW1/4 section 16, T. 30 S., R. 24 E., SLBL&M [figure 2-1]); slabbed core from 8521 feet.

Figure 3-7. Typical peloidal grainstone/ packstone representing moderate-energy, "hard" peloid shoal lithofacies. Lisbon No. B-816 (NE1/4SW1/4 section 16, T. 30 S., R. 24 E., SLBL&M [figure 2-1]); slabbed core from 8463 feet.

Figure 3-8. Typical skeletal/"soft" peloidal wackestone/mudstone representing low-energy, restricted-marine, middle-shelf lithofacies. Lisbon No. B-816 (NE1/4SW1/4 section 16, T. 30 S., R. 24 E., SLBL&M [figure 2-1]); slabbed core from 8549 feet.

Table 3-1. List of well conventional slabbed core examined and described from the Leadville Limestone, Lisbon field, San Juan County, Utah.* See figure 2-1 for well locations.

Well	Location	API No.	Core Interval (feet)	Thin Sections
Lisbon D-816	NE SE 16, T. 30 S., R. 24 E.	43-037-16253	8417-8450	15
Lisbon D-616	C NE NE 16, T. 30 S., R. 24 E.	43-037-15049	8300-9110	13
NW Lisbon B-63	NE NW 3, T. 30 S., R. 24 E.	43-037-11339	9934-10,005	14
Lisbon B-816	NE SW 16, T. 30 S., R. 24 E.	43-037-16244	8463-8697	22
Lisbon B-610	NE NW 10, T. 30 S., R. 24 E.	43-037-16469	7590-8001.5	18

*Repository: Utah Core Research Center.

CHAPTER 4
DIAGENETIC ANALYSIS OF THE LEADVILLE LIMESTONE, LISBON CASE-STUDY FIELD

Thomas C. Chidsey, Jr., and Craig D. Morgan, Utah Geological Survey,
David E. Eby, Eby Petrography & Consulting, Inc.,
Joseph N. Moore, Energy & Geoscience Institute,
Louis H. Taylor, Standard Geological Services, Inc.,
and
John D. Humphrey, Colorado School of Mines

Introduction

The diagenetic fabrics and porosity types found in the various hydrocarbon-bearing rocks of Lisbon field can be indicators of reservoir flow capacity, storage capacity, and untested potential. Diagenetic characterization focused on reservoir heterogeneity, quality, and compartmentalization within the field. All depositional, diagenetic, and porosity information can be combined with the production history in order to analyze the potential for the Leadville Limestone regionally.

The petrographic techniques employed consisted of (1) basic thin section petrographic descriptions, (2) porosity and permeability cross-plot evaluation, (3) scanning electron microscope (SEM) analysis of various dolomites to determine reservoir quality of the dolomites as a function of diagenetic history, and (4) epifluorescence (EF) and cathodoluminescence (CL) petrography for the sequence of diagenesis. Geochemical analysis included (1) fluid inclusion (FI) evaluation to determine the temperatures of secondary dolomite formation and the salinity of the original brines, (2) stable carbon and oxygen isotope analysis of diagenetic components such as cementing minerals and different generations of dolomites, and (3) strontium isotope analysis for tracing the origin of fluids responsible for different diagenetic events.

An ideal diagenetic sequence based on our analysis of Leadville thin sections from Lisbon field is presented in figure 4-1. Leadville reservoir quality at Lisbon is greatly enhanced by dolomitization and dissolution of limestone. There are two basic types of dolomite: very fine, early dolomite and coarse, late dolomite. The early dolomitization and leaching of skeletal grains resulted in low-porosity and/or low-permeablility rocks. Most reservoir rocks within Lisbon field appear to be associated with the second, late type of dolomitization and associated leaching events. Other diagenetic products include pyrobitumen, syntaxial cement, sulfide minerals, anhydrite cement and replacement, and late macrocalcite. Fracturing and brecciation caused by hydrofracturing are widespread within Lisbon field. Sediment-filled cavities, related to karstification of the exposed Leadville, are present in the upper third of the formation. Late dolomitization, sulfides, and brecciation may have developed from hydrothermal events that can greatly improve reservoir quality.

Basic Thin Section Petrographic and Core Plug Petrophysical Analysis

In order to determine the diagenetic histories of the various Leadville rock fabrics, including both reservoir and non-reservoir, 64 thin sections of representative samples were

selected from the conventional cores (figure 2-1 and table 3-1) for petrographic description and later geochemical analysis. Carbonate fabrics were again determined according to Dunham's (1962) and Embry and Klovan's (1971) classification schemes. Pores and pore systems were described using Choquette and Pray's (1970) classification (figure 4-2). Each thin section was photographed with additional close-up photos of (1) typical preserved primary and secondary pore types, (2) cements, (3) sedimentary structures, (4) fractures, and (5) where present, pore-plugging anhydrite, halite, and bitumen.

Thin Section Description and Interpretation

The early diagenetic history of the Leadville sediments, including some early dolomitization and leaching of skeletal grains, resulted in low-porosity and/or low-permeablility rocks. Most of the porosity and permeability associated with hydrocarbon production was developed during deeper subsurface dolomitization and dissolution. Some of these important subsurface processes are shown with the purple bars in figure 4-1 and are discussed below generally in the order in which they occur. For the complete descriptions and photomicrographs of Lisbon thin sections refer to **Deliverable 1-3A – Catalog of Leadville Porosity Types and Diagenesis: Lisbon Field, San Juan County, Utah**.

Syntaxial cement: Syntaxial cementation is an early diagentic event (figure 4-1). This type of cementation is found exclusively as overgrowths on echinoderms (figure 4-3), in this case dominantly crinoids deposited in banks or shoals of the open-marine facies. Crinoid ossicles often appear to be "floating" in cement with little evidence of compaction. If extensive syntaxial cementation has occurred, the result will be a significant reduction of porosity. However, from the thin sections evaluated, it appears that this diagenetic process has been relatively minor.

Dolomitization and porosity development: Two basic types of dolomite have been seen within the cores (figure 4-4A). The first type consists of "stratigraphic" dolomites that preserve original depositional grains and textures. Very fine (<5 μ), interlocking dolomite crystals with no intercrystalline pore spaces are the norm (figure 4-4B). Commonly, this type of dolomite can be correlated across the field in several relatively thin intervals. The second type of dolomite is a much coarser (>10-20 μ), later replacement of all types of limestone and earlier "stratigraphic" dolomites (figure 4-4C). Crosscutting relationships with carbonate bedding and variable dolomite thickness across the field are common. Petrographically, the coarse, second dolomite type consists of crystals with thick, cloudy, inclusion-rich cores and thin, clear overgrowths with planar crystal terminations. Often, these coarser dolomites show saddle dolomite characteristics of curved crystal shape (figure 4-5) and sweeping extinction under cross-polarized lighting. Predating or concomitant with saddle dolomite formation, are pervasive leaching and dissolution episodes that crosscut the carbonate host rocks, and result in late vugs, as well as extensive microporosity. Pyrobitumen appears to coat most intercrystalline dolomite, as well as dissolution pores associated with the second type of dolomite. Most reservoir rocks within Lisbon field appear to be associated with the second, late type of dolomitization and associated leaching events.

Later dolomitization, saddle dolomite, and dolomite cement precipitation may have occurred at progressively higher temperatures, that is, hydothermal dolomite. Hydrothermal events can improve reservoir quality by increasing porosity through dolomitization, leaching,

development of microporosity, and natural fracturing (forming breccia) kept open with various minerals (Smith, 2004; Davies and Smith, 2006; Smith, 2006; Smith and Davies, 2006). Hydrothermal dolomite precipitates under temperature and pressure conditions greater than the ambient temperature and pressure of the host limestone (Davies, 2004; Davies and Smith, 2006; Smith, 2006; Smith and Davies, 2006). The result can be the formation of large, diagenetic-type hydrocarbon traps.

Post-burial brecciation: Fracturing and brecciation are quite common within Lisbon field (figure 4-6 through 4-8). However, brecciation is most commonly caused by hydrofracturing, creating an explosive looking, pulverized rock. The result yields an "autobreccia" as opposed to a collapse breccia. Clasts within an autobreccia have basically remained in place and moved very little. Dolomite clasts are often surrounded by solution-enlarged fractures partially filled with coarse rhombic and saddle dolomites that are coated with pyrobitumen. Areas between clasts can exhibit very good intercrystalline porosity or microporosity or they may filled by low-porosity saddle dolomite cement. Intense bitumen plugging is concurrent or takes place shortly after brecciation. "Reike," or stair-step fractures, are occasionally present, reflecting shear and the explosive fluid expulsion from the buildup of pore pressure.

Karst-related processes: Sediment-filled cavities are relatively common throughout the upper third of the Leadville in Lisbon field (figure 4-9). These cavities or cracks were related to karstification of the exposed Leadville (figure 3-2). Infilling of the cavities by detrital carbonate and siliciclastic sediments occurred before the deposition of the Pennsylvanian Molas Formation. The contact between the transported material and the country rock can be sharp, irregular, and corroded with small associated mud-filled fractures. The transported material consists of poorly sorted detrital quartz grains (silt size), chert fragments, carbonate clasts, clay, and occassional clasts of mud balls (desiccated and cracked). The carbonate muds infilling the karst cavities are largely dolomitized (a later diagenetic process), very finely crystalline, and non-porous. The infilling sometimes displays a crude layering.

Other karst features observed in Leadville thin sections include the presence of "root hair" – thin, sinuous cracks filled with dolomitized mud. Clasts also may have a coating of clay. Both of these features are evidence of a possible, nearby soil zone.

Anhydrite and sulfides: Dissolution pores (molds) and pore throats are sometimes plugged or bridged by lathes of late anhydrite cement (figure 4-10). In the photomicrographs studied, complete plugging of porosity was rare and the overall presence of anhydrite cement and replacement was relatively insignificant for the Leadville Limestone in the Lisbon reservoir rocks.

Possible sulfide minerals are observed in several Leadville thin sections (figure 4-11). They appear as small, angular, brassy crystals. They tend to line moldic pores or form on, and between, rhombic dolomite crystals. These minerals may be associated with hydrothermal fluids responsible for the coarse saddle dolomites. They may also be related to copper mineralization found a few miles to the east at the Lisbon Valley copper mine. The copper deposit includes fracture filling and disseminated copper sulfides (chalcocite, bornite, and covellite) replacing dead oil and pyrite (Hahn and Thorson, 2006).

Late macrocalcite: Macrocalcite, also referred to as poikilotopic calcite, is viewed as late, large, slow-growing crystals (figure 4-12), and although not extensive in the Leadville at Lisbon field, its presence provides some significant insight into the diagenetic history of these rocks. The example shown in figure 4-12 shows an autobreccia that retains small amounts of early, finely crystalline (tight) dolomite replaced by "mini-saddles" and medium crystalline (euhedral) dolomite. Early during this samples' history, it once had intercrystalline porosity that was enhanced by dissolution to form additional pores. Subsequently, the pores were partially filled with coarsely crystalline saddle dolomite and bitumen. Finally, the remaining solution-enlarged pores were occluded by poikilotopic calcite. Poikilotopic calcite may have formed as oil-field water rose following the gas/condensate cap.

Porosity and Permeability Cross Plots

Porosity and permeability data from 380 core plugs were obtained from the five well cores described (figure 2-1 and table 3-1). Cross plots (figures 4-13 through 4-17) of these data are used to (1) determine the most effective pore systems for oil storage versus drainage, (2) identify reservoir heterogeneity, (3) predict potential untested compartments, (4) infer porosity and permeability trends where core-plug data are not available, and (5) match diagenetic processes, pore types, mineralogy, and other attributes to porosity and permeability distribution. Porosity and permeability cross plots were constructed using the available data.

Figure 4-13 is a representative set of core analyses from the Leadville Limestone in Lisbon field. The dominant pore types are intercrystalline, moldic, fracture, and channel. The plot shows two distinct populations of dolomites with respect to permeability and petrographic character. The early, finely crystalline dolomites (with or without isolated molds) display low permeability. The coarser, late dolomites (with or without late dissolution) display high permeability. In addition, analysis of the plot shows that those zones that have been dolomitized have better reservoir potential than those that remain limestone, even where the limestone has been fractured and brecciated.

Scanning Electron Microscopy

In order to further determine the diagenetic histories of the Leadville reservoir at Lisbon field, representative samples were selected from the conventional cores which were used for thin sections. The SEM was used to photograph: (1) typical preserved primary and secondary pore types and pore throats, (2) cements, (3) sedimentary structures, (4) fractures, and (5) pore plugging anhydrite, halite, and bitumen. Of special interest is the identification of possible hydrothermal dolomite and the determination of the most effective pore systems for oil drainage versus storage. Scanning electron microscope analyses were conducted on 12 thin section blanks from the core samples that displayed particular characteristics of interest (table 4-1). For the complete descriptions and SEM images from the Leadville reservoir at Lisbon field refer to **Deliverable 1-3B – Scanning Electron Microscopy, Epifluorescence, Cathodoluminescence, Fluid Inclusions, and Isotopic Studies: Lisbon Field, San Juan County, Utah**.

Porosity Types

All samples exhibit microporosity in the form of intercrystalline (BC) porosity (figure 4-18). Dissolution has contributed to porosity in most samples as well. Dissolution has created moldic (MO), vuggy (VUG), and channel (CH) porosity. Dissolution pores are most often in the mesopore size range (62.5 microns to 4.0 mm.).

Permeability is related to the size and number of pore throats, and, particularly, to the continuity of pore throats. In general, permeability is good in the samples studied, but is limited slightly by mineral cements and pyrobitumen (figure 4-19).

Fractures enhance the permeability in several intervals (figure 4-20). Scanning electron microscopic examination identified fractures in the 8423- and 8442-foot (2567- and 2573-m) intervals of the Lisbon No. D-816 well, and the 8356- and 8682-foot (2547- and 2646-m) intervals of the Lisbon No. D-616 well. In addition to the fractures reported here, petrographic analysis revealed fractures in the 8308- and 8619-foot (2532- and 2627-m) intervals of the Lisbon No. D-616 well, and the 7886-foot (2404-m) interval of the Lisbon No. B-610 well.

Undoubtedly, fractures enhance the permeability in the 8423- and 7886-foot (2567- and 2404-m) samples given their respective measured values of 46 mD and 114 mD. The 83 mD measured permeability of the 7897-foot (2407-m) interval and the 15 mD of the 8426-foot (2568-m) interval suggest that fractures are present in these intervals as well. They were not observed during analysis, however.

Lithology, Diagenesis, and Cements

All samples are dolomite except for the limestone matrix present in the 8308-foot (2532-m) sample of the Lisbon No. D-616 well. That sample, however, contains dolomite as fill material. Secondary materials present include dolomite, calcite, clays, and pyrobitumen. Their presence is discussed below and also included in table 4-1.

Dolomite is the dominant cement (figure 4-18) in all samples except the 8426-foot (2568-m) sample from the Lisbon No. D-816 well, where anhydrite is the abundant cement. The two basic types of dolomite are well displayed by SEM (figure 4-18): the low-porosity and/or low-permeablility, very fine, early dolomite and higher porosity and/or high permeablility, coarse, late dolomite (figure 4-21).

Pores in the 8426-foot (2568-m) sample from the Lisbon No. D-816 well are partially filled with anhydrite (figure 4-22). Anhydrite is also reported from petrographic analaysis of the 8433-foot (2570-m) interval of this well and the 8682-foot (2646-m) sample of the Lisbon No. D-616 well. Scanning electron microscopic analysis indicates that anhydrite is abundant in the 8426-foot (2568-m) sample; it is most likely much less abundant in the other intervals.

Minor euhedral quartz is present in several samples (figure 4-23). Rare illitic clays, possibly illite/smectite mixed-layer clays, are also present. Sulfide mineral(s) containing an unknown cation are present in moderate abundance (figure 4-24). Calcite cement, although rare, was observed in a few samples. The minor constituents of quartz, clays, calcite, and sulfides contribute little to the overall lithology and are relatively insignificant with respect to reservoir quality. The quartz, clay, and calcite cements are rare, and the more abundant sulfide mineral(s) consist of extremely small crystals about 2 microns or smaller.

An approximate diagenetic sequence based on SEM is listed below (not all diagenetic events were identified in every sample). The various diagenetic events are included in table 4-1.

1. Dolomitization

2. Dissolution
3. Dolomite cementation
4. Fracturing
5. Quartz cementation
6. Calcite cementation
7. Clay precipitation
8. Anhydrite cementation
9. Pyrobitumen emplacement
10. Sulfide precipitation

Epifluorescence

Epifluorescence microscopy is a technique that has been used successfully in recent years to provide additional information on diagenesis, pores, and organic matter (including "live" hydrocarbons) within sedimentary rocks. It is a rapid, non-destructive procedure that can be done using a high-quality petrographic (polarizing) microscope equipped with reflected light capabilities. The basic principles and equipment for EF were largely developed in the 1960s and 1970s for applications in coal petrology and palynology (see reviews by van Gijzel, 1967; Teichmuller and Wolf, 1977). All applications depend upon the emission of light (by a material capable of producing fluorescence) that continues only during absorption of the excitation-generating light beam (Rost, 1992; Scholle and Ulmer-Scholle, 2003).

Epifluorescence techniques have been used within industry and research for three objectives. Firstly, EF microscopy has been used extensively for enhancing petrographic observations, including the recognition of depositional and diagenetic fabrics within recrystallized limestone and massive dolomite (see, for instance, Dravis and Yurewicz, 1985; Cercone and Pedone, 1987; Dravis, 1991; LaFlamme, 1992). Secondly, the study of pore structures, microfractures, and microporosity within both carbonates and sandstones has been greatly facilitated by impregnating these voids with epoxy spiked with fluorescing dyes (Yanguas and Dravis, 1985; Gies, 1987; Cather and others, 1989a, 1989b; Soeder, 1990; and Dravis, 1991). Thirdly, the evaluation of "oil shows" (Eby and Hager, 1986; Kirby and Tinker, 1992) and determination of the gravity or type cements and minerals has been facilitated by EF microscopy (Burruss, 1981, 1991; Burruss and others, 1986; Guihaumou and others, 1990; LaVoie and others, 2001). Only the first two objectives were pursued in this study.

Previous Work

There is no known published use of EF microscopy on the Leadville Limestone of the Paradox Basin. However, the published work cited above, applications to carbonate reservoirs listed in Eby and Hager (1986) for a study done within a Permian Basin carbonate field, and case studies documented by Dravis (1988, 1992) provided incentives to apply EF petrography to Leadville reservoir rocks within the Lisbon case-study field.

Methodology

Epifluorescence petrography for this project used incident (reflected) blue-light fluorescence microscopy employing the general procedures outlined by Dravis and Yurewicz

(1985), including the use of the modified "white card" technique outlined by Folk (1987) and Dravis (1991). Ultraviolet (UV) fluorescence did not effectively add any textural or pore structure information that could not otherwise be seen under blue-light excitation, even though some workers utilize UV fluorescence for evaluating fluid inclusions and compositional zoning within dolomite crystals (see Scholle and Ulmer-Scholle, 2003). Fluorescence data and observations collected for this study utilized a Jena (now part of Carl Zeiss) research-grade combination polarizing-reflected light microscope equipped with a high-pressure mercury vapor lamp for EF excitation, a Zeiss IIIRS epifluorescence nosepiece, and a 35-mm camera system. Magnification ranges for examination and photo-documentation were between ~130 and 320x. The EF optical configuration used is similar to that shown in figure 4-25.

The light pathways and mechanics of the EF used in this study have been generally described by Soeder (1990). As described by Burruss (1991), "these excitation wavelengths are reflected to the microscope objective and sample by a dichroic beamsplitter which has a dielectric coating that reflects a specific short wavelength range. Fluorescence emission and reflected short wavelength excitation light is collected by the objective. The dichroic beamsplitter transmits the long wavelength fluorescence emission, but reflects the short wavelengths back toward the light source. The fluorescence emission passes through a barrier filter which removes any remaining short wavelength excitation light." Blue light (~420-490 nm exciter filter/520 nm barrier filter) was used to excite the cuttings and core-chip samples. We have found broad-band, blue-light EF to be the most helpful in observational work on dolomite, although some workers report applications using UV light (330-380 nm exciter filter/420 nm barrier filter) or narrow-band, blue-violet light (400-440 nm exciter filter/480 nm barrier filter). Finally, the greater depth of investigation into a sample by the reflected fluorescence technique than by transmitted polarized light or other forms of reflected light makes it possible to resolve grain boundary and compositional features that are normally not appreciated in cutting or thin-section petrography.

Sample preparation is inexpensive and rapid, involving standard thin section preparation techniques. Thin sections were prepared from representative Leadville fabrics. These thin sections were vacuum- and pressure-impregnated with blue-dyed epoxy (see Gardner, 1980) that was spiked with a fluorescing compound. Microscopy used only uncovered polished surfaces. Examination for each thin section area of interest included photo-documentation under EF and plane-polarized light at the same magnification. Photomicrography of the compositional, textural, and pore structure attributes was done using high-speed film (ISO 800 and 1600) with some bracketing of exposures as camera metering systems do not always reliably read these high-contrast images in the yellow and green light spectrum. Since the image brightness is directly proportional to magnification, the best images are obtained at relatively high magnifications (such as greater than 100x). Low-power fluorescence is often too dim to effectively record on film. These techniques are applicable to thin sections from both core and cuttings samples.

Epifluorescence Petrography of Leadville Limestone Thin Sections

Blue-light, EF microscopy was completed on 15 core samples for a variety of rock textures and diagenetic phases of Leadville limestone and dolomite within Lisbon field. These samples were selected to be representative of compositional, diagenetic, and pore types encountered within the five cored wells (see figure 2-1 for core locations). A detailed

description and interpretation of the fluorescence petrography of each sample follows along with photomicrographs (as figures 4-26 through 4-30) to show representative views under both blue-light EF and plane-polarized light. Short descriptive captions for these photomicrographs are included with each photo pair. For the complete descriptions and EF images from the Leadville reservoir at Lisbon field refer to **Deliverable 1-3B – Scanning Electron Microscopy, Epifluorescence, Cathodoluminescence, Fluid Inclusions, and Isotopic Studies: Lisbon Field, San Juan County, Utah**.

Lisbon No. D-816 well: Blue-light, EF microscopy nicely shows pore spaces and structures that are not readily seen under transmitted, plane-polarized lighting and the range of crystal sizes or shapes within bitumen-rich areas (figure 4-26). Samples from this well are fairly massive dolomite, which is generally non-fluorescent but has a slight hint of fluorescence showing vague relict grains. Some samples display complex zoning, alternating from dull to bright fluorescence within rhombs. Blue-light EF also shows the clear difference between dull replacement dolomite and much lighter replacement dolomite cement. Rare saddle dolomite cements in molds appear to show crystal zonation.

Microfractures cutting through tight dolomite matrix are visible only with blue-light EF. Some pores (isolated molds) are lined with bright, yellow oil film fluorescence possibly from oil staining while others show no oil staining.

Lisbon No. D-616 well: Blue-light, EF microscopy shows replacement dolomite that is fine to medium crystalline with planar to curved crystal faces, weakly yellow fluorescent with possible fluid inclusions (figure 4-27); limestone does not fluoresce. Saddle dolomite cements growing into some of the moldic pores display moderately dull blue fluorescence. Blue-light EF displays replacement rhombic dolomite outlines with high intercrystalline porosity despite the appearance of significant bitumen plugging.

Blue-light, EF microscopy also shows syngenetic dolomite, laminated cryptoalgal (?) mudstone with soft pellets and abundant wispy seam, low-amplitude stylolites moderate yellow fluorescence is observed throughout the samples. Ghosts of original skeltetal/pelletal grains show moderate yellow fluorescence transitioning into coarse replacement dolomite displaying modest intercrystalline porosity. The replacement rhombs have generally dead cores and moderate yellow fluorescent overgrowths.

Lisbon No. B-610 well: Ultraviolet-light, EF microscopy shows two regions within the sample. Region 1 consists of white, syngenetic dolomite with no visible porosity and blue-purple moderate fluorescence. The UV fluorescence nicely shows a variety of corrosion and dissolution fabrics, which sometimes mimic original grain boundaries. Region 2 consists of black, non-fluorescent, finely crystalline dolomite, as well as "floating" large dolomite rhombs that appear to have precipitated out of the finely crystalline ground mass (figure 4-28).

Blue-light EF also displays syngenetic dolomite, both unaltered and corroded, with moderate yellow fluorescence. Within the black dolomite region, the larger floating dolomite rhombs have a dull green fluorescence.

Lisbon No. B-816 well: Blue-light, EF microscopy shows replacement dolomite with highly yellow fluorescent rims (figure 4-29). Saddle dolomite cement has moderate yellow-green fluorescence. Late calcite cements are generally non-fluorescent.

Lisbon NW USA No. B-63 well: Blue-light, EF microscopy shows massive, very finely crystalline, non-porous syngenetic dolomite displaying a mottled dull to medium yellow fluorescence with occasional ghosts of original grain types (can see grain outlines with fluorescence). Dolomitized grains include detrital carbonate (pellets) and siliciclastic (quartz silts and clays) components of the karst cavity infilling (figure 4-30); clay minerals between grains display a pale reddish fluorescence. Outside of the cavity, the host rock is almost pure limestone composed of fossils and coated grains – all calcitic with little visible fluorescence.

Late calcite (poikilotopic) also displays no fluorescence. This late calcite occurs as cements within former isolated molds, fracture fillings, and some replacement of syngenetic dolomitic matrix.

Cathodoluminescence

Cathodoluminescence is the emission of light resulting from the bombardment of materials using a cathode ray (Allan and Wiggins, 1993). This petrographic technique can be an invaluable tool in petrographic studies of carbonate rocks. This technique can provide important information about the complex modification of rock fabrics and porosity within the Leadville Limestone of the Paradox Basin. Diagenesis played a major role in the development of reservoir heterogeneity in Lisbon field as well as throughout all the Leadville fields. Diagenetic processes started during deposition and continued throughout burial history (figure 4-1).

Cathodoluminescence has been used in recent years to provide insights into the chemical differences between preserved remnants of depositional components resulting from various diagenetic events in carbonate rocks as recognized from core examination and thin section petrography. In particular, CL provides visual information on the spatial distribution of certain trace elements, especially manganese (Mn+2) and iron (Fe+2) in calcites and dolomites (Machel and Burton, 1991; Scholle and Ulmer-Scholle, 2003). The visible CL responses are red to orange in color, and their intensity is usually described as non-luminescent, dully luminescent, and brightly luminescent. As a general rule, incorporation of Mn+2 into the calcite lattice stimulates luminescence and the incorporation of Fe+2 quenches or reduces luminescence (Fairchild, 1983; Allan and Wiggins, 1993; Scholle and Ulmer-Scholle, 2003). Qualitative interpretation of CL usually assigns nonluminescent responses to oxidizing settings in which the reduced forms of both Mn and Fe are unavailable for incorporation into the lattices of carbonate mineral precipitates. Oxidized forms of Mn and Fe are not incorporated into calcite or dolomite crystals. Therefore, there is nothing in these crystals to excite luminescence. Bright luminescence is related to carbonate precipitates with high Mn/Fe trace element ratios, typically as a result of reducing environments during early (near-surface) to intermediate stages of burial diagenesis. Dull luminescence seems to happen where the Mn/Fe trace element ratios are present in carbonate precipitates. Thus, dull luminescence is usually thought to be the result of intermediate to late stages of burial diagenesis. It appears that elements other than Mn and Fe do not have any appreciable effect in enhancing or reducing luminescence (Budd and others, 2000).

Particularly useful references on the uses and limitations of CL interpretations in ancient carbonate studies include Sipple and Glover (1965), Frank and others (1982, 1996), Marshall (1988), Hemming and others (1989), Barker and Kopp (1991), Gregg and Karakus (1991), Machel (2000), Lavoie and others (2001), Coniglio and others (2003), and Lavoie and Morin (2004).

Methodology

The analysis done in this study was completed using uncovered, polished thin sections, although rock chips and unpolished thin sections could be used. The equipment needed for CL can be installed on almost any polarizing microscope (see Marshall, 1988; Miller, 1988). A Cambridge Image Technology Ltd. luminoscope (model CLmk3A/4) mounted on an Olympus petrographic microscope (figure 4-31; see also Marshall, 1988) belonging to the Colorado School of Mines Department of Geological Engineering was used for this analysis (figure 4-32). Operating conditions were generally at 10-16kV accelerating potential, 0.5-0.7 mA of beam current and a beam focused at ~2 cm. All the work involved visual observations and some photographic documentation. Photomicrographs were recorded on a digital camera. No attempt was made to measure intensities or spectral information on the CL responses (for example Marshall, 1991; Filippelli and Delaney, 1992) to the Leadville carbonate samples. Image analysis and regional mapping of cement zones (that is "cement stratigraphy") have been done by some workers on carbonate cements (for example Meyers, 1974, 1978, 1991; Dorobek and others, 1987; Cander and others, 1988; Dansereau and Bourque, 2001), but these applications are beyond the scope of diagenesis documentation attempted in this project.

Cathodoluminescence Petrography of Leadville Limestone Thin Sections

Cathodoluminescence examination was completed on four thin-section samples from the Leadville limestone and dolomite within Lisbon field. These thin-section samples were selected to be representative of mineralogical (for example dolomite, calcite, anhydrite, and quartz), compositional, diagenetic, and pore types encountered within typical cores from the field (see figure 2-1 for core locations). For the complete descriptions and CL images from the Leadville reservoir at Lisbon field refer to **Deliverable 1-3B – Scanning Electron Microscopy, Epifluorescence, Cathodoluminescence, Fluid Inclusions, and Isotopic Studies: Lisbon Field, San Juan County, Utah**. The following remarks summarize our findings.

Lisbon No. D-816 well, 8442-8443 feet: Cathodoluminescence shows a wide range of crystal size and growth habits within the dull red luminescing, matrix-replacing dolomite (figure 4-33). The vast majority of the dolomite within areas of fabric selective dolomitization is a deep or intense red color. Between many of the grains, there is a lighter red luminescence where early cements have been dolomitized. Some of the coarser dolomite crystals appear to have an overgrowth of brighter red luminescent material. The range in dolomite rhomb sizes may reflect rapid precipitation. The amount of open porosity under CL is considerably greater than that visible under plane light microscopy. Cathodoluminescence also displays original depositional textures and the outlines of original carbonate grains. Between other grains, there are interparticle pores that are still open. In a few areas, these early pores have been solution-enlarged and lined with a later generation of coarse, rhombic dolomite.

Lisbon No. D-816 well, 8433 feet: Cathodoluminescence imaging was very useful in identifying various generations of dolomite. Two types of CL response are visible within these moderately coarse dolomite crystals. Bright red luminescence can be seen within the interiors of most of the replacement dolomite (figure 4-34). However, many of the crystals exhibit non-luminescent

overgrowths of variable thickness. In addition, some crystals exhibit mostly non-luminescent material. These particular crystals may be largely dolomite cements. Finally, some dolomite crystals exhibit a thin rind of red-luminescing dolomite overlying the non-luminescent overgrowth stage. It is possible that the red luminescing dolomite is the product of the replacement of a previous limestone or earlier dolomite matrix while the non-luminescing crystal additions may be overgrowth cements growing into open pores. Dissolution and corrosion of some crystals is evident between the second (non-luminescent) and the final luminescent rim.

Lisbon No. B-816 well, 8486 feet: Cathodoluminescence imaging was very useful in identifying the presence of saddle dolomites (Radke and Mathis, 1980) within microporous dolomites (figure 4-35). Large dolomite crystals (1.0 to 2.0 mm in diameter) with distinctly curved crystal faces occur as both replacements of finer, earlier dolomites, and as pore-filling cements. These saddle dolomites display dull, red luminescence in their core areas and slightly bright, orange-red luminescence toward their rim areas. In addition, CL makes it possible to see the growth bands in these coarse dolomite crystals due to slight luminescence differences between each growth zone.

In general, the presence of saddle dolomites within a carbonate sample is indicative of the growth of strained, slightly iron-rich, dolomite replacements and cements under elevated temperatures during burial conditions (Radke and Mathis, 1980). Thus, saddle dolomite, as well as the other coarse dolomite crystals with reddish luminescence, are probably late, burial or hydrothermal dolomites. Additional published descriptive work on saddle dolomites using CL may be found in LaVoie and Morin (2004).

Lisbon No. D-616 well, 8308 feet: Sediment-filled cavities are relatively common throughout the upper third of the Leadville Limestone in Lisbon field. These cavities or cracks were formed by karstification of the exposed Leadville. Infilling of the cavities by detrital carbonate and siliciclastic sediments occurred before the deposition of the Pennsylvanian Molas Formation. Cathodoluminescence imaging shows that the contact between the transported material and the limestone country rock can be sharp, irregular, and corroded with small associated mud-filled fractures (figure 4-36). The transported material consists of poorly sorted detrital quartz grains (silt size), chert fragments, carbonate clasts, clay, and occassional clasts of mud balls (desiccated and cracked). The carbonate muds infilling the karst cavities are largely dolomitized (a later diagenetic process), very finely crystalline, and non-porous.

Fluid-Inclusion Systematics of Lisbon Field Samples

During crystal growth, imperfections may trap fluids present in the environment at that time. Later mineral precipitation and deformation, such as the development of fractures, can create additional crystal imperfections that may also trap fluids (figure 4-37). These fluid inclusions are defined as fluid-filled vacuoles, typically 5 to 20 microns in size. They provide pressure, volume, and temperature information about the conditions when the crystal precipitated (Paul Carey and John Parnell, University of Aberdeen, written communication, 2005). The fluids in the inclusion may be connate water, oil, or a sample of the mineralizing fluid. The following properties are assumed not to have changed since an inclusion formed: (1) the composition of the trapped fluid, (2) the density of the trapped fluid, and (3) the volume of the inclusion (Paul Carey and John Parnell, University of Aberdeen, written communication, 2005).

The study of fluid inclusions can help determine (1) the temperature of mineral precipitation, (2) the composition and origin of mineralizing fluids, (3) later history of temperature, pressure, and fluid composition, (4) petroleum migration history, (5) relative timing of porosity occlusion, and (6) deformation event conditions (Paul Carey and John Parnell, University of Aberdeen, written communication, 2005).

Fluid inclusions trapped in calcite, quartz, and dolomite were studied from three wells: Lisbon NW USA No. B-63, Lisbon No. D-616, and Lisbon No. D-816 (figure 2-1). The inclusions were categorized on the basis of origin, number of phases present, and composition. All inclusions were classified as either primary or secondary. Primary inclusions are trapped at the time of mineral growth; secondary inclusions are trapped along healed fractures. Primary inclusions typically define growth zones, although in quartz, large isolated inclusions are typical. All of the inclusions observed contained either one or two fluid phases at room temperature. Inclusions containing brine and vapor are the most common, but single-phase aqueous inclusions, gas-rich inclusions, and inclusions consisting of oil and vapor are present. Single-phase aqueous inclusions are indicative of trapping at temperatures less than 50°C (~122ºF) (Goldstein and Reynolds, 1994).

Fluid-Inclusion Measurements

Heating and freezing measurements were made on doubly polished thick sections and hand picked crystals using a Linkham THSMG 600 freezing and heating stage calibrated with synthetic fluid inclusions. (The data are tabulated in Appendix D of **Deliverable 1-3B – Scanning Electron Microscopy, Epifluorescence, Cathodoluminescence, Fluid Inclusions, and Isotopic Studies: Lisbon Field, San Juan County, Utah**.) The precision of the measurements is estimated to be ± 0.1°C at 0.0°C (32°F) and ± 3°C at 374°C (± 37ºF at 705ºF). Homogenization and ice-melting temperatures were measured. Homogenization temperatures are minimum trapping temperatures. Ice-melting temperatures provide a measure of the fluid salinity. The salinities of the two-phase aqueous inclusions with ice-melting temperatures between 0 and -21.2°C (32 and -6.2ºF) were converted to weight percent NaCl equivalent using the equation of Bodnar (1993). Salinities of inclusions with lower ice-melting temperatures displayed eutectic (first melting) temperatures of <-45°C (-49ºF), indicating the presence of divalent ions (most likely Ca and Mg). These inclusions had ice-melting temperatures as low as about -27°C (~ -17ºF). The equation of Bodnar (1993) cannot be used to calculate the salinities of these fluids. As a first approximation, assuming that only Ca, Na, and water are present in the inclusions, the salinities would be in the range of 25 to 30 weight percent NaCl-$CaCl_2$ equivalent (Yanatieva, 1946). Such high-salinity brines imply interactions with evaporite deposits.

Caveats and Practical Aspects of Fluid-Inclusion Studies

Several factors can affect the utility and validity of fluid-inclusion measurements and these factors can play a significant role in sedimentary environments. Two general tenets of fluid-inclusion research are that: (1) the volume of the cavity has not changed since generation of the vapor bubble, and (2) the bulk composition of the inclusion has remained constant. However, both the volume and compositions of the inclusions can be modified by necking, stretching, refilling, and leakage. As a general rule of thumb, a population of fluid inclusions

that formed contemporaneously (termed a fluid inclusion assemblage by Goldstein and Reynolds, 1994) will yield homogenization temperatures within 15 to 20°C (59-68°F).

All fluid inclusions neck or anneal after trapping as the temperatures decrease. This process typically leads to the splitting of a large inclusion into a number of smaller inclusions. Necking occurring after generation of the vapor bubble is recognized by the petrographic association of inclusions with variable liquid to vapor ratios. Many of the inclusions in calcite and dolomite have variable liquid to vapor ratios. Qualitatively, the presence of all inclusions with vapor bubbles, but variable ratios, suggests necking occurred at elevated temperatures greater than at least 50°C (122°F). Although the homogenization temperatures of necked inclusions are not meaningful, because they can be both greater and lower than the true homogenization temperature, the minimum homogenization temperatures can provide a qualitative measure of the minimum temperatures that have affected the rocks. The salinities of necked inclusions, however, are not greatly affected by necking and can be measured and used. Oil inclusions are less prone to necking than aqueous inclusions, although some secondary inclusions in the latest calcite clearly displayed evidence of necking.

Stretching is the inelastic expansion of the fluid inclusion leading to an increase in its volume. This can lead to the generation or growth of a vapor bubble, which in turn yields an anomalously high temperature of homogenization. The degree of stretching is highly variable even within a single crystal. Its effect is dependent on original fluid inclusion size, shape, location in a crystal, degree of overheating, pressure, and fluid composition. Often a significant percentage of the inclusions will retain their original characteristics. For example, single-phase inclusions, if originally present, will persist after stretching. Stretched inclusions do not yield meaningful homogenization temperatures. The salinities of stretched inclusions, however, can be utilized.

Refilling of fluids may be common but is difficult to recognize. Both the homogenization temperatures and compositions can be utilized. Refilling of fluids can be recognized by comparing the fluid inclusion characteristics of minerals whose relative ages are known.

Leakage of fluids, particularly the liquid phase, from fluid inclusions is also common. Leaked inclusions are typically vapor-rich. Leakage can often be recognized because it will often affect only a small percentage of the total fluid inclusion population.

Fluid Inclusions in Early Calcite

Early calcite represents original fossil material (figure 4-38). It is characteristically coarsely crystalline and decorated with abundant aqueous liquid-rich inclusions with variable liquid to vapor ratios (figure 4-39). Less commonly, oil inclusions are present (figures 4-40 and 4-41). The vast majority of both the aqueous and oil inclusions are randomly distributed throughout the calcite crystals and appear to be primary in origin. Secondary inclusions defining healed fractures are uncommon.

The characteristically variable liquid to vapor ratios of the aqueous inclusions are interpreted as resulting from necking. Reconnaissance homogenization temperature measurements on spatially associated inclusions have temperatures greater than 20°C (>68°F) and are consistent with this interpretation. These homogenization temperatures are not considered meaningful and are not reported here. However, the occurrence of all two-phase

inclusions, in contrast to the presence of numerous single-phase, liquid inclusions in dolomite suggests the inclusions in calcite were trapped at elevated temperatures.

Ice-melting temperatures were measured on the aqueous inclusions in two samples from Lisbon No. D-616 well (figure 4-42). These temperatures ranged from -19.5 to -25.5°C (-3.1 to -13.9ºF) indicating that the fluids were highly saline.

Early calcite containing primary oil inclusions was found in Lisbon No. D-616 well at a depth of 8356 feet (2547 m) (figures 4-40 and 4-41). The color of the oil under fluorescent light suggests it has an API gravity of 35 to 45º (Goldstein and Reynolds, 1994). Twelve primary oil inclusions were measured in a single calcite crystal. All but two yielded homogenization temperatures ranging from 48 to 68°C (118-154ºF). The oil is interpreted as having formed in place from trapped organic material. The homogenization temperatures are minimum trapping temperatures.

Although the aqueous and oil inclusions appear primary in origin, they clearly could not have been present at the time the fossils were deposited. Furthermore, the phase relationships indicate the aqueous inclusions cannot be regarded as original inclusions that have stretched. The most likely explanation for the distribution and character of these calcite-hosted inclusions is that the original calcite has recrystallized and that the fluids were trapped during recrystallization. Oil inclusions in saddle dolomite suggest a similar history.

Fluid Inclusions in Dolomite

Dolomite fills voids and replaces early calcite. Early dolomite is typically fine grained; later saddle dolomite is coarser grained. Small fluid inclusions, most of which are less than a few micrometers in length, are common in dolomite (figure 4-43). These inclusions define growth zones, and consequently are interpreted as being primary in origin. Coarse-grained saddle dolomite frequently contains cloudy cores and clear rims.

Only aqueous inclusions were observed in the early fine-grained dolomite. Later saddle dolomite contains both aqueous and oil inclusions. Although many of the aqueous inclusions appear to contain only a single liquid phase, aqueous inclusions with variable liquid to vapor ratios are not uncommon. Reconnaissance measurements indicate that the two-phase (liquid plus vapor) inclusions commonly have homogenization temperatures ranging from 70 to 135°C (158-275ºF), although inclusions having homogenization temperatures several tens of degrees higher are locally abundant. Fluid inclusions trapped during mineral growth at temperatures greater than 70°C (>158ºF) will typically contain a vapor bubble. The common absence of a vapor bubble in many of the primary inclusions is inconsistent with dolomite formation at elevated temperatures and suggests that (1) the dolomite formed at temperatures of less than about 50°C (~122ºF), (2) the fluid inclusions have re-equilibrated (necked, stretched, or refilled), and (3) the homogenization temperatures of the two-phase inclusions are meaningless. Ice-melting temperatures of inclusions trapped in fine-grained dolomite from depths of 8372 feet (2552 m) in Lisbon No. D-616 well and 8444 feet (2574 m) in Lisbon No. D-816 well and from the clear rims of saddle dolomite from a depth of 9939 feet (3029 m) in Lisbon NW USA No. B-63 well are shown in figure 4-44.

Oil inclusions occur in saddle dolomite from a depth of 9939 feet (3029 m) in Lisbon NW USA No. B-63 well (figure 4-45). The inclusions appear primary, occurring in light colored portions of the crystal. Figure 4-46 shows that the early, dark colored growth zones are truncated by the lighter colored dolomite, suggesting that the dolomite recrystallized during burial. These

relationships indicate that the oil was trapped during recrystallization. Homogenization temperatures of the oil inclusions, which range from 60 to 70°C (140-158°F) (figure 4-47), provide a minimum temperature for this recrystallization.

Fluid Inclusions in Quartz

Quartz occurs as fine- to medium-grained crystals that postdate dolomite. Figure 4-48 shows small quartz crystals filling cavities in dolomite. Larger euhedral quartz crystals encapsulate dolomite and anhydrite (figures 4-49 and 4-50). The anhydrite inclusions are frequently oriented and rounded, indicating they are remnants of large, partially dissolved crystals. Anhydrite has retrograde solubility (deposits as water is heated) whereas quartz has prograde solubility (deposits as fluids cool). These relationships suggest that the anhydrite formed from refluxing brines, while the later laterally or ascending cooling fluids that deposited quartz were undersaturated in anhydrite, leading to its dissolution.

The quartz crystals from a depth of 8356 feet (2547 m) in the Lisbon No. D-616 well commonly contain numerous two-phase aqueous inclusions; rarely, gas-rich and single-phase, liquid-rich inclusions are present. Figures 4-51 and 4-52 show quartz crystals containing primary liquid-rich inclusions. In figure 4-51, primary inclusions define a growth zone within the interior of the crystal. Large isolated primary inclusions, up to 50 micrometers across occur in the quartz crystals shown in figure 4-52. Coexisting liquid- and vapor-rich inclusions were observed in the crystal shown in figure 4-53. Because of the small size of the gas-rich inclusions, it was not possible to estimate their compositions from phase changes during freezing and heating. However, in this environment, the gas is probably methane-rich. No primary oil inclusions were observed in the quartz crystals.

Secondary aqueous inclusions that define healed fractures are common in some of the quartz crystals. The majority of these inclusions contain liquid and vapor at room temperature; rarely single-phase aqueous inclusions are present. As noted above, these single-phase inclusions could represent the local incursion of low-temperature (less than about 50°C [<~ 122°F]) waters.

Homogenization and ice-melting temperatures of quartz-hosted inclusions were measured (figure 4-54). Primary inclusions yielded homogenization temperatures ranging from 118 to 133°C (244-271°F) and ice-melting temperatures of -20.5 to -22.8°C (-4.9 to -9°F). Secondary inclusions yielded lower homogenization temperatures but a much broader range of ice-melting temperatures that overlapped those of the primary inclusions.

The presence of coexisting gas- and liquid-rich inclusions is particularly significant because this suggests that the homogenization temperatures closely approximate the true trapping temperatures (see discussion in Goldstein and Reynolds, 1994). The quartz-hosted inclusions provide the best measure of the maximum burial temperature and depth of any of the minerals studied.

Fluid Inclusions in Late Calcite

Late calcite from depths of 9936 feet, 9991 feet, and 10,005 feet (3028 m, 3045 m, and 3049 m) in Lisbon NW USA No. B-63 well was studied. The calcite encapsulates dolomite (figure 4-55) and fills vugs. The relationships between dolomite, quartz, and calcite are shown in

figure 4-56. These textural relationships imply that the calcite also postdates quartz. As shown in figure 4-55, dissolution of dolomite occurred prior to calcite deposition.

Secondary aqueous and oil inclusions occur in the late calcite. All of the aqueous inclusions display variable liquid to vapor ratios indicative of necking. Ice-melting temperatures of the aqueous inclusions are shown in figure 4-57; see figure 4-58 for comparison of ice-melting temperatures of fluid inclusions in calcite vs. quartz. The majority of the inclusions from depths of 9939 feet and 10,005 feet (3029 m and 3049 m) yielded comparatively high ice-melting temperatures ranging from -5.5 to about -12^{o}C (22.1-~10 ^{o}F), corresponding to salinities of 8.6 to 16 weight percent NaCl equivalent. Inclusions from a depth of 9991.8 feet (3045 m) had higher salinities, up to 18 weight percent NaCl equivalent. These relationships suggest that at least two distinct groups of fluids interacted with the rocks from the Lisbon NW USA No. B-63 well.

Late Oil Inclusions

The youngest significant diagenetic event recorded in the rocks is represented by the presence of the bitumen observed in numerous thin sections. Secondary inclusions trapped in late calcite from a depth of 9936 feet (3028 m) in the Lisbon NW USA No. B-63 well provide unequivocal evidence for a mobile oil phase that postdates calcite deposition. The oil inclusions shown in figure 4-59 display variable liquid to vapor ratios caused by necking. The oil is fluorescent with an estimated API gravity of 35 to 45 ^{o}, based on its color. This contrasts with the produced oil API gravity from 54 to 63°. Similar appearing secondary oil inclusions were observed in calcite from a depth of 8372 feet (2552 m) in the Lisbon No. D-616 well (figure 4-60), although it is not possible to uniquely assign an age to these inclusions. These inclusions yielded consistent homogenization temperatures ranging from 39 to 43^{o}C (102-109^{o}F) (figure 4-61). For comparison, homogenization temperatures of primary oil inclusions are also shown in figure 4-61; see figure 4-62 for comparison of homogenization temperatures of oil inclusions in calcite vs. saddle dolomite.

Stable Carbon and Oxygen Isotope Analysis

Modification of rock fabrics and porosity within the Leadville Limestone in Lisbon field is quite complex. Stable isotope geochemistry has been used in recent years to provide insights into the chemical differences between preserved remnants of depositional components and the various diagenetic events in carbonate rocks, as recognized from core examination and thin section petrography. Figure 4-63 shows a graph of carbon versus oxygen isotope compositions for a range of carbonate rock types from various published sources compiled by Roylance (1990). Broad fields of carbon and oxygen isotope compositions for various carbonate rock settings are indicated, including modern marine (“subsea”) cements, various marine skeletons and sediments, deep-water (“pelagic”) limestone, Pleistocene carbonates, and meteoric carbonates (“speleothems and veins”).

Methodology

Isotopic composition analyses for stable carbon and oxygen, as well as strontium, were completed on a variety of diagenetic phases from Lisbon field core samples (table 4-2).

Individual samples were collected as powdered rock using a Dremel drill equipped with precision bits.

All analyses were completed at the Colorado School of Mines (CSM) Stable Isotope Laboratory, Golden, Colorado. The CSM lab possesses the capabilities of analyzing the stable isotopes of hydrogen, carbon, nitrogen, oxygen, and sulfur (H, C, N, O, and S) from a wide array of sample matrices. The GV Instruments IsoPrime mass spectrometer (figure 4-64) is the keystone around which several on-line preparation devices operate. Traditional dual-inlet applications (waters, carbonates, off-line prepared gases) are prepared with a MultiPrep auto sampler capable of performing carbon dioxide (CO_2) and H_2 equilibration on water samples, and acid digestion of carbonate samples (figure 4-65). A 50-port manifold can also be fitted for dual-inlet analysis of off-line gases. The IsoPrime mass spectrometer is also interfaced with continuous-flow preparation devices, including two elemental analyzers and a trace-gas preconcentrator. The elemental analyzers generate gases by combustion or pyrolysis, which are then carried in an inert stream of helium to the mass spectrometer for analysis of H, C, N, O, and S. Common applications include analysis of phosphates, nitrates, waters, organics, soils, plant and animal matter, sulfides, sulfates, and oils. The trace-gas preconcentrator cryogenically focuses trace quantities of gases for isotopic analysis. Common applications include analysis of methane, carbon dioxide, and nitrous oxide from atmospheric and soil-gas samples.

The internal standard used in the CSM lab is the University of California at Los Angeles (UCLA) Carrara marble. The accepted values for this internal standard were matched consistently during the analysis of the Leadville core samples selected for this study. All isotopic compositions are reported relative to PeeDee Belemnite (PDB) (see Land, 1980, figure 6 for definition relative to Standard Mean Ocean Water [SMOW]).

Stable Carbon and Oxygen Isotopes for Leadville Samples at Lisbon Field

Carbon isotopic compositions for the 25 Leadville Limestone (limestone and dolomite) samples from Lisbon field (table 4-2 and figure 4-66) cluster in a very narrow range around the mean value of –2.95‰ PDB; the range is –1.92 to –6.09‰ PDB (one notable exception of +4.4‰ was excluded). Oxygen isotopic compositions for these samples, however, are more widespread (table 4-2 and figure 4-66). The range is –0.96 to –12.26‰ PDB; the mean value is –4.61‰ PDB.

Stable carbon and oxygen isotope data indicate that all Lisbon Leadville dolomites were likely associated with brines whose composition was enriched in del ^{18}O compared with Late Mississippian seawater. Stable oxygen isotope analyses of dolomites show a linear trend with a fairly narrow range of carbon isotope values (figure 4-66). Figure 4-67 shows a cross plot of the same del ^{13}C/del ^{18}O Leadville data from Lisbon field with the regions of dolomite temperatures of formation suggested by Allan and Wiggins (1993), based upon their interpretation of many ancient dolomites. Note that most of the Leadville data points plot in the region that Allan and Wiggins have called the “overlap of low and high temperature dolomites.”

Stable oxygen isotopes for Mississippian seawater were in the range of –2 to –1‰ (Veizer and others, 1999). Dolomitizing fluid compositions enriched with respect to del ^{18}O are thought to be heavier than normal Mississippian seawater (bracketed by the yellow arrows on figure 4-68). Leadville reflux dolomitization likely resulted from evaporated brines, several per mil heavier than normal seawater (for example modern Arabian Gulf water in the range of 2.5 to 4‰ [Wood and others, 2002]). Assuming similar oxygen enrichment of Mississippian seawater

values gives a dolomitizing fluid in the range of 0.5 to 3‰. This factor, coupled with Leadville dolomite isotope values, constrain Leadville replacement dolomitization temperatures to between 140 and 194°F (60-90°C) (figure 4-68). Saddle dolomite cements were precipitated at temperatures greater that 194°F (>90°C).

Strontium Isotope Analysis

Strontium (Sr) isotope analysis was used to assist with the diagenetic interpretation of different subsurface mineral phases within Leadville Limestone samples from Lisbon field. The interpretation of these analyses will be discussed after the following comments about the nature of the Sr isotope analysis, as well as a description of the analytical technique and laboratory used.

Applications and Background

Strontium isotope analysis is used most frequently as an age-dating tool in marine carbonates. The Sr composition of ancient seawater and its variation through geologic time have been determined from common marine carbonate minerals, especially calcite, aragonite, and dolomite (Brass, 1976; Burke and others, 1982; Allan and Wiggins, 1993).

Among the four known isotopes of Sr, the ratio of $^{87}Sr/^{86}Sr$ is the most useful for tracking the secular changes of seawater Sr. These two isotopes come from separate sources in the earth. Strontium 87 is radiogenic (from the radioactive decay of rubidium 87 with a half-life of about 50 billion years), while ^{86}Sr is non-radiogenic (Faure and Powell, 1972; Faure, 1977). These secular changes in the Sr ratio of seawater are the result of the interplay of tectonism and erosion versus seafloor spreading (Allan and Wiggins, 1993). In general, erosion resulting from increased tectonism increases the ratio of $^{87}Sr/^{86}Sr$; during times of high seafloor spreading the ratio is decreased. The assumed reason for these changes is that continental (sialic) crustal rocks (for example granites, gneisses, and their derivatives such as arkoses) contribute radiogenic Sr ratios (that is relatively high Sr isotopic numbers). On the other hand, mantle (simatic) rocks (for example basalts, other volcanic, undifferentiated basic rock types, and their derivatives such as lithic sandstones) are much less radiogenic (that is relatively low Sr isotopic ratios). The high contribution of Sr into the oceans from highly radiogenic continental materials and less radiogenic mantle minerals, combined with the rapid mixing rate of the oceans and the long oceanic residence time of Sr, have allowed the Sr isotope ratio of seawater to be the same globally at any given time. For useful discussions and explanations of these factors, see (Veizer, 1989; and Allan and Wiggins, 1993, p. 49-52).

Most workers believe that the Sr isotopic composition of seawater throughout the world has changed through geologic time as a function of the relative fluxes in contributions from mantle and continental Sr. The mantle contributions are highest during times of rapid seafloor spreading. The continental contributions are highest during times of orogenesis or during climatic periods of increased erosion of the continents (see, for instance, Veizer, 1989).

Strontium Isotope Age Curve for Marine Carbonate Rocks

The $^{87}Sr/^{86}Sr$ ratio of a carbonate mineral can be measured with great precision (that is to five significant figures). Workers at the Mobil (Oil) Field Research Lab successfully constructed

a reference curve that traced the secular change in the Sr isotopic composition of seawater through all of Phanerozoic time (Burke and others, 1982; Elderfield, 1986; McArthur and Howarth, 2004; see figure 4-69). Index fossil samples were used to construct and constrain the original curve. Originally, the curve served as a reference for Sr isotope dating of marine carbonates without diagnostic index fossils. Cenozoic marine limestones and cherts can be dated with very small margins of error (for example DePaolo and Ingram, 1985; DePaolo, 1986; DePaolo and Finger, 1991) because of the availability of Cenozoic index fossils in good condition and the very steep, monotonic nature of the curve during this time period (figure 4-69). For older marine carbonates, dating is less accurate due to poor preservation of fossils as well as the oscillating trends of the Sr isotope age curve (figure 4-69). The amplitudes and high frequency of these oscillations over geologic time is probably the result of climatic, tectonic-erosional, and seafloor-spreading cycles (Allan and Wiggins, 1993). The Sr isotope curve is most useful for age dating during geologic time intervals when the curve is unidirectional and steep (for instance, during the Permian).

Strontium Isotopes as Tracers for Diagenetic Fluids

Strontium isotopes can have significant value in tracing subsurface fluid movement (Burtner, 1987; Allan and Wiggins, 1993). Marine waters throughout geologic time apparently displayed a relatively narrow range of $^{87}Sr/^{86}Sr$ ratios - from about 0.7068 to 0.7095 (figure 4-69). Any ratios from carbonates that are significantly above or below this range of Phanerozoic seawater $^{87}Sr/^{86}Sr$ ratios indicate contribution by diagenetic waters in carbonate minerals that are of non-marine origin. Higher Sr isotope values indicate addition of radiogenic (high $^{87}Sr/^{86}Sr$ ratio) contaminants from crystalline (granitic or sialic) basement rocks or potassic feldspar-rich siliciclastic sediments (see, for instance Burtner, 1987). Lower Sr isotope values indicate contributions from mafics, ultramafics, and lithic sandstones with calcic plagioclase feldspar (see, for instance, Schultz and others, 1989).

Strontium is a doubly charged cation which easily substitutes into the carbonate crystal lattice (Allan and Wiggins, 1993). When Sr is released by diagenetic processes, it is partitioned into dolomites and carbonate cements in various subsurface settings (figure 4-70). Therefore, Sr analysis is an excellent tool for identifying hydrothermal dolomite.

Strontium Isotopic Ratios for Leadville Samples at Lisbon Field

Three samples of different diagenetic mineral phases were selected for Sr isotopic analysis. Mineral separates were carefully drilled or plucked out of a conventional core segment from the Lisbon NW USA No. B-63 well, Lisbon field (figure 2-1), at a depth of 9939 feet (3030 m). One sample each of (1) replacement, brownish “sucrosic” (rhombic euhedral) dolomite, (2) coarse, white saddle dolomite, and (3) coarse, clear to white calcite spar cement (figure 4-12 is a thin section photomicrograph showing the same mineral phases from 9991.8 feet [3045.4 m]), were analyzed by Geochron Laboratories (a Division of Krueger Enterprises, Inc., Cambridge, MA) for $^{87}Sr/^{86}Sr$ isotopic ratios (table 4-3). The precision of these analyses was reported to six significant figures (that is 0.00000X).

All three samples exhibit highly radiogenic Sr isotopic values, each in excess of 0.711. These values are far higher than the secular range of $^{87}Sr/^{86}Sr$ ratios for marine carbonate fossils and rocks during the Mississippian or for any time during the Phanerozoic (Burke and others,

1982; Allan and Wiggins, 1993; Denison and others, 1994; Bruckschen and others, 1999; McArthur and Howarth, 2004). A plot of the Sr isotope composition for the three Leadville samples from Lisbon field, along with the Phanerozoic marine carbonate curve for Sr ratios, is shown in figure 4-71.

Discussion

It is apparent that the high Sr isotopic ratios for the three late (burial) diagenetic mineral phases indicate contributions from diagenetic waters enriched in ^{87}Sr that were derived from granitic or arkosic sandstone terrains. The most logical terrain for ^{87}Sr enrichment is either Precambrian basement rocks or the Devonian McCracken Sandstone. Both of these sources are at depths considerably below the Leadville reservoir rocks samples for this study. However, early Tertiary reactivation of basement-involved, high-angle normal faults associated with Precambrian tectonics may have allowed hot, deep-seated fluids from the granitic basement or the McCracken Sandstone (figure 4-72) to communicate upwards with the Leadville carbonate section. Brines from evaporites in the Pennsylvanian Paradox Formation may also have entered the Leadville along the large fault bounding the northeast flank of Lisbon field (figures 2-1 and 4-72). It is interesting that these radiogenic fluids were involved in precipitation of replacement "sucrosic" dolomites, saddle dolomites, and late calcite spar cements.

Strontium isotope compositions from many (but not all) burial replacement dolomites are radiogenic (Allan and Wiggins, 1993, p. 95). The high $^{87}Sr/^{86}Sr$ ratio is indicative of allochthonous dolomitizing brines that interacted with potassic feldspars from basement rocks or from arkosic siliciclastic sediments prior to dolomitization. For instance, matrix replacement and white saddle dolomites in Upper Devonian (Frasnian) pinnacle reefs, Alberta Basin, Canada, surrounded by deeper-water facies, contain radiogenic Sr well above the Sr isotope seawater curve (Anderson, 1985; Allan and Wiggins, 1993, figure 95). Burial replacement dolomites in the Ordovician Trenton Formation of southern Michigan, also have Sr isotope similarities to the Leadville at Lisbon field. Reactivation of a basement-involved, Precambrian, left-lateral wrench system allowed brines to migrate from the Silurian Salina Formation along faults and fractures into the Trenton (Allan and Wiggins, 1993). Strontium in Trenton limestone has Ordovician seawater values while dolomite has Silurian seawater values (figure 4-73).

Leadville Limestone Burial History and Possible Heat Sources

Burial history and temperature profiles for the Leadville at Lisbon field provide some guidance as to when important diagenetic and porosity-forming events occurred. These profiles (figure 4-74) were estimated using formation tops derived from well logs, a calculated geothermal gradient from bottom-hole temperatures of Lisbon wells (figure 2-12), regional measured stratigraphic sections, geologic maps, and various publications summarizing the geologic history of the area. The burial history profile shows rapid burial during the Pennsylvanian corresponding to the development of the Paradox Basin. This period is followed by a relatively gradual increase in burial depth, with minor spikes representing times of erosion or non-deposition, until the rapid and maximum depth of burial (16,500 feet [5500 m]) occurred during the Late Cretaceous. The maximum temperature at this time was about 244ºF (118ºC). In addition to the calculated temperature profile, we have inferred anomalous temperature spikes for: (1) late Laramide reactivation along normal faults that extend to basement, and (2)

Oligocene igneous events such as the emplacement of the nearby La Sal and Abajo laccolith complexes, 10 miles (16 km) north and 23 miles (37 km) southwest, respectively, of Lisbon field.

Porous replacement dolomites probably formed during the early and middle portions of the burial history at Lisbon field. Figure 4-75 displays suggested windows for important diagenetic phases in the reservoir history of the Leadville Limestone at Lisbon field: (1) the formation of rhombic dolomites and major intercrystalline ("sucrosic") porosity, (2) saddle dolomite clear rims and cements, (3) euhedral quartz, dissolution of limestone and dolomite matrix, and pyrobitumen development, and (4) late calcite cements (with live oil inclusions). The inferred elevated temperature spikes during maximum burial, late Laramide fault reactivation/uplift, and Oligocene igneous activity may account for the high temperatures responsible for quartz precipitation, sulfide mineralization, pyrobitumen formation, late dissolution of carbonates, and late saddle dolomite cements.

We propose a model with convection cells bounded by basement-rooted faults to transfer heat and fluids from possible crystalline basement, Pennsylvanian evaporites, and Oligocene igneous complexes. Tremendous amounts of water are required to produce the amount, type, and generations of dolomite present at Lisbon field. There is probably not enough water moving through the regional hydrodynamic system to account for the Leadville dolomite. Recycling hot, brine-bearing water in convection cells may have allowed dolomitization to occur. A highly diagrammatic south to north cross section of the greater Lisbon field area (figure 4-72) shows the possible convection cells of the circulation model for ascending warm fluids responsible for saddle dolomite, high-temperature quartz, pyrobitumen, aggressive dissolution of limestone and dolomites, and sulfide mineralization. The basal aquifer for these inferred fault-controlled cells could be the Devonian McCracken Sandstone. This sandstone is locally porous enough to produce oil at Lisbon field. Sources of heat may have been from the Precambrian basement rocks and/or from Oligocene igneous intrusive activity. Some of the mapped faults cutting Lisbon field may have been involved with thermal convection cells for circulating fluids during late burial diagenesis (figure 4-76). Several wells near faults appear to have better reservoir quality, produce greater volumes of oil, and have higher residual bottom-hole temperatures than wells away from these faults.

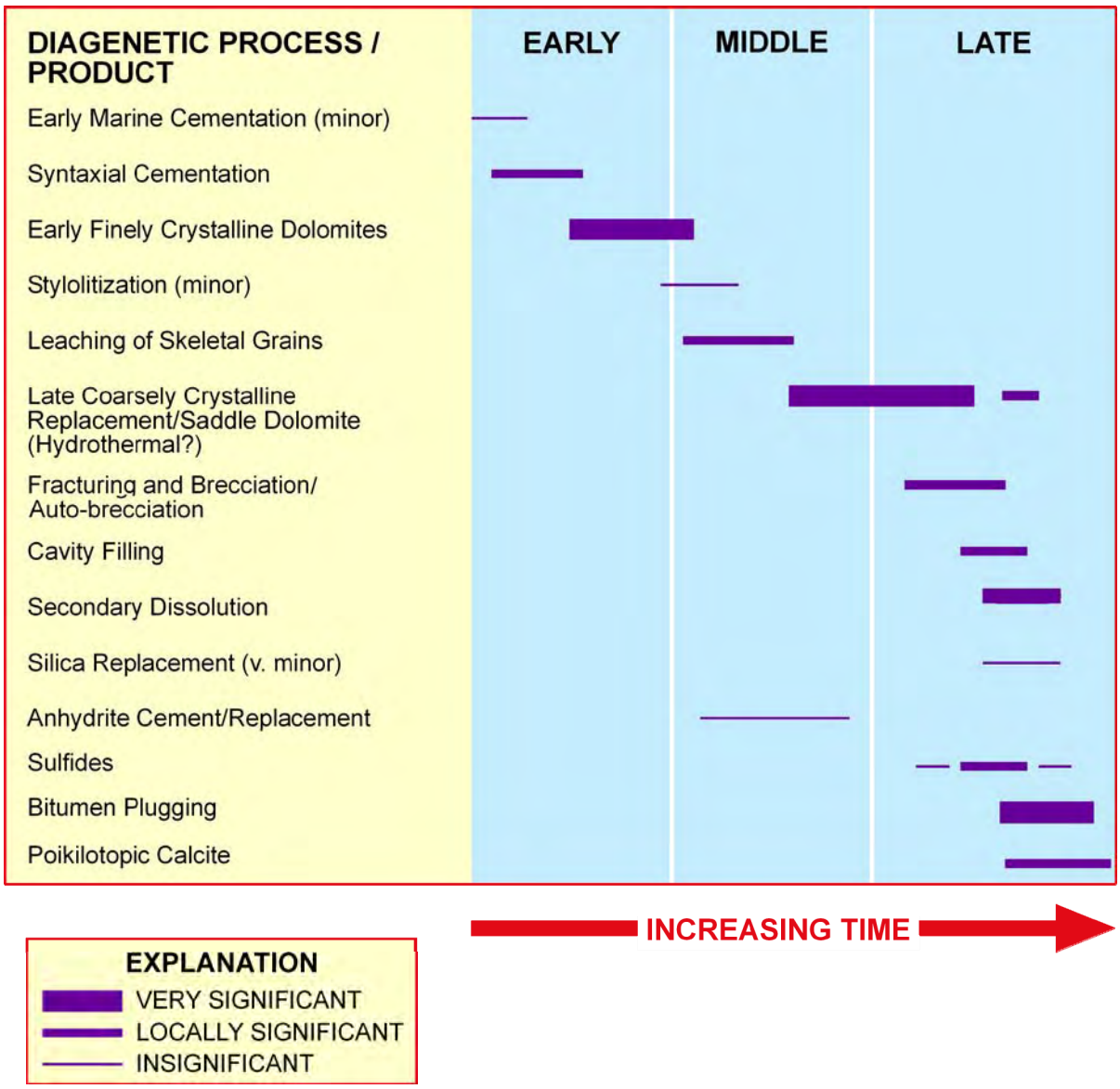

Figure 4-1. Ideal diagenetic sequence through time based on thin section analysis, Leadville Limestone, Lisbon field.

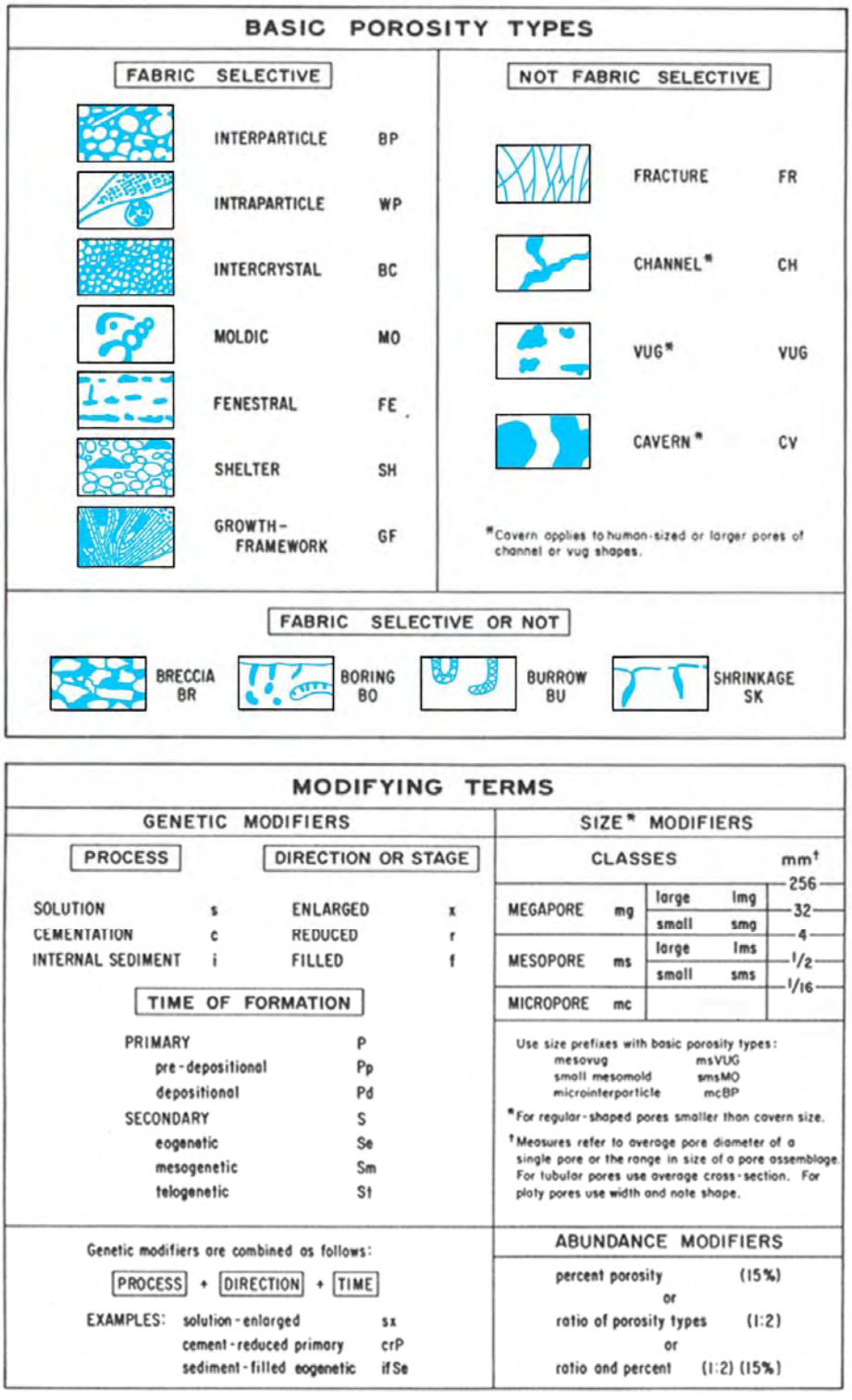

Figure 4-2. Classification of pores and pore systems in carbonate rocks (Choquette and Pray, 1970).

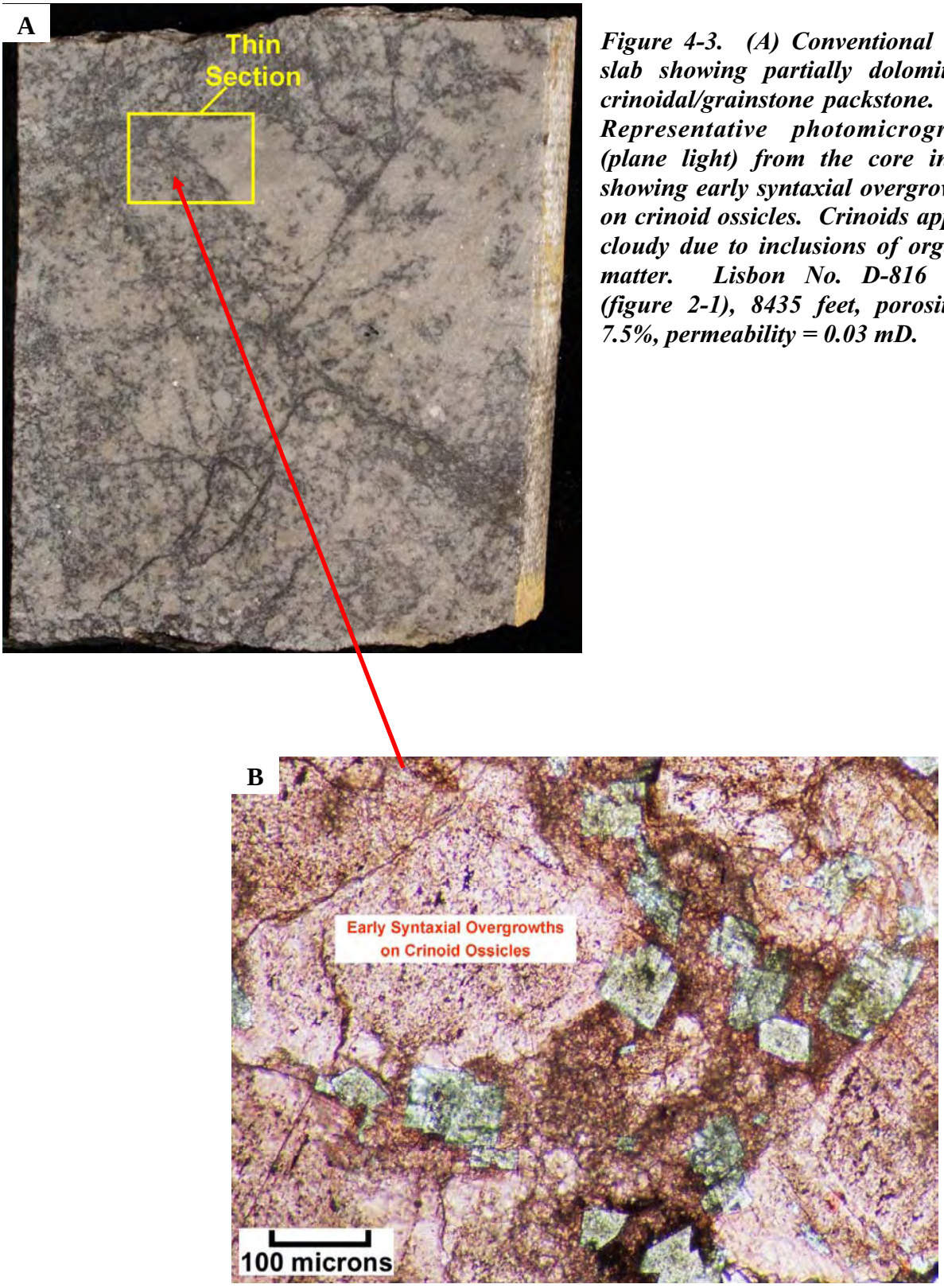

Figure 4-3. (A) Conventional core slab showing partially dolomitized crinoidal/grainstone packstone. (B) Representative photomicrograph (plane light) from the core in A, showing early syntaxial overgrowths on crinoid ossicles. Crinoids appear cloudy due to inclusions of organic matter. Lisbon No. D-816 well (figure 2-1), 8435 feet, porosity = 7.5%, permeability = 0.03 mD.

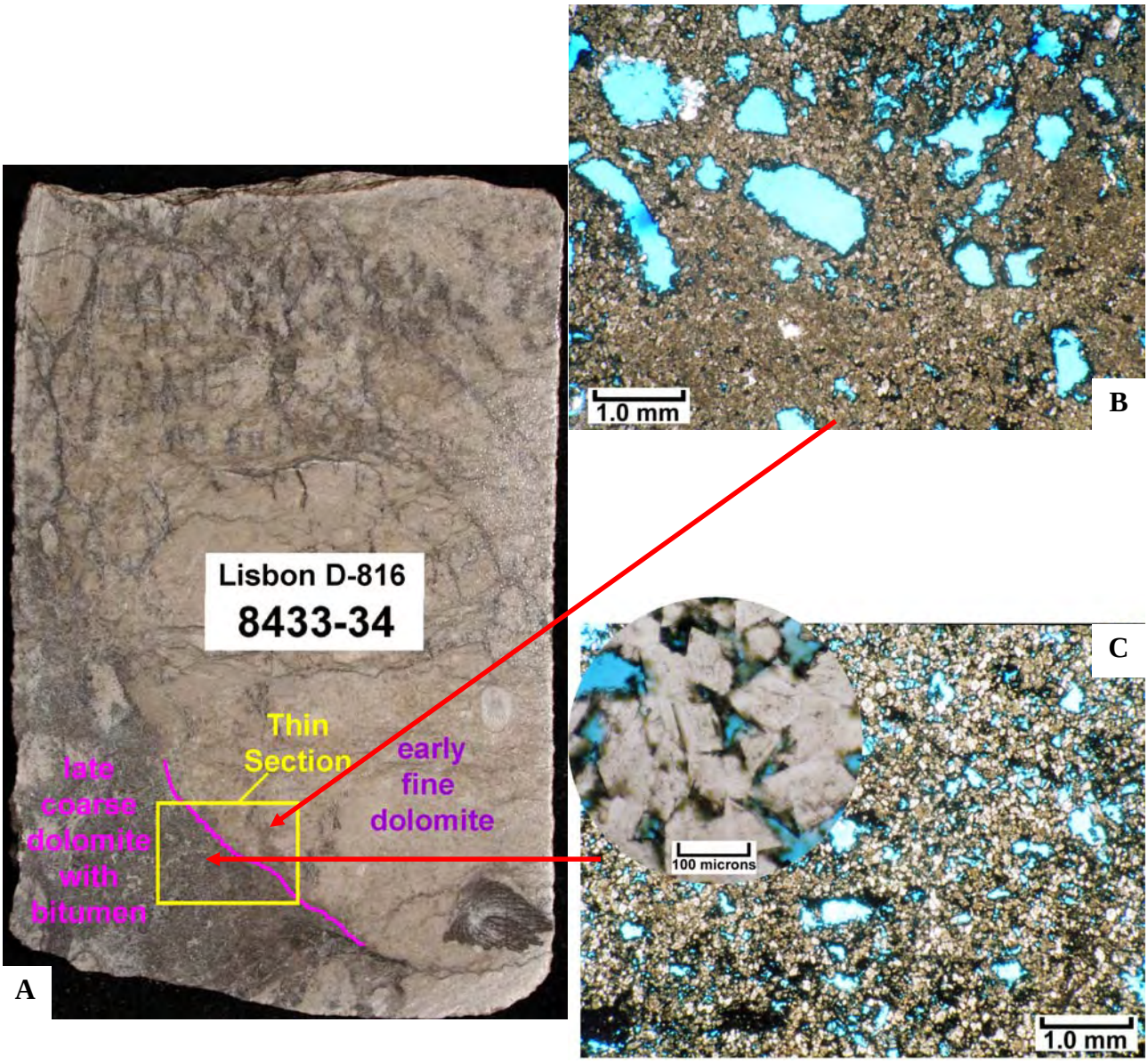

Figure 4-4. (A) Conventional core slab showing tight, fabric selective, very fine early dolomite as well as porous, coarser late dolomite. Most of the late dolomite crystal faces are coated with films of pyrobitumen. Hence, most of the areas of crosscutting coarser dolomites are black in this view. Note the position of the thin section which captures the contact between low-permeability early dolomite (upper right part of the thin section box) and high-permeability late, "black dolomite" (lower left). (B) Representative photomicrograph (plane light) of the tight, finely crystalline dolomite with isolated grain molds. Most of this fabric selective dolomite formed early in the diagenetic history of the skeletal/peloid sediment. (C) Representative photomicrograph (plane light) of the coarser, replacement dolomite (both euhedral rhombs and occasional "saddle" overgrowths [close-up view in inset]). The black (opaque) areas are the result of pyrobitumen films and minor sulfide precipitation. Lisbon No. D-816 well (figure 2-1), 8433 feet, porosity = 2%, permeability <0.1 mD.

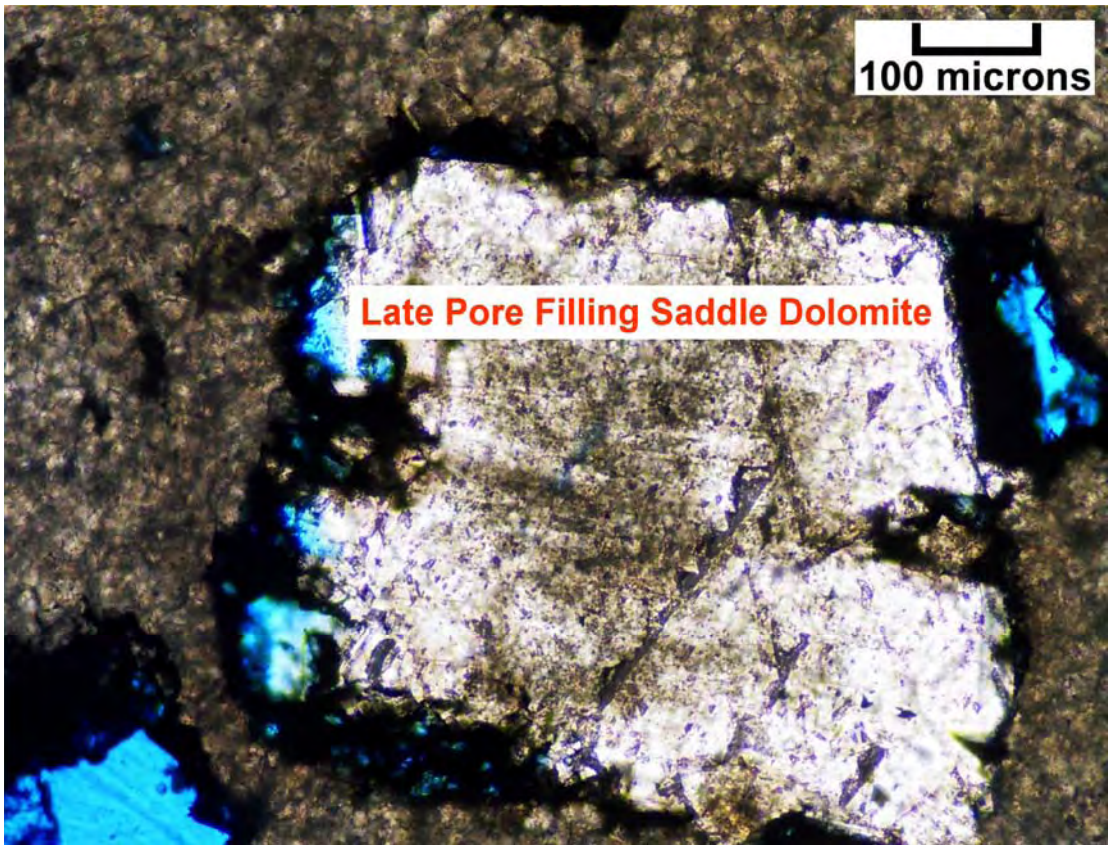

Figure 4-5. Thin section photomicrograph (plane light) showing a saddle dolomite cement that is filling a large pore (either a grain mold or small vug). The dolomite cement has been surrounded by a coating of pyrobitumen (in black). It appears that this late dolomite cement has been partially dissolved or corroded around its margins after the bitumen coating. Lisbon No. D-816 well (figure 2-1), 8421 feet, porosity = 8.3%, permeability = 34 mD.

Figure 4-6. (A) Conventional core slab showing a dolomite "autobreccia" in which the clasts have moved very little. The black material surrounding the in-place clasts is composed of porous late dolomite coated with pyrobitumen. (B) Entire thin section overview from the core in A, showing low-porosity, white dolomite clasts surrounded by solution-enlarged fractures partially filled with coarse rhombic (RD) and saddle dolomites that are coated with pyrobitumen (bit). These black areas between the clasts exhibit very good intercrystalline porosity. The open fracture segments (in blue) between clasts are bridged by coarse, saddle dolomite cements (SDC). (C) Entire thin section overview from the core in A, of black, porous, dolomite clasts surrounded in this case by coarse, low-porosity saddle dolomites. These white dolomites were probably early dolomite (ED) filling space between possible "hydrofactured" replacement dolomites. The black porous dolomites are mostly rhombic (planar) dolomites (RD) coated with thin films of pyrobitumen (bit). Lisbon NW USA No. B-63 well (figure 2-1), 9938.3 feet, porosity = 6.4%, permeability = 54 mD.

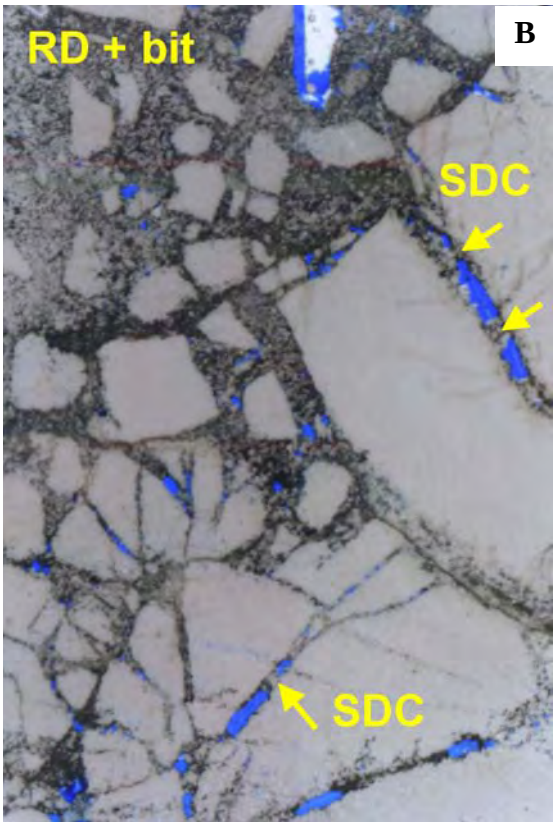

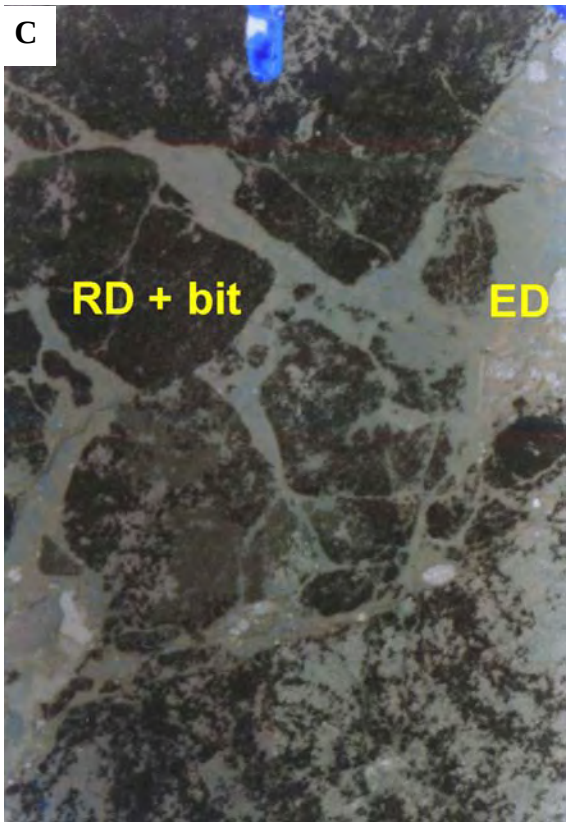

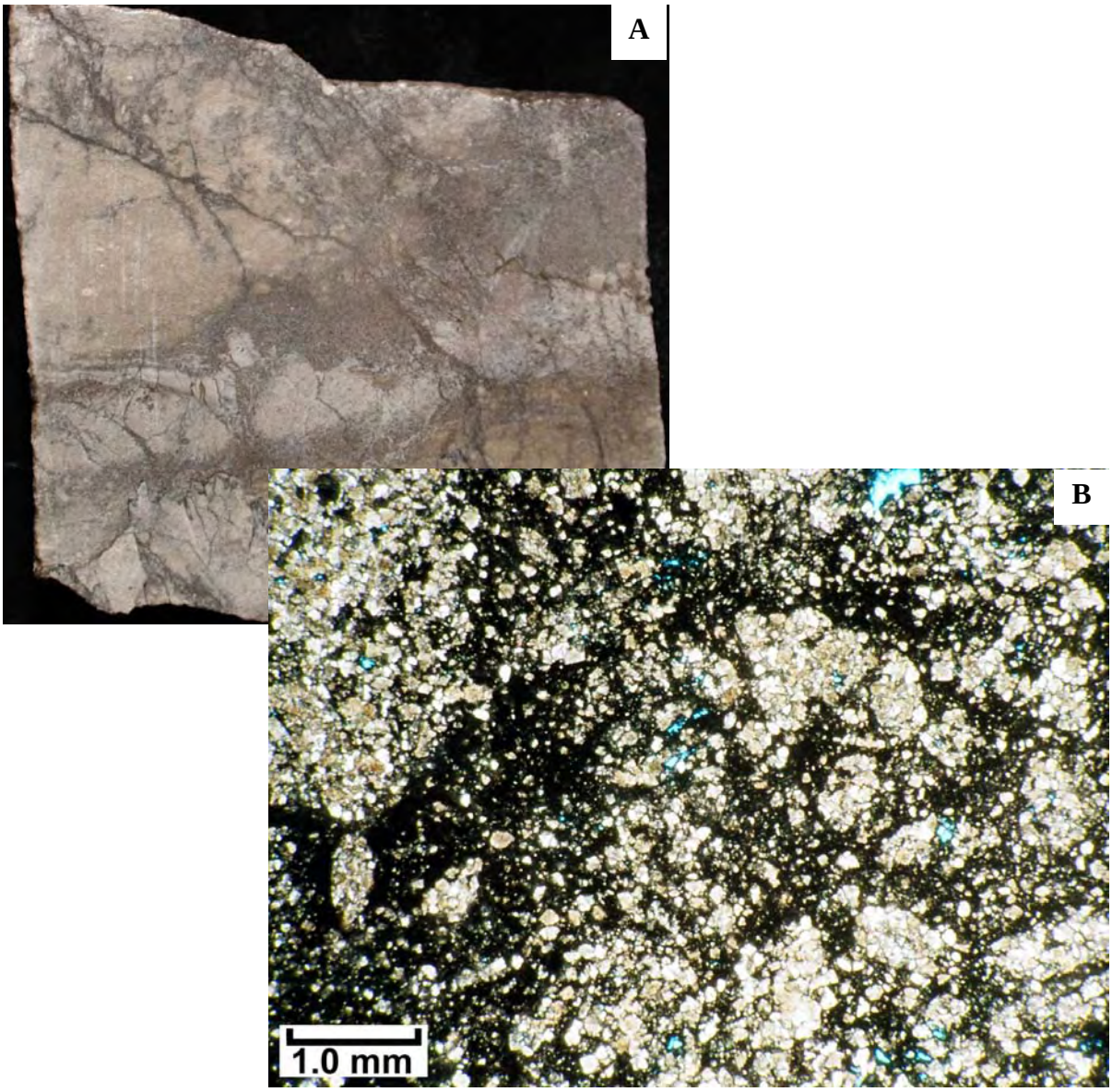

Figure 4-7. (A) Conventional core slab of a dolomitized, peloidal/crinoidal packstone/ wackestone with swarms of fractures marked by black, coarse dolomite. (B) Representative photomicrograph (plane light) from the core in A, showing highly deformed and brecciated dolomite within a bitumen-lined fracture zone. Lisbon No. D-816 well (figure 2-1), 8438.5 feet, porosity = 11%, permeability = 5 mD.

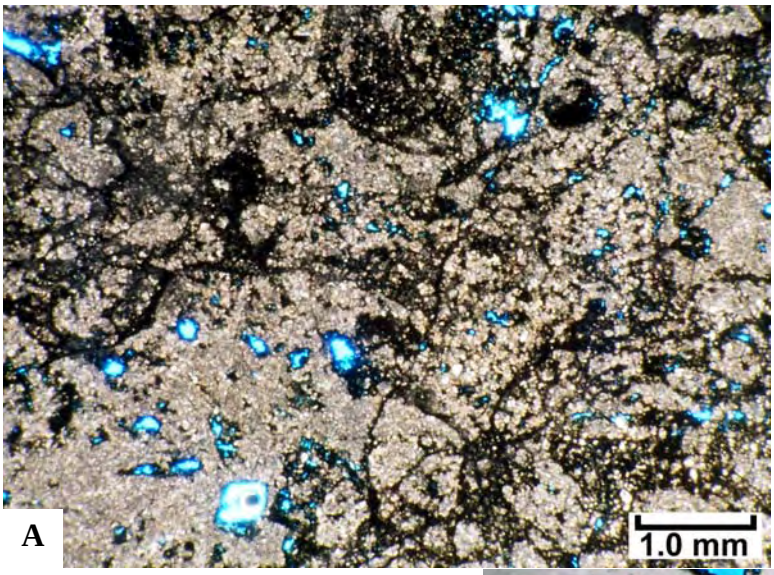

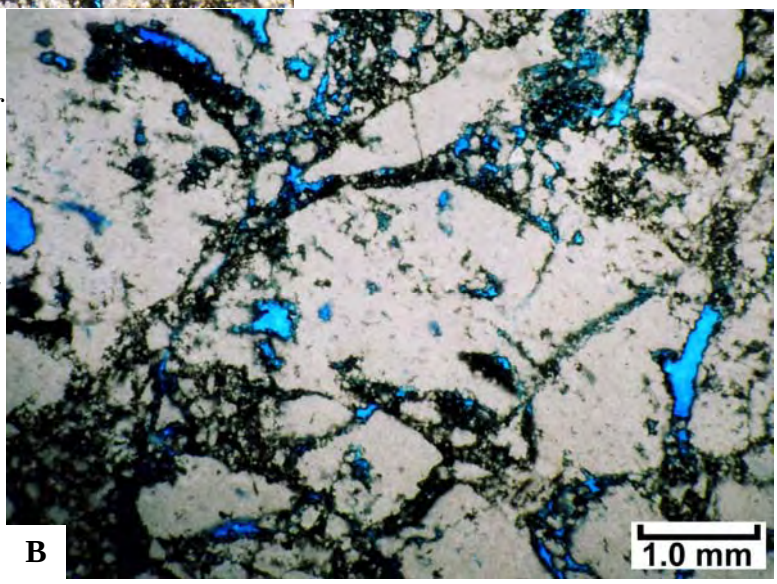

Figure 4-8. (A) Representative photomicrograph (plane light), showing another example of intensely brecciated dolomite within a bitumen-lined fracture zone. (B) Representative photomicrograph (plane light), showing large autoclasts and bitumen in an intensely brecciated dolomite. Lisbon No. D-816 well (figure 2-1), 8423 feet, porosity = 10.5%, permeability = 47 mD.

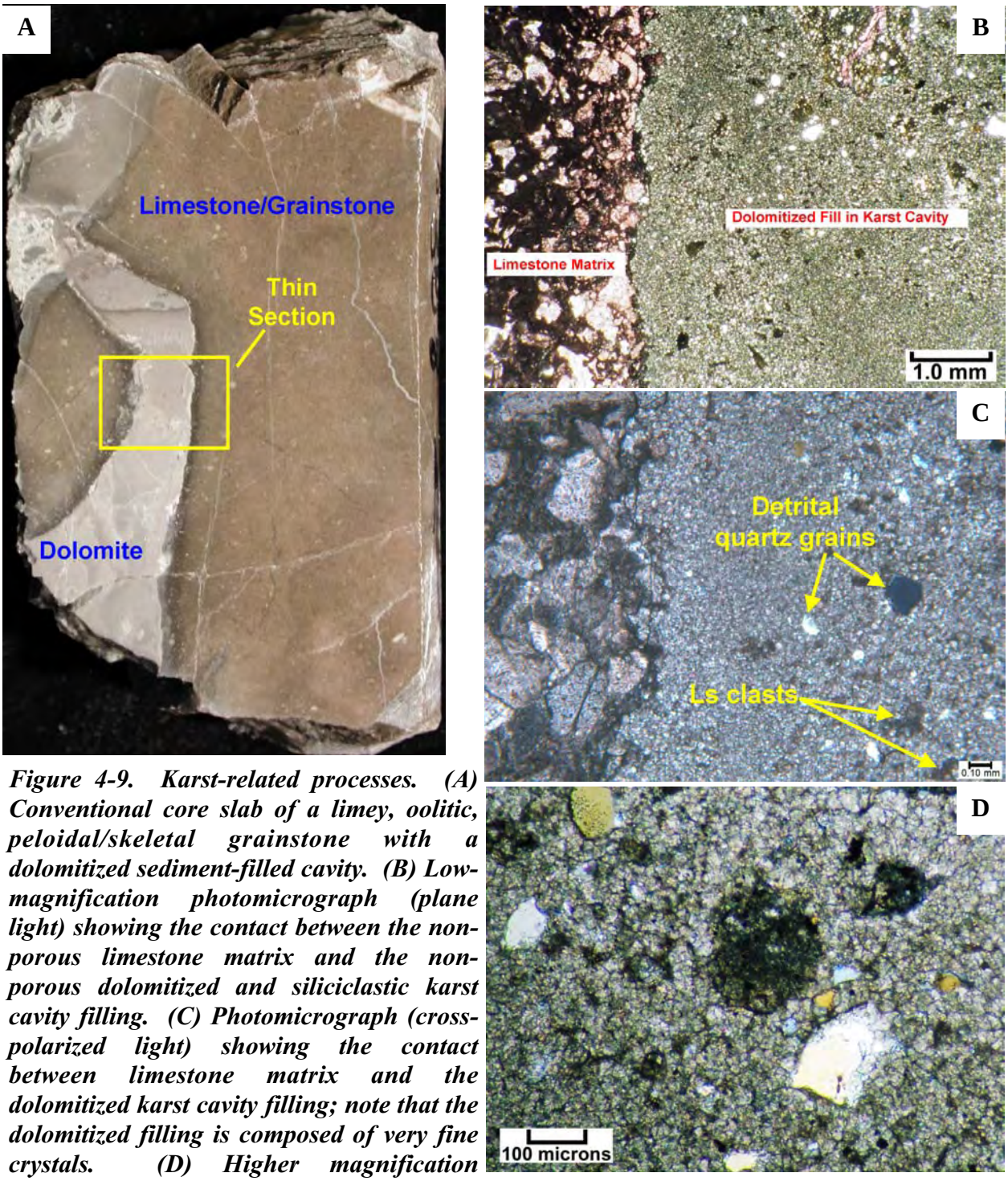

Figure 4-9. Karst-related processes. (A) Conventional core slab of a limey, oolitic, peloidal/skeletal grainstone with a dolomitized sediment-filled cavity. (B) Low-magnification photomicrograph (plane light) showing the contact between the non-porous limestone matrix and the non-porous dolomitized and siliciclastic karst cavity filling. (C) Photomicrograph (cross-polarized light) showing the contact between limestone matrix and the dolomitized karst cavity filling; note that the dolomitized filling is composed of very fine crystals. (D) Higher magnification photomicrograph (plane light) of detrital quartz grains (white) and small carbonate clasts (dark gray) within the tight, dolomitized mud filling the karst cavity. Lisbon No. D-616 well (figure 2-1), 8308-8309 feet, porosity = 1.2%, permeability = 11.1 mD.

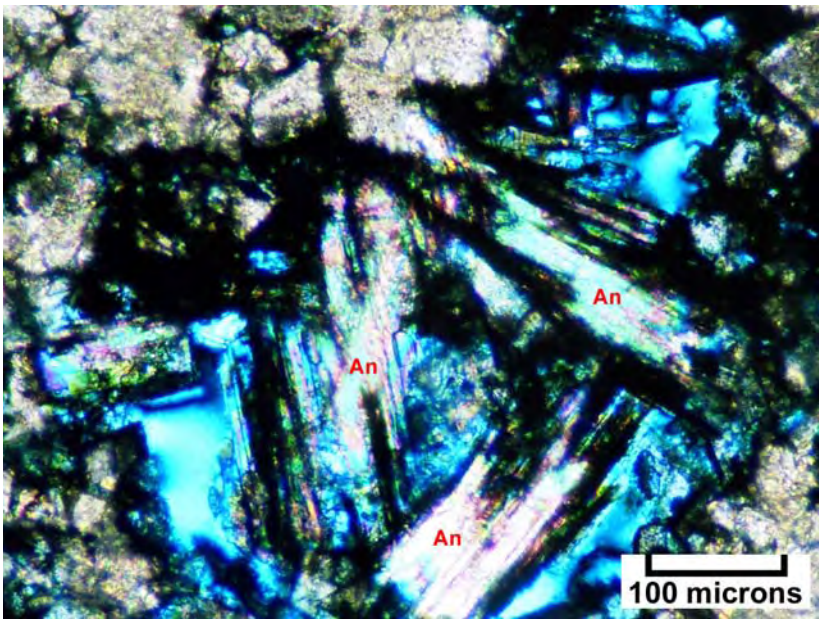

Figure 4-10. Representative photomicrograph (cross-polarized light) showing lathes of late anhydrite cement (An, in the pastel colors) filling a dissolution pore. The unfilled portions of the pore are seen in the blue areas. Lisbon No. D-816 well (figure 2-1), 8426-8431 feet, porosity = 11.1%, permeability = 15 mD.

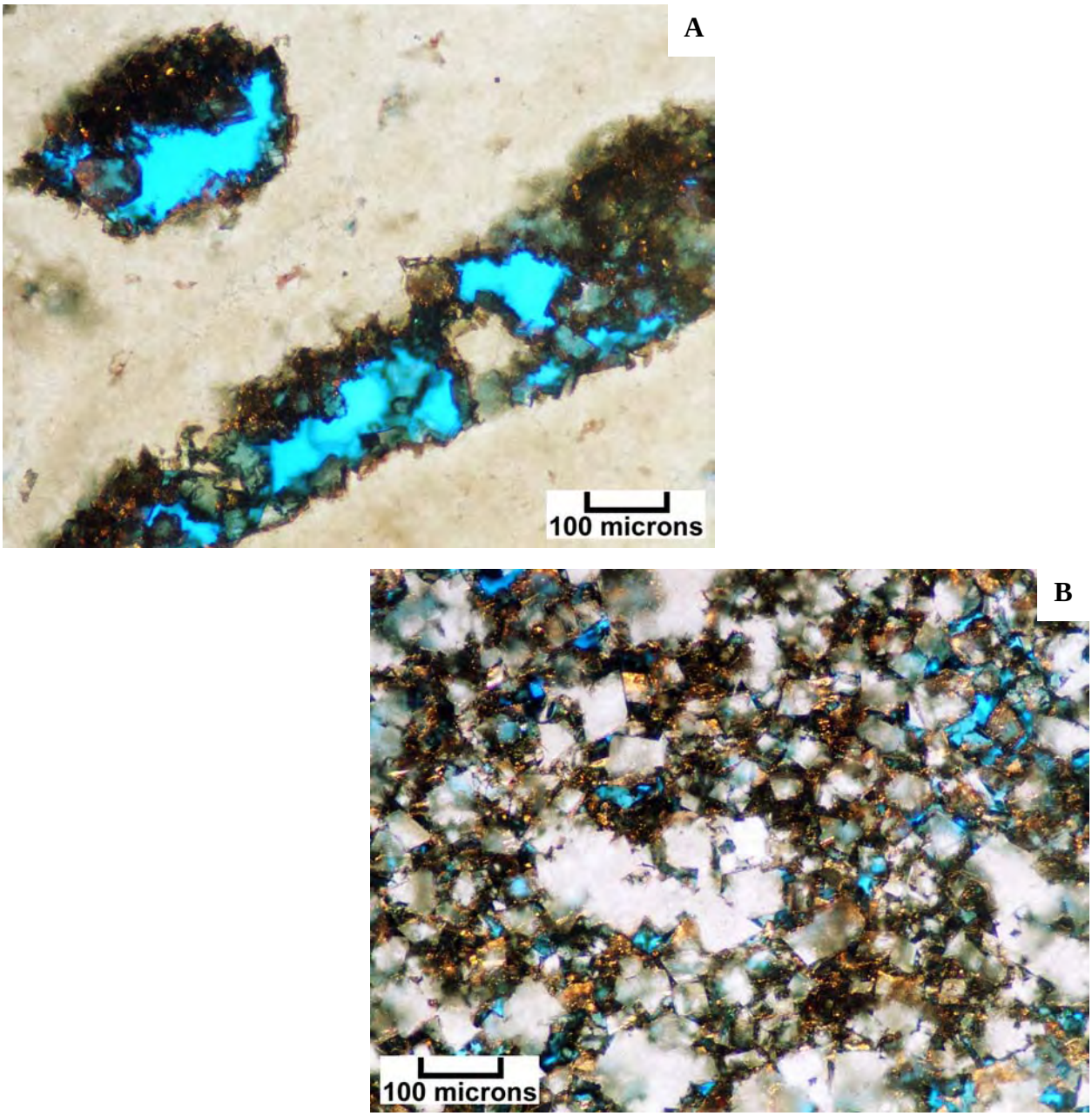

Figure 4-11. Possible sulfide mineralization within the Leadvlle Limestone at Lisbon field. (A) Photomicrograph ("white card" and reflected light) showing moldic pore lined with black pyrobitumen and possible sulfide minerals (small brassy crystals). Lisbon No. D-816 well (figure 5), 8444-8445 feet, porosity = 6.6 percent, permeability = 7 mD. (B) Photomicrograph ("white card" and reflected light) showing black pyrobitumen and sulfide minerals on and between rhombic dolomite crystals (in white and light gray). Lisbon No. D-816 well (figure 2-1), 8446-8447 feet, porosity = 13%, permeability = 59 mD.

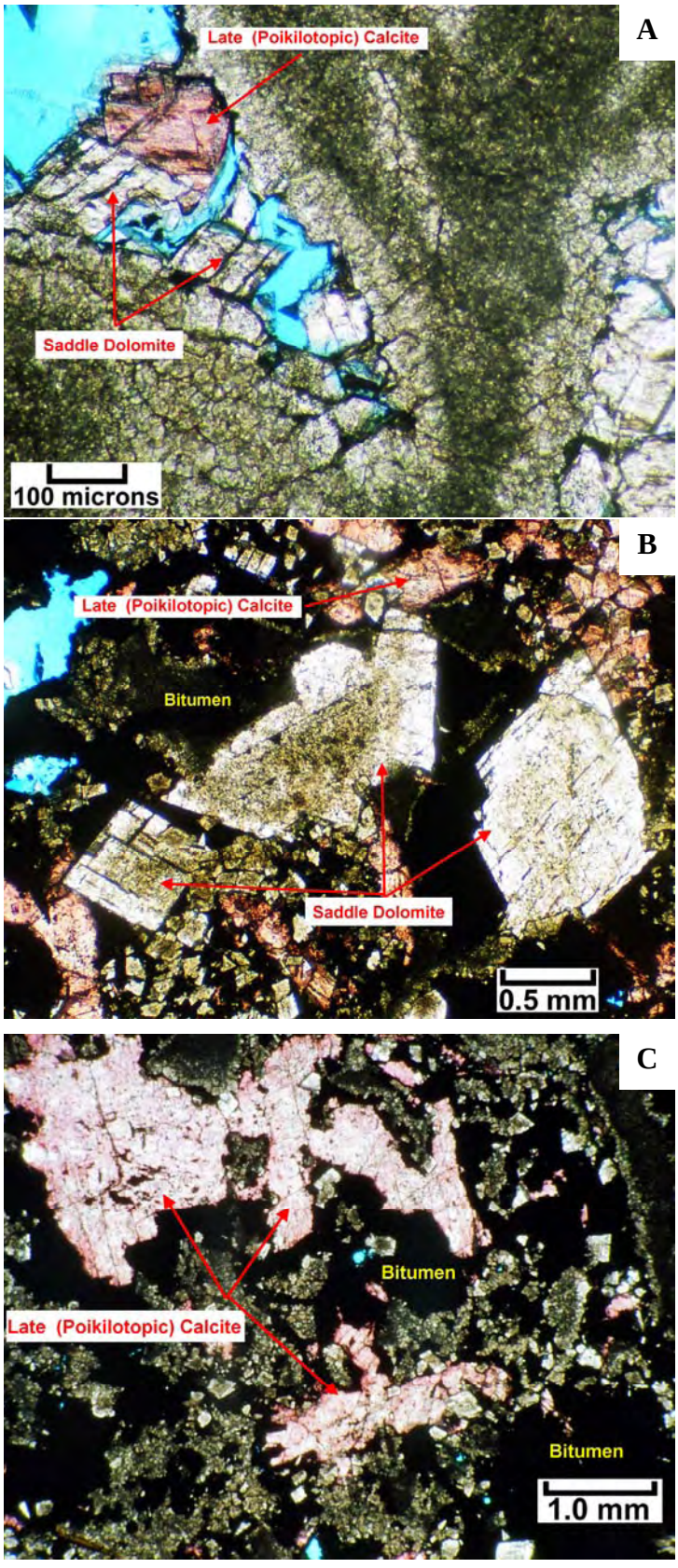

Figure 4-12. (A) Photomicrograph (plane light) showing coarse, white saddle dolomite crystals and a single, coarse, clear late macrocalcite cement crystal (stained red) filling a portion of a large dissolution pore (blue) in a finely crystalline, sucrosic replacement dolomite matrix. Northwest Lisbon No. B-63 well (figure 2-1), 9991.8 feet, porosity = 6.2%, permeability = 0.3 mD. (B) Photomicrograph (plane light) showing coarse rhombic and saddle replacement dolomite that displays cloudy cores and clear rims. Dissolution pores are filled with pyrobitumen (black) and late macrocalcite (stained red). An additional episode of dissolution can be seen as the open (blue) pores that appear to post-date most of the pyrobitumen emplacement. (C) Dissolution pores filled completely with bitumen (black) and late macrocalcite (stained red) that resemble saddle dolomite molds. B and C from Northwest Lisbon No. B-63 well, 10,004-10,005 feet, porosity = 14.4%, permeability = 1.9 mD.

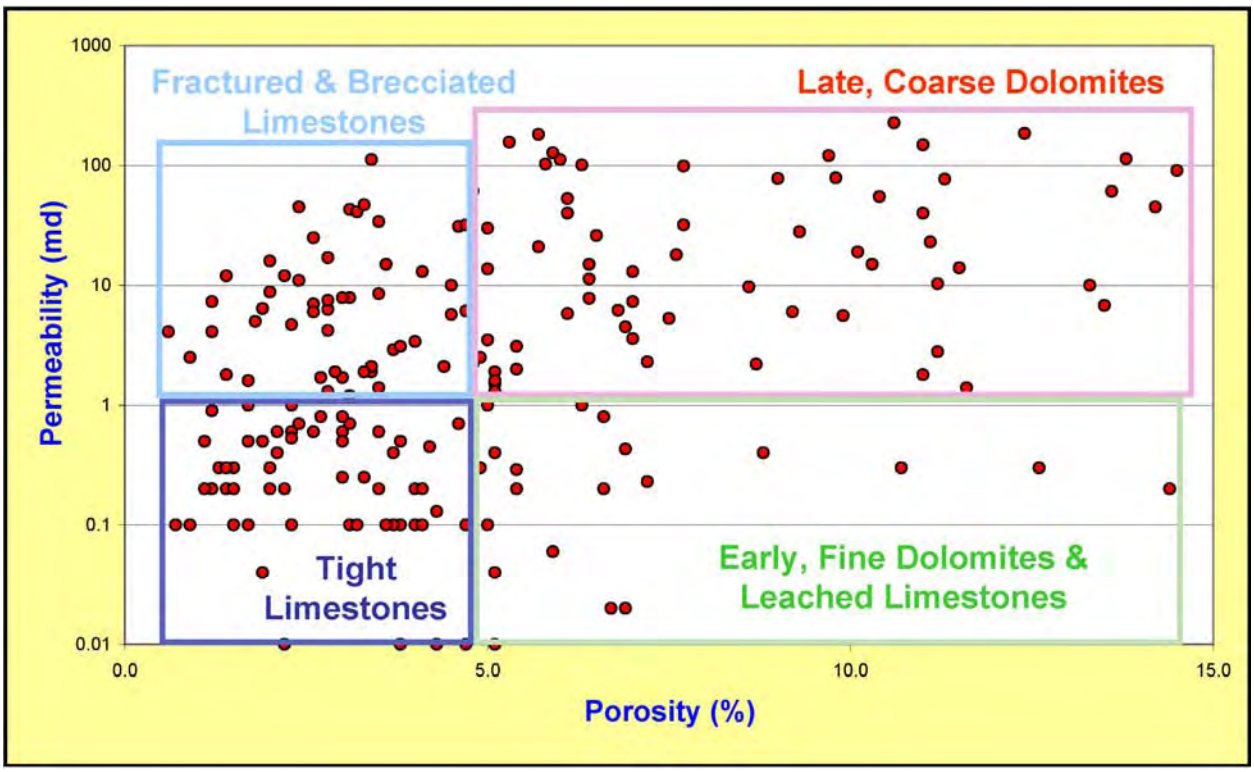

Figure 4-13. Lisbon Unit No. B-610 well permeability versus porosity cross plot by diagenesis.

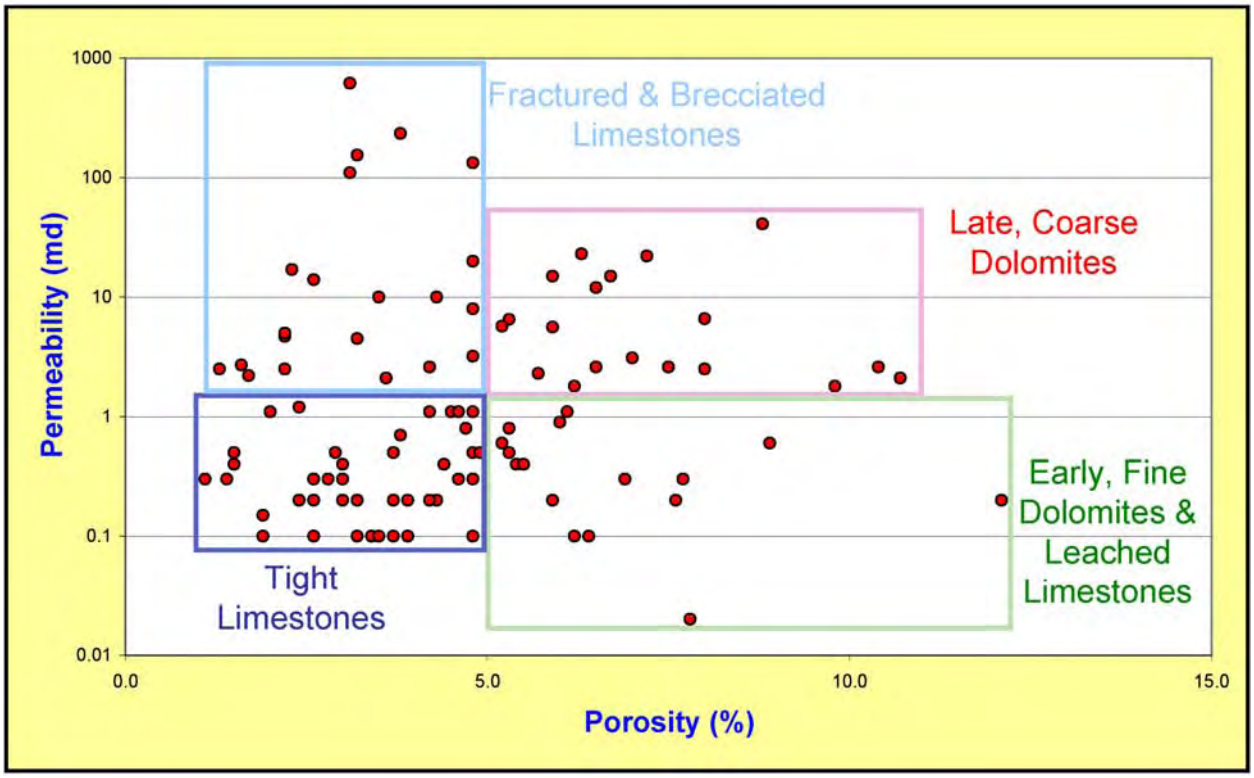

Figure 4-14. Lisbon Unit No. B-816 well permeability versus porosity cross plot by diagenesis.

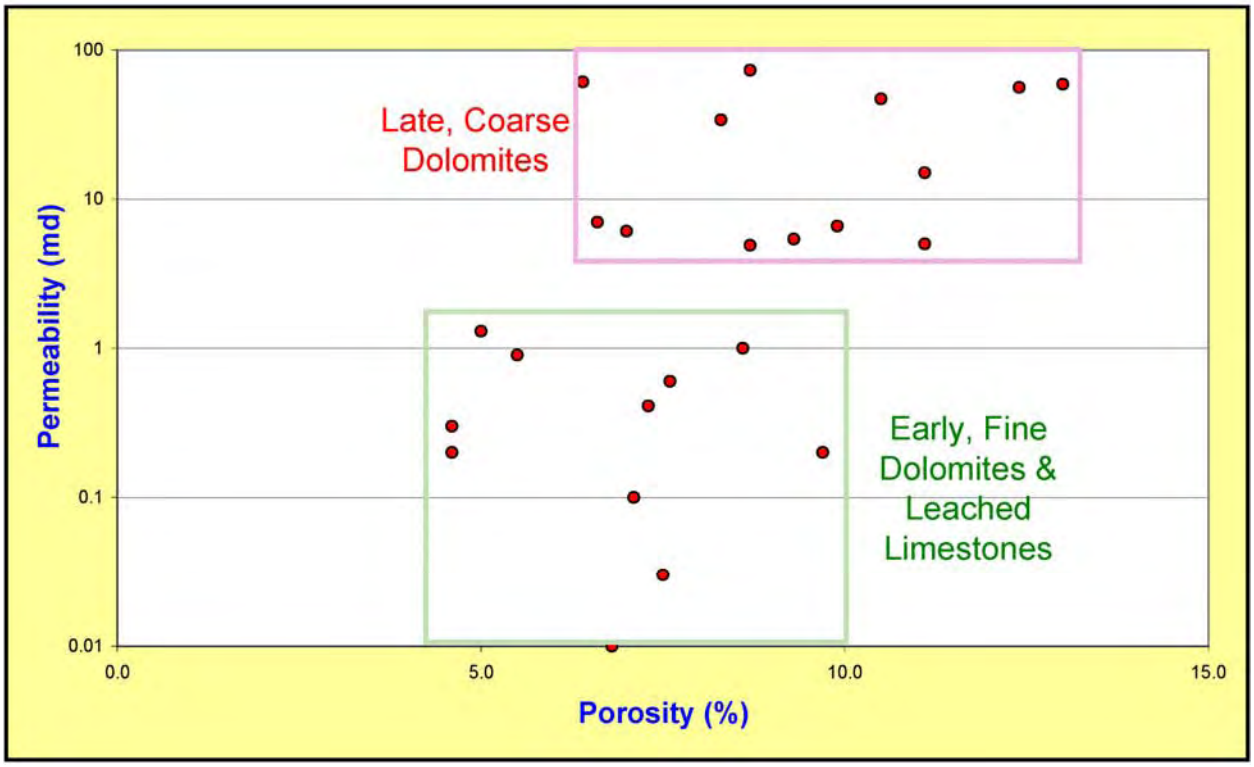

Figure 4-15. Lisbon Unit No. D-816 well permeability versus porosity cross plot by diagenesis.

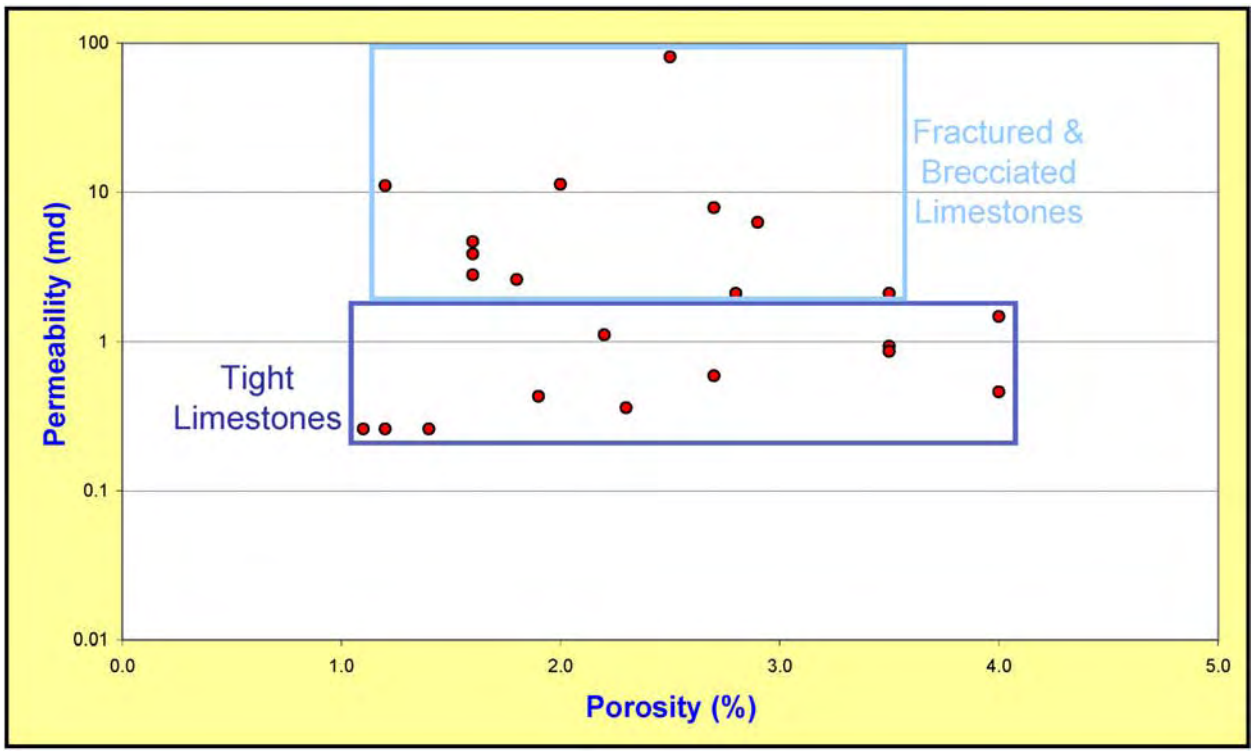

Figure 4-16. Lisbon Unit No. D-616 well permeability versus porosity cross plot by diagenesis.

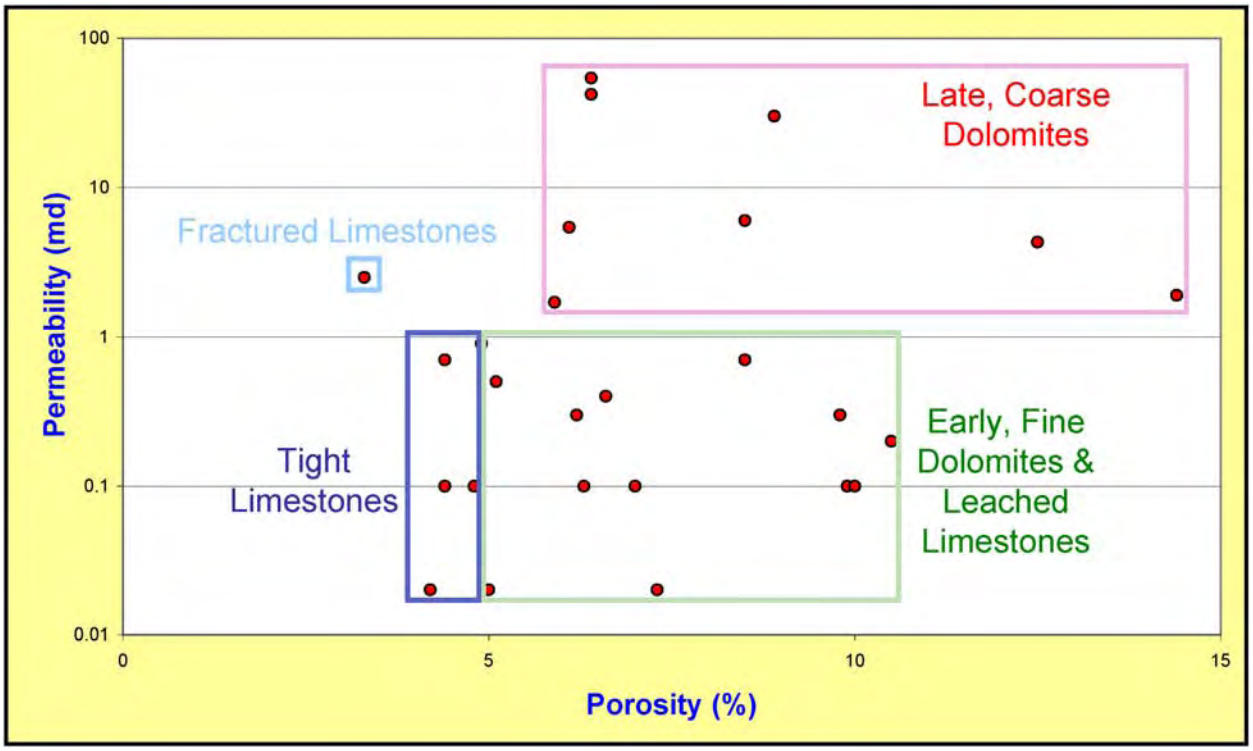

Figure 4-17. Lisbon Unit No. B-63 well permeability versus porosity cross plot by diagenesis.

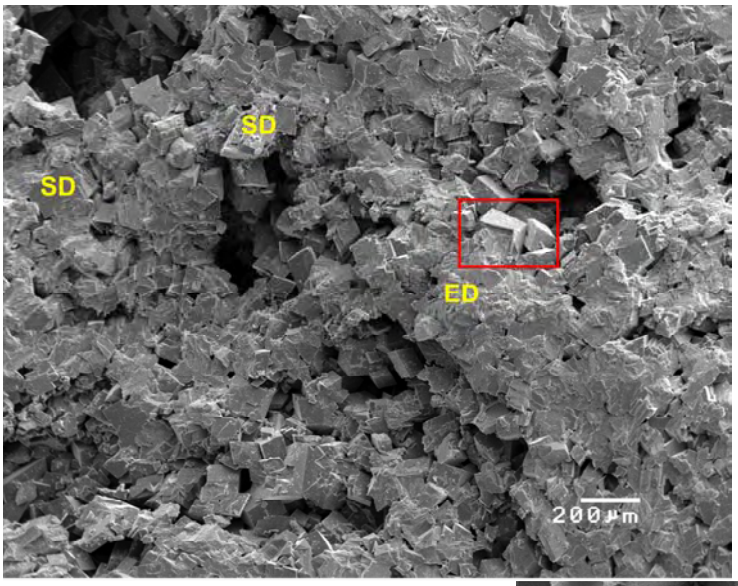

Figure 4-18. Scanning electron microscope photomicrograph of a core plug from 8433 feet, Lisbon No. D-816 well, showing typical Leadville dolomites at Lisbon field. Note the very fine, tight early dolomites (ED) that have been replaced with late, rhombic and saddle (SD) dolomites. There is a significant porosity increase associated with the late dolomite replacement. Scale bar represents 200 microns (0.2 mm). Porosity = 2%; permeability < 0.1 mD based on core-plug analysis.

Figure 4-19. Scanning electron microscope photomicrograph of a core plug from 7886 feet, Lisbon No. B-610 well, showing probable pyrobitumen (P) coating the rhombic dolomite crystal in the center. Pyrobitumen coats many other dolomite crystals as well. Scale bar represents 10 microns (0.01 mm). Porosity = 13.8%; permeability = 114 mD based on core-plug analysis.

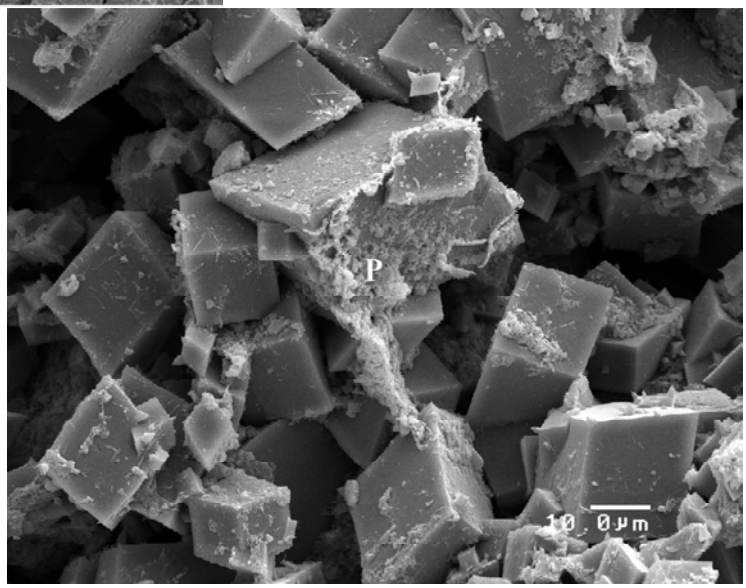

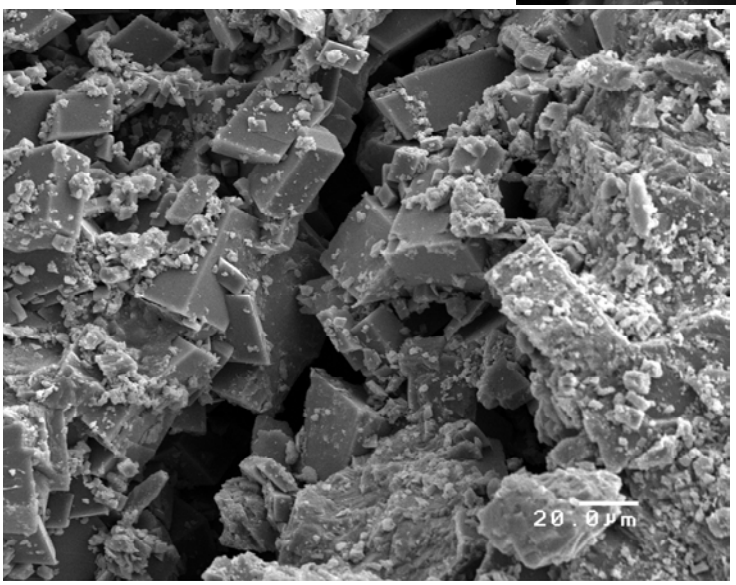

Figure 4-20. Scanning electron microscope photomicrograph of a core plug from 8423 feet, Lisbon No. D-816 well, showing enlargement of a fracture partially filled with secondary dolomite. Scale bar represents 20 microns (0.02 mm). Porosity = 10.5%; permeability = 47 mD based on core-plug analysis.

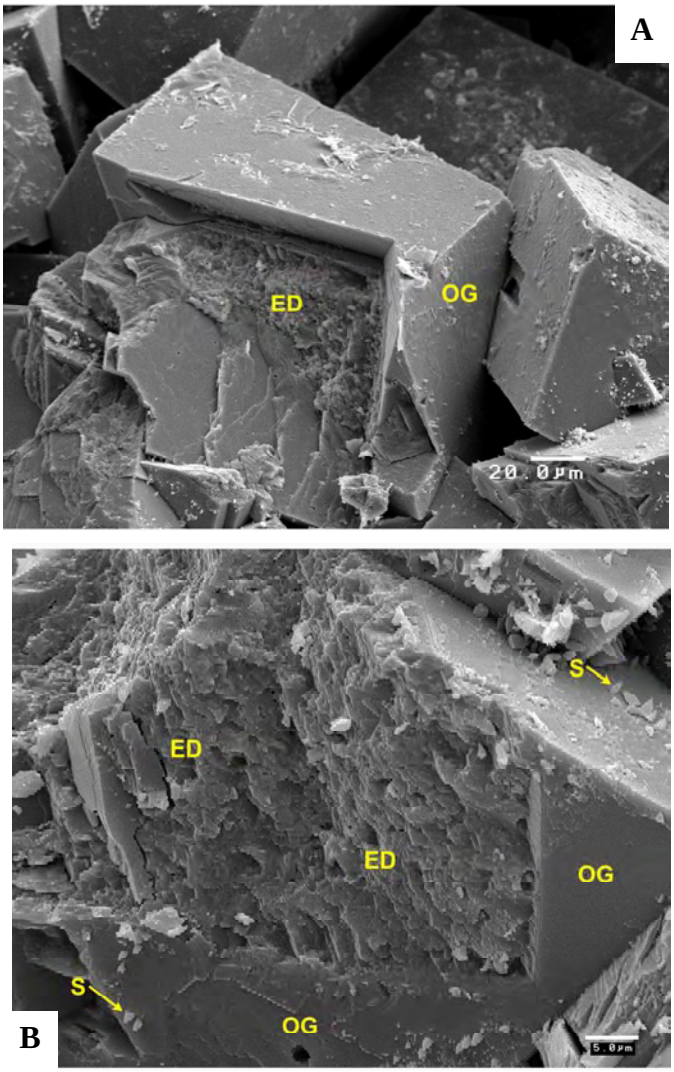

Figure 4-21. Scanning electron microscope photomicrograph of a core plug from 8433 feet shown in figure 4-18 (see red box), Lisbon No. D-816 well. A – Closeup shows the composition of typical replacement rhombic dolomites. The core of each rhombic crystal is composed of a dense remnant of fine, early dolomite (ED), which is surrounded by a euhedral dolomite overgrowth (OG). The rhombic dolomite faces are often covered with a thin film of pyrobitumen. Scale bar represents 20 microns (0.02 mm). B – High magnification across a section of poorly crystalline, early dolomite core (ED) and dense overgrowth (OG) that forms the dolomite into coarser rhombs. The very small, angular decorations on the crystal surfaces may very well be small sulfide precipitates (S). Scale bar represents 5 microns (0.005 mm). Porosity = 2%; permeability < 0.1 mD based on core-plug analysis.

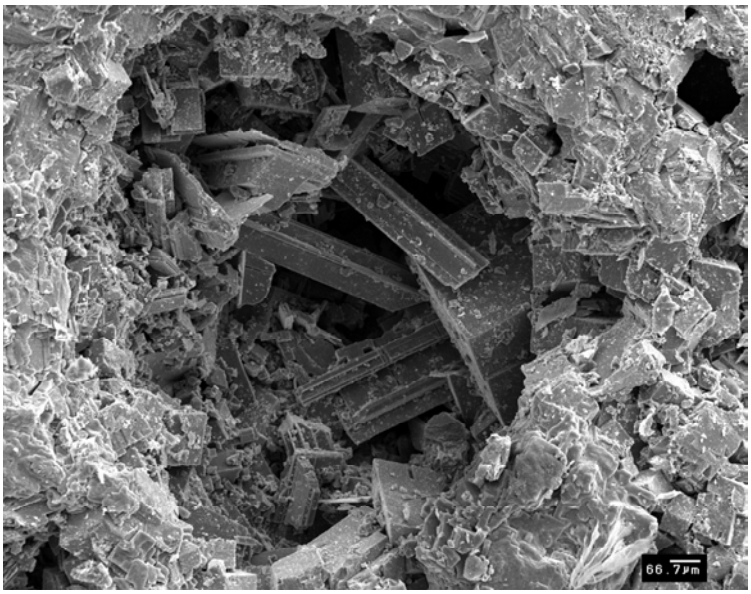

Figure 4-22. Scanning electron microscope photomicrograph of a core plug from 8426 feet, Lisbon No. D-816 well, showing anhydrite cement lathes partially filling a small dissolution vug. Scale bar represents 66.7 microns (0.067 mm). Porosity = 11.1%; permeability = 15 mD based on core-plug analysis.

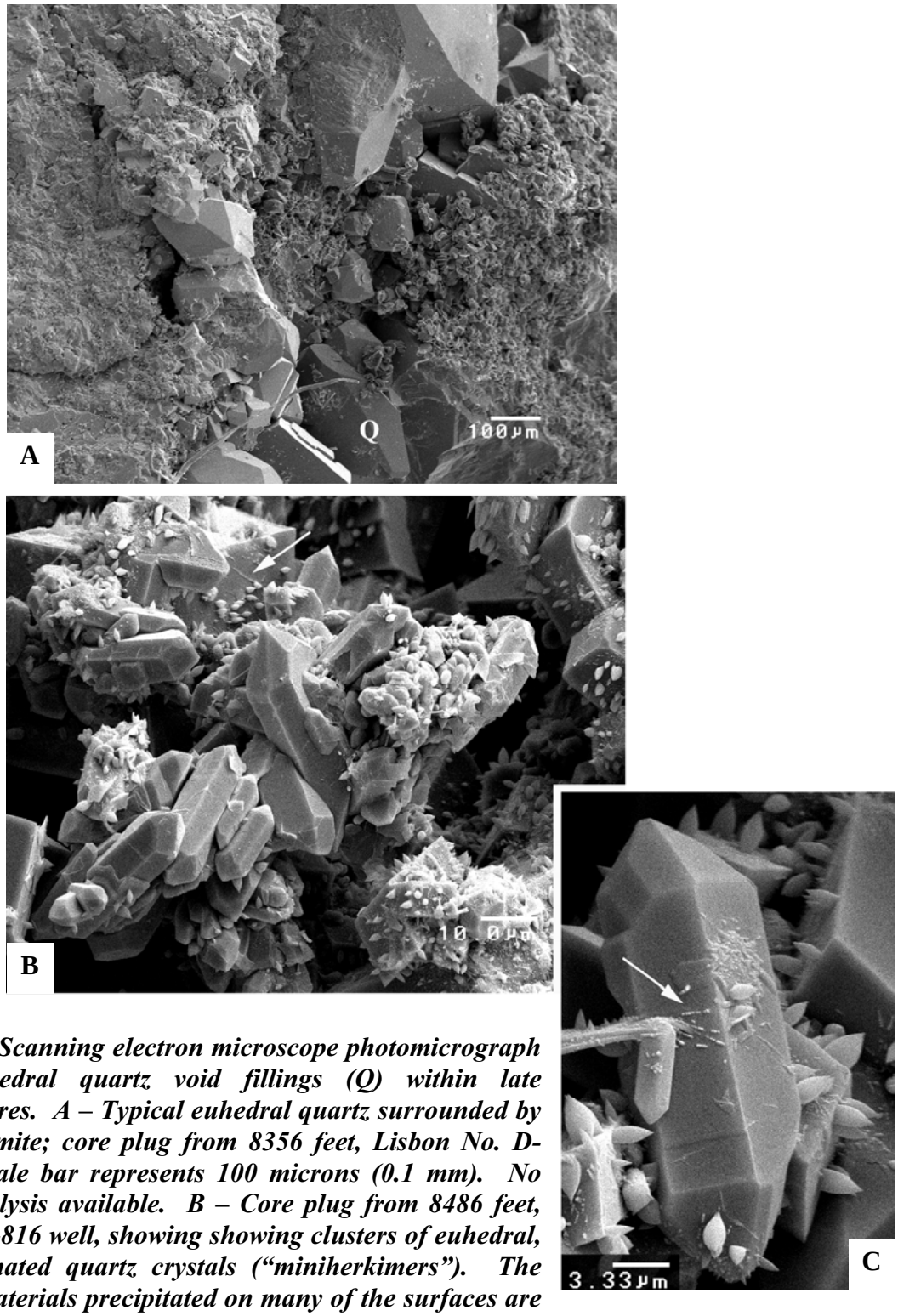

Figure 4-23. Scanning electron microscope photomicrograph showing euhedral quartz void fillings (Q) within late dissolution pores. A – Typical euhedral quartz surrounded by rhombic dolomite; core plug from 8356 feet, Lisbon No. D-616 well. Scale bar represents 100 microns (0.1 mm). No core-plug analysis available. B – Core plug from 8486 feet, Lisbon No. D-816 well, showing showing clusters of euhedral, doubly terminated quartz crystals ("miniherkimers"). The small spiky materials precipitated on many of the surfaces are either pyrobitumen or sulfide minerals. Scale bar represents 10 microns (0.01 mm). Porosity = 5.9%; permeability = 0.2 mD based on core-plug analysis. C - Closeup of a typical doubly terminated quartz crystal from same core sample in B. The linear features (arrow) and the spiky materials on many of the crystal surfaces are composed of either pyrobitumen or sulfide minerals.

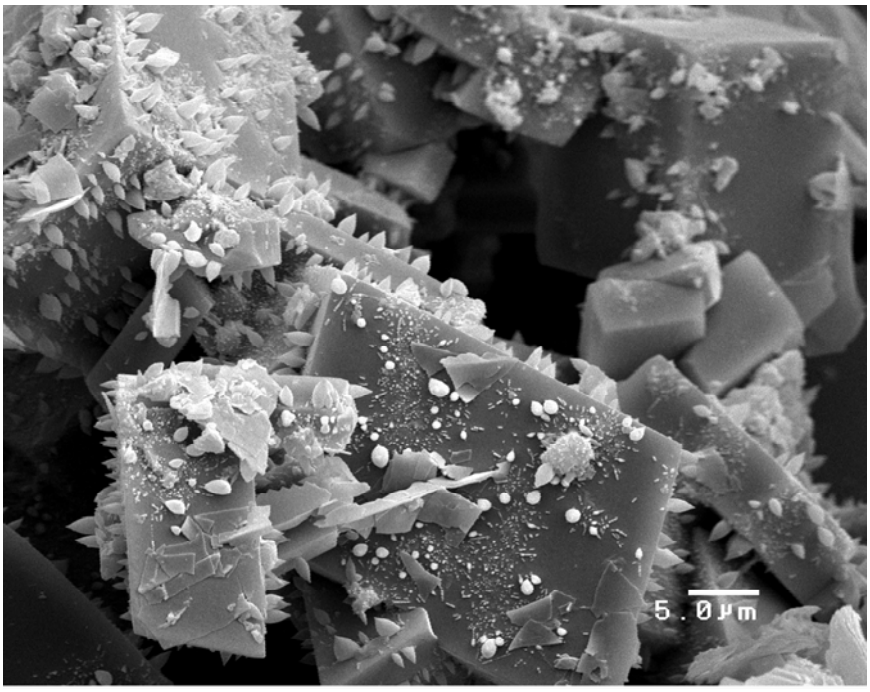

Figure 4-24. Scanning electron microscope photomicrograph of a core plug from 8442 feet, Lisbon No. D-816 well, showing possible sulfide minerals on large dolomite rhombs. Scale bar represents 5 microns (0.005 mm). Porosity = 8.6%; permeability = 1.0 mD based on core-plug analysis.

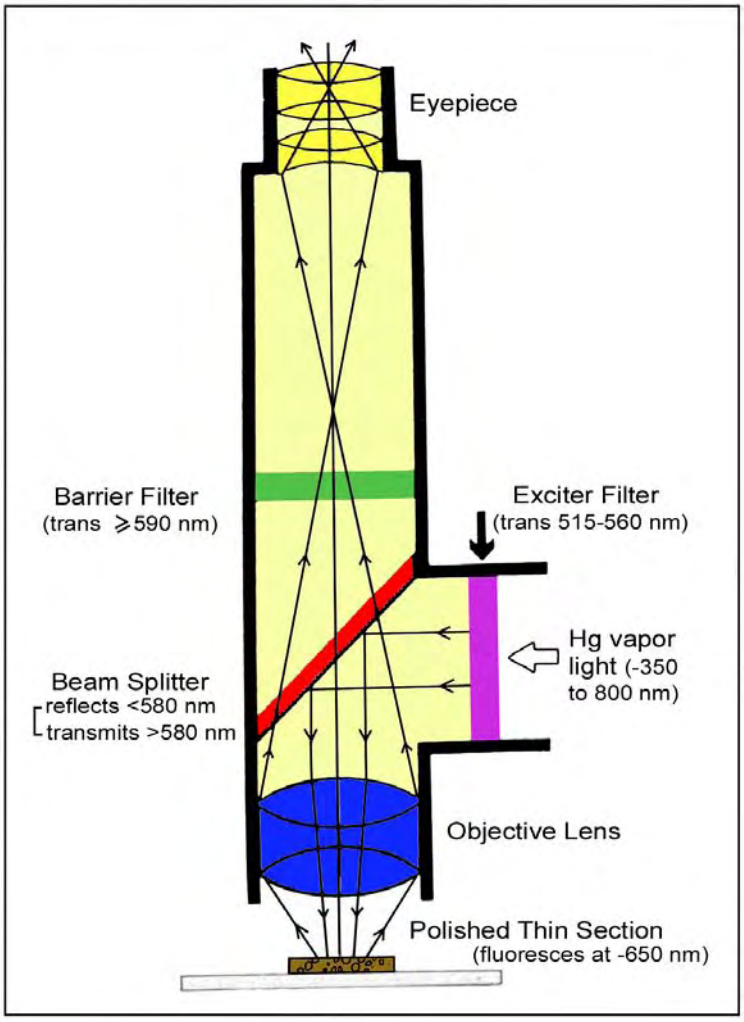

Figure 4-25. Generalized microscope optical configuration for observing fluorescence under incident light (modified from Soeder, 1990).

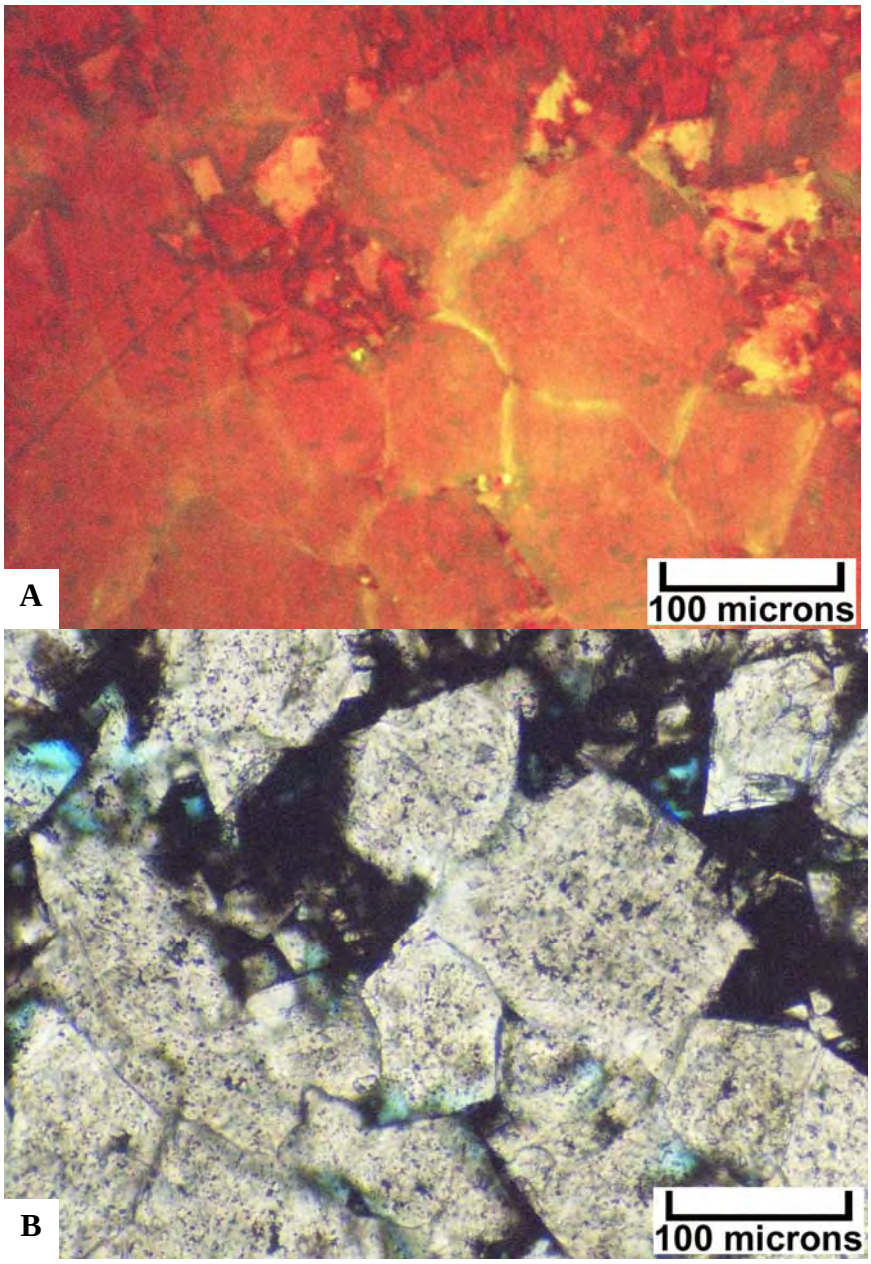

Figure 4-26. Photomicrographs from Lisbon No. D-816 well at 8435.8 feet. A – Epifluorescence under moderate magnification, showing a representative area showing fluorescence zonation within coarse dolomite crystals. The reddish areas are pores with abundant bitumen linings and plugging (see figure 4-26B). Fluorescence petrography makes it possible to clearly see the dolomite crystals versus the pore space. In places, very small rhombic outlines of dolomite crystals can be resolved. Many of these pores appear to be completely surrounded by an interlocking network of dolomite crystals. B - The same field of view as above is shown under plane light at the same magnification. Note that the black (and opaque) areas composed of bitumen mask the crystal boundaries of the dolomite as well as individual pore outlines. The white and gray areas are remnants of the dolomite matrix that are not masked by the bitumen. Only a small amount of pore space (blue-dyed areas) can be seen in this view compared to the fluorescence photomicrograph above.

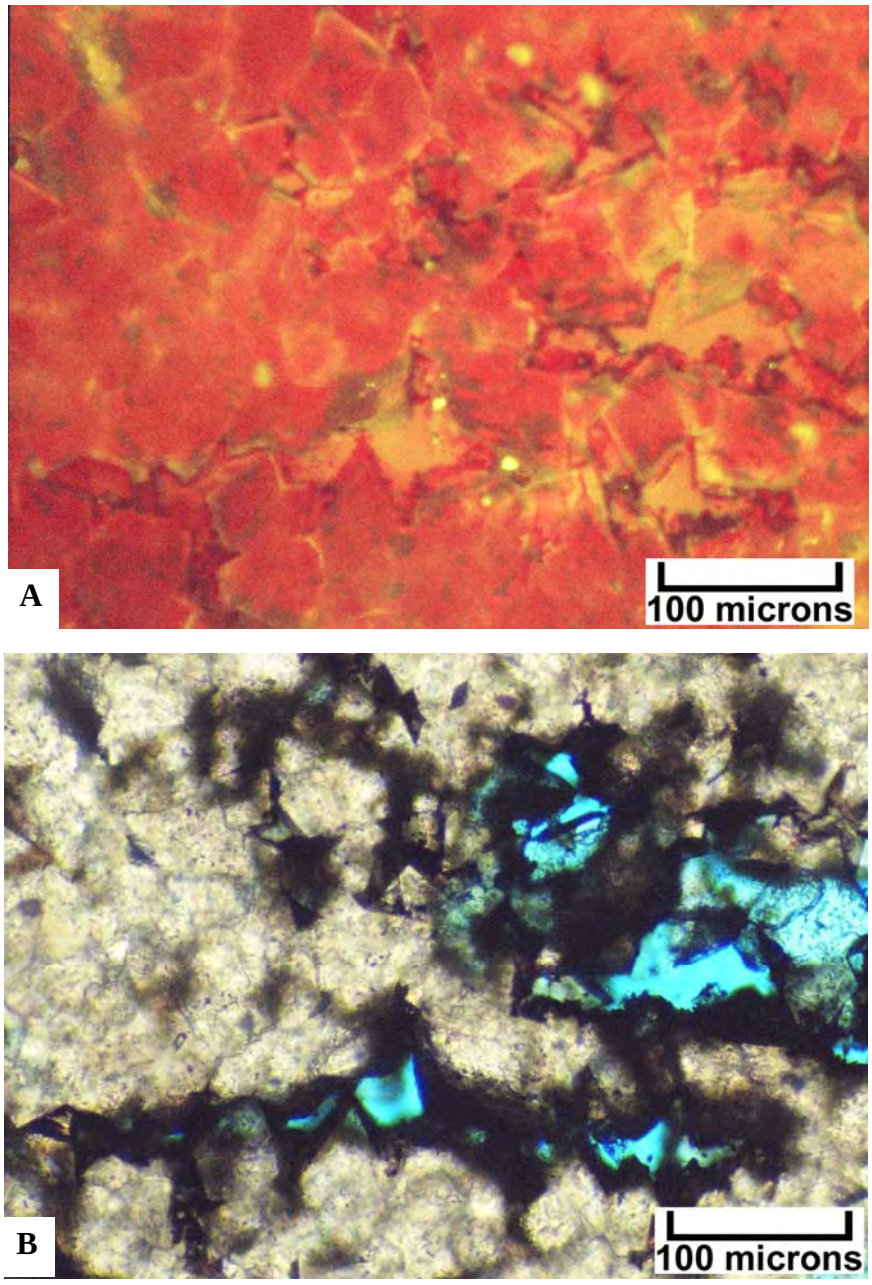

Figure 4-27. Photomicrographs from Lisbon No. D-616 well at 8435.8 feet. A – Epifluorescence under moderate magnification, showing fine- to medium-sized crystals of replacement dolomite. The rhombs display dead cores and fluorescent rims. B - The same field of view as above is shown under plane light at the same magnification. Again, note that the black (and opaque) areas composed of bitumen mask the crystal boundaries of the dolomite as well as individual pore outlines.

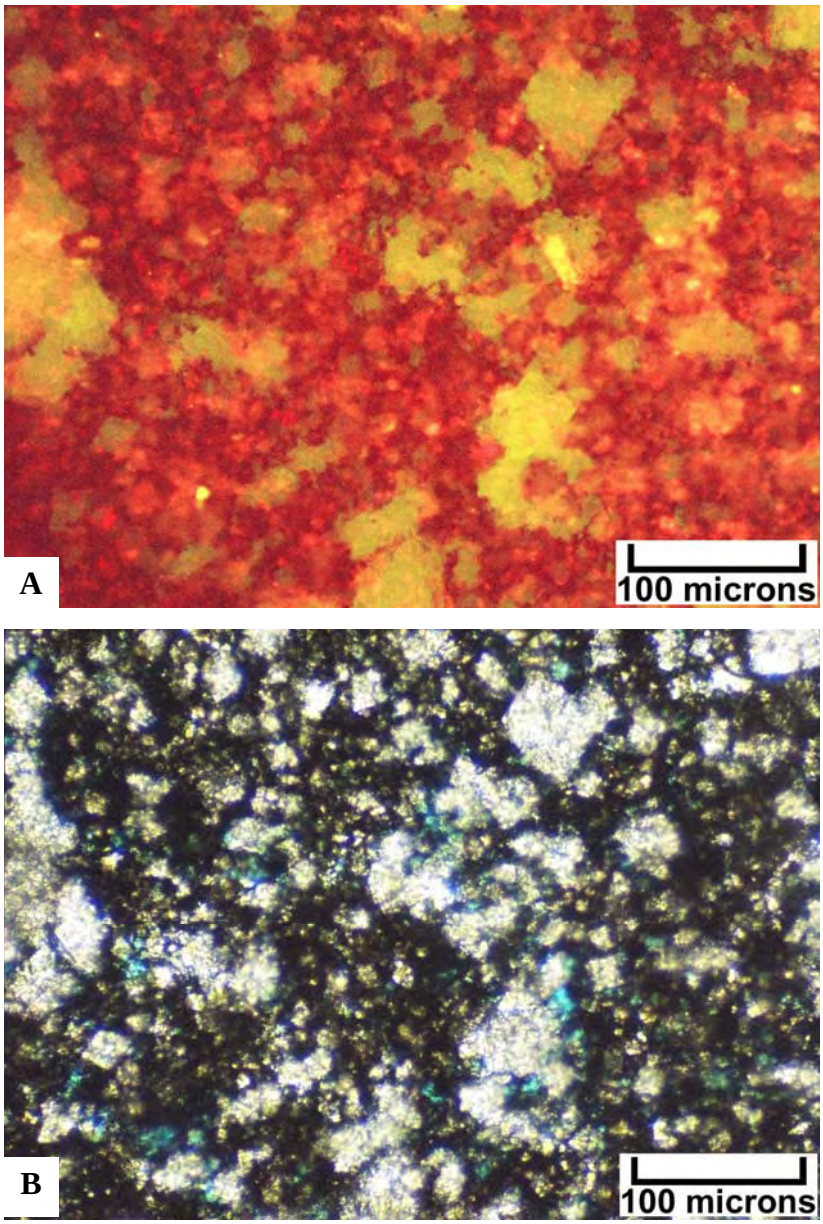

Figure 4-28. Photomicrographs from Lisbon No. B-610 well at 7897 feet. A – Epifluorescence under moderate magnification, showing individual, yellow-fluorescing dolomite rhombs "floating" in a non-fluorescing dolomite matrix. B - The same field of view as above is shown under plane light at the same magnification.

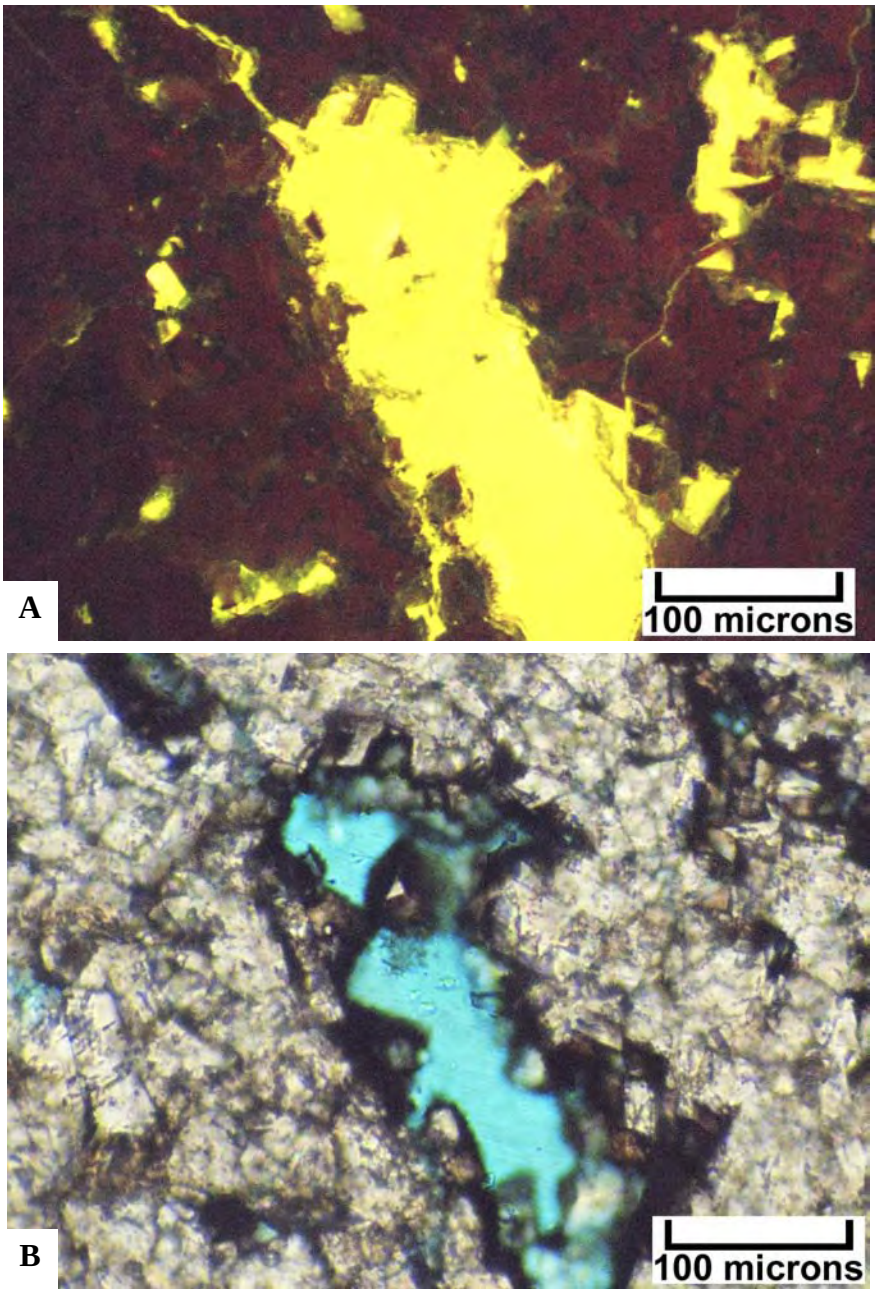

Figure 4-29. Photomicrographs from Lisbon No. B-816 well at 8486 feet. A – Epifluorescence under moderate magnification, showing zoned, rhombic replacement dolomite with dead cores and highly fluorescent rims. B - The same field of view as above is shown under plane light at the same magnification. Note the large solution pore (blue area).

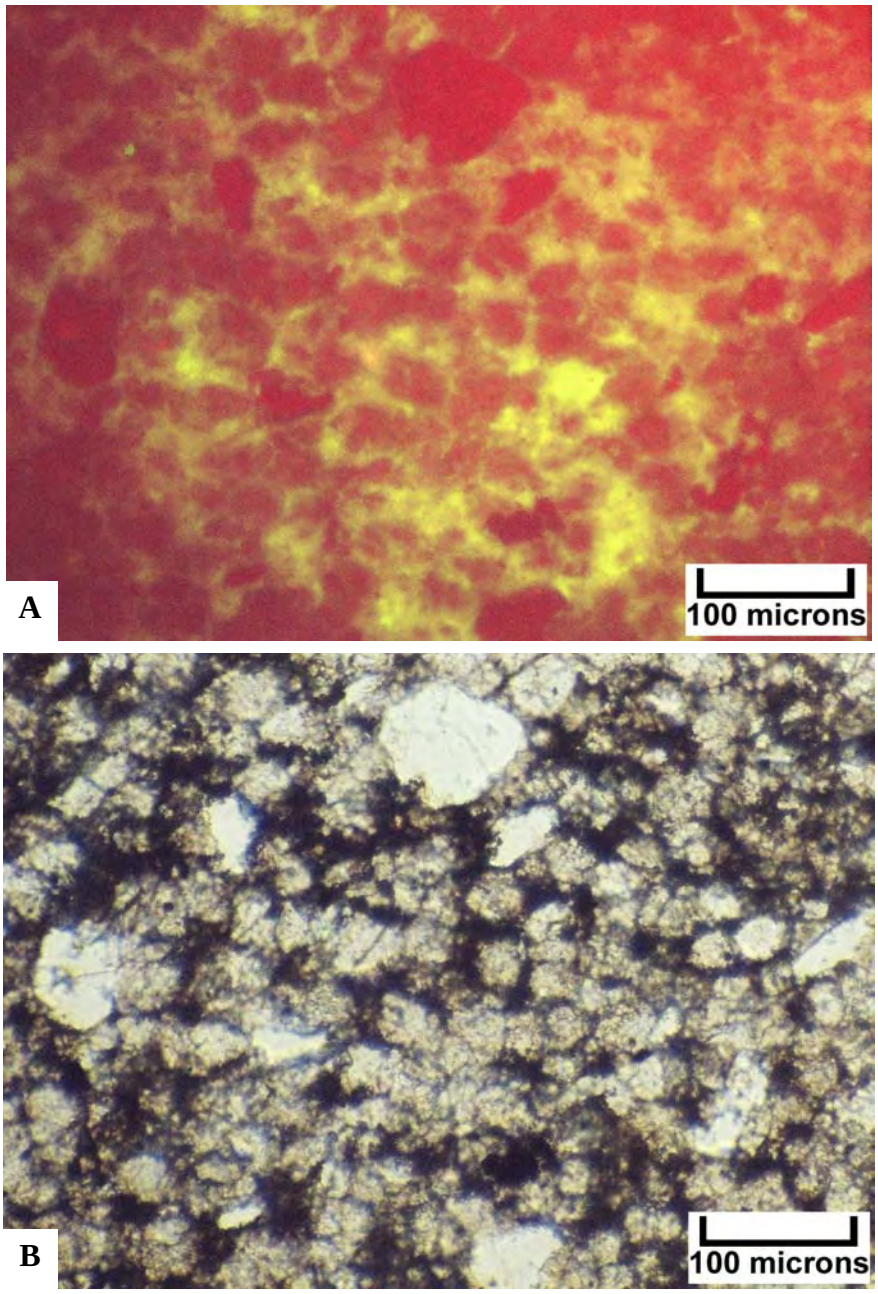

Figure 4-30. Photomicrographs from Lisbon NW USA No. B-63 well at 9935.6 feet. A – Epifluorescence under moderate magnification, showing dolomitized detrital fill within a karst cavity. B - The same field of view as above is shown under plane light at the same magnification. Note the large quartz grains, and angular limestone and dolomite clasts. These clasts do not fluoresce.

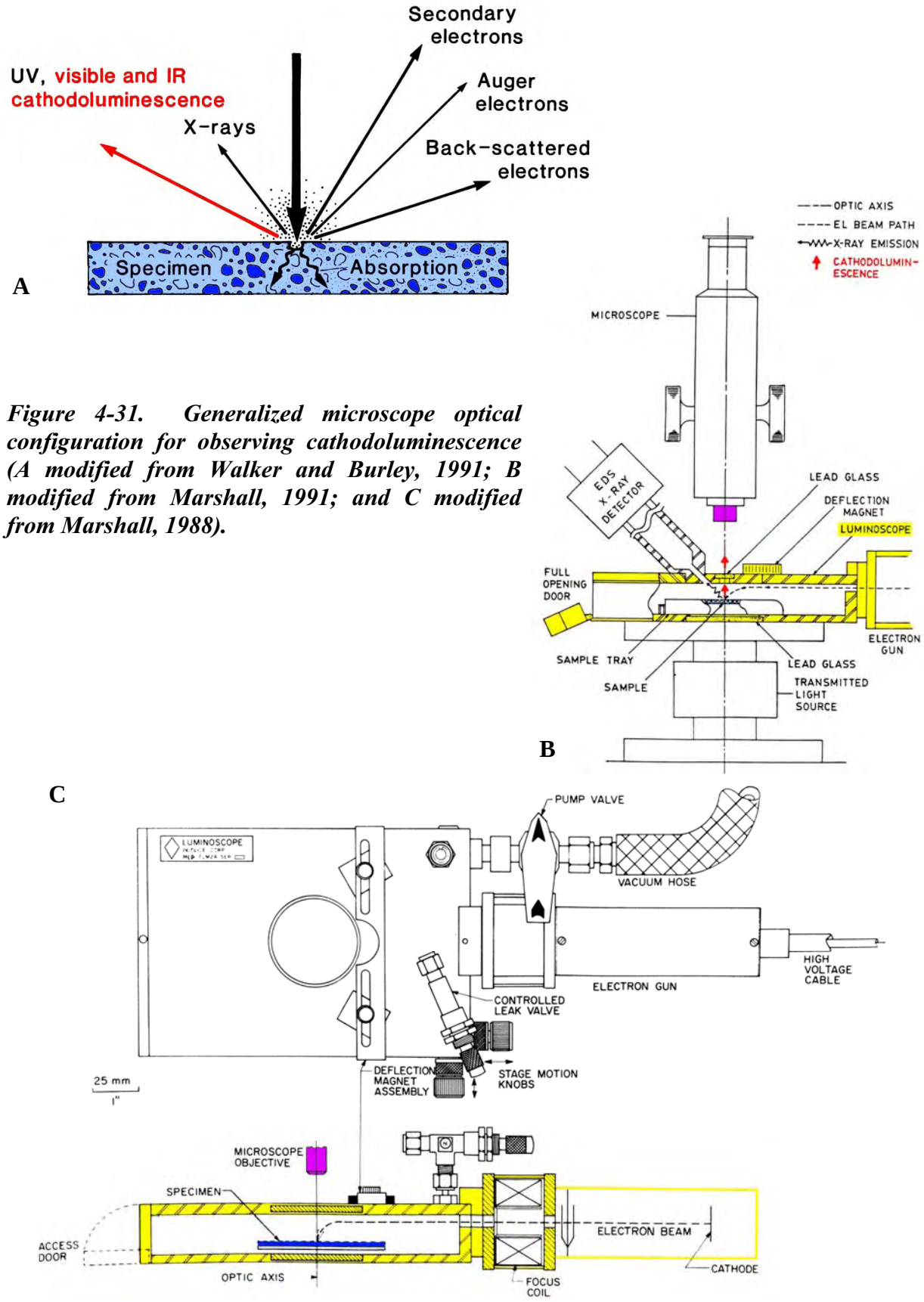

Figure 4-31. Generalized microscope optical configuration for observing cathodoluminescence (A modified from Walker and Burley, 1991; B modified from Marshall, 1991; and C modified from Marshall, 1988).

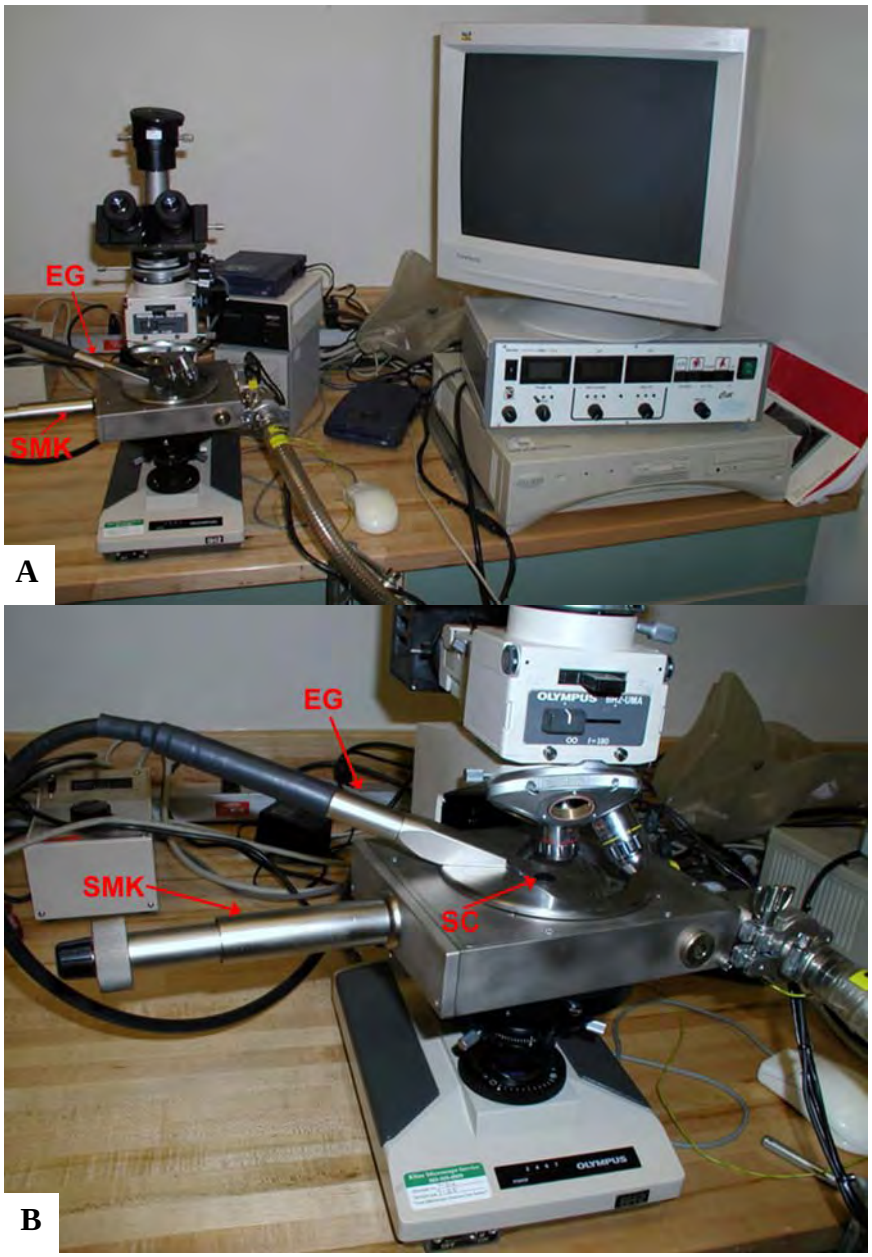

Figure 4-32. Colorado School of Mines cathodoluminescence setup used for the Leadville samples from Lisbon field. A - Cambridge Image Technology Ltd. CLmk3A/4 cathodoluminescence instrument is mounted on an Olympus BH2 petrographic microscope. The electron gun (EG) can be seen in the inclined position to the left of the sample chamber. The stage motion knob (SMK) is the silver cylinder to the left of the sample chamber. The hose to the vacuum pump can be seen to the right of the chamber. The front panel controls (beneath the video monitor) include (from left to right) the diagnostic selector, vacuum and diagnostic metering, gun current metering, Gun kV metering, and main power switch. The video monitor and CPU were used for handling and displaying the CL images captured by a digital camera. B - Closeup of the cathodoluminescence instrument sample chamber (SC), electron gun (EG) and stage motion knob (SMK) mounted on an Olympus BH2 petrographic microscope.

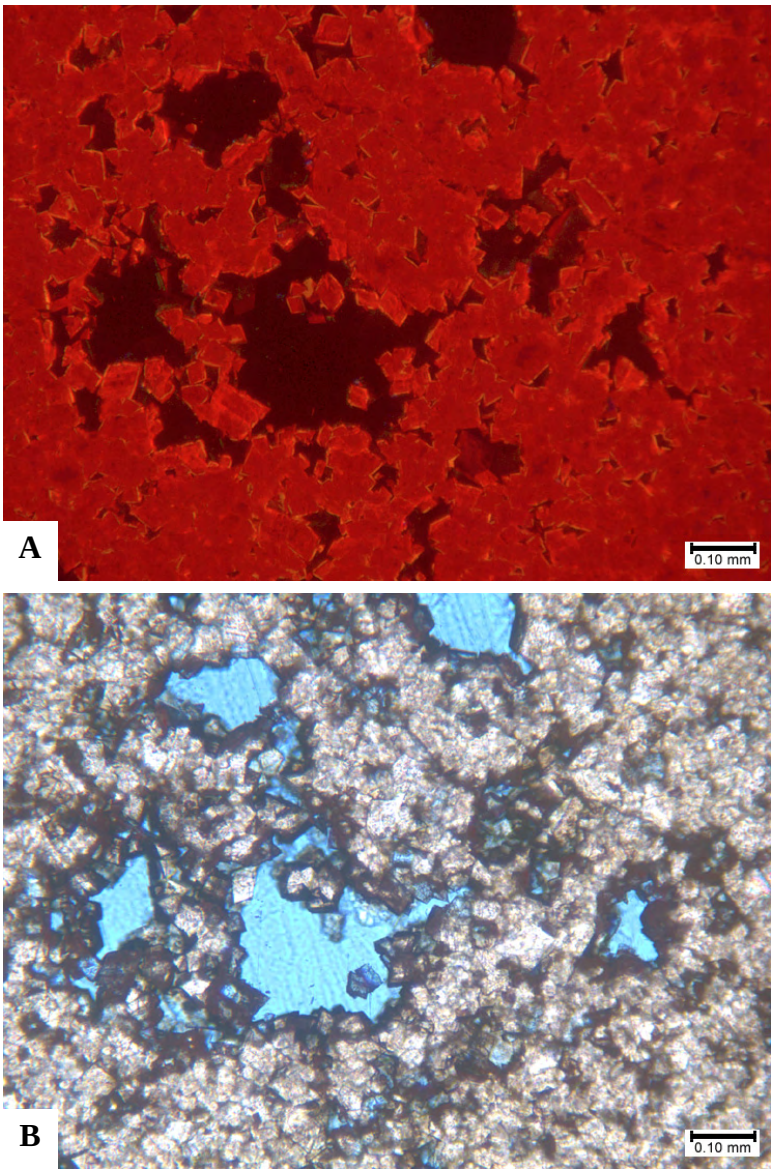

Figure 4-33. Photomicrographs from Lisbon No. D-816 well at 8442-8443 feet. A - Cathodoluminescence shows sharp outlines between the dolomite crystals and adjoining pore spaces. Note that the porosity (seen in black) in this sample seems to be a combination of intercrystalline space and solution-enlarged molds. The vast majority of the dolomite seen here consists of bright red luminescing dolomite with only occasional thin rinds of dull luminescing overgrowth. There are also rare non-luminescing dolomite cement crystals within some of the smaller pore spaces (see, for instance, the cement occluding a small pore in the lower center of this image). Finally, note that "ghosts" of former grains such as "hard" peloids can be seen in the luminescing pattern of the dolomites in the upper right corner of this view. B - The same field of view under plane light. The outlines of the dolomite crystals are not nearly as distinct and crisp here as in the previous CL view. In fact, it is difficult to pick out the crystal outlines or faces in this type of lighting. Black pyrobitumen makes is difficult to see the smaller, but important, intercrystalline pores. The larger solution-enlarged molds in blue are easy to see, but their interconnection through the smaller intercrystalline space is better seen under CL imaging.

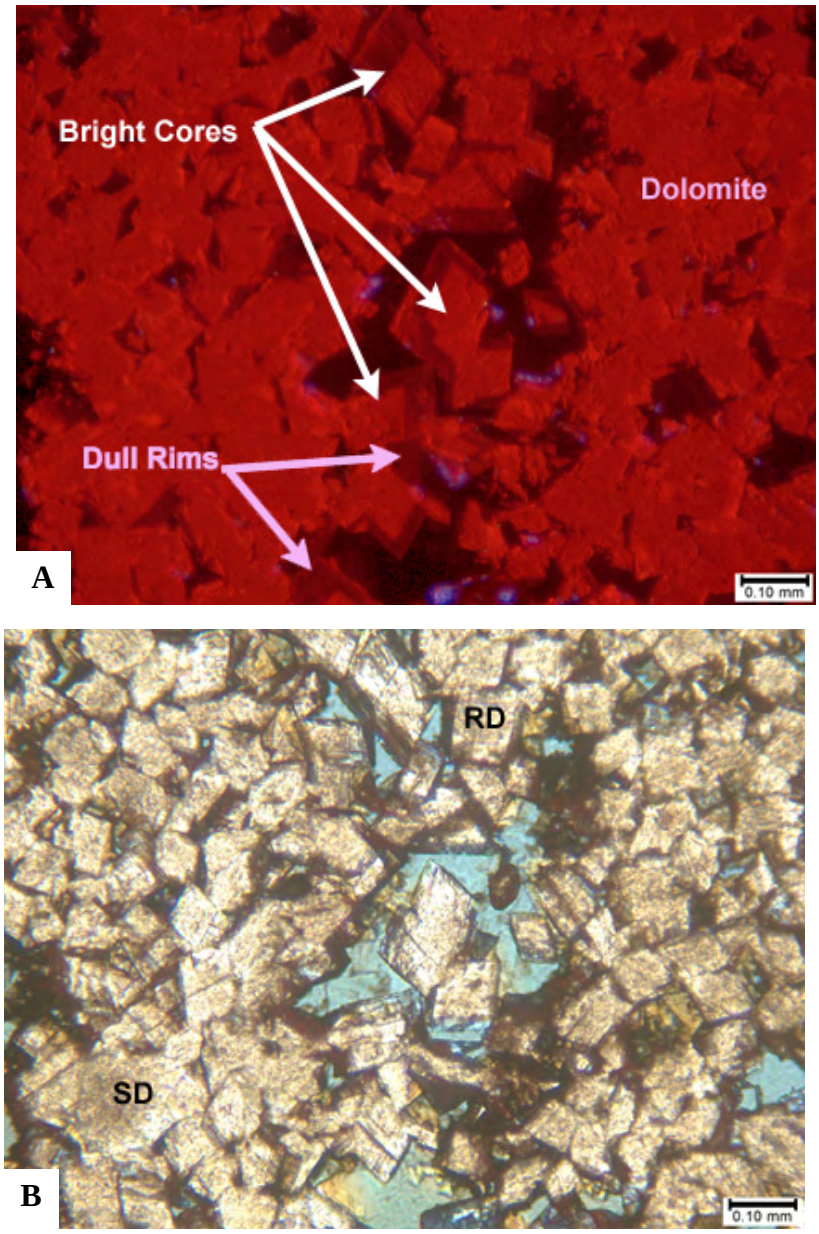

Figure 4-34. Photomicrographs from Lisbon No. D-816 well at 8433 feet. A - This CL image shows beautiful luminescence zonation of many of the dolomite crystals, especially in a band from the top center to the bottom center of the image. Note the bright red luminescing dolomite cores surrounded by rim zones of non-fluorescent overgrowth. The black areas on this image are currently open pore spaces. B - The same field of view under plane light showing replacement dolomite (RD) and saddle dolomite (SD). The dolomite crystals shown here are well formed with planar crystal faces and generally rhombic outlines. Note that some crystal terminations may display curved (or saddle) outlines. Plane light does not make it possible to distinguish the crystal composition zonation imaged in the CL photomicrograph. The black areas within this field of view are due to pyrobitumen coatings on many of the dolomite crystal surfaces. The blues areas between many of the replacement dolomite crystals are open pores.

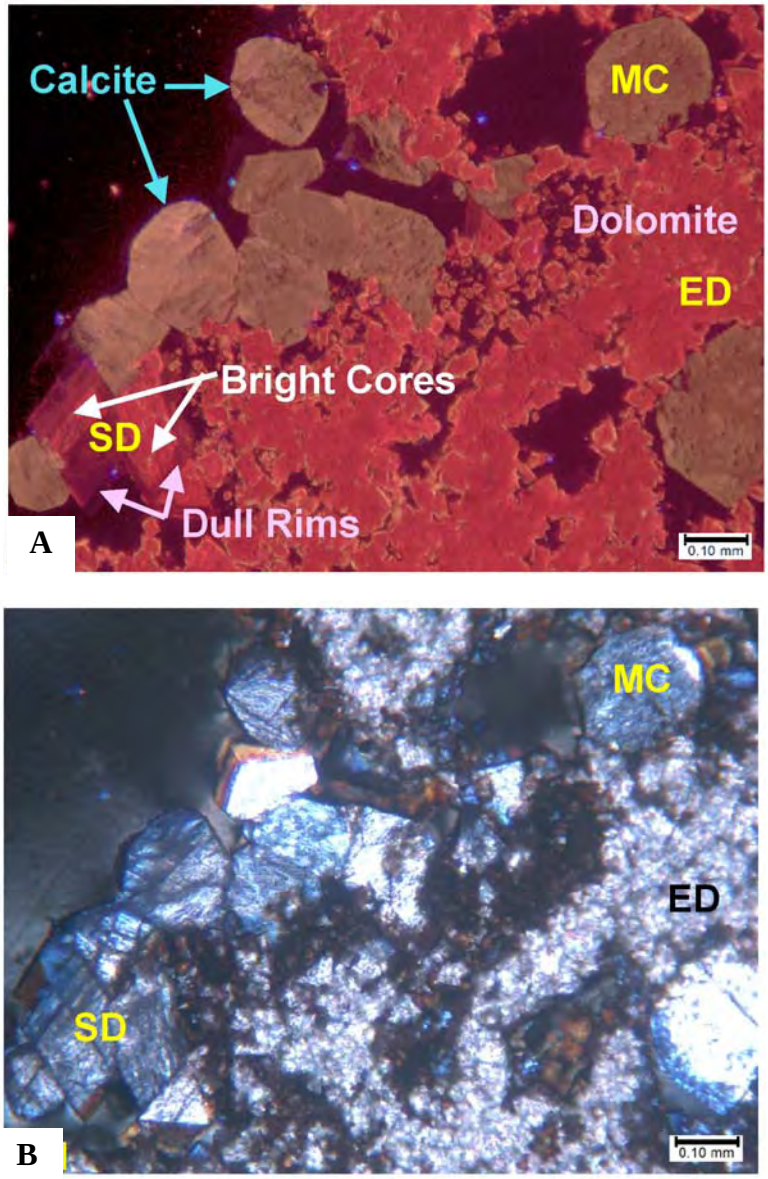

Figure 4-35. Photomicrographs from Lisbon No. B-816 well at 8486 feet. A - This area of high matrix porosity (in black) shows early replacement dolomite (ED) that displays intense red luminescence. Some of these replacement crystals display very thin orange overgrowths. However, some of the largest dolomite rhombs (saddle dolomite [SD]) in this field of view display a coarser crystal zonation in which the bright red luminescent core is overgrown with thick, dull luminescent rims (see the lower left corner of this photomicrograph). Finally, note the large, late calcite spar crystals (macrocalcite [MC]) with orange luminescence within the large pores from lower left to upper right as well as in the lower right portion of this view. B - The same field of view under crossed nicols. Note that some of the large dolomite crystals in the lower left portion of this image display sweeping extinction and possibly curved crystal faces that are consistent with probable saddle dolomites. The replacement dolomites throughout most of this field of view are too small or too inclusion-rich to distinguish extinction patterns. The late calcite spar cements generally display straight extinction.

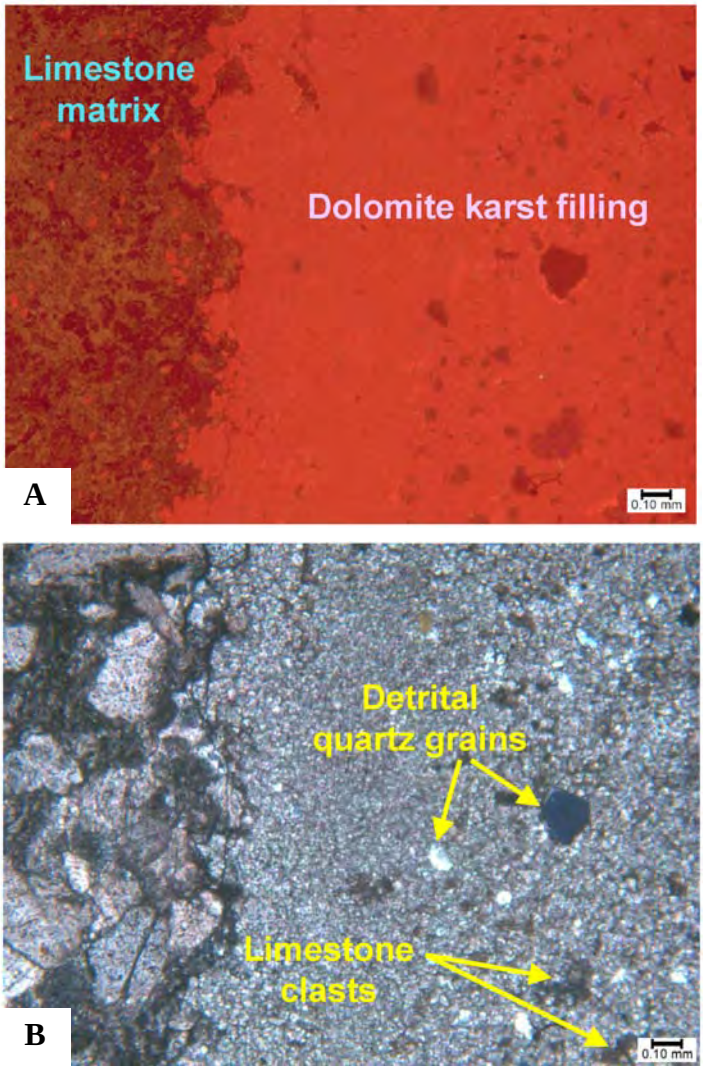

Figure 4-36. Photomicrographs from Lisbon No. D-616 well at 8308 feet. A - This low-magnification image nicely shows a sharp contact that runs from top to bottom toward the left side of the photomicrograph. The bright red field is composed mostly of dolomite, while the field with the orangish cast (to the left) is almost entirely limestone. The dolomite area is composed of carbonate grains and sediments that have filled a karst-related crack or cavity. The poorly sorted, angular grains that are seen "floating" within the dolomite field are a combination of detrital siliciclastic (mostly quartz) grains and lithified limestone clasts. The limestone field along the left side of the photomicrograph is composed of non-luminescent skeletal (crinoid-rich) sediments with orangish cements. Neither the dolomite with siliclastic sediments nor the limestone display any visible matrix porosity. The contact between the dolomite and limestone fields is irregular but sharp. Finally, there are few scattered replacement dolomite rhombs (also with red luminescence) within the well-cemented limestone. B - The same field of view under crossed nicols. Note that the siliciclastic grains within the microcrystalline dolomite field display plane extinction positions with colors ranging from white to yellow to dark gray. The polygonal grain in the right center contains overgrowths that form a prismatic quartz form in cross section. In the limestone field to the left, many of the fossils are surrounded by straight extinction syntaxial cements.

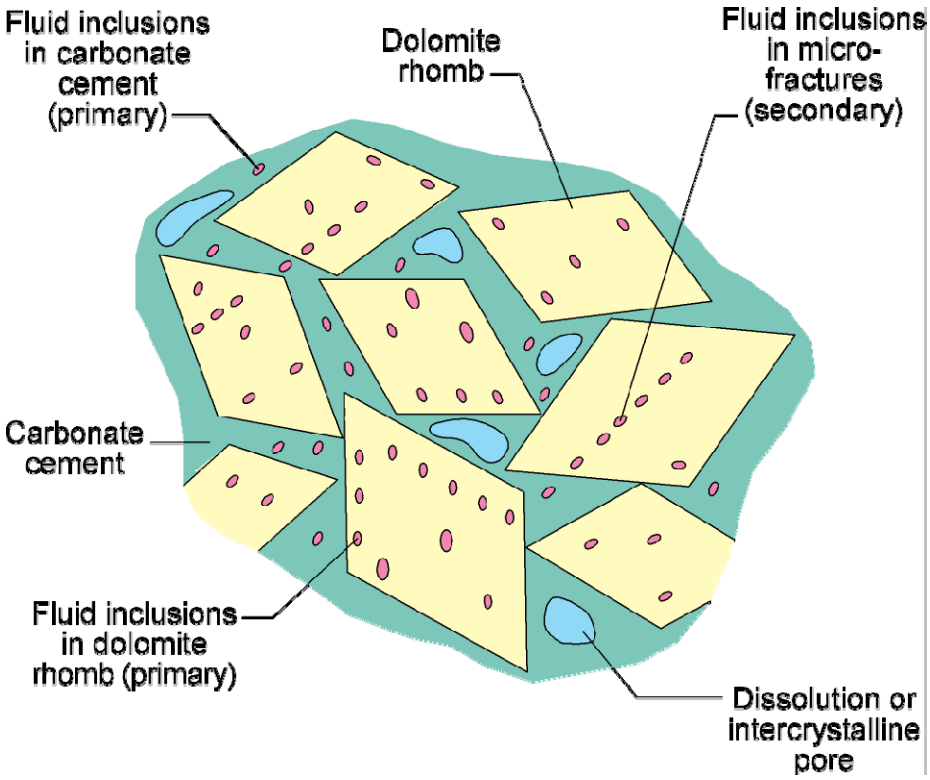

Figure 4-37. Schematic diagram of basic fluid inclusion types.

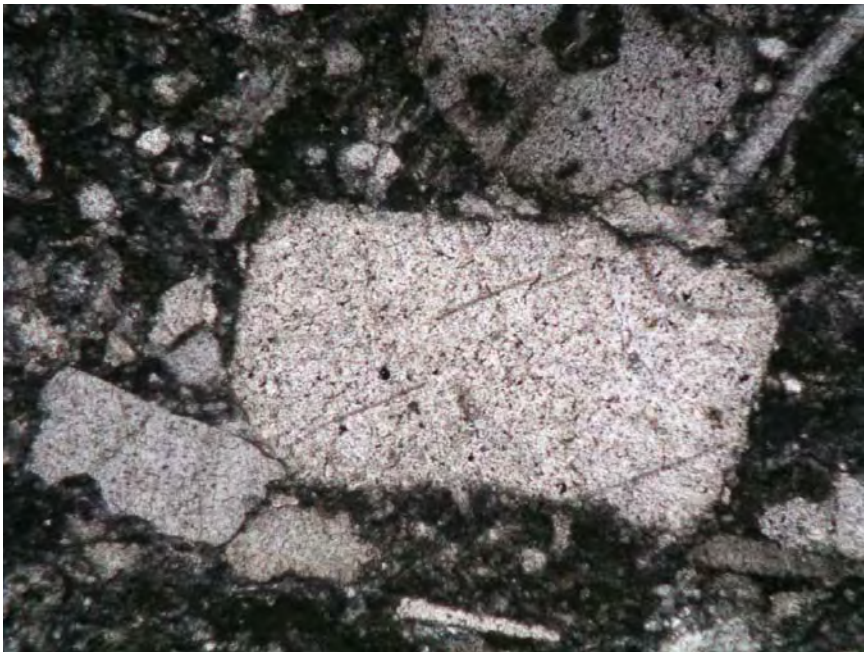

Figure 4-38. Early calcite from the Lisbon No. D-616 well at 8356 feet. The mottled appearance of the calcite is due to abundant fluid inclusions. Width of image is 3.3 mm.

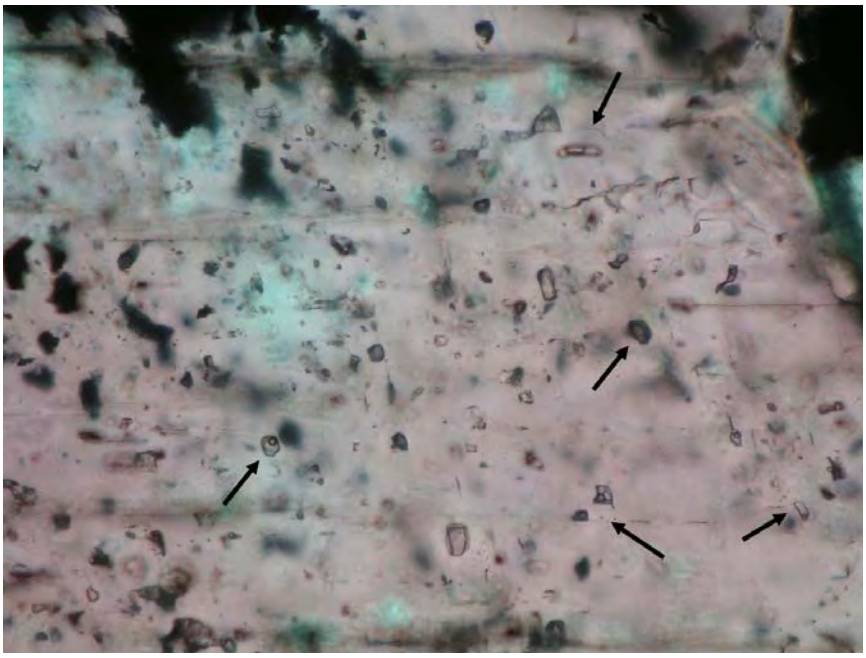

Figure 4-39. Fluid inclusions in early calcite from the Lisbon No. D-616 well at 8356 feet. Arrows point to inclusions with different liquid to vapor ratios, resulting from necking after trapping. Width of image is 0.7 mm.

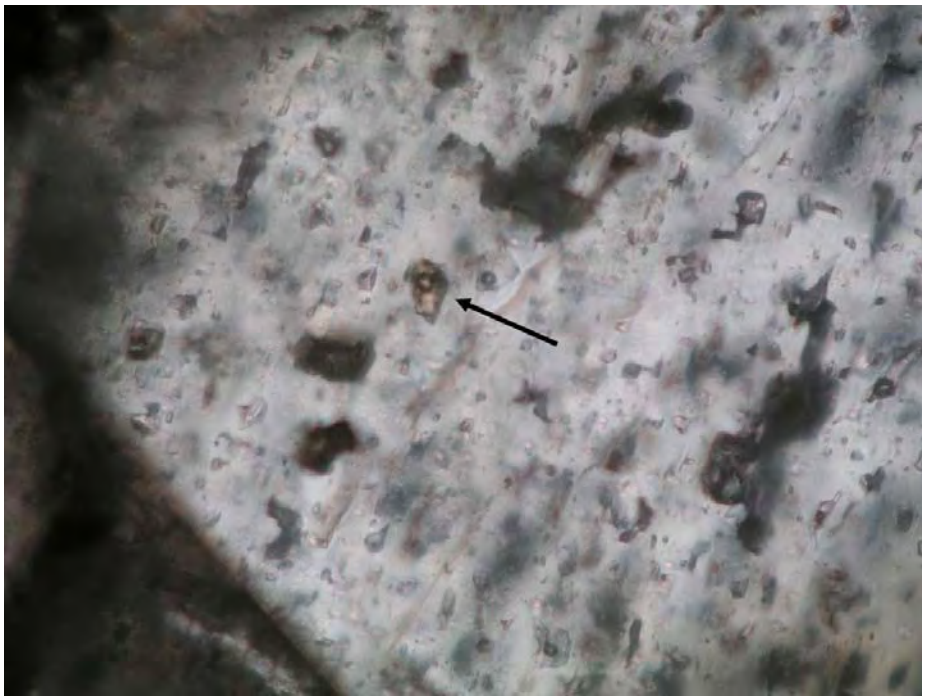

Figure 4-40. Brown primary oil inclusion (arrow) in calcite from the Lisbon No. D-616 well at 8356 feet. Clear inclusions are aqueous. Width of image is 0.3 mm.

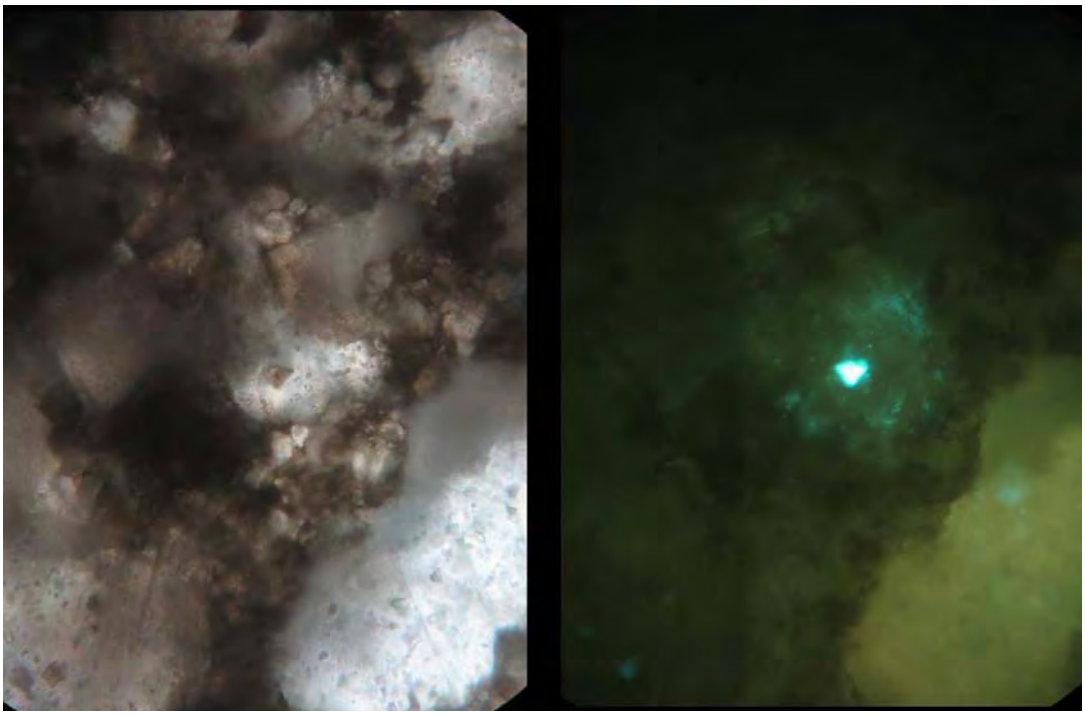

Figure 4-41. Primary oil inclusion in calcite from the Lisbon No. D-616 well at 8356 feet. Right-hand image taken under fluorescent light shows that the oil is live. Height of image is 0.3 mm.

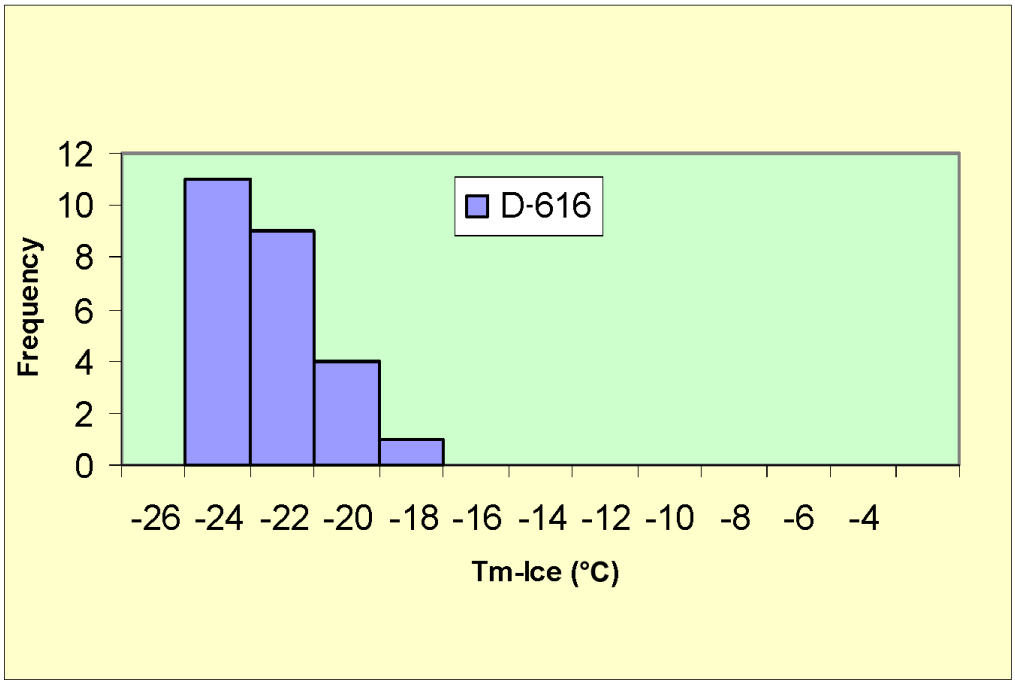

Figure 4-42. Ice-melting temperatures of fluid inclusions in early calcite from the Lisbon No. D-616 well at 8356 feet and 8372 feet.

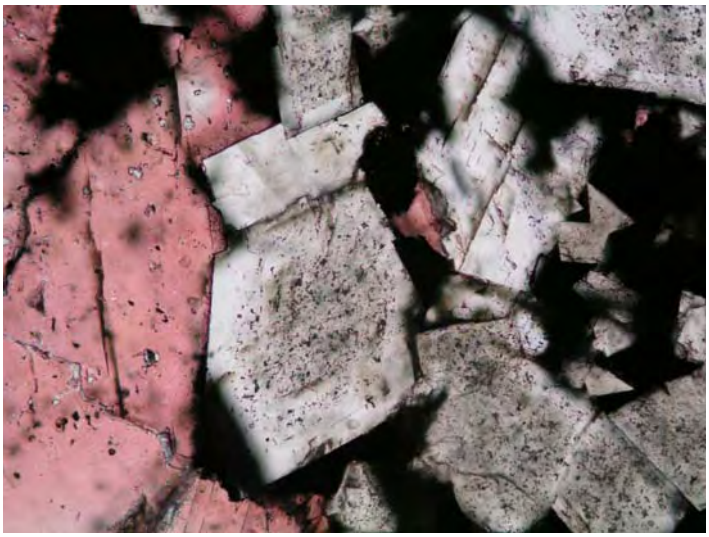

Figure 4-43. Dolomite (colorless) and calcite (red) from the Lisbon NW USA No. B-63 well at 10,004 feet. The cloudy appearance of the dolomite is due to abundant fluid inclusions. Saddle dolomites (center of photo) typically have cloudy cores and clear rims. Width of image is 0.7 mm.

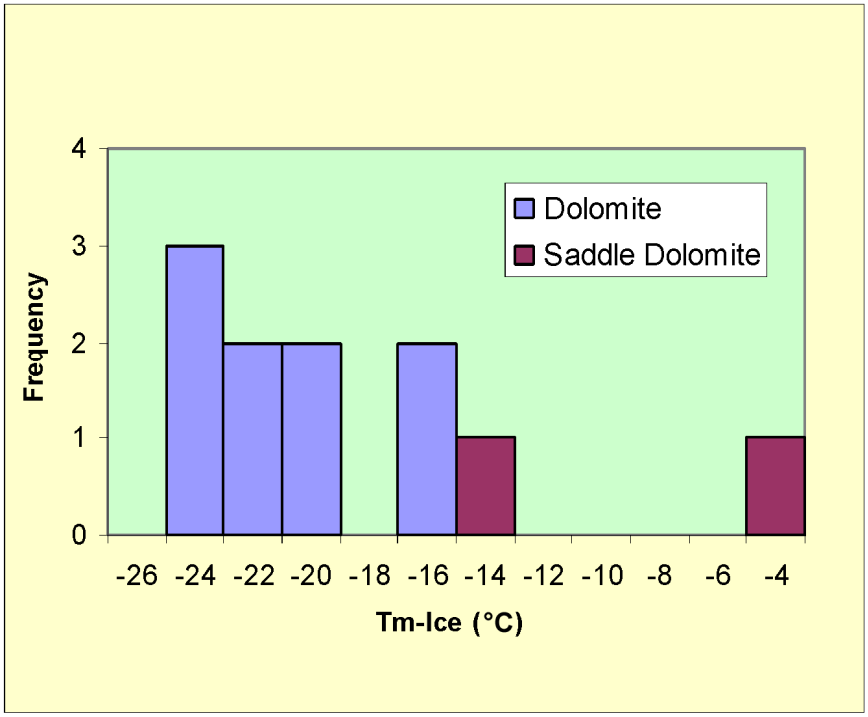

Figure 4-44. Ice-melting temperatures of dolomite-hosted fluid inclusions. Samples from depths of 8372 feet in the Lisbon No. D-616 well, 8444 feet in the Lisbon No. D-816 well, and from the clear rims of saddle dolomite from a depth of 9939 feet in the Lisbon NW USA No. B-63 well.

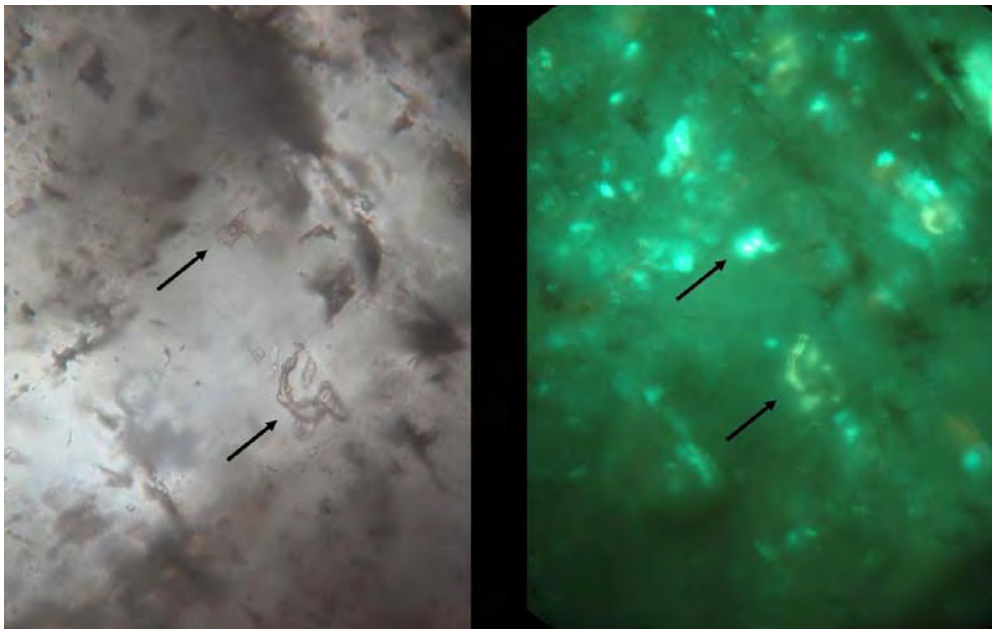

Figure 4-45. Oil inclusions in saddle dolomite from the Lisbon NW USA No. B-63 well at 9939 feet. Arrows point to two of the inclusions; others are apparent in the right-hand image taken under fluorescent light. Height of images is 0.3 mm.

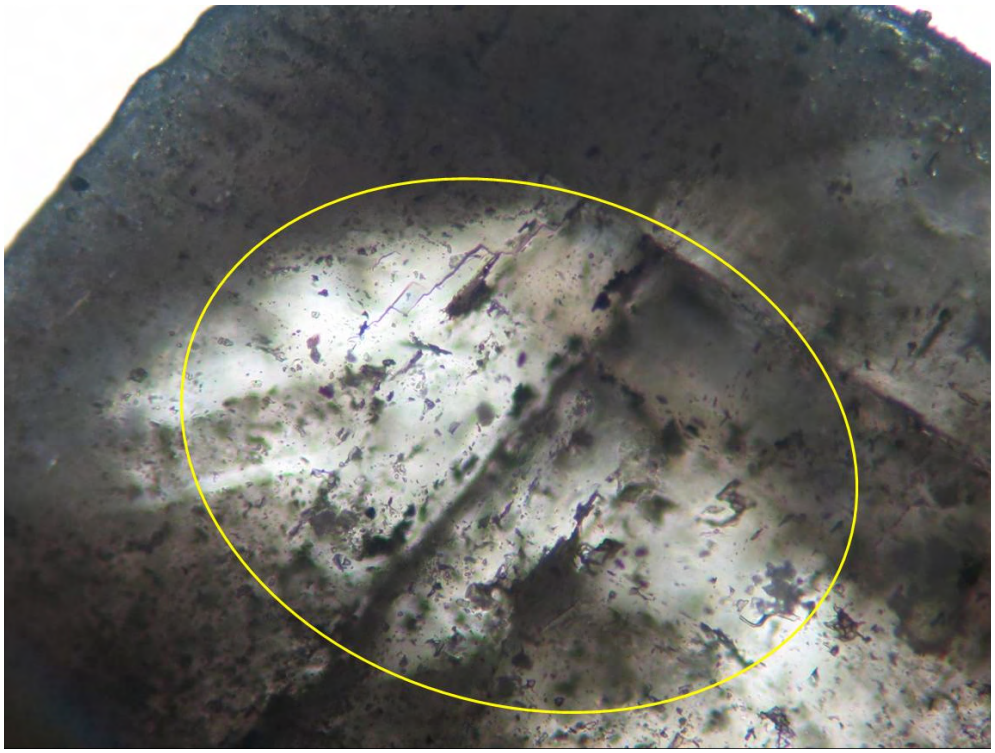

Figure 4-46. Low-magnification image of saddle dolomite shown in figure 4-45. Dark growth zones are truncated near the left side of the oval. Oil inclusions in figure 4-45 occur in the light colored dolomite on right side of oval. Width of image is 0.7 mm.

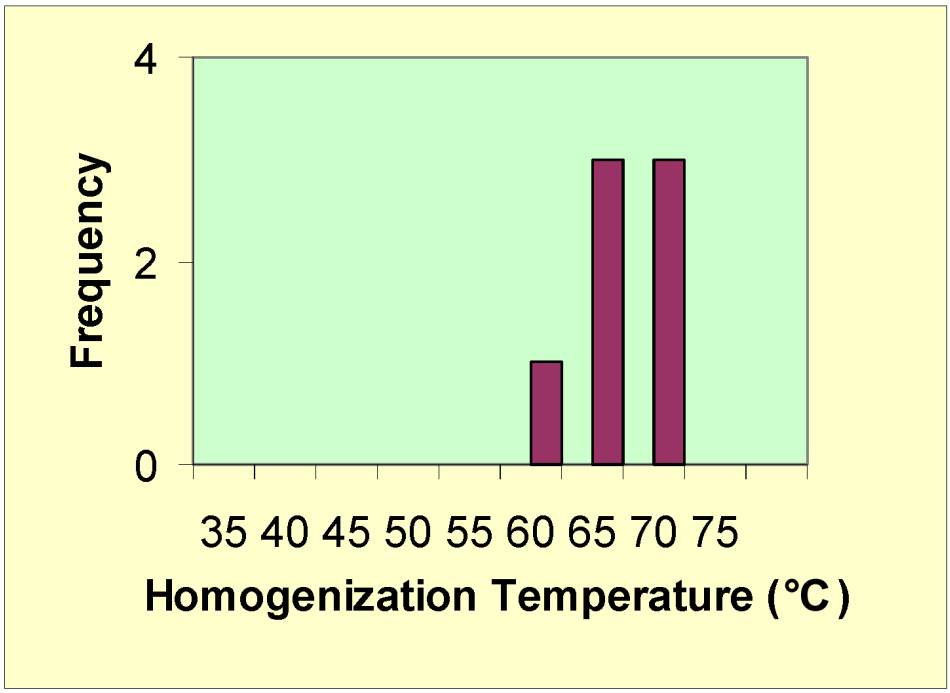

Figure 4-47. Homogenization temperatures of oil inclusions trapped in saddle dolomite from the Lisbon NW USA No. B-63 well at 9939 feet.

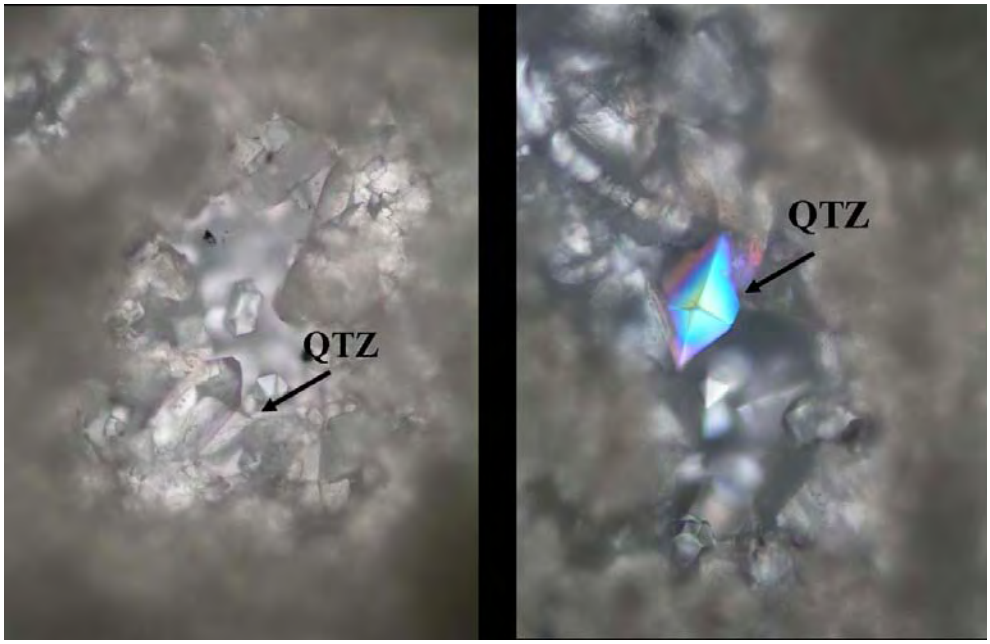

Figure 4-48. Quartz crystals partially filling a cavity in dolomite from the Lisbon NW USA No. B-63 well at 9981 feet. The right-hand image was taken under partially crossed nicols. Height of images 0.7 mm.

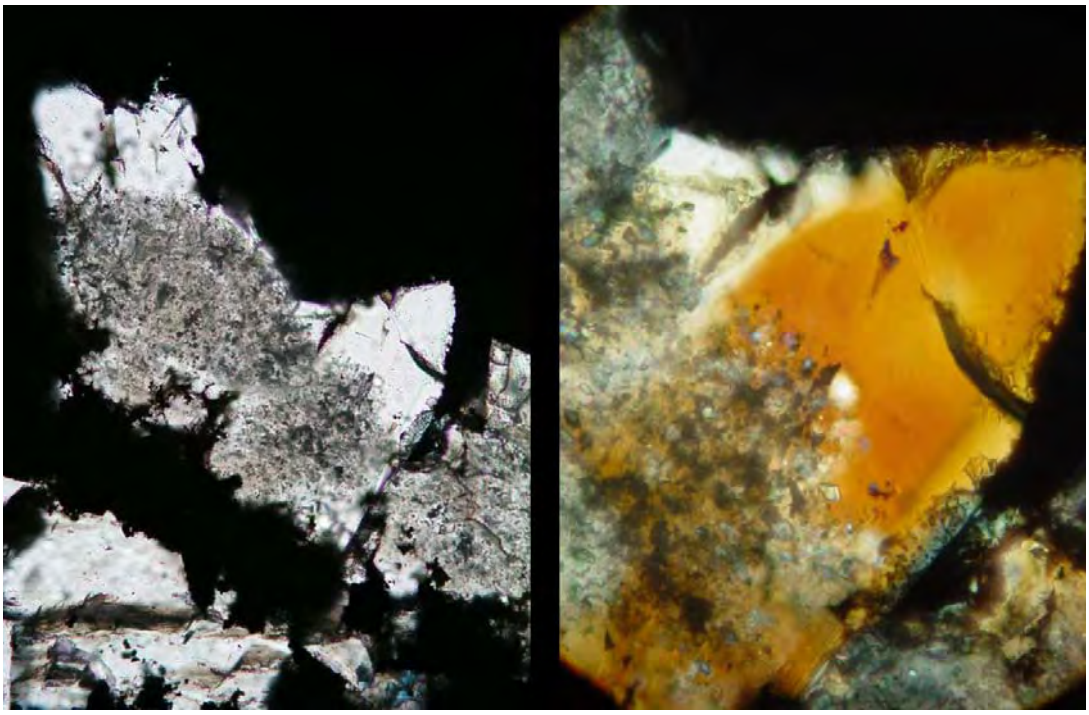

Figure 4-49. Quartz encapsulating dolomite from the Lisbon NW USA No. B-63 well at 10,004 feet. Height of images is 1.3 mm (left) and 0.7 mm (right). Right-hand image taken under crossed nicols.

Figure 4-50. Coarse-grained quartz crystal from the Lisbon No. D-616 well at 8356 feet. Small oriented grains of anhydrite are encapsulated in the quartz. Width of image is 1.3 mm.

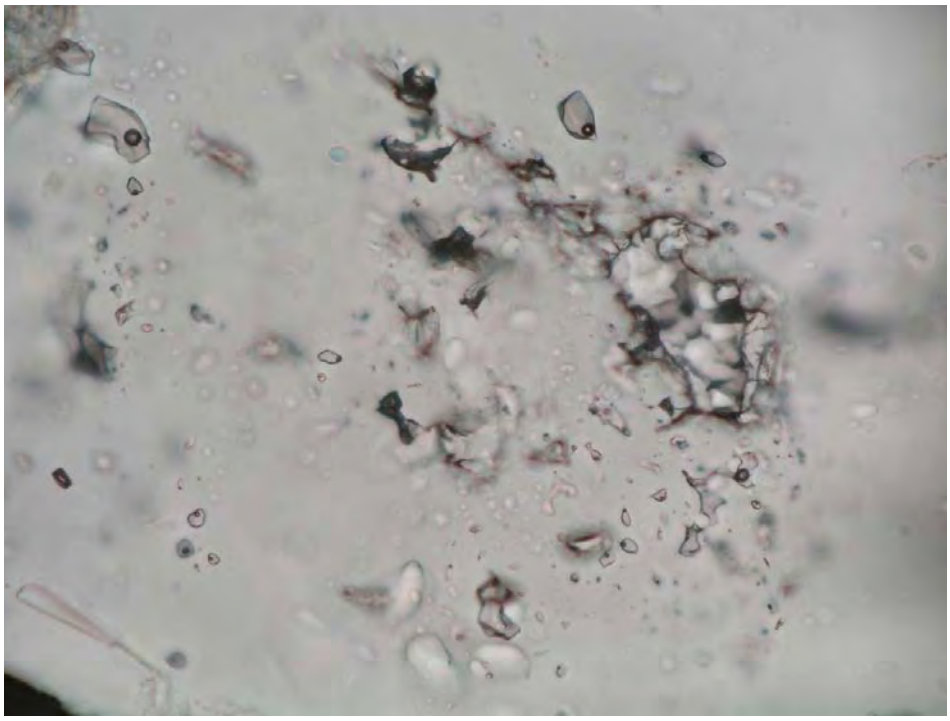

Figure 4-51. Two-phase, liquid-rich inclusions defining a growth zone in the interior of a quartz crystal from the Lisbon No. D-616 well at 8356 feet. The large, irregular cavity on the right may have been initially filled with anhydrite. Width of image is 0.3 mm.

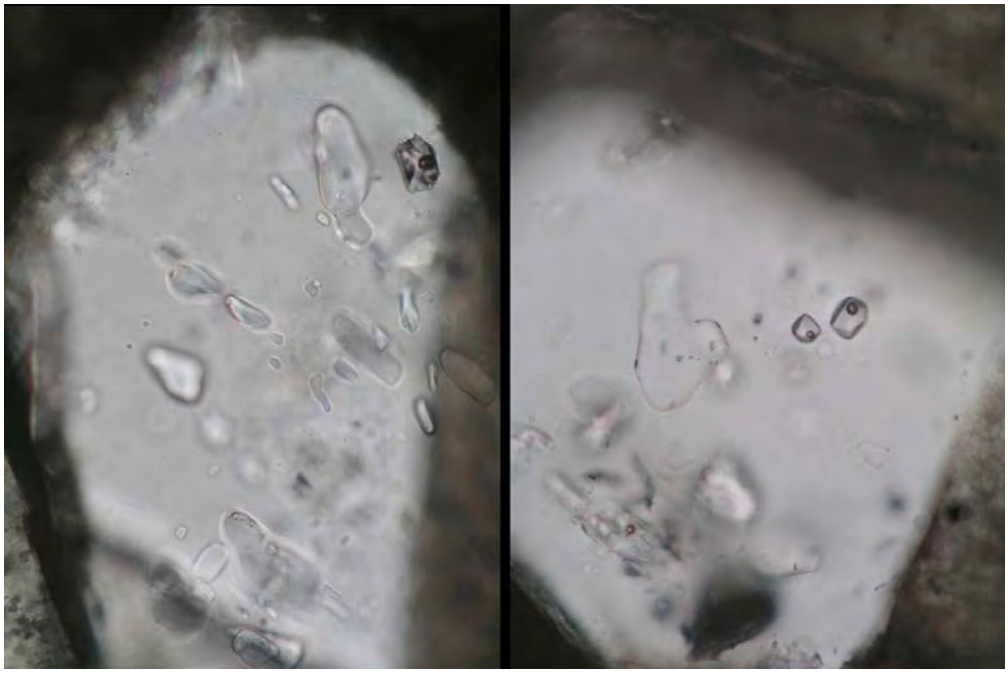

Figure 4-52. Primary liquid-rich inclusions in quartz from the Lisbon No. D-616 well at 8356 feet. Height of image is 0.3 mm. Irregular shaped inclusions are anhydrite.

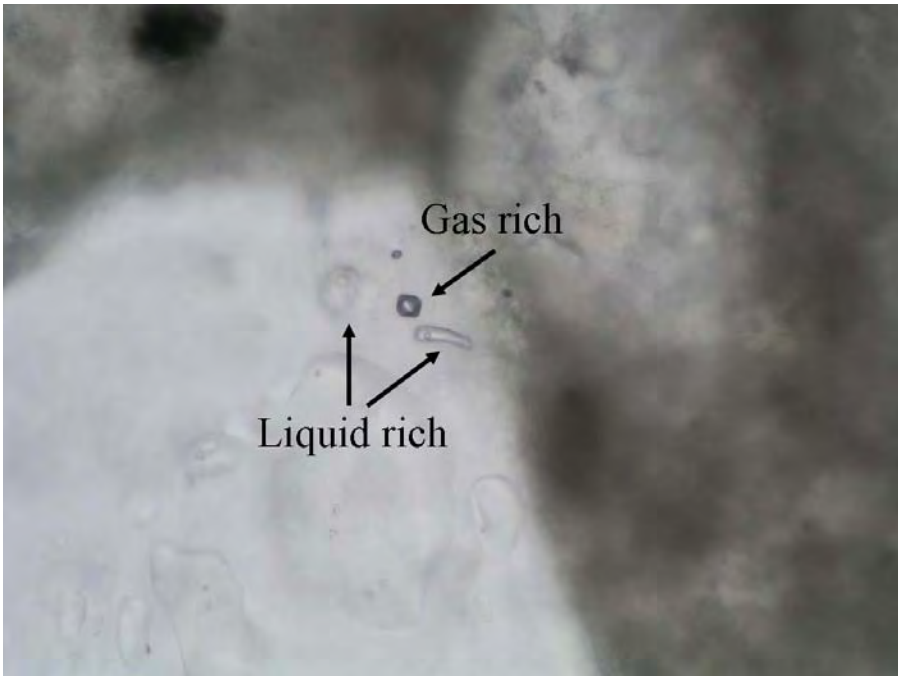

Figure 4-53. Coexisting primary liquid- and gas-rich inclusions in quartz from the Lisbon No. D-616 well at 8356 feet. Width of image is 0.3 mm.

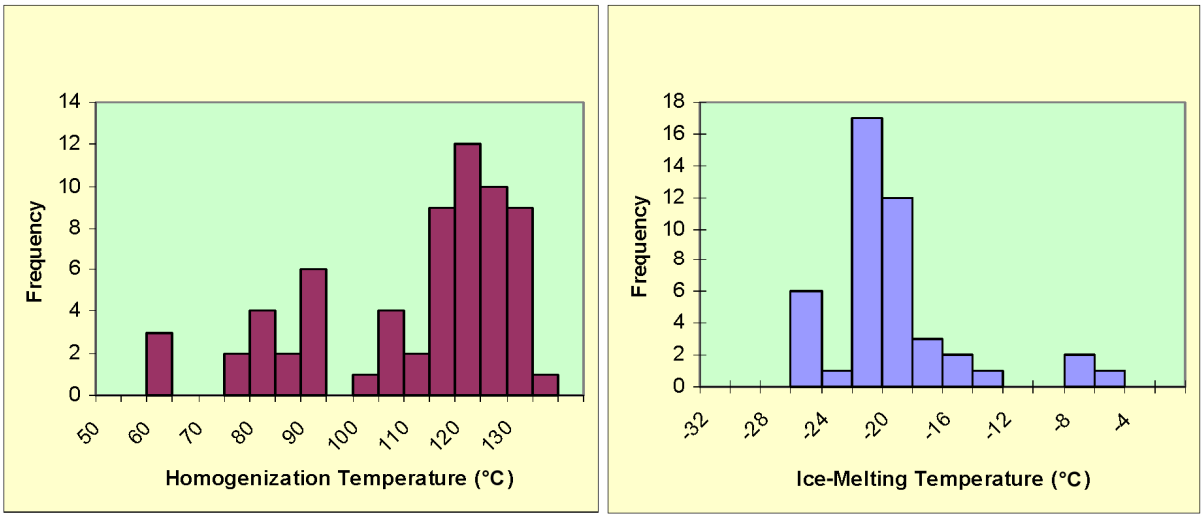

Figure 4-54. Homogenization (A) and ice-melting (B) temperatures of quartz-hosted aqueous inclusions from the Lisbon No. D-616 well at 8356 feet.

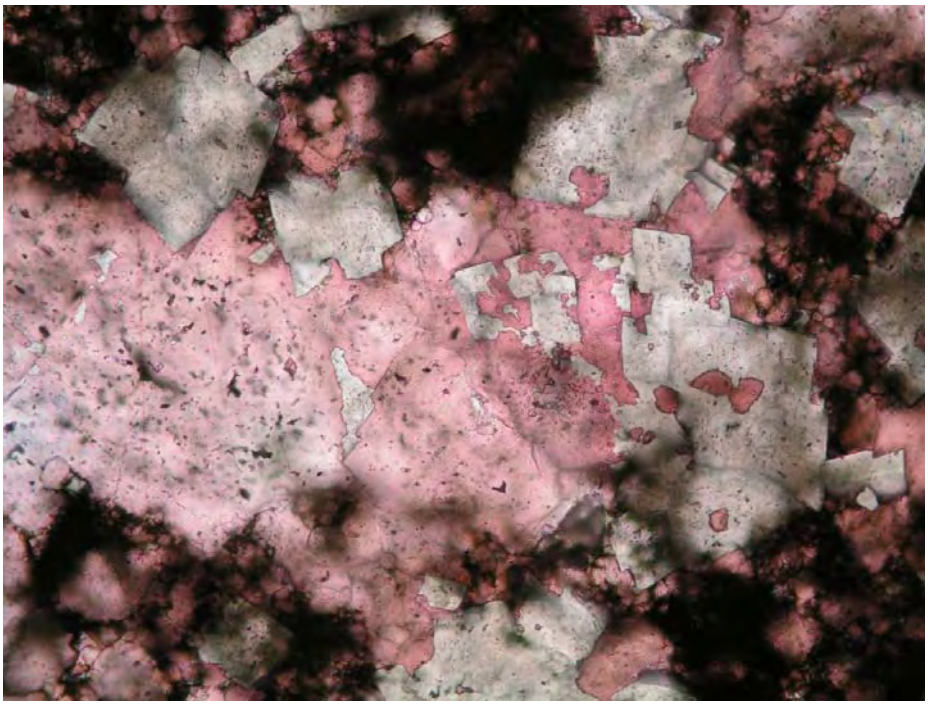

Figure 4-55. Corroded and dissolved dolomite (white) encapsulated in calcite (pink) from the Lisbon NW USA No. B-63 at 9936 feet. Width of image is 1.3 mm.

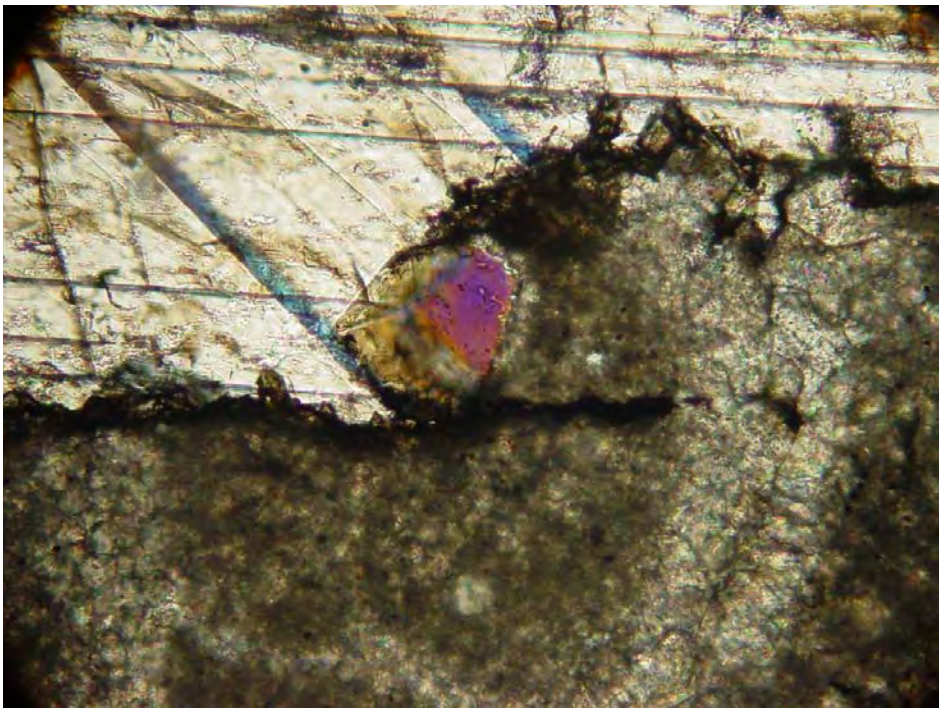

Figure 4-56. Coarse-grained calcite (upper half of image) that appears to postdate quartz (purple crystal in center) and dolomite (lower half of image). Lisbon NW USA No. B-63 well at 10,004 feet. Width of image is 0.7 mm.

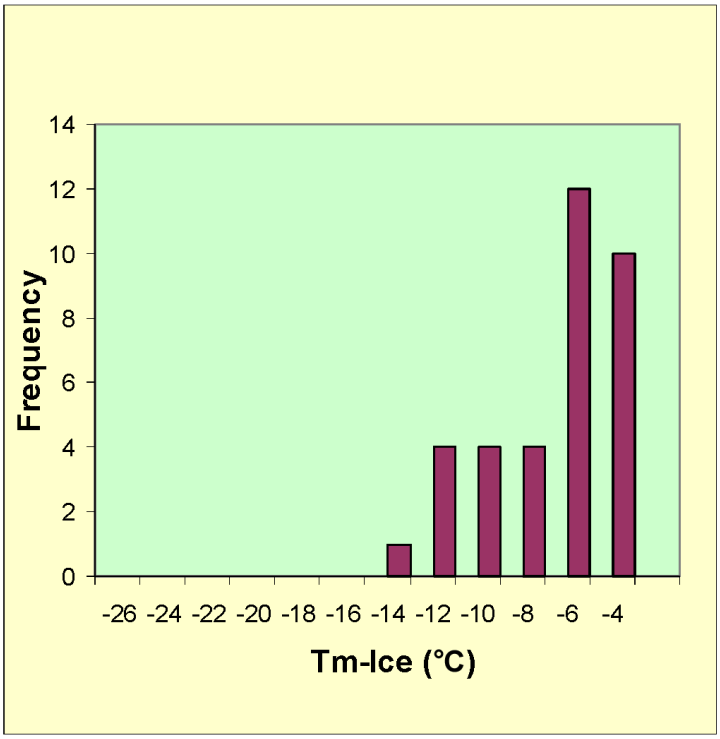

Figure 4-57. Ice-melting temperatures of late, calcite-hosted fluid inclusions from the Lisbon NW USA No. B-63 well.

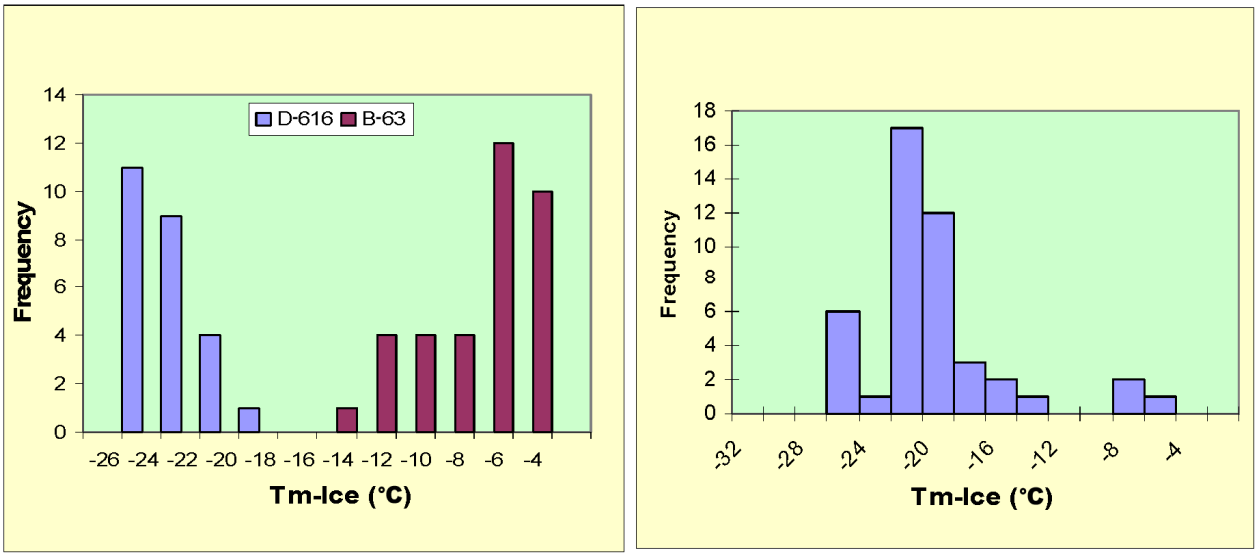

Figure 4-58. Comparison of ice-melting temperatures of fluid inclusions in calcite (A) and quartz (B) from the Lisbon No. D-616 well.

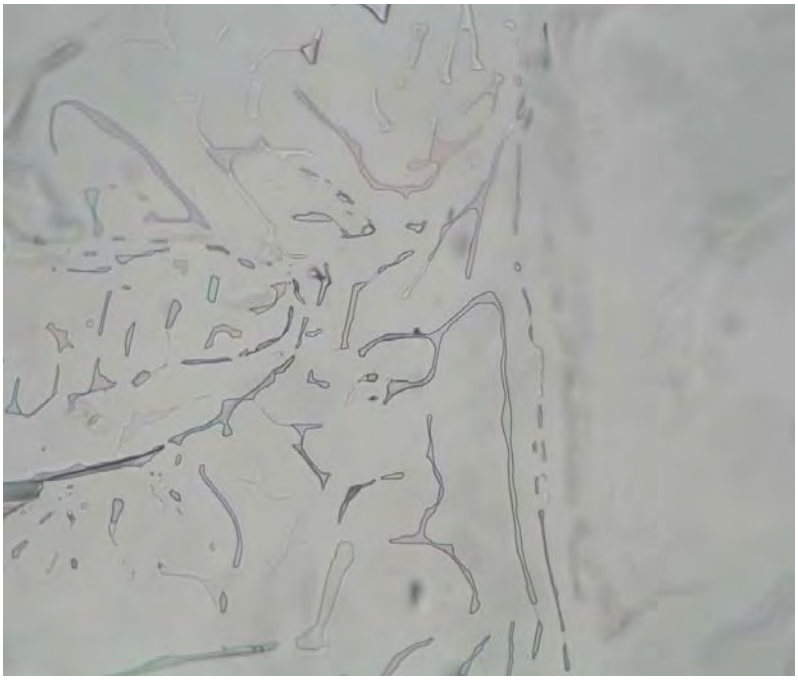

Figure 4-59. Secondary oil inclusions in late calcite from the Lisbon NW USA No. B-63 well at 9936 feet. The inclusions are necked. The large brown inclusion at bottom center contains only liquid; others contain variable ratios of liquid and gas. Width of image is 0.7 mm.

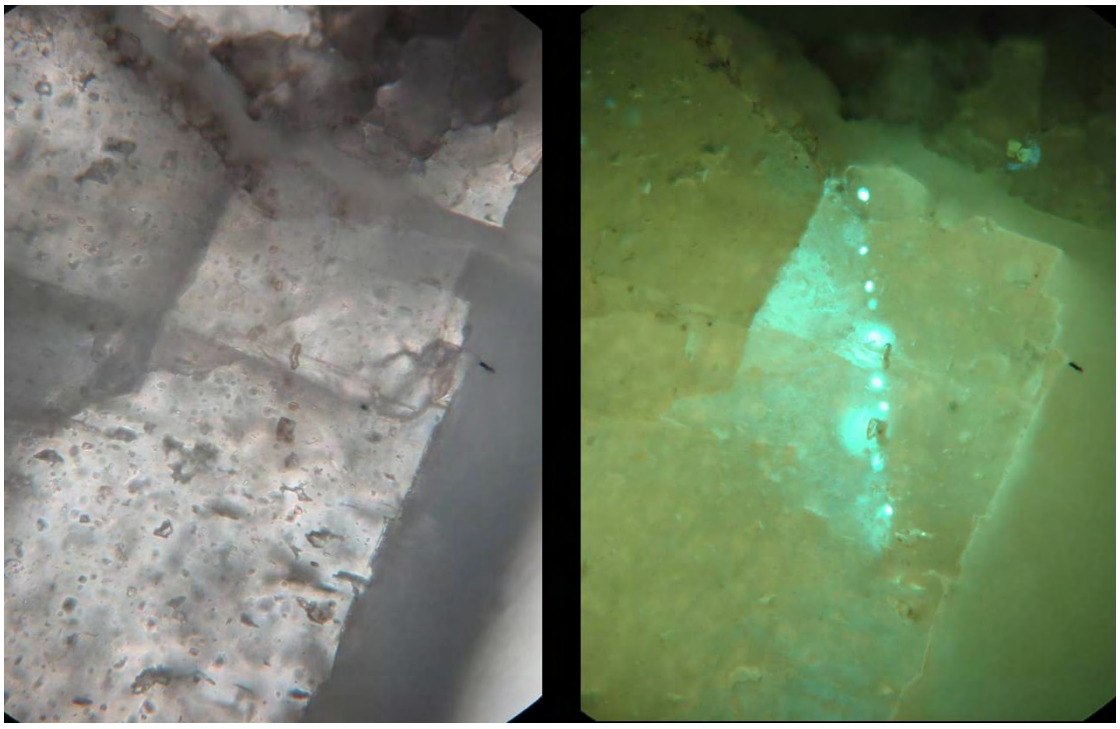

Figure 4-60. Secondary oil inclusions in calcite from the Lisbon No. D-616 well at 8372 feet. The height of each image is 0.3 mm. Right-hand image was taken under fluorescent light.

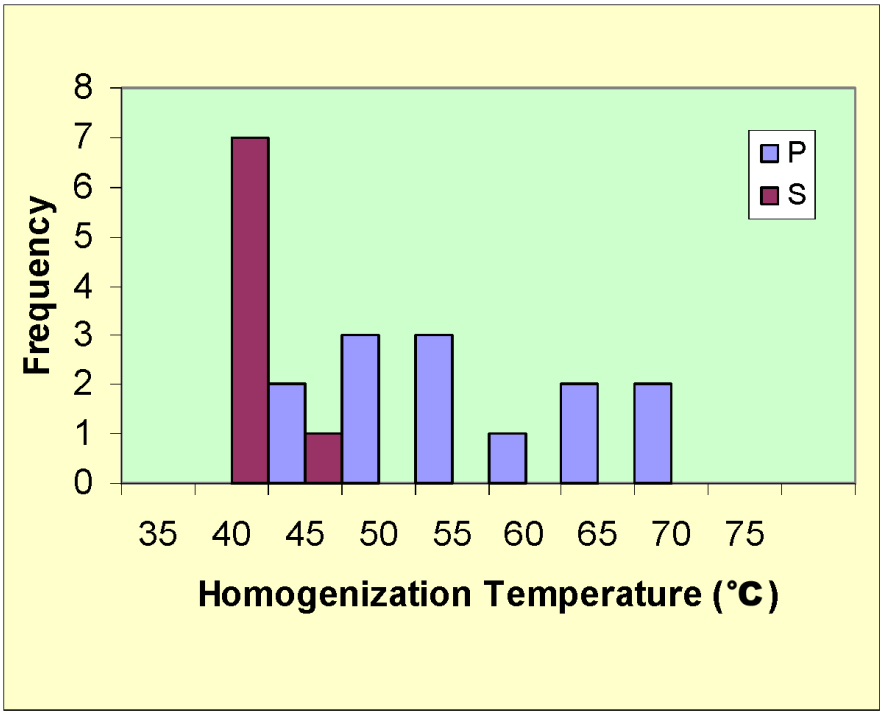

Figure 4-61. Comparison of homogenization temperatures of primary (P) and secondary (S) oil inclusions in calcite.

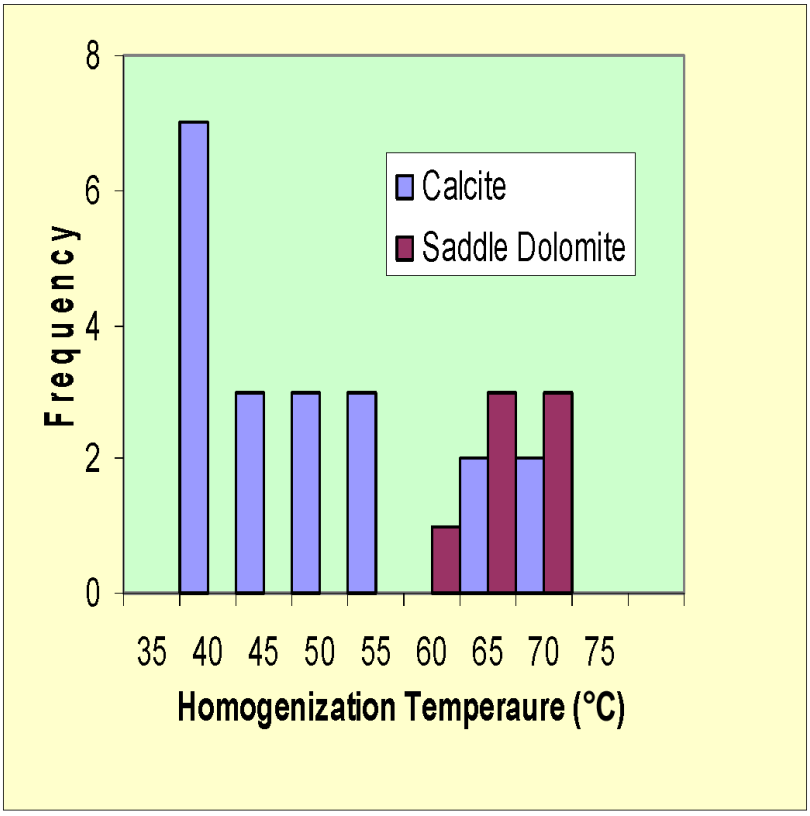

Figure 4-62. Comparison of homogenization temperatures of oil inclusions in calcite and saddle dolomite. All inclusions are primary except 35 to 40°C inclusions in calcite.

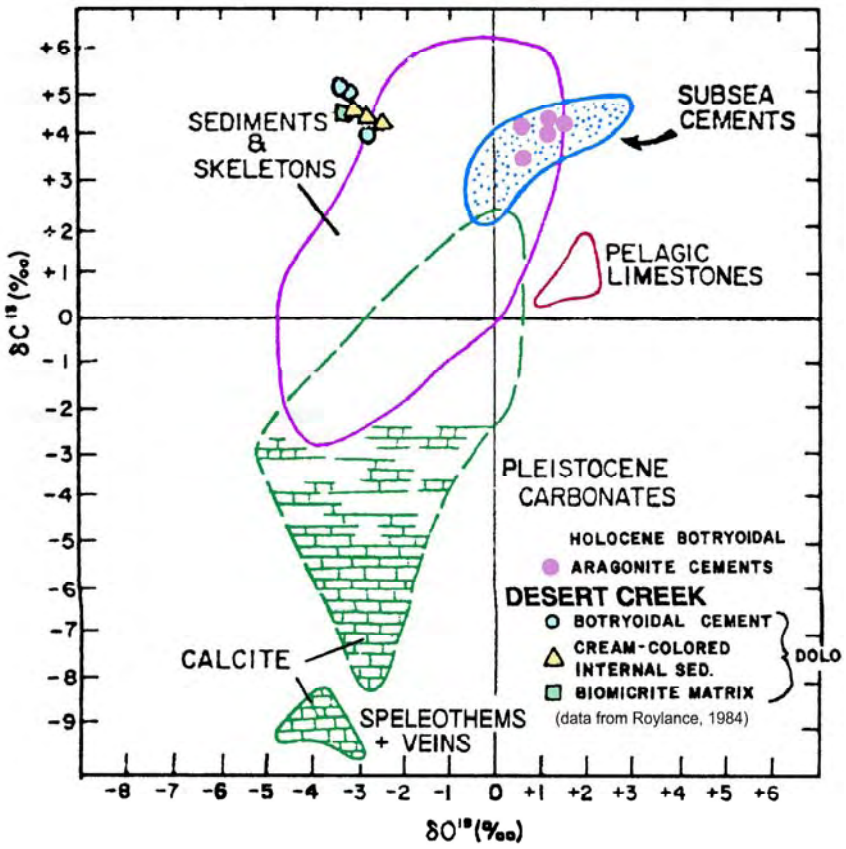

Figure 4-63. Graph of carbon versus oxygen isotope compositions. Other compositional facies compiled from various published work (modified from James and Ginsburg, 1979, by Roylance, 1990).

Figure 4-64. The CSM Stable Isotope Laboratory's GV Instruments IsoPrime stable isotope ratio mass spectrometer. Several peripheral devices are interfaced with the IsoPrime for both dual-inlet and continuous flow applications.

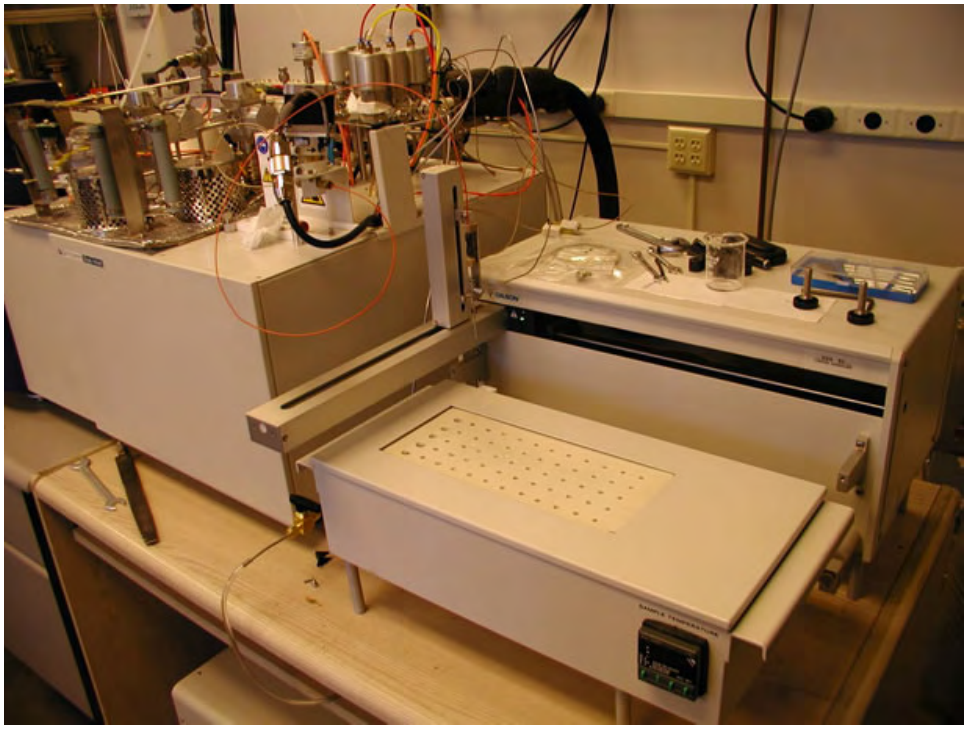

Figure 4-65. MultiPrep intended for high-precision dual-inlet analysis of carbon and oxygen isotopes of carbonate samples, and oxygen isotopes for waters by traditional equilibration techniques. Sample sizes for carbonates ranges from 10 to 100 ug – water samples are 200 ul.

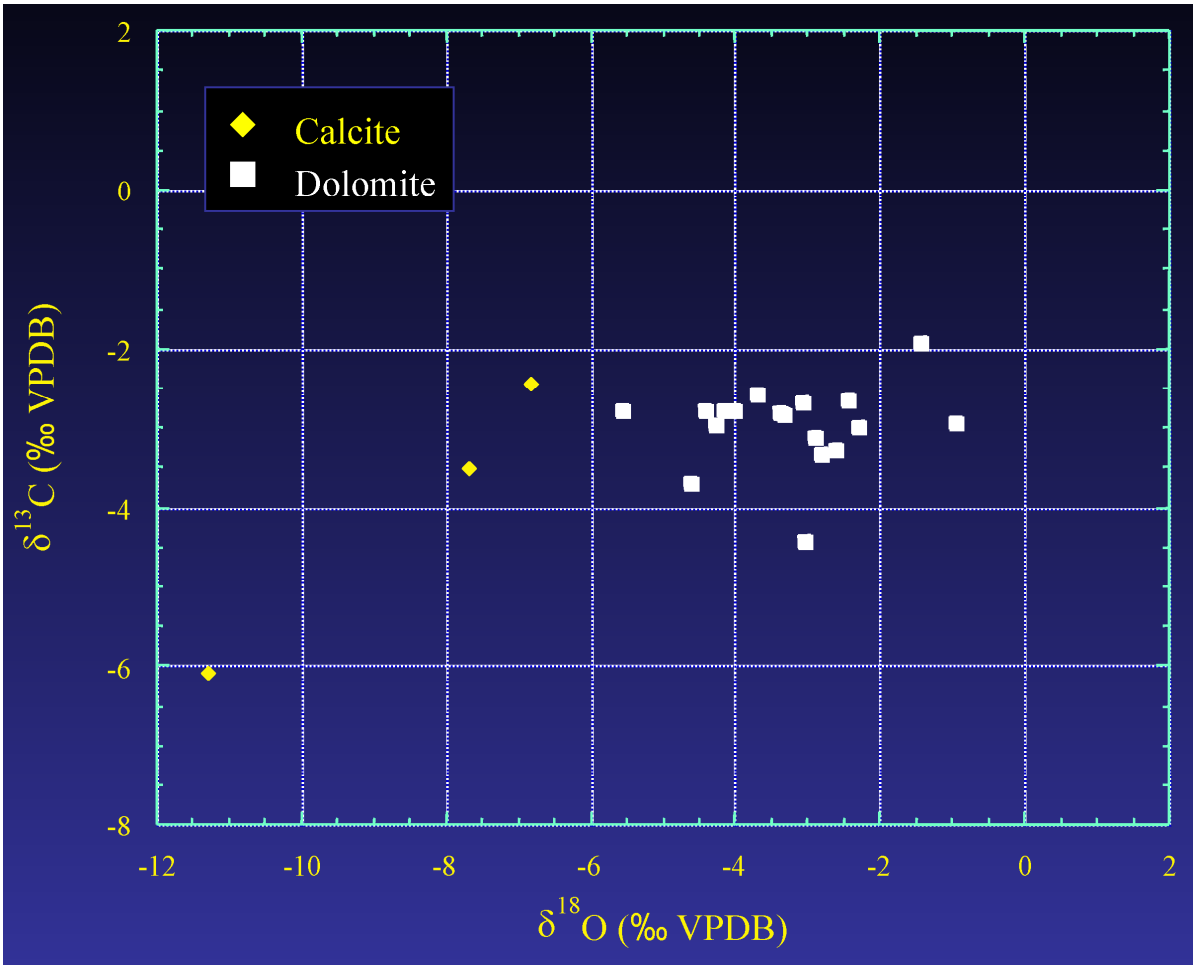

Figure 4-66. Graph of stable carbon versus oxygen isotopic compositions for Leadville dolomite and calcite from Lisbon field. Sample numbers 17 and 24 not shown.

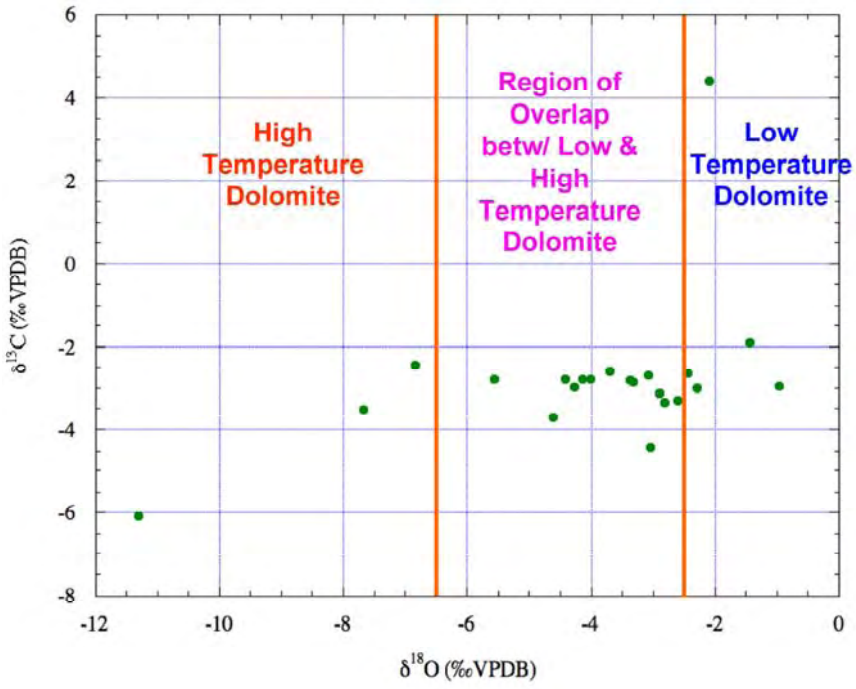

Figure 4-67. Cross plot of the del ^{13}C/del ^{18}O Leadville data from Lisbon field with the regions of dolomite temperatures of formation suggested by Allan and Wiggins (1993).

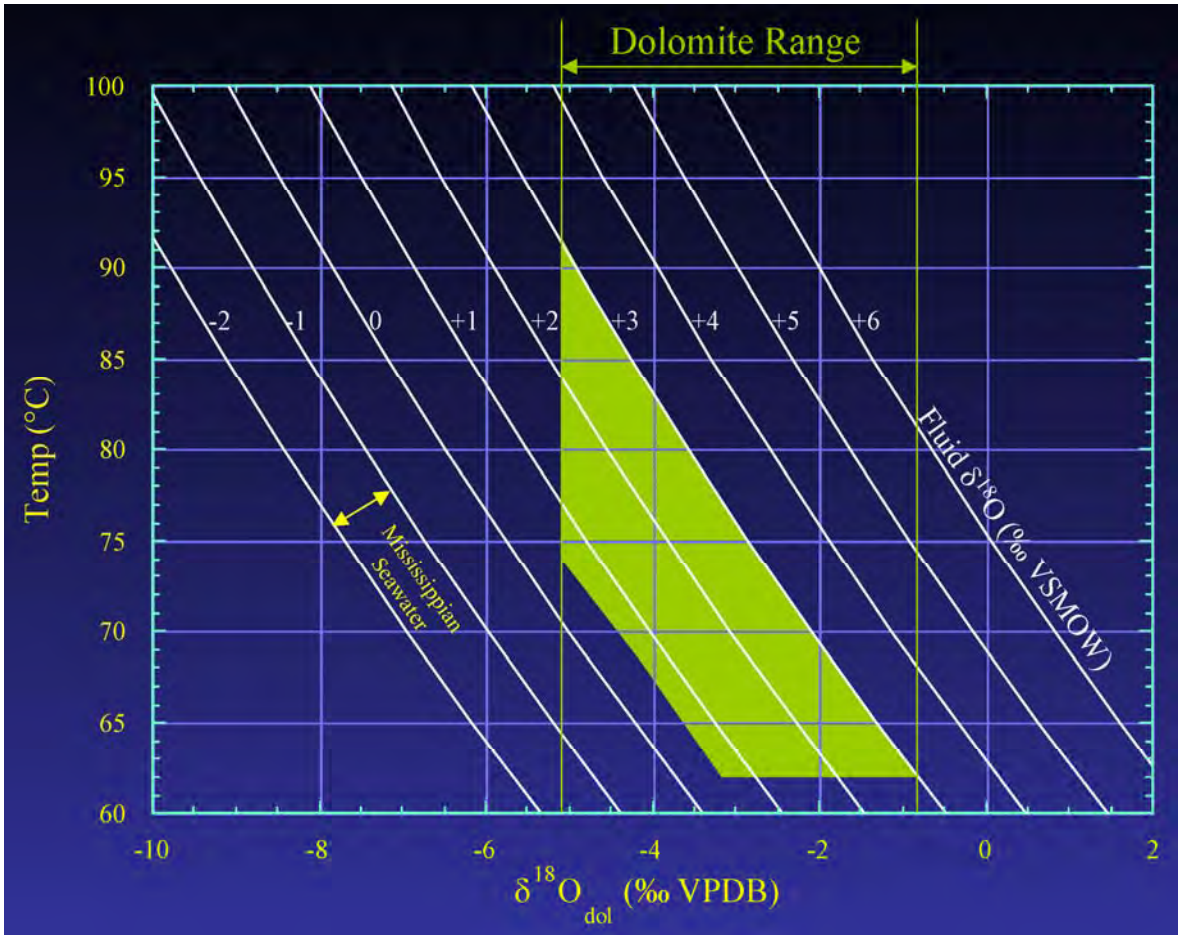

Figure 4-68. Graph of dolomite stable oxygen isotope values versus temperature data. The green field shows our estimate of del ^{18}O of dolomitizing fluids at between 0.5 and 3.0‰. Precipitation temperatures were up to about 90°C (~194°F).

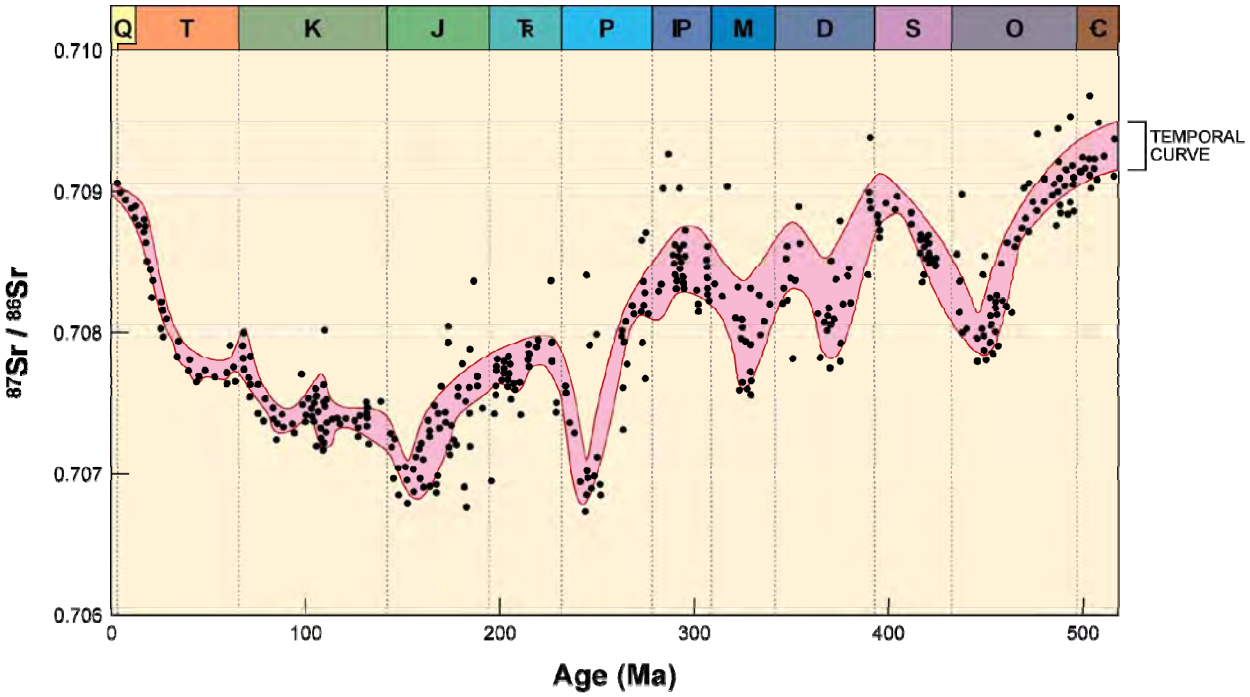

Figure 4-69. Strontium isotope seawater composition curve (from Burke and others, 1982; Elderfield, 1986; Allan and Wiggins, 1993).

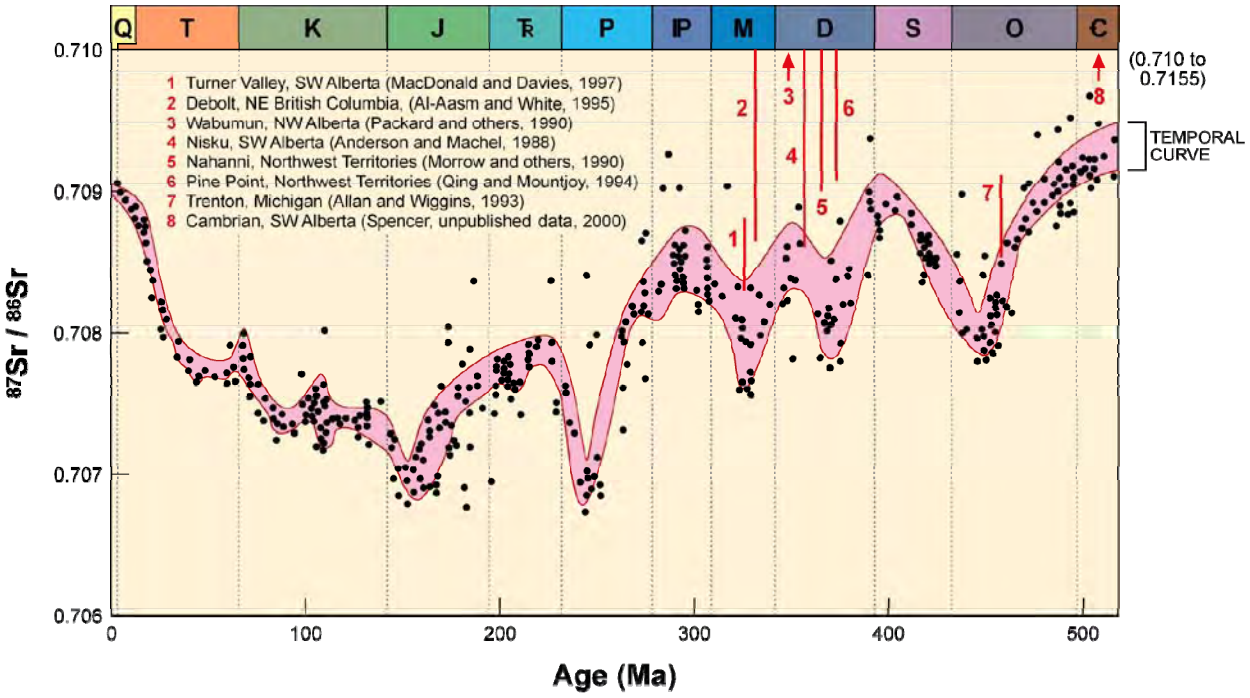

Figure 4-70. Strontium isotope compositions of saddle dolomites from the Canadian Rockies and Michigan Basin (from McArthur and Howard, 2004).

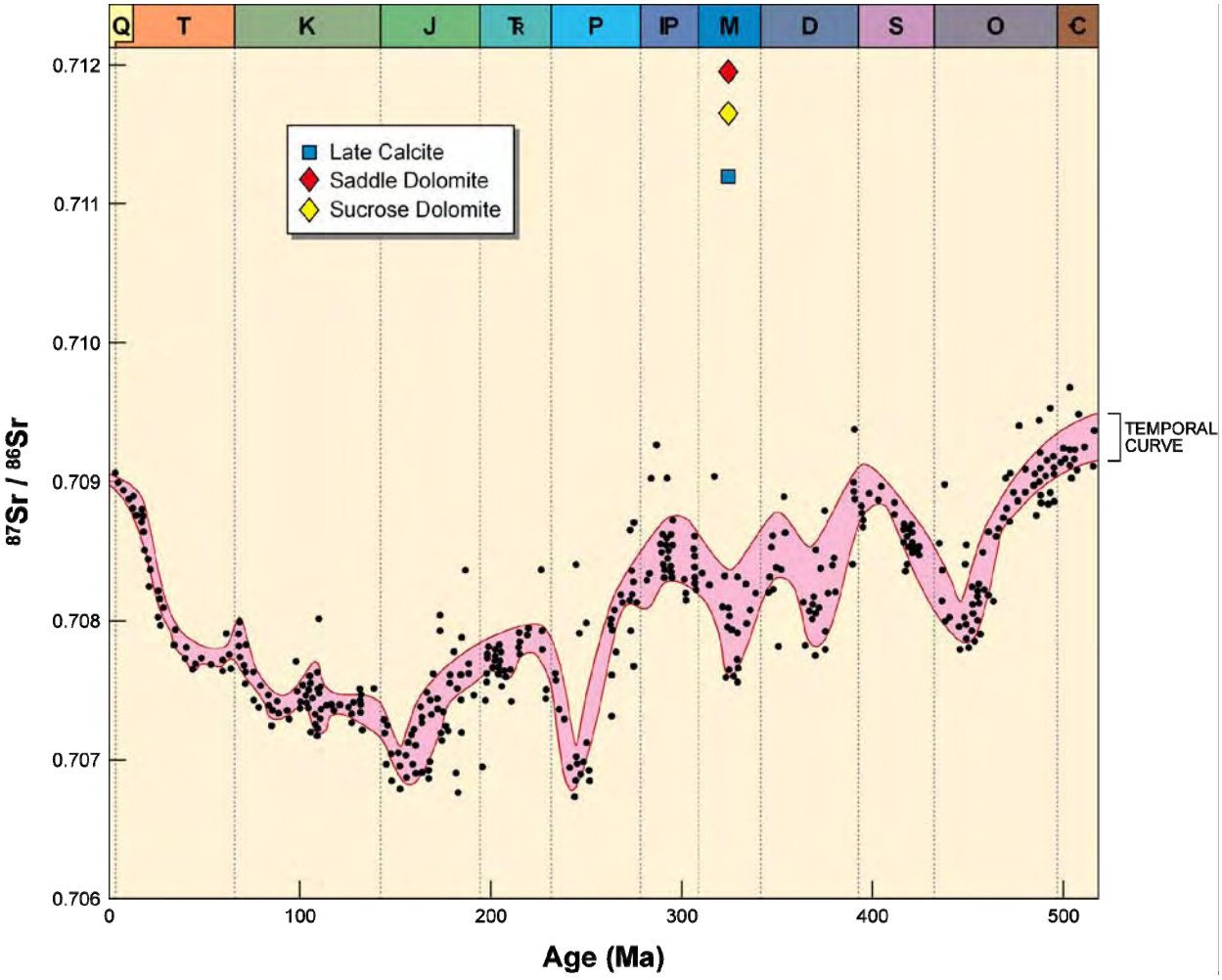

Figure 4-71. A plot of the Sr isotope composition for the three Leadville samples from Lisbon field along with the Phanerozoic marine carbonate curve for Sr ratios (modified from Allan and Wiggins, 1993).

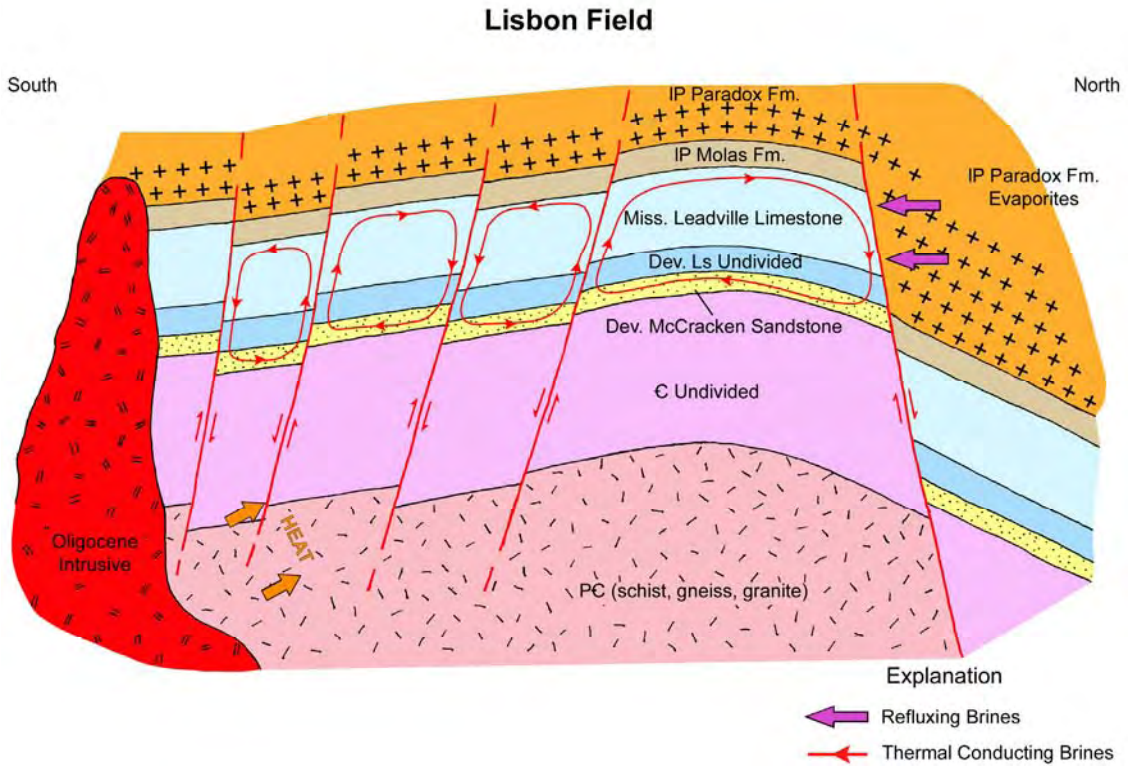

Figure 4-72. Possible heat sources and convection cells for late dolomitization of the Leadville Limestone in Lisbon field.

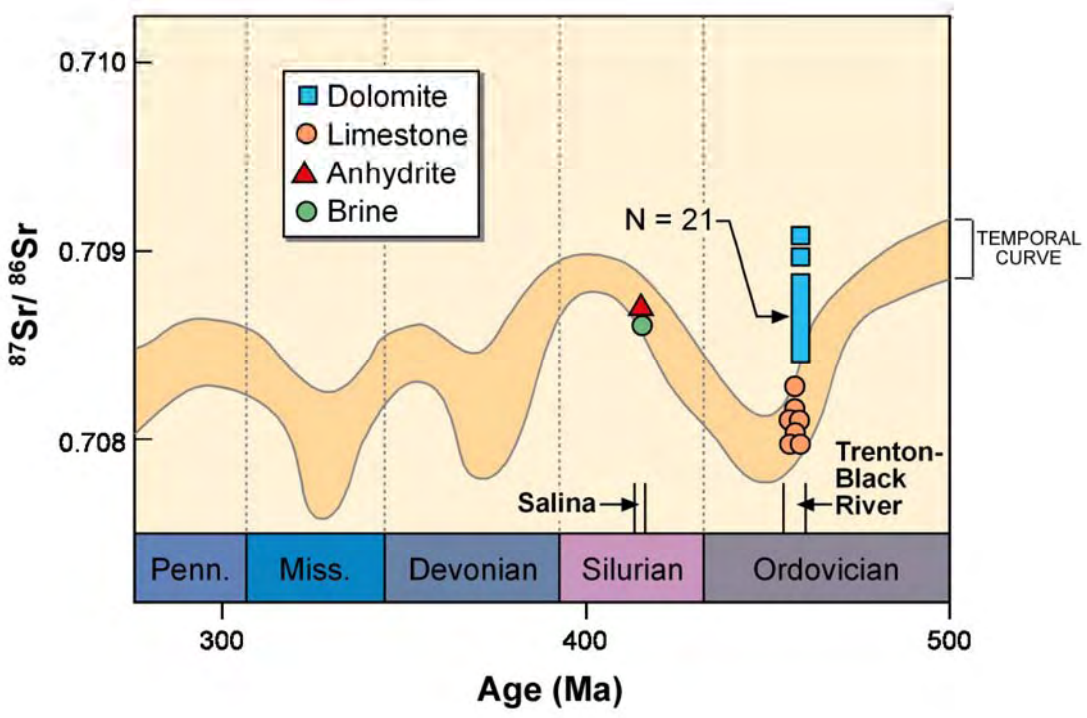

Figure 4-73. Strontium isotope values for limestone and dolomite of the Ordovician Trenton Formation and anhydrite and brine from the Silurian Salina Formation (from Allan and Wiggins, 1993).

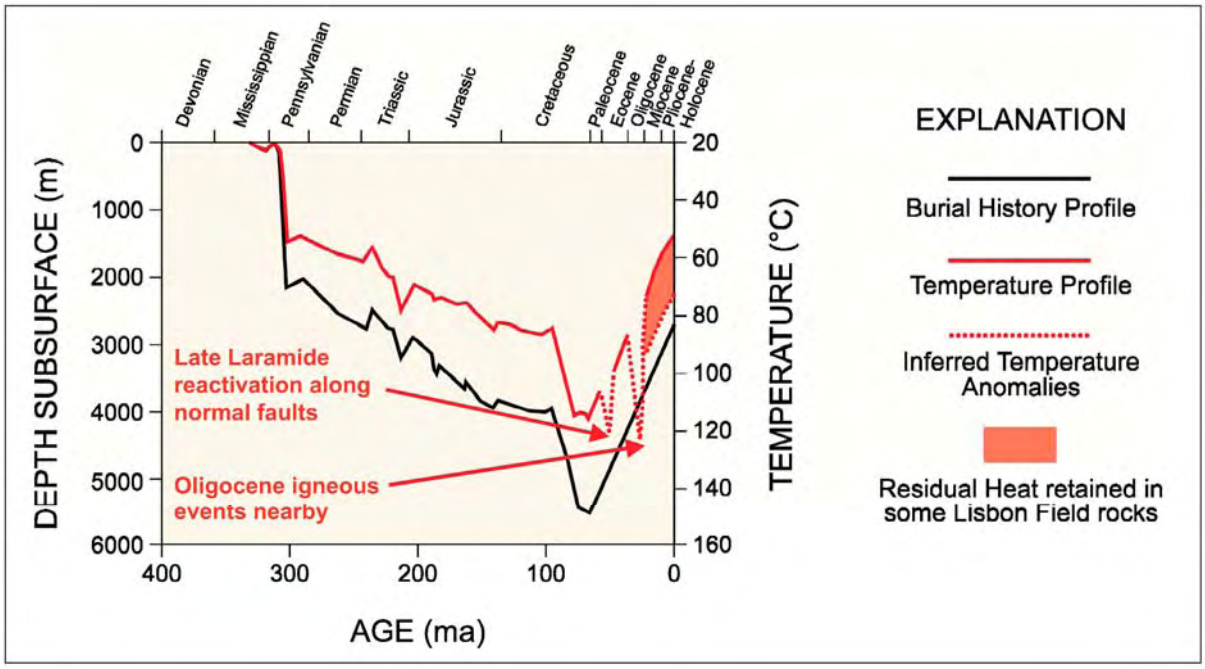

Figure 4-74. Burial history and temperature profile for Lisbon field.

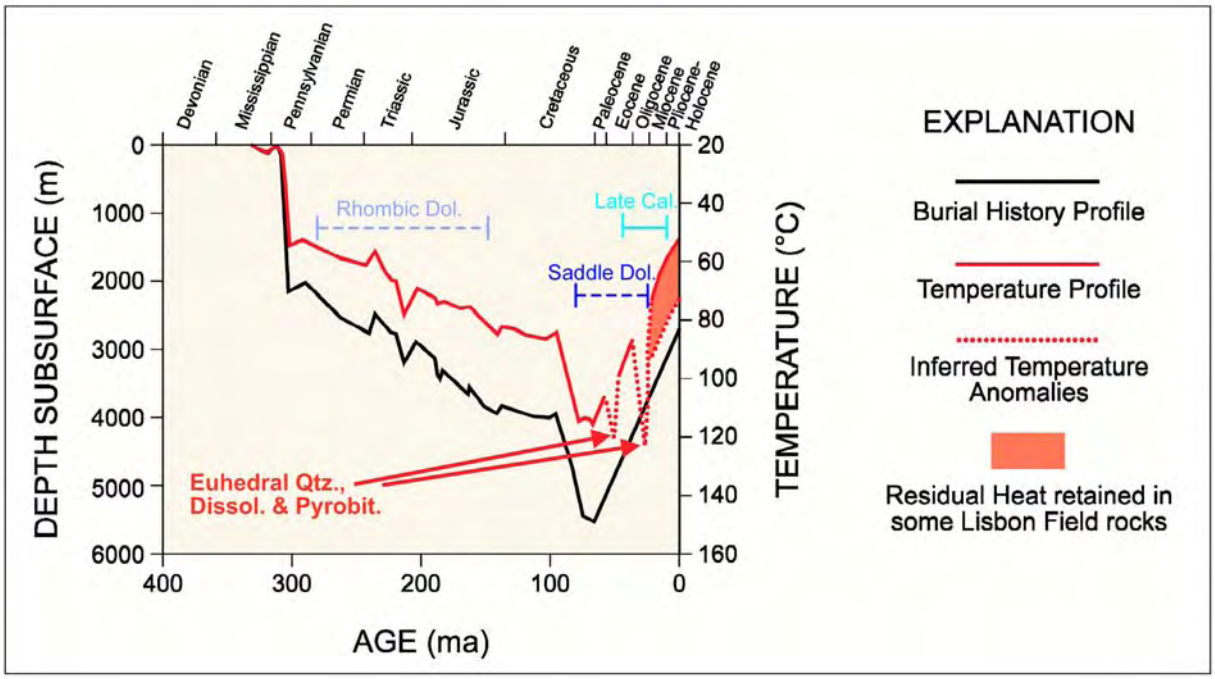

Figure 4-75. Burial history and temperature profiles with inferred diagenetic windows at Lisbon field.

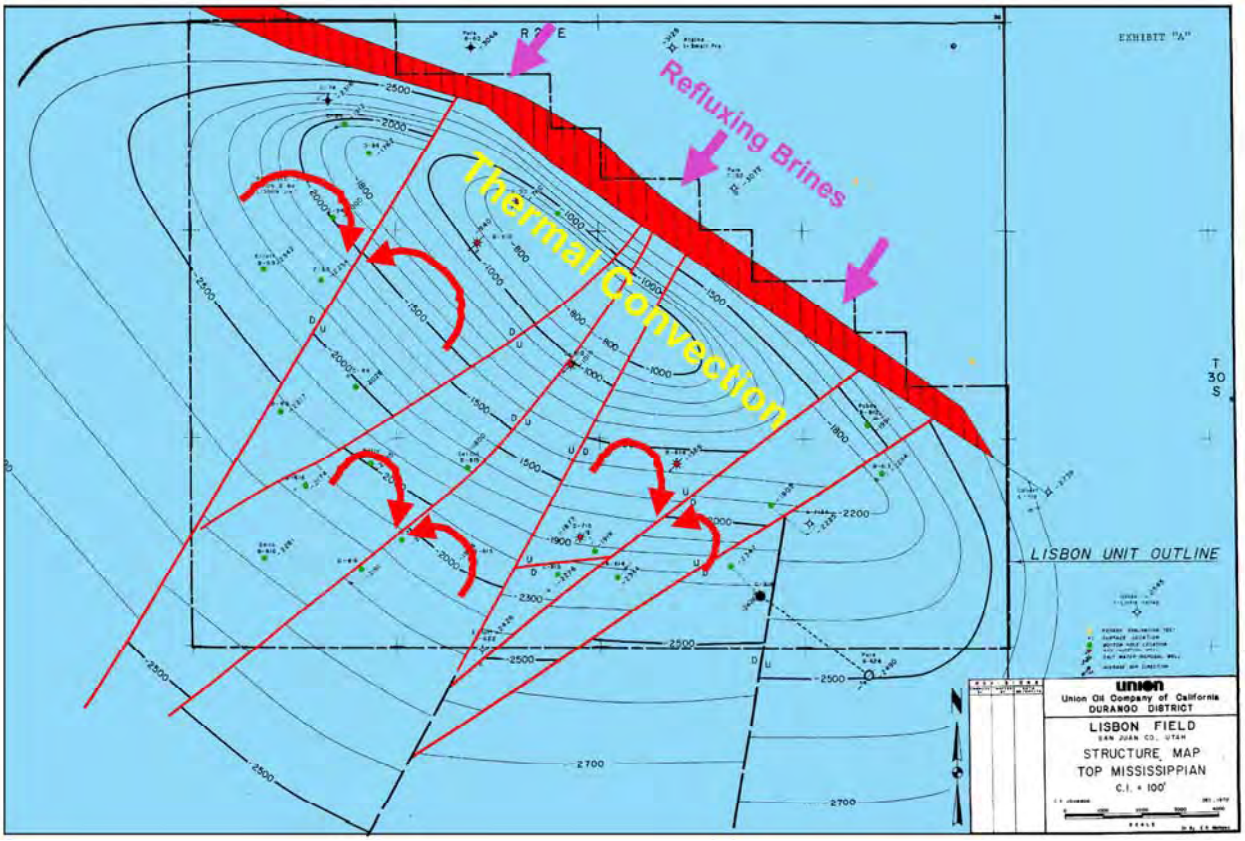

Figure 4-76. Top of structure of the Leadville Limestone, Lisbon field, showing possible thermal convection cells between small, northeast-southwest-trending normal faults (modified from C.F. Johnson, Union Oil Company of California files, 1970; courtesy of Tom Brown, Inc.).

Table 4-1. Summary of characteristics observed with scanning electron microscopy in samples from the Lisbon No. D-816, Lisbon No. D-616, and Lisbon No. B-610 wells, Lisbon field, San Juan County, Utah.

Well	Lisbon D-816					Lisbon D-616					Lisbon B-610	
DEPTH (ft)	8423'	8426'	8433'	8442'	8486'	8308'	8356'	8559'	8619'	8682'	7886'	7897'
POROSITY												
Intergranular (Micro) (BC)	X	X	X	X	X	X	X	X	X	X	X	X
Dissolution (MO)	X	X	X	X	X		X		X		X	X
Dissolution (VUG)		X	X	X	X				X		X	X
Dissolution (CH)											X	
Fractures	X			X		X	X		X	X	X	
CEMENTS												
Anhydrite		X	X							X		
Calcite					X	X	X				X	
Quartz					X	X	X		X			
Dolomite	X	X	X	X	X	X	X	X	X	X	X	X
Illitic Clay	X					?				X		X
Pyrobitumen	X	X	X	X	X				X			
Sulfides	X		X	X	X				X		X	X
DIAGENESIS												
Dolomitization	X	X	X	X	X	X	X		X	X	X	X
Dissolution	X	X	X	X	X	X	X		X	X	X	X
Calcite Cementation					X	X	X					
Quartz Cementation					X	X	X		X			
Illitic clay Deposition	X					X			X	X	X	X
Anhydrite Cementation		X	X							X		
Pyrobitumen Emplacement	X	X	X	X	X				X			
Fracturing	X			X		X	X		X	X	X	
Data from SEM, EDS, and optical microscopy by Standard Geological Services, Inc. and petrography by Eby Petrography & Consulting.												

Table 4-2. Stable carbon and oxygen isotope data from the Mississippian Leadville Limestone, Lisbon field core samples.

Sample No.	Well	Depth (ft)	del ^{13}C	del ^{18}O	Comments
1	B-63	9960.6	-2.441	-6.830	Late calcite
2	B-63	9960.6	-1.918	-1.435	Syngenetic dolomite
3	B-63	10,004-05	-6.092	-11.297	Late calcite
4	D-816	8444-45	-2.696	-3.069	Dolomite cement
5	D-816	8444-45	-2.648	-2.441	Replacement dolomite
6	D-816	8444-45	-3.008	-2.287	Matrix dolomite
7	D-816	8421	-2.584	-3.699	Dolomite cement
8	D-816	8421	-2.978	-4.265	Replacement dolomite
9	D-616	8356-57	-3.709	-4.613	Saddle dolomite in fractures
10	D-616	8356-57	-2.793	-4.422	Limestone matrix/crinoids
11	D-816	8433	-2.815	-3.375	Late replacement matrix dolomite
12	B-610	7897	-2.951	-0.963	White, tight early dolomite
13	B-610	7897	-3.348	-2.808	Black, porous late dolomite
14	B-610	7886	-3.294	-2.601	White, tight early dolomite
15	B-610	7886	-3.126	-2.890	Black, porous late dolomite
16	D-616	8559	-2.851	-3.313	Black, porous late replacement dolomite
17	D-616	8682	4.407	-2.086	Syngenetic dolomite
18	B-63	9935.6	-2.795	-4.012	Dolomite (possible cross-cutting karst sediment fill)
19	B-63	9935.6	-2.785	-5.564	Limestone, peloidal/skeletal grainstone; sampled only black non-skeletal grains which appear microporous
20	D-616	8308-09	-4.418	-3.038	Dolomitized sediment within karst cavity
21	D-616	8308-09	-2.783	-4.147	Limestone country rock
22	B-63	9991.8	-3.510	-7.668	Late calcite, poikliotopic
23	B-63	9939	-3.499	-7.644	Saddle dolomite
24	B-63	9909	-4.794	-12.255	Late calcite
25	D-616	8308	-4.224	-2.694	Karst-fill dolomite

Table 4-3. Strontium isotopic data from the Lisbon NW USA No. B-63 well core samples.

Sample No.	Well	Depth (ft)	$^{87}Sr/^{86}Sr$	Comments
1	B-63	9939	0.712068	Late calcite
2	B-63	9939	0.711961	Saddle dolomite
3	B-63	9939	0.711464	Matrix sucrosic dolomite

EXPLORATION TECHNIQUES FOR THE MISSISSIPPIAN LEADVILLE LIMESTONE PLAY

CHAPTER 5
NEW TECHNIQUES FOR NEW DISCOVERIES – SURFACE GEOCHEMICAL SURVEYS IN THE LISBON CASE-STUDY FIELD AND LIGHTNING DRAW SOUTHEAST FIELD AREAS, SAN JUAN COUNTY, UTAH

David M. Seneshen, Direct Geochemica/Vista Geoscience,
and
Thomas C. Chidsey, Jr., Craig D. Morgan, and Michael D. Vanden Berg,
Utah Geological Survey

Introduction

Surface exploration methods, such as geochemical, magnetic, and remote sensing, have increasingly proven to significantly reduce petroleum exploration risks and finding costs. These methods, and numerous case histories, are summarized by Schumacher and LeSchack (2002). Surface geochemical surveys in the Michigan and Williston Basins helped identify areas of poorly drained or by-passed oil in pinnacle reef fields (Wood and others, 2001, 2002), which are comparable in many aspects to the depositional environment of the Leadville Limestone in the Paradox Basin. Surface geochemical methods detected hydrocarbon microseepage over Grant Canyon field, Nevada, and these methods are also being used to define potential faulted, carbonate reservoirs in western Utah (Seneshen and others, 2006). Anomalies are relatively easy to identify and are conclusive about the presence of subsurface hydrocarbon deposits.

The potential for additional hydrocarbon reserves in the Paradox Basin is enormous, but the high cost of 3D seismic exploration methods in environmentally sensitive areas with extensive outcrops deters small independents from exploring for Leadville hydrocarbon reservoirs. Lisbon field (figure 1-3) is ideal for a surface geochemical survey. Besides active hydrocarbon production from beneath the easily accessible area, the surface geology is similar to the subsurface structure of the field (figures 2-1, 5-1, 5-2, and 5-3). In addition, nearby Lightning Draw Southeast field (figures 1-3, 5-2, and 5-3) is also accessible and is at or near original reservoir pressure making it an excellent test site to evaluate hydrocarbon seepage in comparison with that at Lisbon.

Remote sensing studies over Lisbon field have documented the presence of seep-induced alteration to near-surface soils and sediments (Merin and Segal, 1989; Segal and Merin, 1989). Other work has shown the potential of remote-sensing techniques for identifying kaolinite-enriched, bleached redbed Triassic Wingate sandstones over productive parts of Lisbon field (Conel and Alley, 1985; Segal and others, 1986). These studies used Landsat Thematic Mapper (TM) data to recognize the presence of kaolinite as well as reduced iron (that is, bleached redbed sandstones). A ratio of TM bands 2/3 was used to define variations in ferric-iron content, while a band 5/7 ratio was used to highlight variations in clay content. Because vegetation also exhibits high band 2/3 ratio values, it can be confused with bleached rocks. Vegetation also shows high band 5/7 ratio values that can be confused with clay-rich rocks. Other than this work, there are no published surface geochemical studies in the Lisbon field area. The UGS therefore contracted Direct Geochemical/Vista Geoscience to test the effectiveness of several conventional and unconventional surface geochemical methods in the Lisbon area. The main

objective for testing these techniques was to find effective, low-cost, non-invasive geochemical exploration methods to prescreen large areas of the Paradox Basin for subsequent geophysical surveys and lease acquisition, and also act as a follow-up to classify geophysical anomalies as "productive or barren," specifically for the Leadville Limestone or other subsurface reservoir exploration programs.

The premise behind surface geochemical exploration for petroleum is that light volatile hydrocarbons (that is, C_1 to C_5) ascend rapidly to the surface from a pressured reservoir as buoyant colloidal-size "microbubbles" along water-filled fractures, joints, and bedding planes (Price, 1986; Klusman, 1993; Saunders and others, 1999). Studies over gas-storage reservoirs support the rapid development of soil-gas hydrocarbon anomalies over a charged reservoir, and the rapid depletion of such anomalies once the reservoir has been depleted (Coleman and others, 1977). Partial aerobic and anaerobic bacterial consumption of the ascending hydrocarbons produces carbon dioxide and hydrogen sulfide that can significantly alter the chemical and mineralogical composition of overlying sediments (Schumacher, 1996). Changes to overlying soils and sediments can include (1) precipitation of isotopically light calcite, pyrite, pyrrhotite, and uranium, sulfur, and iron (magnetic) oxides, (2) bleaching of redbeds through the removal of Fe^{3+} by reduced fluids, (3) conversion of illitic clays and feldspars to kaolinite and removal of potassium by acidic, reduced fluids, and (4) variations in the major and trace element chemistry of soil and vegetation (Saunders and others, 1999). Chemical reactions that produce the various minerals found in "reduced chimneys" above petroleum reservoirs are shown in figure 5-4.

Various techniques have been tested over oil and gas reservoirs to search for direct and indirect indications of hydrocarbon microseepage. These techniques include analysis of (1) soil hydrocarbon fluorescence (Herbert, 1984), (2) hydrocarbons adsorbed to and occluded in soils (Horvitz, 1985), (3) carbonate (CO_2) and soil salts (Duchscherer, 1986), (4) major and trace elements of soils (Duchscherer, 1984), (5) hydrocarbon-consuming bacteria in soils (Price, 1993), (6) gas concentrations (for example, hydrocarbons, helium, and so forth) and stable isotopic composition of hydrocarbons in pore-space soil air (Roberts and others, 1976; Bammel and others, 1994), (7) passive gas collections (Potter and others, 1996), and (8) vegetation for trace elements (Klusman and others, 1992).

Time and budget constraints did not allow for testing of all of the above-mentioned techniques. The direct and indirect geochemical methods chosen for testing over the Lisbon area were based on the available sample media, composition of produced gas, and analytical methods offered by Direct Geochemical at the time. For example, the produced Leadville gas is rich in carbon dioxide and helium compared with overlying formations. It was therefore decided to analyze free-gas samples over Lightning Draw Southeast field, San Juan County, Utah, for carbon dioxide and helium in addition to hydrocarbons. Direct methods included the assessment of hydrocarbon compositional signatures in surface soils, outcrop fracture-fill soils and lichen, and 6-foot (2 m) deep free-gas samples. Indirect methods are those not related to hydrocarbons such as the evaluation of major/trace element and anion chemistry of soils and outcrop-fracture fill soils and lichen to look for alteration effects resulting from hydrocarbon microseepage.

This surface geochemical study over Leadville hydrocarbon reservoirs focused on testing both "direct and indirect" methods over known "productive and non-productive areas." The techniques tested in this study are termed "new" mainly because they have not been tested previously in the Lisbon area. Some of the sampling and analytical techniques are in fact methods that have not been previously employed for hydrocarbon exploration. One truly new technique tested is Direct Geochemical's proprietary thermal desorption hydrocarbon analysis of

soil samples and the unique interpretation of the data. Also, organic and inorganic analyses of outcrop fracture-fill vegetation is introduced here as a new technique for geochemical exploration for oil and gas reservoirs.

Lisbon and Lightning Draw Southeast Areas, San Juan County, Utah

Lisbon field (described in detail in Chapters 2 through 4), San Juan County, Utah (figure 1-3) accounts for most of the Leadville oil production in the Paradox Basin. The reservoir characteristics, particularly its diagenetic overprinting and history, and Leadville lithofacies can be applied regionally to other fields and exploration trends in the Paradox Basin. A major northwest-southeast-trending anticline (tens of miles in length) along the Lisbon fault, displaces the Pennsylvanian Honaker Trail Formation against Cretaceous strata (figures 5-2 and 5-3). Four miles (6.4 km) to the southwestof Lisbon field, the recently discovered Lightning Draw Southeast field (figure 1-3) its similar to Lisbon in terms of Leadville reservoir lithology, structure, and gas composition (table 5-1).

The Leadville reservoirs in Lisbon and Lightning Draw Southeast fields are separated from upper Paleozoic and Mesozoic strata by cyclic evaporites in the Pennsylvanian Paradox Formation (figure 1-2). These conditions are typical of what might be expected when exploring for similar drilling targets in the basin. Three factors create reservoir heterogeneity within productive zones: (1) variations in carbonate fabrics and facies, (2) diagenesis (including karstification and late-stage bitumen plugging), and (3) fracturing. The extent of these factors and how they are combined affect the degree to which they create barriers to fluid flow laterally and vertically – possibly to the surface.

Lightning Draw Southeast (LDSE) field consists of two Leadville wells producing, primarily gas and condensate, along with barren dry wells off structure (figure 5-5). Like the Lisbon trap, the LDSE trap is also an elongate, but relatively small, asymmetric, northwest-trending anticline (no surface expression), with nearly 250 feet (75 m) of structural closure. The structure is bounded on the southwest flank by a high-angle, basement-influenced reverse fault (figures 5-3 and 5-5). A northwest-trending syncline separates the LDSE and Lisbon anticlines in the subsurface.

Producing units at LDSE are similar to Lisbon field in terms of depositional environments, carbonate fabrics, and diagenesis. There are two principal Leadville zones at LDSE field: an upper zone primarily of fossiliferous limestone with crinoids, brachiopods, and coated grains forming skeletal wackestone to packstone and some grainstone fabrics; and a lower zone of dolomitized mudstone with large rhombic to sucrosic dolomite crystals. Diagenesis consists of hydrothermal dolomitization, bitumen coating, and fracturing. The producing interval is confined to the upper zone although both have some units over 6% porosity. The net reservoir thickness is about 40 feet (12 m) over an approximate 320-acre (130 ha) area. Porosity over the perforated interval averages 17%, and permeability averages 13 mD. The drive mechanism is an expanding gas cap; water saturation is 21%. The bottom-hole temperature is 136ºF (58ºC).

The Leadville Limestone reservoir at LDSE field was first discovered by Texaco in 1980 in the 8826-foot (2690 m) deep Evelyn Chambers Government No. 1 well, NE1/4NE1/4 section 6, T. 31 S., R. 24 E., SLBL&M (figure 5-5). The Mississippian interval tested 1.72 MMCFGPD (0.05 MCMGPD) and the upper and lower Ismay zones of the Pennsylvanian Paradox Formation tested 12 BOPD (condensate) (1.9 m^3), 4.5 MCFGPD (0.1 MCMGPD), and 60 bbls of water per

day (BWPD) (9.5 m^3). ST Oil Company re-perforated the Leadville interval in Evelyn Chambers Government No. 1 well in May 2004, but production statistics are unavailable.

Subsequently, ST Oil Company completed the Federal No. 1-31 well, NW1/4SW1/4 section 31, T. 30 S., R. 24 E., SLBL&M (figures 5-3 and 5-5), in December 2004 with an IFP of 18 BOPD (condensate) (3 m^3), 1543 MCFGPD (44 MCMPD), and 5 BWPD (0.8 m^3). The API gravity of the condensate is 50º. The original reservoir field pressure was 1100 psi (7585 kPa). The well also intersected 34 feet and 29 feet (10 m and 8.8 m) of pay in the upper and lower Ismay zones, respectively. There is currently one producing (Evelyn Chambers Government No. 1 well) and one shut-in (Federal No. 1-31) gas/condensate well from the Leadville Limestone in the field. Cumulative Leadville production as of September 1, 2008, was 3585 bbls of condensate (570 m^3), 353,061 MCFG (9999 MCMG) and 4868 BW (774 m^3) (Utah Division of Oil, Gas and Mining, 2008).

In comparison with the Lisbon field, the LDSE field contains a lower concentration of hydrocarbons and more nitrogen and helium (table 5-1), and it has productive intervals in the overlying Ismay zone. The crosscutting, normal faults at Lisbon are not evident at LDSE from the limited drilling to date.

Jointing

Jointing is best developed in the Jurassic Wingate and Navajo Sandstones (figure 5-6), and is also present in the intervening Kayenta Formation although not as pronounced. Joints may be thin (millimeter to centimeter) or several feet in width (figure 5-7) and tens of feet or miles in length. They may also occur as (1) parallel (figure 5-6), (2) blocky or rectalinear joint sets (figures 5-7B, 5-8A, and 5-8B), and (3) curvilinear polygonal, often with several orders of size or generation (figure 5-8C). Joint sets in the area generally are vertical to near vertical. Many small joints contain very little soil, although enough to support bryophytes (mosses) and lichen growth where there is sufficient moisture (figure 5-8). Some small joints are filled with thin (a few millimeters) silica or calcite veins (figure 5-7C); those joints observed over the gas cap area near the Lisbon No. C-910 well (SW1/4SE1/4 section 10, T. 30 S., R. 24 E., SLBL&M) have halos of possible iron/manganese-bearing minerals around calcite (figure 5-7D). Large joint sets often contain brecciated sandstone and fault gouge-like material.

In the Lisbon field area, joint orientation in the Wingate Sandstone on the southwest-dipping flank of the Lisbon surface anticline and over the gas cap is dominantly northwest-southeast (figure 5-9A), parallel to the regional structural trends. In the relatively flat-lying Navajo Sandstone farther southwest of the surface structure and over the oil leg, the dominant joint trend is nearly perpendicular, east-northeast - west-southwest, to the orientation over the gas cap (figure 5-9B). Joint sets in flat-lying Navajo over the water leg southwest of the field display a dominant east-west orientation (figure 5-9C).

In the LDSE field area, the Navajo Sandstone is also relatively flat lying. Two sets of joints are found near the Federal No. 1-31 well. Their orientations are generally north-south and northwest-southeast (figure 5-10A). Two joint sets are also found in the Navajo to the southeast near the Evelyn Chambers Government No. 1 well with orientations trending northwest-southeast and northeast-southwest (figure 5-10B).

Methodology for the Geochemical Survey

Sample Collection

Surface soils are easily accessible by truck or on foot in the Lisbon and LDSE field areas. Permission was obtained from the field operator, EnCana Oil & Gas (USA) Inc., and the U.S. Bureau of Land Management to conduct the surface geochemical sampling program in the Lisbon field area. A safety orientation was provided by EnCana at the Lisbon Gas Plant, and a hydrogen sulfide (H_2S) monitor was lent to the sampling crew. Some sampling sites were relocated and the grid adjusted farther to the west to avoid an H_2S pipeline in Lisbon field.

The sample site locations were planned weeks in advance of the survey. The sample points were digitized off a topographical base using Surfer™ and a table of Universal Transverse Mercator (UTM), North America Datum 1927 (NAD27) coordinates was created and imported into Excel™. The coordinates and topographical maps were generated in Garmin™-compatible format and uploaded to Global Positioning System (GPS) units for use in the field. The field sampler would then walk to the designated sample site displayed on the GPS. At each sample site the UTM coordinates were recorded in the memory of the GPS and written in a field notebook. Field notes recorded included sample depth, soil color, and texture, and signs of possible contamination from nearby wells, gas condensers, paved roads, and so forth.

Collection of surface soils: Two surface soil types are evident in the study area. In outcrop-rich areas (shown as Mesozoic and Paleozoic geological units on figure 5-11), the thin soils that sporadically cover bedrock are classified as Rizozo-Rock Outcrop-Ildefonso types (Lammers, 1991). The dominant vegetation on these thin soils is piñon, Utah juniper, big sagebrush, Mormon tea, and galleta. Shallow Rizozo soils, formed from residual and eolian deposits, are a yellowish-red gravelly, fine-grained, sandy loam. Samples collected from depths of 8 to 12 inches (20-31 cm) are reddish-brown, sandy loam, clay loam, and fine-grained sandy loam (figure 5-12A). In broader valleys (eolian and alluvium deposits on figure 5-11), there is a mixture of Begay-Windwhistle-Ildefonso soil types (Lammers, 1991). Vegetation is primarily big sagebrush, spiny hopsage, snakeweed, and blue grama. These soils form on alluvium and eolian deposits derived mainly from sandstones and at surface consist of reddish-brown fine sandy loam. Subsoils collected from 8 to 12 inches (20-31 cm) depth are yellowish-red, loamy, fine-grained sand.

Surface soil samples were collected at 1500-foot (500 m) intervals on a 16-square-mile (42 km^2) rectangular grid over and around Lisbon field (figure 5-11). A total of 307 samples were collected over the field and 101 samples off the field. The survey was then expanded to include the collection of soils at 656-foot (200 m) intervals on a grid of northwest-southeast and northeast-southwest lines over LDSE (figure 5-11). A total of 53 samples were collected over LDSE and 66 samples off the field. All sample location coordinates, geological units under the soil, and sample identification information are included in Appendix C – Lisbon-Lightning Draw Surface Geochemical Data.

The sample intervals chosen were based on the size of the fields themselves. The sampling grid and lines extend well beyond the proven limits of Lisbon and LDSE fields to ensure adequate background data. The areas chosen therefore sufficiently covered the gas caps, oil leg (present only at Lisbon), and background "barren" areas including the footwalls of the northeast-bounding normal fault and the southwest-bounding reverse fault of Lisbon and LDSE fields, respectively (figures 5-3 and 5-11).

Along the grid and lines, shallow (generally 8- to 12-inch [20-30 cm] deep) soil samples were collected with a spade or tree-planting shovel over a 6-square-foot area (0.6 m^2) at each site (figure 5-12A). Care was taken to avoid sampling material sluffed off the surface. The soils were placed and stored in airtight, Teflon-sealed glass soil jars to prevent hydrocarbon contamination during transport to the laboratory. In addition to the jar samples, soils were also collected in plastic Zip-loc bags for major/trace element and anion analyses. Some sample sites had to be offset because of lack of soil in outcrop areas. Evidence of surface alteration (for example, stressed vegetation) that could be attributed to hydrocarbon seepage and fracturing was also noted. Backup samples were also collected from each site and stored in plastic bags. Sample sites around wells were located topographically high relative to the well pad to reduce the possibility of contamination (figure 5-13).

At Lisbon field, 90 samples were collected around two gas wells in the gas cap, two productive oil wells in the oil leg, and two barren dry wells (figures 5-1 and 5-11), 15 samples at each well site. The two gas wells are the Lisbon No. C-910 well (SW1/4SE1/4 section 10, T. 30 S., R. 24 E., SLBL&M), which has produced 23,952 bbls of oil (3808 m^3) and 26.4 BCFG (0.75 BCMG), and the Lisbon No. D-810 (NW Lisbon USA No. A-2) well (NE1/4SE1/4 section 10, T. 30 S., R. 24 E., SLBL&M), which has produced 21,631 bbls of oil (3439 m^3) and 23.2 BCFG (0.66 BCMG) (Utah Division of Oil, Gas and Mining, 2008). The two oil wells are the Lisbon No. C-99 well (SW1/4SE1/4 section 9, T. 30 S., R. 24 E., SLBL&M), which has produced 503,915 bbls of oil (80,122 m^3) and 12.9 BCFG (0.37 BCMG), and the Lisbon No. D-716 well (SW1/4SE1/4 section 10, T. 30 S., R. 24 E., SLBL&M), which has produced 556,660 bbls of oil (88,509 m^3) and 10.2 BCFG (0.29 BCMG) (Utah Division of Oil, Gas and Mining, 2008). The barren dry wells include one to the west of the field in the water leg (the No. 21-4 Federal, NW1/4NW1/4 section 21, T. 30 S., R. 24 E., SLBL&M) and the other is northeast of the field on the low side of the fault which parallels the structure (the No. 1 State-Small Fry, NE1/4NW1/4 section 2, T. 30 S., R. 24 E., SLBL&M).

At LDSE field, 45 samples were collected around two gas wells over the gas cap and two barren dry wells (figures 5-5 and 5-11), 10 to 15 samples at each well site. The two gas wells are the Federal No. 1-31 well, which has produced 495 bbls of condensate (79 m^3) and 0.08 BCFG (0.002 BCMG) (currently shut-in), and the Evelyn Chambers Government No. 1 well, which has produced 3090 bbls of condensate (491 m^3) and 0.28 BCFG (0.01 BCMG) (Utah Division of Oil, Gas and Mining, 2008). The barren dry wells include the No. 2 White Rock Unit 1 well and No. 1 Hatch Wash Unit (NW1/4SE1/4 section 30, T. 30 S., R. 24 E., SLBL&M) north of the field in the water leg.

Collection of outcrop fracture-fill lichen, mosses, and soil: Joints in outcrops may provide pathways for hydrocarbon microseepage to the surface, which may be evident in the soils and vegetation that fill the joints (figures 5-6, 5-7, and 5-8). Thus, the sampling program was further expanded to collect soil and vegetative tissue samples from the joints for additional hydrocarbon and elemental analysis over barren and productive parts of both Lisbon and LDSE fields (figure 5-14).

Soil samples (33 samples, see Appendix C for details) from joints required the same amount (that is, 4 ounces [110 g]) of sample material as was taken along the grid, but they were harder to acquire. Representative samples were often only obtained by scraping sandy soil out of the joints with a stainless steel spoon, knife, or flathead screwdriver (figure 5-12). Where the joints were narrow with sparse soils or the soil zone especially shallow, this process frequently

required sampling along tens of feet in order to acquire enough material. Joints with established vegetation generally have deeper soils and better sampling opportunities.

Bryophytes and lichen commonly grow along thin joints in the area where there are higher than ambient amounts of moisture (figure 5-8). These plants may also show a geochemical signature in their tissues indicative of underlying hydrocarbons or subsurface mineralization, so they were also sampled (30 samples) to compare with the analyses of the soils that support them (figure 5-12). Two species of bryophytes and one species of lichen grow along joints in the area. The bryophytes fit into the genera *Grimmia* (possibly *Grimmia wrightii*) and *Bryum*. Both are common soil crust mosses. The lichen is *Collema tenax* – an abundant and common soil crust lichen in the intermountain western United States (Larry St. Clair, Monte L. Bean Life Science Museum, Brigham Young University, written communication, October 28, 2006).

Collection of 6-Foot-Deep Free-Gas Samples: Free-gas samples (see Appendix C for location and other details) were collected at 15- to 300-foot intervals (5-100 m) over LDSE field and in off-structure areas using the following protocol (figure 5-15):

1. Drill to at least a 6-foot (2 m) depth (10 feet [3 m] preferably) in unconsolidated overburden using the Geoprobe percussion (hammer) drill with 1-inch (2.54 centimeter) diameter pipe (figure 5-15).

2. Insert polyethylene tubing into rod and secure it to a retractable point at the bottom of the rod.

3. Purge the soil air at least three times with a plastic 40 cc syringe to clear the tubing of ambient air (figure 5-15).

4. Draw soil air (free gas) up using the syringe and force it into a 1-liter Tedlar bag (for hydrocarbon and fixed-gas analyses) and/or lead-lined CO_2 cartridge (for helium analysis).

Samples were collected from 6-foot (2 m) depth using the GeoProbe method to capture the in-situ soil air with minimal influence from dilution by atmospheric gases.

Laboratory Analysis

The surface soils, bryophytes, and lichen were dried at 122°F (50°C) and sieved to <63 microns. Equal splits of the sieved samples were then weighed out into air-tight 20 cc glass vials for thermal desorption at constant temperature for a constant time. Equal aliquots of headspace gas were injected into a Hewlett-Packard 5890 gas chromatograph with flame ionization and photo ionization detectors (GC-FID/PID) for analysis of 38 hydrocarbon compounds in the C_1 to C_{12} range (table 5-2; Appendix C). The organic carbon content of the samples was estimated using a gravimetric technique (loss on ignition [LOI]).

In addition, a solvent extract of sieved soil splits was analyzed by synchronous scanned fluorescence (SSF), which measures relative amounts of heavy (C_6 to C_{40}) aromatic hydrocarbons (Appendix C). Synchronous scanning fluorescence technique is a very cost-effective way to analyze soils for traces of the much heavier liquid hydrocarbons without the

high cost of elaborate extraction techniques and high-resolution gas chromatography. Solvent extracts of the soils are scanned from wavelengths of 250 nm to 500 nm. Hydrocarbons that fluoresce in oils are the ringed aromatic compounds and can be grouped by the number of (benzene type) rings chained together. These groups have fluorescence spectra maxima that increase in wavelength approximately with increasing ring numbers as shown in figure 5-16. Splits of the dried and sieved soil samples were also dissolved in aqua regia acid and the supernatant was analyzed for 53 major and trace elements (table 5-2) by inductively-coupled-plasma mass spectrometry and emission spectroscopy (ICP/MS and ICP/ES). Samples were also analyzed for seven anion species using a deionized water extraction and ion chromatography (table 5-2).

The free-gas samples were drawn from the Tedlar bags and cartridges with a 5-cc syringe and analyzed for 19 hydrocarbons in the C_1 to C_8 range using the GC-FID instrument (Appendix C). Gas from the Tedlar bags and lead-lined cartridges were also analyzed for fixed gases (CO_2, CO, O_2, N_2, He, and H_2) using a Varian CP-4900 gas chromatograph with a thermal conductivity detector (GC-TCD).

The precision and accuracy of the hydrocarbon, organic carbon, major/trace element, and anion analyses was between ±10 to 20% for a 95% confidence level based on the analysis of laboratory duplicates and standard reference materials at 10% frequency.

Interpretation and Mapping

The organic and inorganic data were compiled in an Excel spreadsheet for interpretation. The hydrocarbon and elemental compositions of near-surface soil gas and soils can reflect the character of subsurface petroleum accumulations and faults. It is important to identify and correlate the numerous near-surface compounds and elements with their sources—particularly petroleum accumulations. Different accumulations yield different near-surface compositional signatures, which can be used to determine if the accumulation is in the oil or gas range. Factor and discriminant analysis were used in this study to reduce the complex mixtures of organic and inorganic variables to a smaller number of interpretable variables.

Both factor and discriminant analysis are multivariate statistical tools that allow the evaluation of large numbers of data variables simultaneously. Multivariate analysis of the data was performed in Statistica 8.0. These multivariate tools permit the user to appreciate the existence of particular organic and inorganic associations that may reflect compositionally unique microseepage and mineralizing processes. In oil and gas exploration, this is important because the presence of oil or gas in the subsurface is rarely imaged by one or two variables.

Factor analysis summarizes the data set in a series of mathematical “vectors” or “factors,” which are combinations of co-varying variables in multivariate space. The derived factors (when combined together) account for all or most of the variation in the dataset, but in fewer variables than are in the dataset. For example, there may be 15 variables measured in a dataset, but these may be reduced to five factors, which account for most of the variance in the individual variables. Factors are ranked in descending order of the amount of variance they account for in the dataset. Factor 1 accounts for the most variance, factor 2 the second greatest, and so on. For each factor, it is possible to identify the mixture of variables (components) and their relative importance. In oil and gas producing basins, it is common for factor analysis to result in at least one factor reflecting a mixture of light (C_1 to C_4) hydrocarbons (that can be related to “gas”), and at least one reflecting a mixture of heavy (C_5 to C_x) hydrocarbons (that can be related to “oil”).

Factor loadings are the correlation coefficients between the variables and the factors. The more a variable is correlated with a particular factor (that is, correlated group of variables in multivariate space), the higher the factor loadings will be for that variable. Factors are plotted spatially as "factor scores," which represent the degree of correlation of variables in particular samples with the derived factors.

Forward, stepwise, discriminant analysis was used to discriminate the compositional character of microseepage over productive and barren areas using the C_1 to C_{12} hydrocarbon variables from soil samples over known productive and barren areas (that is, training sets). In the case of soil samples, the compositional character of the "adsorbed" microseepage over dry and barren areas reflects an alteration effect on soils as a result of continuous or episodic microseepage and hydrocarbon degradation over long periods of time. In essence, discriminant analysis is used to distinguish between the unique multi-component alteration signature imparted to soils over barren and productive areas from prolonged microseepage. The analysis derives a "discriminant function" or linear combination of variables that separates the compositional character of microseepage between "productive and barren" areas. The form of the discriminant function, also called a *canonical root*, is a latent variable which is created as a linear combination of discriminating (independent) variables, such that $L = b_1x_1 + b_2x_2 + ... + b_nx_n + c$, where the b's are discriminant coefficients, the x's are discriminating variables, and c is a constant. The discriminant coefficients are used to assess the relative classifying importance of the independent variables. If microseepage can be distinguished between "productive and barren" areas based on statistical significance tests (for example, Wilk's Lambda, F-tests) and cross-validation, then the discriminant function can be used to classify samples from "unknown" areas into productive or barren categories. The forward, stepwise, discriminant analysis eliminates variables from the function that have minimal influence on the discrimination based on F-test and Wilk's Lambda statistics. These predictions are represented as discriminant scores or probabilities of a particular sample falling into either barren or productive clusters.

In some cases, the absolute concentrations of organic and inorganic variables in soils and free gas can be spatially correlated with underlying hydrocarbon reservoirs, and may actually reflect charge in the reservoir rather than an "alteration-effect" on soils as a result of hydrocarbon microseepage over long periods of time. In the Lisbon study, absolute concentrations of organic and inorganic variables have been transformed to Z-scores to better evaluate contrast in the data. The Z-scores are derived by subtracting the population mean for a particular variable from the concentration of that variable for a particular sample and then dividing by the population standard deviation. This reduces the data to a mean of zero and the Z-scores then represent standard deviations above a mean of zero (that is, Standard Normal Distribution). In this study, the absolute concentrations of organic and inorganic variables over Lisbon are significantly higher than those over LDSE field possibly because of more intense microseepage and the presence of exposed uranium mineralization. Z-scores were therefore calculated separately for the Lisbon and LDSE datasets to more fully appreciate the subtle, but significant, anomalies at LDSE. The absolute concentrations (in parts per million and parts per billion) of hydrocarbons and fixed gases in free gas over LDSE are plotted, however, to emphasize the low concentration of species in these samples.

Organic and inorganic variables, and the factor and discriminant scores and free-gas concentrations are plotted on a geological background as proportional symbols using ArcGIS 9.2™. Only those variables and scores that show a spatial correlation with the Lisbon and/or LDSE fields are presented here. There are several inorganic variables, for instance, that are

spatially correlated with specific geological units (for example, rare earth element anomalies in soils over the arkosic Permian Cutler Formation), the meaning of which is beyond the scope of this study.

Results of the Geochemical Survey

The results of the study are very encouraging in that both organic and inorganic anomalies are spatially associated with parts of Lisbon and LDSE fields (table 5-3). Although several variables are anomalous over parts of the fields, only those most coherent anomalies will be presented. Throughout the presentation of results the number of anomalous samples relative to total number of samples over and off the field structures will be given to express the effectiveness of the various techniques for predicting oil and gas potential over Leadville reservoirs.

Thermally Desorbed Hydrocarbons (Surface Soils)

Absolute hydrocarbon concentrations: Several "live oil" hydrocarbon concentration anomalies are evident over both the Lisbon and LDSE areas relative to background "water-leg" areas (table 5-3). Toluene, for instance, is anomalous in the central part of the Lisbon field where normal faults are most abundant and closely spaced and also in the northwest part of the field on the west side of a normal fault (figure 5-17). The anomalies occur mainly over the Jurassic/Triassic Wingate Sandstone and Jurassic Kayenta Formation, but a few anomalous samples are also found over the Permian Cutler Group, Triassic Chinle Formation, and Jurassic Navajo Sandstone (figure 5-17). The anomalies cover 13% of the total samples over the field, and 6% of samples off the field also report as anomalous.

At LDSE field, toluene anomalies trend parallel to joint sets in Navajo Sandstone and over the reverse fault bounding the field to the southwest (figure 5-17). Anomalous samples comprise 13% of samples over the field and 12% of samples off the field. Anomalous samples occur over the Navajo (n = 10), Quaternary stream alluvium (n = 3), and the Slick Rock Member of the Jurassic Entrada Sandstone (n = 2).

Discriminant analysis results: Although several hydrocarbons in surface soils are spatially associated with the Leadville oil and gas fields, the anomalies are somewhat sporadic and some fall outside the limits of the fields. Discriminant analysis was therefore used to determine (1) if a linear combination of variables distinguishes microseepage over the oil and gas fields from that over the water legs, (2) which hydrocarbon variables best discriminate between oil, gas, and water production, (3) if discriminant scores (probabilities) better map the surface expression of the two fields, and (4) if separate discriminant functions for the fields predict one another (that is, cross-validate).

Three-component discriminant analysis: The first discriminant analysis model distinguishes hydrocarbon microseepage between the gas cap (samples at the Lisbon No. D-810 well), oil leg (samples at the Lisbon No. C-99 well), and water leg (several samples) at Lisbon field (figure 5-18). In this model, the microseepage over the gas cap is distinguished from that over the oil and water legs, and pentane, benzene, and propane are the most important variables for this discrimination (figure 5-19). The microseepage character of the less productive oil leg shows

less distinct separation from the water leg than the gas cap does (figure 5-19). Toluene contributes most to the weak discrimination of microseepage between the Lisbon oil and water legs. Soils around the very productive Lisbon No. C-910 gas well (table 5-1) and other parts of the gas cap predict as gas-prone and dry wells predict as dry.

Soil samples that fall into the "gas" category cluster mainly in the upper part of the Lisbon anticline where most of the gas production comes from (figure 5-19). Anomalous samples make up 16% of samples over the field and 7% of samples off the field (table 5-4). The anomalies are clustered in the normal-faulted, east-central part of the field, along the northeastern faulted margin of the field, and west of a normal fault in the northwest part of the field (figure 5-19). The anomalies mainly occur over the Wingate and Kayenta Formations, but sporadic anomalies are also found over the Cutler Group, Chinle Formation, and Navajo Sandstone.

Two samples over Navajo Sandstone and Quaternary stream alluvium near the top of the LDSE anticline also predict as having "Lisbon gas" type compositional character (figure 5-19). These comprise a smaller proportion of the samples over the field compared with Lisbon field, but none of the samples off the field are incorrectly classified as having "Lisbon gas" character (table 5-4).

Samples around the Lisbon No. D-716 oil well, Federal No. 1-31 gas well, and Evelyn Chambers No. 1 gas/condensate well are predicted as oil-prone (figure 5-20). The anomalous samples comprise 7% of the samples over Lisbon field and 8% of the samples over LDSE field, and none of the samples are incorrectly classified over either field (table 5-4). Anomalous samples over Lisbon occur over Navajo Sandstone and those over LDSE field are over Quaternary stream alluvium.

Two-component discriminant analysis: The second discriminant analysis model tests for differences in microseepage between productive "gas/oil" parts of Lisbon field and the water leg (figure 5-21). Samples around productive wells (Federal No. 1-31 and Evelyn Chambers No. 1) in LDSE field are also compared with the Lisbon water-leg samples (figure 5-21). Ethane and *n*-butane are important variables for discriminating between the productive part of Lisbon and the water leg.

Samples with anomalous Lisbon gas/oil probabilities (that is, samples with similar compositional character to productive parts of Lisbon field) comprise 20% of Lisbon field samples and there is a clustering of anomalies in the central, northwest, and southeast parts of the field (figure 5-22; table 5-4). A smaller proportion of anomalous samples (12%) fall outside of the productive limits of the field. The majority of anomalous samples within the field are over the Wingate and Kayenta Formations and isolated anomalies within and outside the field occur over Quaternary stream and eolian deposits, and the Cutler Group, Chile Formation, and Navajo Sandstone. At LDSE, 26% of samples over the field are predicted as having productive "Lisbon-like" compositional character (figure 5-22; table 5-4). Three anomalous samples (5% of samples off the field) are also evident off the field to the northeast (figure 5-22; table 5-4). Two of the 17 anomalous samples occur over Navajo Sandstone and the remainder are over Quaternary stream alluvium.

The microseepage over the productive part of LDSE field is distinct from that over the Lisbon water leg, and ethane and *n*-butane again are the most influential discriminating variables (figure 5-23). Ethylene, methane, pentane, and propane are also important variables for discrimination. Samples with anomalous LDSE gas probability comprise 38% of samples over

the field and 3% of samples off the field (figure 5-23; table 5-4). One of the 20 anomalous samples occurs over Navajo Sandstone, and the remaining samplers are situated over Quaternary stream alluvium. A smaller proportion of samples over and off Lisbon field predict as having "LDSE-like" compositional character (figure 23; table 5-4). Anomalies over the field are mainly over Wingate and Kayenta Formations with one sample situated over Navajo Sandstone. The two samples outside the productive limits of the field occur over the Wingate and Chinle Formations.

Thermally Desorbed Hydrocarbons (Outcrop Fracture-Fill Lichen and Soils)

Several hydrocarbons are anomalous in outcrop fracture-fill lichen and soils over Lisbon and LDSE fields as opposed to the Lisbon water-leg (table 5-3). As for the surface soils, discriminant analysis was performed on thermally desorbed C_1 to C_{12} data from the outcrop lichen and soils to determine if the microseepage over Lisbon and LDSE fields is compositionally distinct from that over the Lisbon water leg and, if so, to identify which variables contribute most to the discrimination. It is also important to determine if discriminant functions developed for both fields predict each other (that is, cross-validation). The discriminant scores (probabilities) are again plotted to evaluate the spatial association of anomalies with productive and non-productive areas.

Outcrop fracture-fill lichen: Outcrop lichen samples over the gas cap, oil leg, and water leg at Lisbon field were analyzed for compositional differences in a three-component discriminant model, and then samples over LDSE field were compared with those over the Lisbon water leg (figure 5-24). Lichen samples over the Lisbon gas cap, oil leg, and water leg are clearly different in terms of their compositional character as shown on the canonical score plot in figure 5-25. The canonical scores for each sample in the plot are derived by inserting the hydrocarbon concentrations into the two discriminant functions (that is, Roots 1 and 2). In the case of outcrop lichen, methane contributes most to the discrimination of the gas cap from the oil and water legs, and propane is the most important variable for separating the oil leg from the gas cap and water leg (figure 5-25). One of the seven lichen samples (14%) over the top of the LDSE anticline (that is, near the Federal No. 1-31 gas well) falls into the productive Lisbon gas cap category (figure 5-25; table 5-5). Three out of seven (43%) lichen samples at a lower structural level on the anticline (that is, near the Evelyn Chambers No. 1 gas/condensate well predict to have Lisbon oil leg compositional character (figure 5-26; table 5-5).

When the lichen samples over LDSE gas field are compared with those over the Lisbon water leg, nine of eleven (82%) samples over the productive parts of the Lisbon field are predicted as having LDSE gas potential (figure 5-27; table 5-5). Important variables that contribute to the distinction between samples over LDSE field and the Lisbon water leg are ethane, *n*-hexane, propane, ethylene, *n*-butylbenzene, and ethylbenzene (figure 5-27).

Outcrop fracture-fill soils: The same discriminant models were tested on C_1 to C_{12} data from outcrop fracture-fill soils collected over the Lisbon gas cap, oil leg, and water leg, and LDSE field with the only difference being that more soils were available over the Lisbon gas cap than were lichen samples (compare figures 5-24 and 5-28). The compositional character of microseepage between the Lisbon gas cap, oil leg, and water leg is even more distinct (that is, more separation between canonical score clusters) than that shown by the lichen training set

samples (compare figures 5-25 and 5-29). As for the outcrop lichen samples, variables in outcrop soils that contribute most to the discrimination of the gas cap and oil leg are methane and propane, respectively. A higher percentage of the outcrop soils over the LDSE field (71%) predict as Lisbon gas-prone as compared with that predicted by the lichen samples (14%). None of the outcrop soils over LDSE fall into the Lisbon oil leg category (figure 5-30; table 5-6).

Outcrop soils over LDSE field are compositionally distinct from the Lisbon water leg, but fewer of the Lisbon field outcrop soils (50%) predict as Lighting Draw Southeast gas as compared with the 82% of the Lisbon lichen samples that predicted as LDSE gas-prone (figure 5-31). Variables that significantly contribute to the discrimination of microseepage in outcrop soils over LDSE field and the Lisbon water leg are *n*-pentane, *n*-butane, and ethylbenzene.

Fluorescence of Solvent-Extractable Aromatic Hydrocarbons (Surface Soils)

Lisbon oil samples (from Lisbon No. C-99 and Lisbon No. D-716 wells) have condensate to medium gravity oil fluorescence spectral patterns, and they can therefore be classified as "light oils" (figures 5-32a and 5-32b). Background and anomalous fluorescence patterns are clearly distinguished in surface soils. In background areas, peak wavelengths are low intensity and below the 300 nm single-ring aromatic wavelength (figures 5-16 and 5-32c). Synchronous scanned fluorescence spectra in anomalous areas are more intense and extend to longer, multi-ring aromatic wavelengths (figures 5-32d and 5-32e). Soil samples with these anomalous spectra contain light oil that has been weathered through chemical and biological oxidation processes. As weathering progresses, the once fresh light oil (as in figures 5-32a and 5-32b) gradually loses its light single and double ring aromatic compounds leaving a residue of 3- to 6-ring aromatics that fluoresce in the 395 to 470 nm range (figures 5-32d and 5-32e). Asphalt dust from paved roads can add intensity to peaks in the 350 to 450 nm range thereby producing false anomalies (figure 5-32f). Soil samples collected near paved roads in this study were therefore removed from the database prior to interpreting the SSF data.

Factor analysis reveals high loadings for the 395 nm, 431 nm, and 470 nm peaks (that is, heavy 4- to 6-ring aromatic residue in weathered light oil). Samples with high correlation of these fluorescence peaks (that is, high 395 to 470 nm factor scores) are clustered in the central and eastern part of Lisbon field where closely spaced normal faults are most abundant (figure 5-33). One anomaly cluster, in the central part of the field, is parallel to a northeast-oriented normal fault in the Lisbon anticline and the joint set in the oil leg (figure 5-33). Most anomalies occur over Wingate Sandstone, but isolated anomalies are also found over the Chinle, Kayenta, and Navajo Formations. Anomalous samples comprise 10% and 3% of the samples over and off the field, respectively.

Anomalous 395 to 470 nm factor scores are also evident in 17% of the samples over LDSE field, and orientation of the 0.6-mile-long (1-km) anomaly in the southeast part of the field is sub-parallel to joint sets in Navajo Sandstone (figure 5-33). They occur mainly over Quaternary stream alluvium with the exception of the southeasternmost anomaly, which is situated over Navajo Sandstone (figure 5-33).

Hydrocarbons and Fixed Gases (Free-Gas Samples)

Hydrocarbon concentration anomalies in free-gas samples show a distinct spatial correlation with productive parts of LDSE gas field. For example, high-contrast propane

anomalies are evident in three samples (19%) over a distance of 600 feet (200 m) (figure 5-34, table 5-7). Isohexane is also anomalous in two adjacent samples over a distance of 450 feet (150 m) and in one isolated sample over the gas field (figure 5-35). None of the free-gas samples off-structure are anomalous in hydrocarbons (figures 5-34 and 5-35). Hydrogen is anomalous in six (38%) samples for a distance of 1200 ft (400 m) over the top of the LDSE anticline and in one (7%) sample off-structure (figure 5-36, table 5-7). Carbon dioxide, which is a significant component of the produced gas (table 5-1), is anomalous in eight (50%) free-gas samples for a distance of 1500 feet (500 m) over the LDSE anticline and in four (27%) samples off-structure (figure 5-37, table 5-7). Helium, which is also concentrated in the produced gas (table 5-1), is above ambient levels (>5.2 parts per million [ppm]) in six samples off-structure at LDSE field and in three samples over the water leg of Lisbon field (figure 5-38). This represents 60% of the samples collected off the LDSE field (table 5-7).

Acid-Extractable Metals (Surface and Outcrop Fracture-Fill Soils)

Major and trace element anomalies in surface and outcrop soils and lichen are evident over both Lisbon and LDSE fields (table 5-3). A larger variety of trace metals are anomalous in surface soils over LDSE compared with soils over Lisbon. Elements that show a distinct spatial correlation with Lisbon and/or LDSE fields are cadmium, uranium, molybdenum, vanadium, manganese, lead, mercury, and organic carbon (table 5-8).

Factor analysis reveals two heavy metal element associations that are spatially associated with Lisbon and LDSE fields. The first factor has high loadings for cadmium, uranium, and molybdenum, and moderate loadings for vanadium, manganese, and lead (figure 5-39). Samples that show correlation of these elements form a 1.2-mile-long (2 km), northeast-trending anomaly cluster mainly over the Chinle Formation along a canyon in the east-central part of Lisbon field (figure 5-39). The canyon has a similar orientation to the dominant joint set in Navajo Sandstone over the Lisbon oil leg (figure 5-39). These anomalous samples comprise 3% and 2% of the samples over and off Lisbon field, respectively. A higher proportion of anomalous samples are evident in Quaternary stream alluvium over LDSE field (figure 5-39, table 5-8). The 0.6-mile-long (1 km) anomaly over the southeast half of the field is subparallel to joint sets in Navajo and it is spatially correlated with heavy aromatic hydrocarbon anomalies shown in figure 5-33. Only 3% of samples off the field report as anomalous and these occur over Quaternary stream alluvium and Navajo (figure 5-39; table 5-8).

The second factor shows high loadings for mercury, organic carbon, and lead. These elements are correlated (that is, factor scores >1) in 12% and 8% of samples over and off Lisbon field, respectively (figure 5-40, table 5-8). Anomalies are evident mainly over the Wingate and Kayenta Formations in the upper part of the Lisbon anticline (figure 5-40). Although the anomalies are clustered in the northwest, central, and southeast parts of the field, their overall trend is northwest, which is similar to the joint set in Wingate sandstones. A higher proportion of anomalous samples are evident over LDSE field and, as for the heavy aromatic hydrocarbons and cadmium-uranium-molybdenum-vanadium-manganese-lead (Cd-U-Mo-V-Mn-Pb) element association, the anomalies cluster over the southeast half of the field (figure 5-40, table 5-8). The majority of the anomalous samples occur over alluvium, but two anomalies are also situated over Navajo Sandstone. The trend of the anomalies is similar to the joint sets in Navajo outcrops. A small proportion of the anomalous samples fall outside of LDSE field (table 5-8).

Fluoride is anomalous in 38% of surface soils over LDSE field and 4% of soils off the field. The anomalies, which roughly parallel the northwest joint sets, are confined to Quaternary alluvium and cluster near the Federal No. 1-31 and Evelyn Chambers No. 1 wells and in the central part of the field. In comparison, only a small proportion of samples on and off the Lisbon field are anomalous in fluoride (figure 5-41, table 5-8). Anomalies at Lisbon field occur over Quaternary stream and eolian deposits and the Cutler Group, Wingate Sandstone, Kayenta Formation, and Navajo Sandstone.

Arsenic is anomalous in 49% of surface soils over LDSE field and 15% of soils off the field. The anomalies occur over Quaternary stream and eolian alluvium deposits and the Navajo Sandstone and Carmel Formation. The anomalies trend both northwest and northeast, which is parallel to the major joint sets. In comparison, only one sample over the Chinle Formation on Lisbon field is anomalous in arsenic (figure 5-42).

Discussion

The main objective of this study was to determine if low cost, surface geochemical methods are applicable to Leadville Limestone hydrocarbon exploration. Our data show that all of the methods tested result in anomalies that are spatially correlated with Lisbon and LDSE fields. Before any conclusions can be drawn, however, further discussion of the results is necessary to explore possible origins for the observed anomalies. The following observations in particular require further discussion.

Hydrocarbon Anomalies

Aromatic and alkane hydrocarbon anomalies are spatially correlated with both Lisbon and LDSE fields. There is a clustering of anomalies in the central part of Lisbon where normal faults are more abundant and clusters are also evident west of a normal fault at the northwest end of the field. At Lighting Draw Southeast, the anomalies trend parallel to the field-bounding reverse fault and anomaly clusters are evident near the Federal No. 1-31 and Evelyn Chambers No. 1 wells, and also off structure. The fluorescence spectral pattern of aromatic hydrocarbon anomalies suggests the presence of weathered light oil in the soil samples. These hydrocarbon anomalies could represent (1) surface contamination developed over past and present production at Lisbon and LDSE fields, and/or (2) the surface expression of past and present hydrocarbon microseepage along joints in sub-cropping sandstones. Factors that favor surface contamination as a source of the anomalies are that anomalies are found in proximity to producing and shut-in well sites and some anomalies are situated downwind of producing well sites. Factors that preclude surface contamination as a source of the anomalies are:

1. While some anomalies occur near production, there are several productive and shut-in wells without hydrocarbon anomalies in soils.

2. There are strong toluene anomalies in soils over the northwest part of Lisbon field that are upwind of production.

3. The heavy aromatic (3- to 6-ring) hydrocarbon anomaly over the southeast half of LDSE field extends for 0.6 mile (1 km) upwind of the Evelyn Chambers No. 1 gas/condensate well.

The anomalies most likely therefore represent volatile and liquid hydrocarbon seeps that ascend along joints in outcropping and sub-cropping sandstones with possible control by the crosscutting normal faults at Lisbon field and the bounding reverse fault and joint sets at LDSE field. The hydrocarbon anomalies are subparallel to preferred joint orientations and the majority of anomalies are found in northwest-trending stream alluvium. This northwest-trending channel is a major topographic feature in the area, which may reflect an underlying fault.

Discriminant Analysis Models

Discriminant analysis is a useful tool for distinguishing the microseepage over Lisbon and LDSE fields from that of the Lisbon water leg. There is a compositional link between microseepage at Lisbon and Lighting Draw Southeast as demonstrated by the various discriminant models using different sample media. Variables that most influence the distinction between productive and water-wet areas are mainly light hydrocarbons in the C_1 to C_6 range, and this is not surprising considering the composition of the produced gas and that lighter volatile hydrocarbons have a better chance of making it to the surface. The three-component discriminant model for Lisbon field, which compares samples around individual gas and oil wells with those over the water leg correctly predicts a few samples over LDSE field as having gas or oil potential. The two-component model, which compares an array of samples over the gas cap and oil leg of Lisbon with the water leg, predicts hydrocarbon potential in significantly more samples over LDSE. Rather than only using samples collected at well sites as training sets, a better approach is therefore to use an array of samples that are more representative of microseepage over the productive area. This is important from an exploration standpoint because small targets like LDSE are easier to find if more samples are predicted as having hydrocarbon potential. In the subsequent model, which compares samples over LDSE field with those over the Lisbon water leg, several samples over Lisbon field are predicted as having hydrocarbon potential. The fact that both Leadville fields predict one another adds confidence to the discriminant models and implies that they can be used in untested areas of the Paradox Basin to assess hydrocarbon potential in Leadville Limestone.

The outcrop fracture-fill soils and lichen better discriminate between the Lisbon gas cap, oil leg, and water leg than do the surface soils. In both outcrop lichen and soils, the most important variable for predicting gas and oil are methane and propane, respectively. The better discrimination power of these sample media probably reflect the fact that they are situated directly on the avenues for ascending microseepage. The outcrop soils better predict the gas-prone nature of LDSE field using Lisbon gas-cap samples as a training set. On the other hand, the outcrop lichen better predict the productive gas cap at Lisbon using LDSE samples as a training set.

Free Gas Results

More direct evidence of current-day hydrocarbon seepage over LDSE field is provided by the high contrast, light (C_2 to C_6) alkane hydrocarbon anomalies in free-gas samples. These hydrocarbon anomalies are encompassed by more extensive hydrogen and carbon dioxide anomalies (figure 5-43). Anomalous helium ($\pm$ CO_2 and H_2) concentrations in free-gas samples are only found outside the productive limits of LDSE and Lisbon fields (figure 5-43).

The source of the hydrocarbons, carbon dioxide, and hydrogen anomalies over LDSE field could be (1) weakly productive intervals in the upper and lower Ismay zone, (2) very productive intervals within the Leadville Limestone, or (3) a combination of both reservoirs. The anomalous carbon dioxide over the reservoir could reflect input from the oxidation of Pennsylvanian and/or Mississippian hydrocarbons and Mississippian carbon dioxide. The fact that the carbon dioxide anomaly is wider than the hydrocarbon anomaly favors input from an additional Mississippian source. Hydrogen is actually a common constituent of oil and gas reservoirs (Zinger, 1962), and it could therefore be derived from the Ismay and/or Leadville reservoirs. Hydrogen could certainly come from the Leadville considering its small molecular size and mobility in the subsurface. Helium, which is strongly enriched in produced Leadville gas, is only anomalous over the margins of the LDSE and Lisbon reservoirs. This fact could imply that the hydrocarbons, carbon dioxide, and hydrogen over the productive part of LDSE field are mainly sourced in the Ismay zone. The helium ($+CO_2$) at the margins of the reservoirs may ascend along fractured zones at the margins of salt diapers formed as a result of subsidence. Helium anomalies in free gas around the Red Wing Creek oil field in North Dakota were documented by Pogorski and Quirt (1981). Fracture zones at the margins of oil and gas reservoirs have also been implicated as a source of the halo anomalies around oil and gas fields (Duchscherer, 1984, 1986).

Trace Metal and Anion Results

The Cd-U-Mo-V-Mn-Pb element association observed over productive parts of Lisbon and LDSE fields may have separate origins and emplacement mechanisms. Anomalies in the canyon with exposed Chinle Formation and the historic uranium mine workings (Wood, 1968; Chenoweth, 1990, 1996) are probably sourced from the Chinle and mine tailings (figure 5-44). This is supported by the fact that the strongest uranium anomalies (up to 43.4 ppm) are spatially correlated with abandoned mine shafts and adits and exposed Chinle in the canyon (figure 5-44).

The anomalous element association is also evident in Quaternary stream alluvium over LDSE field where it also correlates with anomalous heavy aromatic hydrocarbons. The source of this anomaly could be (1) mechanical and chemical dispersion of these elements from abandoned uranium mines in the Salt Wash Member of the Jurassic Morrison Formation 3 miles (5 km) to the east (figure 5-44) or (2) from the underlying Chinle Formation. Factors in support of chemical dispersion from Salt Wash uranium deposits are (1) the anomalies are in a stream channel that accesses exposed uranium mineralization and oil workings, (2) there is one anomaly off structure and up drainage of LDSE field, and (3) there is an organic carbon build-up (high LOI and heavy aromatics) over the southeast part of the field, which would act as a sink for mechanically and chemically dispersed metals. Factors that negate the Salt Wash uranium deposits as a source of the anomalies in stream alluvium are (1) the uranium contents of the soils are very low (<1.1 ppm), (2) it is unlikely that all of these elements would chemically disperse and precipitate together to form anomlies that are compositionally similar to the Chinle, and (3) there should be more anomalies in upstream areas if the elements were mechanically and chemically dispersed from the Salt Wash deposits on Deerhead Mesa to the south. A more likely source of the multi-element anomaly is the underlying Chinle. The Evelyn Chambers No. 1 well intersected 98 feet (30 m) of the Chinle. Hydrocarbon and brine fluids that ascended a probable fault underlying the northwest-trending channel probably leached and transported these heavy metals to the surface. Mercury, lead, and fluoride are also spatially associated with the anomaly

over the southeast part of the field and a similar origin is therefore invoked. The fluoride anomalies could reflect ascending brines, and the mercury and lead could be derived from the oil seep itself or perhaps the organic-rich black shales of the Paradox Formation it ascends through. The source of the wider dispersed arsenic anomaly over and around LDSE field is unclear. Trace amounts of arsenic are present in crude oil samples, so perhaps this is its source.

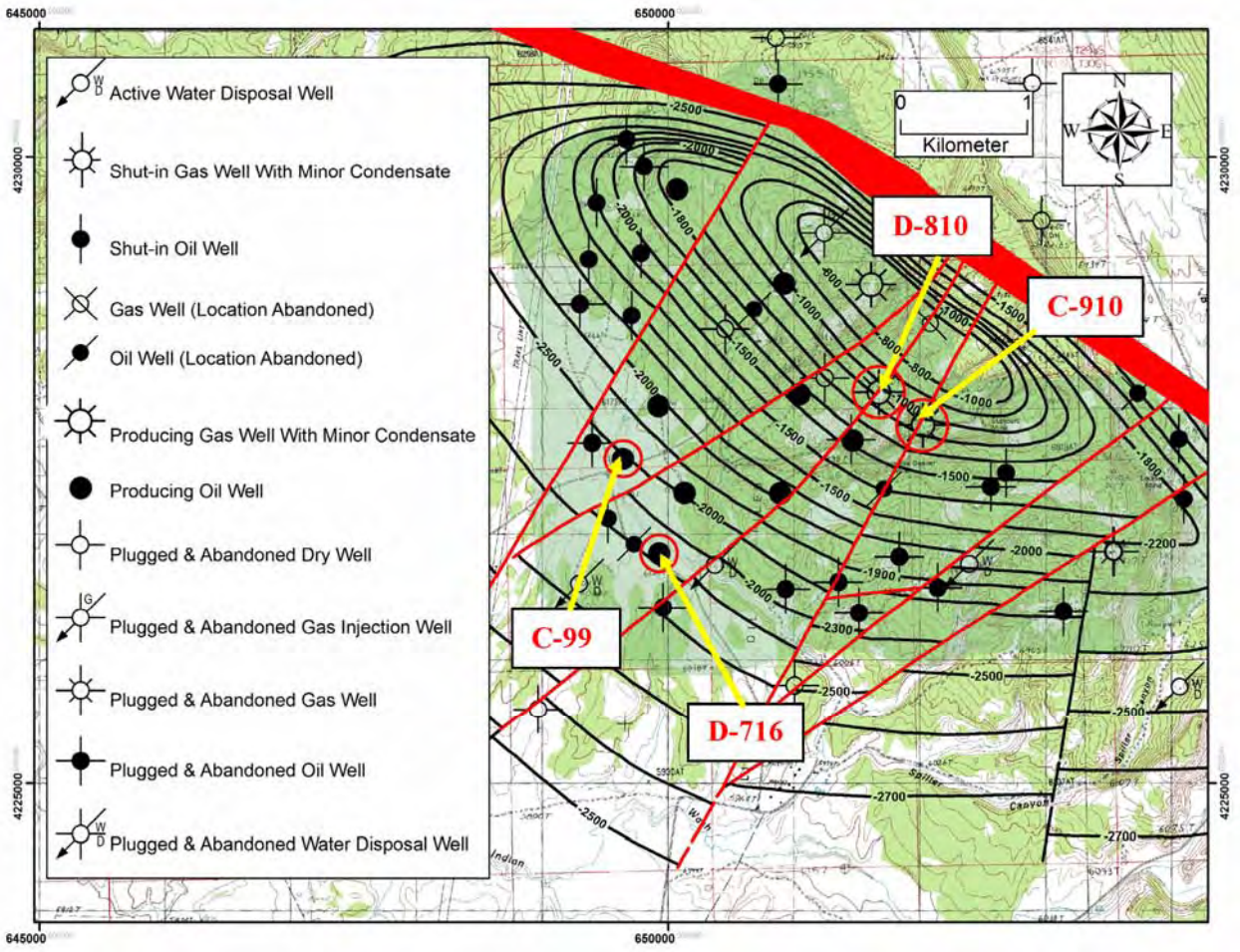

Figure 5-1. Structure contour map of the Leadville Limestone, Lisbon field, San Juan County, Utah (modified from C.F. Johnson, Union Oil Company of California files, 1970; courtesy of Tom Brown, Inc.), superimposed over the topographic base; the contour interval is 100 feet and the datum is sea level. Included on the map are well locations (well sites identified where detailed sampling was conducted); Lisbon oil field outline shaded bluish green. Base map: La Sal 30' X 60' topographic quadrangle map, U.S. Geological Survey. See figure 1-3 for location of Lisbon field in the Paradox Basin.

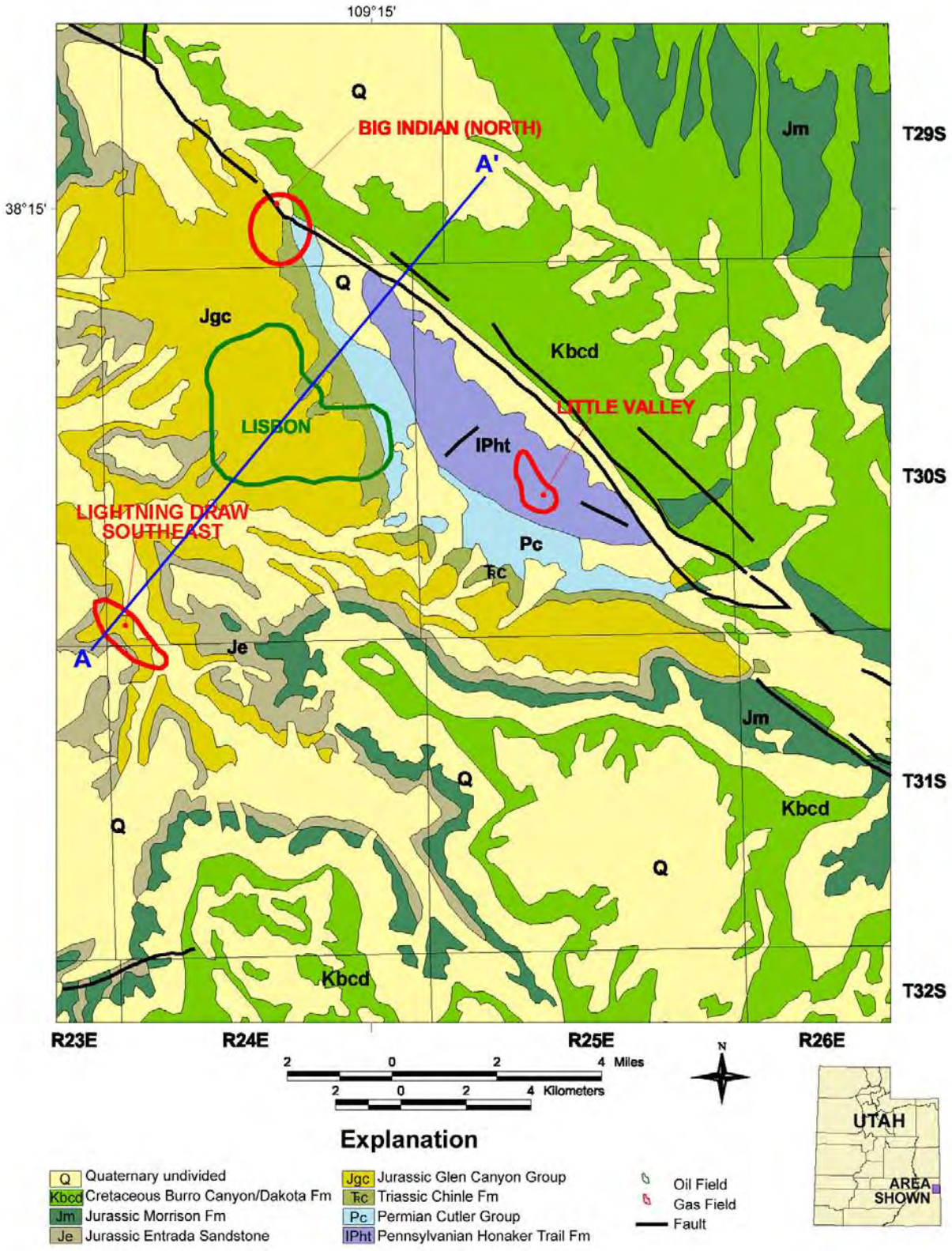

Figure 5-2. General surface geology of the Lisbon field area (modified from Hintze and others, 2000). Cross section A-A' shown on figure 5-3.

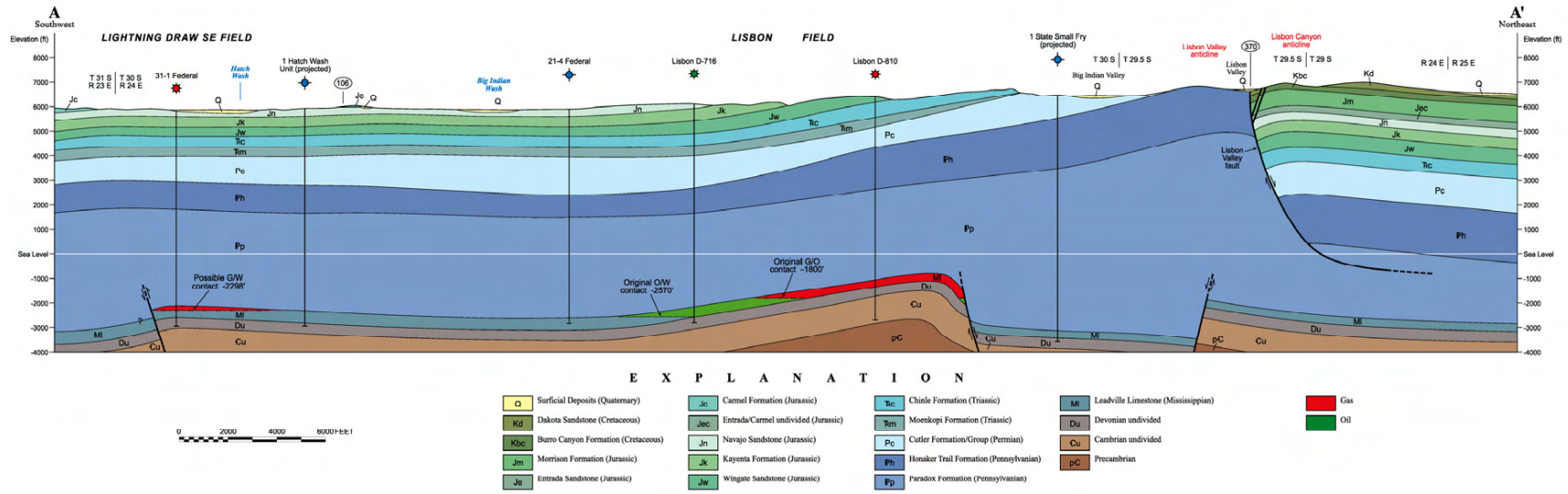

Figure 5-3. Detailed cross section through the Lisbon and Lightning Draw Southeast fields showing the fault-bounded Leadville Limestone hydrocarbon reservoirs. Line of section shown on figure 5-2. G/O contact = gas-oil contact, O/W contact = oil-water contact, G/W contact = gas-water contact.

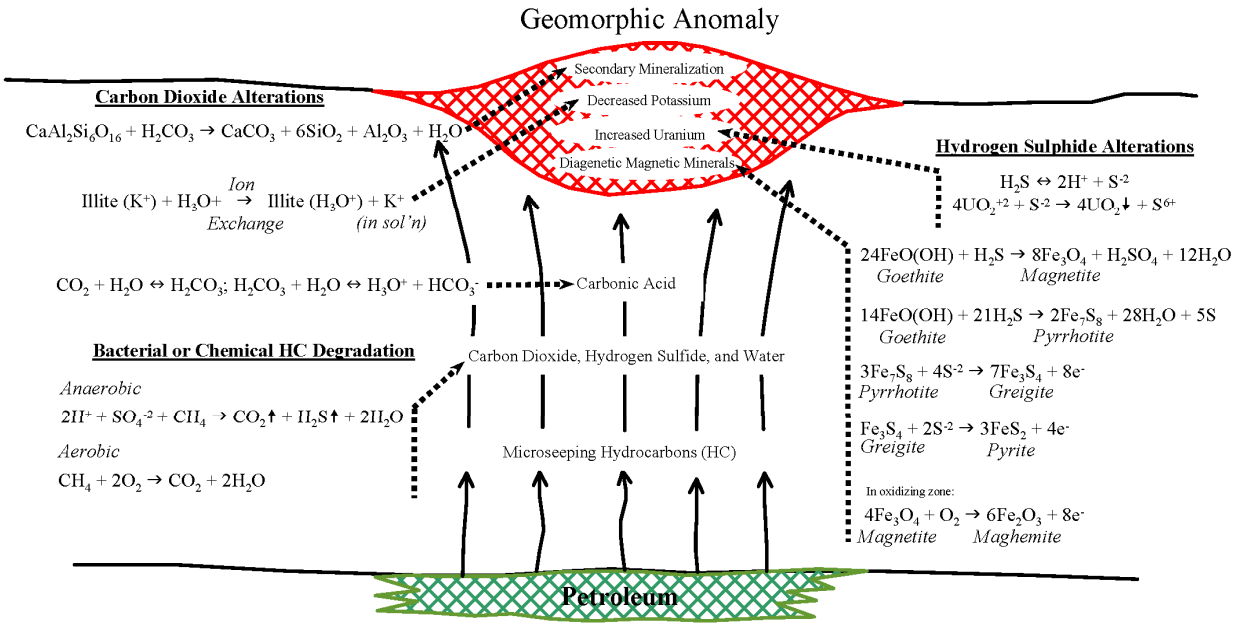

Figure 5-4. Model of hydrocarbon microseepage-related alteration over petroleum deposits (modified after Saunders and others, 1999).

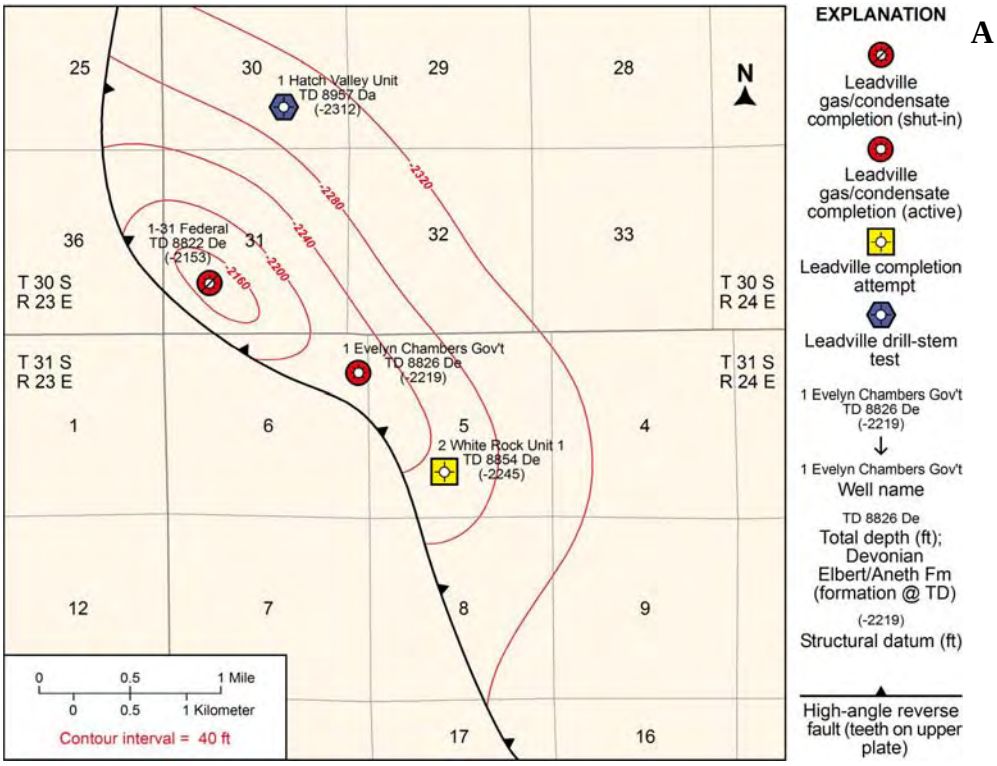

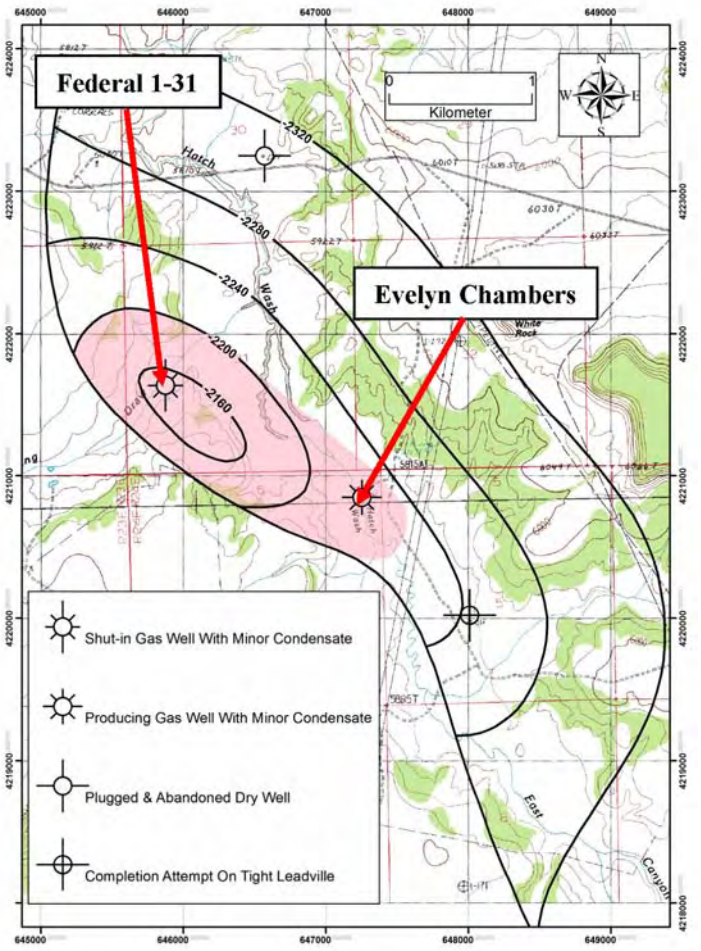

Figure 5-5. A – Structure contour map of the Leadville Limestone, Lightning Draw Southeast field, San Juan County, Utah (modified from a fault map provided courtesy of ST Oil Company). B – Top of structure of the Leadville Limestone superimposed over the topographic base, well locations (well sites identified where detailed sampling was conducted), and Lightning Draw Southeast field outline (shaded pink). The contour interval is 40 feet and the datum is sea level. Base map: La Sal 30' X 60' topographic quadrangle map, U.S. Geological Survey. See figure 1-3 for location of Lightning Draw Southeast field in the Paradox Basin.

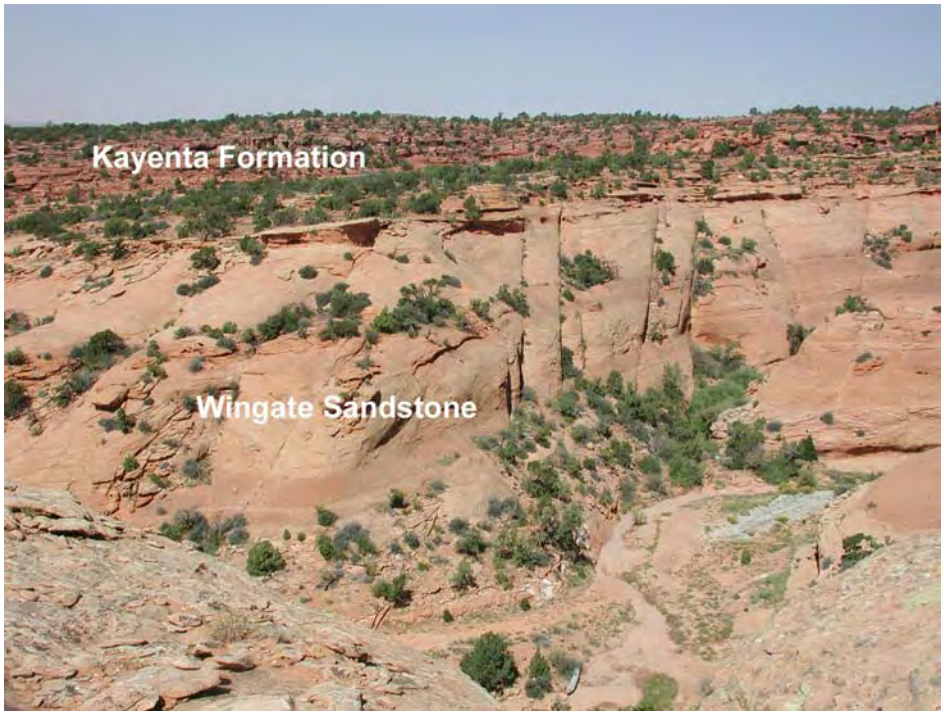

Figure 5-6. Subvertical joints in the Jurassic Wingate Sandstone from Lisbon field; view to the northwest. The contact with the overlying Jurassic Kayenta Formation is sharp. Note that the continuation of these joints into the Kayenta is not as obvious.

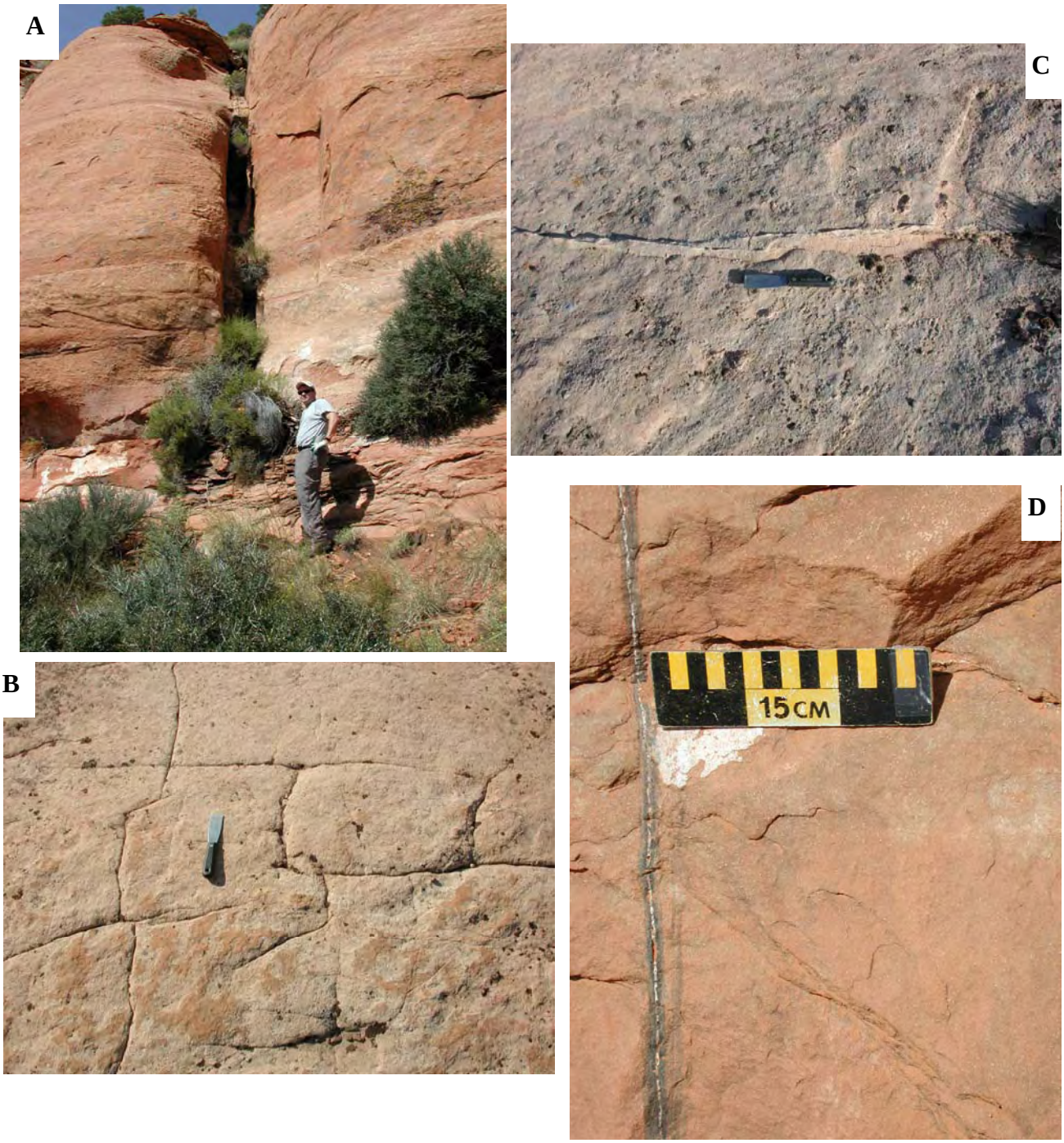

Figure 5-7. Examples of joints in the Lisbon field area. A – Large, probable region-scale joint in the Wingate Sandstone over the gas cap. B – Blocky or rectalinear joint sets in the Navajo Sandstone over the water leg. C – Thin silica vein in a joint over the water leg. D – Very thin calcite vein with a halo of possible iron/manganese-bearing minerals over the gas cap. Figures 5-7A and 5-7D are near the Lisbon No. C-910 well (SW1/4SE1/4 section 10, T. 30 S., R. 24 E., SLBL&M); figures 5-7B and 5-7C are near the No. 21-4 Federal well (NW1/4NW1/4 section 21, T. 30 S., R. 24 E., SLBL&M).

Figure 5-8. Bryophytes (mosses) and lichen that commonly grow along thin, moisture-rich joints in sandstone outcrops in the Lisbon area. A – Close-up of bryophytes (Grimmia [possibly Grimmia wrightii] and Bryum) and lichen (Collema tenax) along a joint in the Wingate Sandstone near the Lisbon No. D-810 (NW Lisbon USA No. A-2) well (NE1/4SE1/4 section 10, T. 30 S., R. 24 E., SLBL&M) over the gas cap of Lisbon field. B – Bryophytes and lichen along a thin joint in the Jurassic Navajo Sandstone over the oil leg of Lisbon field. The Lisbon No. D-716 well (SE1/4NE1/4 section 16, T. 30 S., R. 24 E., SLBL&M) and southwest dipping flank of the Lisbon anticline (Kayenta Formation) are in the background. C – Bryophytes and lichen along curvilinear, polygonal joints in the Navajo Sandstone near the No. 21-4 Federal well (NW1/4NW1/4 section 21, T. 30 S., R. 24 E., SLBL&M) over the water leg of Lisbon field.

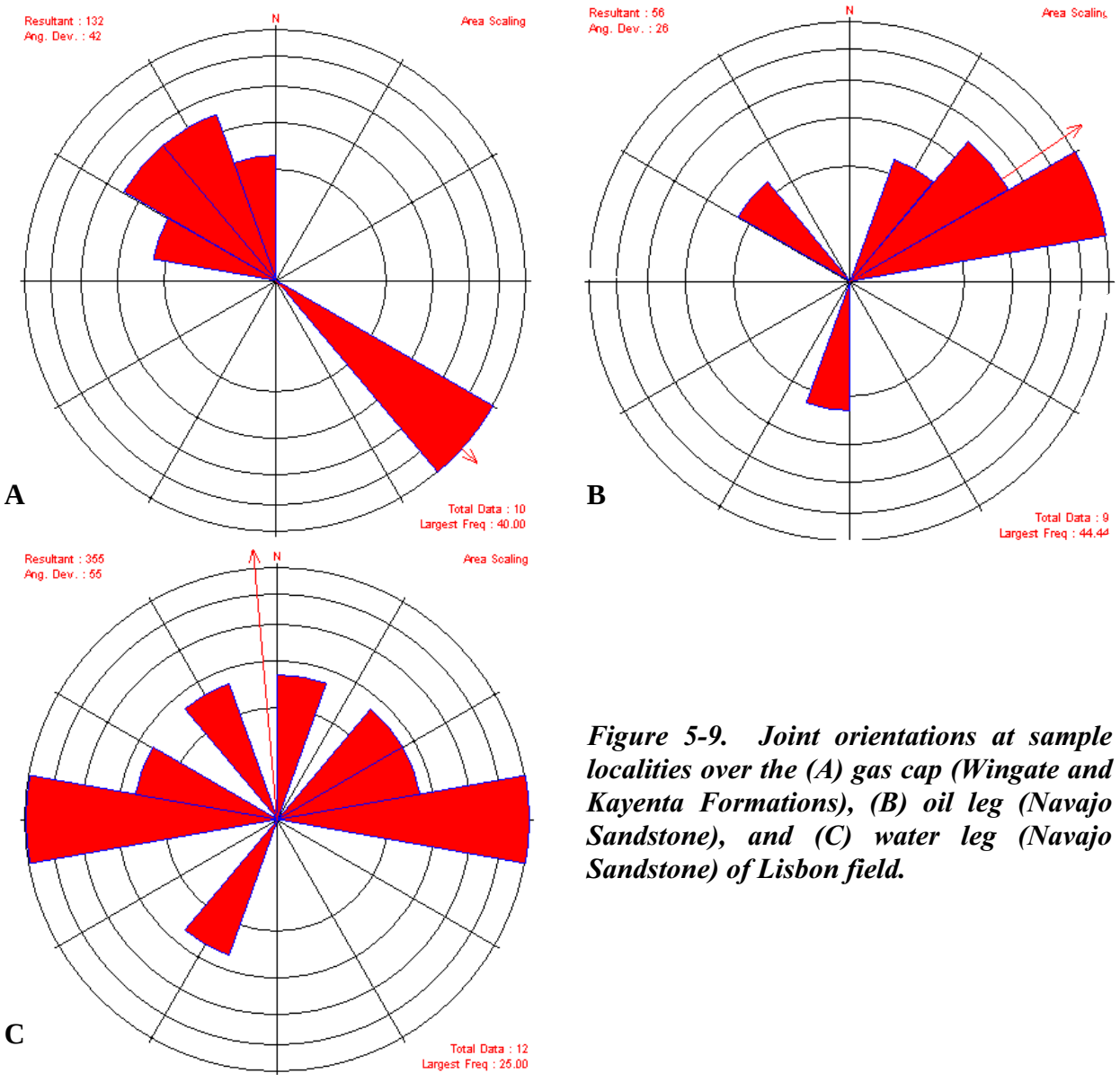

Figure 5-9. Joint orientations at sample localities over the (A) gas cap (Wingate and Kayenta Formations), (B) oil leg (Navajo Sandstone), and (C) water leg (Navajo Sandstone) of Lisbon field.

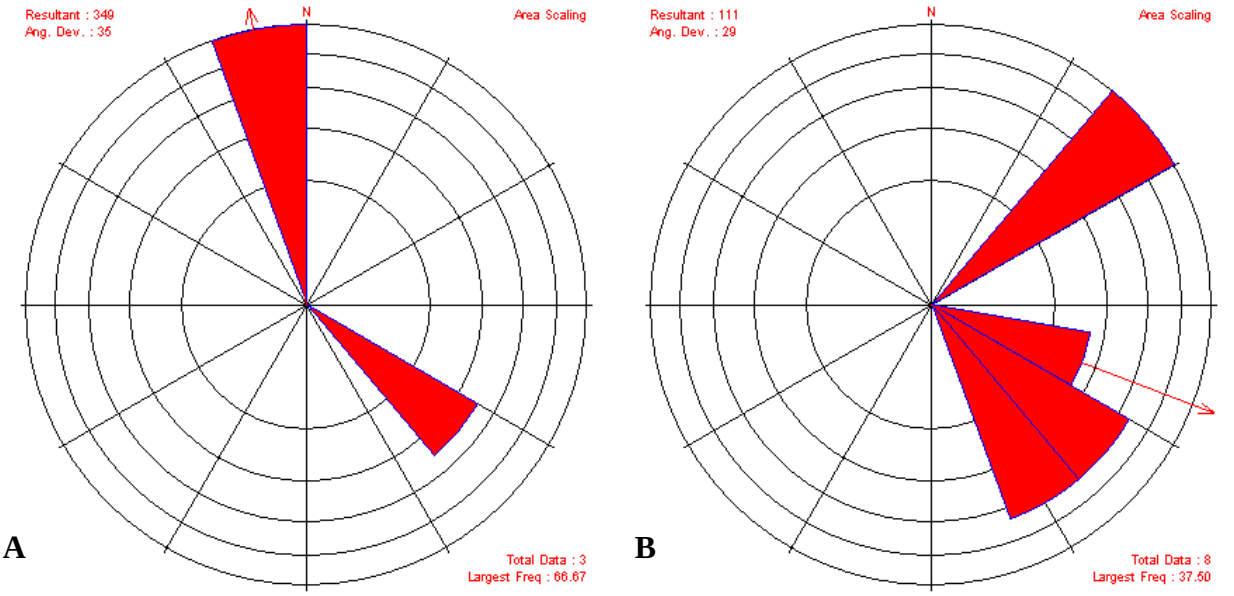

Figure 5-10. Joint orientations at sample localities near the (A) Federal No. 1-31 well (NW1/4SW1/4 section 31, T. 30 S., R. 24 E., SLBL&M), and (B) Evelyn Chambers Government No. 1 well (NE1/4NE1/4 section 6, T. 31 S., R. 24 E., SLBL&M) at Lightning Draw Southeast field.

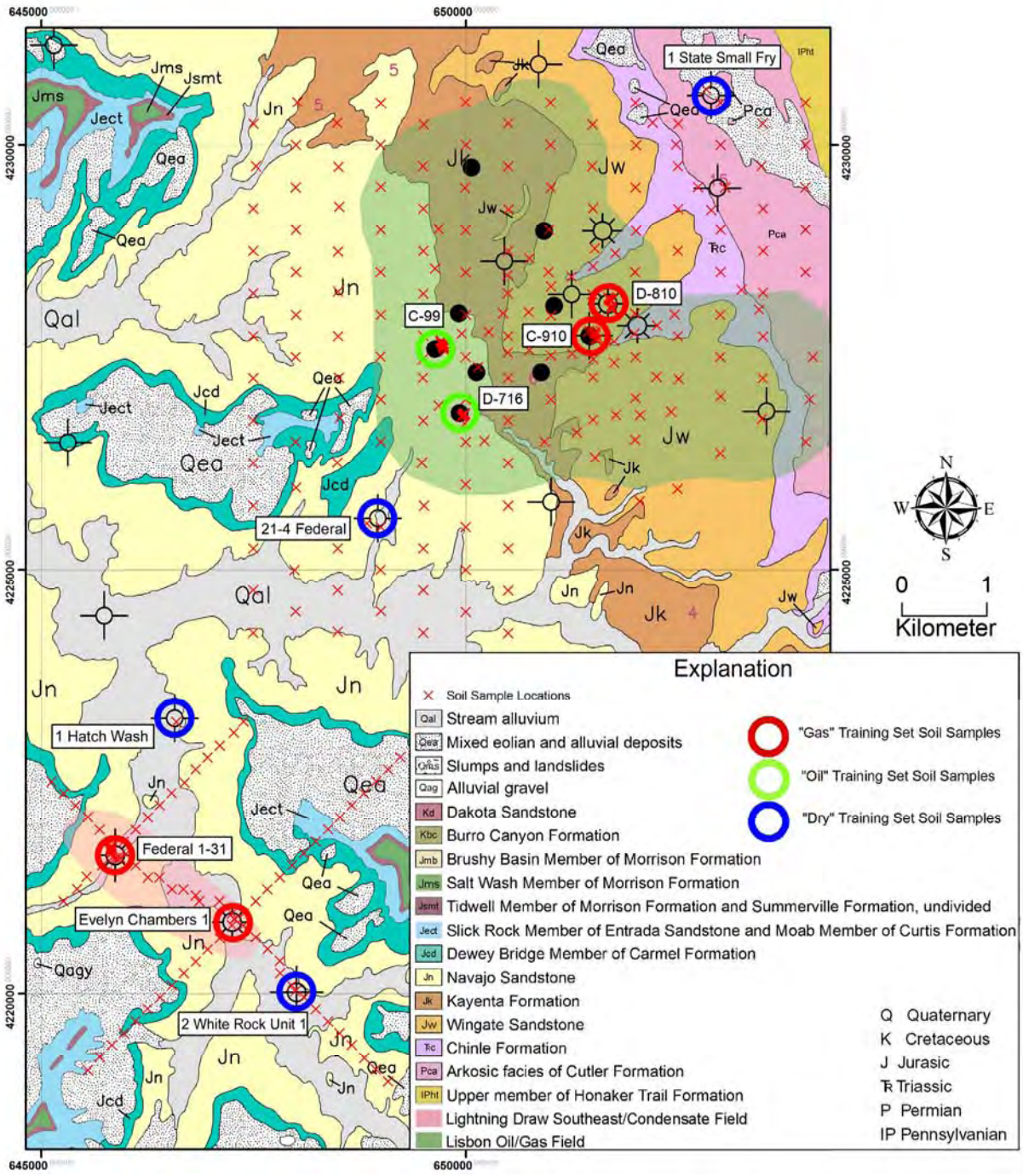

Figure 5-11. Distribution of grid, line, and training set soil samples collected over and around the Lisbon and Lightning Draw Southeast fields, superimposed over geologic map modified from Doelling (2005); see figure 5-1 for explanation of well symbols.

A

B

Figure 5-12. Sampling methods used in the Lisbon/Lightning Draw Southeast area. A – Collection of shallow, reddish-brown, fine-grained, sandy loam from 8- to 12-inch depth on Wingate Sandstone outcrop. These samples are referred to as "surface soils" throughout this report. B – Along joints, soil, sand, bryophytes, and lichen were sampled using a flathead screwdriver, knife, or stainless steel spoon.

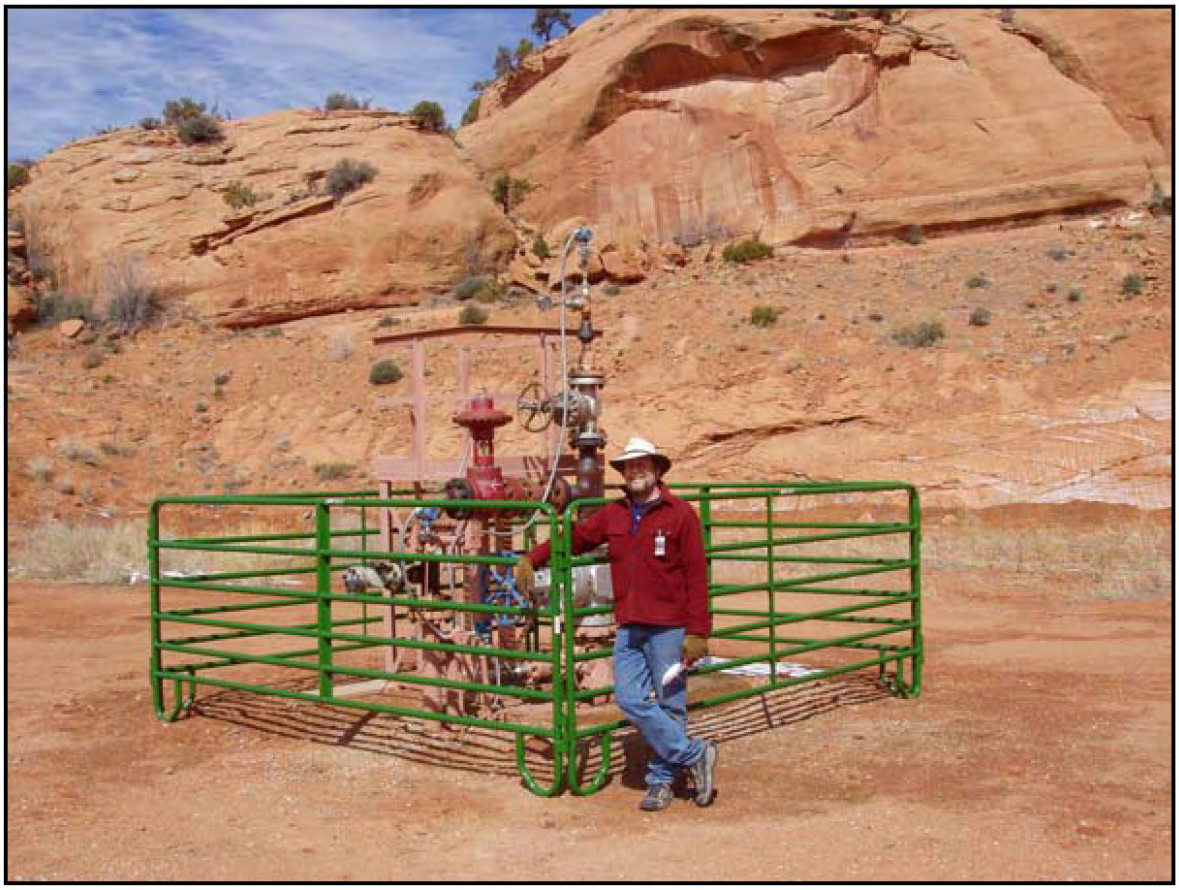

Figure 5-13. The Lisbon No. C-910 well, which produces 7 MMCF/D of low-Btu (≈ 670) sour gas with considerable amounts of N_2 and CO_2 (see table 5-1). Soils samples were collected from the ledge above the well pad to avoid contamination.

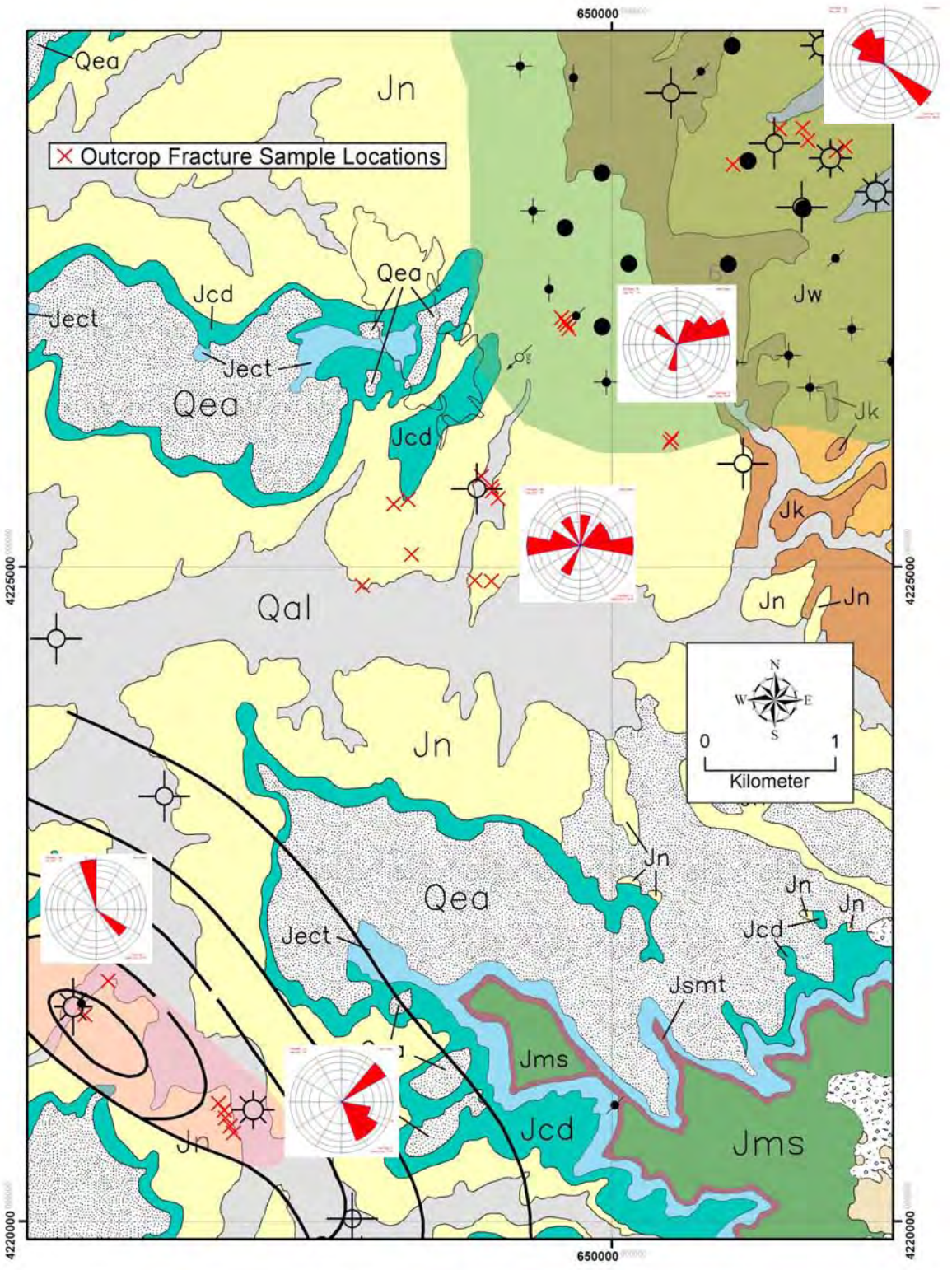

Figure 5-14. Outcrop fracture-fill lichen and soil sample locations over the Lisbon gas cap, oil leg, and water leg, and over the Lightning Draw Southeast field (shown in pink). Dominant joint orientations at sample site areas are also indicated. Surface geology modified from Doelling (2005); see figures 5-1 and 5-11 for explanations of well symbols and geologic units. Form line contours based on structure contour map of the Leadville Limestone shown on figure 5-5.

Figure 5-15. Location of 6-foot-deep free-gas samples over and off Lightning Draw Southeast field (shown in pink). The samples were collected with a Geoprobe "Direct-Push" drill and gas was extracted through plastic tubing (inset photos), which was inserted into the 1-inch steel pipes. Surface geology modified from Doelling (2005); see figures 5-1 and 5-11 for explanations of well symbols and geologic units. Form line contours based on structure contour map of the Leadville Limestone shown on figure 5-5.

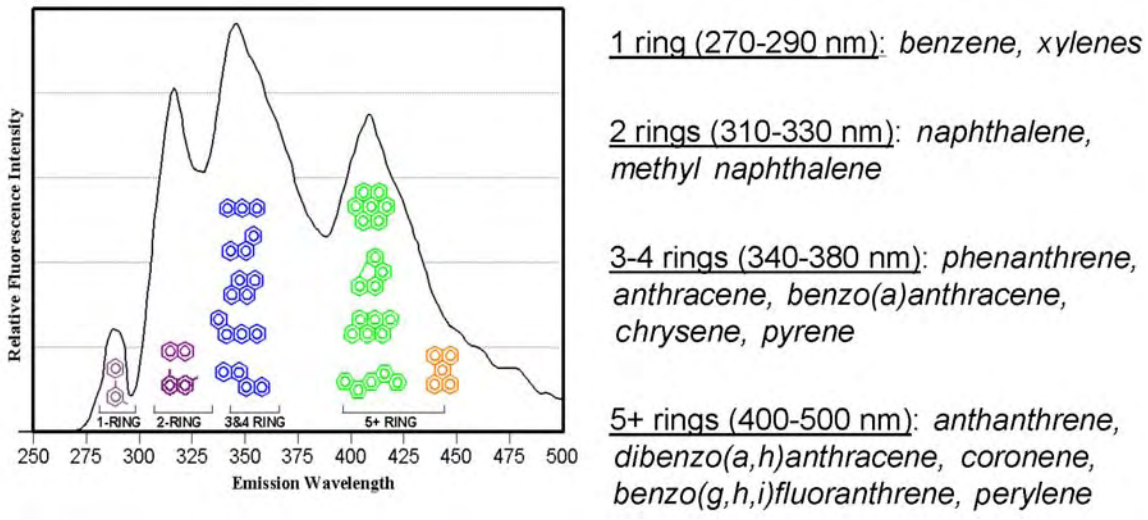

Figure 5-16. Schematic of synchronous scanned fluorescence spectra depicting the aromatic hydrocarbons and corresponding emission wavelengths.

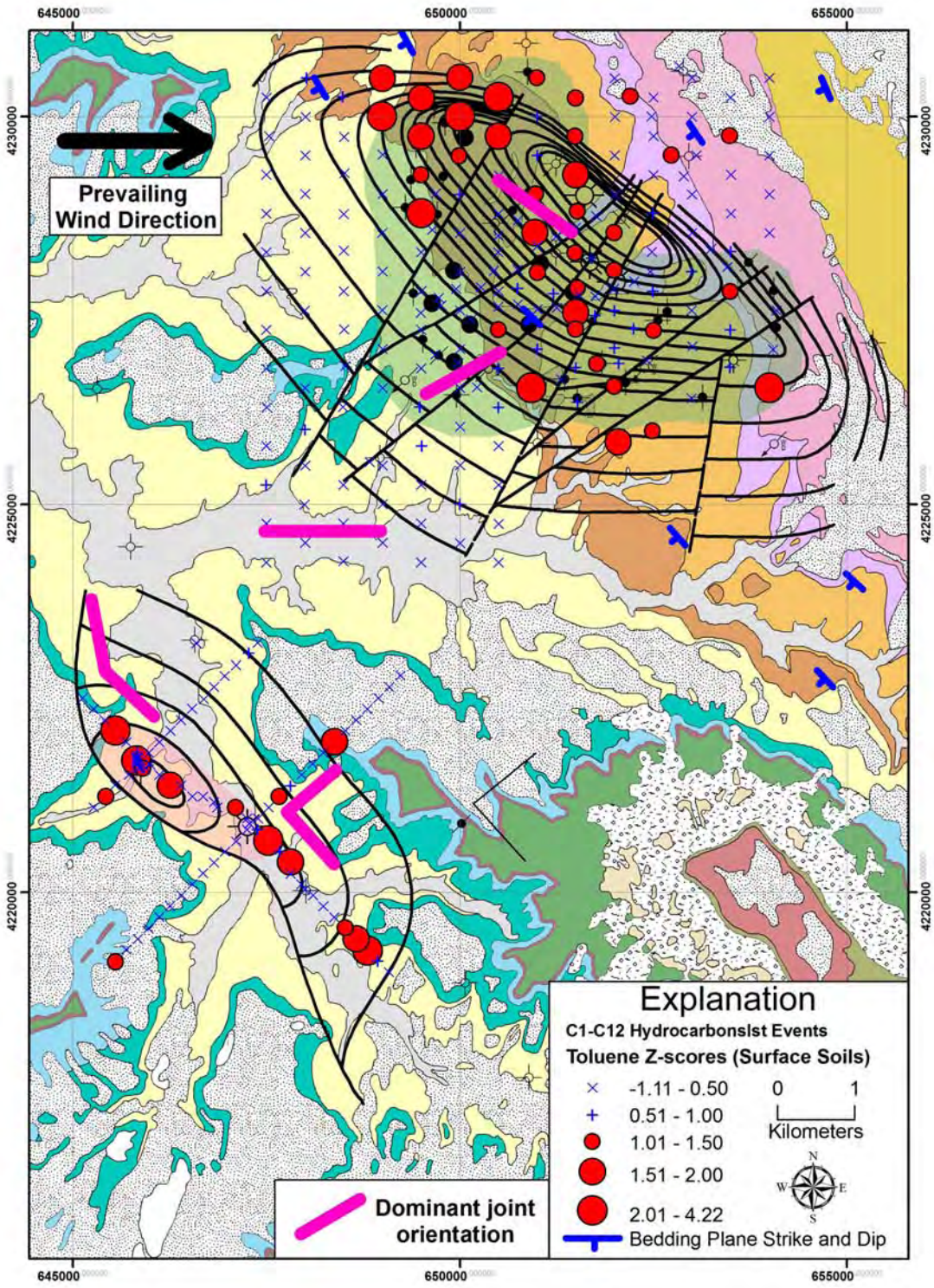

Figure 5-17. Distribution of toluene Z-scores in surface soils over the Lisbon and Lightning Draw Southeast fields. See figure 5-11 for description of geologic units (geologic base modified from Doelling, 2005) and figure 5-1 for explanations of well symbols; form line contours based on structure contour maps of the Leadville Limestone shown on figures 5-1 and 5-5. Lisbon and Lightning Draw southeast fields shown in bluish green and pink, respectively.

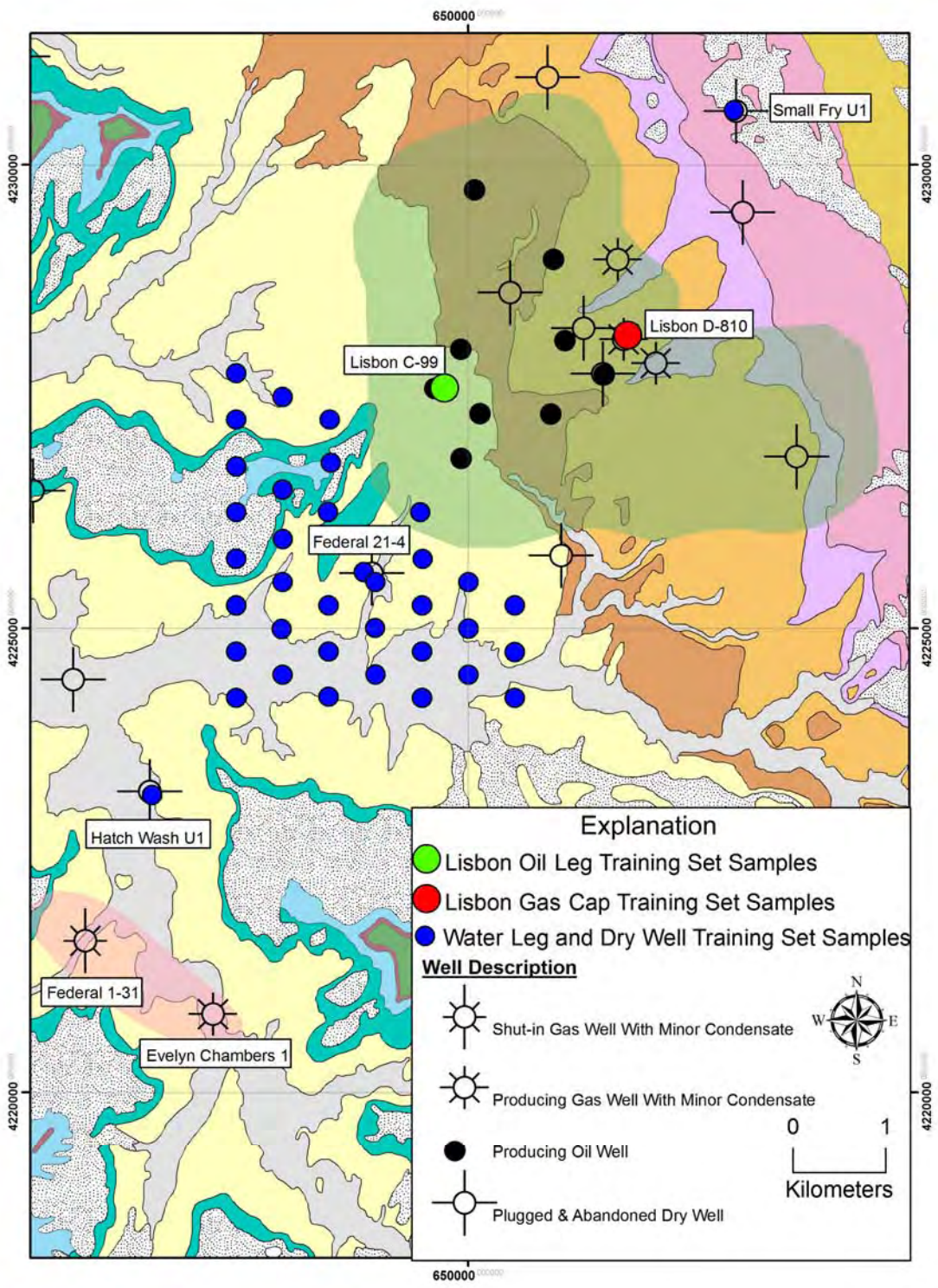

Figure 5-18. Surface soil training set samples used for three-component Lisbon gas cap versus oil leg versus water leg discriminant analysis model. See figure 5-11 for description of geologic units (geologic base modified from Doelling, 2005). Lisbon and Lightning Draw southeast fields shown in bluish green and pink, respectively.

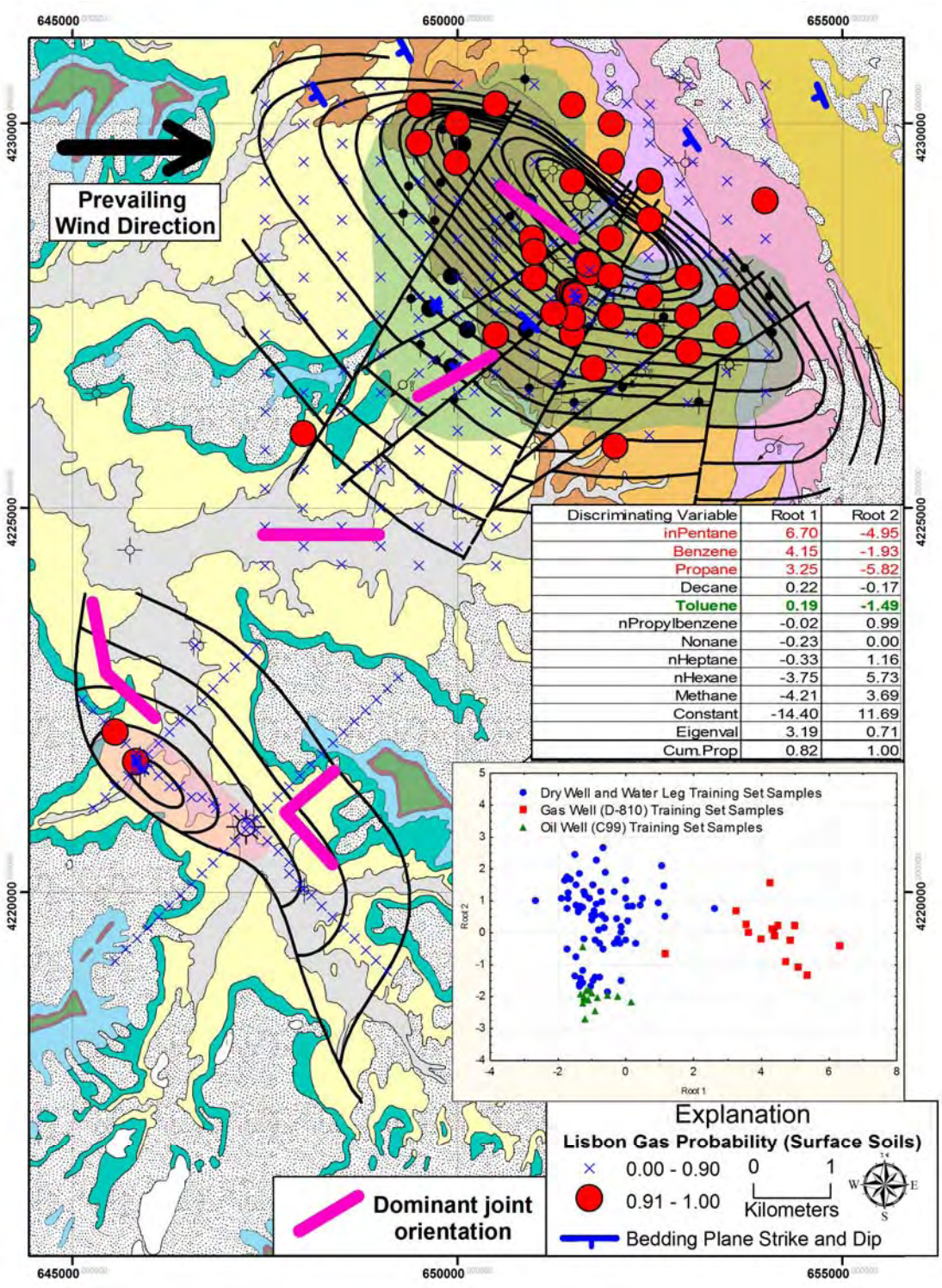

Figure 5-19. Distribution of Lisbon gas-oil probabilities derived from three-component discriminant analysis of thermally desorbed C_1-C_{12} hydrocarbons from surface soils. See figure 5-11 for description of geologic units (geologic base modified from Doelling, 2005) and figure 5-1 for explanations of well symbols; form line contours based on structure contour maps of the Leadville Limestone shown on figures 5-1 and 5-5. Lisbon and Lightning Draw southeast fields shown in bluish green and pink, respectively.

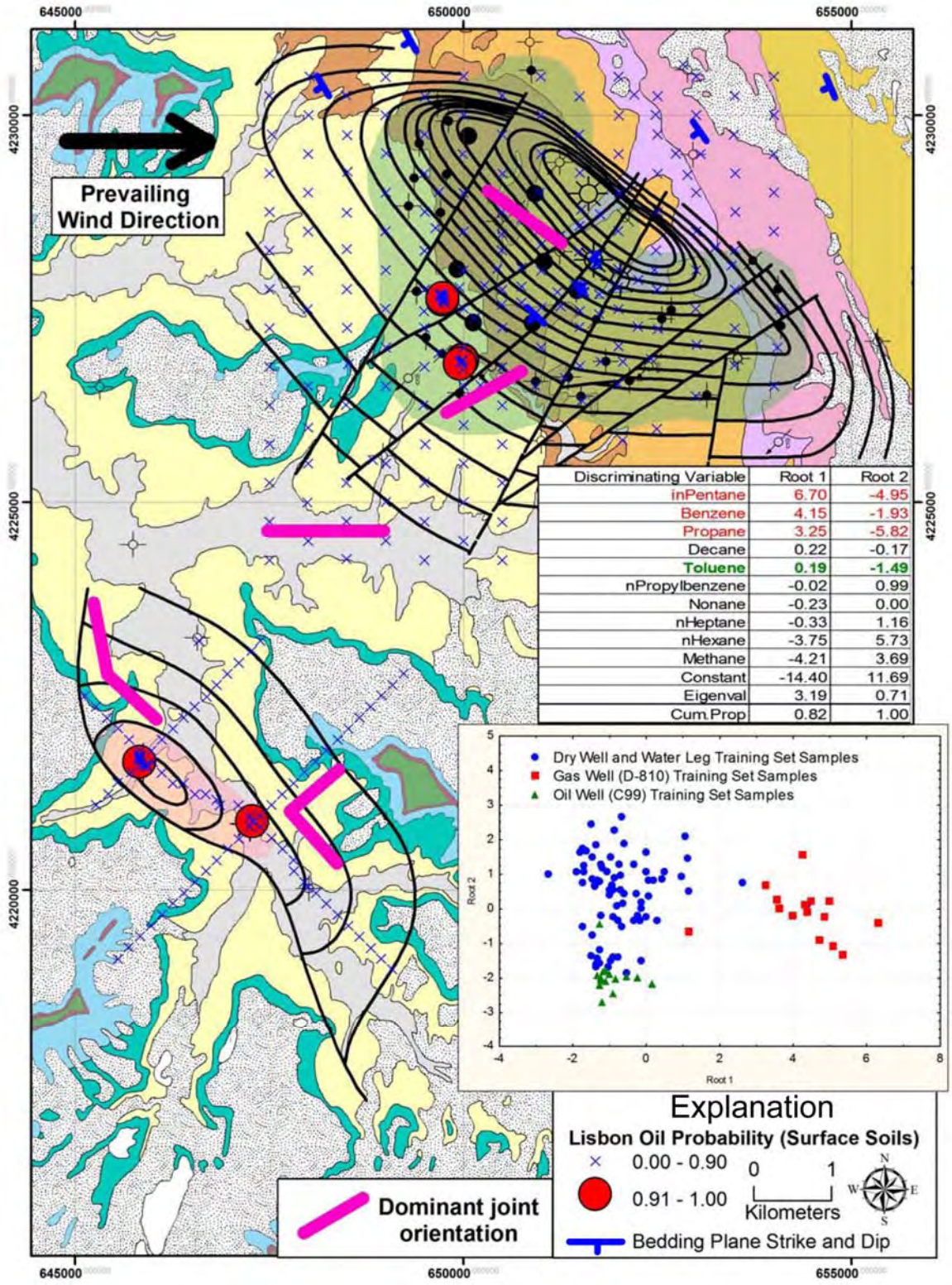

Figure 5-20. Distribution of Lisbon oil probabilities derived from three-component discriminant analysis of thermally desorbed C_1-C_{12} hydrocarbons from surface soils. See figure 5-11 for description of geologic units (geologic base modified from Doelling, 2005) and figure 5-1 for explanations of well symbols; form line contours based on structure contour maps of the Leadville Limestone shown on figures 5-1 and 5-5. Lisbon and Lightning Draw southeast fields shown in bluish green and pink, respectively.

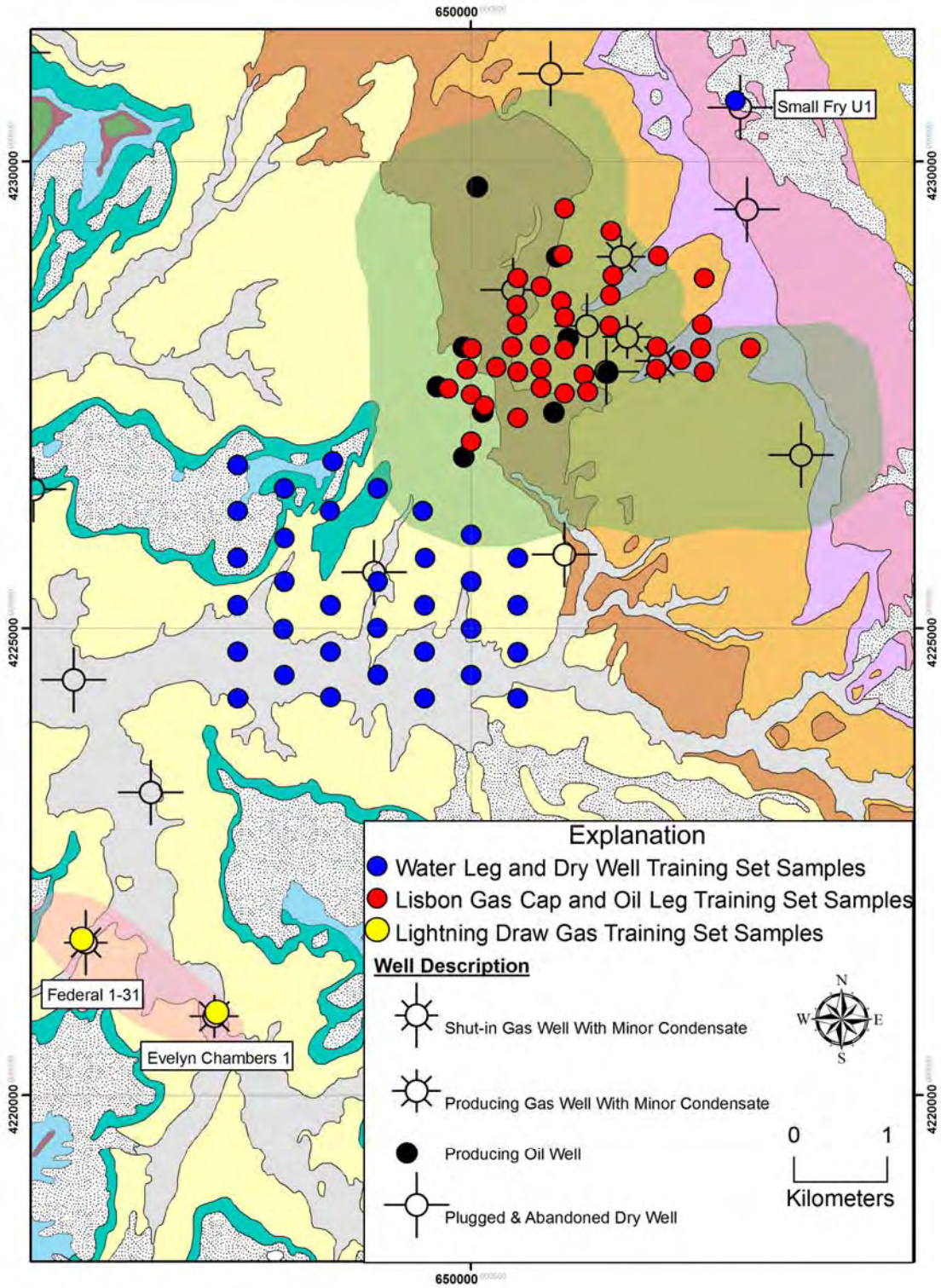

Figure 5-21. Surface soil training set samples used for two component Lisbon gas cap/ oil leg versus water leg and Lightning Draw Southeast gas versus Lisbon water leg discriminant analysis models. See figure 5-11 for description of geologic units (geologic base modified from Doelling, 2005). Lisbon and Lightning Draw southeast fields shown in bluish green and pink, respectively.

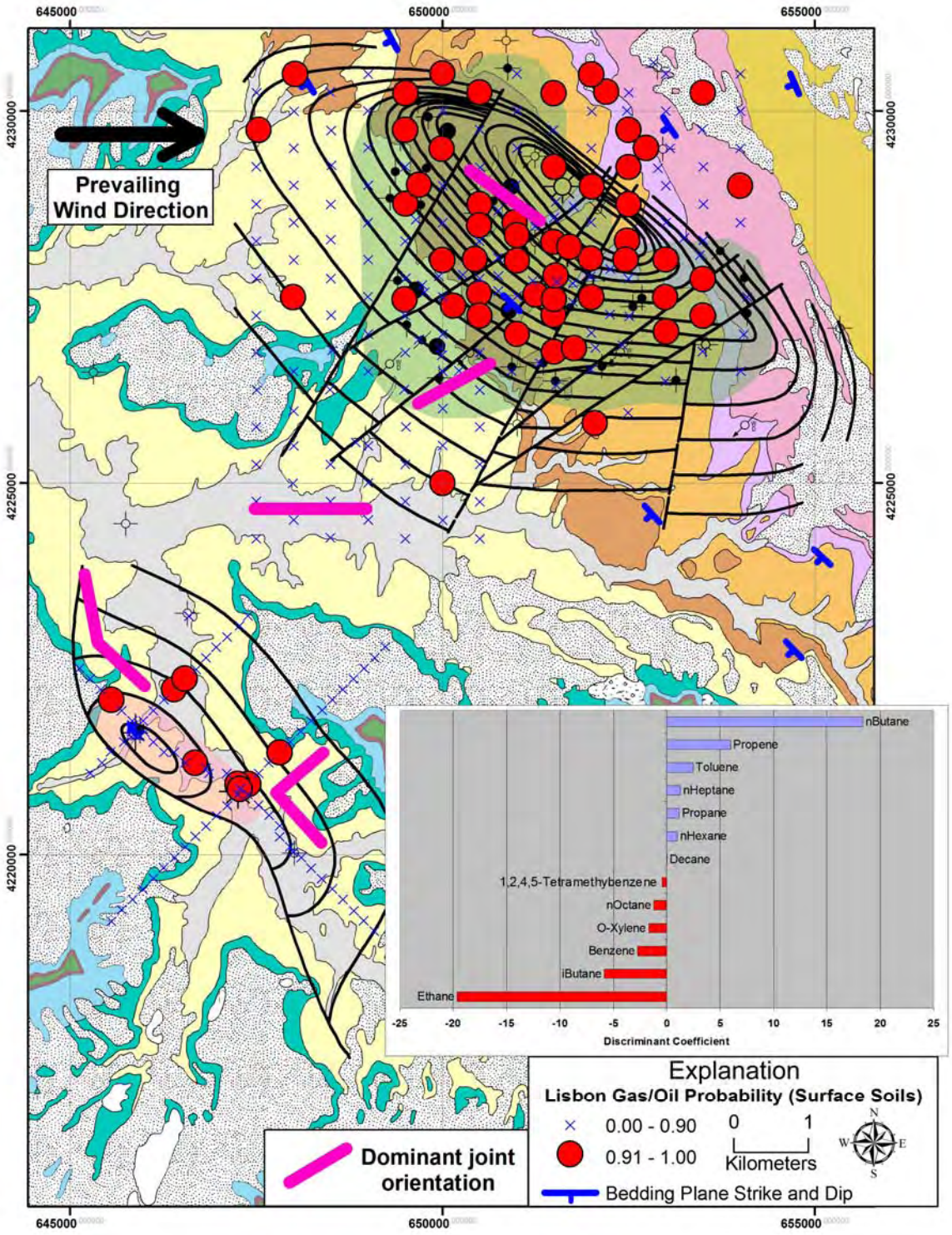

Figure 5-22. Distribution of Lisbon gas-oil probabilities derived from two-component discriminant analysis of thermally desorbed C_1 to C_{12} hydrocarbon from surface soils. See figure 5-11 for description of geologic units (geologic base modified from Doelling, 2005) and figure 5-1 for explanations of well symbols; form line contours based on structure contour maps of the Leadville Limestone shown on figures 5-1 and 5-5. Lisbon and Lightning Draw southeast fields shown in bluish green and pink, respectively.

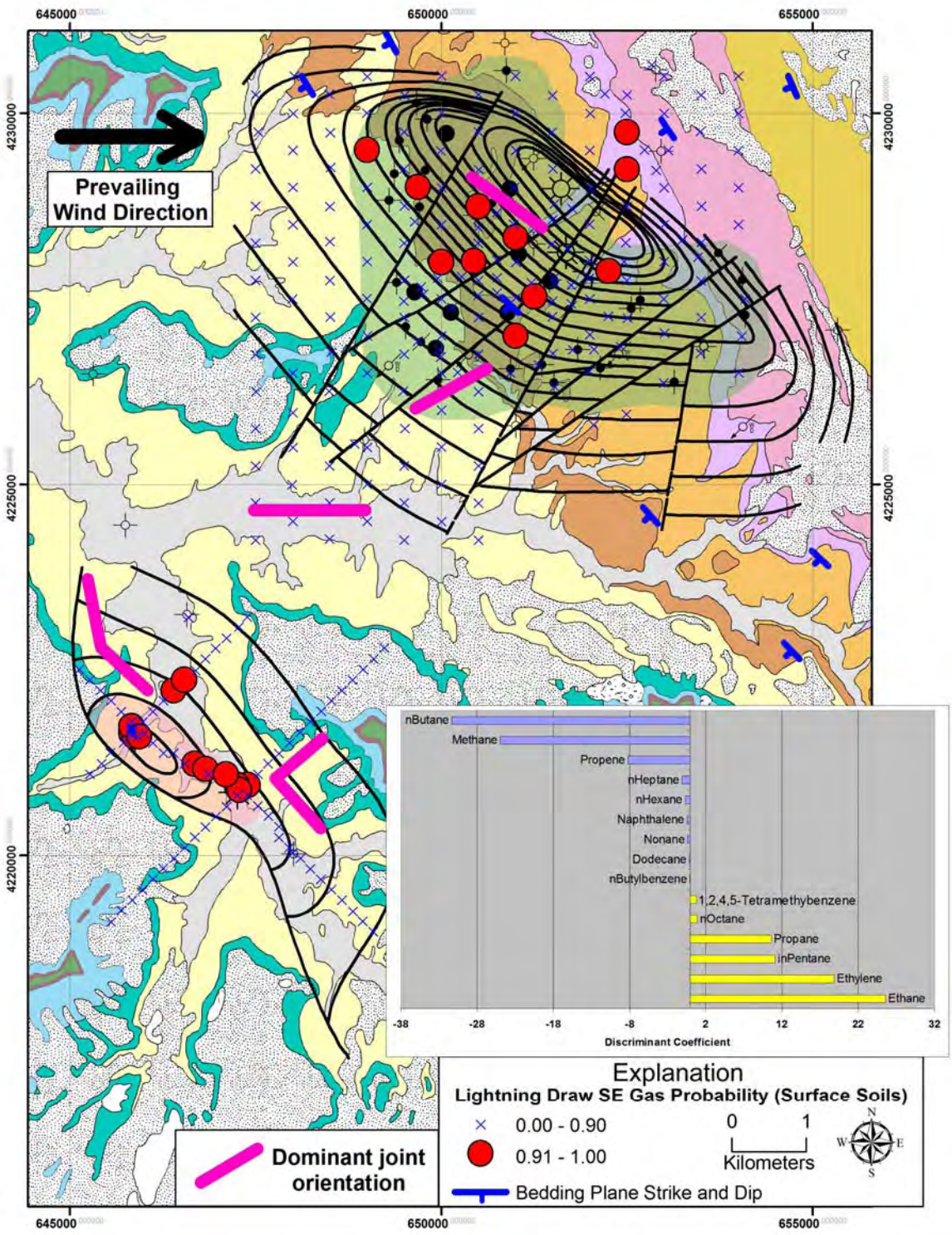

Figure 5-23. Distribution of Lightning Draw Southeast gas probabilities derived from two-component discriminant analysis of thermally desorbed C_1 to C_{12} hydrocarbon from surface soils. See figure 5-11 for description of geologic units (geologic base modified from Doelling, 2005) and figure 5-1 for explanations of well symbols; form line contours based on structure contour maps of the Leadville Limestone shown on figures 5-1 and 5-5. Lisbon and Lightning Draw southeast fields shown in bluish green and pink, respectively.

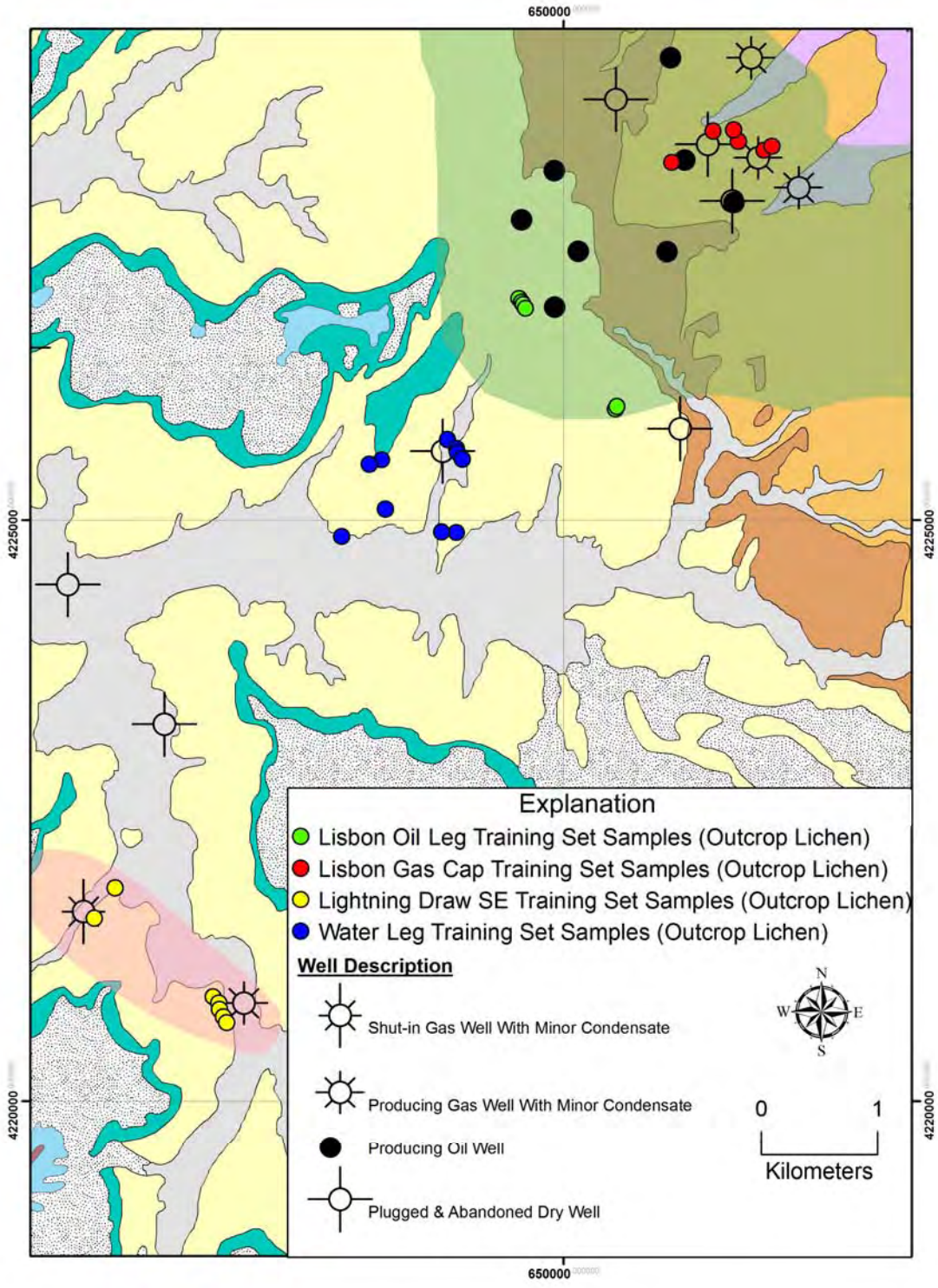

Figure 5-24. Outcrop lichen training set samples used for three-component Lisbon gas cap versus oil leg versus water leg and two-component Lightning Draw Southeast gas versus Lisbon water leg discriminant analysis models. See figure 5-11 for description of geologic units (geologic base modified from Doelling, 2005). Lisbon and Lightning Draw southeast fields shown in bluish green and pink, respectively.

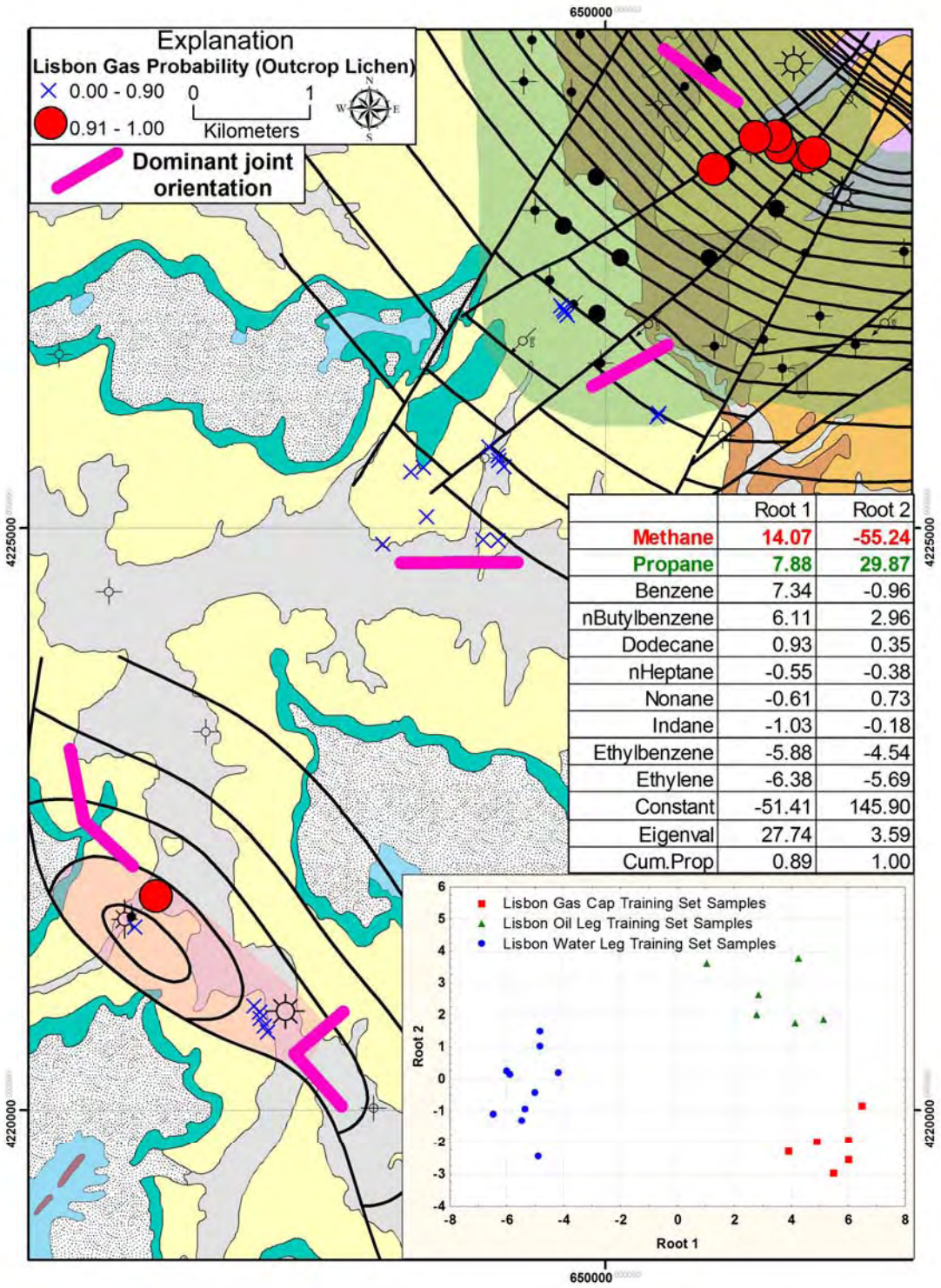

Figure 5-25. Distribution of Lisbon gas probability derived from three-component discriminant analysis of thermally desorbed C_1 to C_{12} hydrocarbon from outcrop lichen samples. See figure 5-11 for description of geologic units (geologic base modified from Doelling, 2005) and figure 5-1 for explanations of well symbols; form line contours based on structure contour maps of the Leadville Limestone shown on figures 5-1 and 5-5. Lisbon and Lightning Draw southeast fields shown in bluish green and pink, respectively.

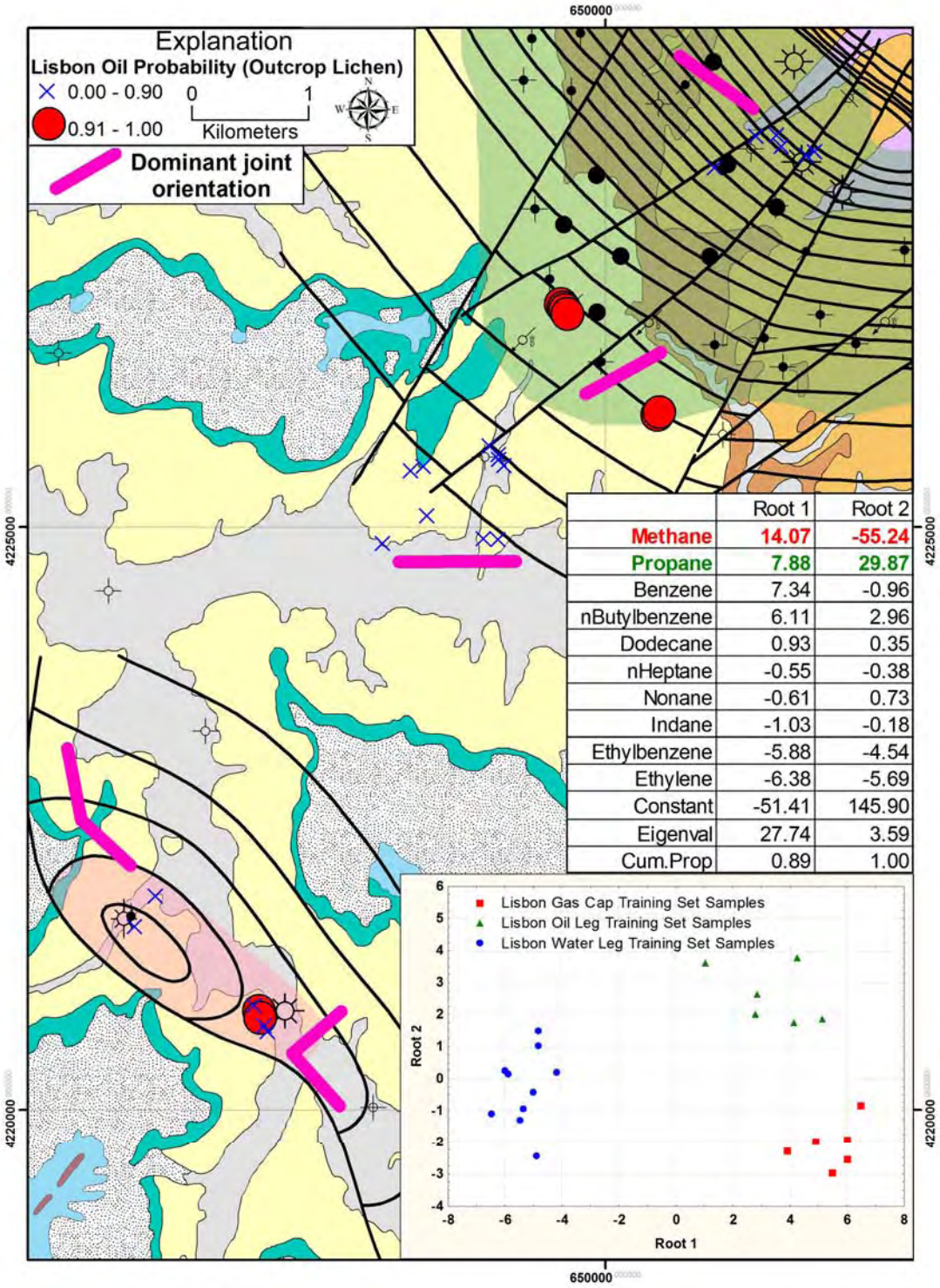

Figure 5-26. Distribution of Lisbon oil probability derived from three-component discriminant analysis of thermally desorbed C_1 to C_{12} hydrocarbon from outcrop lichen samples. See figure 5-11 for description of geologic units (geologic base modified from Doelling, 2005) and figure 5-1 for explanations of well symbols; form line contours based on structure contour maps of the Leadville Limestone shown on figures 5-1 and 5-5. Lisbon and Lightning Draw southeast fields shown in bluish green and pink, respectively.

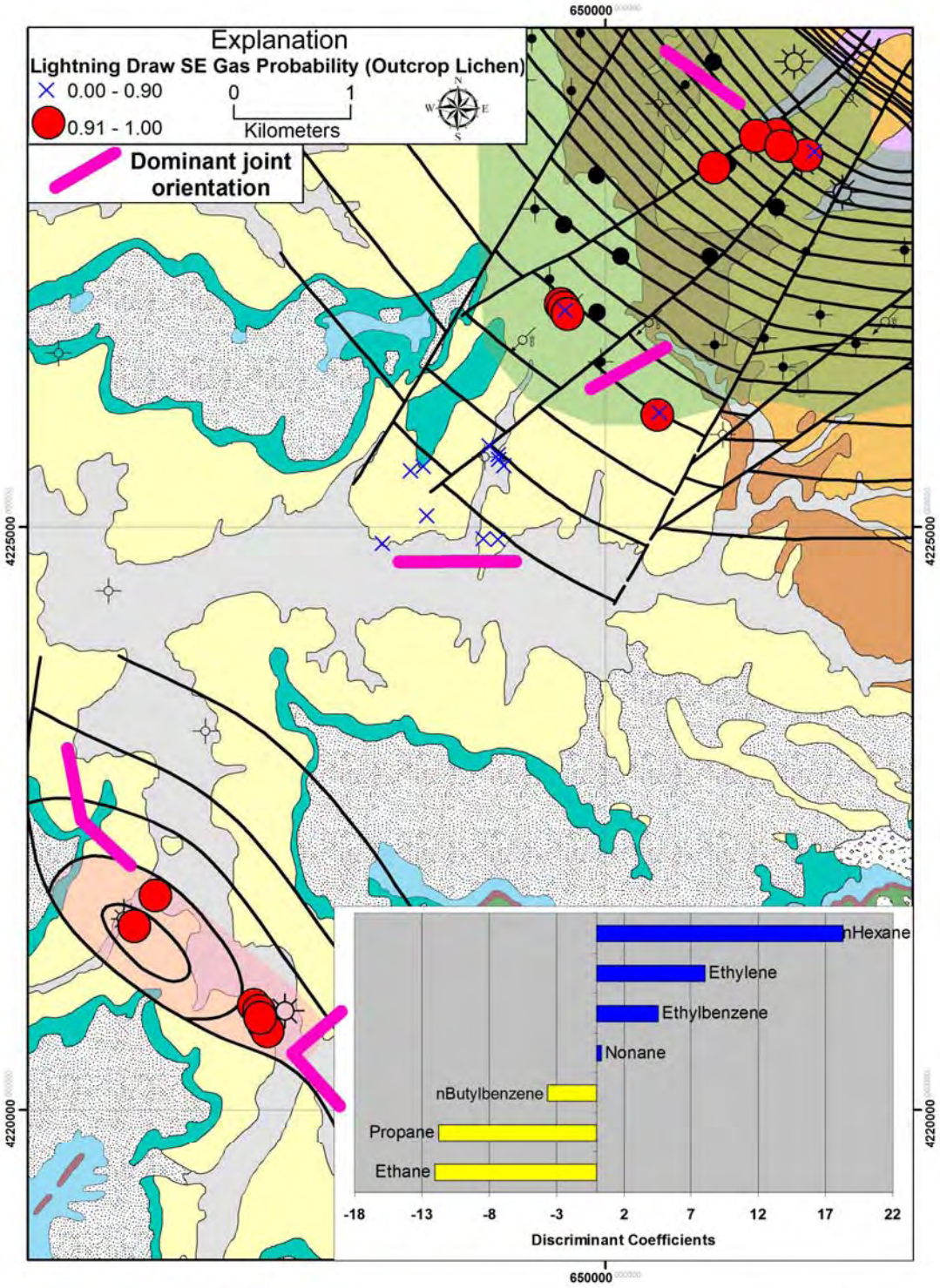

Figure 5-27. Distribution of Lightning Draw Southeast gas probabilities derived from two-component discriminant analysis of thermally desorbed C_1 to C_{12} hydrocarbon from outcrop lichen samples. See figure 5-11 for description of geologic units (geologic base modified from Doelling, 2005) and figure 5-1 for explanations of well symbols; form line contours based on structure contour maps of the Leadville Limestone shown on figures 5-1 and 5-5. Lisbon and Lightning Draw southeast fields shown in bluish green and pink, respectively.

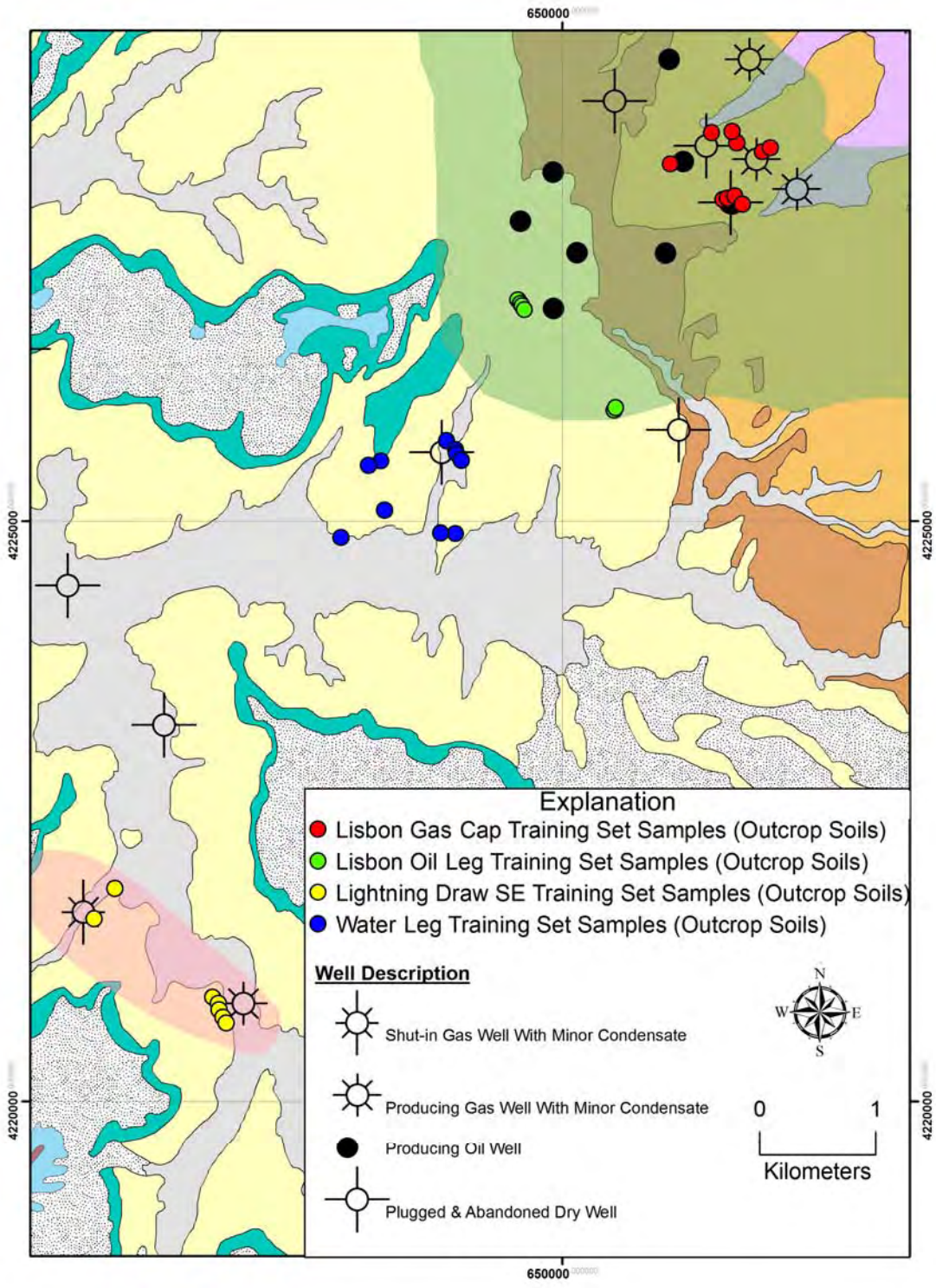

Figure 5-28. Outcrop soil training set samples used for three-component Lisbon gas cap versus oil leg versus water leg and two-component Lightning Draw Southeast gas versus Lisbon water leg discriminant analysis models. See figure 5-11 for description of geologic units (geologic base modified from Doelling, 2005). Lisbon and Lightning Draw southeast fields shown in bluish green and pink, respectively.

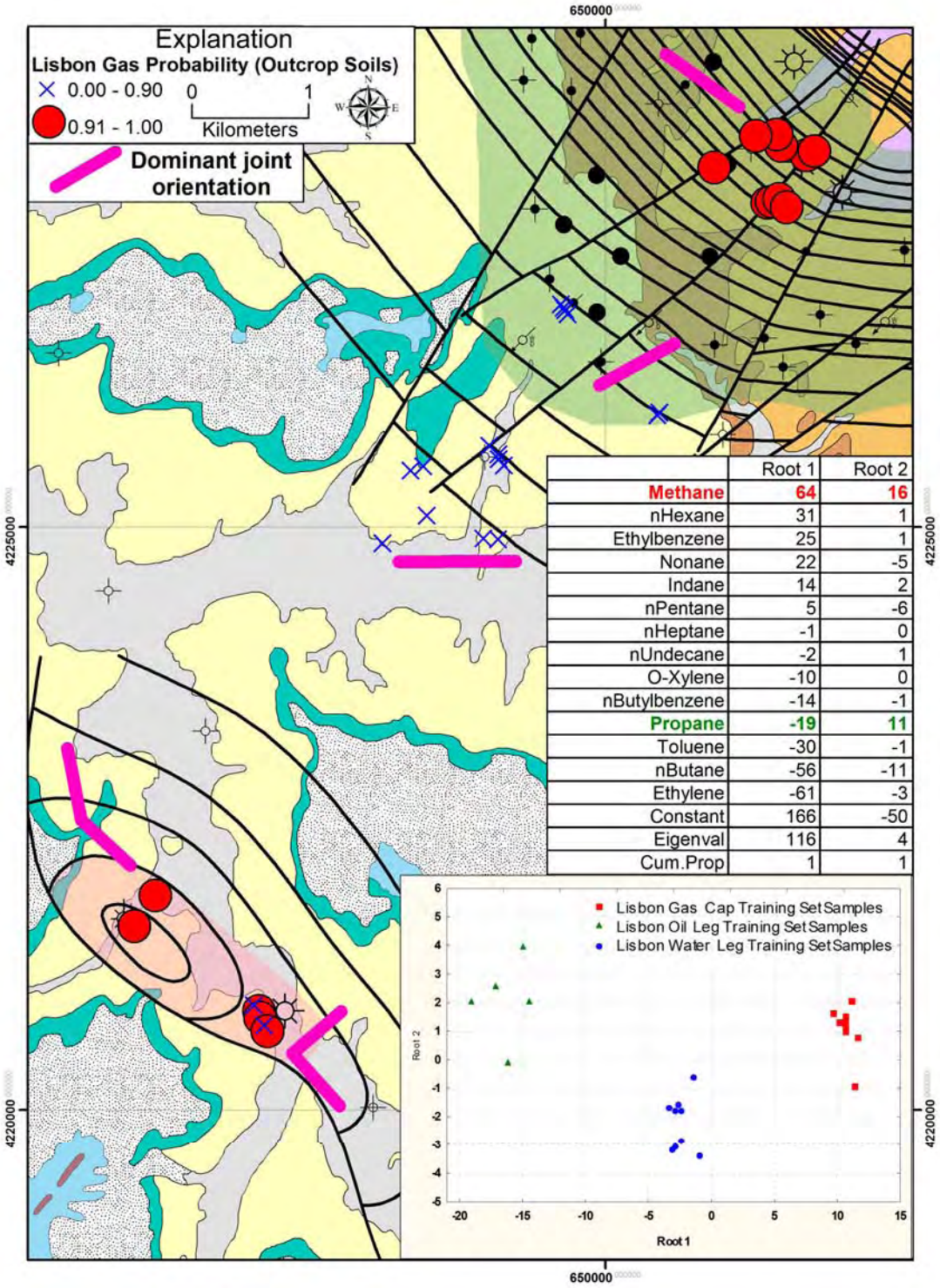

Figure 5-29. Distribution of Lisbon gas probability derived from three-component discriminant analysis of thermally desorbed C_1 to C_{12} hydrocarbon from outcrop soil samples. See figure 5-11 for description of geologic units (geologic base modified from Doelling, 2005) and figure 5-1 for explanations of well symbols; form line contours based on structure contour maps of the Leadville Limestone shown on figures 5-1 and 5-5. Lisbon and Lightning Draw southeast fields shown in bluish green and pink, respectively.

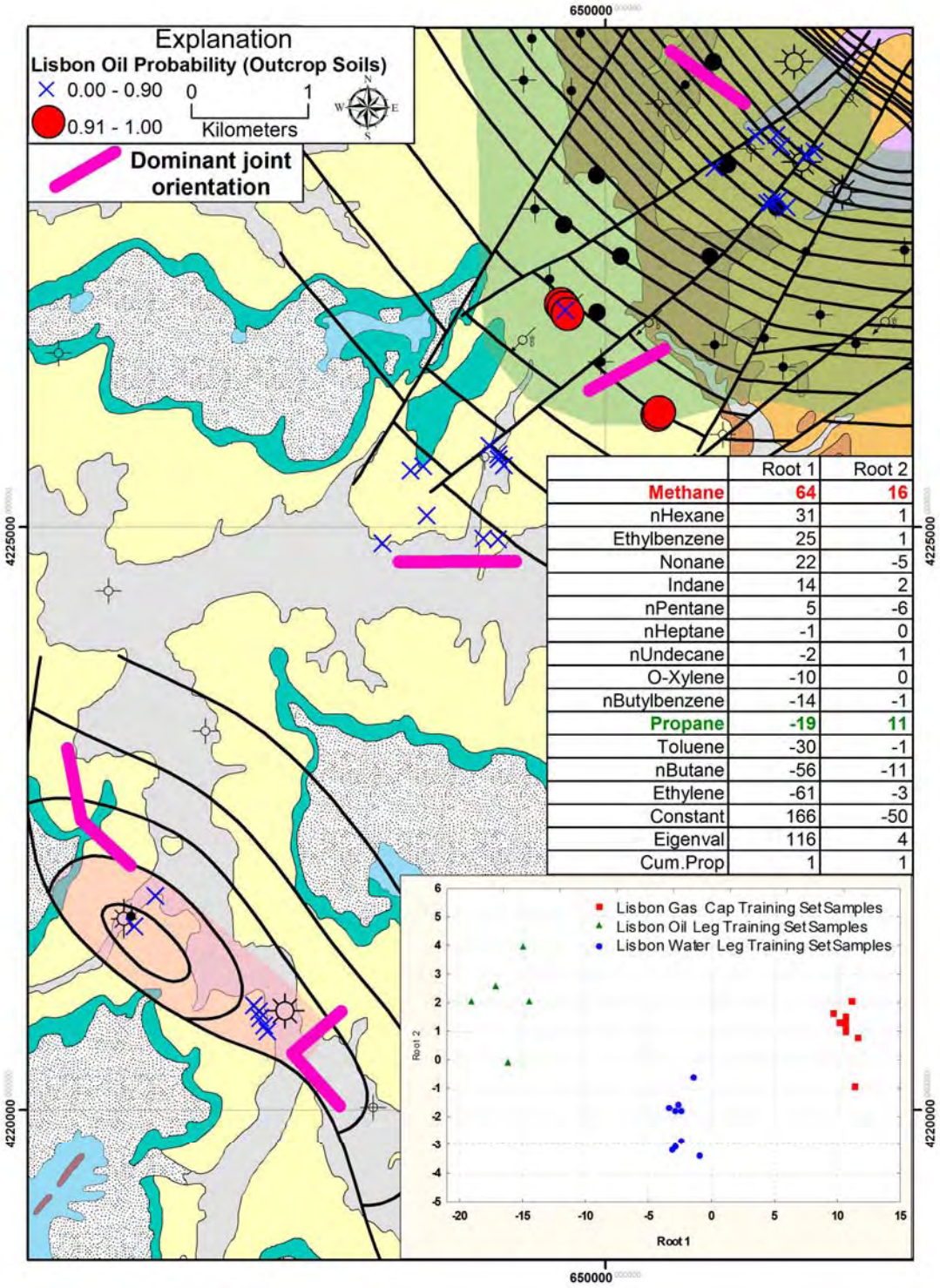

	Root 1	Root 2
Methane	64	16
nHexane	31	1
Ethylbenzene	25	1
Nonane	22	-5
Indane	14	2
nPentane	5	-6
nHeptane	-1	0
nUndecane	-2	1
O-Xylene	-10	0
nButylbenzene	-14	-1
Propane	-19	11
Toluene	-30	-1
nButane	-56	-11
Ethylene	-61	-3
Constant	166	-50
Eigenval	116	4
Cum.Prop	1	1

Figure 5-30. Distribution of Lisbon oil probability derived from three-component discriminant analysis of thermally desorbed C_1 to C_{12} hydrocarbon from outcrop soil samples. See figure 5-11 for description of geologic units (geologic base modified from Doelling, 2005) and figure 5-1 for explanations of well symbols; form line contours based on structure contour maps of the Leadville Limestone shown on figures 5-1 and 5-5. Lisbon and Lightning Draw southeast fields shown in bluish green and pink, respectively.

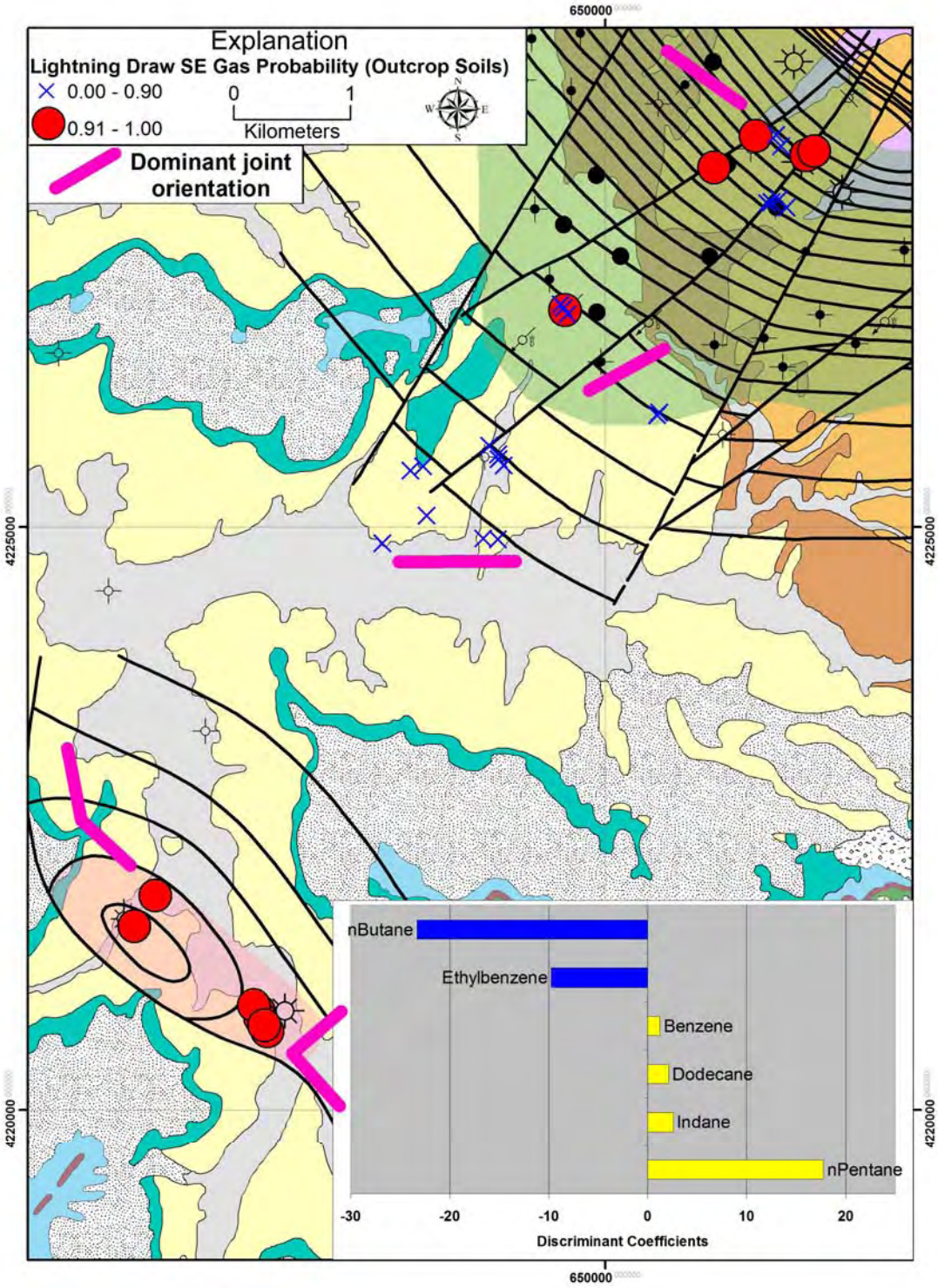

Figure 5-31. Distribution of Lightning Draw Southeast gas probabilities derived from two-component discriminant analysis of thermally desorbed C_1 to C_{12} hydrocarbon from outcrop soil samples. See figure 5-11 for description of geologic units (geologic base modified from Doelling, 2005) and figure 5-1 for explanations of well symbols; form line contours based on structure contour maps of the Leadville Limestone shown on figures 5-1 and 5-5. Lisbon and Lightning Draw southeast fields shown in bluish green and pink, respectively.

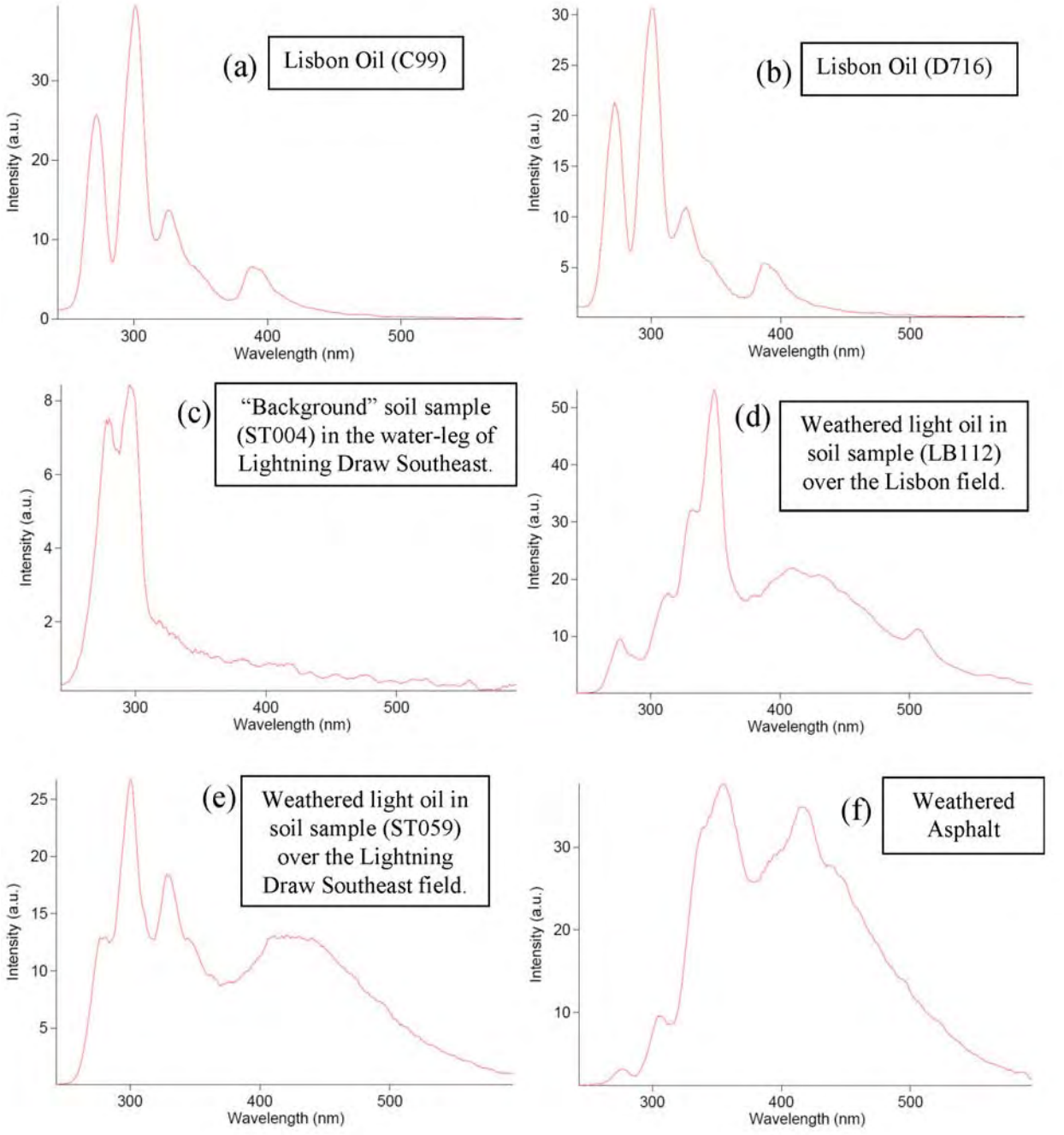

Figure 5-32. Synchronous scanned fluorescence spectra for Lisbon oil (a and b), background soil sample (c), weathered oil in soil over Lisbon field (d), weathered oil in soil over Lightning Draw Southeast field (e), and weathered asphalt (f).

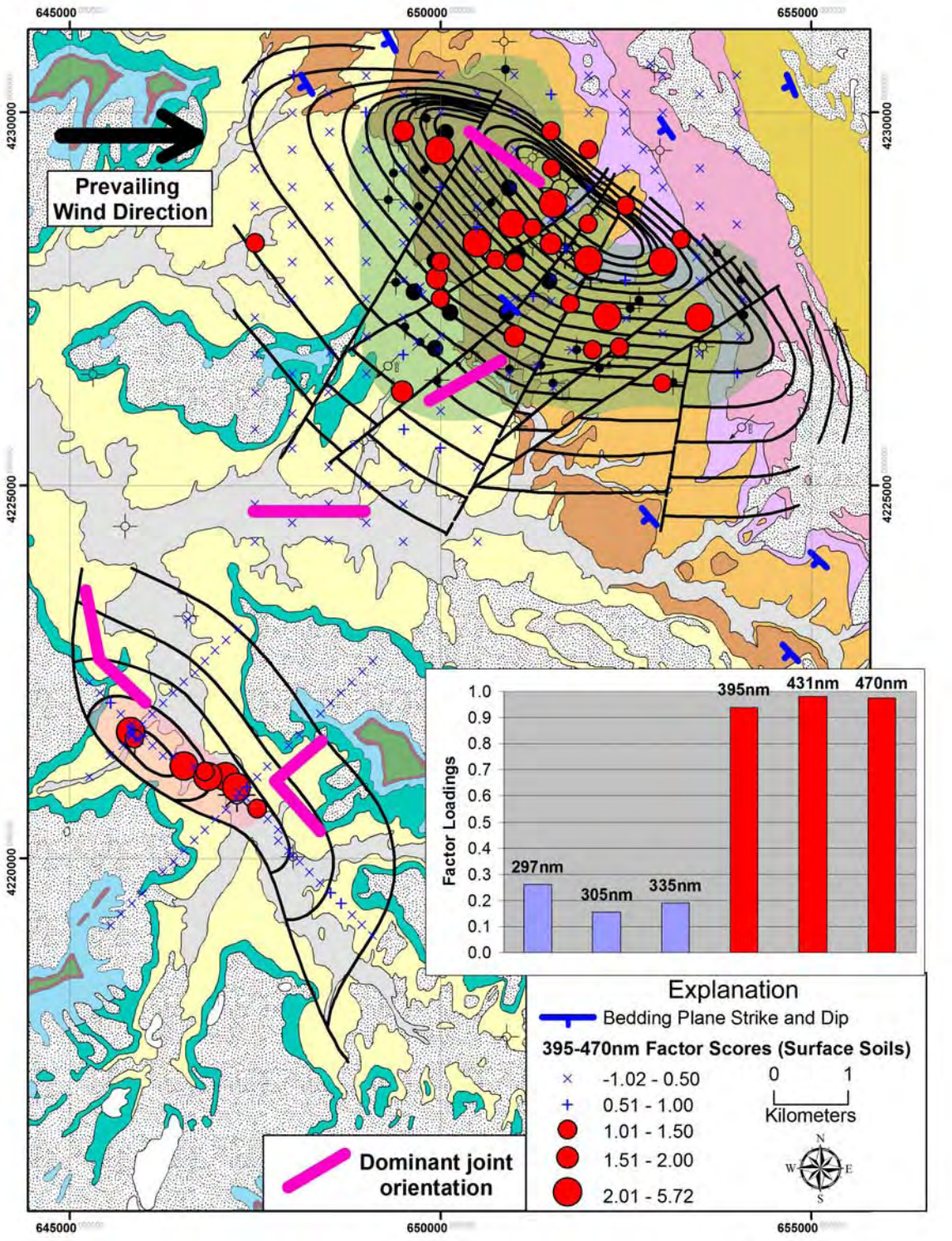

Figure 5-33. Distribution of 395 to 470 nm factor scores (3- to 6-ring aromatics) in surface soils over Lisbon and Lightning Draw Southeast fields (shown in bluish green and pink, respectively). See figure 5-11 for description of geologic units (geologic base modified from Doelling, 2005) and figure 5-1 for explanations of well symbols; form line contours based on structure contour maps of the Leadville Limestone shown on figures 5-1 and 5-5.

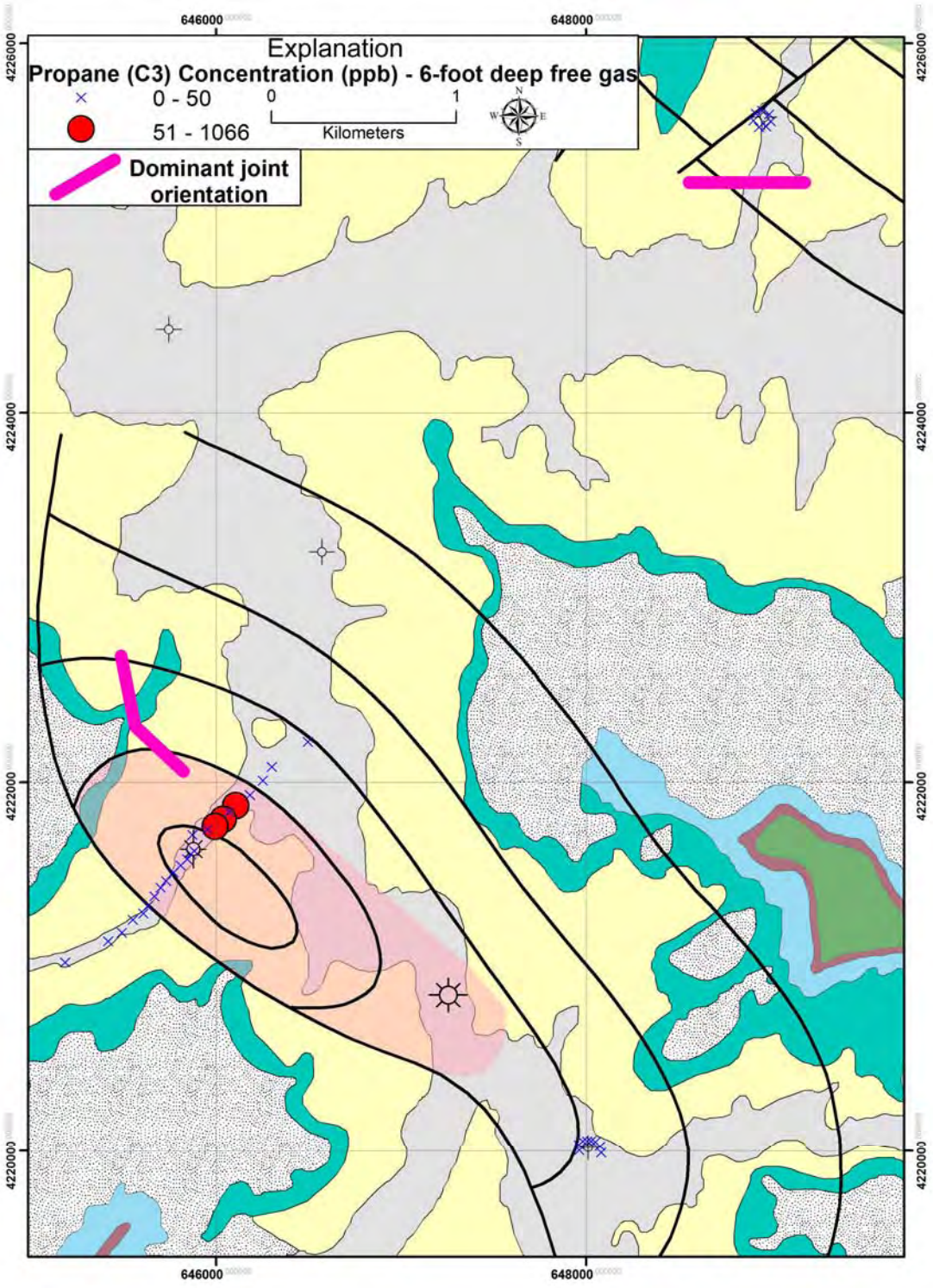

Figure 5-34. Distribution of propane concentrations in 6-foot-deep free gas over Lightning Draw Southeast field (shown in pink) and background areas. See figure 5-11 for description of geologic units (geologic base modified from Doelling, 2005) and figure 5-1 for explanations of well symbols; form line contours based on structure contour map of the Leadville Limestone shown on figure 5-5.

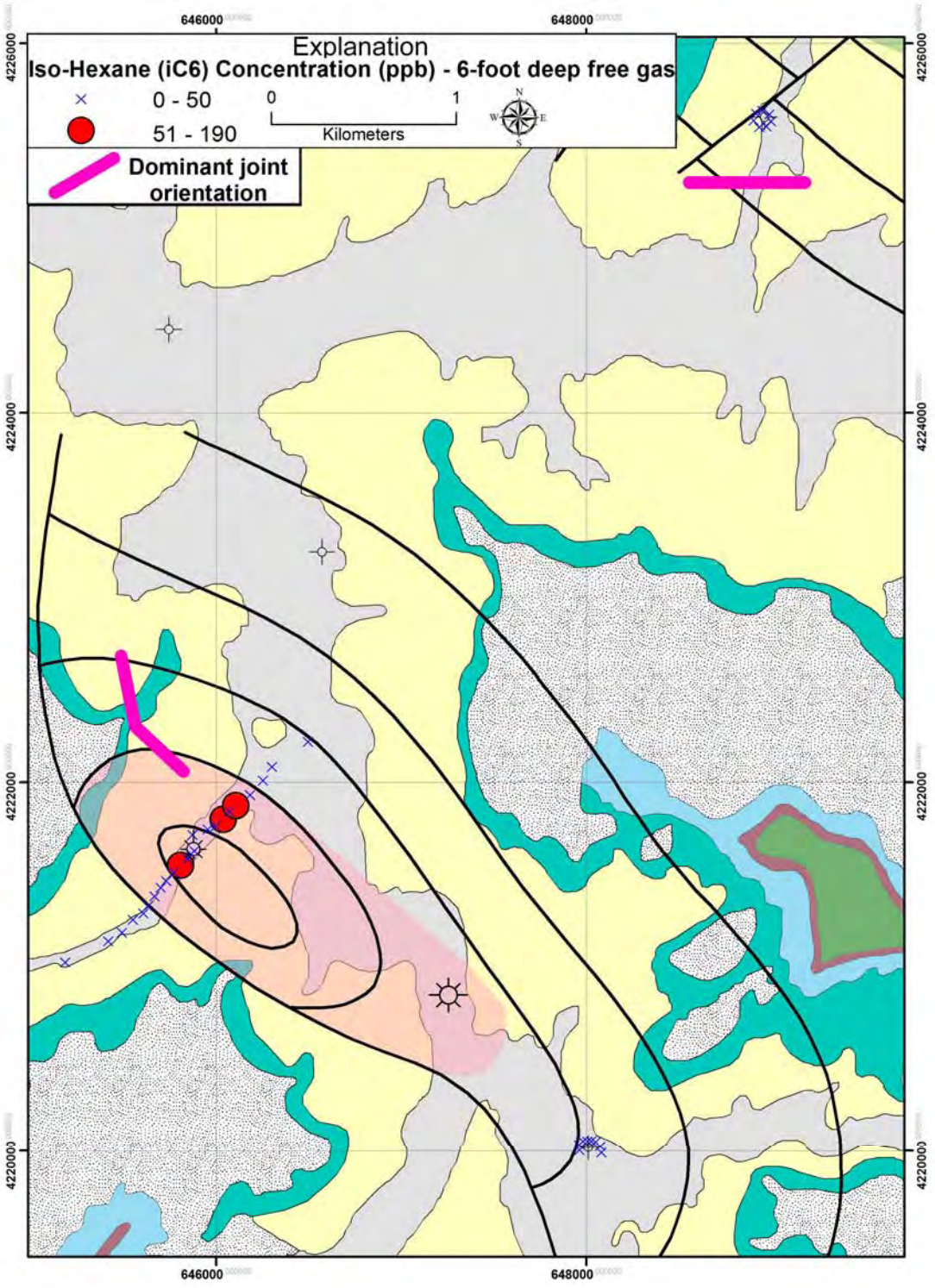

Figure 5-35. Distribution of isohexane concentrations in 6-foot-deep free gas over Lightning Draw Southeast field (shown in pink) and background areas. See figure 5-11 for description of geologic units (geologic base modified from Doelling, 2005) and figure 5-1 for explanations of well symbols; form line contours based on structure contour map of the Leadville Limestone shown on figure 5-5.

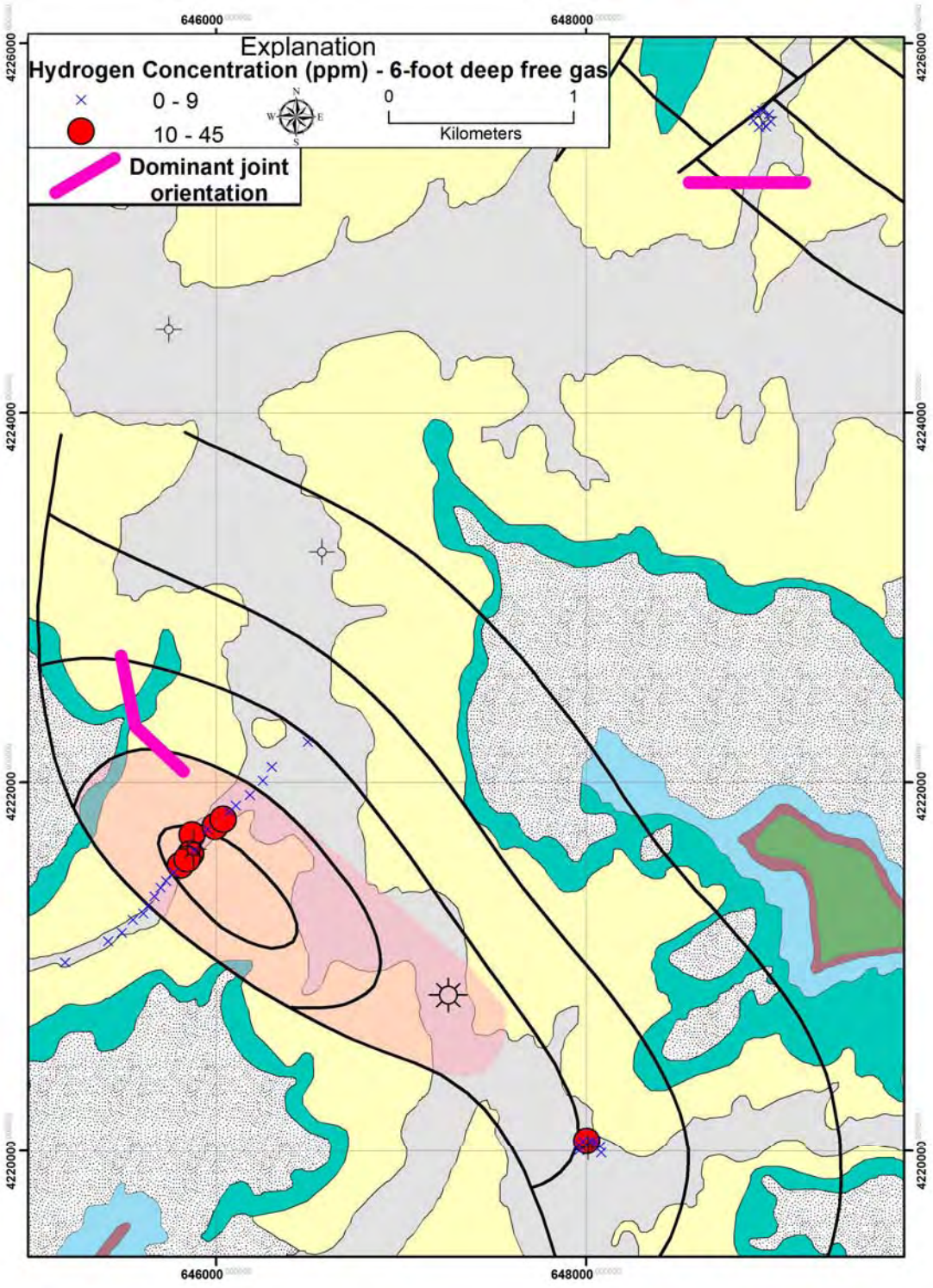

Figure 5-36. Distribution of hydrogen concentrations in 6-foot-deep free gas over Lightning Draw Southeast field (shown in pink) and background areas. See figure 5-11 for description of geologic units (geologic base modified from Doelling, 2005) and figure 5-1 for explanations of well symbols; form line contours based on structure contour map of the Leadville Limestone shown on figure 5-5.

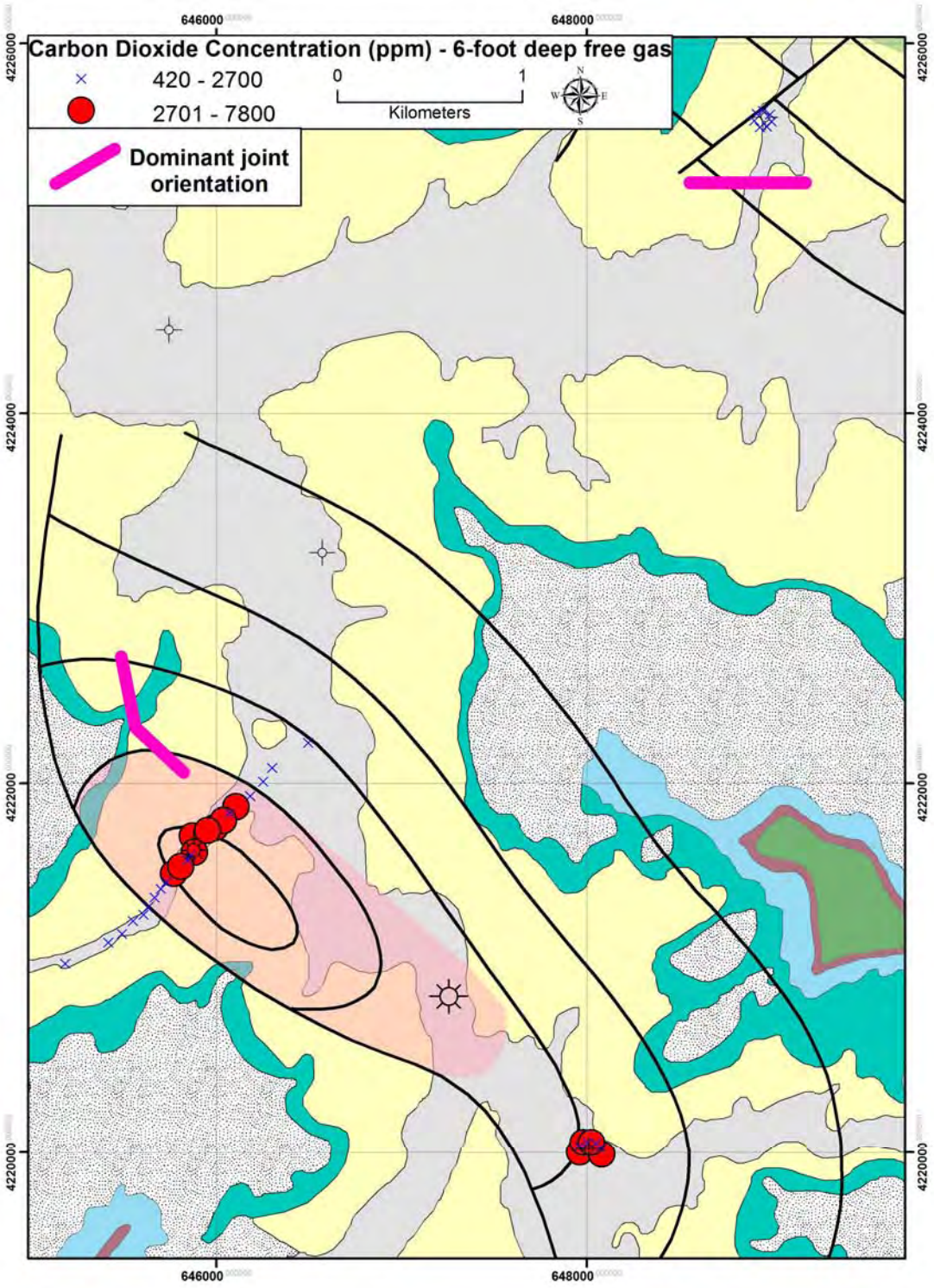

Figure 5-37. Distribution of carbon dioxide concentrations in 6-foot-deep free gas over Lightning Draw Southeast field (shown in pink) and background areas. See figure 5-11 for description of geologic units (geologic base modified from Doelling, 2005) and figure 5-1 for explanations of well symbols; form line contours based on structure contour map of the Leadville Limestone shown on figure 5-5.

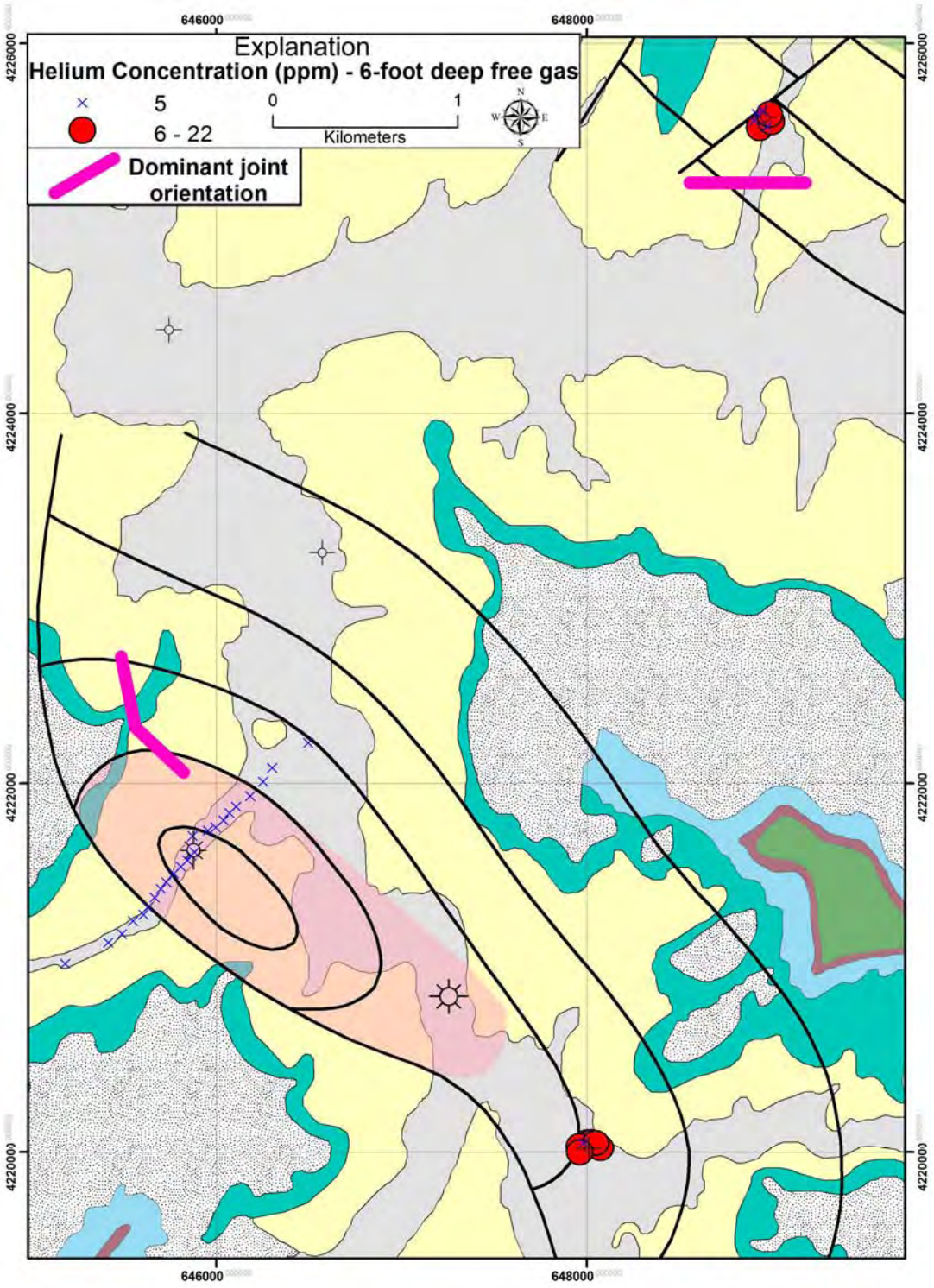

Figure 5-38. Distribution of helium concentrations in 6-foot-deep free gas over Lightning Draw Southeast field (shown in pink) and background areas. See figure 5-11 for description of geologic units (geologic base modified from Doelling, 2005) and figure 5-1 for explanations of well symbols; form line contours based on structure contour map of the Leadville Limestone shown on figure 5-5.

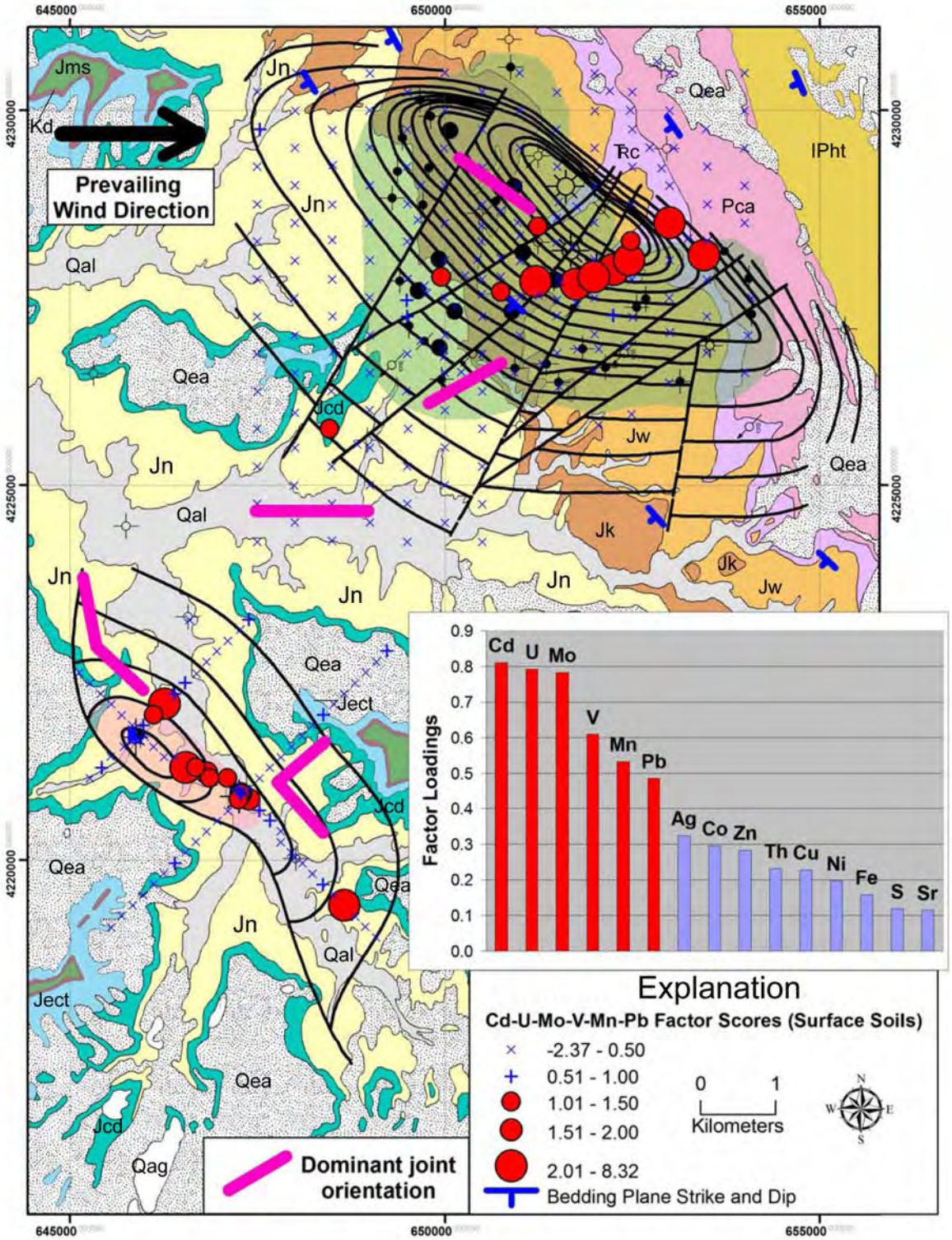

Figure 5-39. Distribution of cadmium-uranium-molybdenum-vanadium-manganese-lead factor scores in surface soils over Lisbon and Lightning Draw Southeast fields (shown in bluish green and pink, respectively). See figure 5-11 for description of geologic units (geologic base modified from Doelling, 2005) and figure 5-1 for explanations of well symbols; form line contours based on structure contour maps of the Leadville Limestone shown on figures 5-1 and 5-5.

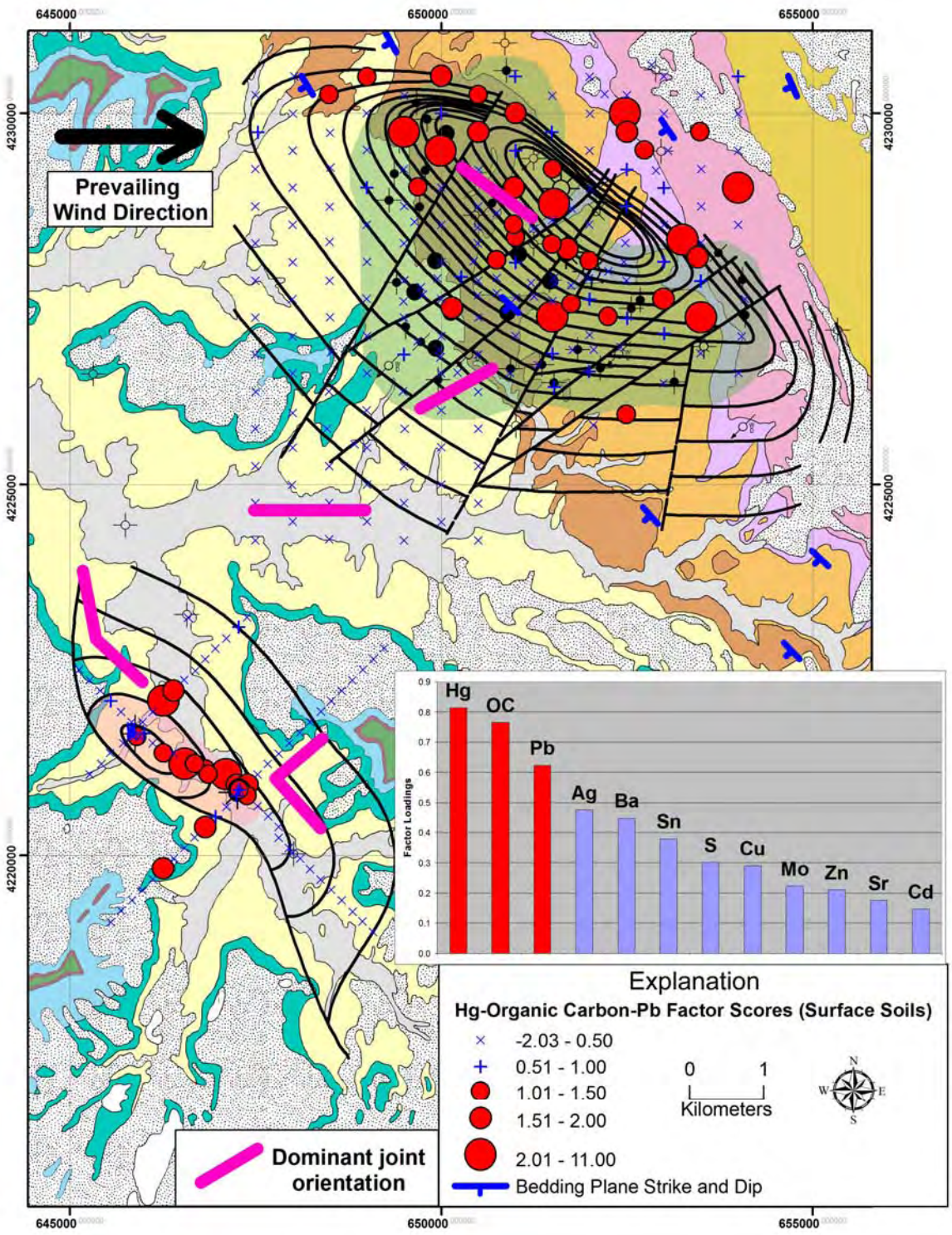

Figure 5-40. Distribution of mercury-organic carbon-lead factor scores in surface soils over Lisbon and Lightning Draw Southeast fields (shown in bluish green and pink, respectively). See figure 5-11 for description of geologic units (geologic base modified from Doelling, 2005) and figure 5-1 for explanations of well symbols; form line contours based on structure contour maps of the Leadville Limestone shown on figures 5-1 and 5-5.

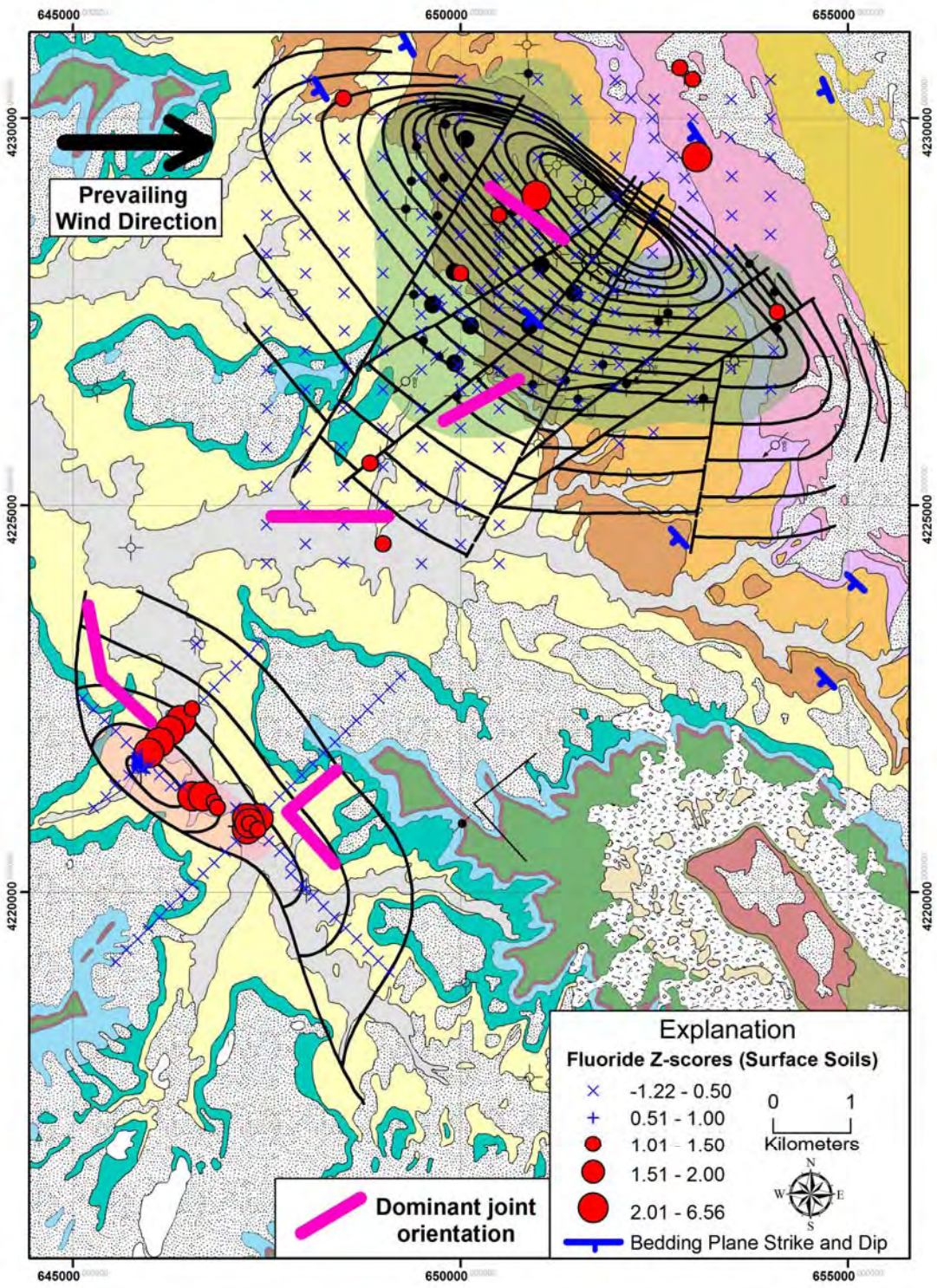

Figure 5-41. Distribution of fluoride Z-scores in surface soils over Lisbon and Lightning Draw Southeast fields (shown in bluish green and pink, respectively). See figure 5-11 for description of geologic units (geologic base modified from Doelling, 2005) and figure 5-1 for explanations of well symbols; form line contours based on structure contour maps of the Leadville Limestone shown on figures 5-1 and 5-5.

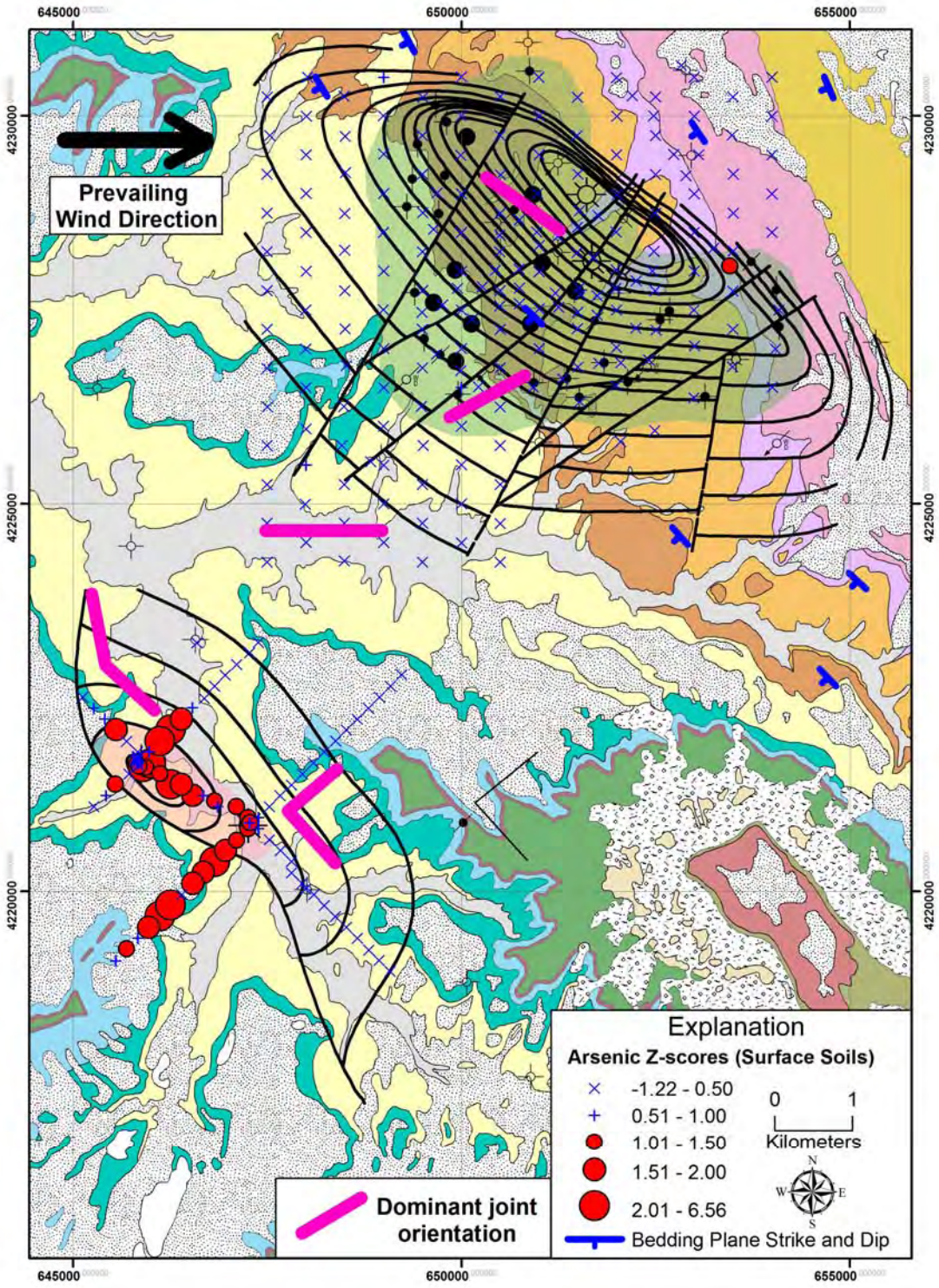

Figure 5-42. Distribution of arsenic Z-scores in surface soils over Lisbon and Lightning Draw Southeast fields (shown in bluish green and pink, respectively). See figure 5-11 for description of geologic units (geologic base modified from Doelling, 2005) and figure 5-1 for explanations of well symbols; form line contours based on structure contour maps of the Leadville Limestone shown on figures 5-1 and 5-5.

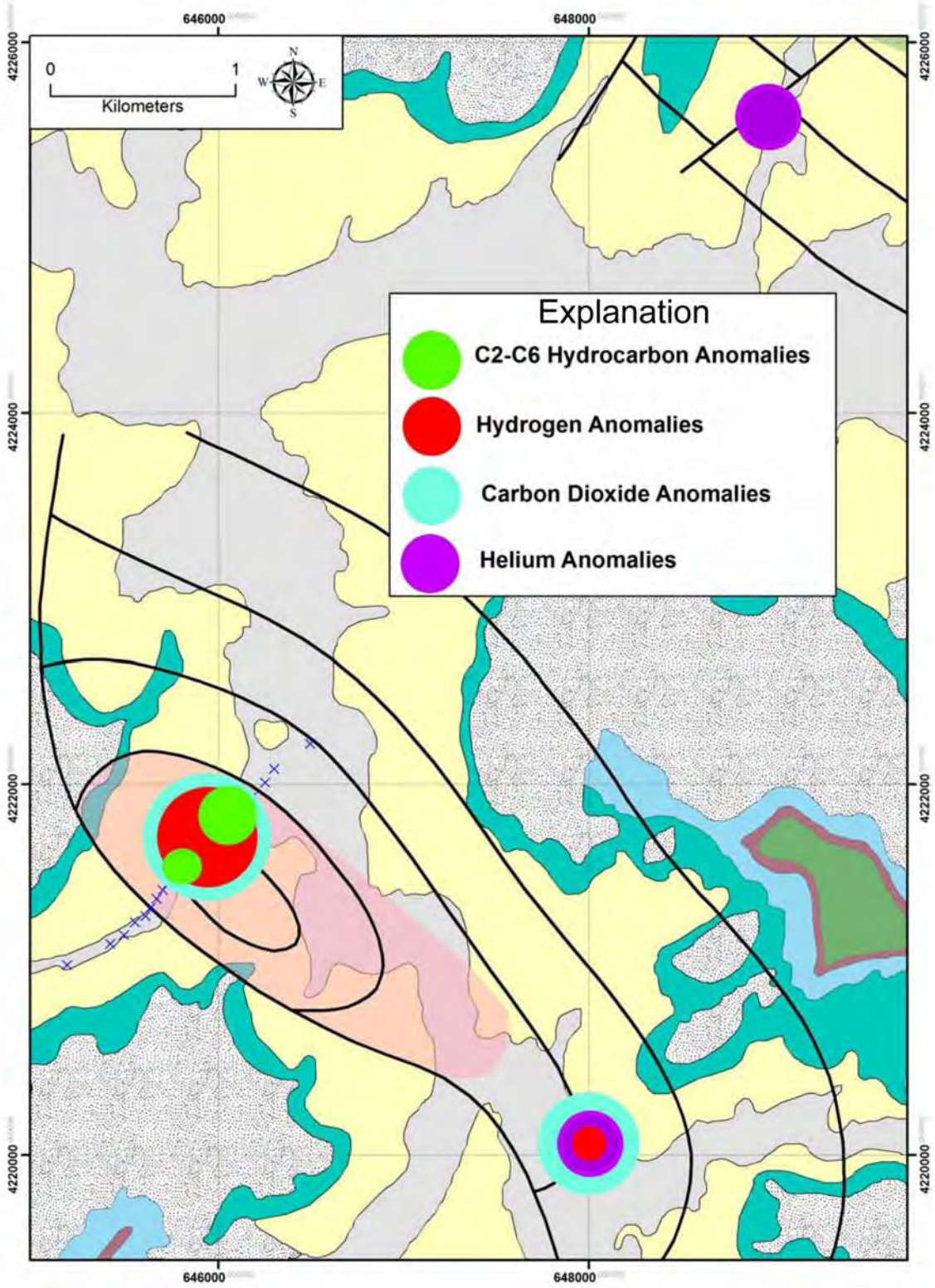

Figure 5-43. Distribution of hydrocarbon and fixed-gas anomalies in free gas over Lightning Draw Southeast field (shown in pink). See figure 5-11 for description of geologic units (geologic base modified from Doelling, 2005). Form line contours based on structure contour map of the Leadville Limestone shown on figures 5-5.

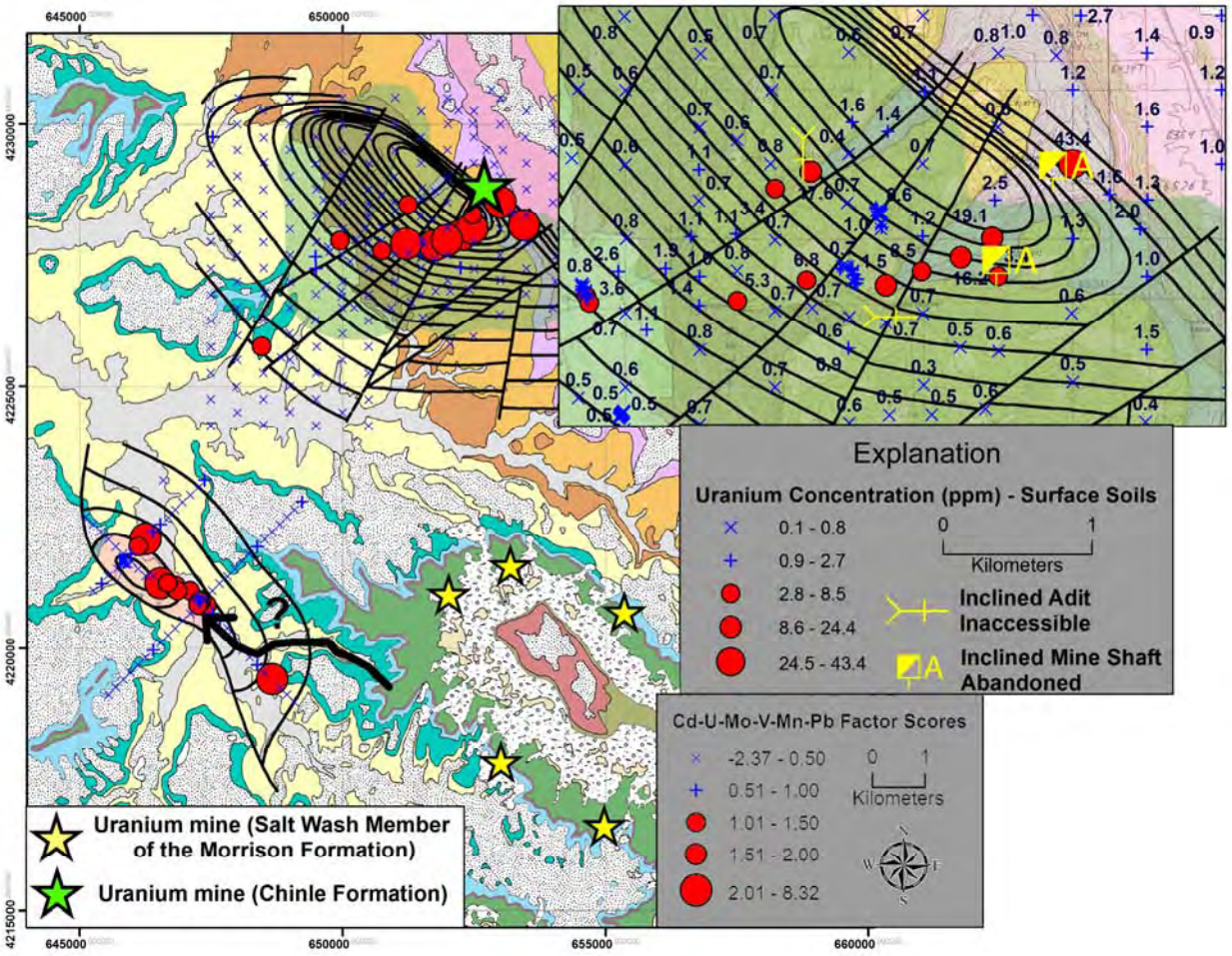

Figure 5-44. Distribution of cadmium-uranium-molybdenum-vanadium-manganese-lead factor scores in surface soils over Lisbon and Lightning Draw Southeast fields (shown in bluish green and pink, respectively) and location of uranium mines. See figure 5-11 for description of geologic units (geologic base modified from Doelling, 2005) and figure 5-1 for explanations of well symbols; form line contours based on structure contour maps of the Leadville Limestone shown on figures 5-1 and 5-5.

Table 5-1. Produced gas compositions (weight percent) from Lisbon and Lightning Draw Southeast fields. Courtesy of EnCana Oil & Gas (USA) Inc and ST Oil Company.

	Lisbon Gas Cap		Lisbon Oil Leg		Lightning Draw Southeast Gas	
Well No.	**D-810**	**C-910**	**C-99**	**D-716**	**Federal 1-31**	**Evelyn Chambers Gov. 1**
Cumulative Production* (September 1, 2008)	23.2 BCFG 21,631 BO	26.4 BCFG 23,952 BO	12.9 BCFG 503,915 BO	10.2 BCFG 556,660 BO	0.08 BCFG 495 BO	0.28 BCFG 3090 BO
Methane	36.16	38.28	37.83	40.27	27.01	23.97
Ethane	7.44	8.39	8.87	8.63	4.85	3.90
Propane	2.76	2.45	4.88	4.40	3.26	2.59
Isobutane	0.48	0.40	0.93	0.83	0.71	0.60
Normal Butane	0.26	0.21	0.48	0.45	0.40	0.34
Isopentane	0.29	0.22	0.55	0.51	0.50	0.41
Normal Pentane	0.35	0.27	0.67	0.62	0.58	0.46
Carbon Dioxide	23.58	28.78	30.89	27.69	27.02	36.64
Hydrogen Sulfide	1.37	1.00	0.20	0.28	0.00	0.00
Nitrogen	25.97	18.85	13.18	14.66	33.48	29.20
Helium	0.70	0.66	0.53	0.66	1.42	1.40
Hexanes+	0.62	0.50	0.99	1.00	0.77	0.48
Total	99.97	100.00	100.00	100.00	100.00	100.00

* Utah Division of Oil, Gas and Mining (2008).

Table 5-2. Components reported by four analytical methods.

C_1-C_{12} Hydrocarbons	Seven Anions	53 Major and Trace Elements	Synchronous Scanned Fluorescence
methane, ethane, ethene, propane, propene, i-butane, n-butane, butene, i-pentane, n-pentane, pentene, i-hexane, n-hexane, hexene, i-heptane, n-heptane, heptene, i-octane, n-octane, benzene, n-butylbenzene, cyclohexane, n-decane, n-dodecane, ethylbenzene, m-ethyltoluene, p-ethyltoluene, indane, naphthalene, n-nonane, n-propylbenzene, 1,2,4,5-tetramethylbenzene, toluene, 1,2,4-trimethylbenzene, 1,3,5-trimethylbenzene, n-undecane, m-xylene, p-xylene, and o-xylene.	fluoride, chloride, bromide, nitrite, nitrate, phosphate, sulfate	Ag, Al, As, Au, B, Be, Bi, Ca, Cd, Ce, Co, Cr, Cs, Cu, Fe, Ga, Ge, Hf, Hg, I, In, K, La, Li, Mg, Mn, Mo, Na, Nb, Ni, P, Pb, Pd, Pt, Rb, Re, S, Sb, Sc, Se, Sn, Sr, Ta, Te, Th, Ti, Tl, U, V, W, Y, Zn, Zr	Fluorescence intensities in the 250 to 500 nm range that correspond to condensate, medium-gravity oil, and low-gravity oil. Allows fingerprint matching with produced oils in the area.

Table 5-3. Organic and inorganic anomaly types identified in different sample media over Lisbon and Lightning Draw Southeast fields.

	Lisbon Field	Lightning Draw Southeast Field
Surface Soils	methane, ethane, ethene, propane, propene, i-butane, n-butane, butene, i-pentane, n-pentane, pentene, i-hexane, n-hexane, hexene, i-heptane, n-heptane, heptene, i-octane, n-octane, benzene, n-butylbenzene, cyclohexane, n-decane, n-dodecane, ethylbenzene, m-ethyltoluene, p-ethyltoluene, indane, naphthalene, n-nonane, n-propylbenzene, 1,2,4,5-tetramethylbenzene, toluene, 1,2,4-trimethylbenzene, 1,2,5-trimethylbenzene, n-undecane, m-xylene, p-xylene, and o-xylene Bi, Cd, Hg, Mo, Pb, U, V 297-305 nm factor scores, 395-470 nm factor scores	methane, ethane, ethene, propane, propene, i-butane, n-butane, butene, i-pentane, n-pentane, pentene, i-hexane, n-hexane, hexene, i-heptane, n-octane, benzene, n-butylbenzene, n-decane, n-dodecane, ethylbenzene, m-ethyltoluene, p-ethyltoluene, indane, naphthalene, n-nonane, n-propylbenzene, 1,2,4,5-tetramethylbenzene, toluene, 1,2,4-trimethylbenzene, 1,3,5-trimethylbenzene, n-undecane, m-xylene, p-xylene, and o-xylene Ag, Al, As, Be, Bi, Co, Cu, Ga, Hf, Hg, La, Li, Mo, Pb, Sc, Sn, Sr, Tl, U, V, Zn, Zr 297-305 nm factor scores, 395-470 nm factor scores
Outcrop Lichen	ethane, ethene, propene, i-butane, butene, pentene, hexene, benzene, n-butylbenzene, n-decane, ethylbenzene, m-ethyltoluene, p-ethyltoluene, indane, naphthalene, n-nonane, n-propylbenzene, 1,2,4,5-tetramethylbenzene, toluene, 1,2,4-trimethylbenzene, 1,2,5-trimethylbenzene, m-xylene, p-xylene, and o-xylene Ag, Al, As, Au, B, Ba, Bi, Co, Cu, Ga, Hf, K, La, Li, Mo, Na, Pb, Re, Sb, Sc, Sn, Sr, Th, Ti, Tl, U, V, Y, Zn, Zr 305 nm Intensity	methane, ethane, ethene, propene, i-butane, butene, pentene, hexene, benzene, indane, naphthalene, 1,2,4-trimethylbenzene, 1,2,5-trimethylbenzene, o-xylene. Ag, Al, As, B, Ba, Bi, Co, Cu, Ga, Hf, K, Li, Mo, Na, Pb, Sb, Sc, Sr, Th, Tl, Zr 305 nm Intensity
Outcrop Soils	methane, ethane, propane, propene, butene, pentene, hexene, n-octane, n-butylbenzene, m-ethyltoluene, p-ethyltoluene, naphthalene, 1,2,4,5-tetramethylbenzene, 1,2,4-trimethylbenzene, 1,2,5-trimethylbenzene, n-undecane, n-dodecane Ag, Cl, Na, NO_4, Re, S, Se, SO_4, U, Y 305 and 335 nm Intensity	methane, ethane, ethene, propane, propene, butene, pentene, hexene, n-octane, ethylbenzene, n-butylbenzene, m-ethyltoluene, p-ethyltoluene, indane, naphthalene, 1,2,4,5-tetramethylbenzene, 1,2,4-trimethylbenzene, 1,2,5-trimethylbenzene, n-undecane, m-xylene, p-xylene, Ag, As, Co, S, Se, Y
Free Gas	No free gas collected	ethane, propane, propene, i-butane, n-butane, i-pentane, n-pentane, i-hexane, hydrogen, carbon dioxide helium, carbon dioxide, and hydrogen at margins of reservoirs

Table 5-4. Correct and incorrect classifications for discriminant models (surface soils). Orange shading represents the field being predicted by the model.

Model	Correct classification (% of samples over field)		Incorrect classification (% of samples off field)	
	Lisbon	Lightning Draw SE	Lisbon	Lightning Draw SE
Lisbon Gas Probability	16	4	7	0
Lisbon Oil Probability	7	8	0	0
Lisbon Gas/Oil Probability	20	26	12	5
Lightning Draw SE Gas Probability	3	38	2	3

Table 5-5. Correct and incorrect classifications for discriminant models (outcrop facture-fill lichen). Orange shading represents the field being predicted by the model.

Model	Correct Classification (% of samples over field)		Incorrect Classification (% of samples off field)	
	Lisbon	Lightning Draw SE	Lisbon	Lightning Draw SE
Lisbon Gas Probability	100	14	0	0
Lisbon Oil Probability	100	28	0	0
Lightning Draw SE Gas Probability	75	100	0	0

Table 5-6. Correct and incorrect classifications for discriminant models (outcrop facture-fill soils). Orange shading represents the field being predicted by the model.

Model	Correct Classification (% of samples over field)		Incorrect Classification (% of samples off field)	
	Lisbon	Lightning Draw SE	Lisbon	Lightning Draw SE
Lisbon Gas Probability	100	71	0	0
Lisbon Oil Probability	83	0	0	0
Lightning Draw SE Gas Probability	50	100	0	0

Table 5-7. Percent of anomalous free-gas samples over and off Lightning Draw Southeast field.

Variable	% of anomalous samples over field	% of anomalous samples off field
Propane	19	0
Iso-Hexane	19	0
Hydrogen	38	7
Carbon Dioxide	50	27
Helium	0	60

Table 5-8. Percent of anomalous soil samples over and off Lightning Draw Southeast field.

Variable	%anomalous samples over field/total samples over field x 100)		%anomalous samples off field/total samples off field x 100)	
	Lisbon	Lightning Draw SE	Lisbon	Lightning Draw SE
Cd-U-Mo-V-Mn-Pb Factor Scores	3	21	2	3
Hg-Organic Carbon-Pb Factor Scores	12	23	8	6
Fluoride Z-scores	1	38	6	4
Arsenic Z-scores	1	49	0	15

CHAPTER 6
POTENTIAL OIL-PRONE AREAS IN THE PARADOX FOLD AND FAULT BELT, UTAH, BASED ON SHOWS IN DRILL CUTTINGS USING EPIFLUORESCENCE MICROSCOPY TECHNIQUES

David E. Eby, Eby Petrography & Consulting, Inc.,
and
Thomas C. Chidsey, Jr., and
Craig D. Morgan, Utah Geological Survey

Introduction

Potential oil-prone areas for the Mississippian Leadville Limestone were identified in the northern Paradox Basin (Paradox fold and fault belt), Utah, based on hydrocarbon shows using low-cost epifluorescence (EF) techniques. The trapping mechanisms for Leadville producing fields in this region are usually anticlines bounded by large, basement-involved normal faults. Epifluorescence microscopy is a technique used to provide information on diagenesis, pore types, and organic matter (including "live" hydrocarbons) within sedimentary rocks. It is a rapid, non-destructive procedure that uses a petrographic microscope equipped with reflected-light capabilities, a Hg-vapor light, and appropriate filtering. For an overview of EF principles, previous work, and methodology, refer to Chapter 4.

Sampling Compilation, Examination, and Evaluation

Wells penetrating the Leadville Limestone in the Utah part of the Paradox fold and fault belt were plotted and all Leadville well cuttings available from the collection at the Utah Core Research Center were compiled. Cuttings were examined under a binocular microscope and porous samples of dolomite and some limestone were selected from various zones over the Leadville section (figure 6-1): generally four to ten samples per depth interval from each well. The cuttings were placed on Petrologs™, a small plastic, self-adhesive compartmentalized cutting storage unit, for EF examination (figure 6-2). (All Petrologs™ containing Leadville cuttings from the project are stored at the Utah Core Research Center and are available to the public.) Thus, sample preparation is inexpensive and rapid.

Approximately 900 cutting samples were selected from 32 wells penetrating the Leadville Limestone (six producing gas, condensate, and oil wells, as well as 26 non-productive wells) throughout the region (table 6-1; see Appendix D for detailed descriptions, binocular microscope images of selected cuttings, and thin section photomicrographs). These cuttings display mainly intercrystalline porosity, occasional small vugs or molds, and other pore types (figure 6-3). Oil staining, bitumen, and stylolites are also observed (figure 6-3).

Examination of cuttings included photo-documentation under EF and plane-polarized light at the same magnification. Photomicrography of the compositional, textural, and pore structure attributes was done using high-speed film (ISO 800 and 1600) with some bracketing of exposures as camera metering systems do not always reliably read these high-contrast images in the yellow and green light spectrum. Since the image brightness is directly proportional to

magnification, the best images are obtained at relatively high magnifications (such as greater than 100X). Low-power fluorescence is often too dim to effectively record on film.

Epifluorescence petrography makes it possible to clearly identify hydrocarbon shows in Leadville cuttings selected for study. A qualitative visual rating scale (a range and average) based on EF evaluation was applied to the group of cuttings from each depth in each well (table 6-2 and figure 6-4). Using the qualitative visual rating scale, the highest maximum and highest average EF reading from each well were plotted and mapped (figures 6-5 and 6-6).

Discussion

Epifluorescence allows one to observe the presence of any soluble hydrocarbons. Samples displaying fluorescence represent areas where hydrocarbons may have migrated or accumulated. The best fluorescence, when present, was gold and occurred in high porosity (figure 6-4A), low permeability dolomites (thus the major reason the collection effort concentrated on porous dolomites). Pale-yellow fluorescence indicated possible high-gravity oil (figure 6-4B). If no fluorescence was observed in porous dolomites, the samples were also good representatives of areas where hydrocarbons had not migrated or accumulated. Bitumen (pyrobitumen) was common in many samples. It has no activity within the hydrocarbon molecules and therefore does not fluoresce (figure 6-4D).

As expected, productive Leadville wells (fields such as Lisbon and Salt Wash) have cuttings distinguished by generally higher EF readings (figures 6-5 and 6-6). However, a regional southeast-northwest trend of relatively high EF from Leadville cuttings parallels the southwestern part of the Paradox fold and fault belt from Lisbon field to west of the town of Green River. A visual reading of 2.0 to 3.0 for the highest maximum EF (figure 6-5) and 2.0 to 2.5 for the highest average EF (figure 6-6) occur in this region. The northeastern part of the fold and fault belt shows a regional trend of low EF including a large area of essentially no EF (a visual reading of less than 0.4 for the maximum highest average EF) centered around the town of Moab (figure 6-6).

These EF maps imply hydrocarbon migration and dolomitization was associated with regional northwest-trending faults and fracture zones, which created potential oil-prone areas along the southwest trend. Hydrocarbons may have migrated from organic-rich shales in the Pennsylvanian Paradox Formation where they are in contact with the Leadville Limestone along faults. Hydrothermal alteration associated with these faults and related fracture zones may have generated late, porous dolomite and thus produced diagenetic traps indicated by EF.

Alternative interpretations for the lack of significant EF in the northeast trend is the possibility that (1) most hydrocarbons may have been flushed out to the southwest by hydrodynamic processes, and (2) the northeast part of the Paradox fold and fault belt has passed the oil window and gone into the dry gas/post-oil window stage maturation. A final explanation is that these EF trends could be related to facies or karst development in the Leadville Limestone. At any rate, the mapping of hydrocarbon shows based on EF indicates exploration efforts should be concentrated in suggested oil-prone areas along the southwest part of the Paradox fold and fault belt.

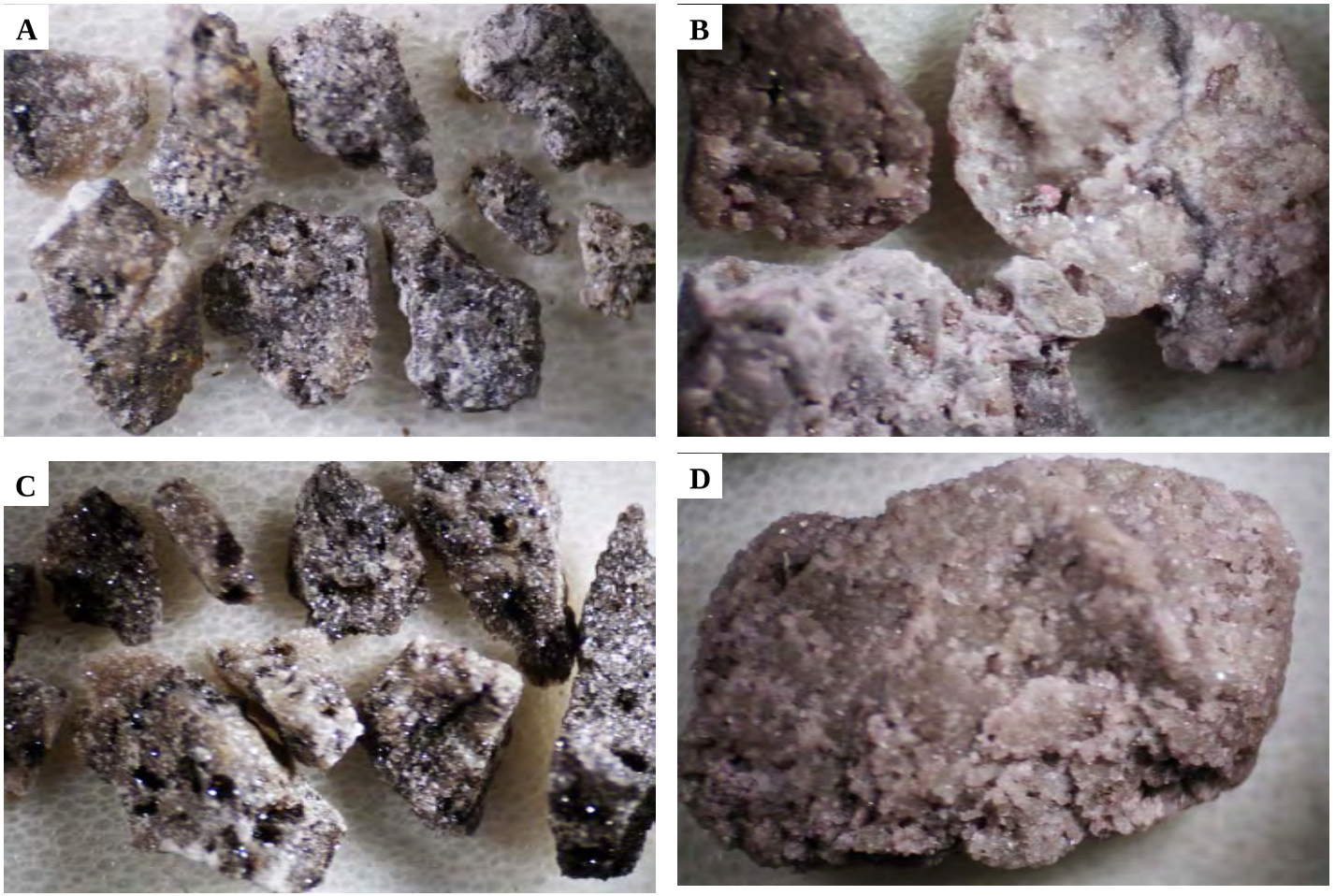

Figure 6-1. Examples of cuttings selected from various Leadville zones as observed with a binocular microscope. A – Overview of dolomite cuttings (16X) from 9410 to 9420 feet containing porosity and bitumen in the Pure Spiller Canyon State 1 well (SW1/4SW1/4 section 16, T. 30 S., R. 25 E., [SLBL&M], San Juan County). B – Overview of dolomite cuttings (13X) from 7800 to 7810 feet containing porosity and stylolites in the Hatch Mesa 1 well (SE1/4SW1/4 section 22, T. 28 S., R. 21 E., SLBL&M, San Juan County). C – Overview of dolomite cuttings (12X) from 10,020 to 10,023 feet containing porosity and bitumen in the Pure USA Big Indian 1 well (SE1/4SE1/4 section 33, T. 29 S., R. 24 E., SLBL&M, San Juan County). D – Single white dolomite cutting (14X) with good intercrystalline porosity from 7790 to 7800 feet containing porosity and stylolites in the Hatch Mesa 1 well.

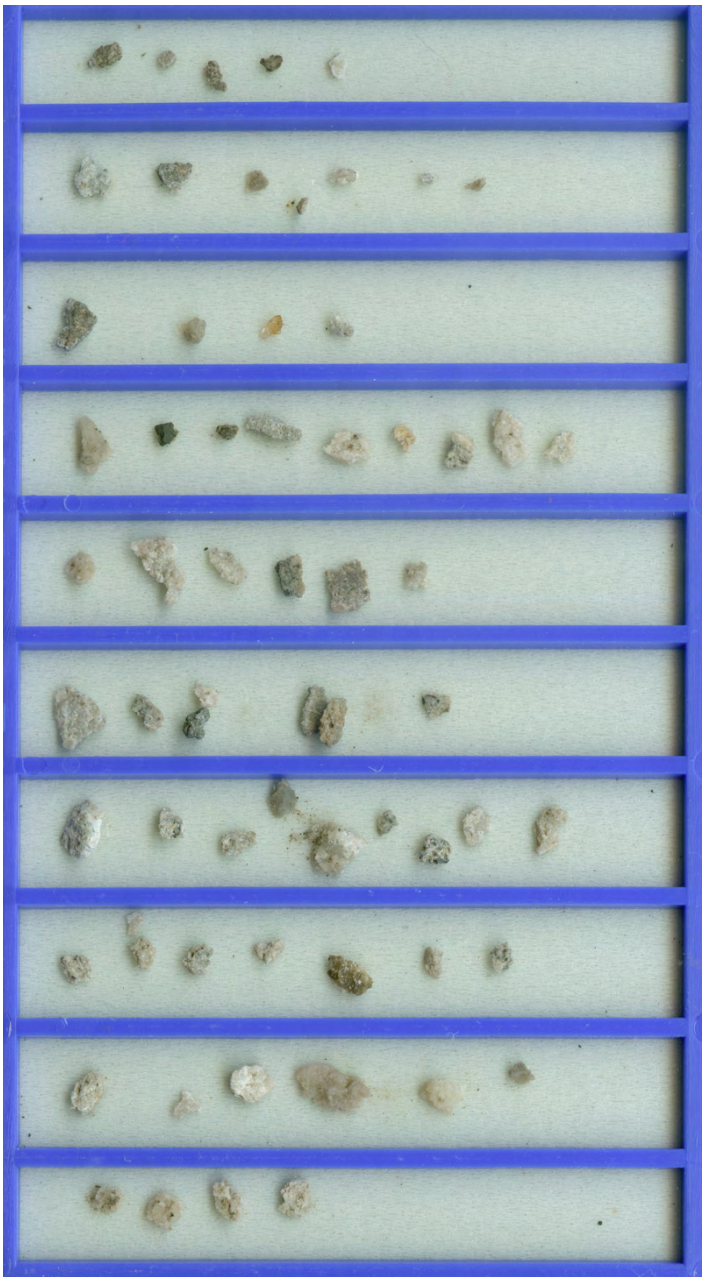

Figure 6-2. Example of cuttings selected from various Leadville zones between 6875 to 7075 feet, Pure Mineral Point 1 well (section 7, T. 26 S., R. 18 E., [SLBL&M], Grand County), placed on Petrologs™ for epifluorescence examination.

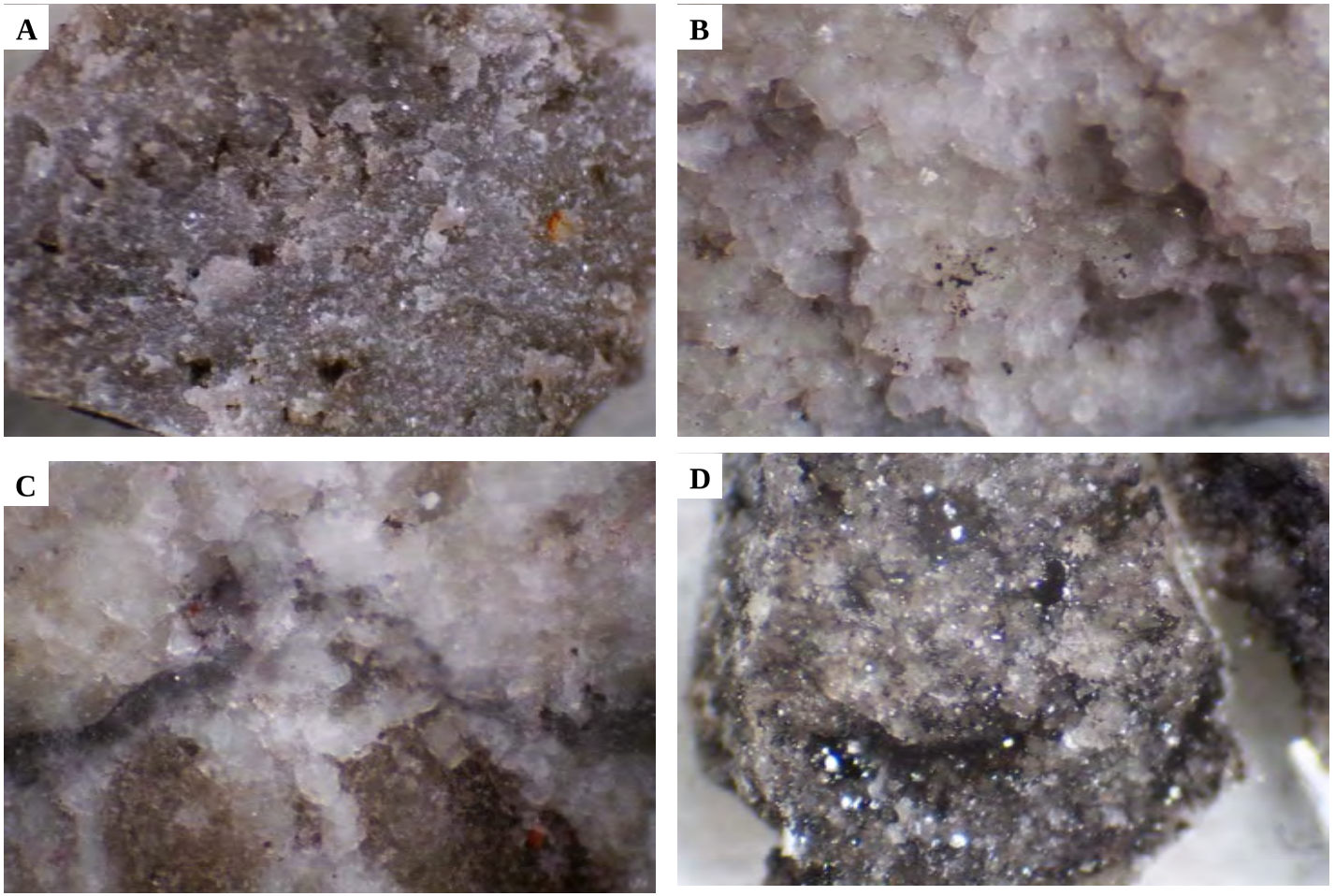

Figure 6-3. Close-up views of petrographic characteristics of Leadville cuttings as observed with a binocular microscope. A – Large, single sample of tight dolomite with widely spaced small vugs from 7780 to 7790 feet in the Hatch Mesa 1 well (SE1/4SW1/4 section 22, T. 28 S., R. 21 E., SLBL&M, San Juan County). B – Sample of white dolomite with good intercrystalline porosity from 7790 to 7800 feet contain porosity and bitumen in the Hatch Mesa 1 well; note possible sulfide replacement (opaque). C – Sample showing stylolite overprinted with dolomite replacement from 7800 to 7810 feet in the Hatch Mesa 1 well; note possible sulfide replacement. D – Sample showing dolomite containing small vugs and intercrystalline porosity lined with bitumen from 10,020 to 10,023 feet in the Pure USA Big Indian 1 well (SE1/4SE1/4 section 33, T. 29 S., R. 24 E., SLBL&M, San Juan County).

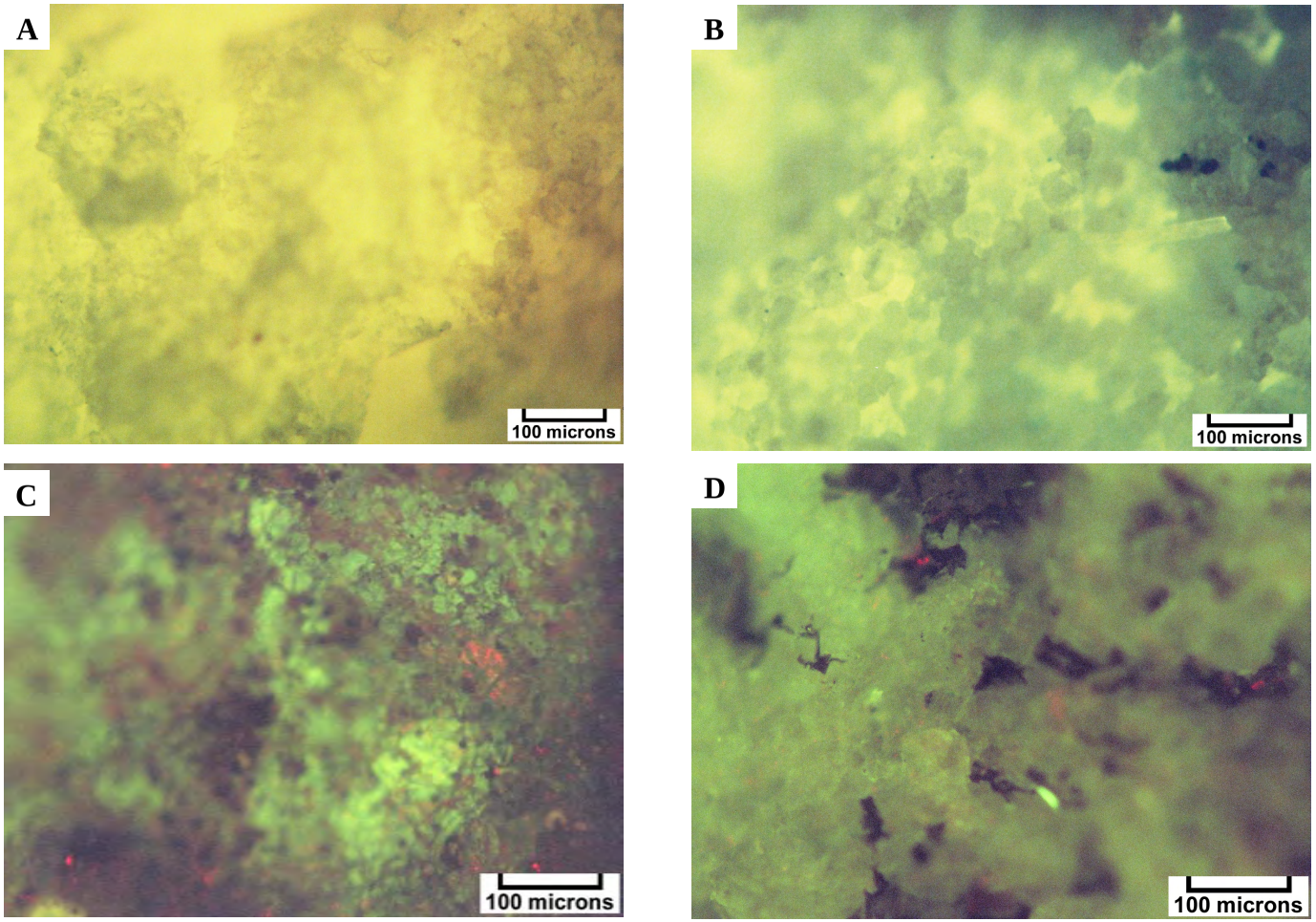

Figure 6-4. Photomicrographs under moderate magnification showing examples of visually rated epifluorescence. A – Bright fluorescence, rated 3.0, in medium crystalline dolomite with fair to good intercrystalline porosity from 5935 to 5945 feet in the Federal Hatt 1 well (SE1/4SE1/4 section 19, T. 23 S., R. 14 E., SLBL&M, Emery County). B – Moderate fluorescence, rated 2.0, fine to medium crystalline dolomite from 10,240 to 10,250 feet in the Gulf Muleshoe 1 well (section 2, T. 28 S., R. 23 E., SLBL&M, San Juan County). C – Weak fluorescence, rated 1.0, medium to coarsely crystalline dolomite with fairly good bitumen-lined, intercrystalline porosity from 9150 to 9160 feet in the Pure Spiller Canyon 1 well (SW1/4SW1/4 section 16, T. 30 S., R. 25 E., SLBL&M, San Juan County); note abundant iron distribution (red), bitumen is black. D – No to very weak fluorescence, rated 0.2, medium to coarsely crystalline dolomite containing bitumen and iron from 10,020 to 10,023 feet in the Pure USA Big Indian 1 well (SE1/4SE1/4 section 33, T. 29 S., R. 24 E., SLBL&M, San Juan County).

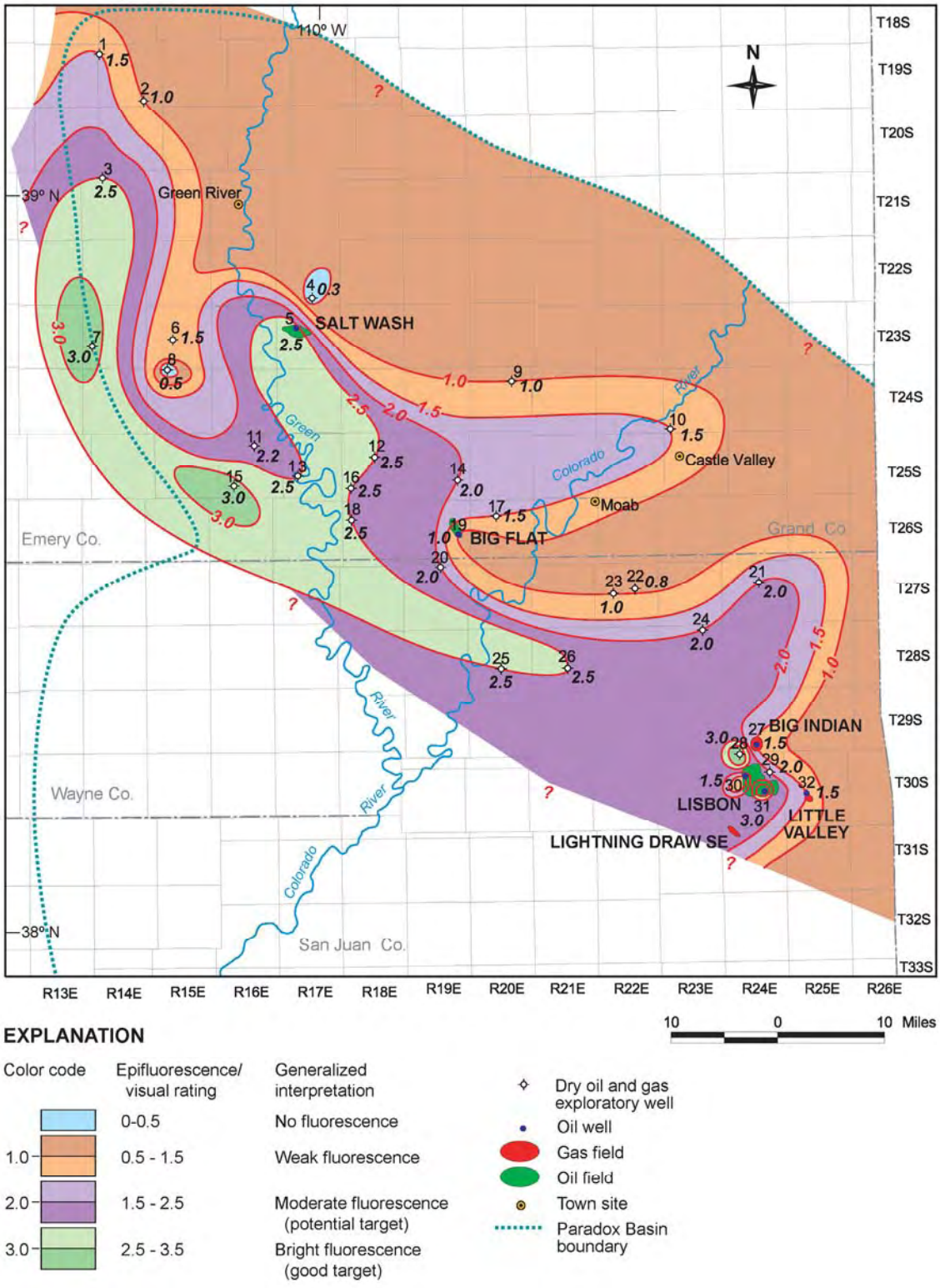

Figure 6-5. Map of the highest maximum epifluorescence based on visual rating of well cuttings, Paradox fold and fault belt, Utah.

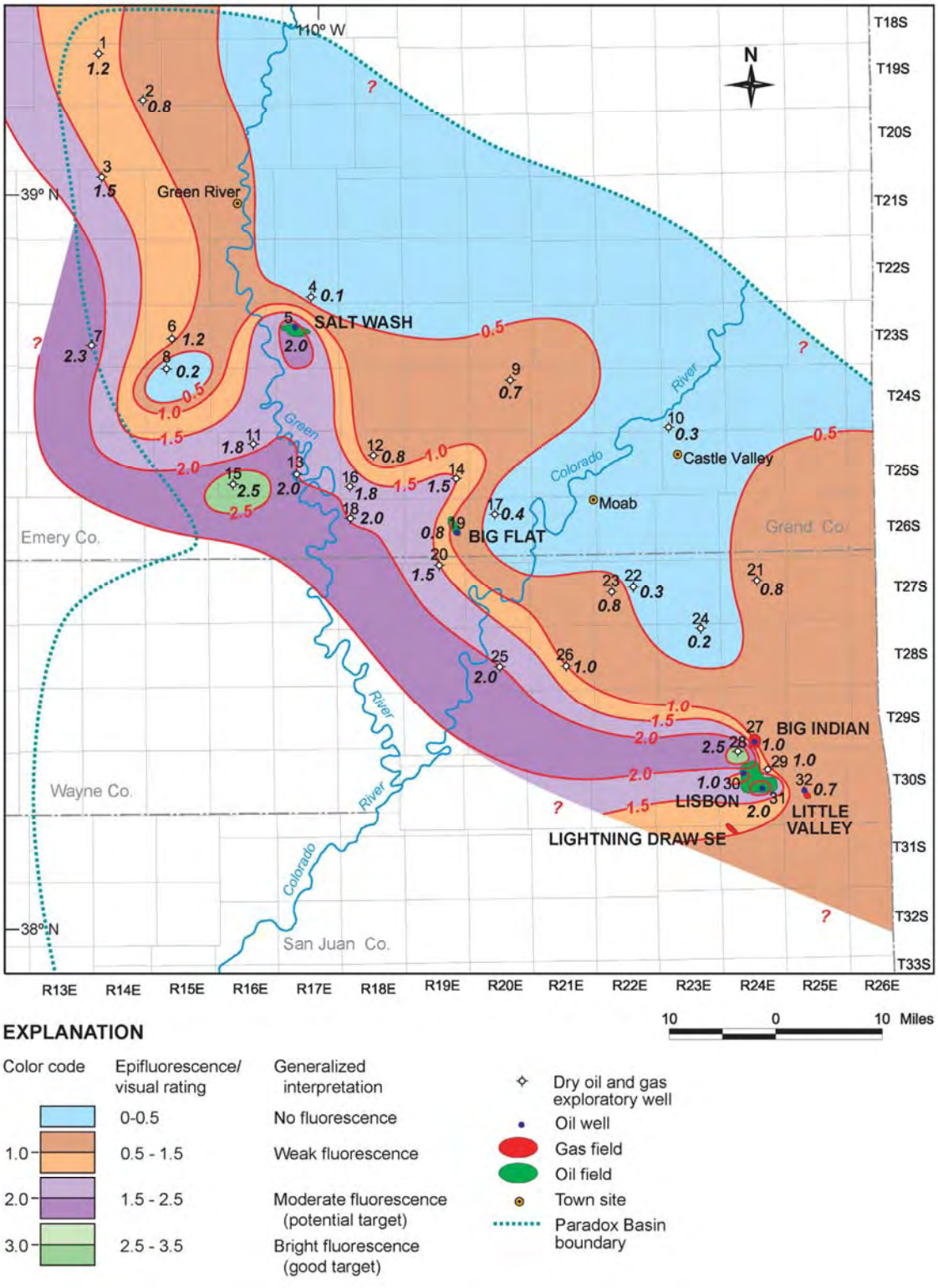

Figure 6-6. Map of the highest average epifluorescence based on visual rating of well cuttings, Paradox fold and fault belt, Utah.

Table 6-1. Wells in the Paradox fold and fault belt, Utah, containing Leadville Limestone cuttings evaluated using epifluorescence techniques. N = number of samples.

Map #	Well Name	Location	County	Interval (ft)	N	Visual EF Rating	
						Highest Maximum	Highest Average
1	Woodside 1	SESE 12 19S 13E	Emery	6580-6750	23	1.5	1.2
2	Hatch Sphinx Unit 1-A	SWNW 35 19S 14E	Emery	8670-8715	45	1.0	0.8
3	Denison Mines 5-1	5 21S 14E	Emery	5830-5870	23	2.5	1.5
4	Salt Wash 22-34	34 22S 17E	Grand	10070-10085	16	0.3	0.1
5	Government Smoot 1	CSENE 17 23S 17E	Grand	8732-8737	16	2.5	2.0
6	Chaffin 1	NENW 21 23S 15E	Emery	7460-7540	26	1.5	1.2
7	Federal Hatt 1	SESE 19 23S 14 E	Emery	5905-6020	33	3.0	2.3
8	Gov 45-5	5 24S 15E	Emery	6899-6935	5	0.5	0.2
9	State 12-11	SWNW 11 24S 20E	Grand	11810-11850	50	1.0	0.7
10	Federal 31	NWSE 31 24S 23E	Grand	10450-10760	27	1.5	0.3
11	Gruvers Mesa 2	10 25S 16E	Emery	6750-6910	32	2.2	1.8
12	McRae Fed 1	SWSW 10 25S 18E	Grand	8485-8550	8	2.5	0.8
13	Bow Knot Unit 1	NESE 20 25S 17.5E	Grand	6075-6400	31	2.5	2.0
14	Big Flat/Bartlett Flat 1	NENE 26 25S 19 E	Grand	8560-8650	17	2.0	1.5
15	Lookout Point 1	SWSW 29 25S 16E	Emery	6380-6520	22	3.0	2.5
16	Fed Bowknoll 1	NESE 30 25S 18 E	Grand	7375-7390	12	2.5	1.8
17	Long Canyon 1	NENW 9 26S 20E	Grand	7560-7630	44	1.5	0.4
18	Mineral Point 1	7 26S 18E	Grand	6875-7075	65	2.5	2.0
19	Big Flat 3	NENE 23 26S 19E	Grand	7714-7725	51	1.0	0.8
20	Federal Ornsby 1	NWNE 3 27S 19E	Wayne	7740-7810	25	2.0	1.5
21	Gold Basin 1	NWNW 15 27S 24E	San Juan	14300-14410	37	2.0	0.8
22	Putnam 1	SENE 15 27S 22 E	San Juan	7410-7490	30	0.8	0.3
23	Unit 1 Bridger Sack Mesa	SESE 17 27S 22 E	San Juan	7030-7070	53	1.0	0.8
24	Muleshoe 1	2 28S 23E	San Juan	10240-10280	9	2.0	0.2
25	Lockhard Fed 1	SW 22 28S 20E	San Juan	5130-5050	37	2.5	2.0
26	Hatch Mesa 1	SESW 22 28S 21E	San Juan	7780-7820	23	2.5	1.0
27	USA Big Indian 1	NWSESE 33 29S 24E	San Juan	9960-10090	55	1.5	1.0
28	State 1	32 29.5S 24E	San Juan	9835-9852	16	3.0	2.5
29	NW Lisbon St. A	2 30S 24E	San Juan	9710-9725	12	2.0	1.0
30	Lisbon Valley C-1	NENW 9 30S 24E	San Juan	8765-70	20	1.5	1.0
31	Lisbon 814-A	CNWSW 14 30S 24E	San Juan	8870-8930	80	3.0	2.0
32	Spiller Canyon State 1	SWSW 16 30S 25E	San Juan	9080-9420	75	1.5	0.7

Table 6-2. Key to the epifluorescence qualitative visual "rating" scale.

Rating	Generalized Interpretation
0 – 0.5	No Fluorescence: Not capable of oil production. May be wet, if not a gas-bearing zone.
1.0 – 1.5	Weak Fluorescence: An "oil" show. Indicative of oil in the system, but not necessarily capable of production. Some dull or weak fluorescence may exist in a wet zone (especially if there is "speckled" fluorescence) or in a mixed oil/water zone.
2.0 – 2.5	Moderate Fluorescence: A good indication of oil within this zone. Probably capable of some oil production if there is adequate porosity and permeability.
3.0 – 3.5	Bright Fluorescence: A very good to excellent indication of oil within this zone. Should be capable of some oil production if there is adequate porosity and permeability.
3.5 – 4.0	Very Bright, Intense Fluorescence: Also a very good to excellent indication of oil within this zone. However, some very bright fluorescence may indicate very tight oil-bearing rocks or mature, oil-generating source rocks.

REGIONAL STUDIES OF THE MISSISSIPPIAN LEADVILLE LIMESTONE

CHAPTER 7
REGIONAL CORRELATION AND FACIES OF THE LEADVILLE LIMESTONE IN THE PARADOX BASIN AND NEIGHBORING AREA

Craig D. Morgan and Thomas C. Chidsey, Jr.,
Utah Geological Survey

Introduction

The Leadville Limestone in the Paradox Basin (Four Corners area) is a shallow, open-marine carbonate shelf deposit. The formation thins from the northwest to the southeast due to depositional onlap onto the shelf and erosion during periods when the shelf was subaerially exposed. The Leadville can be divided into informal upper and lower members separated by a regional disconformity within the formation (figure 2-3). According to Baars (1966) this disconformity can be correlated throughout the Paradox Basin. Mitchell (1961) noted that the contact between the upper and lower members at Lisbon field is unconformable and characterized by an abundance of chert clasts.

The traps for hydrocarbons in the Leadville are faults and fault-related anticlines. As a result, hydrocarbon production and most drilling oil shows are found along the northwest trending Paradox fold and fault belt (figure 1-1). Stratigraphically and diagenetically trapped accumulations of oil may exist in the Leadville, but these types of traps have not been a significant exploration play because their lack of surface expression makes their identification difficult.

Stratigraphy of the Leadville Limestone

The Paradox Basin is within the west-central part of the Colorado Plateau physiographic province. The basin area is often referred to as the Four Corners area because it is where the boundary of four states, Utah, Arizona, New Mexico, and Colorado, all join.

The Mississippian (late Kinderhookian through Osagean to early Meramecian) Leadville Limestone is a shallow, open marine carbonate-shelf deposit (figure 7-1). The same deposits are referred to as the Redwall Limestone (Grand Canyon nomenclature) in parts of the study area, but for convenience we use Leadville Limestone in this report. Unconformities separate the Leadville from the Devonian Ouray Limestone below and the Pennsylvanian Hermosa Group above (figure 7-1).

The Leadville Limestone thins from more than 700 feet (200 m) in the northwest corner of the Paradox Basin to less than 200 feet (60 m) in the southeast corner of the basin (figures 7-2 through 7-4). Parker and Roberts (1963) demonstrated that there is both erosional wedging out and depositional thinning of individual limestone members of the Leadville in a southeasterly direction. On figure 7-2, Leadville thicknesses are generalized and thus, many areas of local fault-related thinning are not displayed.

Paleodeposition and Lithology of the Leadville Limestone

During the Mississippian, the Colorado Plateau was covered by a shallow-shelf marine bank or platform with the shelf break into the deeper starved basin west of the Four Corners area (figures 7-5 and 7-6). The platform was an area of extensive carbonate deposition of nearly pure limestone implying arid conditions in the shallow sea lying south of the paleoequator (Blakey and Ranney, 2008). Little sand or mud was transported into the shallow, clear sea, providing favorable sites for the growth of lime-secreting marine organisms such as brachiopods, bryozoans, corals, and crinoids and other echinoderms (figure 7-7) (Blakey and Ranney, 2008). Leadville facies include open marine (crinoidal banks or oolitic shoals and Waulsortian-type buildups), middle shelf, and restricted marine (peloidal muds) based on evaluation of cores from regional exploration wells and Leadville fields in Utah (figure 7-2) (stored at the UGS's Utah Core Research Center). In the interior of the Leadville carbonate bank, conditions were right for early marine reflux dolomitization from magnesium-bearing brines (figure 7-5). During the Late Mississippian, the entire carbonate platform in southeastern Utah and southwestern Colorado was subjected to subaerial erosion resulting in formation of a lateritic regolith (Welsh and Bissell, 1979) (figures 7-8 and 7-9). Brecciation and sediment-filled cavities, related to karstification of the exposed Leadville, are relatively common throughout the upper third of the formation.

The Leadville carbonate bank is composed of oolitic, pelletal, birdseye, micritic, stromatolitic, and fossiliferous carbonates. Some of the Leadville Limestone is dolomitized (both early and late [possibly due to hydrothermal conditions]), crosscutting lithologies within the interior of the bank (Welsh and Bissell, 1979). The oil reservoir at Big Flat field is an example of a dolomitized Waulsortian mound on the shallow-shelf bank (Welsh and Bissell, 1979). At Lisbon field (figures 1-1 and 7-2), the dolomitic lower member is composed of mudstone, wackestone, packstone, and grainstone deposited in shallow-marine, subtidal, supratidal, and intertidal environments (Fouret, 1996). Porosity in the lower member is developed between dolomite rhombs and in vugs formed by solution of fossil material. The upper member is composed of mudstone, packstone, grainstone, and terrigenous clastics also deposited in subtidal, supratidal, and intertidal environments (Fouret, 1996). Reservoir rocks in the upper member are dolomitized crinoidal carbonate-mud deposits (Baars, 1966). For the complete descriptions of Lisbon reservoir depostional environments and diagenetic history, refer to Chapters 3 and 4.

Structural Setting

Faulting within the basin began in the Middle Pennsylvanian and was associated with the development of the Uncompahgre Highlands and Ancestral Rocky Mountains, although minor fault movement and related topography may have begun in the Mississippian. In areas of greatest paleorelief the Leadville is completely missing as a result of nondeposition or subsequent erosion (Baars, 1966).

Periodic movement along "blind," northwest-trending, basement-involved faults affected deposition of the Leadville Limestone. Ahr (1989) and Wilson (1975) presented evidence that structure may have influenced deposition of the Waulsortian mound facies in the Leadville. Crinoid banks accumulated in shallow-water environments on upthrown fault blocks or other paleotopographic highs.

Hydrocarbon Potential

Hydrocarbon production from the Leadville Limestone has been from fault and fault-related anticlinal traps. The production and most of the drilling oil shows have been from wells in the northwest-trending Paradox fold and fault belt. Buried fault blocks have been the most common target for exploration of hydrocarbons in the Leadville because they have a proven history of success and fault blocks can be identified on gravity, aeromagnetic, and seismic geophysical data. Stratigraphic oil accumulations may exist to the west and southwest of the fold and fault belt. Traps may be formed by porous Waulsortian mounds or other carbonate buildups, where porosity is further enhanced by early dolomitization. Traps may also be developed in the regolith deposits in both the upper and lower members. Diagenetic traps formed from late, possibly hydrothermal dolomite may be present especially along major fault trends (figure 1-1).

Subtle stratigraphic and diagenetic traps are difficult to identify in the Paradox Basin and, therefore, have not been significant exploration targets. Surface geochemical surveys and high-resolution 3D seismic may improve the ability of explorationists to identify these traps.

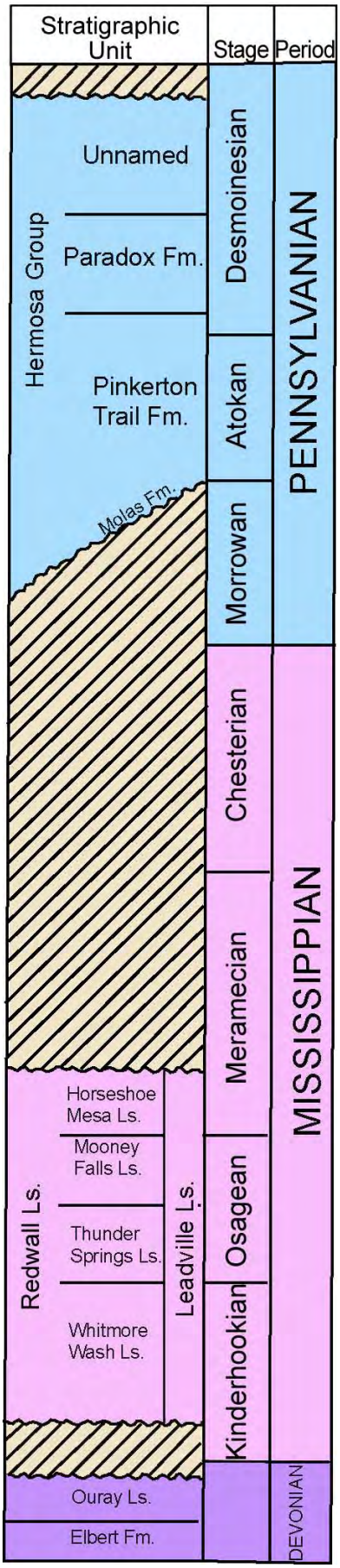

Figure 7-1. Devonian through Middle Pennsylvanian stratigraphic column for the Paradox Basin. Modified from Welsh and Bissell (1979).

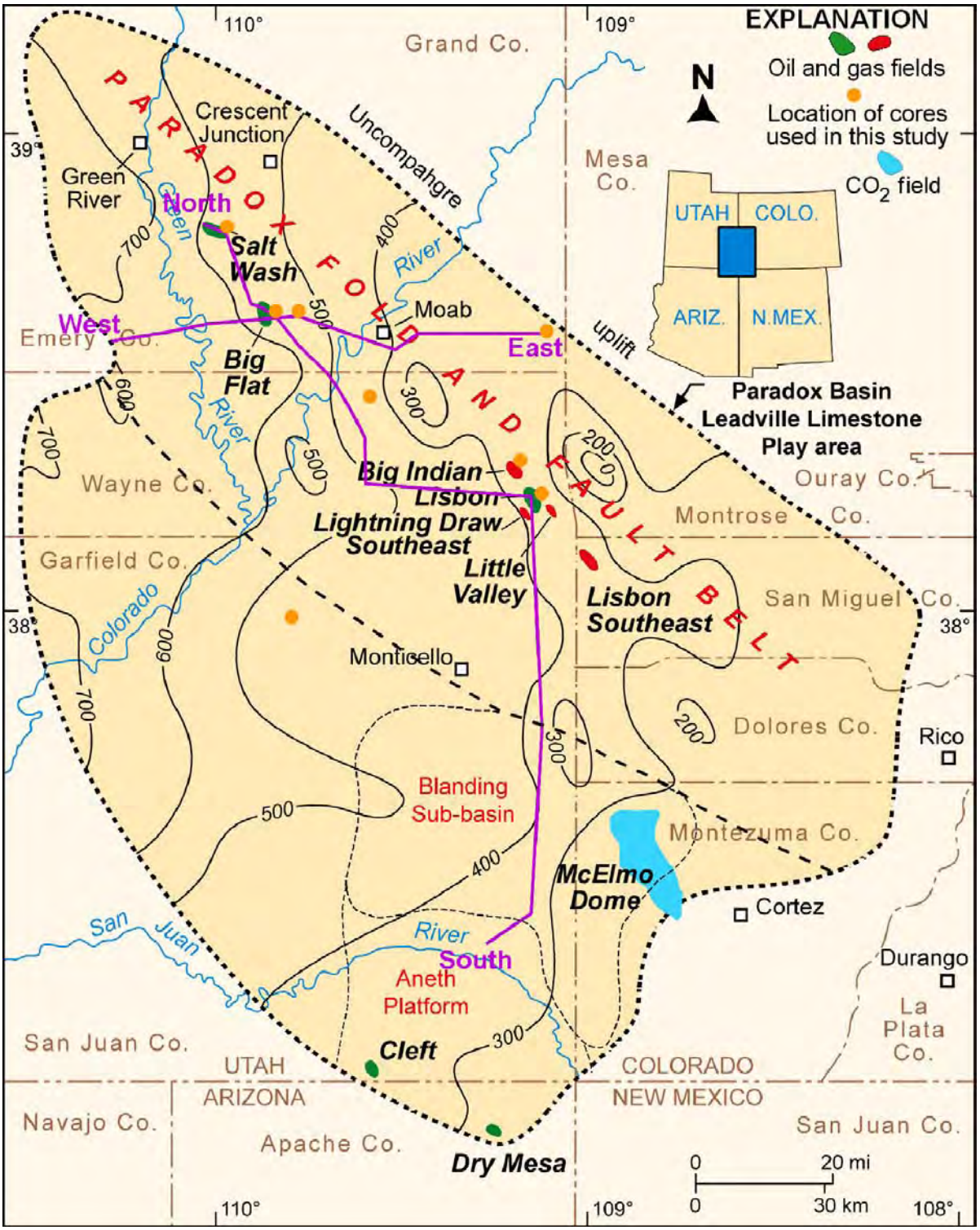

Figure 7-2. Thickness of the Mississippian Leadville Limestone, Utah and Colorado; contour interval is 100 feet (modified from Parker and Roberts, 1963). Thicknesses are generalized, and many areas of local fault-related thinning are not displayed. Also shown are oil (green) and gas (red) fields that produce from the Leadville and location of cores from regional exploration wells and Leadville fields used in the study. Locations of north-to-south cross section (figure 7-3) and east-to-west cross section (figure 7-4) in purple.

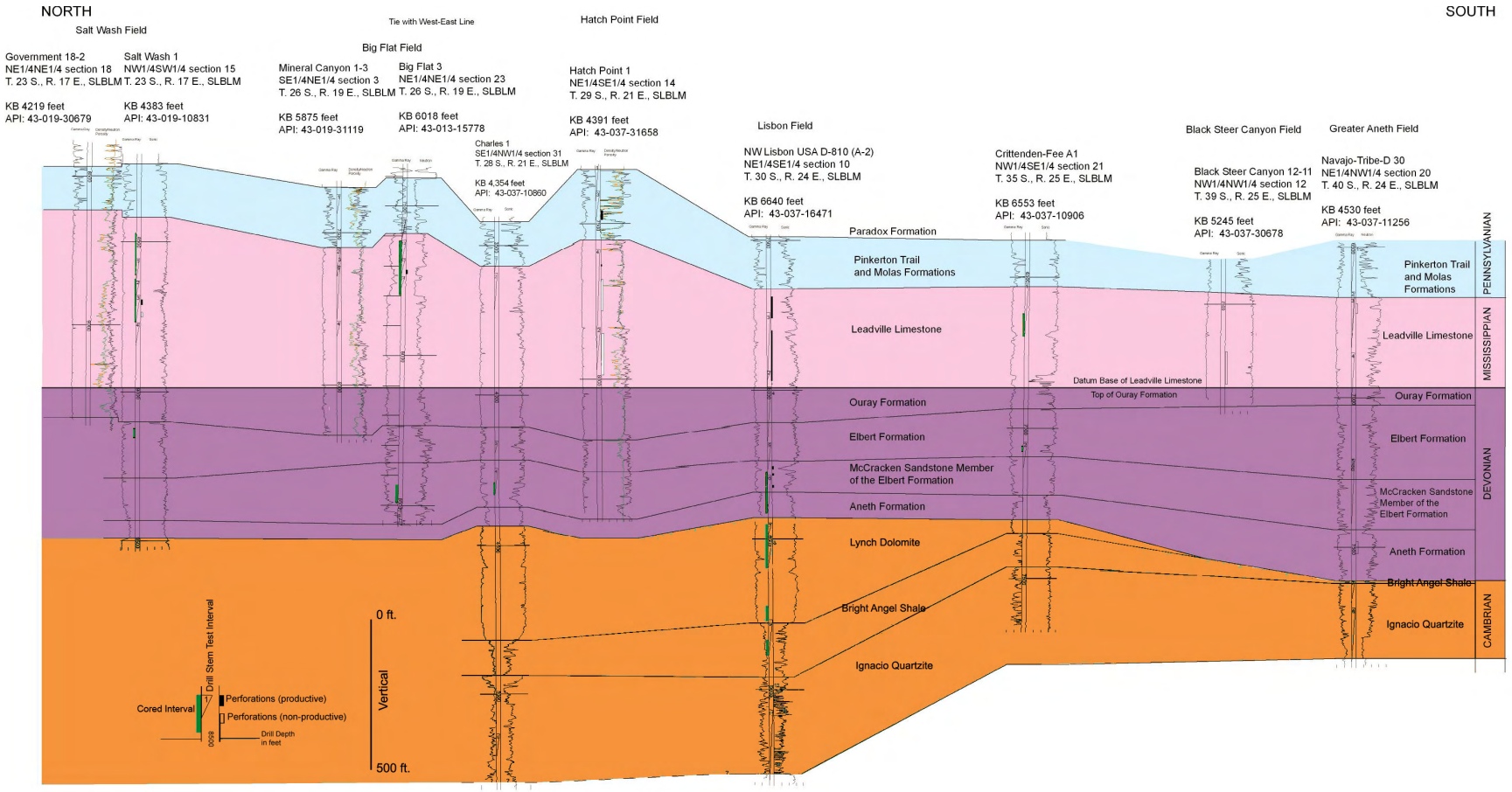

Figure 7-3. North-south stratigraphic cross section through the Utah portion of the Paradox Basin showing regional Paleozoic correlations. No horizontal scale. See figure 7-2 for location of cross section.

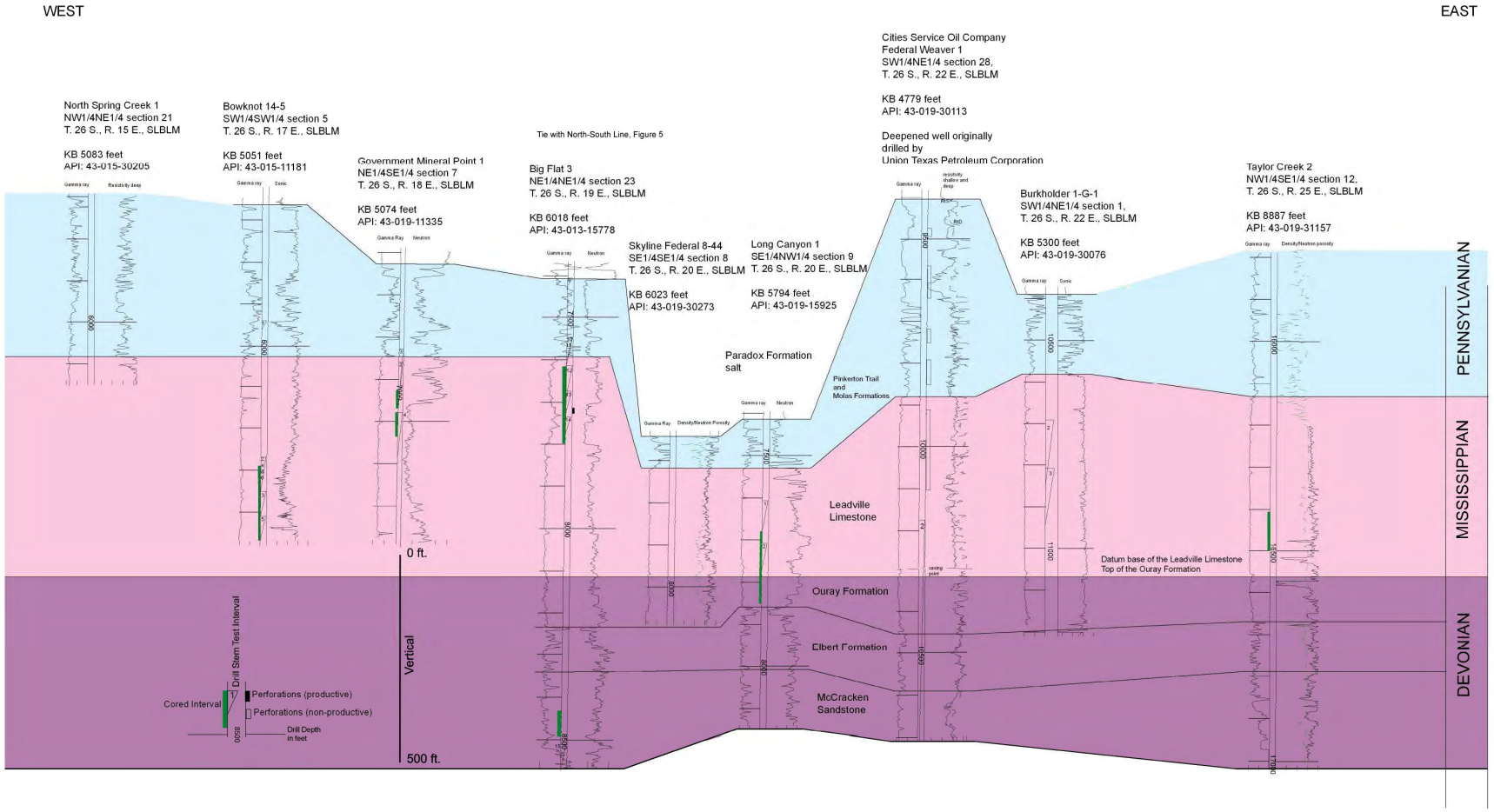

Figure 7-4. East-west stratigraphic cross section through the Utah portion of the Paradox Basin showing regional Paleozoic correlations. No horizontal scale. See figure 7-2 for location of cross section.

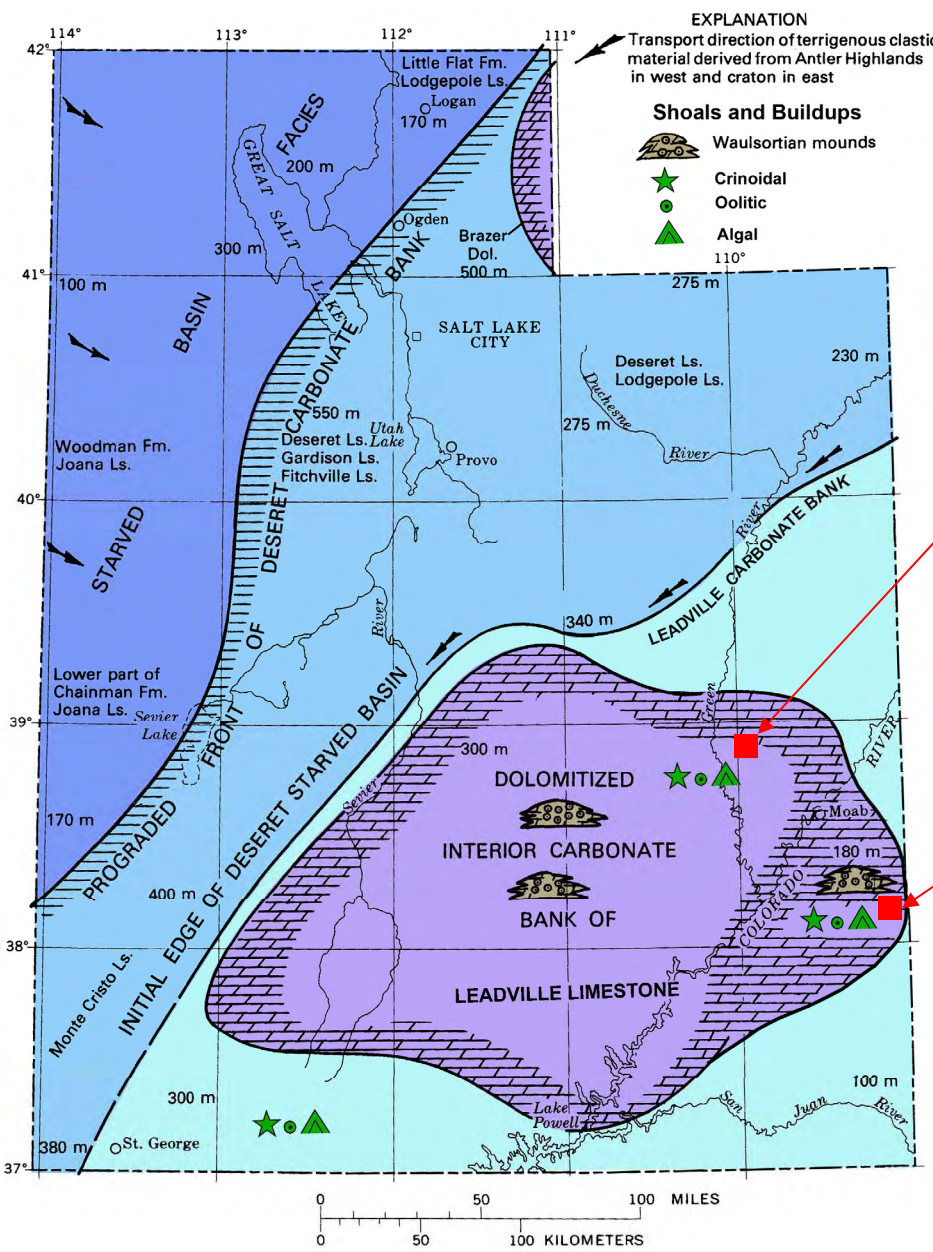

Figure 7-5. Paleogeographic map of Utah showing approximate present thicknesses in meters of deposits of the late Kinderhookian through Osagean into early Meramecian time. Modified from Welsh and Bissell (1979). A - Crinoidal/skeletal packstone to grainstone representing a shallow crinoidal shoal; Salt Wash No. 1 Floy well, 9469 feet. B - Porous algal boundstone to mudstone representing a possible Waulsortian mound; No. 1 Big Indian well, 10,081 feet.

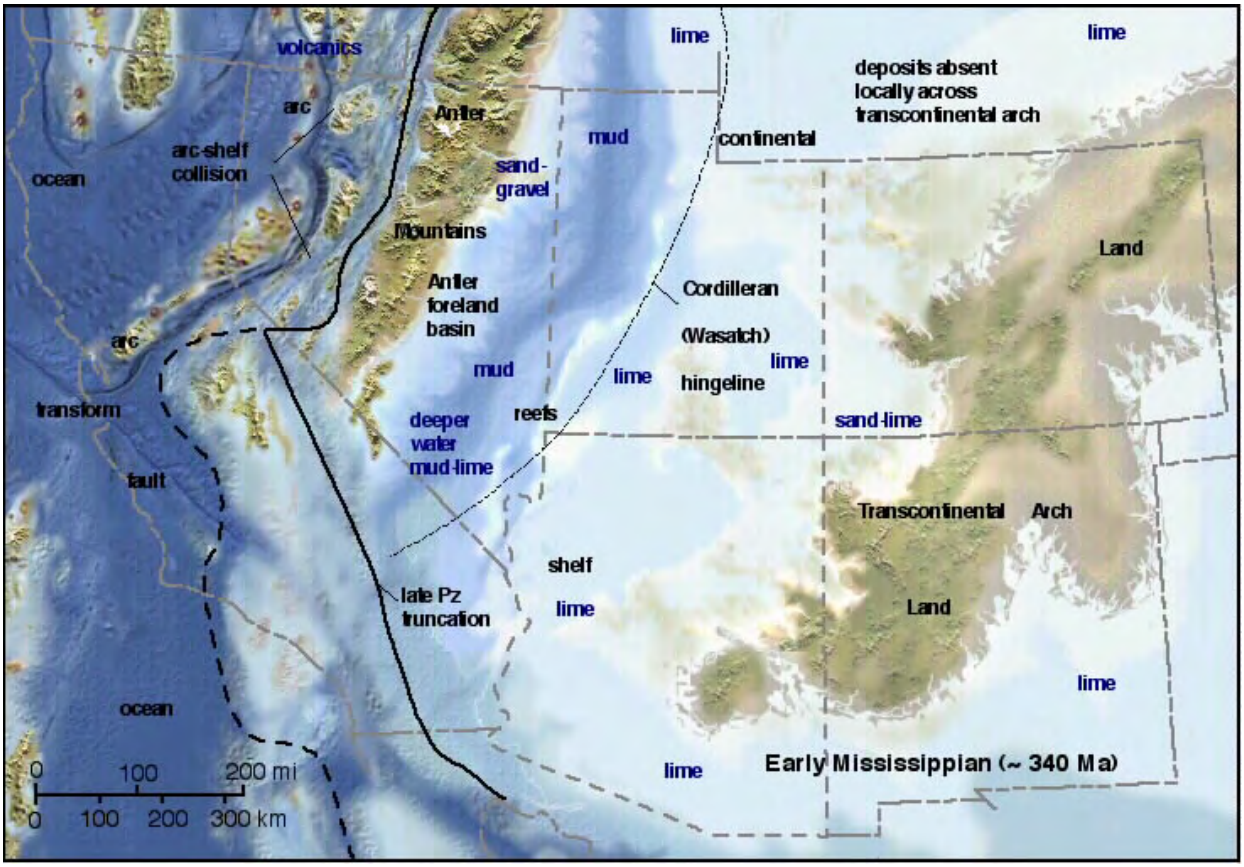

Figure 7-6. Paleogeographic map of the southwest U.S. during the Early Mississippian. From Blakey, http://jan.ucc.nau.edu/~rcb7/, accessed December 2008.

Figure 7-7. Diorama of a Mississippian crinoid meadow. Illinois State Museum, http://www.museum.state.il.us/exhibits/changes/htmls/tropical/underwater_mississippian.html.

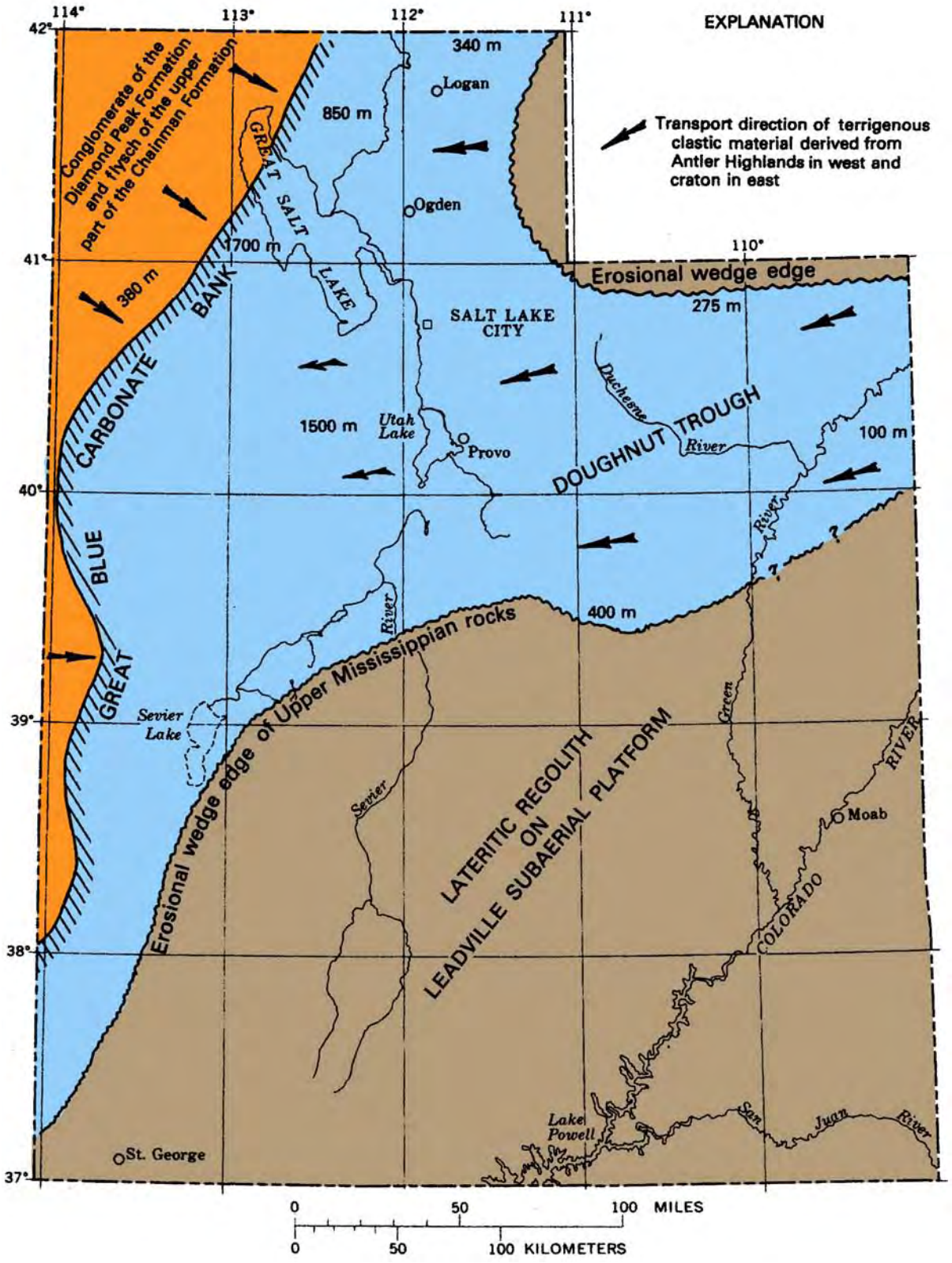

Figure 7-8. Paleogeographic map of Utah showing approximate present thicknesses in meters of upper Meramecian to upper Chesterian deposits. After Welsh and Bissell (1979).

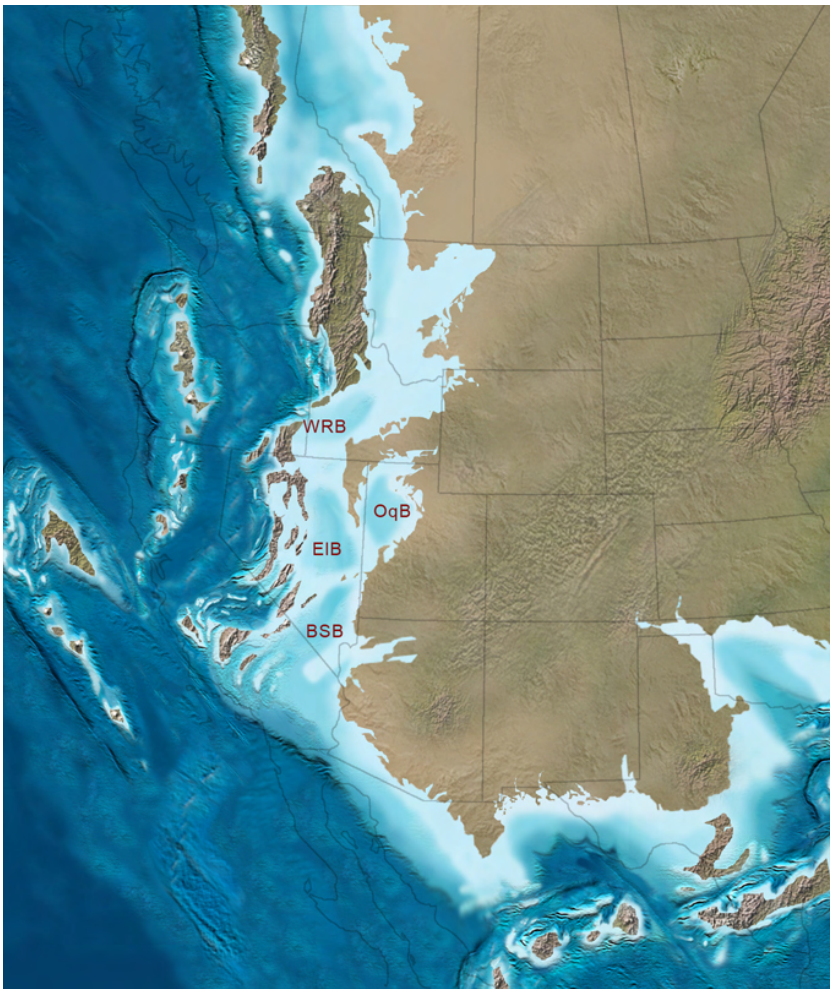

Figure 7-9. Paleogeographic map of the western U.S. during the Late Mississippian to Early Pennsylvanian when the Mississippian Leadville Limestone carbonate platform was subaerially exposed resulting in erosion and formation of a lateritic regolith in the Four Corners area. WRB = Wood River Basin, OqB = Oquirrh Basin, BSB = Bird Springs Basin, and ElB = Ely Basin. From Blakey, http://jan.ucc.nau.edu/~rcb7/, accessed December 2008.

CHAPTER 8
OUTCROP RESERVOIR ANALOGS FOR THE MISSISSIPPIAN LEADVILLE LIMESTONE: SOUTH FLANK OF THE UINTA MOUNTAINS, UTAH

David E. Eby, Eby Petrography & Consulting, Inc.,
and
Thomas C. Chidsey, Jr., Utah Geological Survey

Introduction

Utah is fortunate that representative outcrop analogs (depositional or diagenetic) for the Leadville Limestone play are present near the Paradox Basin. Production-scale analogs provide an excellent view, often in 3D, of reservoir-facies characteristics, geometry, distribution, diagenetic characteristics, and nature of boundaries, all of which contribute to the overall heterogeneity of reservoir rocks. The specific objectives of this chapter are to: (1) increase understanding of vertical and lateral facies variations and relationships within Leadville reservoirs, (2) describe the lithologic and diagenetic characteristics, (3) determine the morphology, internal geometries, and possible permeability and porosity distributions, (4) identify potential impediments and barriers to fluid flow, and (5) determine the causes of brecciation features.

An outcrop-analog model, combined with the details of internal lithofacies characteristics, can be used as a "template" for evaluating data from conventional core, geophysical and petrophysical logs, and seismic surveys. When combined with subsurface geological and production data, the analog model will improve development drilling and production strategies, reservoir-simulation models, reserve calculations, and design and implementation of secondary/tertiary oil recovery programs and other best practices used in the Leadville oil fields of Paradox Basin.

South Flank of the Uinta Mountains, Utah

Although not exposed in southeastern Utah, Mississippian rocks equivalent to the Leadville Limestone crop out in the northern and western parts of the state (figure 8-1). These formations include the Madison, Gardison, Deseret, and Humbug Formations (figure 8-2), which have generally the same characteristics as the Leadville. These provide production-scale analogs of the facies and diagenetic characteristics, geometry, distribution, and nature of boundaries contributing to the overall heterogeneity of Leadville reservoir rocks. Excellent examples of Leadville-equivalent rocks (Madison, Deseret, or Humbug) are found along the south flank of the Uinta Mountains where they are up to 600 feet (200 m) thick (figures 8-1 and 8-2). However, it is important to note that the Madison, Deseret, or Humbug Formations have often been mapped interchangeably along the south flank region, but for simplicity they will be collectively referred to as the Madison Limestone in this report.

General Characteristics

The Madison and equivalent formations were deposited in a shallow, warm-water, relatively high energy, epeiric sea that extensively covered a large part of the craton. The Madison is mostly light- to dark-gray, fine- to coarse-crystalline, cherty limestone (figure 8-3A). Dolomitic units are gray to tan, sucrosic to crystalline, and medium bedded with occasional silty partings; both limestone and dolomite are the prime reservoir lithologies for the Leadville Limestone. Chert is typically light gray, forming lenses and nodules. In the Whiterocks Canyon area (figure 8-1), the Madison contains some thin-bedded, tan, calcareous, fine- to medium-grained sandstone (Kinney, 1955). The most common carbonate fabrics of the Madison include peloidal, skeletal, and oolitic grainstone, packstone, and wackestone; rudstone and floatstone are also present. Cross-bedded grainstones of crinoid debris are referred to as encrinites.
Mudstones appear as microcrystalline and cryptocrystalline limestone and dolomite. The Madison is generally thick to massive and unevenly bedded, forming vertical cliffs and dip slopes.

Marine fauna in the Madison Limestone are represented by corals, brachiopods, pelecypods, bryozoans, and crinoids (Rowley and Hansen, 1979); however, fossils are relatively rare in some areas. Other common biota include algae, ostracods, forams, and gastropods. Depositional environments include tidal-flat mud; deeper, subtidal, burrowed, pellet muds; shallow, subtidal bay; beach/foreshore; oolitic shoal; storm-dominated, outer shelf, crinoid shoals; low-energy, open-marine, muddy intershoal; low-energy, open-marine, outer shelf above storm wave base. Oolitic and crinoid shoals or banks produce carbonate buildups.

The contact between Madison, Deseret, or Humbug Formations with the overlying Mississippian Doughnut Shale is marked by a major unconformity (Hintze, 1993). This is the same unconformity found at the top of the Leadville Limestone in the Paradox Basin and the equivalent Redwall Limestone in the Grand Canyon (McKee, 1969). The unconformity on the south flank of the Uinta Mountains displays many of the same features recognized in Leadville cores (see Chapter 4) and Grand Canyon Redwall outcrops. Subaerial exposure resulted in development of karst topography, commonly expressed in outcrop as a surface of relief, carbonate breccia-filled paleosinkholes and collapse features, and terra rosa (cave fill) near the top of the Madison/Deseret/Humbug section.

The upper Madison has numerous “young,” actively forming caverns, sinkholes, and springs (figure 8-2). Controls on these features are vertical joints, fractures, and selected bedding planes rather than the unconformity at the top of the Mississippian (Hamblin and Rigby, 1968). Underground drainage is common and larger caves are related to sinking streams (White, 1979). In addition, high dolomite content can influence cave development (White, 1979). Many units display dissolution activity in the form of large and small vugs (figures 8-3B and 8-3C).

The Madison Limestone contains local zones of breccia due to either collapse or natural hydrofracturing. Breccia associated with sediment-filled collapsed cavities is relatively common. These cavities are related to paleokarstification of the Madison when exposed during Late Mississippian time. Brecciation caused by explosive natural hydrofracturing, created the same shattered-looking, pulverized rock also identified in Lisbon cores. Possible breccia pipes may be related to past hydrothermal activity.

Fracturing is common in the Madison Limestone. It is best expressed as closely spaced, vertical fractures throughout thin- to medium-thick beds or as swarms associated with large and

small faults and collapse features. Stylolites, jointing, and fractures are also present creating rock sections with high heterogeneity (figures 8-3A, 8-3B, and 8-3D).

Study Sites

Three sites were selected for detailed outcrop studies (figure 8-4): (1) South Fork Provo River, (2) Dry Fork Canyon, and (3) Crouse Reservoir/Diamond Mountain Plateau. Each study site has a unique set of depositional lithofacies and post-depositional characteristics in the Madison Limestone that are identical or very similar to those observed in Leadville Limestone cores from Lisbon field in the Paradox Basin (figure 1-3). Samples were collected for slabbing and thin section analysis. Two short stratigraphic sections (less than 120 feet [40 m]) were measured, using a compass, tape, or Jacob staff, at study sites 2 and 3 (see Appendix E) specifically targeting lithofacies. Dockal (1980) published ten nearly complete measured sections of the Madison from the canyons around the core of the Uinta Mountains and they serve as an excellent reference set for further comparison.

Study Site 1 – South Fork Provo River: The South Fork Provo River study site is located in the western end of the south flank of the Uinta Mountains, Wasatch County (figure 8-4). It is a series of roadcuts along the east side of Highway 35, about 11 miles (18 km) east of the town of Francis, and about 25 miles (40 km) northwest of the town of Hanna, Utah (figure 8-5).

The Madison Limestone at study site 1 is typically dark- to light-gray limestone consisting of skeletal grainstone to packstone (figure 8-6A). Skeletal grains are composed of broken crinoids and rugose corals representing a high-energy, open-marine environment. Some units contain in-place *Syringopora* coral and burrows (figure 8-6B) indicating a lower-energy environment. Other units are dolomitized and include chert nodules (figure 8-6C). Vertical fractures are also common (figure 8-6D).

The most striking feature at study site 1 is a large breccia pipe (figure 8-7). The pipe is about 17 feet (6 m) wide at the base of the outcrop and cuts through about 30 feet (10 m) of Madison section. It is highly brecciated with small to large clasts surrounded by pulverized rock (figure 8-8A). Calcite veins, dolomitized zones, and vugs are widespread (figure 8-8B). The contact with the unaltered limestone country rock is sharp. Vertical, often calcite-filled, fractures are prevalent on both sides of the breccia pipe. Thin sections reveal the presence of mini-Herkimer quartz crystals (figure 8-8C), which were also found in Leadville cores from Lisbon field. There, the mini-Herkimer crystals had high-temperature fluid inclusions (see Chapter 4). Their presence suggests a high-temperature event has occurred at study site 1.

The poorly exposed top of the section, presumably the unconformity with the overlying Doughnut Shale, reveals probable paleokarst features. Brecciation (collapse) is extensive (figures 8-9A and 8-9B) but without the calcite veins, dolomization, and explosive characteristic of a breccia pipe. Terra rosa red weathering profiles are also common (figure 8-9C).

Study Site 2 - Dry Fork Canyon: The Dry Fork Canyon study site is located in the east-central part of the south flank of the Uinta Mountains, Uintah County (figure 8-4), about 20 miles (32 km) northwest of the town of Vernal, Utah. It includes a measured stratigraphic section (Appendix E) and several noteworthy outcrops along the Red Cloud Loop Road where it forks and turns up Brownie Canyon (figure 8-10).

The Dry Fork Canyon stratigraphic section demonstrates the incredible heterogeneity as well as the cyclicity (possibly two shoaling upwards cycles) of the Madison Limestone depositional environments within only a 40-foot-thick (12 m) outcrop (figures 8-11A and 8-11B). The Madison at this site is predominately dolomite. The base of the section is oolitic/hard pellet grainstone with distinctive pock-marked weathering. It has well-defined, planar to low-angle, cross-stratification; the upper 6 inches (15 cm) may contain beach rock and semi-lithified rip-up clasts (figure 8-12A). The depositional environment was a beach/foreshore. The next unit is a calcareous, peloidal/skeletal packstone to grainstone (figure 8-12B) with hard pellets, benthic forams, and other microfossils. Bedding is wavy to bioturbated and the top may be channelized. The depositional environment was stable, shallow, subtidal bay. The section coarsens up to oolitic/hard pellet grainstone with small- to medium-scale cross-stratification (figure 8-12C) representing an oolitic shoal. Tidal-flat mud and deeper, subtidal, burrowed, pellet mud (figure 8-12D) overlie the oolitic shoal consisting of soft pellet mudstone with crinkly continuous cryptalgal laminates and skeletal microfossils (ostracods and benthic forams). These sediments are overlain by thin-bedded to bioturbated, pelloidal/skeletal packstone to grainstone with endothyrid forams (figure 8-12E) and other microfossils indicating return to a stable, shallow, subtidal bay. The cycle continues to coarsen upward with low- to medium-angle cross-stratified oolitic grainstone of an oolitic shoal (figures 8-12F and 8-12G). The upper surface of the oolitic grainstone appears to be rippled to channelized with "cookie-chip-like" muddy rip-up clasts and fossil fragments in the troughs. Local nodular calcite masses may be relic evaporite structures. The top of the Dry Fork Canyon section is mudstone with continuous cryptalgal laminates (figure 8-12G), pellets, possible desiccation cracks and rip-up clasts, and no fossils, all features indicative of a peritidal tidal-flat mud.

Several interesting post-depositional features can also be found in the study site 2 area. A megabreccia is exposed at the west end of the same Madison outcrop where the section was described (figure 8-13A). The breccia represents a paleokarst collapse feature where limestone and dolomite clasts are set in a tight muddy matrix. In thin section (figure 8-13B), this breccia appears very similar to collapse breccia seen in core from Lisbon field (compare to figure 4-9). The undisturbed country rock is a dolomitized, cross-bedded, oolitic grainstone (oolite shoal) capped by low-angle, stratified grainstone (foreshore) (figure 8-13A). An outcrop along the road a short distance up Brownies Canyon from the measured section displays spectacular, high-amplitude, bed-parallel stylolites in bioturbated mudstone (figure 8-14).

Study Site 3 – Crouse Reservoir/Diamond Mountain Plateau: The Crouse Reservoir/Diamond Mountain Plateau study site is located in the eastern part of the south flank of the Uinta Mountains, Uintah County (figure 8-4), about 29 miles (47 km) northeast of Vernal. It also includes a measured stratigraphic section (Appendix E) and a key outcrop of brecciation on the west side of the improved gravel road to Crouse Reservoir (figure 8-15).

Units of entirely limestone in the Madison Limestone stratigraphic section show cycles of three depositional environments within the 116-foot-thick (35 m) outcrop (figures 8-16A and 8-16B): (1) storm-dominated, outer-shelf, crinoid shoals, (2) low-energy, open-marine, muddy intershoal, and (3) low-energy, open-marine, outer-shelf above storm wave base. Storm-dominated, outer-shelf, crinoid shoals consist of well-sorted, coarse sand to granule size crinoid fragments in wavy-thin to medium- or large-scale cross-bedded grainstone (encrinite) (figures 8-17A and 8-17B). The upper contact is often sharp with undulatory topography, possible small-scale interference ripples, and small rugose corals on top. Syntaxial cements are well developed.

Low-energy, open-marine, muddy intershoal depositional environments are represented by burrowed, soft peloid/crinoid wackestone to packstone (figures 8-17C and 8-17D) containing some well-preserved fenestrate bryozoans. Low-energy, open-marine, outer-shelf, above storm wave base depositional environments consists of skeletal wackestone to packstone with grainstone burrow infills of biogenetic skeletal material. Burrow fillings occur at several scales. The larger burrow networks are open burrows filled with coarse, stormed-pumped shells (tubular tempestites) (figures 8-17E and 8-17F). Within muds are well-preserved, articulated. crinoid columnals and fenestrate bryozoans. Locally abundant nodular cherts probably follow burrow systems.

The most unique feature at study site 3 is a ridge with two sags dominated by intense breccia zones (pipes?) (figures 8-15, 8-18, and 8-19). The zones are about 75 to 100 feet (25-30 m) wide composed of coarse dolomite. They are characterized by coarse calcite and vein-like mineralization (figures 8-20 and 8-21A). Dolomitization and leaching of the matrix limestone has occurred throughout the zones (figure 8-21B). These distinctive elements imply a hydrothermal event rather than a paleokarst collapse origin for the breccia zones.

Discussion

All of the Madison Limestone depositional environments described from outcrops above are also observed in Leadville cores from Lisbon field (see Chapter 3). Good porosity/permeability encrinites and oolitic buildups represent the best reservoir analog units, while low-porosity/permeability, open-marine packstone and wackestone represent the worst reservoir analog units, unless they have experienced dolomitization (hydrothermal) that results in increased reservoir quality. Paleokarst features also can enhance reservoir quality. Breccia pipes and fractures enhance reservoir quality. The post-burial breccias associated with hydrothermal events, fracturing, and dissolution in the Leadville Limestone yield the best reservoir development at Lisbon field (see Chapter 4).

The breccia pipes and zones discovered at study sites 1 and 3 are likely the result of hydrothermal actively in the geologic past. The presence of the basal Cambrian Tintic Quartzite or Lodore Sandstone (figure 8-1B) as aquifers are important contributors to the hydrothermal story. The Tintic is a very coarse to granular, or pebble, sandstone with moderate sorted, subrounded, roller to spherical, monocrystalline and polycrystalline quartz grains. It has thin to thick cross-bedding, is moderately indurated, and contains a few shaley partings which have small amounts of mica and some feeding trails (Dockal, 1980). Its contact with overlying Mississippian Madison is fairly sharp. The Lodore is a very fine to medium-grained, well-sorted, very thinly bedded to cross-bedded (with somewhat undulatory surfaces) sandstone marked by argillaceous partings (figure 8-22). Quartz grains are subrounded to spherical. The Lodore can be calcareous and slightly ferruginous. The top appears to be eroded (Dockal, 1980). Both the Lodore and Tintic can have porous and permeable units. They served as aquifers supplying hot water to the former hydrothermal system.

Recent 3D numerical models of seafloor hydrothermal convection demonstrate that convection cells organize themselves into pipelike upflow zones surrounded by narrow zones of warm downflow (Coumou and others, 2008). Recharge can occur over an extensive area or along faults as water migration pathways. The Tintic Quartzite is mapped on the western end of the Uinta Mountains while the Lodore Sandstone is present on the eastern end. Through the central part of the south flank of the Uinta Mountains, porous Cambrian sandstone is missing and

the Mississippian lies unconformably on middle Neoproterozoic Red Pine Shale (as observed in Whiterocks Canyon [figure 8-1]). No hydrothermal breccia zones or pipes are found in the central part of the south flank, lending credence to the concept that aquifers in the Tintic and Lodore were a required condition for past hydrothermal activity to have occurred. Thus, when targeting Leadville Limestone areas for potential hydrothermal dolomite and enhanced reservoir quality due to hydrofracturing, the presence of an aquifer below may be a necessary ingredient.

A

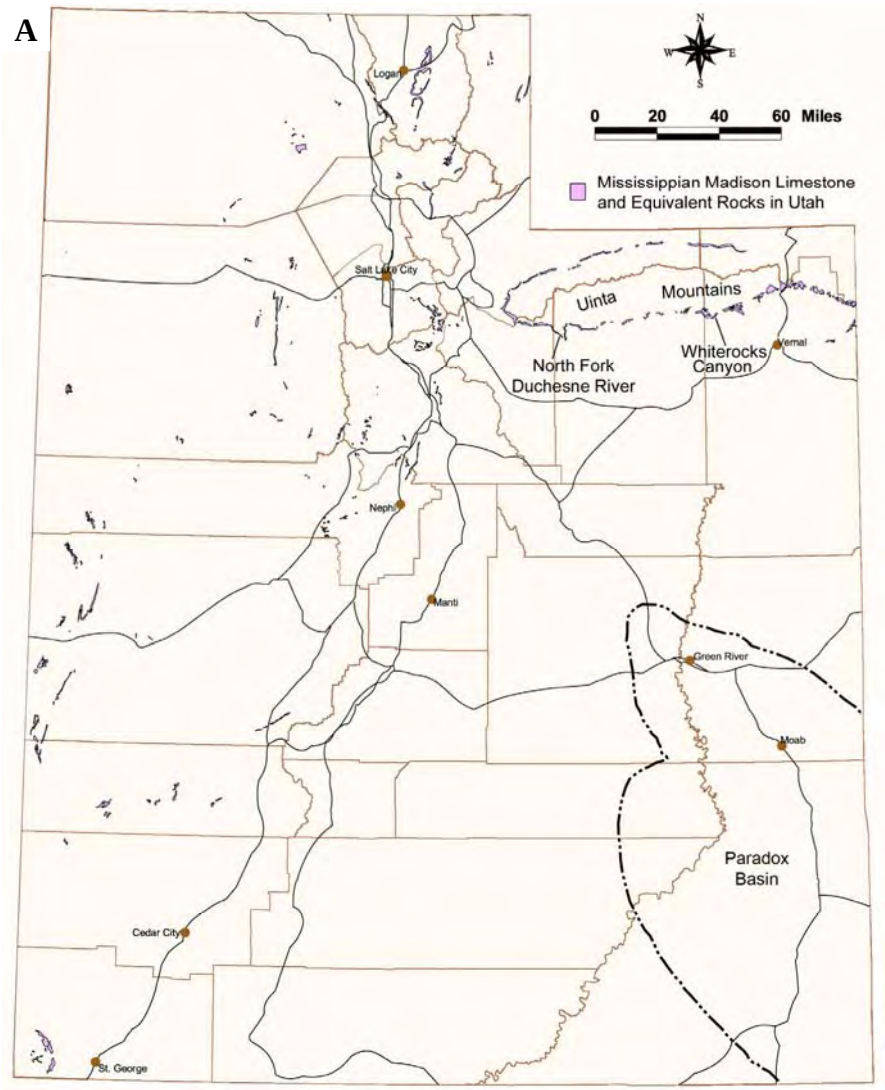

B

Age	Formation		Thickness	Lithology
PENN	Morgan Fm	Upper Mbr	600-650'	
		Lower Mbr	150-250'	
	Round Valley Ls		200-350'	
MISS	Doughnut Shale		100-180'	
	Humbug Fm		150-200'	
	Madison Ls		600'	
Є	Lodore Fm		400-600'	

Figure 8-1. A - Location of Mississippian rock outcrops in Utah equivalent to the Leadville Limestone of the Paradox Basin. B - Stratigraphic column of a portion of the Paleozoic section along the south flank of the Uinta Mountains (modified from Hintze, 1993).

Figure 8-2. Mississippian Deseret Limestone forming a jagged, vertical cliff, North Fork of the Duchesne River, Duchesne County, Utah. Note the cavernous nature of the outcrop. See figure 8-1A for location of North Fork of the Duchesne River area.

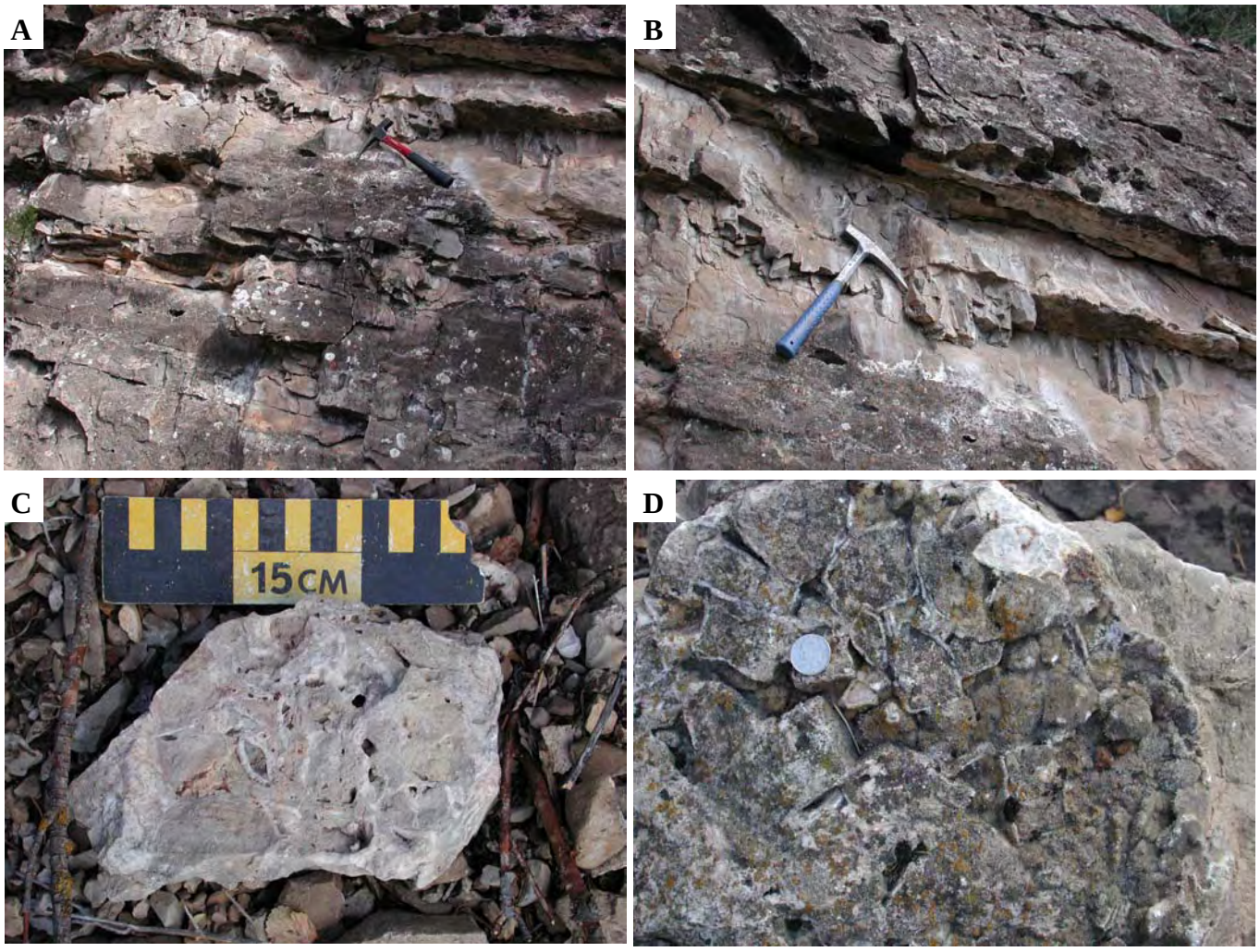

Figure 8-3. Characteristics of the Mississippian Madison Limestone along the south flank of the Uinta Mountains, Uintah County, Utah. A – Typical exposure of light- to dark-gray, medium-bedded, fine- to coarse-crystalline, limestone and dolomite containing fractures, stylolites, and crinoid hash, Whiterocks Canyon. B – Vugs and fractures in limestone and dolomitic units, Whiterocks Canyon. C – Close-up of open and calcite-filled vugs in limestone matrix, Whiterocks Canyon. D – Close-up of small-scale, calcite-filled rectilinear fractures in limestone matrix, Whiterocks Canyon. See figure 8-1 for location of Whiterocks Canyon.

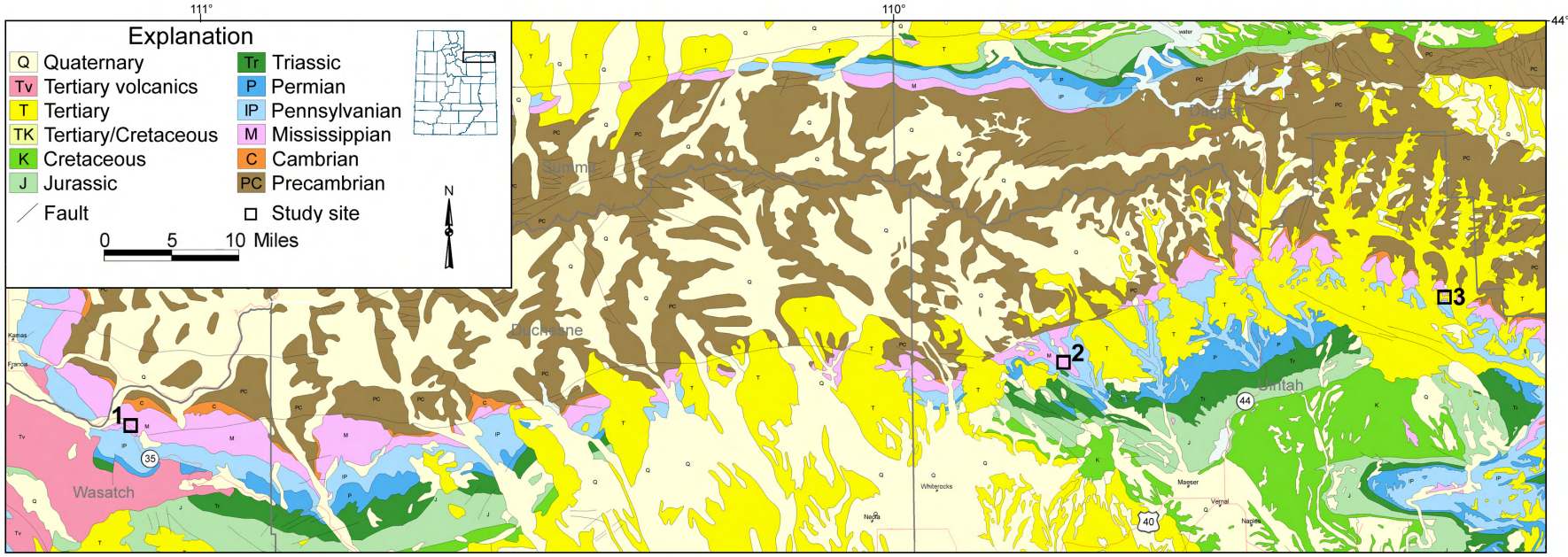

Figure 8-4. Generalized geologic map of the Uinta Mountains, northeastern Utah, showing the location of the Mississippian Madison study sites. Modified from Hintze and others, 2000.

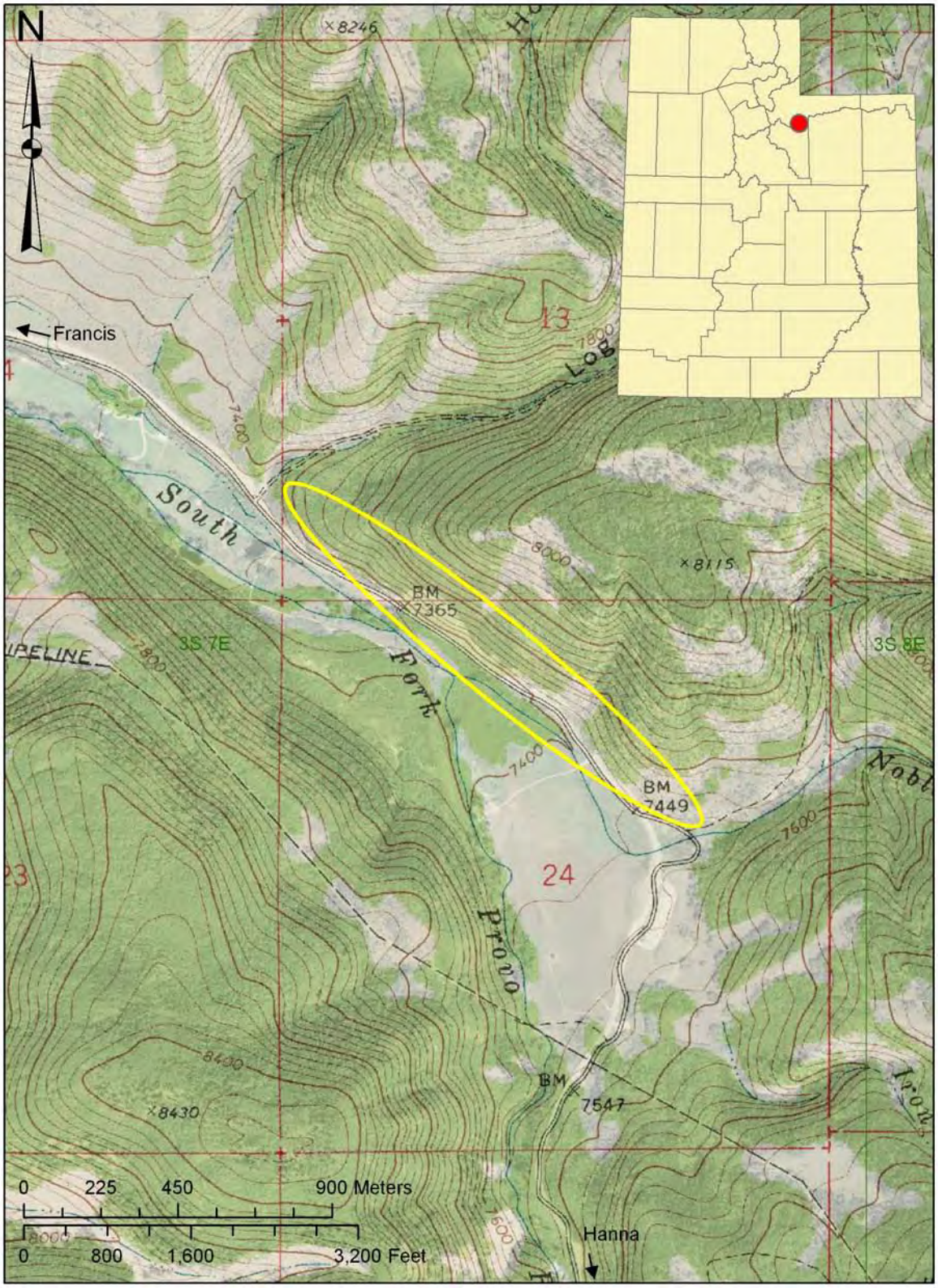

Figure 8-5. Location of South Fork Provo River study site (elongated yellow oval). Base map: Soapstone Basin l:24,000 topographic quadrangle map, U.S. Geological Survey.

Figure 8-6. Typical characteristics of the Madison Limestone at study site 1. A – Skeletal (crinoid and rugose coral) grainstone and packstone. B – In-place <u>Syringopora</u> coral. C – Chert nodules in dolomitized packstone. D – Vertical fractures.

Figure 8-7. Large breccia pipe penetrating the Madison Limestone at study site 1. Note pulverized nature of the material that comprises the pipe, the sharp contact with the country rock and parallel, calcite-filled vertical fractures.

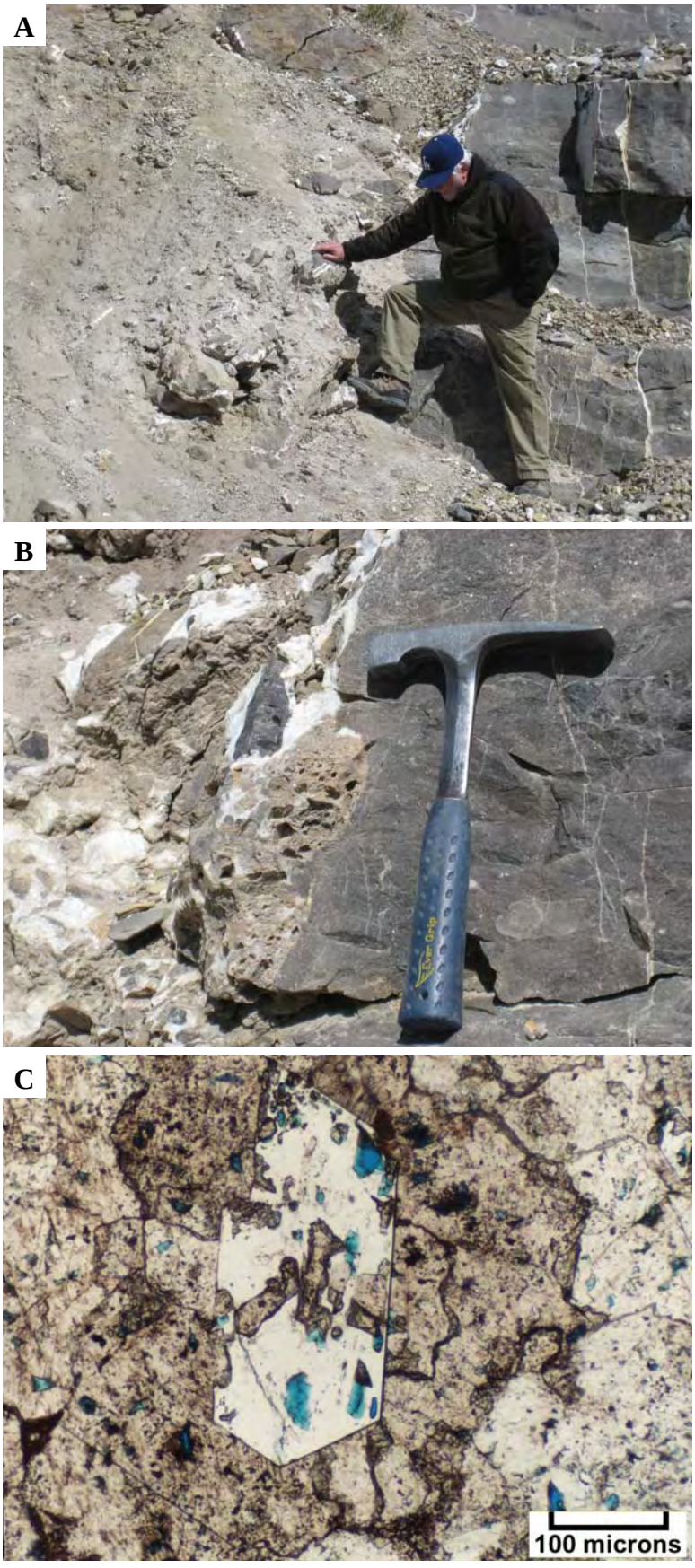

Figure 8-8. Characteristics of the explosive breccia pipe at study site 1. A – Brecciated rock in shattered-looking, pulverized groundmass. B – Close-up of sharp contact with unaltered limestone country rock. Note vuggy dolomite and white calcite veins. C – Photomicrograph (plane light) of dolomite containing a mini-Herkimer quartz crystal suggesting a high-temperature event.

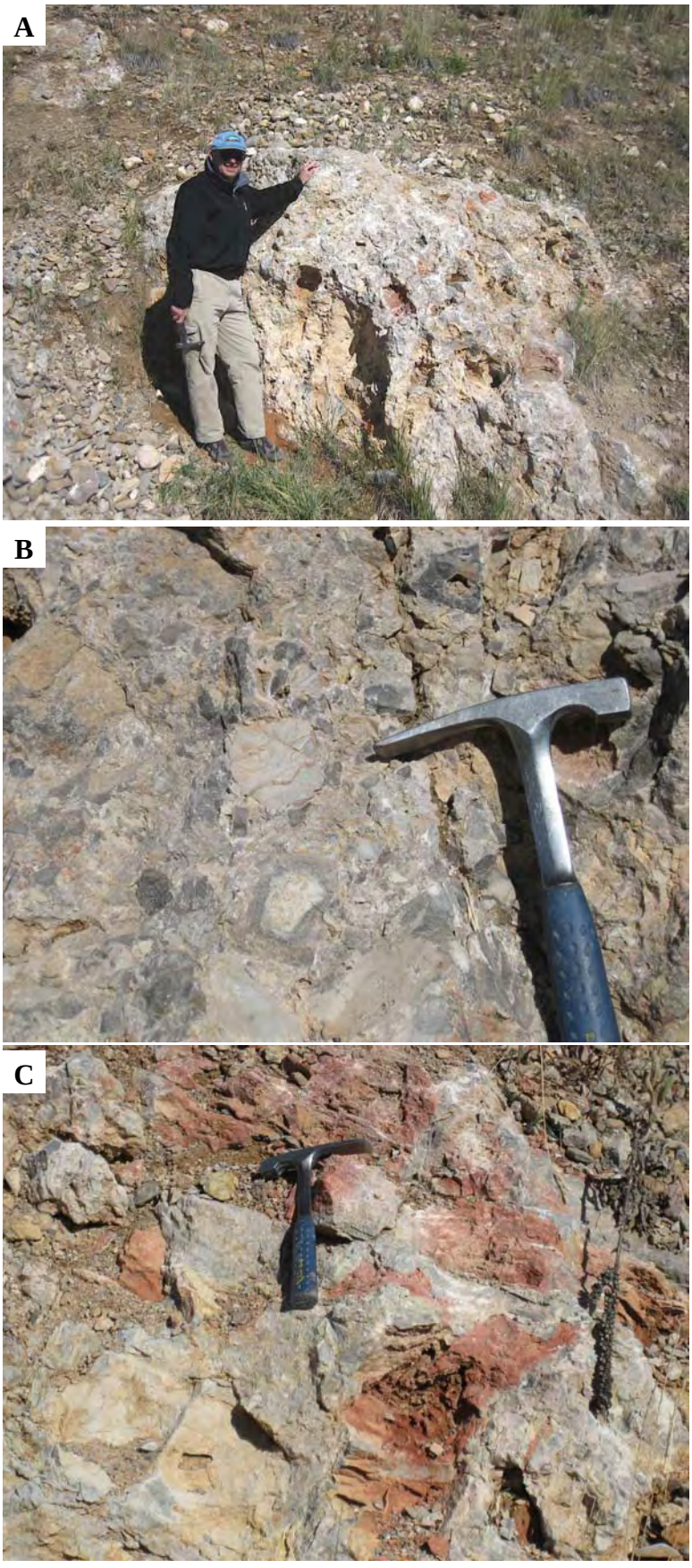

Figure 8-9. Paleokarst characteristics at study site 1. A – Extensive collapse brecciation. B – Close-up of limestone breccia clasts. Note the lack of calcite veins and dolomite. C – Terra rosa weathering.

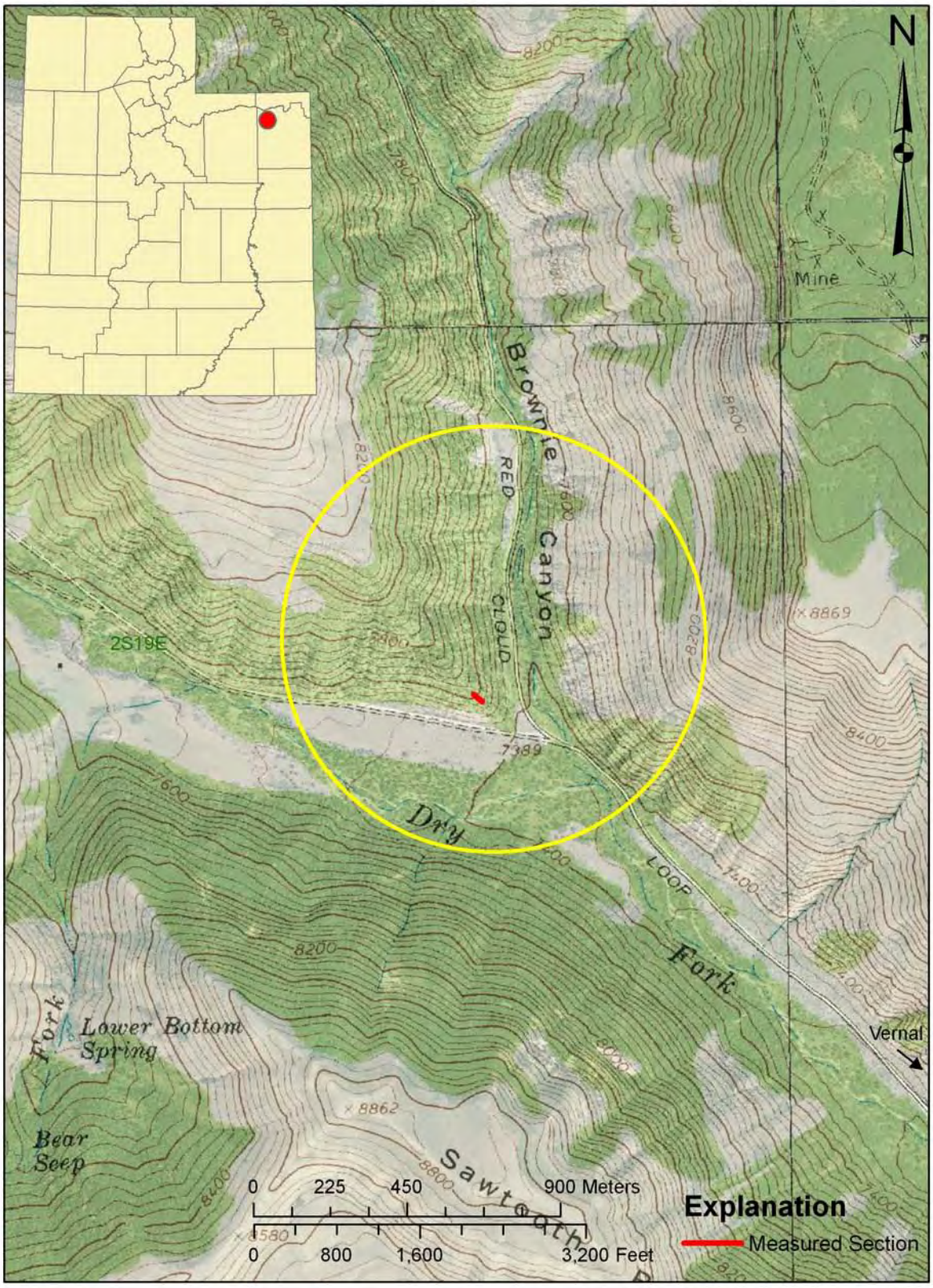

Figure 8-10. Location of the Dry Fork study site (yellow circle). Base map: Lake Mountain 1:24,000 topographic quadrangle map, U.S. Geological Survey.

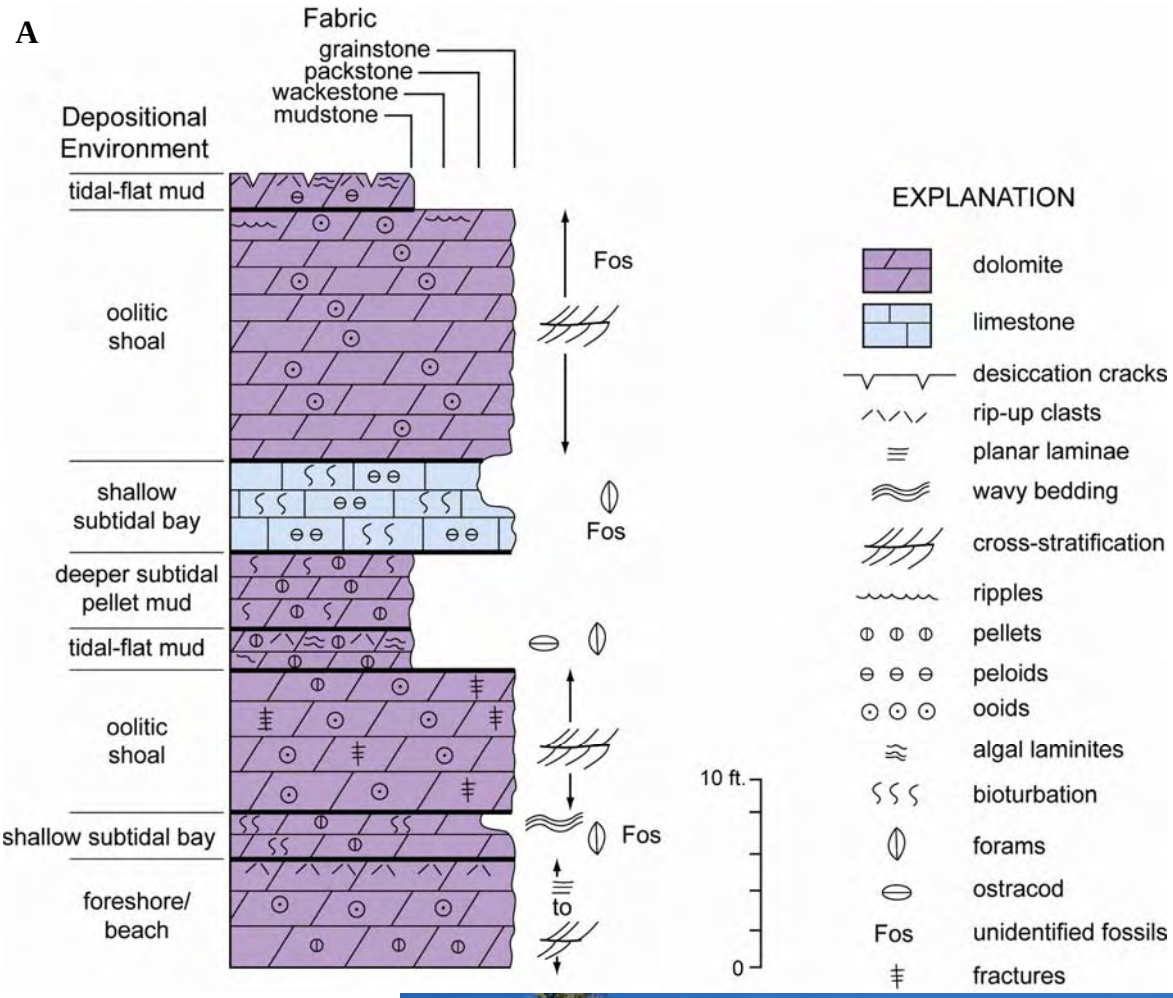

Figure 8-11. Madison Limestone section at study site 2. A – Stratigraphic column from the Madison Limestone 2 showing carbonate fabrics and textures, fossils, and depositional environments. B – Outcrop of measured stratigraphic section.

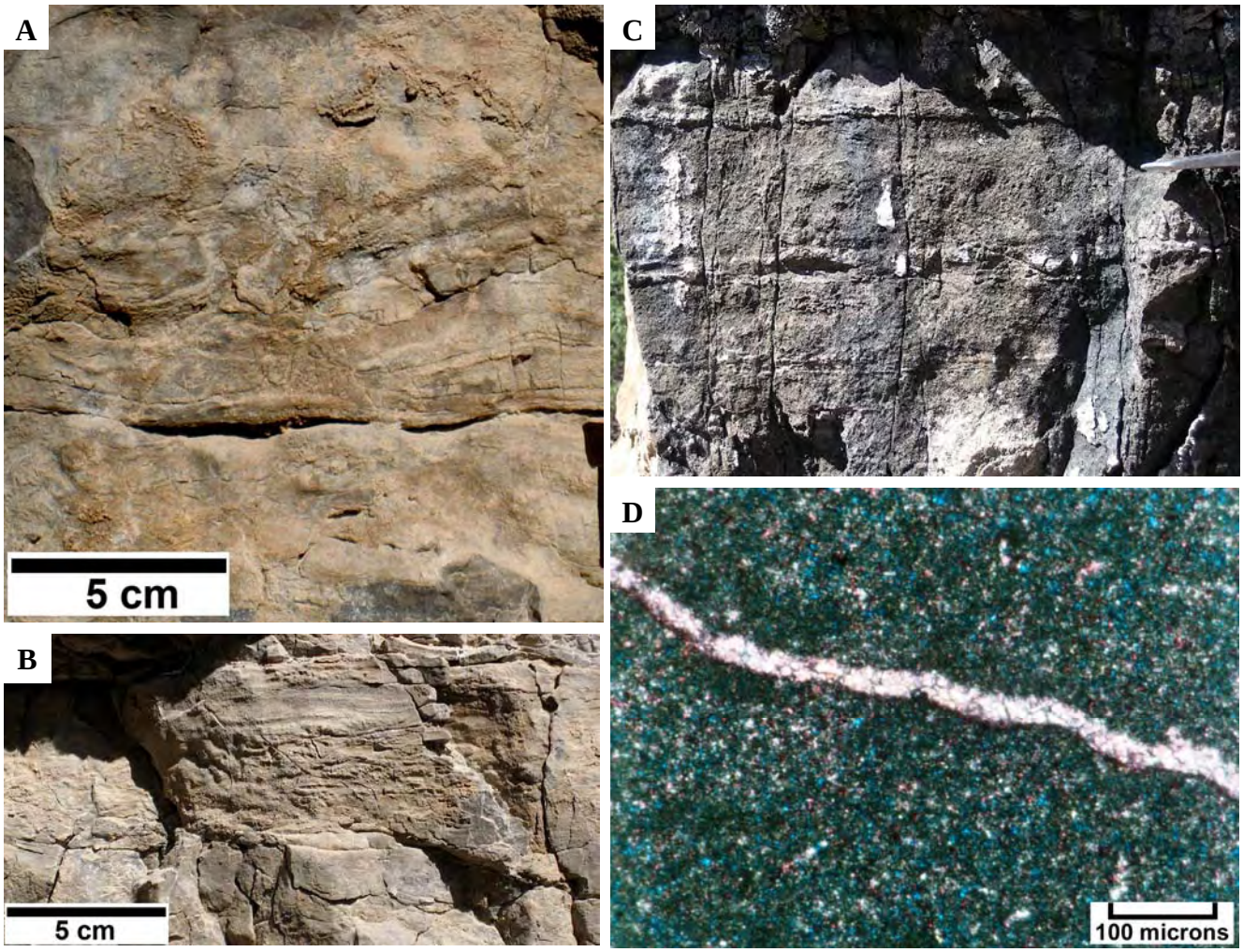

Figure 8-12. Examples of Madison lithofacies from study site 2. A – Oolitic/hard pellet grainstone with "beachrock" clasts. B – Peloidal/skeletal packetone/grainstone of a stable. Shallow, subtidal bay. C – Oolitic/hard pellet grainstone with small- to medium-scale cross-bedding. Note closely spaced swarms of vertical fractures. D – Photomicrograph (plane light) of soft pellet mudstone (note dolomite-filled fracture across the image) containing organic material representing deeper-water subtidal mud. E – Photomicrograph (plane light) of endothyrid forams in a peloidal/skeletal grainstone. F – Oolitic grainstone with "cookie-chip-like" rip-up clasts. G – Photomicrograph (plane light) of a highly dolomitized grainstone with relic ooids. H – Photomicrograph (plane light) of dolomitic mudstone with cryptalgal laminates.

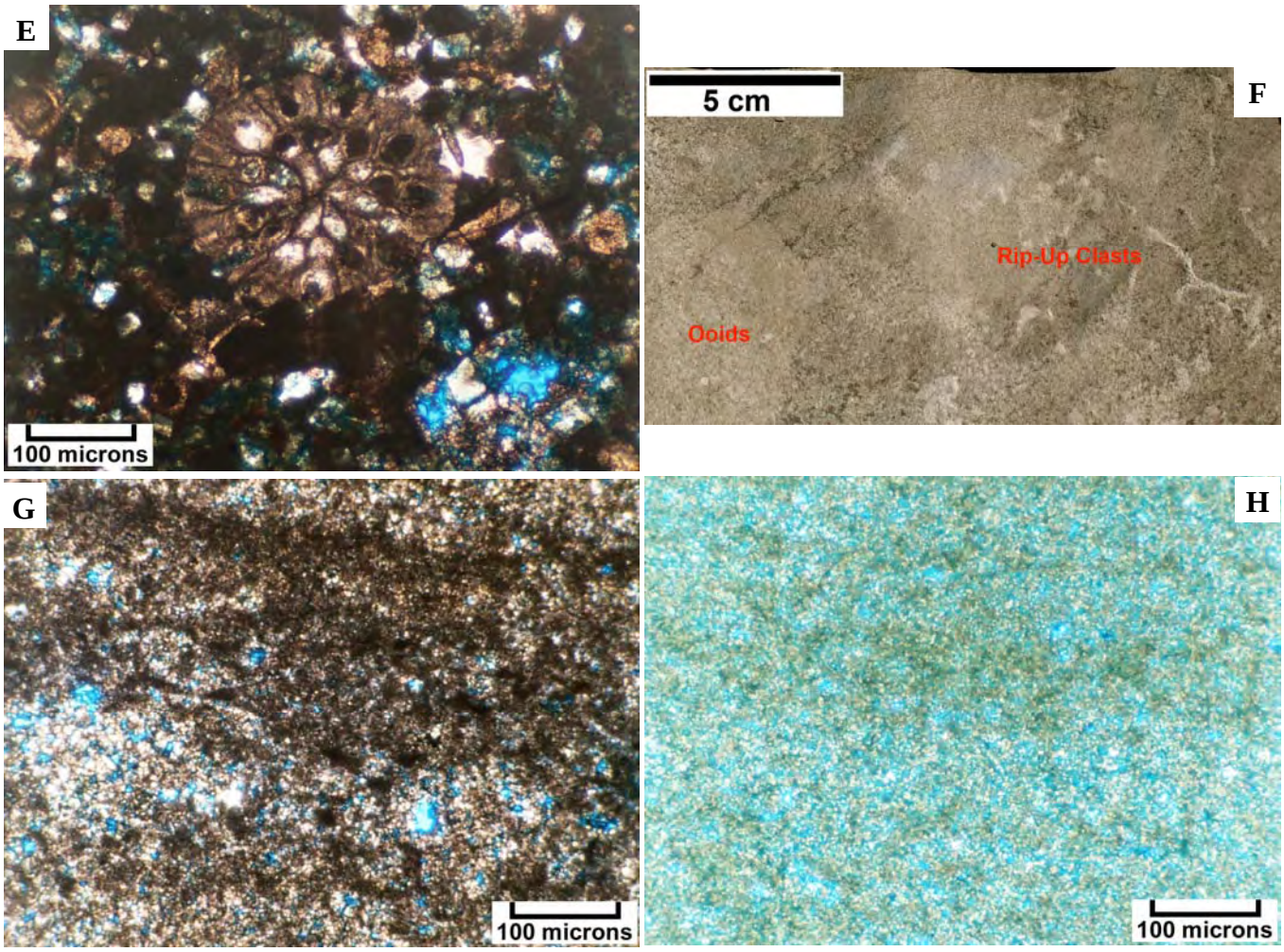

Figure 8-12 continued. Examples of Madison lithofacies from study site 2. A – Oolitic/hard pellet grainstone with "beachrock" clasts. B – Peloidal/skeletal packetone/grainstone of a stable. Shallow, subtidal bay. C – Oolitic/hard pellet grainstone with small- to medium-scale cross-bedding. Note closely spaced swarms of vertical fractures. D – Photomicrograph (plane light) of soft pellet mudstone (note dolomite-filled fracture across the image) containing organic material representing deeper-water subtidal mud. E – Photomicrograph (plane light) of endothyrid forams in a peloidal/skeletal grainstone. F – Oolitic grainstone with "cookie-chip-like" rip-up clasts. G – Photomicrograph (plane light) of a highly dolomitized grainstone with relic ooids. H – Photomicrograph (plane light) of dolomitic mudstone with cryptalgal laminates.

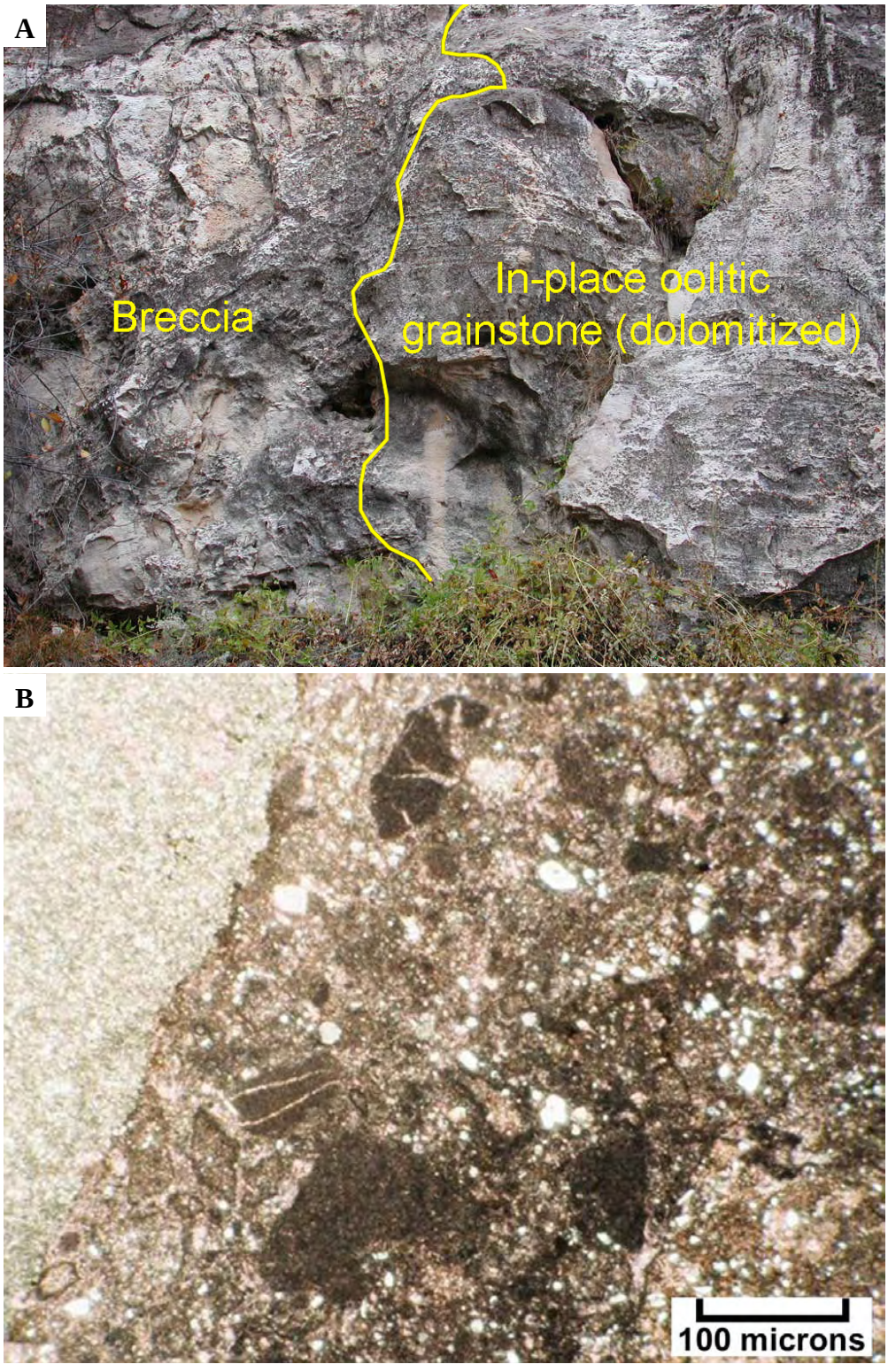

Figure 8-13. Megabreccia in study site 2. A – Small-scale oolitic shoal and collapse breccia (outcrop is approximately 10 feet [3 m] high). B – Photomicrograph (plane light) showing the contact between dolomitic grainstone (light gray, upper left) and the dolomitized karst cavity filling of small carbonate clasts.

Figure 8-14. High-amplitude, bed-parallel stylolites in bioturbated mudstone (closeup of stylolites shown in inset).

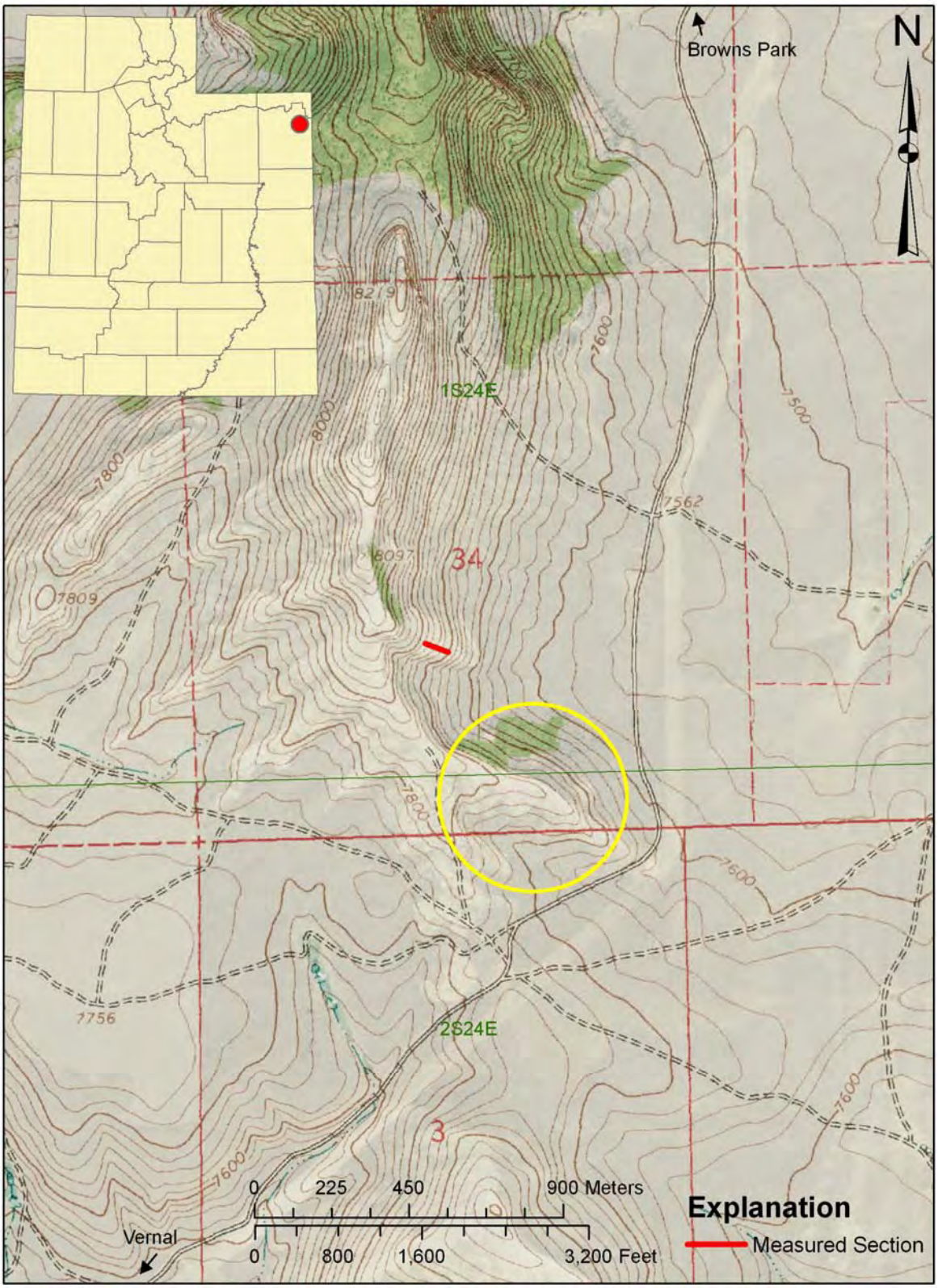

Figure 8-15. Location of Crouse Reservoir/Diamond Mountain Plateau study site (key brecciated outcrop indicated with yellow circle). Base map: Crouse Reservoir 1:24,000 topographic quadrangle map, U.S. Geological Survey.

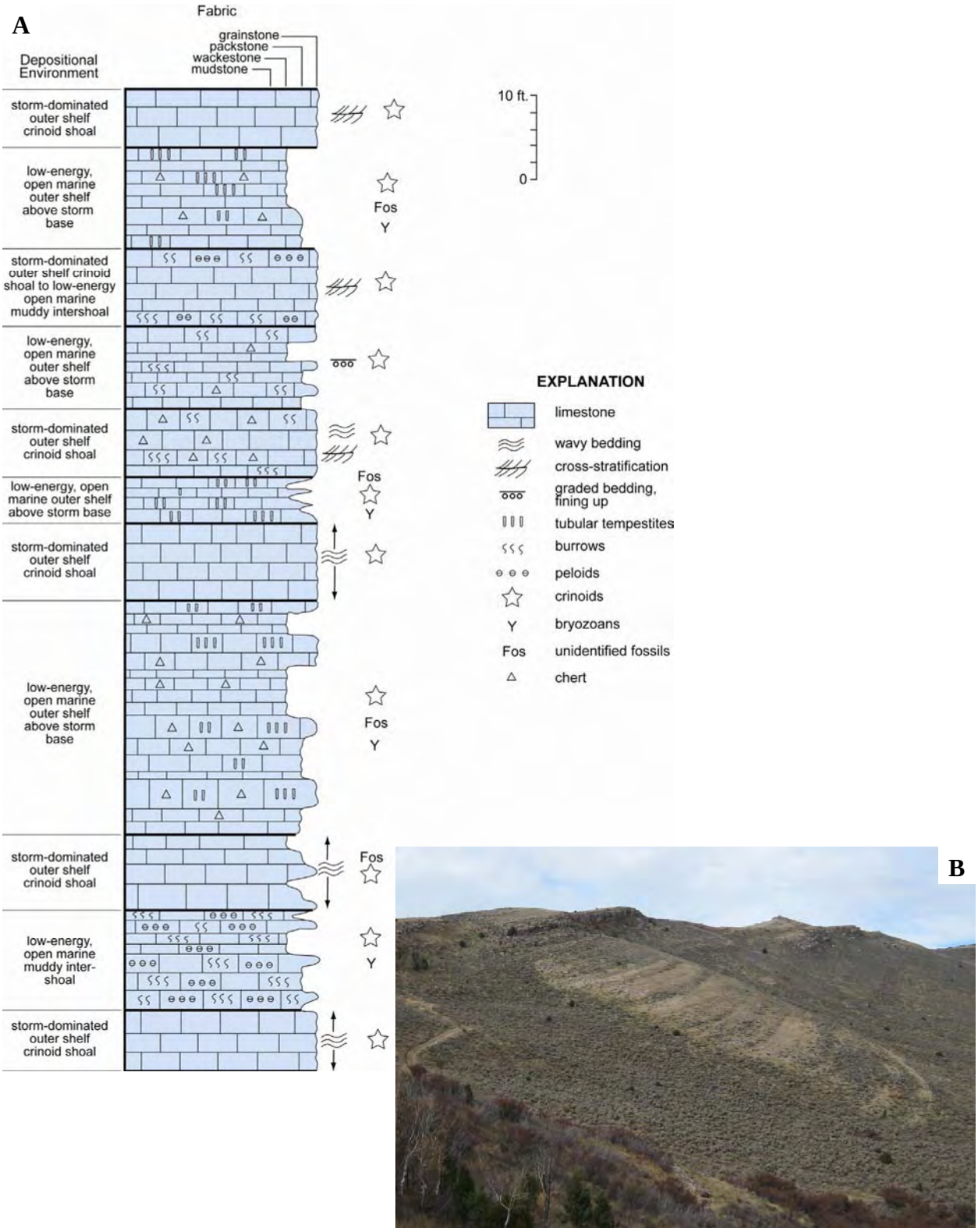

Figure 8-16. Madison Limestone section at study site 3. A – Stratigraphic column from the Madison Limestone at study site 3 showing carbonate fabrics and textures, fossils, and depositional environments. B – Outcrop of measured stratigraphic section.

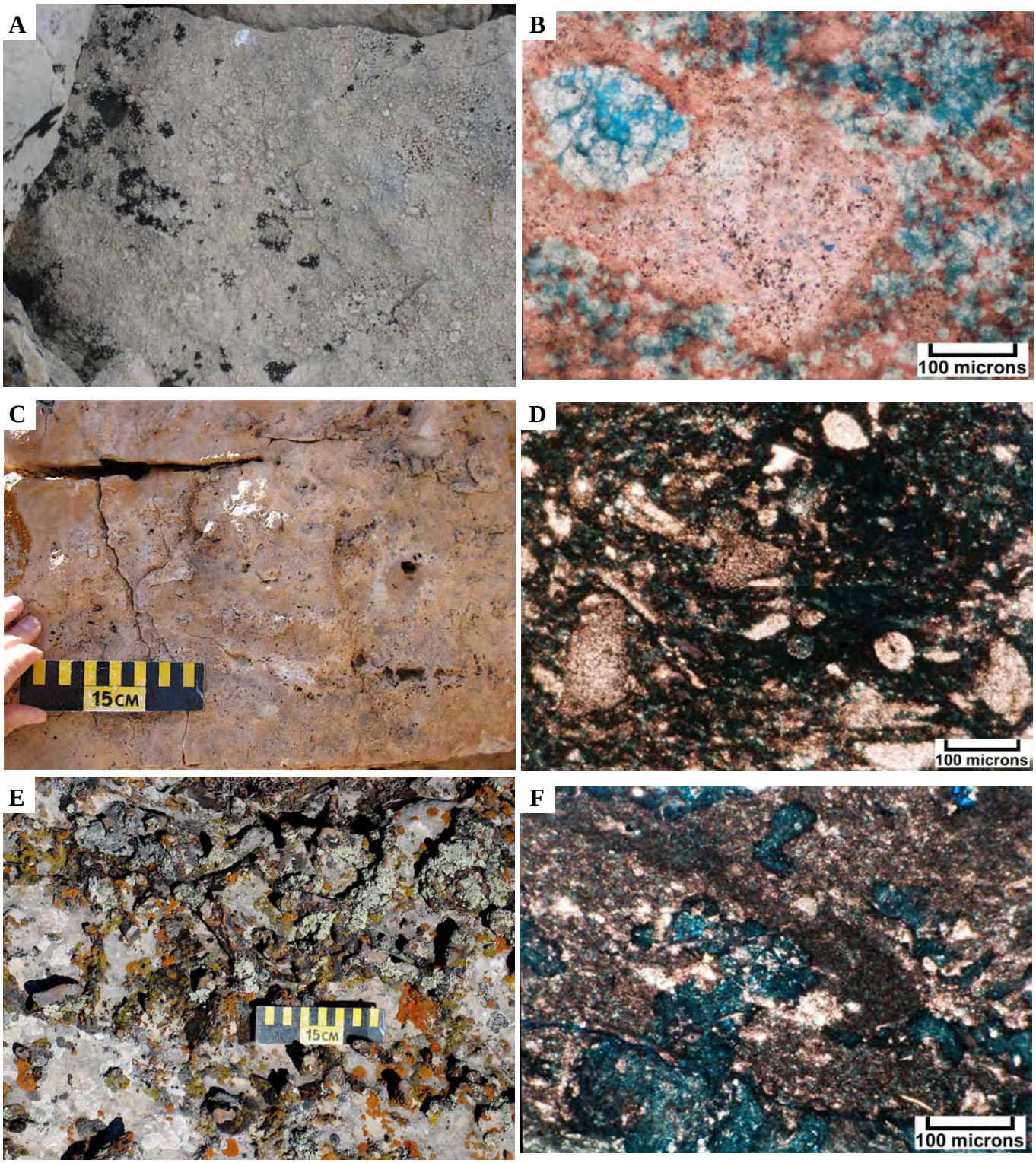

Figure 8-17. Examples of Madison lithofacies from study site 3. A – Coarse-grained, skeletal/ crinoidal grainstone (encrinite). B – Photomicrograph (plane light) of a crinoid columnal within a typical limestone encrinite. Note some syntaxial cement overgrowths. C – Typical burrowed soft peloid/crinoid packstone. D – Photomicrograph (plane light) of a low-energy, open-marine peloidal wackestone. E – Weathered out tubular tempestites in a skeletal packstone. F – Photomicrograph (plane light) of a tubular tempestite containing skeletal debris.

Figure 8-18. Topographic sags at the sites of major breccia zones (pipes?) along a ridge of Madison Limestone (view to the southeast).

Figure 8-19. Slabbed specimen of highly brecciated rock typical of that present at study site 3.

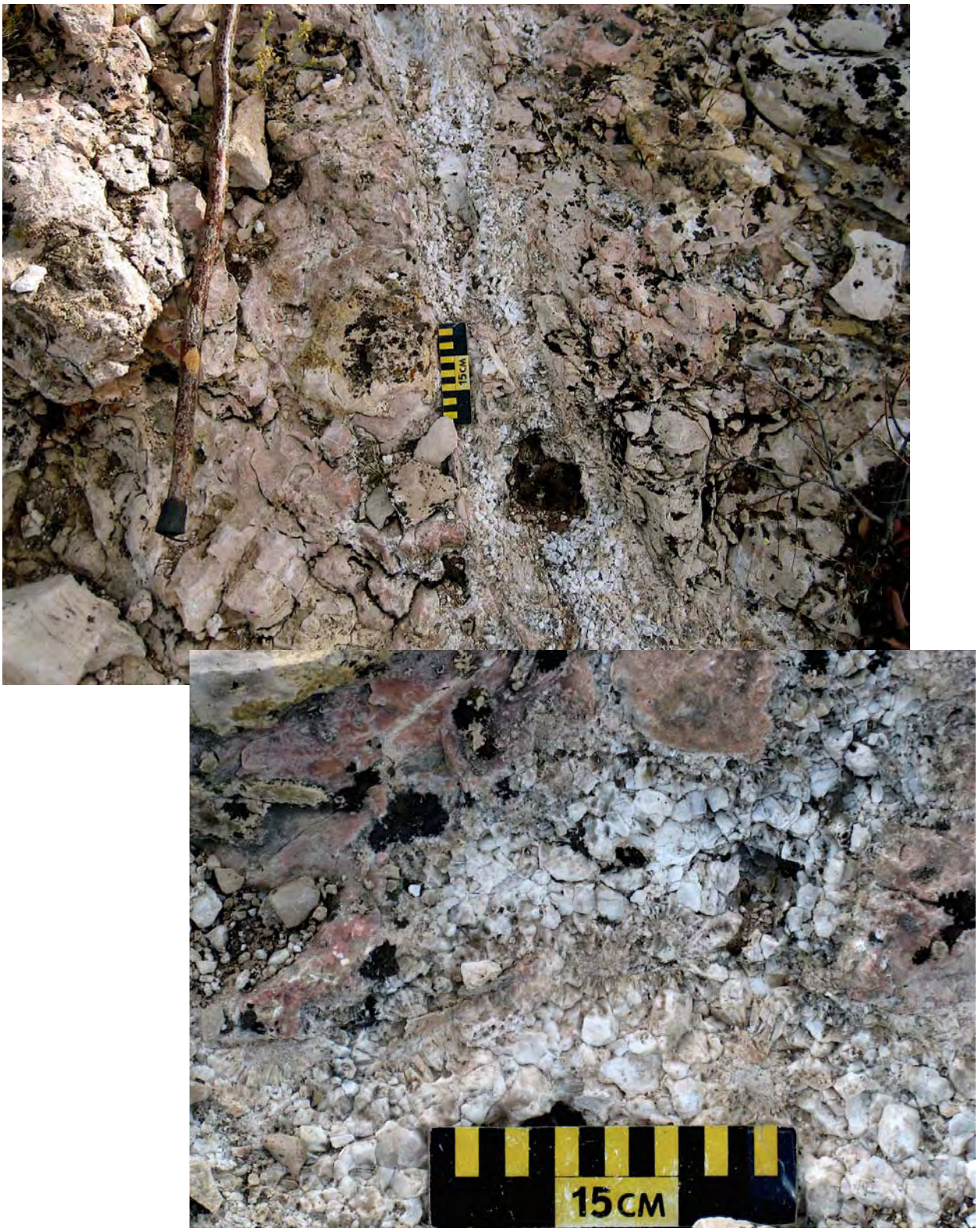

Figure 8-20. Coarse calcite vein in a highly brecciated dolomitic matrix. Inset: close-up shown of large, representative, calcite crystals.

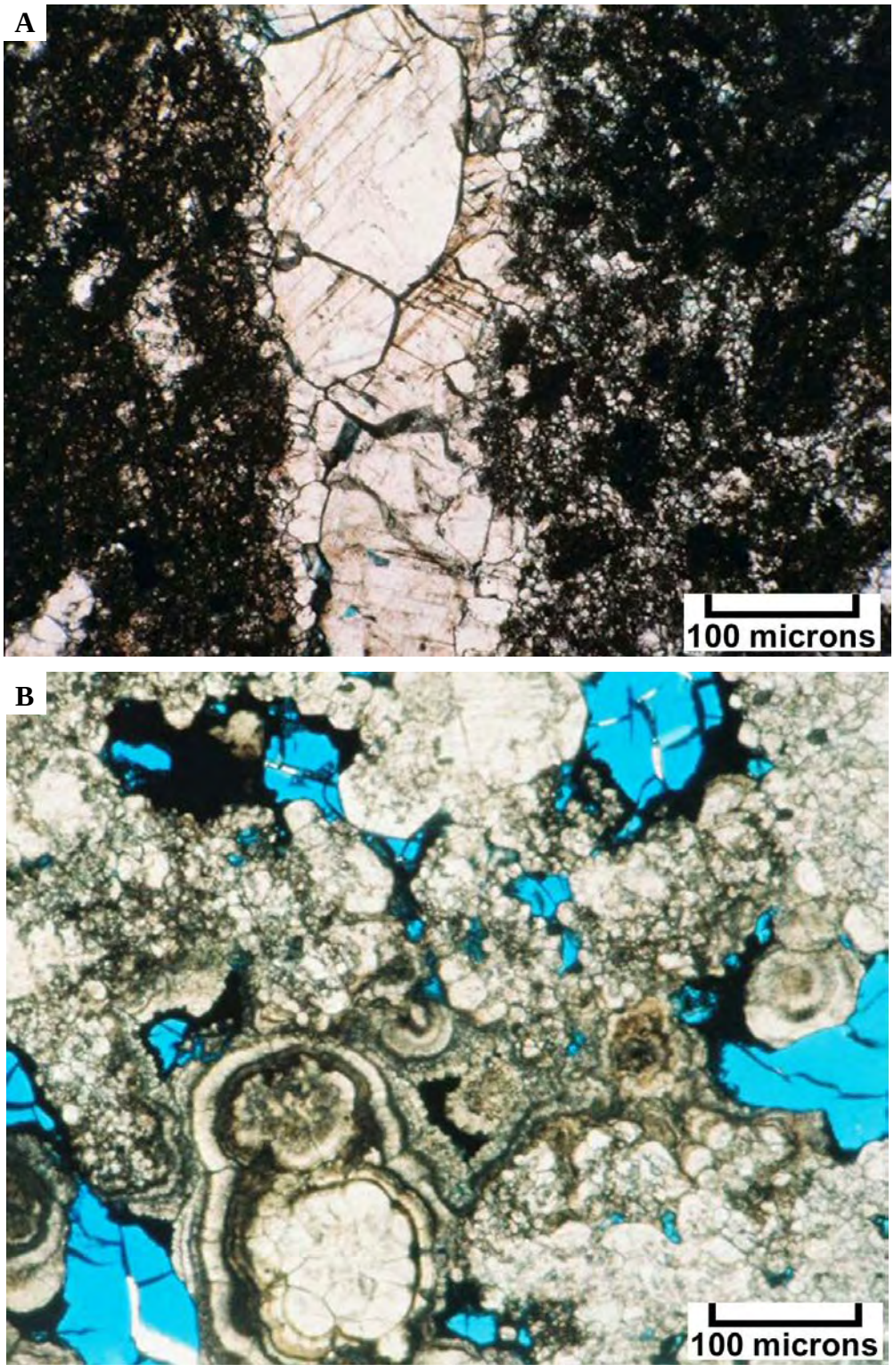

Figure 8-21. Photomicrographs (plane light) from breccia samples at study site 3. A - Vein of coarse calcite in a tight dolomitic matrix. B - Unusual concentric dolomite cement (high temperature?) overgrowths in a dolomitic breccia matrix.

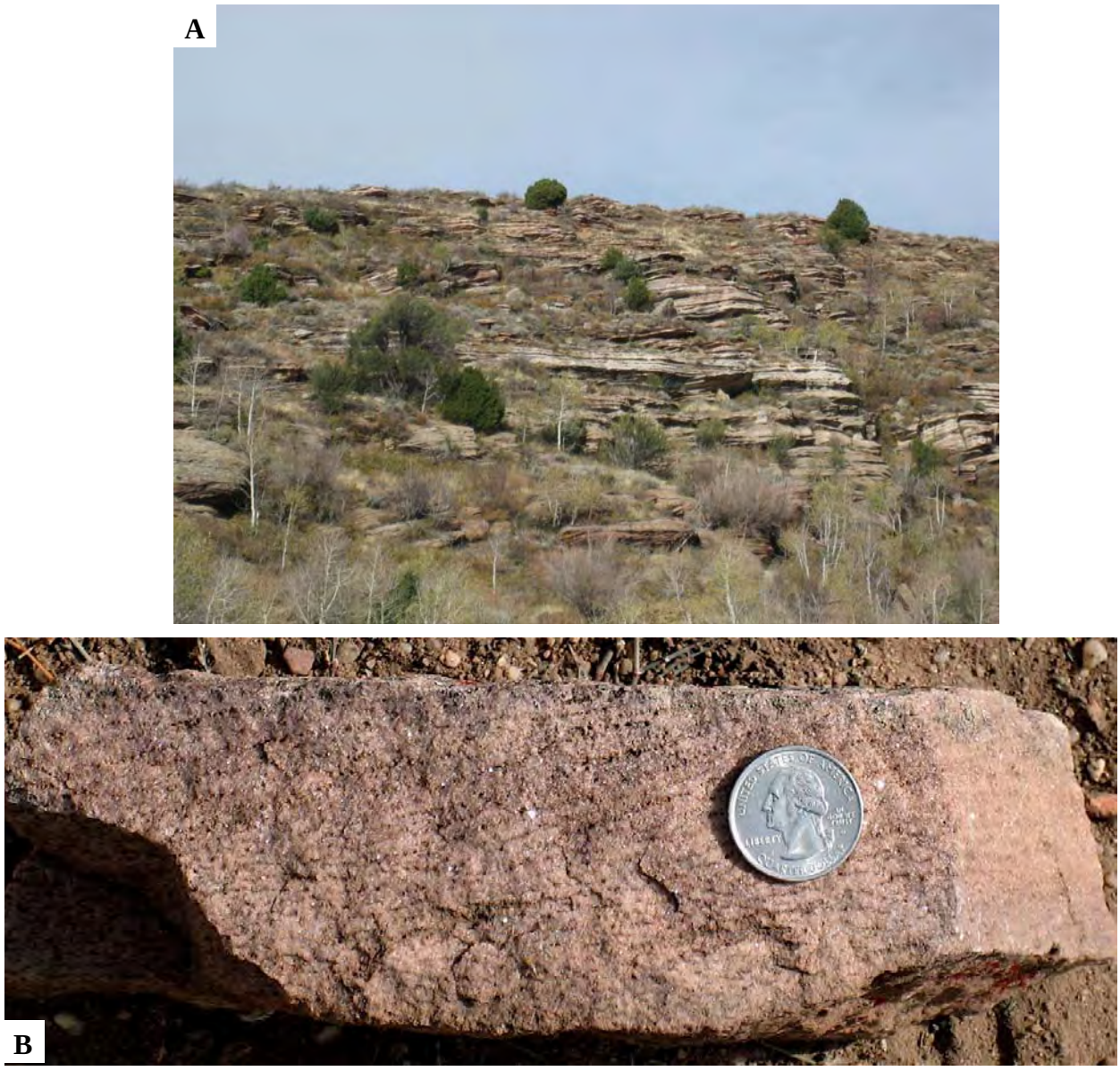

Figure 8-22. Basal Cambrian Lodore Sandstone. A - Outcrop of thin-bedded Lodore Sandstone north of study site 3, southwest of Crouse Reservoir. B - Lodore Sandstone hand sample of very fine grained, well sorted, cross-bedded, slightly ferruginous sandstone.

CHAPTER 9
MODERN RESERVOIR ANALOGS FOR THE MISSISSIPPIAN LEADVILLE LIMESTONE: SOUTHERN FLORIDA AND THE BAHAMAS

Thomas C. Chidsey, Jr., Utah Geological Survey

Introduction

The oil production from the Mississippian Leadville Limestone of the Paradox Basin is from a variety of warm, shallow-shelf, carbonate depositional environments as described in previous chapters. Deposition of the Leadville and other carbonate formations was widespread in Paleozoic and Mesozoic epeiric seas. However, there are relatively few places on Earth where shallow-marine carbonates are actively being deposited on a major scale and over millions of years. Platform-scale carbonate deposition today is restricted to the southern Florida-Bahamas region, the Yucatan, the Arabian Gulf, and Australia.

Leadville environments have modern analogs in the southern Florida-Bahamas region – a world class natural laboratory to study "tropical" carbonate depositional systems (figure 9-1). This region represents a time horizon from which one can observe carbonate deposition, the conditions (physical, biological, and chemical) which create various carbonate sediments, and the processes by which the deposits change. Understanding the facies types, distribution, geometry, and depositional patterns of these modern analogs helps to better (1) determine sediment source and accumulation, (2) estimate reservoir heterogeneity and capacity, (3) establish initial pore-space characteristics, and (4) identify areas regionally that have the greatest petroleum potential of the Leadville Limestone.

Basic Principles of Carbonate Deposition – Carbonate Factories and Platforms

Southern Florida and the Bahamas are carbonate "factories." Carbonate production is at a maximum in the carbonate-factory areas. Noel P. James, pre-eminent scholar in the processes that produce modern limestone, stated "Carbonates are born, not made." They result from biological and biochemical processes (S. Ritter, Brigham Young University, verbal communication, 2008). Carbonate minerals are secreted by plants and animals. Some carbonate sediment is created by direct precipitation from seawater (Bosence and Wilson, 2005). Skeletal materials become particles and accumulations become limestone.

Three basic rules control the nature (formation, distribution, and deposition) of carbonate depositional systems (Schlager, 1992): (1) carbonate sediments are largely organic in origin, (2) carbonate systems can build wave-resistant structures, and (3) they undergo extensive diagenetic alteration. The rate at which organisms and plants produce carbonate sediment depends on latitude, temperature, salinity, oxygen content, water depth, acidity (pH), sunlight intensity, turbidity, water circulation, partial pressure of carbon dioxide (pCO_2), and nutrient supply.

Most carbonates are produced close to where they are deposited as opposed to typical siliciclastic sediments. However, storms, tides, and currents will transport large quantities of fine sediment in adjacent areas (including both shallow- and deep-water settings). Carbonate factories develop where clean, shallow (<300 feet [100 m]) marine waters cover large platforms;

the highest sediment productivity occurs at water depth less than 30 feet (10 m) (S. Ritter, Brigham Young University, written communication, 2008).

Carbonate platforms are recent and ancient thick deposits of carbonate rocks (Bosence and Wilson, 2005). Factors that influence differences in the platforms upon which warm-water carbonates are deposited include (1) climate, (2) platform morphology (such as ramp or rimmed attached platforms or isolated unattached platforms), (3) lithology (carbonate only, carbonate/siliciclastic, or carbonate/evaporate), (4) fauna, (5) subsidence, (6) siliciclastic source, and (7) eustacy (greenhouse, icehouse, or transitional) (S. Ritter, Brigham Young University, verbal communication, 2008).

There are three main types of carbonate factories: (1) warm water, (2) cool water, and (3) pelagic (Bosence and Wilson, 2005). The southern Florida and Bahamas region is a warm-water carbonate factory. The Leadville Limestone was most likely deposited in a warm-water carbonate factory during Mississippian time on an epeiric attached platform, that is, an extensive cratonic area covered by a shallow sea (figures 7-5 and 7-6). Warm-water carbonate factories are located generally between low latitudes (30° north and 30° south; both presently and in the geologic past). Shallow-marine tropical waters support rapidly calcifying communities of organisms that use photosynthesis for energy. Examples of these communities include calcified green and red algae, and corals with symbiotic algae. Forams, mollusks, sponges, and echinoderms are also common members of such communities. These communities build shallow-water coral reefs, shoals composed of skeletal grains, and other types of carbonate buildups.

The warm water is also often supersaturated with respect to calcium carbonate which can be precipitated to form carbonate grains such as ooids, peloids, grapestone, and carbonate mud. Shallow warm-water carbonate accumulation rates range from about 0.6 to 24 feet (0.2-8 m) per 1000 years and can keep pace with a rise in sea level when the rate of sediment production is highest (Bosence and Wilson, 2005).

Taphonomic Processes

Another key aspect of using modern carbonate analogs to better interpret the lithofacies of the Leadville Limestone is using tropical taphonomy to take biofacies (biotic coummunities) to lithofacies (carbonate sediments). Taphonomic processes (biostratinomy) take place after an organism dies but before its final burial. These processes are largely destructive (bioerosion) and include physical, biological, and chemical effects. As a result, much of the information about the biotic community is lost, but the gain is a depositional environment with information “encoded.” Thus, the sedimentary lithofacies mimic the former biological communities.

Physical processes consist of reorientation, transport, breakage, disarticulation, and exhumation. Biological processes consist of decay, scavenging, bioturbation, boring, and encrustation. Chemical processes consist of corrosion, dissolution, and recrystallization. The roles of organisms in these processes may be ecological, sedimentological, or diagenetic. Ecologic roles of organisms are that of a primary producer, grazer, predator, or filter feeder. Sedimentalogical organism roles include sand makers, mud makers, sediment binders, sediment bafflers, frame builders, sediment eaters, burrowers, borers, and encrusters. Diagenetic roles consist of producing aragonite versus calcite, micritization, and grain borer (S. Ritter, Brigham Young University, verbal communication, 2008).

Warm Water Biologic Communities

Although the organisms in warm-water carbonate settings today are different from those of the past due to organic evolution, the roles of sediment producer, modifier, and so forth, have remained largely unchanged through time (S. Ritter, Brigham Young University, written communication, 2008). According to Enos (1977), "for modern ecology to have maximum applicability to ancient limestone, consideration should be given to evolutionary replacement. Replacement is the adaption of an organism or groups to approximately duplicate the way of life of an earlier group. Replacement may result from successful competition with the earlier group or from simply filling an available ecological niche, long since vacated by the earlier group." Examples include Paleozoic tabulate corals and modern scleractinian corals, or the Pennsylvanian green algae *Ivanovia* and the modern green algae *Halimeda*. Southern Florida and the Bahamas team with a wide variety of life to fill the ecological, sedimentalogical, and diagenetic roles (described above) which have counterparts in the Leadville Limestone.

Protozoans

Protozoans are mainly foraminifera. The majority of the shelf foraminifera belong to two families: Miliolidae and Peneroplidae. They are mobile benthonic forms that live on grass (figure 9-2) and in/or on sediment (Enos, 1977).

Plants

Plants include algae and vascular plants. Calcareous algae are classified based on pigmentation, composition, and habit. They consist of three phyla; (1) Cyanophyta (blue-green algae), (2) Rhodophyta (red algae), and (3) Chlorophyta (green algae). The blue-green algae form algal mats in supratidal environments (figure 9-3) and act as binding material. The red algae make up about 10% of the calcareous algae while the bulk of the volume of sediment produced from calcareous algae comes from the green algae (figures 9-4 and 9-5). The segmented green algae *Halimeda* (figure 9-5) is a sand maker found in relatively high-energy environments. Multiple generations grow each year. It is a major producer of carbonate sediment – estimated to be as much as 22,000 grains per year per 11 square feet (1 m^2) or 65% of the sediment is some areas (S. Ritter, Brigham Young University, 2008). Mud-making green algae include *Penicillus*, *Udotea*, and *Rhipocephalus* (figures 9-4 and 9-6). *Penicillus* and *Udotea* produce needles of aragonite when they die. *Penicillus* ("shaving brush") is the major contributor of fine aragonite mud; the similarity of Holocene muds and many ancient lime muds (textures, structures, and fossils) implies that these plants have been a significant source of fine-grained sediment in the geologic past (Stockman and others, 1967), including possibly Leadville Limestone. The most common red algae is *Neogoniolithon* typically found on shelf margins. It can be flat, saucer-shaped crusts to erect, branching plants (figure 9-7) (Enos, 1977).

Vascular plants include sea grasses (angiosperms) and mangroves. The most widespread sea grass is *Thalassia testudinium* (turtle grass) (figure 9-8), which requires adequate sunlight and stable, thick sediment for its root system. Turtle grass plays an important role as a baffle and sediment trap (Enos, 1977). Mangroves are classified as red (*Rhizopora mangle*) with roots going down (figure 9-9) and black (*Avecinnia*) with roots going up (figure 9-10) which form around the edges of islands, lagoons, and marshes. These plants can ultimately form peat.

Invertebrates

Invertebrates include the phylums Porifera (sponges), Cnidaria, and Mollusca. Sponges generally require a hard surface for attachment. The larger sponges contain siliceous spicules. Their contribution overall as a sediment constituent is low. Phylum Cnidaria represents the most important invertebrates in warm-water carbonate platforms – the corals. The three main classes are Hydrozoa (fire corals), Scyphozoa (jellyfish), and Anthozoa which includes the order Scleractinia (Triassic through modern corals). Hydrozoans are common but only the fire coral Millepora secretes a calcareous skeleton (figure 9-11) (Enos, 1977). They may be branching or bladed requiring a firm substrate in high-energy environments. Alcyonaria (also known as Octocroallia because they have eight-fold symmetry) is a subclass of Anthozoa. They include sea fans, sea whips (figure 9-12), sea pens, sea feathers, and soft corals. Alcyonarians grow on dead coral or rubble in outer reefs and patch reefs around living coral where the water is shallow and has strong wave action. When they die, many species disaggregate and become sediment consisting of little rods.

The spectacular reefs of the southern Florida-Bahamas region are primarily built by scleractinian corals (hard corals). These corals are zoned and grow in a variety of sub-environments. The chief framework builder of the outer reefs is the massive, branching *Acropora palmata* (moosehorn coral) occurring where there is maximum wave action and water circulation on the reef crest (figure 9-13A). *Acropora cervicornis* (elkhorn coral) (figure 9-13A) and *Porites porites* (finger coral) (figure 9-13B) are found in quieter waters of the outer reef and back reef areas. The branches of elkhorn and moosehorn corals often break off, especially due to storms or when they die, forming rubble zones in the back reef, reef front, and forereef areas. *Porites* also occurs on patch reefs in the back reef and lagoonal areas where it is well-rooted or attached. Massive head corals are the dominant forms in patch reefs but can also grow in sheltered parts of outer reefs. The most abundant head coral in patch reefs is the large, massive *Montastrea annularis* (star coral) (figure 9-13C). Other common patch reef corals are *Diploria* (brain coral) (figure 9-13D) and *Siderastrea* (golfball coral) (figure 9-13E). Some patch reef corals, such as *Siderastrea* and *Porites*, also occur in semi-restricted environments where they may be widely distributed but populations are sparse and their size small. In addition, small *Porites* and *Siderastrea* are very abundant around muddy shoals (main mud mounds) or tidal channels (Enos, 1977). Some corals are mud tolerant such as *Manicina* (rose coral) (figure 9-13F), which are comparable to Paleozoic horn (rugose) corals common in the Leadville Limestone (figure 3-4).

The phylum Mollusca, particularly gastropods (snails) and bivalves (clams and oysters), are significant contributors of sand-size skeletal grains. While skeletal grains from crinoids may have been prevalent to create shoals in the Mississippian, gastropods, for example, are a major contributor now (figure 9-14). Molluscs are varied, abundant, and good ecological guides (Enos, 1977).

Of the arthropods, the crustaceans are the most significant. They live in all marine environments in the carbonate platform. They contribute huge amounts of fecal pellets into the carbonate system and are major burrowers, particularly the shrimp *Callianassa* (figure 9-15). Ostracods are common in restricted inner shelf areas.

Echinoderms are also common in all marine environments and include echinoids (sea urchins and sand dollars), holothurians (sea cucumbers), ophiuroids (brittle stars), and

asterozoans (star fishes). Yet, in comparison to Paleozoic environments, their modern contribution is relatively minor. Sand-size calcite plates from sand dollars (figure 9-16) can yield significant quantities of carbonate sand in some areas. Annelid worms affect carbonate deposits of platforms by burrowing, pelleting, and boring (Enos, 1977). Bryozoans, so common in the Paleozoic fossil record, play a relatively minor role in modern carbonate environments.

Southern Florida – Florida Bay to the Outer Reef

Southern Florida provides an opportunity to examine transgressive depositional conditions and sediments across several facies belts ranging from the Everglades to shelf-edge barrier reefs, including supratidal algal flats, restricted marine mudbanks and "lakes," tidal channels, and outer shelf sand bodies (Ball, 1967). Here one can observe two complementary facets of each environment: (1) the influence of physical and biological processes on the distribution of marine plants and animals, and (2) the relationship between the organisms that inhabit the area and the type of sediment and sedimentary textures produced in each environment.

Southern Florida is an attached, rimmed carbonate platform (figures 9-17 and 9-18). This shallow shelf, warm-water carbonate factory lies on the late Pleistocene Key Largo Limestone. The Key Largo Limestone reef forms the present-day Florida Keys, the islands that separate the modern arcuate reef tract from Florida Bay. From northwest to southeast, the platform consists of mangrove swamps and supratidal flats (Everglades), an inner shelf (Florida Bay), inner and outer shelf margins, and a shallow slope into the Straits of Florida (figures 9-17 and 9-18) (Enos, 1977).

Southern Florida has a semi-humid to sub-tropical climate (40 to 45 inches [100-114 cm] of rain per year) with a wet season from July to December (Bosence and Wilson, 2005). Southeast trade winds during the summer swing to the northeast during the winter generating bottom currents of 1.5 feet (0.5 m) per second. The region is within the microtidal range (2 feet [0.7 m]) and tidal currents only affect channels and flood-tidal deltas except during storms (S. Ritter, Brigham Young University, verbal communication, 2008). The platform hinterland (Everglades) is large with an abundance of fresh water.

Florida Bay

Florida Bay is triangular shaped due to barriers that restrict circulation (figure 9-17) (Enos and Perkins, 1979). Water depths range from 0 to 10 feet (0-3 m) and maximum local relief is 12 feet (4 m). Water circulation is restricted with periodic tides only on the margins. The surface water temperature ranges from 59° to 104° F (15-40 C°) and the salinity varies from 10 to 70 parts per thousand (‰). Plankton and nutrient availability is low and the turbidity is generally high (S. Ritter, Brigham Young University, verbal communication, 2008).

There are four hydrological influences on the environmental characteristics of Florida Bay: (1) the Gulf of Mexico, (2) the reef tract, (3) the Everglades, and (4) the bay itself. Waters and biota in the bay are derived from the Gulf of Mexico to west, the Atlantic Ocean (Straits of Florida) through breaks in the exposed Pleistocene reef tract (the Florida Keys) to the south and east, and the Everglades to the north. The Gulf of Mexico has the greatest effect although broad carbonate mud banks restrict tidal action. Tidal channels through the Keys into the bay represent high-energy environments that support a high diversity of larger organisms (gastropods, clams,

and corals) in deposits of *Halimeda*-produced sand that are relatively free of mud (which has been winnowed out by currents). In the Everglades, fresh water accumulates during the rainy season then flows southward into the northern part of the bay during the winter, thus significantly lowering the salinity to as little as 10‰ from a summer high of 50‰. Such a wide range limits the biota of the bay (S. Ritter, Brigham Young University, verbal communication, 2008). The honeycomb nature of the mud-bank distribution within the bay (figure 9-17), further restrict currents, salinity, tides, and so forth.

A variety of sedimentary environments are represented in Florida Bay as part of a transgressive record: (1) fresh-water pond, (2) coastal mangrove swamp, (3) broad, shallow bay basins ("lake"), (4) mud bank, and (5) island. From our work on the Leadville Limestone, we recognize the shallow bay basins and mud banks (mounds) as modern analogs which are described in the following sections.

Shallow bay basins ("lakes"): Broad shallow bay basins, locally known as "lakes" occupy about 90% of the total area of Florida Bay (Stockman and others, 1967). In the eastern part of the bay, these shallow basins are polygonal (figures 9-19 and 9-20) due to the honeycomb nature of the surrounding mud mounds, and cover an area typically of 2 to 8 square miles (5-21 km^2). They are 3 to 7 feet deep (1-2 m) with an average sediment thickness of only 6 inches (15 cm) composed of shelly sediment on Pleistocene bedrock (Stockman and others, 1967; Enos and Perkins, 1979). Limited wave action and currents are strong enough to winnow out fine material which is deposited on the leeward side of mud mounds. Over 70% of the sand-size sediment consists of molluscan skeletal fragments (figure 9-21) (Ginsburg, 1956). This environment does not support a large and diverse biotic community. Sea grasses are lacking but the sediment is completely burrowed by worms and crustaceans. The mud that is present is pelleted by these organisms (Shinn, 1968; Enos and Perkins, 1979).

The shallow bay basins in the western part of Florida Bay receive a strong influence from the Gulf of Mexico. Sediment is thicker and contains up to 3 feet (1 m) of mud which supports turtle grass (further trapping mud) and a larger, diverse fauna. The deposits within the shallow bay basins of Florida Bay would produce skeletal-peloidal packstone, wackestone, and mudstone like these found in the Leadville (see figures 3-1 and 3-8).

Mud mounds (mud banks): Mud mounds (or mud banks as they are often referred to in the literature) are prominent features in Florida Bay. They represent localized accumulations of muddy biogenic carbonate sediments built up by winter storm winds from the northeast (figure 9-22). The windward sides are steeper and covered by a thin skeletal lag. The muddy leeward sides slope more gently and are stabilized with turtle grass (Enos and Perkins, 1979). Mounds migrate slowly in the leeward direction (Bosence, 1995; Bosence and Wilson, 2005). Mound tops are flat and awash at low tides. Some mounds build up to sea level to become islands colonized by mangroves. Saline ponds and algal mats are also common on the mud-mound islands. Mud mound thicknesses range from 6 to 12 feet (2-4 m) (Enos and Perkins, 1979).

The green algae *Pennicillus* is responsible for the production of one-third of the aragonite mud in the mounds (Stockman and others, 1967). Other sedimentary particles include poorly sorted shell fragments and pellets. Mound sediments are completely burrowed and the upper zones penetrated by roots and rhizomes of turtle grass (Enos and Perkins, 1979).

Mud mounds contain sedimentological, paleontological, and geochemical records of past conditions in Florida Bay (Robert B. Halley, U.S. Geological Survey, verbal communication,

1998). Therefore, such records likely exist in Mississippian Waulsortian-type (mud mound) buildups. The deposits that make up Florida Bay mud mounds would produce skeletal/pelletal wackestone and locally packstone or mudstone (see figures 3-1 and 3-5) as found in the Leadville.

Reef Tract

The southern Florida attached platform has a rimmed margin formed by the arcuate reef track band (figures 9-17 and 9-18). Water depths range from 0 to 300 feet (0-100 m) and maximum local relief is 30 feet (10 m). Water circulation is open with semi-diurnal tide exchange with the Florida current. The surface water temperature ranges from 59° to 91° F (15°-33°C) and the salinity varies from 32 to 38‰. Plankton and nutrient availability is normal for the tropics and the turbidity is periodically high in the lagoonal part of the shelf margin (S. Ritter, Brigham Young University, verbal communication, 2008).

The reef track is 150 miles (240 km) long and averages 4 miles (6 km) in width. It coincides with the inner and outer shelf margins (figure 9-18). Sedimentary environments include the seaward forereef, discontinuous outer barrier reef (subdivided into a reef front, reef crest, and reef flat), and back reef consisting of a sand apron and lagoon (containing patch reefs and sand shoals). The differences among these environments are due to water depth and circulation which also is reflected in sediment types and biological communities. Areas of mud accumulation (mud mounds) are found in front of the Keys representing a transition from open-marine conditions to those of Florida Bay.

There are no barrier reefs known in the Leadville Limestone. However, from our work, we recognize the marine mud mounds, patch reefs, and sand shoals in the reef tract as modern analogs which are described in the following sections.

Mud mounds: Besides being a dominant feature of Florida Bay, mud mounds or carbonate mud banks, have also formed in the inner shelf margin of the reef tract. They have similar characteristics to the mud mounds in Florida Bay. Examples include Rodriguez Key and Tavernier Key (figure 9-17). Rodriguez Key is a flat-topped island, about 1.5 miles (2.4 km) long and 0.7 miles (1.1 km) wide, with the surface varying around mean sea level. The axis of the island is covered with black mangroves and the margins with red mangroves. Surrounding the windward side of Rodriguez Key are three biologic zones (figure 9-23): (1) an inner zone of turtle grass and green algae (*Halimeda, Penicillus, Udotea,* and *Rhipocephalus*) in the bank environment, (2) a middle zone of finger coral (*Porites*) and thickets of branching red algae (*Neogoniolithon*) in windward bank margin, and (3) and an outer zone of turtle grass and green algae in the off-bank environment (Turmel and Swanson, 1976; Bosence, 1985).

The mound is composed of skeletal calcite mud produced principally by green algae (Turmel and Swanson, 1976). The maximum thickness of the sediments is 15 feet (5 m). The mound developed over a topographic low in the underlying Key Largo Limestone. This low filled with mud which was probably stabilized by turtle grass resulting in eventual mound development – a possible key for predicting mud mounds in the Mississippian. The resulting sediments outward from the island are (1) mixtures of lime mud and skeletal sand, (2) skeletal sand and gravel and (3) lime mud and skeletal sand.

Patch reefs: Patch reefs are common in the inner shelf margin of the reef tract lagoon and back reef areas (figure 9-18). Though small in area, many are named such as Hens and Chicken reef, for example. They rise 10 or more feet (3 m+) above the sea floor to within 6 to 12 feet (2-4 m) of the surface. Patch reefs are circular to elliptical in plan view and can range up to several hundred feet in length (S. Ritter, Brigham Young University, written communication, 2008). They develop over slight topographic highs, changes in slope, or on the rims of depressions (Enos, 1977). Ecologically, patch reefs require similar conditions for development as barrier reefs except for lower wave energy.

Patch reefs may include large and small corals of *Montastrea annularis* (star coral), *Porites* (finger coral), *Siderastrea* (golfball coral), and *Diploria* (brain coral). Alcyonarians (sea fans and sea whips) grow on dead coral which is often encrusted with coralline algae. Patch reefs are usually surrounded by an apron of rubble and sand grains produced by physical erosion (currents and wave action) and bioerosion (by sponges, worms, parrot fish, echinoids, and molluscs). The bottom of the lagoon where patch reefs grow is usually skeletal containing 10 to 60% lime mud produced by the green, mud-making algae and trapped by carpets of turtle grass.

Carbonate sand shoals: Calcareous sand shoals, such as White Bank (figures 9-17 and 9-18), lie between the outer reef and the inner shelf margin. Sand deposits are thin, clean, and ripple marked (figure 9-24) (and probably cross-bedded), and the grain size is medium to coarse (figure 9-25). The ripples are usually oscillation types formed from normal current and tidal conditions (Enos, 1977). Water depths of the shoals are 12 feet (4 m) or less. Skeletal sand accumulates in depressions or on topographic highs. The sediment is derived from the outer reef and transported landward (Enos, 1977), thus the size of the shoal is proportional to that of the nearby outer reef. However, some sediment is produced within the sand shoals from sand dollar echinoids. Worms, crustaceans, and molluscs also inhabit carbonate sand shoals.

White Bank is the largest carbonate sand shoal along the reef tract. It is 1 mile (1.6 km) wide and 20 miles (32 km) long. Large carbonate sand shoals, similar to White Bank, were common in the Leadville Limestone. Instead of skeletal grains of coral and mollusc fragments, the Leadville shoals consisted of crinoid columnals (see figures 3-1 and 3-4).

Great Bahama Bank – Andros Island Area

The Great Bahama Bank, centered around Andros Island, provides another opportunity to examine classic examples of modern carbonate deposition in an unattached, isolated, rimmed carbonate platform (figure 9-26). These include the origin, sedimentary dynamics, and reservoir properties of ooid shoals, carbonate tidal flats, and the Earth's third longest barrier reef.

The Bahama platform is composed of Pleistocene limestone that lies above 19,000 feet (6000 m) of Tertiary and Cretaceous limestone and dolomite. They represent continuous carbonate deposition for nearly 135 million years on a basement of oceanic (basaltic) crust. Holocene sediments reach a thickness of no more than 10 feet (3 m) (S. Ritter, Brigham Young University, verbal communication, 2008). The platform is separated from other isolated platforms by wide, deep channels that are in actuality canyons that were maintained during platform deposition (the Dolomites in northern Italy are an ancient example).

Like southern Florida, the Bahamas climate is semi-humid to subtropical. The Bahamas are within the northeasterly trade-wind belt. The platform is in the microtidal range of 2.5 feet (0.8 m) and the water depths are 0 to 30 feet (0-10 m). The surface water temperature ranges

from 72° to 88°F (22°-31°C). Open-marine waters have an average salinity of 36‰.

Basic Depositional Setting

From east to west, the Great Bahama Bank consists of the following features: (1) the barrier reef with a steep reef front dropping rapidly into the Tongue of the Ocean, which reaches a depth of 8000 feet (2500 m), (2) a narrow lagoon, (3) Andros Island composed of exposed Pleistocene limestone with modern carbonate tidal flats on the western side, (4) the shelf lagoon over 40 miles (60 km) wide, and (5) oolitic shoals (figure 9-27). The maximum storm wave energy and turbulence takes place at the barrier reef on the east side of the platform. Current velocity and wave action are low in the shelf lagoon, but still very important in depositional processes. Turbulence due to tidal currents, not waves, increases along the rimming oolitic shoals (Bosence and Wilson, 2005).

The biological communities within the Great Bahama Bank vary according to water depth, temperature, salinity, wave and tidal energy, substrate, and other living organisms. When comparing the distribution of biotic communities (figure 9-28) with facies (figure 9-27) there appears an obvious correlation and interdependency between the two. In the case of the Great Bahama Bank, a direct relationship exists between biologic communities and two physical factors – wave action (turbulence) and substrate – and therefore facies (Newell and others, 1959; Purdy, 1963).

Platform Facies

The Great Bahama Bank has many of the same facies, with some differences, as the southern Florida platform reef tract. The barrier and patch reefs have similar biological communities and generate similar sediments. However, Bahamian carbonate sand shoals are distributed completely different than sand shoals of the Florida reef tract and their composition is almost entirely of ooids. Sand shoals rim the shelf lagoon which is also very dissimilar to lagoons along the Florida reef tract. From our work on the Leadville Limestone, we recognized ooid shoals and shelf lagoonal sedimentation as modern analogs which are described in the following section.

Oolitic Shoals: The oolitic shoals of the Great Bahama Bank (platform) are almost pure ooids. Ooids grow as concentric rings around a nucleus of a fecal pellet or shell fragment in water of elevated temperature and salinity. Wave action is not required for calcite to precipitate as layers on the ooids as previously thought. Calcite precipitation forms ooids by a chemical reaction dependent on pH and the calcium and bicarbonate concentrations in seawater (Dave Tingey, Brigham Young University, verbal communication, 2008). Ooid shoals tend to initiate on topographic highs, but their facies distribution and geometry is due to syndepositional processes (Grammer and others, 2001). Waves suspend the finer sediments and the tides sweep them off the platform (Milliman and others, 1993). Thus, a tide-dominated system yields a grain-dominated facies, such as the ooid shoals (Eugene Rankey, Iowa State University, verbal communication, 2009). Currents and wave action distribute and build ooids into shoals that follow the leeward margins of the platform (figures 9-26 and 9-27; also see figure 3-1) in shallow water where there are no reefs.

Joulter's Cay off the north end of Andros Island (figures 9-29 and 9-30A) is a world class

geosite to examine modern ooid shoals and their characteristics. The ooid shoals display flat-topped, bi-directional current ripples due to shallow tidal currents (figures 9-30A and 9-30B). Megaripples are also present in deeper water shoals. Ripple orientation is fairly random as one traverses from area to area across the shoals. Small tidal pools display (figure 9-30C) small-scale tidal deltas and tidal channels. Shoals are cross-bedded and often show a slight variation in ooid size from very fine (figure 9-30A inset) to coarse in different parts of the shoal complex. There are some thin zones of shell hash and coated grains. The shoal complex is active and thickens to the east. Bioturbation is intermittent, perhaps occurring every 30 feet (10 m), mainly by the rapidly burrowing bivalve *Tivela abaconia* (figure 9-30D). Only a few large starfish can be found grazing in the shallow water of the shoals.

Prolonged subaerial exposure leads to the establishment of stable grain flats (figure 9-30E). They generally thicken west at Joulters Cay and consist of very fine grained ooids and peloids. Red mangroves colonize the surface and *Callianassa* burrows are common along tidal channels. A large tidal channel is located at the south end of the Joulter's Cay shoal complex (figures 9-29 and 9-30F). Oncolites (algal balls) form within the channel. The dominant flow of currents in the channel is northeasterly toward the open sea where an ebb-tidal delta is built (figure 9-29).

Shallow-shelf lagoon: West of Andros Island, the semi-restricted, shallow-shelf lagoon of the Bahama platform covers an area of 3900 square miles (10,000 km^2) (figures 9-26, 9-27, and 9-31A). The water temperature and salinity are elevated compared to surrounding open-marine waters. Salinity increases up to 46‰ toward Andros Island. Currents decrease toward Andros Island and wave energy becomes negligible. Therefore ripples and cross-bedding are absent in the sediments. Carbonate (aragonite) muds are produced from direct precipitation in seawater (Bosence and Wilson, 2005). However, the "mud" is mainly composed of peloids (fecal pellets) and grapestone (aggregates of shell fragments and peloids, coated and cemented by aragonite) which would produce grainstone and packstone in the rock record. These sediments are widely distributed across the shallow-shelf lagoon (figure 9-27).

Mud and pellet mud facies dominate the lagoon directly west of Andros Island, while grapestone facies are found north to northwest and south to southwest of the island (figure 9-27) (Newell and others, 1959; Purdy, 1963). Tidal channels from tidal flats in northwestern Andros Island can produce small pellet shoals in the shallowest parts of the lagoon, in Red Bay for example (figure 9-31B). Exposed sediments also may experience early marine dolomitzation (figure 9-31C).

In the lagoon, turtle grass is locally dense. *Halimeda* and the mud-making *Penicillus, Udotea,* and *Rhipocephalus* green algae are significant contributors to the sediment mix. Fauna are sparse, limited to a few species of sponges, molluscs, echinoids, and rose coral (*Manicina*). Burrowing by worms and *Callianassa* is massive and the presence of these organisms is responsible for the peloids that make up the major portion of the sediments in the lagoon.

The sediments and facies observed in the Bahama platform shallow-shelf lagoon are very similar to those found in the Leadville Limestone (figures 3-1). They would produce carbonate fabrics ranging from peloidal grainstone to mudstone (see figures 3-6, 3-7, and 3-8), all having reservoir potential.

Carbonate tidal flats: As with other facies on the Bahama platform, the carbonate tidal flats on the northwest part of Andros Island are spectacular features. They have been the subject of

numerous studies such as Shinn and Lloyd (1969), Hardie and Shinn (1986), Reid and Browne (1991), Rankey (2002), Rankey and Morgan (2002), and Rankey and others (2004), to name just a few.

The Andros Island carbonate tidal flats consist of three tidal zones: (1) subtidal, (2) intertidal, and (3) supratidal (Shinn and Lloyd, 1969). Sediment in the subtidal zone is deposited below low tide in channels (figure 9-32A) and the nearby lagoon. Sediment in tidal channels is mainly thin skeletal (shells) sands, and scours can reach Pleistocene bedrock. Channels contain thickets of turtle grass and *Callianassa* burrows. Sediment in the intertidal zone is deposited between normal low and normal high tide as soft peloid grains and laminated algal mats (figure 9-32B). Mudcracks develop on algal mats during dry periods; they then provide "pastures" for grazing gastropods (figure 9-14). Sediment in the supratidal zone is deposited above normal high tide but within the range of spring and storm tides. The sediment forms channel levees (figure 9-32A), beach ridges, marshes, and ponds (figure 9-32C). Levee sediments are often heavily burrowed (figure 9-32D).

Carbonate tidal flats are laterally extensive along strike and represent part of a shallowing upward cycle (Grammer and others, 2001). Paleo tidal flat deposits are productive in Williston Basin fields and other carbonate reservoirs (Roehl, 1967). Recognizing the modern characteristics of carbonate tidal flats in the Leadville Limestone may provide additional target areas for drilling.

Figure 9-1. Landsat image of southern Florida and the Bahama Islands. Photo courtesy of Scott Ritter, Brigham Young University.

Figure 9-2. Underwater photograph of forams attached to sea grass, Florida Bay. Photo courtesy of Scott Ritter, Brigham Young University.

Figure 9-3. Algal mats (blue-green algae) in a supratidal environment on Cotton Key, one of many islands in Florida Bay. Photo courtesy of Scott Ritter, Brigham Young University.

Figure 9-4. Underwater photograph of the green algae <u>Halimeda</u> and <u>Penicillus</u> growing on the sandy bottom of Florida Bay. Photo courtesy of Scott Ritter, Brigham Young University.

Figure 9-5. Closeup of Halimeda (A) and the sand grains (B) it makes. Photo on right courtesy of Scott Ritter, Brigham Young University.

Figure 9-6. Mud-making green algae (from left to right) <u>Penicillus</u>, <u>Udotea</u>, and <u>Rhipocephalus</u>. Photo courtesy of Scott Ritter, Brigham Young University.

Figure 9-7. Underwater photograph of the branching red algae <u>Neogoniolithon</u> near Rodriquez Bank, Florida. Photo courtesy of Scott Ritter, Brigham Young University.

Figure 9-8. Underwater photograph of turtle grass (Thalassia) illustrating its ability to act as a sediment trap, Florida Bay. Photo courtesy of Scott Ritter, Brigham Young University.

Figure 9-9. Red mangrove (Rhizopora mangle), Florida Bay area. Photo courtesy of Scott Ritter, Brigham Young University.

Figure 9-10. Black mangrove (<u>Avecinnia</u>), Florida Bay area. Photo courtesy of Scott Ritter, Brigham Young University.

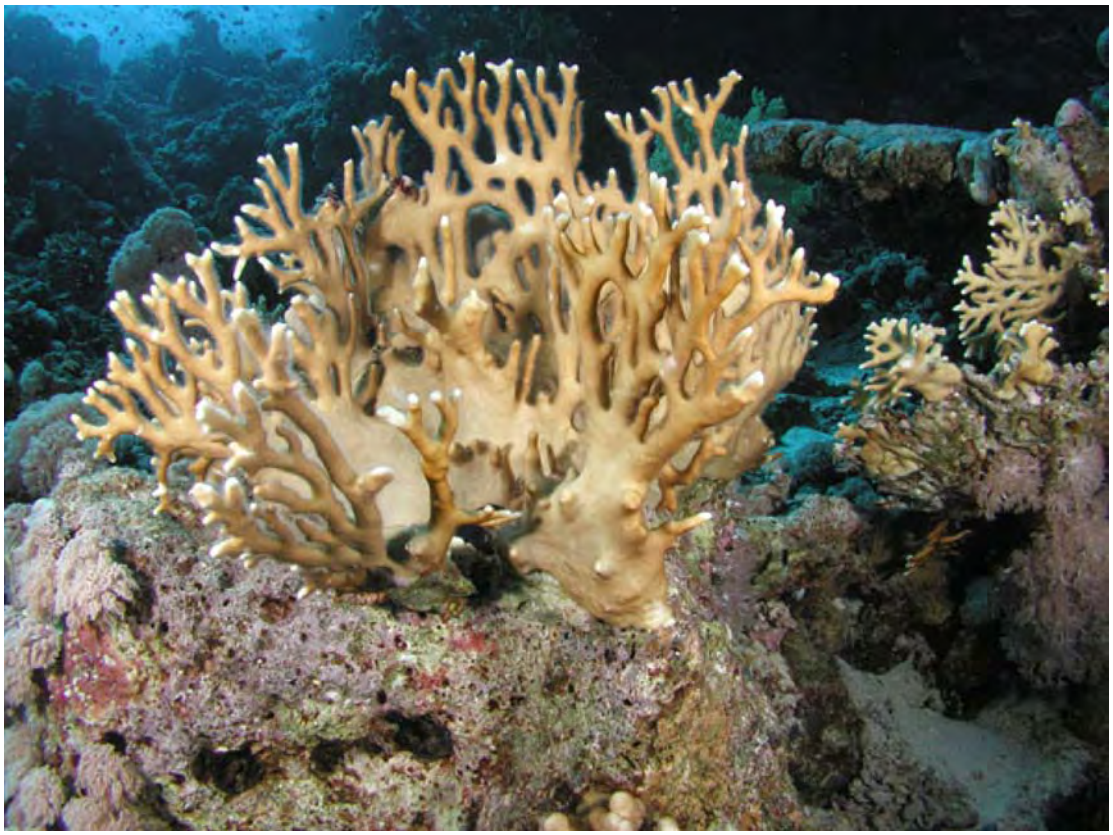

Figure 9-11. Underwater photograph of the branching fire coral <u>Millepora</u>. Photo courtesy of Scott Ritter, Brigham Young University.

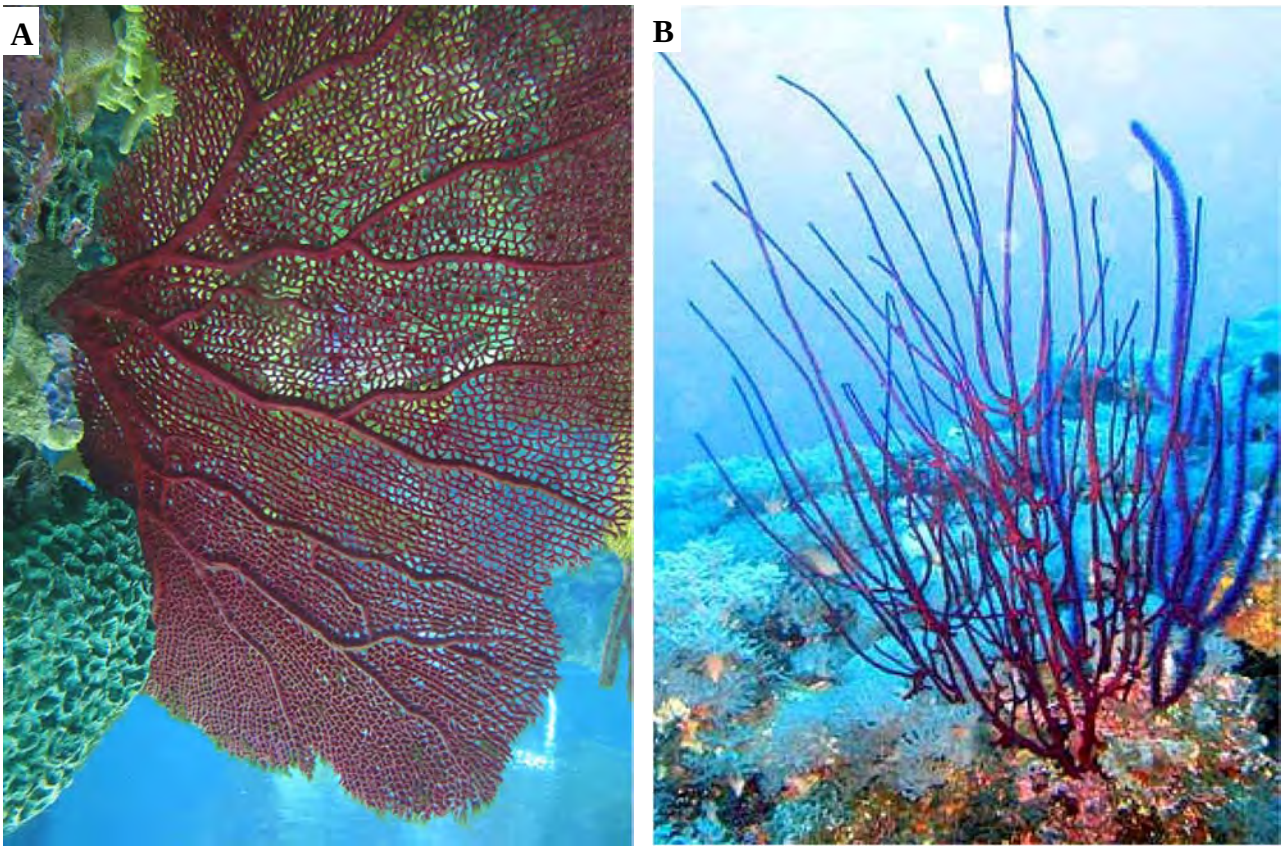

Figure 9-12. Underwater photographs of alcyonarian sea fans (A) and sea whips (B). Photo courtesy of Scott Ritter, Brigham Young University.

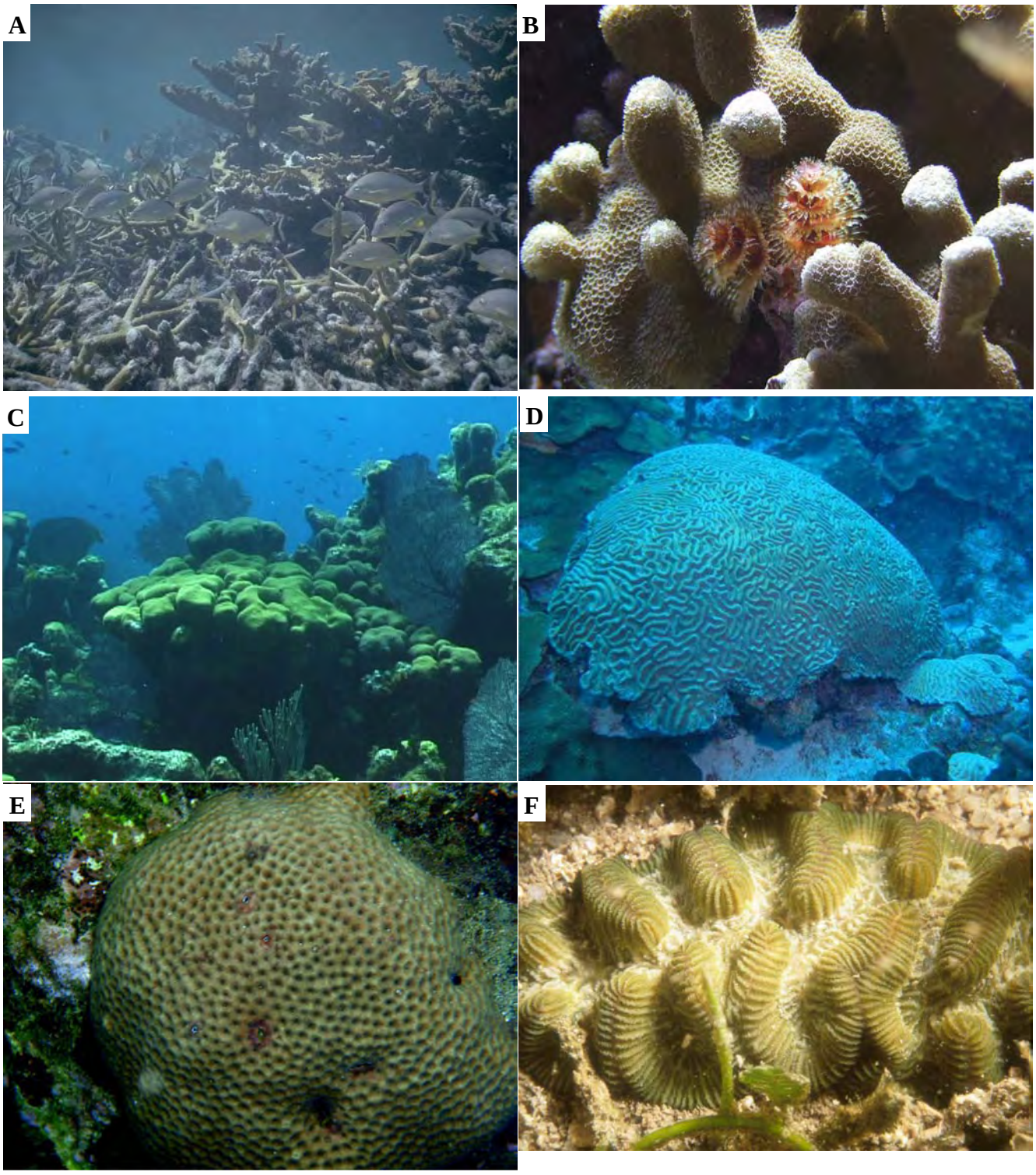

Figure 9-13. Underwater photographs of various scleractinian corals: A – moosehorn (Acropora palmata) and elkhorn (Acropora cervicornis) corals, B – finger coral (Porites), C – star coral (Montastrea annularis), D – brain coral (Diploria), E – golfball coral (Siderastrea), and F – rose coral (Manicina). Photo courtesy of Scott Ritter, Brigham Young University.

Figure 9-14. Large concentration of small, high spiral gastropods which feed on the algal matts of the intertidal zone in the carbonate tidal flats, northwest side of Andros Island, Bahamas. This deposit would ultimately yield a skeletal packstone to wackestone in the rock record.

Figure 9-15. Underwater photograph showing numerous mounds made by the burrowing shrimp <u>Callianassa</u> (inset), Bahamas. Photo courtesy of Scott Ritter, Brigham Young University.

Figure 9-16. Typical grain-making sand dollar echinoid. Photo courtesy of Scott Ritter, Brigham Young University.

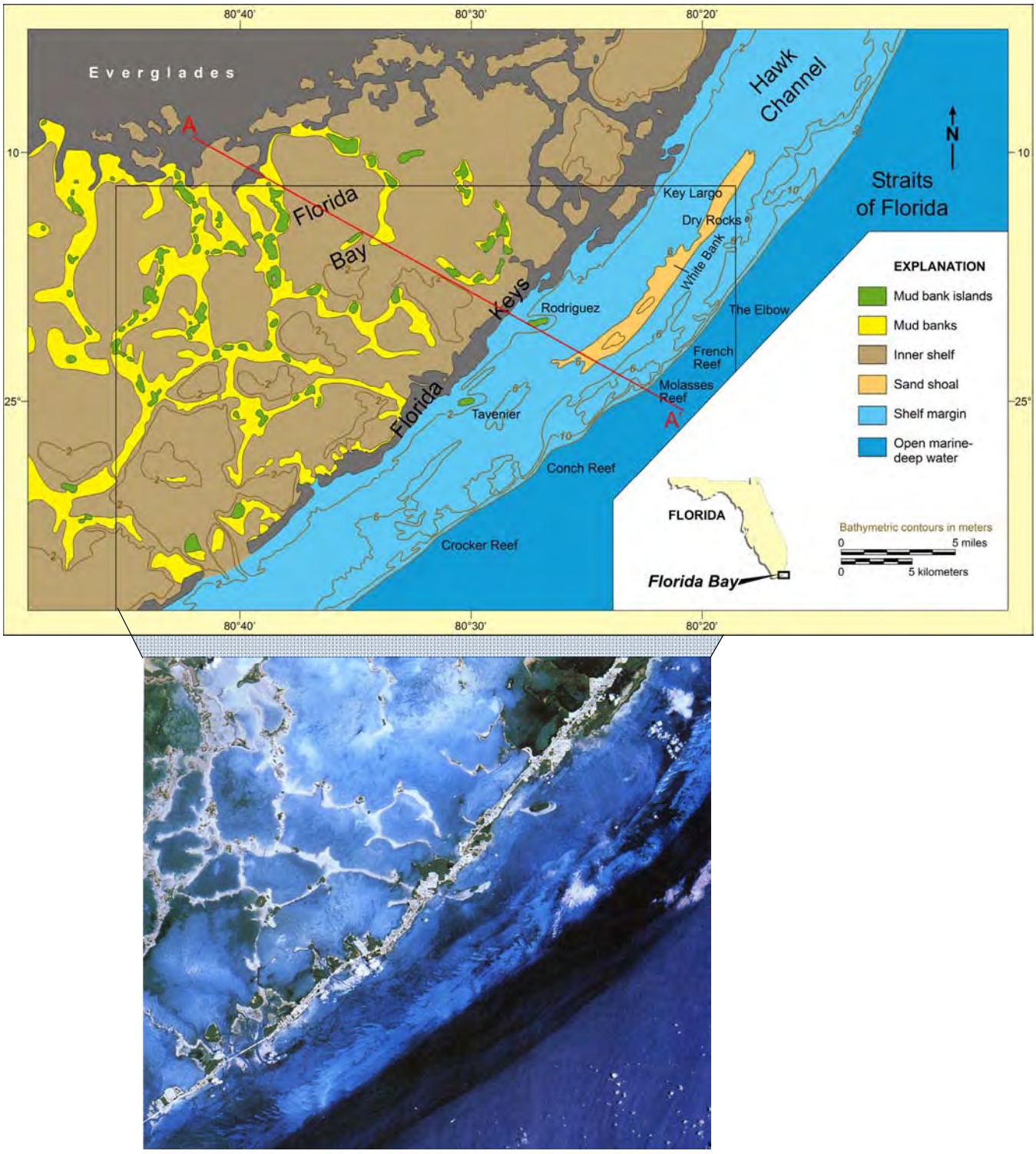

Figure 9-17. Features of the southern Florida attached, rimmed carbonate platform including bathymetry, the Florida Keys (Pleistocene reefs of the Key Largo Limestone), major depositional environments, and modern reefs (modified from Ginsburg, 1956). Cross section A-A' shown on figure 9-18. Map projected from regional Landsat image below.

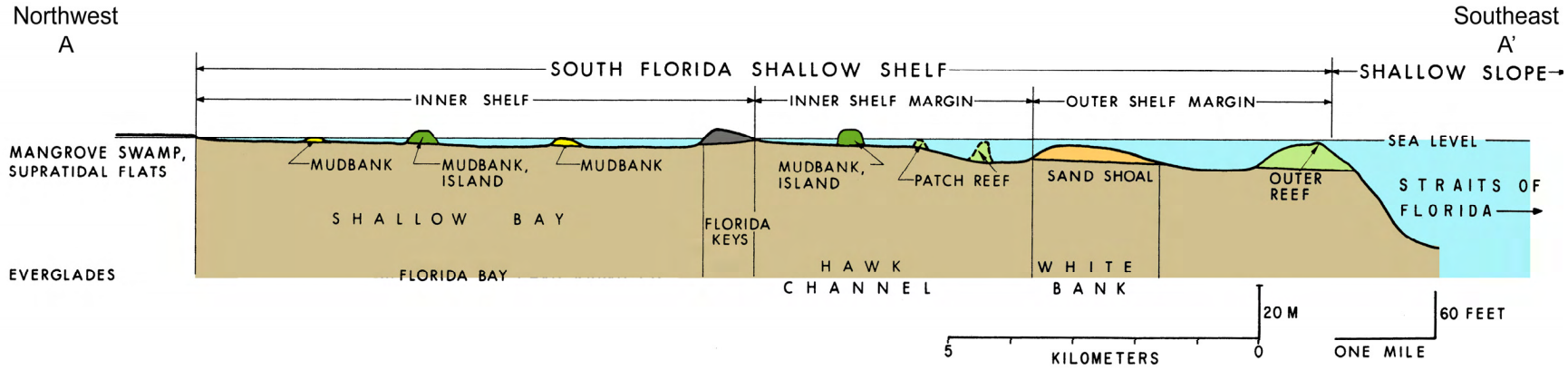

Figure 9-18. Generalized northwest-southeast cross section through the southern Florida attached, rimmed carbonate platform displaying major features and depositional environments (modified from Enos, 1977). Line of section shown on figure 9-17.

Figure 9-19. Oblique aerial view of Florida Bay shallow bay basins ("lakes"), mud mounds, and islands. Photo courtesy of Scott Ritter, Brigham Young University.

Figure 9-20. Typical view of Florida Bay from sea level of a shallow bay basin and islands (Keys).

Figure 9-21. Sieved samples of coarse, shelly sediment from the shallow bay basin near Sign Bank, Florida Bay.

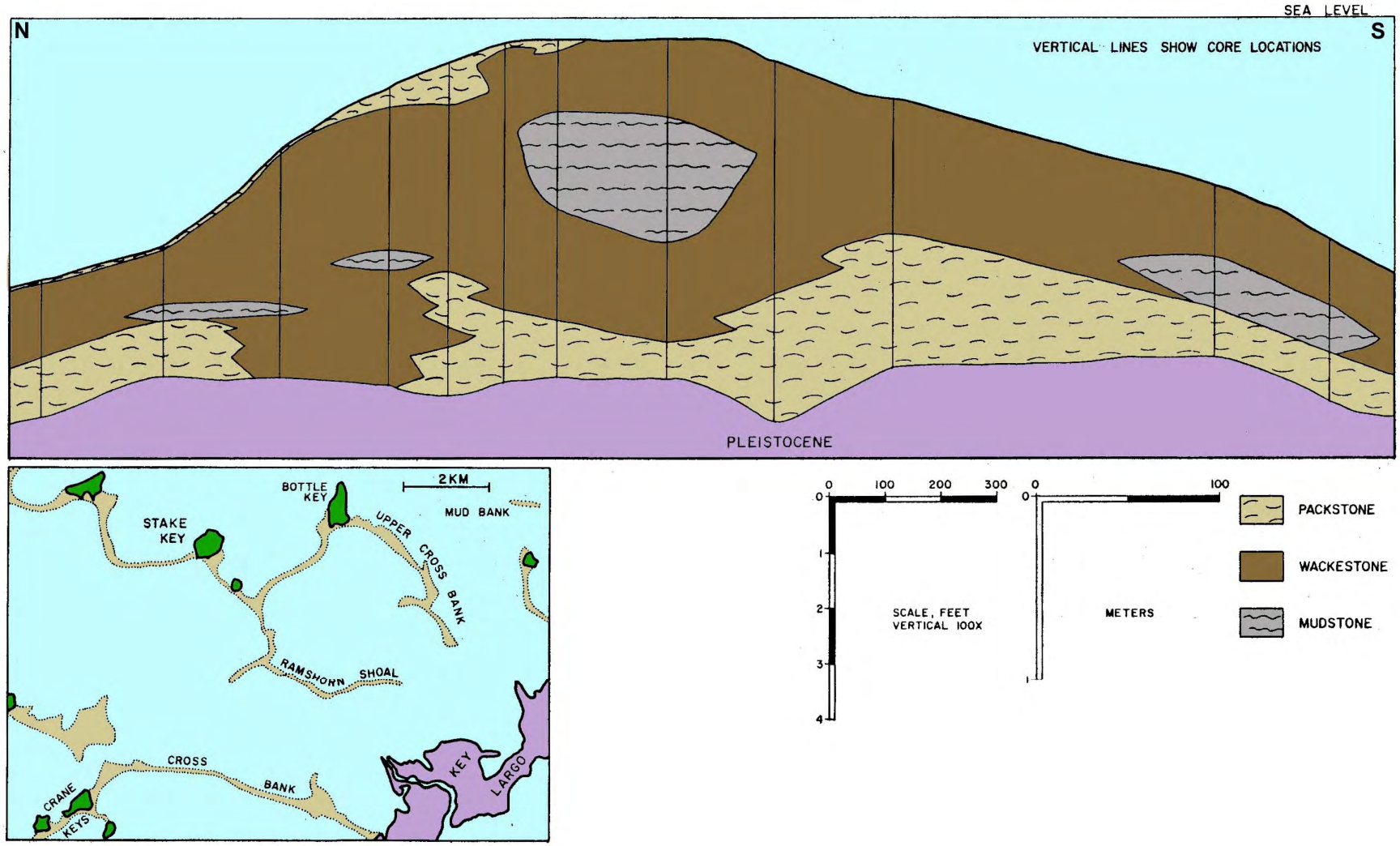

Figure 9-22. Generalized cross section through Cross Bank, a typical Florida Bay mud mound. The steeper north, windward side is capped by a layer of shelly sediment that would produce a packstone. Modified from Enos and Perkins (1979).

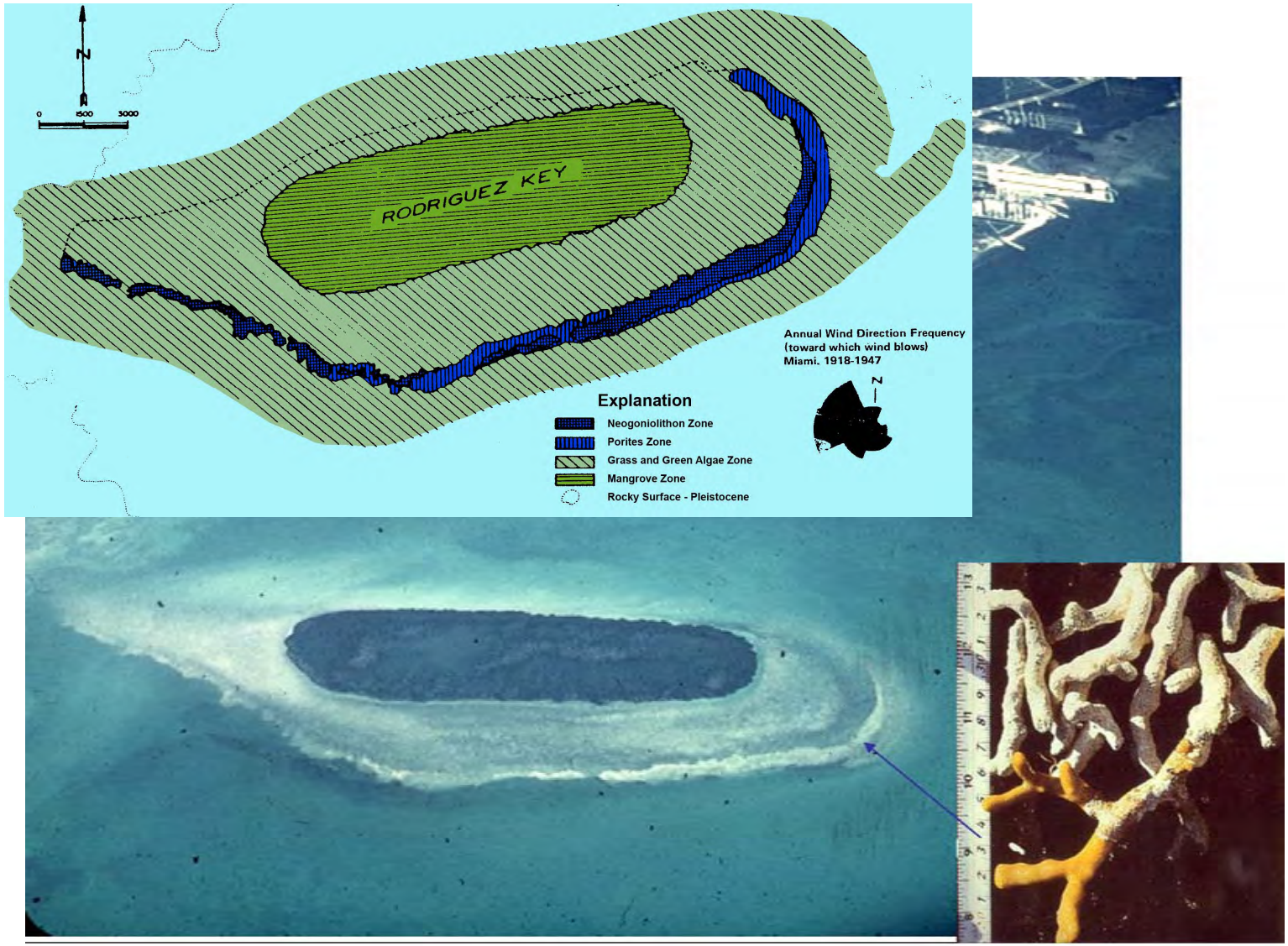

Figure 9-23. Generalized map of sediments and environments of Rodriguez Key. Inset photograph of Neogoniolithon. Modified from Turmel and Swanson (1976).

Figure 9-24. Underwater photograph of clean, rippled, calcareous sands of the White Bank sand shoal.

Figure 9-25. Coarse, clean skeletal (primarily coral) sand grains from the White Bank sand shoal.

Figure 9-26. Landsat image of the Great Bahama Bank and the Bahama Islands. Photo courtesy of Scott Ritter, Brigham Young University.

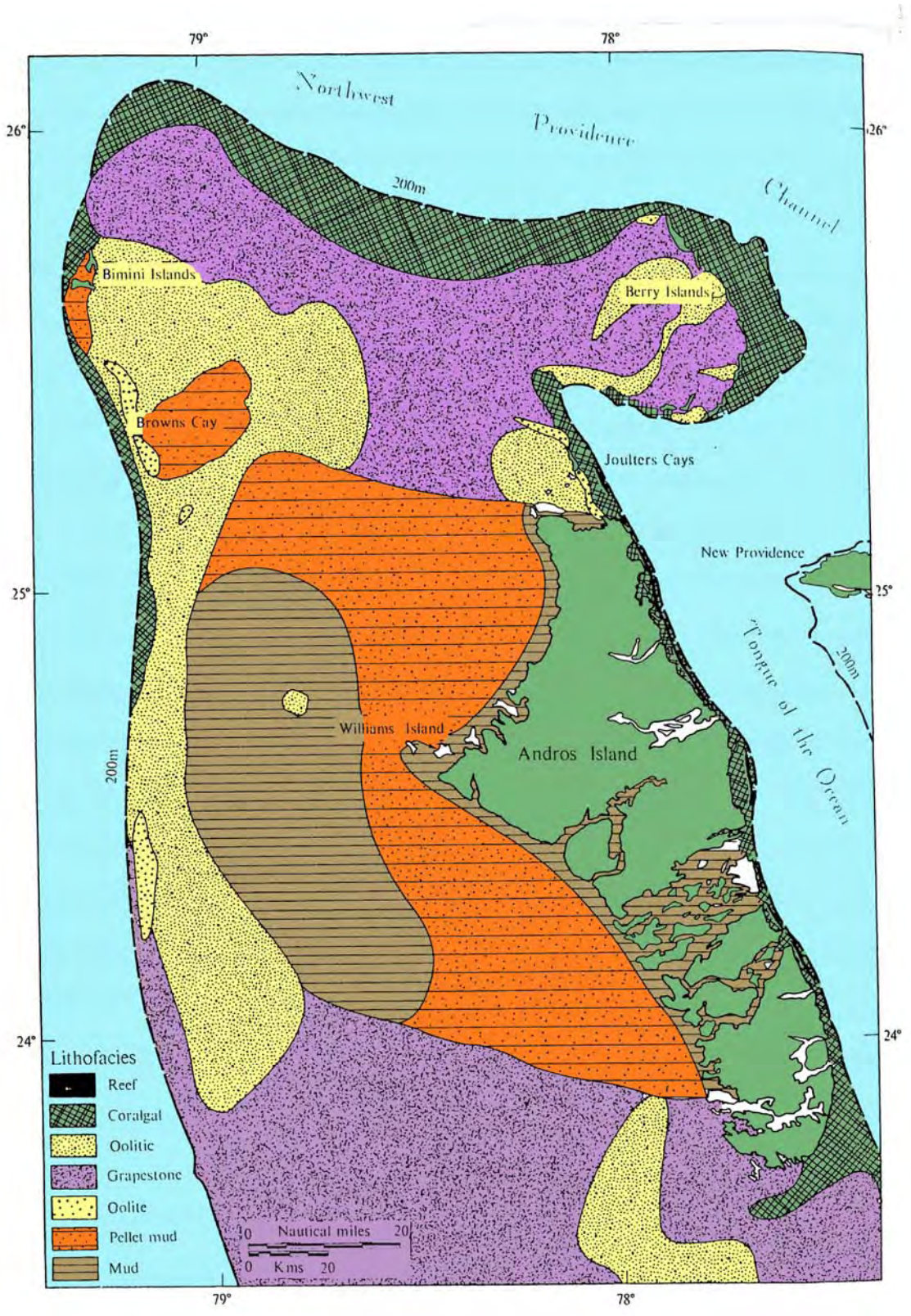

Figure 9-27. Generalized facies map of the Great Bahama Bank. Modified from Newell and others (1959); Purdy (1963).

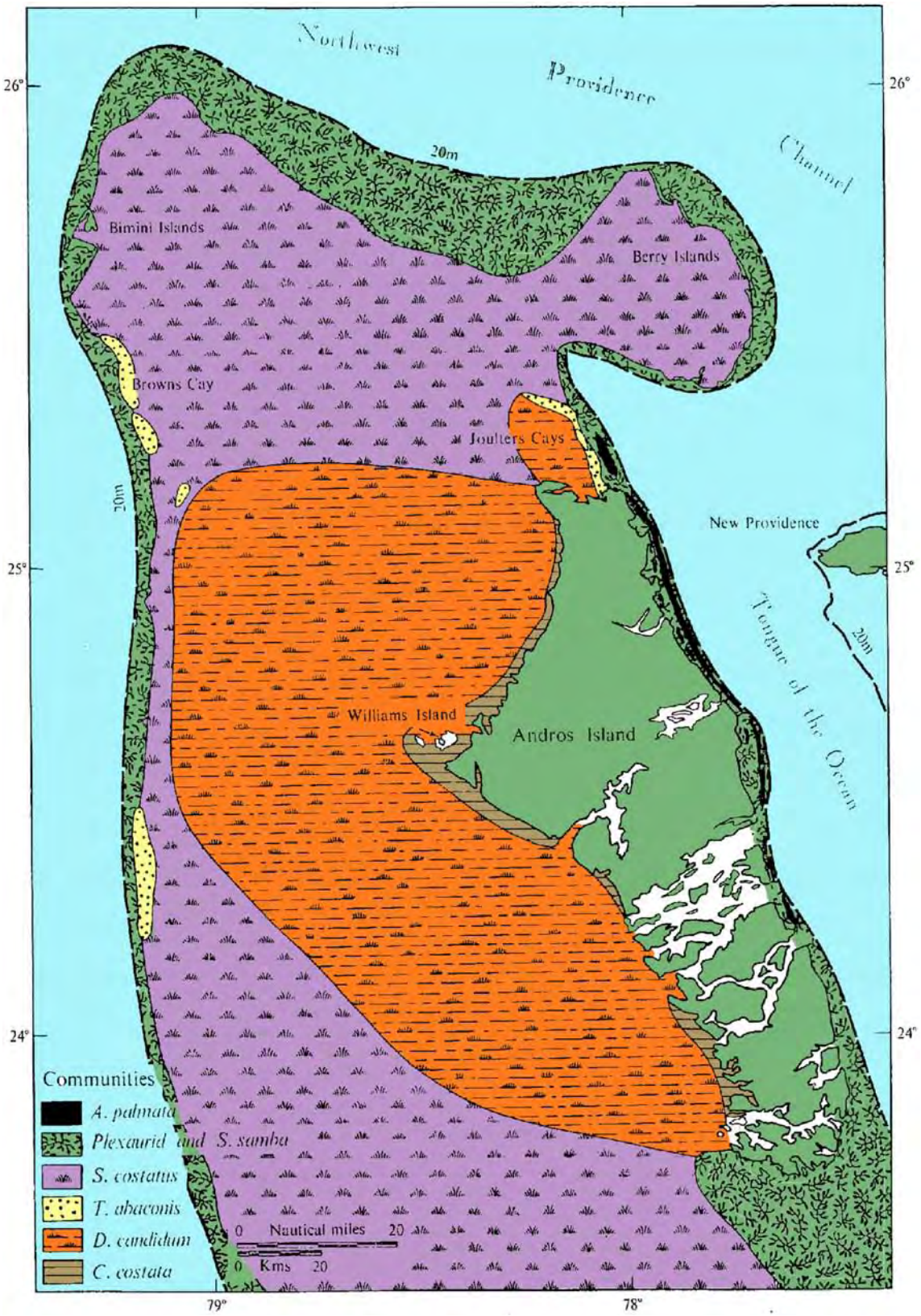

Figure 9-28. Biological communities on the Great Bahama Bank. Modified from Newell and others (1959).

Figure 9-29. Landsat image of the Joulter's Cay ooid shoal complex and the north end of Andros Island. Photo courtesy of Scott Ritter, Brigham Young University.

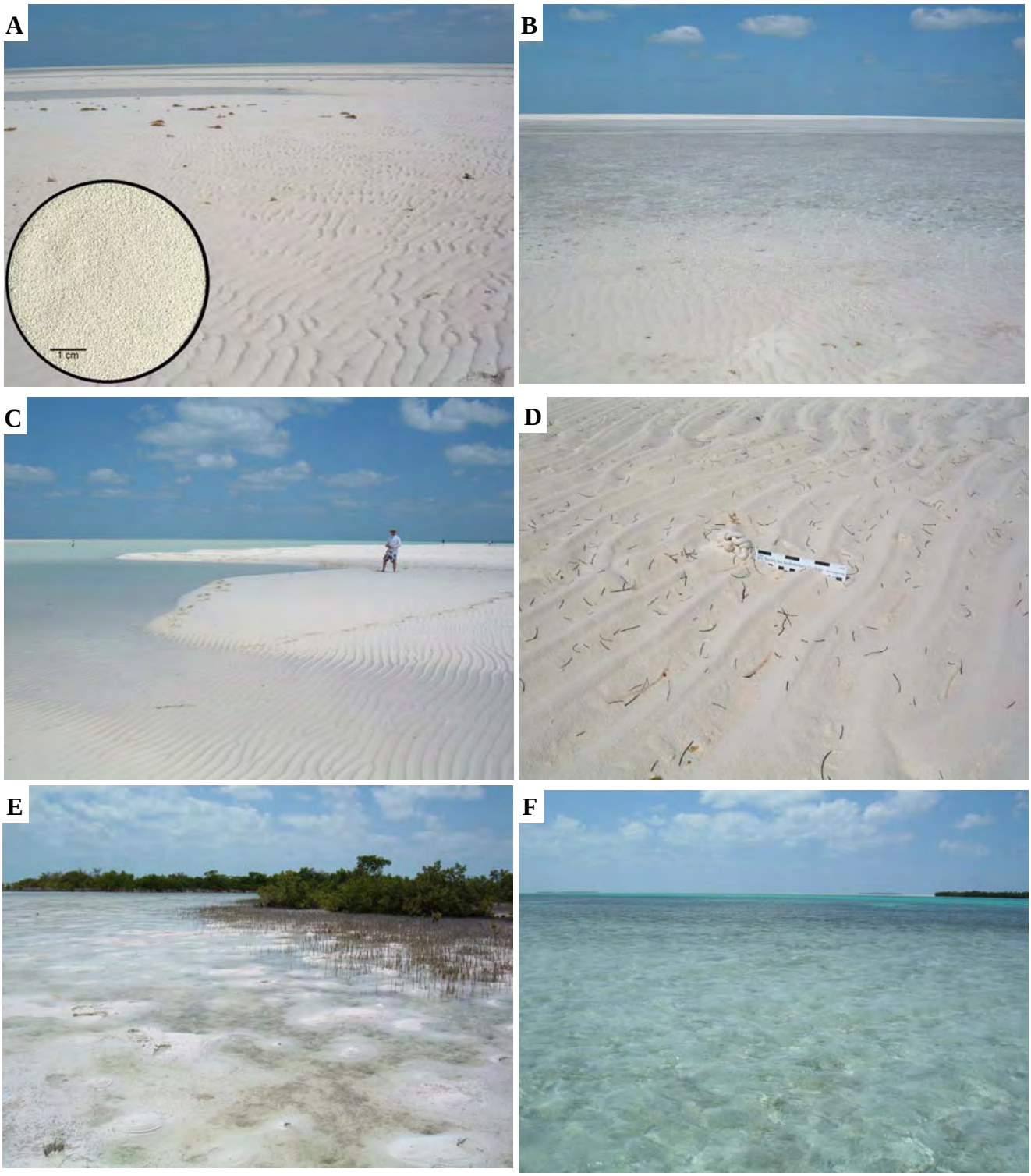

Figure 9-30. Joulter's Cay ooid shoal complex. A – Ooid shoals as far as the eye can see (view to the north). Flat topped current ripples due to flood-tidal currents. Inset is closeup of typical Joulter's Cay ooids. B – Slightly flooded ooid shoals forming bi-directional current ripples. C – Shallow tidal pools and rippled, exposed shoals of ooids (cross-bedded). D – Small burrow by the bivalve Tivela abaconia in rippled ooid sediments. E – Stablized grain flats composed of ooids and peloids, colonized by red mangroves. Note numerous active Callianassa burrows. F – Tidal channel that leads to northeasterly directed ebb-tidal delta.

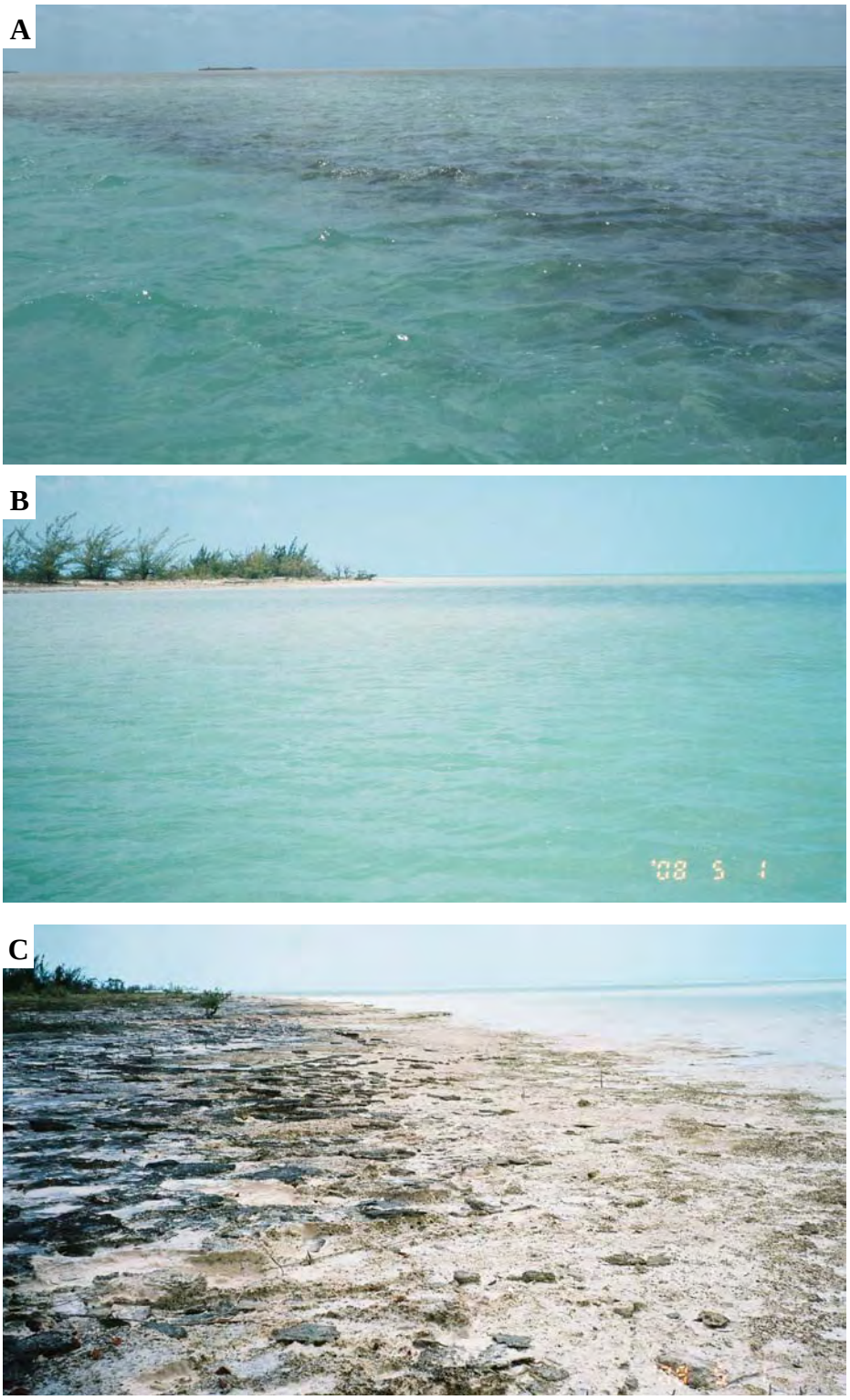

Figure 9-31. Great Bahama Bank shelf lagoon. A – View to the west of the 40-mile-wide lagoon where carbonate pellet-bearing muds are actively being deposited. B – Red Bay part of the shelf lagoon and pellet shoals near the mouth of a tidal channel from a tidal flat along the northwest coast of Andros Island (view to the southwest). C – Exposed pellet-bearing muds from the shelf lagoon undergoing early marine dolomitization.

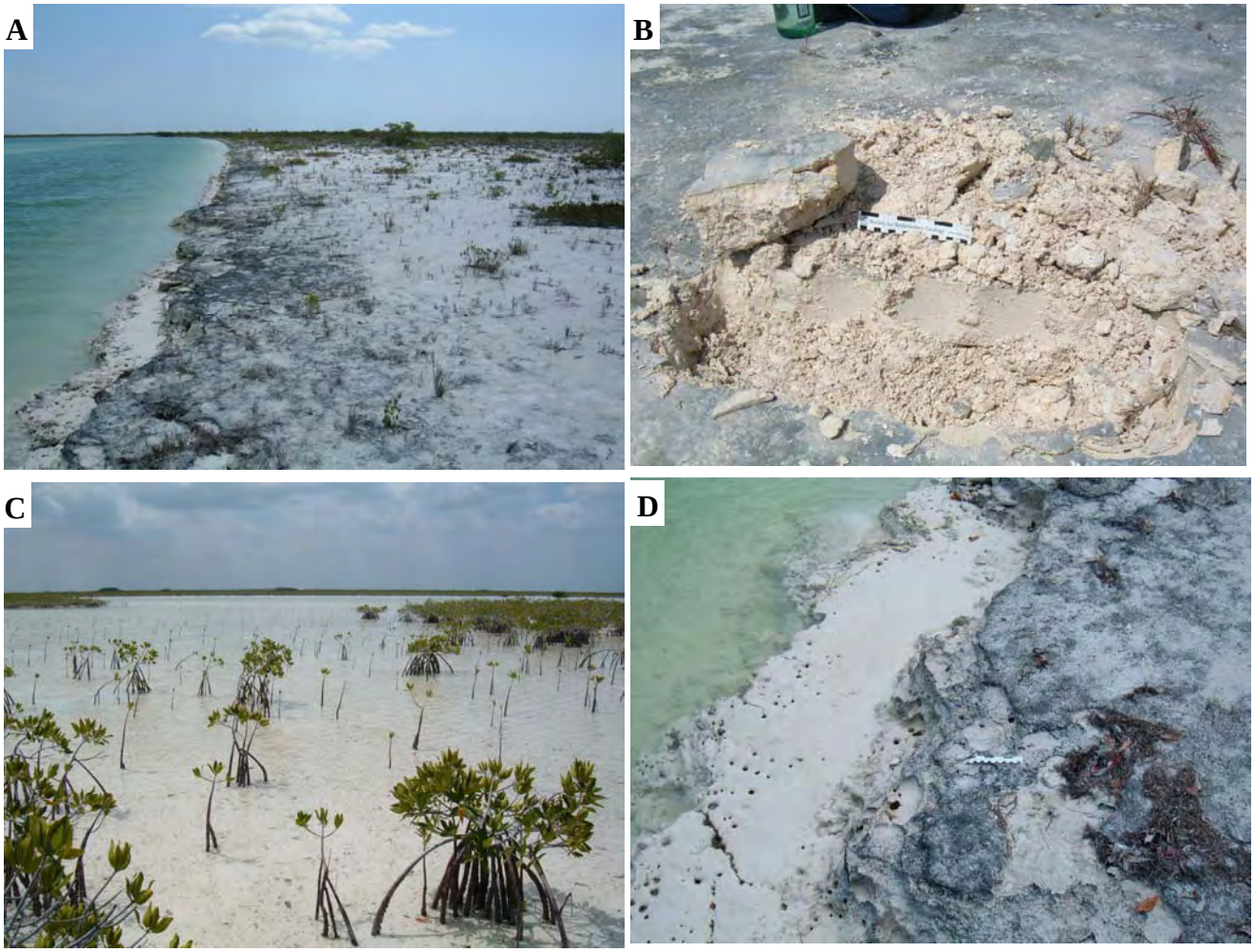

Figure 9-32. Carbonate tidal flats, Three Creeks area on the northwest side of Andros Island. A – Tidal channel (subtidal zone) and levee (supratidal zone) composed of carbonate, pellet-bearing mud. B – Algal mats and laminated, soft peloid grains in the intertidal zone of the tidal flats. C – Shallow ponds within the supratidal zone. D – Burrowing on the tidal channel levee deposits.

CHAPTER 10
MISSISSIPPIAN/DEVONIAN AND PENNSYLVANIAN BRINE CHEMISTRY AND TRENDS WITHIN THE PARADOX BASIN, UTAH

J. Wallace Gwynn, Utah Geological Survey

Introduction

The focus of this chapter is the chemistry and changes in chemistry of the brines found in the Mississippian/Devonian and Pennsylvanian formations in the Paradox Basin. From analyses of this information inferences can be made as to the migration history, including possible pathways and direction, of hydrocarbons in the Leadville Limestone.

Chemical data for Mississippian/Devonian and Pennsylvanian oil-well brines from the Paradox Basin were obtained from published literature; Utah Division of Oil, Gas and Mining files; oil companies; and various other sources (Breit, no date; Gwynn, 1995). These data include analyses from production, drill-stem, swab, and other types of well tests. Considerable effort was expended to ensure that the analyses from Gwynn (1995) were within a mole imbalance of less than 5%. The mole imbalances of the samples from Breit (no date) were not determined. Data are displayed as (1) histograms to show the elevation intervals of the samples, (2) Piper and Stiff diagrams to show the distribution of the major cations and anions, and (3) scatter plots overlain by best-fit lines to show the north-to-south variations of these ions within the Paradox Basin.

Previous studies on the brine chemistry of the Paradox Basin include those of Hanshaw and Hill (1969), Huntoon (1979), Howells (1990), and Spangler and others (1996). Howells (1990) provides detailed information on the stratigraphy within San Juan County, including the maximum reported strata thickness, lithology, and hydrologic characteristics and significance of the various formations. Spangler and others (1996) provide information on the hydrology, chemical quality, and salinity in the Jurassic Navajo Sandstone aquifer in the Greater Aneth field area (figure 1-1).

Mississippian – Devonian Brines

The distribution of Mississippian-Devonian sample locations is shown in figure 10-1. The majority of the samples are located in the northern portion of the Paradox Basin within Grand, Emery, Wayne, and San Juan Counties. A smaller number of samples are found in the southern portion of the Paradox Basin (the southeast corner of San Juan County) in the Greater Aneth field area. The elevation of the "top of the sampled interval" for the majority of the samples lies within the -4000 (subsea) to 2000-foot (-1200 to 600 m) elevation interval, as shown in figure 10-2. This appears to be a much broader elevation range than for the Pennsylvanian samples, but the sampled intervals for the northern and southern areas are probably much different.

The distribution of the chemical composition of the Mississippian/Devonian brine samples is shown in the Piper and Stiff diagrams for the Mississippian, Devonian, and combined Mississippian and Devonian samples (figures 10-3 and 10-4). The cation components of the brines are predominantly sodium (Na) with minor amounts of calcium (Ca) and magnesium (Mg). The anion components in the brine are dominantly chloride (Cl) with a small number of

brine samples having relatively high concentrations of sulfate (SO_4). Bicarbonate (HCO_3) is uniformly very low in these brines. Brines departing from the general trends are found mainly in San Juan and Wayne Counties.

Scatter plots (figures 10-5 and 10-6) show the elevation of the top of the sample interval, the chemistry of the samples (as individual ions), and total dissolved solids (TDS) versus their UTM-northing positions (from 4325000 on the north to 4075000 on the south). Fifth-degree polynomial best-fit lines indicate data trends from north (left) to south (right) through the length of the Paradox Basin.

Pennsylvanian Brines

The distribution of the wells from which the Pennsylvanian brine samples were collected is shown in figure 10-7. The majority of the samples are located in the southern portion of the Paradox Basin (the southeast corner of San Juan County), in and around the Greater Aneth and Bug fields (figure 1-1). A few scattered samples are also within or near the central and northern portions of the basin. The top of the sampled interval for the majority of the samples lies at about zero to 1000 feet (0-300 m) above mean sea level as shown in figure 10-8.

The distribution of the chemical composition of the Pennsylvanian brine samples is shown on Piper and Stiff diagrams (figures 10-9 and 10-10). The cations in most brine samples are Na-rich with a few samples containing greater percentages of Ca and to a lesser extent Mg. The anion components in the brine are Cl dominated with a smaller number of samples containing relatively high concentrations of SO_4. Bicarbonate is very low in these brines. Brines departing from the general trends are found mainly in San Juan and Wayne Counties. The high salinity of Pennsylvanian brines is probably due to their association with the bedded salts in the Paradox Formation.

Based on scatter plots (figures 10-11 and 10-12), the few Pennsylvanian samples present in the northern portion of the Paradox Basin suggest lower concentrations of Na, Mg, Ca, Cl, TDS, and higher SO_4 as compared to brine samples from the Bug and Greater Aneth field areas. The elevation of the top of the sampled interval in the northern portion of the basin is somewhat lower than it is in the vicinity of Bug field, but higher than in the Greater Aneth field area.

Sodium, Mg, Ca, Cl, and TDS concentrations approach a maximum value in the area of Bug field, and then show decreasing concentration southward through the Greater Aneth field area. Bicarbonate and SO_4 concentrations both reach minimum values between Bug field and the Greater Aneth field area, but then rise southward toward T. 43 S., SLBL&M.

Direction of Brine Movement

Hanshaw and Hill (1969) provide a detailed discussion of the geochemistry and hydrodynamics of the Paradox Basin region, and include potentiometric maps of the Mississippian Leadville Limestone; the Pennsylvanian Pinkerton Trail, Paradox, and Honaker Trail Formations of the Hermosa Group; and the Permian formations. In their discussion, they summarize the areas of recharge and movement of ground water as follows:

> The principal areas of recharge to aquifers in the Paradox Basin are the west flank of the San Juan Mountains and the west flank of the Uncompahgre uplift. The direction of ground-water movement in each unit studied [Mississippian rocks, Pinkerton Trail

Limestone, Paradox Member of the Hermosa Formation, Honaker Trail Formation, and the Permian formations] is principally southwestward toward the topographically low outcrop areas along the Colorado River in Arizona. However, at any point in the basin, flow may be in some other direction owing to the influence of intrabasin recharge areas or local obstructions to flow, such as faults or dikes. Many structurally and topographically high areas within the basin are above the regional potentiometric surface; recharge in these areas will drain rapidly off the highs and adjust to the regional water level.

Discussion

Table 10-1 gives averaged values for ground elevation, top and bottom elevation of the sampled interval, TDS, and ions for individual counties, and for township intervals within San Juan County. Based on the data in table 10-1, the following can be said:

1. For Mississippian/Devonian brines, the samples from Grand County have the highest average TDS values, followed by San Juan, Emery, and Garfield. For Pennsylvanian brines, the samples from Grand County also have the highest average TDS of all the counties in the study area, followed by San Juan, Emery, and Wayne.

2. The Na, Mg, Ca, and Cl contents of the Pennsylvanian brines are consistently higher, in a given county or township interval (for instance T. 40 S., SLBL&M, in San Juan County), than the Mississippian/Devonian brines in the same interval, while the average values for SO_4 and HCO_3 are lower.

3. From the Piper and Stiff diagrams (figures 10-3A, 10-3B, 10-4, 10-9, and 10-10), it can be concluded that the brines in both the Mississippian/Devonian and Pennsylvanian systems are mainly NaCl in nature, with end-member samples whose cations contain about 70% Ca and 30% Mg, and whose anion makeup approaches a high-SO_4 brine. From the scatter plots (figures 10-5, 10-6, 10-11, and 10-12), it appears that these end-member brines are found to the south of the Greater Aneth field area.

A comparison of the various average chemistries in table 10-1 is difficult to visualize because of the varied salt concentrations of the samples. Table 10-2 gives these data on a dry-weight basis. Based on these data, the following conclusions can be drawn regarding the Mississippian/Devonian and Pennsylvanian brine chemistries in the various counties:

1. The Mississippian/Devonian brines from Grand, Emery, and San Juan Counties are very similar, even though the TDS concentration of the Grand County brines is considerably higher than either Emery or San Juan County. Garfield County brines, like the Wayne County brines, are totally dissimilar.

2. The Pennsylvanian brines from Grand and San Juan Counties are very similar, even though the TDS concentration of the Grand County brines is considerably higher. The brines from Emery and Wayne Counties are not similar to the brines of the other two counties, and the brines from Wayne County are totally dissimilar.

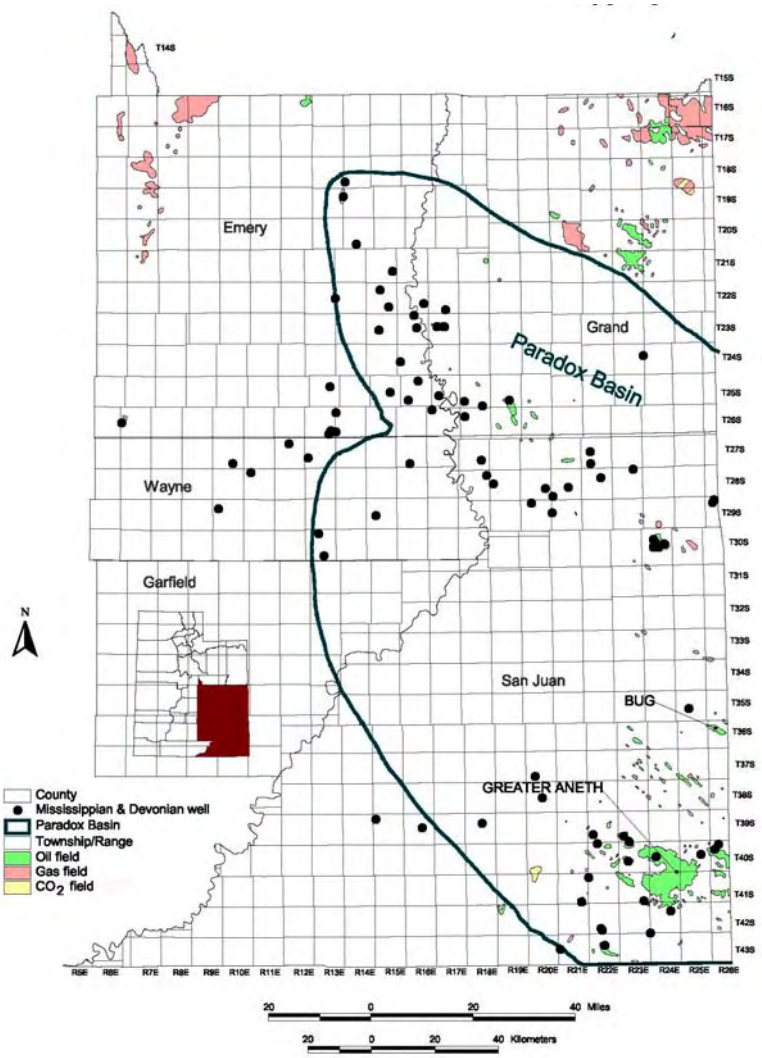

Figure 10-1. Locations of Mississippian/Devonian samples (wells), and oil and gas fields in the Paradox Basin and vicinity, Utah.

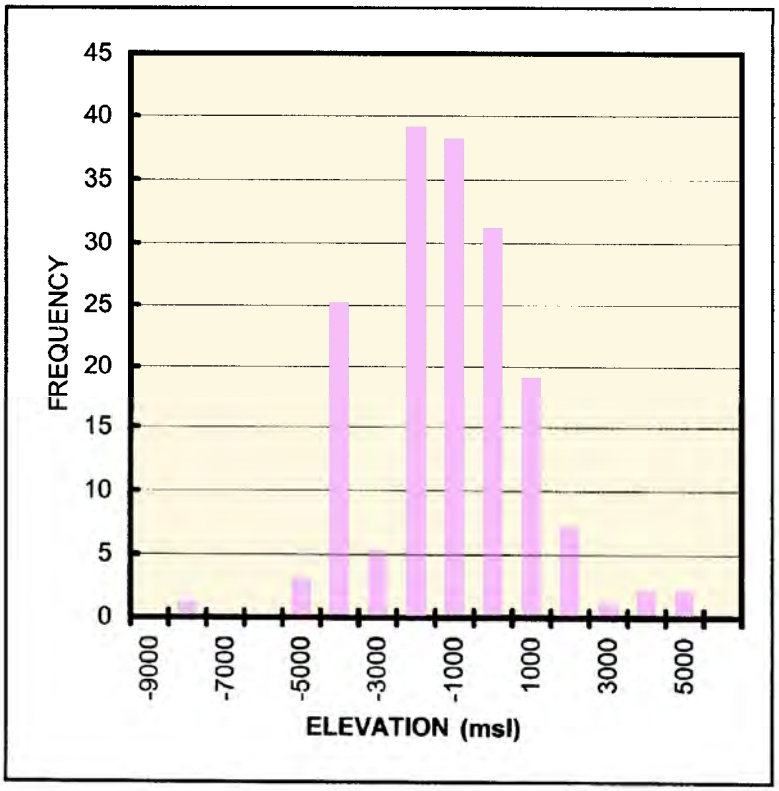

Figure 10-2. Elevation of the top of the sampled interval for the Mississippian/Devonian brine samples.

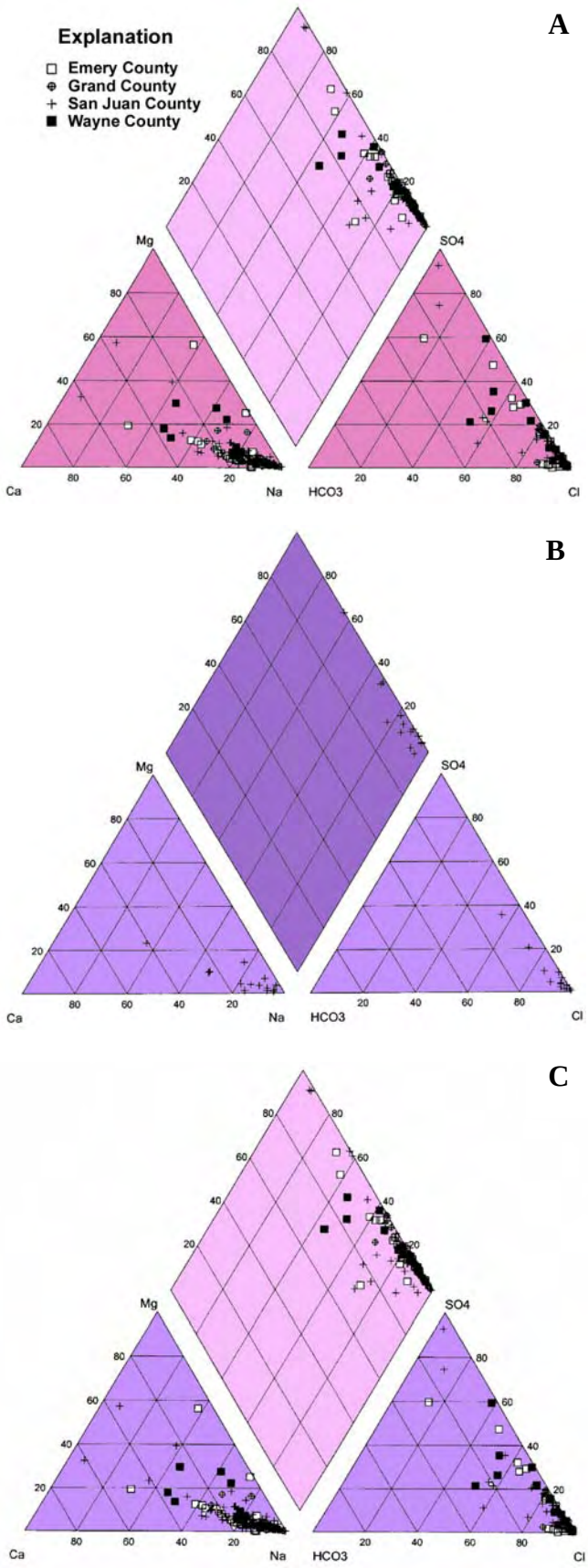

Figure 10-3. Piper diagrams showing the composition of (A) Mississippian brines, (B) Devonian brines, and (C) Mississippian and Devonian brines combined, in the Paradox Basin and vicinity, Utah.

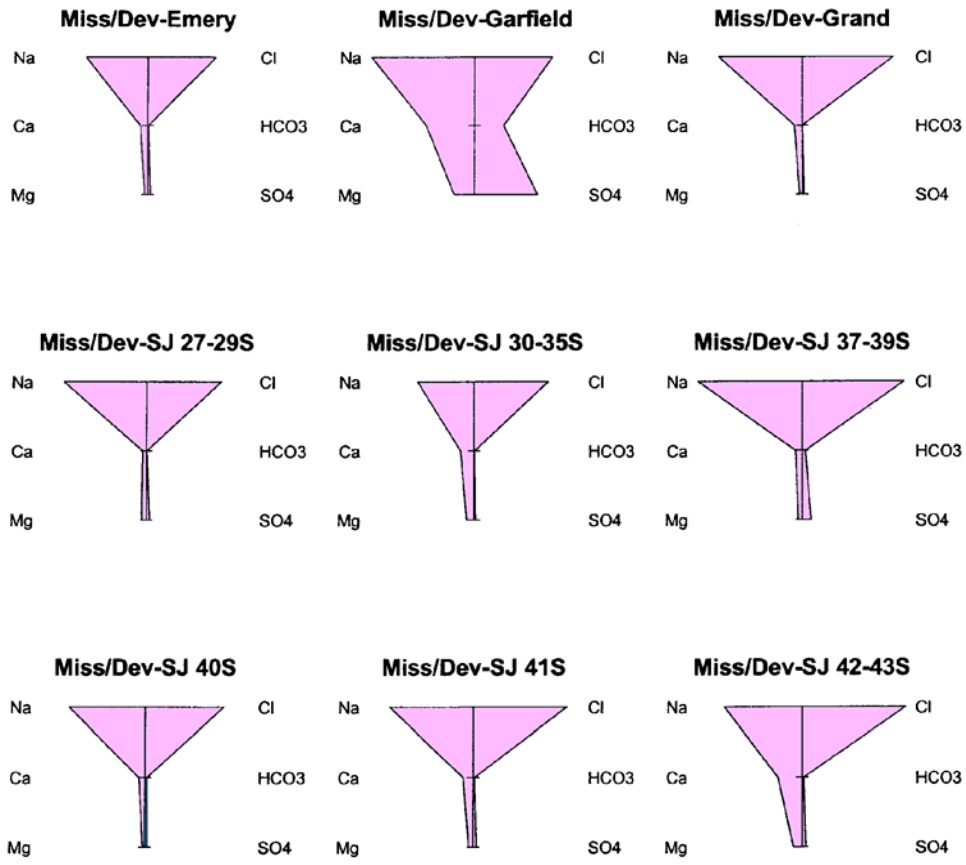

Figure 10-4. Stiff diagrams for Mississippian and Devonian (Miss/Dev) brines combined, by county (SJ = San Juan County). The township interval within San Juan County is indicated above the diagram. The field width of the county represents the range interval.

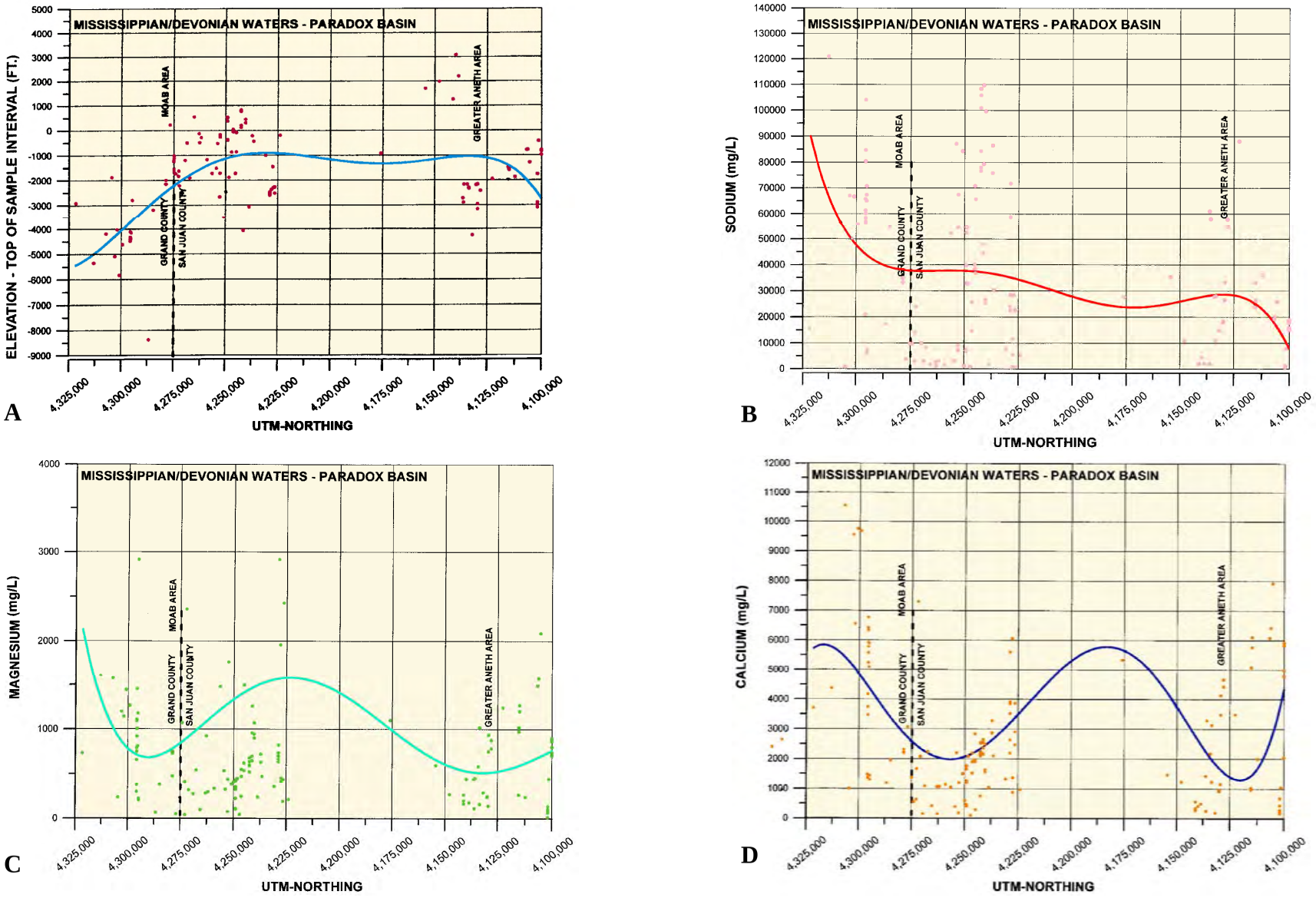

Figure 10-5. Scatter plots showing the elevation of the top of the sample interval (A), and sodium (B), magnesium (C), and calcium (D) concentrations versus geographic location (UTM-northing) for the Mississippian/Devonian samples. Fifth-degree polynomial best-fit lines indicate data trends from north (left) to south (right) through the length of the Paradox Basin. The general Greater Aneth and Moab areas are shown, as well as the Grand-San Juan County line.

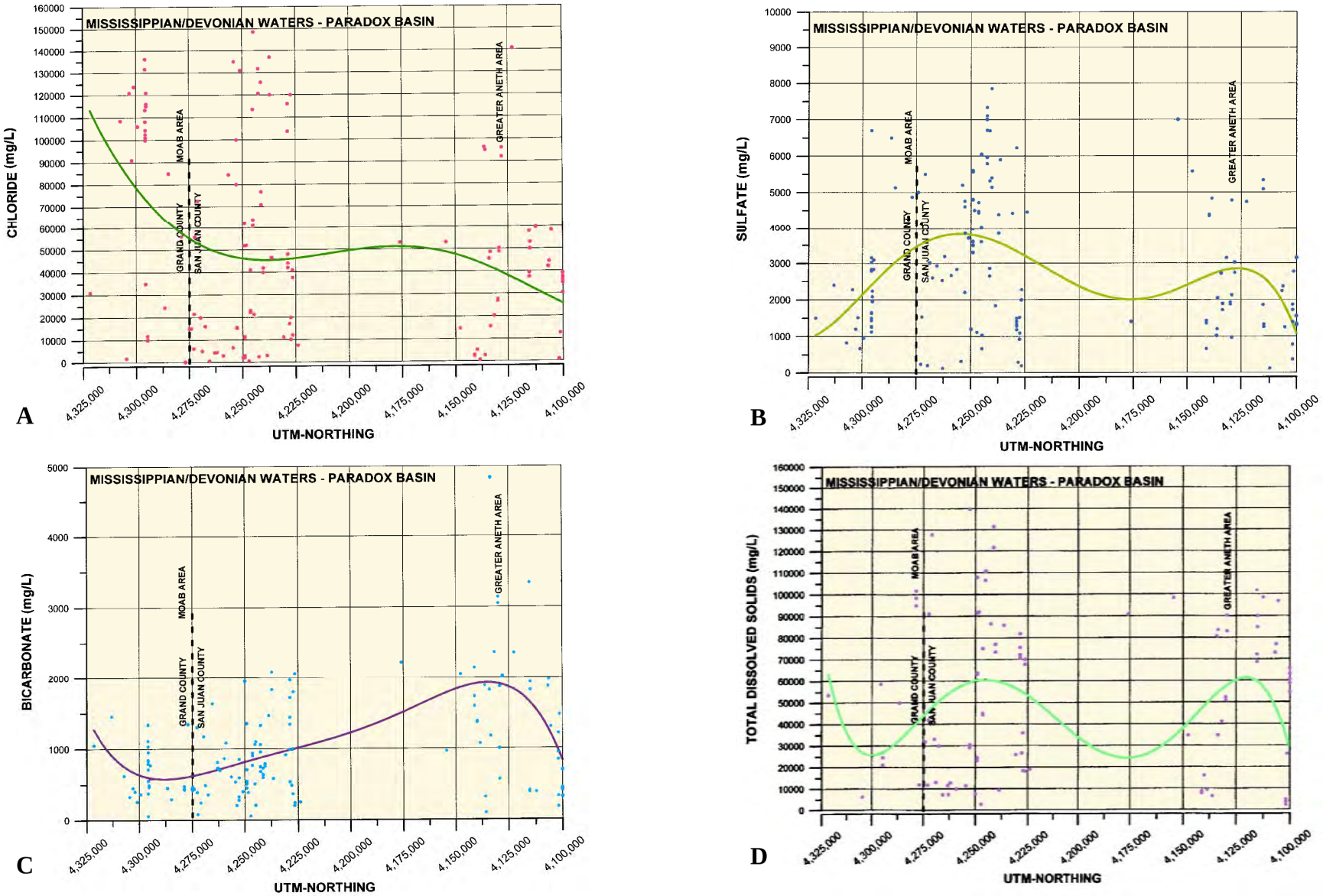

Figure 10-6. Scatter plots of chloride (A), sulfate (B), bicarbonate (C), and total dissolved solids (D) concentrations versus geographic location (UTM-northing) for the Mississippian/Devonian samples. Fifth-degree polynomial best-fit lines indicate data trends from north (left) to south (right) through the length of the Paradox Basin. The general Greater Aneth and Moab areas are shown, as well as the Grand-San Juan County line.

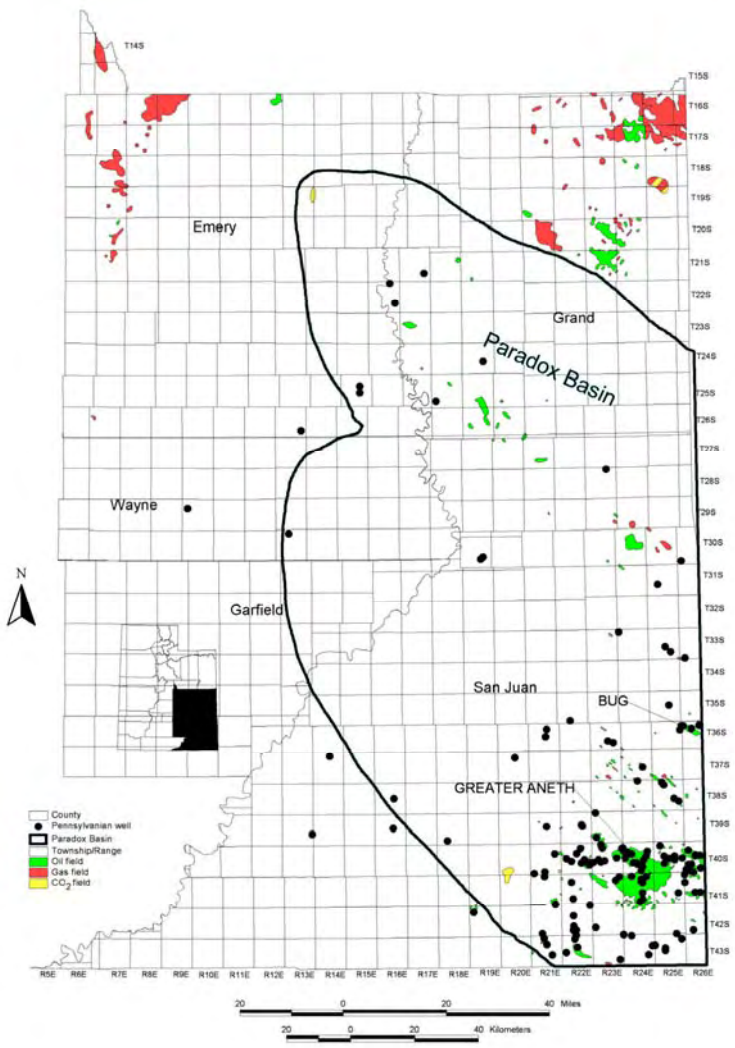

Figure 10-7. Locations of Pennsylvanian brine samples (wells), and oil and gas fields in the Paradox Basin and vicinity, Utah.

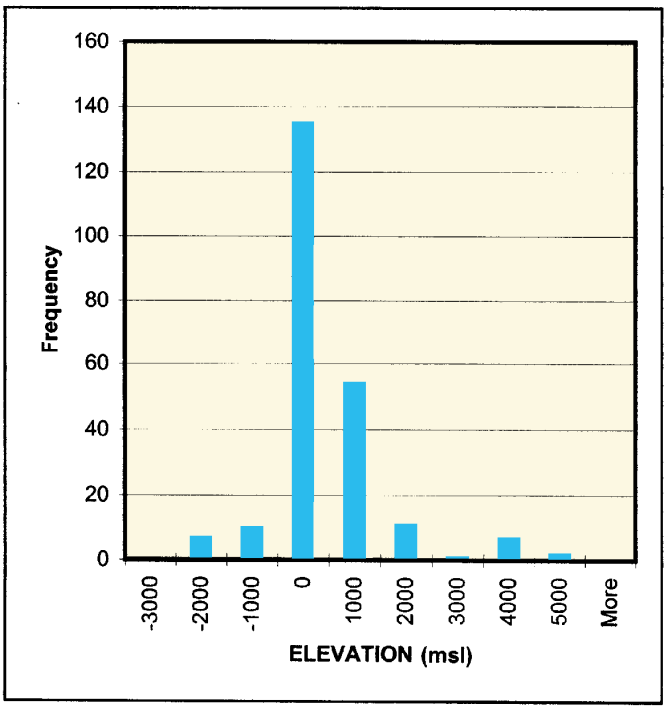

Figure 10-8. Elevation of the top of sampled interval for Pennsylvanian brine samples.

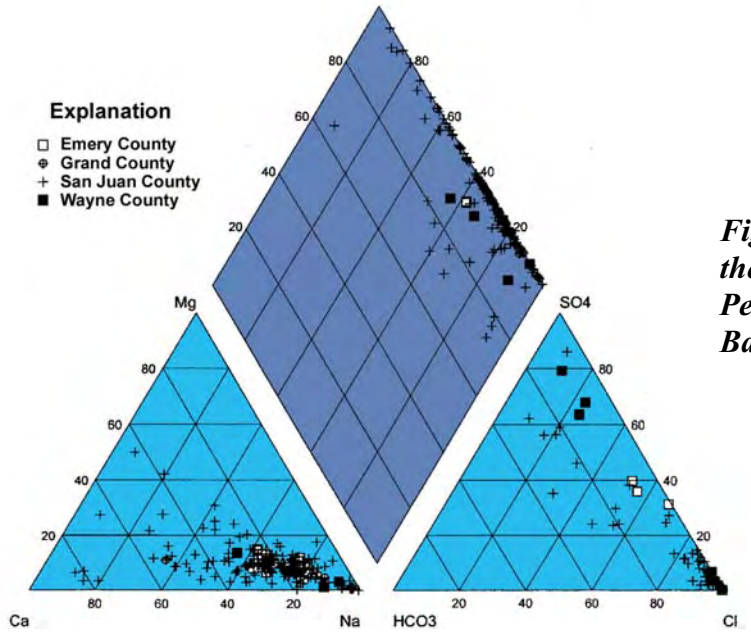

Figure 10-9. Piper diagram showing the chemical composition of the Pennsylvanian brines in the Paradox Basin by county.

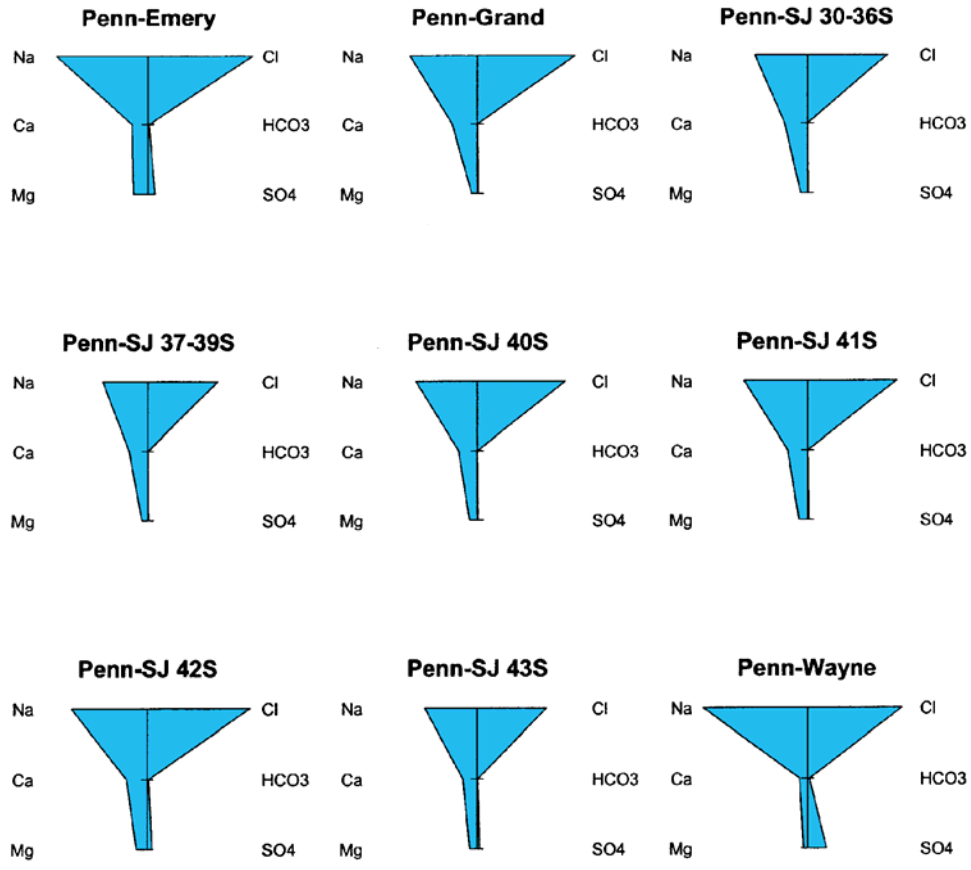

Figure 10-10. Stiff diagrams for Pennsylvanian (Penn) brines, by county (SJ = San Juan County). The township interval within San Juan County is indicated above the diagram. The field width of the county represents the range interval.

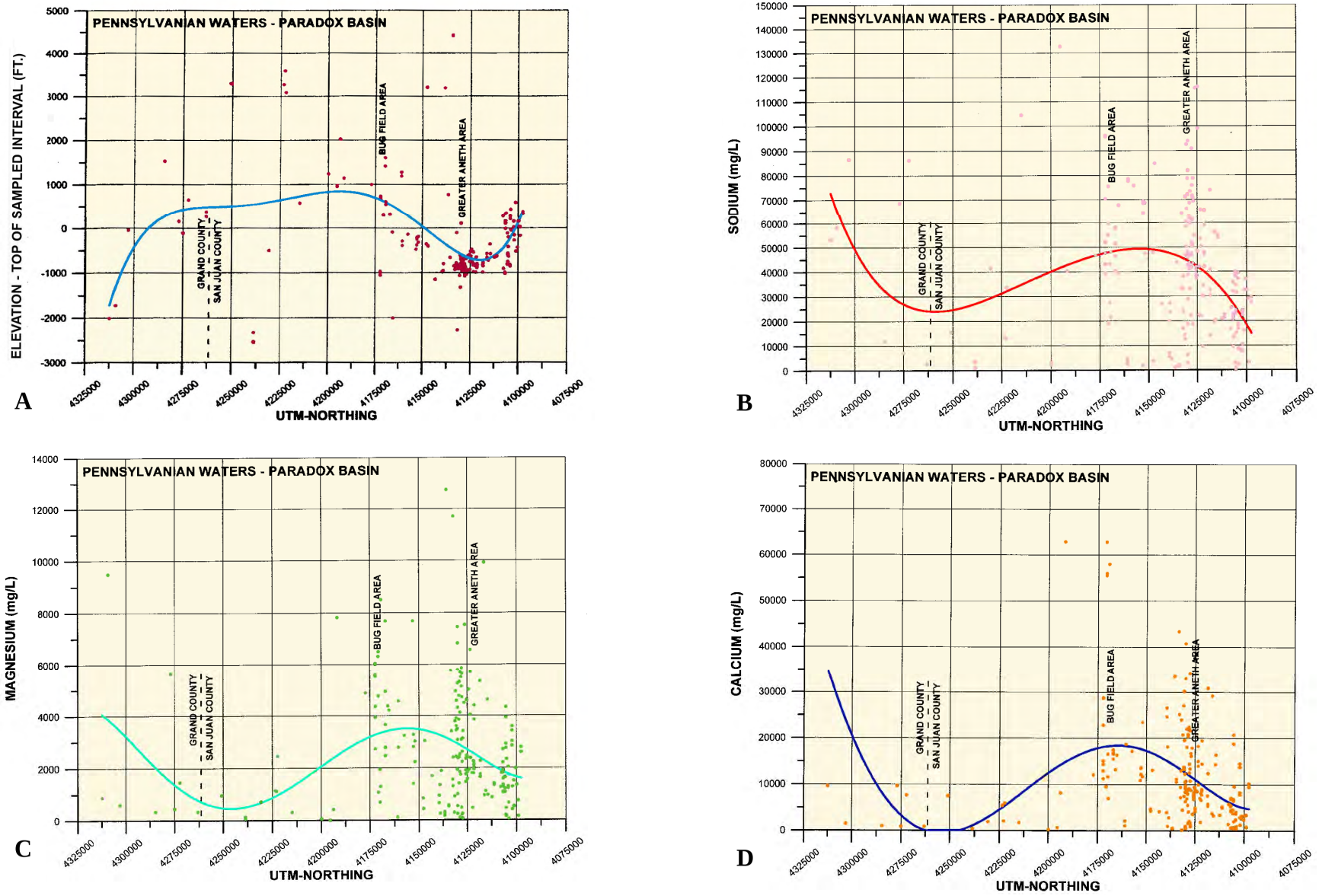

Figure 10-11. Scatter plots showing the elevation of the top of the sample interval (A), and sodium (B), magnesium (C), and calcium (D) concentrations versus geographic location (UTM-northing) for the Pennsylvanian samples. Fifth-degree polynomial best-fit lines indicate data trends from north (left) to south (right) through the length of the Paradox Basin. The general areas of the Greater Aneth and Bug fields are shown, as well as the Grand-San Juan County line.

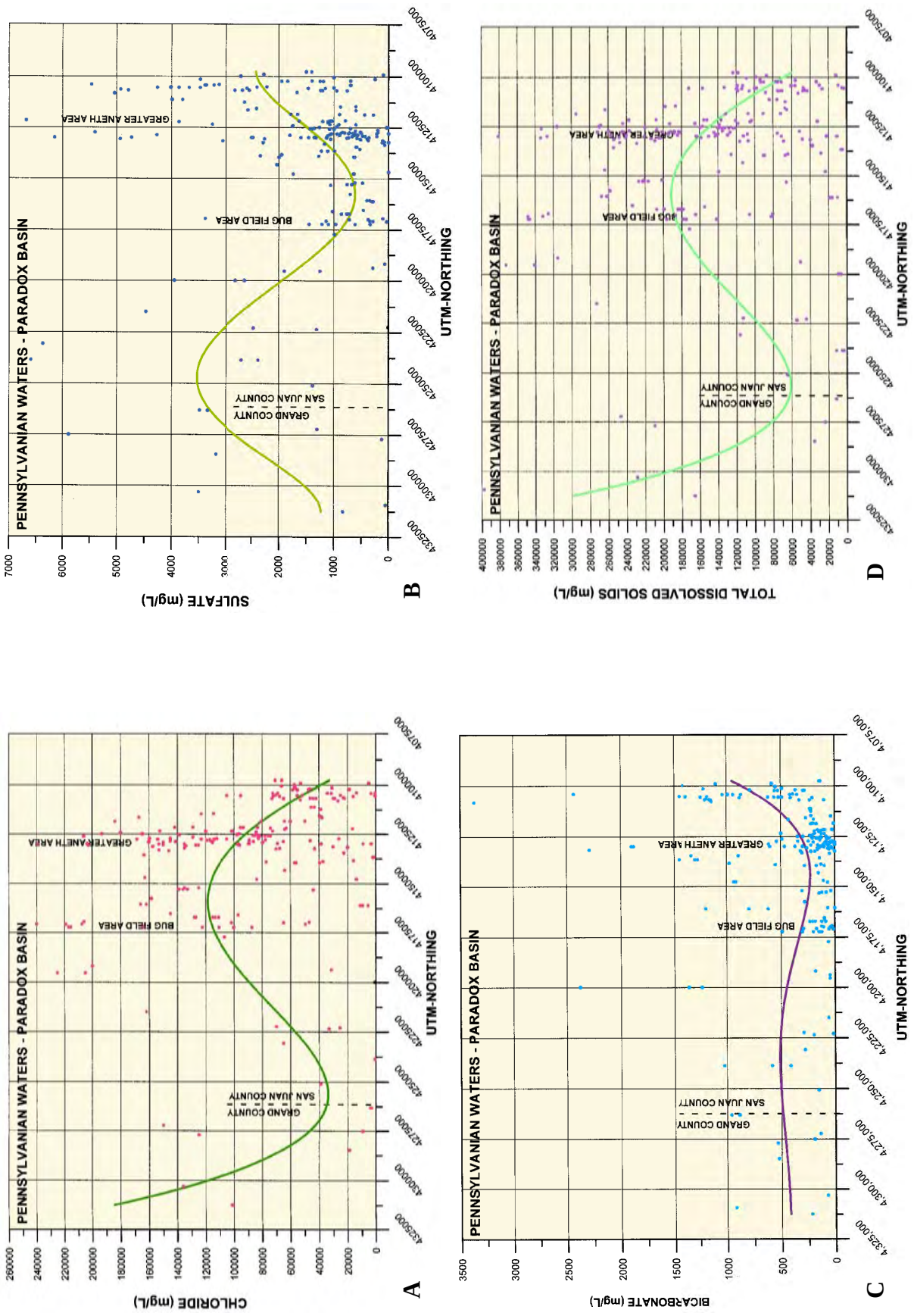

Figure 10-12. Scatter plots of chloride (A), sulfate (B), bicarbonate (C), and total dissolved solids (D) concentrations versus geographic location (UTM-northing) for the Pennsylvanian samples. Fifth-degree polynomial best-fit lines indicate data trends from north (left) to south (right) through the length of the Paradox Basin. The general areas of the Greater Aneth and Bug fields are shown, as well as the Grand-San Juan County line.

Table 10-1. Brine sample location, averaged ground elevation, top and bottom elevation of the sampled interval, TDS, and ions for individual counties, and for township intervals within San Juan County.

COUNTY	AGE	TWP-INTERVAL	ELEV	TOP-ELEV	BOT-ELEV	TDS	Na	Mg	Ca	Cl	SO_4	HCO_3
Grand	Penn	Grand	4518	-321	-385	214249	59288	2550	19198	131066	1772	375
Emery	Penn	Emery	5160	172	92	64339	20317	1690	3084	35399	3206	645
Wayne	Penn	Wayne	4892	-1976	-2056	34699	11815	246	788	16763	4510	577
San Juan	Penn	SJ 30-36S	6319	953	1004	177196	45717	3102	17185	109702	1228	262
San Juan	Penn	SJ 37-39S	5226	503	434	115110	30044	2003	10679	71006	878	501
San Juan	Penn	SJ 40S	4781	-825	-888	190857	53925	3611	14187	117895	1050	189
San Juan	Penn	SJ 41S	4721	-800	-868	148979	41502	2997	11241	91442	1627	172
San Juan	Penn	SJ 42S	4987	-170	-314	71723	20231	1511	4775	41637	2675	894
San Juan	Penn	SJ 43S	5202	-199	-257	79159	22916	1692	5379	46398	2332	739
		SJ Average	5206	-90	-148	130504	35723	2486	10574	79680	1632	460
Emery	Miss/Dev	Emery	4852	-2116	-2250	81229	27407	741	2906	46963	2432	710
Garfield	Miss/Dev	Garfield	5936	-1268	-1322	7472	1595	164	650	1848	2018	1197
Grand	Miss/Dev	Grand	4561	-4089	-4116	156376	54959	876	4481	92829	2578	651
San Juan	Miss/Dev	SJ 27-29S	5630	-798	-893	141402	55153	1643	2191	77243	4546	719
San Juan	Miss/Dev	SJ 30-35S	6320	-2300	-2422	84321	24886	1651	5004	50137	1637	966
San Juan	Miss/Dev	SJ 37-39S	5617	1090	1001	52048	18284	349	997	27727	3266	1426
San Juan	Miss/Dev	SJ 40S	4608	-2594	-2718	95537	33750	474	2234	54115	2463	2501
San Juan	Miss/Dev	SJ 41S	4848	-1759	-1872	109684	36913	996	3742	63057	3269	1707
San Juan	Miss/Dev	SJ 42-43S	5070	-873	-946	66618	18705	1071	5033	38828	1869	1113
		SJ Average	5349	-1206	-1308	91602	31282	1031	3200	51851	2842	1405

TWP-interval = township interval. A single county name means the average of all samples within that county.
SJ = San Juan County.
ELEV = Average ground elevation of all sampling sites.
TOP-ELEV, BOT-ELEV = Average elevations of the top and bottom of the sampled intervals.
TDS = Total dissolved solids, reported in mg/L.
Individual ion values are reported in mg/L.

Table 10-2. Total dissolved solids (mg/L) and ions on a dry-weight-percent basis for brines from the Paradox Basin, Utah, by county.

Mississippian/Devonian Brine

Area	TDS	Na	Mg	Ca	Cl	SO_4	HCO_3
Grand Co	156376	35	1	3	59	2	<1
Emery Co	81229	34	1	4	58	3	1
Garfield Co	7472	21	2	9	25	27	16
All of San Juan Co	91602	34	1	3	57	3	2

Pennsylvanian Brine

Area	TDS	Na	Mg	Ca	Cl	SO_4	HCO_3
Grand Co	214249	28	1	9	61	1	<1
Emery Co	64339	32	3	5	55	5	1
Wayne Co	34699	34	1	2	48	13	2
All of San Juan Co	130504	28	2	8	62	1	<1

CHAPTER 11
REGIONAL MIDDLE PALEOZOIC HYDRODYNAMIC PRESSURE REGIME OF THE PARADOX BASIN, UTAH AND COLORADO

Richard G. Allis, Craig D. Morgan, Sonja Heuscher, and Ammon McDonald,
Utah Geological Survey

Introduction

Recently there has been increased interest in exploring for potential reservoirs of oil and gas in Mississippian rocks of the Paradox Basin. Although most oil in the basin has been found in carbonate buildups (algal mounds) of the Pennsylvanian, the northwest-trending fold and fault belt near the northern margin of the basin contains several Mississippian oil and gas fields, the largest being Lisbon, Utah (figures 1-1 and 1-3). McElmo Dome (figures 1-1 and 1-3), southwest Colorado, near the southeast margin of the basin is a major producer of carbon dioxide (CO_2) from the Mississippian (Gerling, 1983; Tremain, 1993). Two minor oil fields (abandoned) occur near the southern margin of the basin, close to the Utah-Arizona state line.

One factor providing insight to recent secondary or tertiary migration of oil within the Mississippian is the present hydrodynamic condition. A horizontal pressure gradient within relatively permeable reservoir rock may indicate significant water movement that displaces trapped oil, whereas abnormally high pressures could indicate hydrocarbon generation and accumulation in relatively low-permeability rocks.

The only prior systematic compilation of pressure trends within the Mississippian system of the Paradox Basin appears to be by Hanshaw and Hill (1969). They studied the potentiometric trends in seven "aquifers" ranging in age between the Cambrian-Devonian and the Permian. Their potentiometric map for the Mississippian (reproduced as figure 11-1) shows a head gradient of about 2400 feet (730 m) between the Utah-Colorado state line and east margin of the Paradox Basin adjacent to the San Juan Mountains (that is, head increasing eastwards). This was interpreted as a major recharge area in the vicinity of the mountains. An area to the southwest of the Abajo Mountains near the northern end of the Monument upwarp (figure 1-1) is shown as having more than 1000 feet (300 m) of head above the surrounding region of southeast Utah. The authors noted that hydrology here is complicated, with mixed evidence of oil wells that were dry to at least the Mississippian, and other wells that indicated an elevated water column.

The compilation by Hanshaw and Hill (1969) has several limitations, which were acknowledged by the authors at that time. Firstly, it is dependent on analysis of only about 600 drill-stem tests (DSTs) supplied by oil companies from wells drilled up until 1961. Of these, about 300 were usable, so the number of DSTs for a particular horizon's potentiometric map is presumably a small fraction of these. Unfortunately, the maps do not show the data points used to constrain the contours. Secondly, the authors chose to present the pressure measurements in the form of a potentiometric surface obtained by converting the pressure to a freshwater column. While the overall pressure trends should be reasonable, the local elevation of the column is less useful.

Several thousand more wells have been drilled in the Paradox Basin since 1961, and many had DSTs performed on various formations. The purpose of this study was to review this data and compile a new map of pressure variations across the Mississippian of the basin. This

study will improve the understanding of geological constraints on fluid flow within the largely carbonate units of the Paleozoic part of the geologic section. Over much of the basin, the Mississippian section is known as the Leadville Limestone, and it is underlain by Devonian limestone of the Ouray and Elbert Formations (Hintze, 1993). Some oil exploration reports from wells to the south of the basin refer to the Mississippian Redwall Limestone, and occasionally the name Madison Limestone is used. The Leadville Limestone is overlain by a thin shale (Molas Formation, <150 feet [46 m] thick) at the base of the Pennsylvanian, and this is overlain by the Hermosa Group containing the main oil-producing units of the basin (Paradox Formation). A stratigraphic column for the central Paradox Basin is shown in figure 11-2.

The Leadville Limestone does not crop out in the Paradox Basin, but it occurs at about 1000 feet (300 m) depth in the Cataract Canyon section of the Colorado River, just downstream of the junction with the Green River (the oldest outcrops in Cataract Canyon are evaporites of the Paradox Formation). On the northeastern margin of the basin, the Leadville Limestone occurs at more than 15,000 feet (4600 m) depth, close to where it is faulted against the Uncompahgre uplift. The carbonate deposition represents a time when there was a stable cratonic platform, prior to the development of a paleoforedeep structure that formed the Paradox Basin. Across much of the eastern half of the basin the Mississippian is overlain by 7000 to 10,000 feet (2100-3000 m) of mostly Pennsylvanian and Permian strata. These cover rocks include low-permeability units of shale, anhydrite, and salt of the Paradox Formation, so there is the potential for significant overpressure in the underlying Mississippian over the eastern half of the basin, and therefore potential for significant lateral variations in fluid pressure here. Simplified maps of the depth to Leadville Limestone (figure 11-3), and structural contours on the top of the Leadville Limestone (figure 11-4) show the gross trends of the Laramide uplifts and the regional erosion patterns across the basin. Note that the contours on both maps are based only on picks of the top of the Leadville in oil exploration wells, and there is no account for local incision in canyons or local faulting and folding. East of the Colorado River in the Monument upwarp, and west of the Green River in the San Rafael Swell, the top of the Leadville rises to 5000 feet (1500 m) above sea level (ft asl [m asl]). This elevation is 1000 feet (300 m) above the level of these sections of the Colorado River and the Green River (3800 to 4000 ft asl [1160-1200 m asl]), which are presumably controlling at least the near-surface hydrology in these areas.

Data Source and Methodology

About 5000 DST reports compiled by PI/Dwights Plus-IHS Energy/Well Data (2008) were used for this pressure compilation. The "shut-in" pressure values included with this report have been used without further correction for recovery to equilibrium. This is a very noisy dataset, so criteria were applied to screen out obviously inaccurate data. The most common source of error is incomplete pressure recovery because of low permeability, either due to local mud-cake problems or inherently low permeability in the formation (Bredehoeft, 1965; Nelson, 2002). If the shut-in time was less than 30 minutes, or there was no shut-in time recorded, the shut-in pressure was discarded. While the 30-minute threshold sometimes appeared to indicate reliable data for the most permeable formations such as the Leadville Limestone, it was far too short for low-permeability rocks. Even after 240 to 300 minutes, pressures in all reported "salt" formations and some "shale" formations were still clearly far from equilibrium. Most DSTs reported an "initial" and a "final" shut-in pressure, and in such cases the larger of the two values was chosen. The topographically lowest part of the Paradox Basin is the Colorado River, and

this should control the minimum pressure in the basin. Any pressure values less than about 70% of hydrostatic pressure beneath the Colorado River were therefore eliminated. Any DSTs that did not identify the formation being tested, or had incomplete depth information, were also eliminated.

As a result of this screening process, between 50 and 75% of the pressure data were removed from further study. To allow further averaging of the pressure data, the Paradox Basin was subdivided into six, one-degree quadrangles (figure 11-5), and the pressure data were plotted at the elevation of the DST (midpoint of the open interval). This resulted in as few as 27 data points for the Mississippian in the Glen Canyon quadrangle, which has no producing fields, and 614 data points in the Aneth quadrangle. In all, there were 1529 pressure points spread over the six quadrangles. To investigate the vertical pressure trends in each quadrangle, the data were subdivided on the basis of geological time. The Paleozoic was split into the periods Mississippian and older, Pennsylvanian, Permian, and where appropriate, a Mesozoic era was included. The total number of Mississippian and older pressure values is 395, representing less than 10% of the initial DST dataset for the Paradox Basin.

Pressure Trends by Quadrangle

Figures 11-6 through 11-11 show the vertical pressure trends for each quadrangle, and a map of the well locations where the DSTs were made. Sometimes more than one DST is from the same well, and within oil and gas fields, wells are close together and occasionally obscure other well locations. To facilitate comparison between the quadrangles, each graph has the same reference line superimposed on it based on a composite pressure trend for the Mississippian and older strata discussed in a later section. This composite trend line has a slope of 0.47 pounds per square inch/foot (psi/ft [10.6 kPa/m), which is almost 10% above the hydrostatic gradient for fresh water. It is equivalent to a static pressure gradient in a column of water with a salinity of 100,000 to 150,000 mg/kg (J.W. Gwynn, UGS, verbal communication, June 2008) which is reasonable for the Paleozoic section of the Paradox Basin. Shallow ground water in the Paradox Valley, Colorado, has an average dissolved solids concentration of 250,000 mg/kg (Chafin, 2002). However, the springs and geysers near the town of Green River in the north part of the basin have concentrations of 11,000 to about 20,000 mg/kg (Baer and Rigby, 1978; Shipton and others, 2004), so there is probably a gradient in salinity across the basin. Note that the main source of error with DST shut-in pressures is failure to completely come to equilibrium during the test, and for the pressure to be less than actual pressure. These uncertainties are such that the inferred pressure gradient of 0.47 psi/ft (10.6 kPa/m) has an estimated 10% uncertainty.

Glen Canyon Quadrangle

The DST pressure data from the Mississippian and older strata are sparse for the Glen Canyon quadrangle (figure 11-6A), but consistent with a hydrostatic trend when compared with data from the surrounding quadrangles. Although there is a suggestion that the deeper pressures (that is, below sea level) may be less than the regional trend shown on the graph (figure 11-6B), this is considered unlikely since this area is in the hydrologically lowest part of the Paradox Basin (Colorado River at 3800 ft asl [1160 m]). Pennsylvanian and Permian formations are largely consistent with the one hydrostatic trend extending from near-surface to at least -4000 ft asl (-1200 m asl). Two Pennsylvanian pressure values at shallow depth suggest a locally perched

water table near the surface (head at close to 5000 ft asl [1520 m asl]). Both of these pressure points are from wells on the eastern boundary of the quadrangle, and are consistent with a near-surface pressure trend that is more strongly identified on the adjacent quadrangle (Aneth). Hanshaw and Hall (1969) reported that several exploration wells drilled east of Cataract Canyon on the northern end of the Monument upwarp encountered dry conditions down into the Mississippian, which as figure 11-4 shows, suggests the deep head is at an elevation of less than 4000 to 5000 ft asl (1200-1500 m asl), and consistent with the trend in figure 11-6.

West Green River Quadrangle

The DST pressure data for the West Green River quadrangle (figure 11-7A) indicate one linear trend from a shallow water table elevation of about 4000 ft asl (1200 m asl) in the Triassic to the deepest Mississippian at -6000 ft asl (-1800 m asl) (figure 11-7B). The slope is 0.47 psi/ft (10.6 kPa/m), consistent with saline water. It is likely that the pressure trend is 100 to 200 psi (690-1380 kPa) higher than the composite trend shown on the graph. This is because of the tendency for DST shut-in pressure to underestimate the actual pressure. In addition, in the northeast corner of the quadrangle immediately east of the Green River, saline water and CO_2 flow to the surface in the form of springs and geyser activity in abandoned wells. These fluids are interpreted to originate from deep within the Paradox Basin (Heath, 2004; Shipton and others, 2004; Allis and others, 2005). The elevation of the springs and overflowing wells is 4050 ft asl (1230 m asl), implying a hydrostatic trend at least 250 ft (75 m) (about 100 psi [690 pKa]) higher than the composite trend on the graph. There may be locally higher pressures within the Pennsylvanian section, with a few pressure points 500 psi (3450 kPa) higher than the regional trend.

Aneth Quadrangle

A relatively large amount of data from the Pennsylvanian exists in the Aneth quadrangle (figure 11-8A) because of the intensive drilling that has occurred in Greater Aneth and other oil fields in the Blanding sub-basin (figure 1-1). The Mississippian data are split into two sets: those below sea level (typically > 5000 feet [1500 m] depth) and those above sea level (1000 to 3500 ft asl [300-1100 m asl]). The former are in the eastern half of the quadrangle, the latter are mostly in the western half (Monument upwarp). Both sets of data are consistent with a regionally extensive pressure trend with a head at 3800 ft asl (1160 m asl), the average elevation of the Colorado River in the adjacent Glen Canyon quadrangle. The Pennsylvanian data show more scatter, with most data clustering close to the underlying Mississippian pressure trend (figure 11-8B). However, there is also clear evidence of overpressures of up to 2000 psi (13,790 kPa) relative to the Mississippian trend. This is likely related to locally lower permeability and hydrocarbon generation within the Pennsylvanian section. The Permian pressure data suggest a hydrostatic gradient with control by surface recharge from a ground elevation of 4500 to 5000 ft asl (1400-1500 m asl). The elevation of the San Juan River near Aneth field is 4400 ft asl (1340 m asl). The Mississippian pressure trend in parts of the quadrangle where it is situated above sea level (mostly western half) is between 500 and 1000 psi (3450-6900 kPa) lower than where the Permian section occurs at a similar elevation (mostly eastern half).

Note that the pressure trends in the higher elevation areas in the north of the quadrangle (Abajo Mountains) are unknown. However, Kirby (2008) reported that ground water levels in

the vicinity of the city of Blanding (10 to 15 miles [16-24 km] south of the Abajo Mountains) range between 6400 ft asl (1950 m asl) in the north to 5300 ft asl (1600 m asl) near Blanding. The ground water is "perched" within the Dakota and Burro Canyon Formations (Cretaceous) on top of the underlying Morrison Formation (Upper Jurassic). Recent ground-water wells drilled into the Navajo Sandstone (Lower Jurassic) near Blanding have water levels close to 5400 ft asl (1800 m asl), and encountered good quality drinking water (Loughlin Water Associates, verbal communication, 2008). Both of these Mesozoic aquifers appear to be perched relative to water in Permian and underlying formations.

Lisbon Quadrangle

The Lisbon quadrangle contains more Mississippian pressure data (figure 11-9A) than the others because of the Mississippian oil and gas fields in the Paradox fold and fault belt (figure 1-3). The pressure trend (figure 11-9B) is consistent with, and largely controls (because of the amount of data), the composite pressure trend for the basin. Pennsylvanian pressure data are very scattered, but as in the Aneth quadrangle, there is evidence of local overpressuring by up to about 1000 psi (6900 kPa). The Permian and Mesozoic pressures suggest a trend that is systematically higher than the Mississippian trend, but due to poor data quality, it is unclear whether there is one aquifer trend or locally varying pressure trends with zero-pressure intercepts between 4500 and about 6000 ft asl (1370-1800 m).

Dolores Quadrangle

In the Dolores quadrangle, although some Mississippian DST pressure data (figure 11-10A) lie close to the composite pressure trend, most data lie at higher pressures (figure 11-10B). The same higher-pressure pattern occurs in the Permian-Pennsylvanian and the Mesozoic sections. The scatter in the Mesozoic section appears to be smaller than that in the underlying sections, and these data suggest zero-pressure head elevations of between 4000 and 7000 ft asl (1220-2130 m asl). The northeast portion of the quadrangle has higher ground elevations associated with the western flank of the San Juan Mountains, which range up to 14,000 ft asl (4260 m asl) to the east of the quadrangle. The deeper trends (Permian and below) are up to about 2000 psi (13,790 kPa) above the composite pressure trend. The well locations for most of these higher-pressure DSTs are situated in the northeast portion of the quadrangle, suggesting the effects of recharge from the San Juan Mountains to the east.

Cortez Quadrangle

The DST pressure data are scattered in the Cortez quadrangle, although the deep Mississippian pressures are constrained by data from injection wells drilled by the U.S. Bureau of Reclamation near the Dolores River in the Paradox Valley, western Colorado (figure 11-11A). Here, the three DSTs on figure 11-11B imply a pressure of 6300 psi (43,400 kPa) at an elevation of -9500 ft asl (-2900 m). This agrees with the undisturbed pressures quoted by Ake and others (2005) of 6235 psi (43,000 kPa) at 9200 ft (2800 m) below sea level for the deep wells in the Paradox Valley. It confirms that the Mississippian near the western edge of this quadrangle has pressures similar to the composite trend in the rest of the Paradox Basin farther west. However, there are other Mississippian pressure data up to about 1000 psi (7000 kPa) higher than the

composite trend, and two points almost 2000 psi (13,900 kPa) higher. Inspection of the well locations of those DSTs shows them to be in the eastern half of the quadrangle. The same pattern applies to the Pennsylvanian and Permian DSTs. A hydrostatic pressure trend that is an upper boundary to the DSTs would have a zero-pressure intercept of about 8000 ft asl (2400 m asl). The Uncompahgre uplift that diagonally traverses the quadrangle rises to over 9000 ft asl (2700 m asl). Recharge on the uplift may be contributing to the higher pressures apparently occurring in the quadrangle.

Composite Mississippian Pressure Trend

Figure 11-12 compiles all the Mississippian DST pressure data onto one graph, coded by quadrangle. A linear trend is apparent over an elevation range of 14,000 ft (4300 m), with a slope of 0.47 psi/ft (10.6 kPa/m) as discussed above. To clarify the pattern of a small amount of data plotting at significantly higher pressures than this trend, figure 11-13 examines the amplitude of the pressure departure from the composite trend against the ground elevation of the well with the DST measurement. This indicates that a systematic pattern of increased pressure departure (that is, higher pressures) with higher ground elevation occurs in the Cortez and Dolores quadrangles. Elsewhere, there is not a significant correlation.

Interpretation

For most of the Paradox Basin, an area of at least 100 by 100 miles (260 by 260 km) including the Glen Canyon, West Green River, Aneth, and Lisbon quadrangles, the Mississippian pressure regime is remarkably uniform, close to hydrostatic, and independent of laterally varying pressure in overlying formations. This implies relatively high permeability, presumably because of interconnected fractures throughout the section and development of karst topography at the top due to subaerial exposure at the end of the Mississippian. The zero-pressure head on this pressure regime varies between 4000 ft asl (1200 m asl) in the north (West Green River quadrangle) and 3800 ft asl (1200 m asl) in the two southern quadrangles. This corresponds to the elevation of the adjacent sections of the Colorado and Green Rivers, which are acting as the pressure control for this entire region.

In the West Green River quadrangle adjacent to the Green River, saline water (11,000 to 20,000 mg/kg total dissolved solids) flows to the surface at several localities, indicating a major discharge point for the basin. Presumably the stretch of the Colorado River south of the junction with the Green River (Cataract Canyon, possibly extending into Glen Canyon/Lake Powell) is also a zone of hydrological connection, and potentially major discharge, for the Mississippian. Any discharge is presumably obscured by the confined, high flow of the Colorado River within the canyon here. Large-scale intrusion of Paradox salt has deformed the canyon (Needles District of Canyonlands National Park), and faults link the northern Monument upwarp to Cataract Canyon (Lewis and Campbell, 1965). The top of the Mississippian section is within about 1000 feet (300 m) of the river level here, when elevations from the wells (figure 11-3) are interpolated and compared to the river elevation. In the Monument upwarp, the top of the Mississippian section rises to 5000 ft asl (1500 m asl).

Near the eastern margin of the Paradox Basin, the pressure in the Mississippian section increases compared to the regional trend elsewhere by as much as 2000 psi (14,000 kPa) (figure 11-14). This rise in pressure occurs adjacent to the San Juan Mountains farther east, and

presumably represents a major recharge area to the Mississippian and older section. There is no evidence of hydrological transition or boundary zones to the Mississippian section in the north or the west of the studied area. However, there probably are other recharge areas beyond the northwest and west of the six quadrangles studied in this report, perhaps beyond the conventional boundaries of the Paradox Basin as shown in figure 1-1. Around the north and northeast boundaries, the Mississippian dips beneath the Uinta Basin and may also be faulted against the Uncompahgre uplift, so significant recharge from this direction seems unlikely.

The broad, uniform pressure regime within the Mississippian raises questions about how long it has existed and its implications for past oil and gas migration. Its widespread permeability suggests that it could have been a major fairway for hydrocarbon migration at various times in the past. The top of the Mississippian in the major anticlines in and adjacent to the Paradox Basin (figure 11-4) is situated above the zero-pressure intercept for the regional pressure trend discussed above. This means that if any fluids are still present, they are likely to be at a low pressure and possibly discontinuous. Depending on the vertical permeability of the overlying strata, the Mississippian could be air-filled (dry) as reported by Hanshaw and Hill (1969) for some wells on the Monument upwarp. However, this may not have been the case several million years ago. Down-cutting by the Colorado River system has hydrologically intercepted the Mississippian section. Using characteristic incision rates of 1 foot/thousand years (0.6 to 1.6 ft [0.18-0.5 m] per 1000 years – see Davis and others, 2001; Hanks and others, 2001; Marchetti and Cerling, 2001; Willis and Biek, 2001; Pederson and others, 2002), several million years ago there would have been several thousand feet more of section overlying and potentially sealing the Mississippian. Today's relative underpressure of the Mississippian relative to the Pennsylvanian and Permian as seen in the Aneth quadrangle would not have been present, and the hydrodynamic gradient could have been in a different direction. That is, the large-scale fluid flow that is inferred to be occurring today towards the Colorado River would not have been occurring, and the Mississippian would have been fully saturated within the Paradox Basin, and could have held significant quantities of oil and gas within the structural highs. Some of this volume of oil could be preserved as the tar sand deposits (Tar Sand Triangle, White Canyon, and Ten Mile Wash), found along the western margin of the Paradox Basin, that may have been a larger pool trapped in what is now partially breached Monument upwarp.

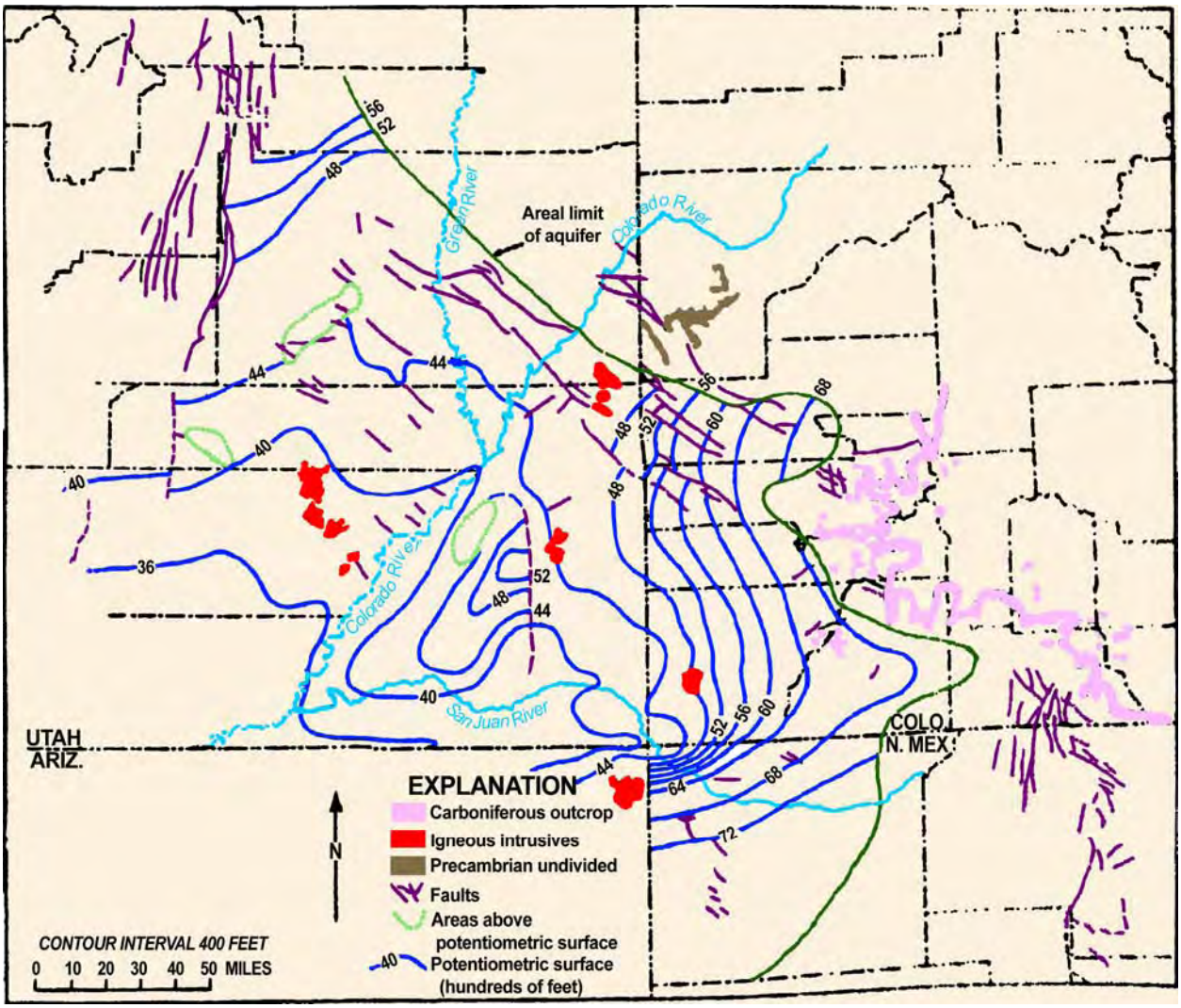

Figure 11-1. Potentiometric map for the Mississippian derived from oil and gas DST pressure data up to 1961 (from Hanshaw and Hall, 1969).

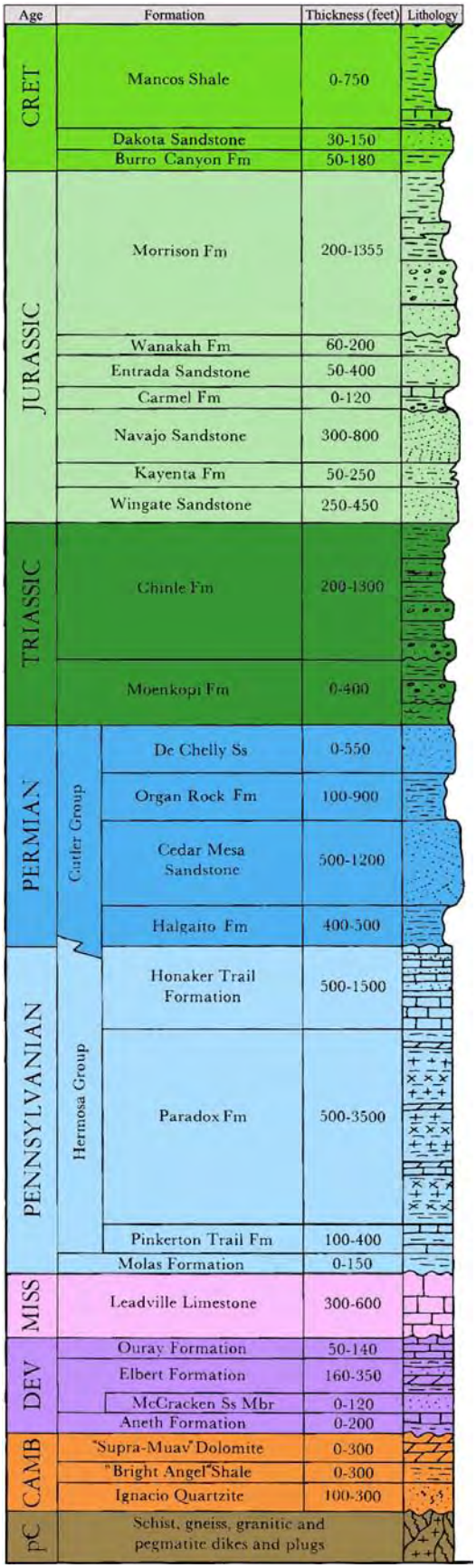

Figure 11-2. Stratigraphic section for the central Paradox Basin near Monticello, Utah (after Hintze, 1993).

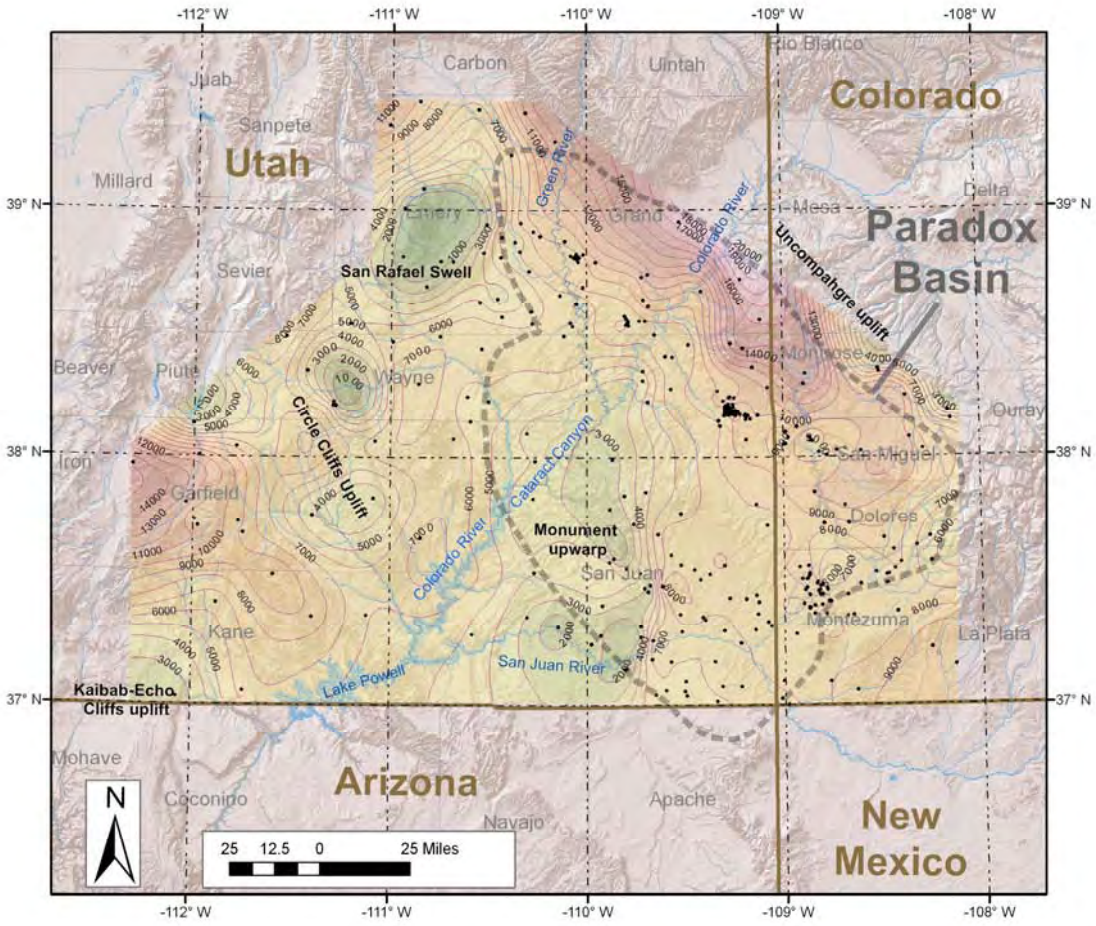

Figure 11-3. Depth to top of the Mississippian Leadville Limestone derived from oil and gas exploration wells. Note that the contours do not consider local topographic relief between the wells, such as the Colorado River canyon and mountains. Contour interval is 1000 feet.

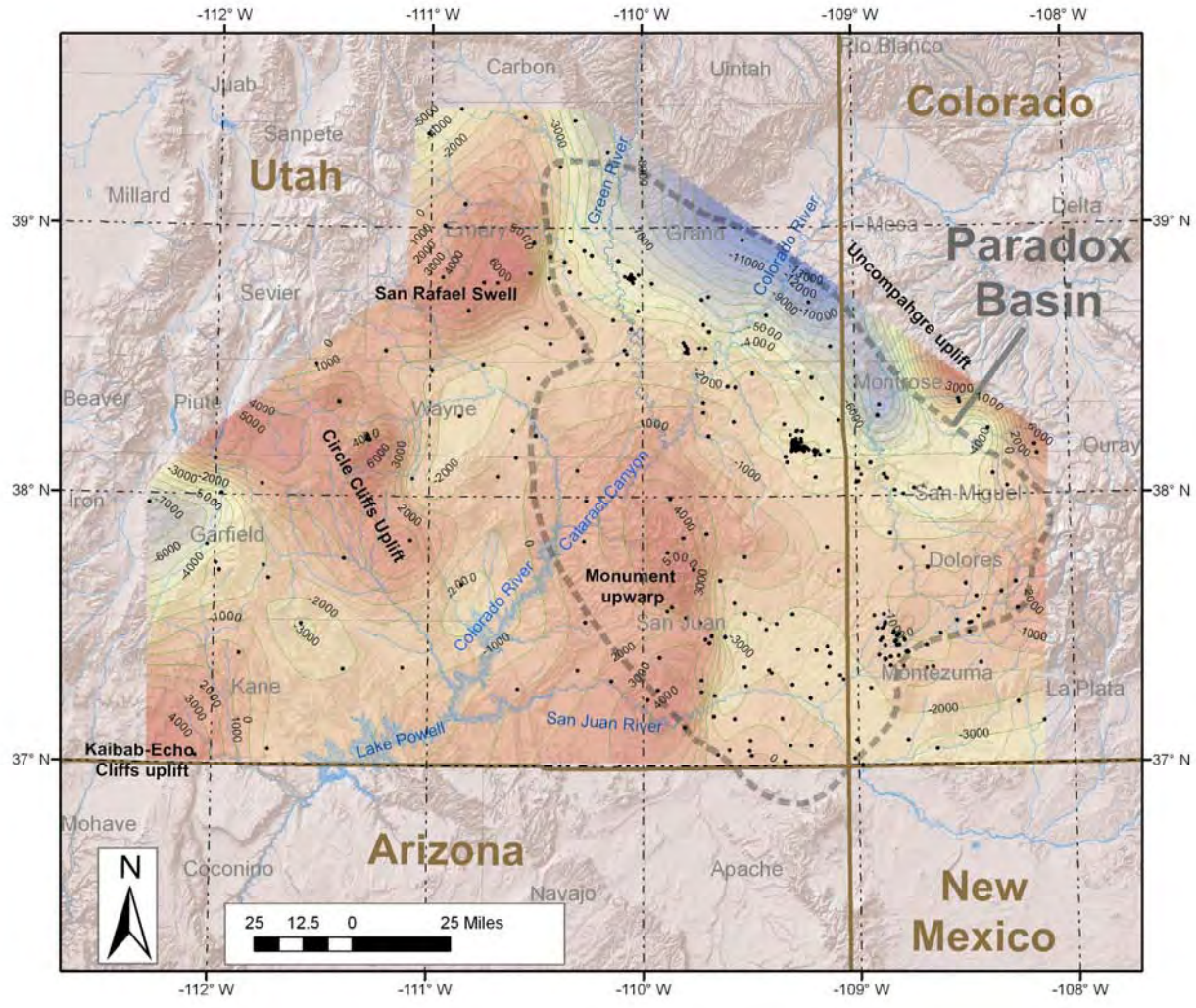

Figure 11-4. Structural contours on the top of the Leadville Limestone derived from oil and gas exploration wells. Note that the contours do not consider fault offsets and folding between the wells. The contour interval is 1000 feet (relative to sea level). The structural highs correspond to Laramide uplifts.

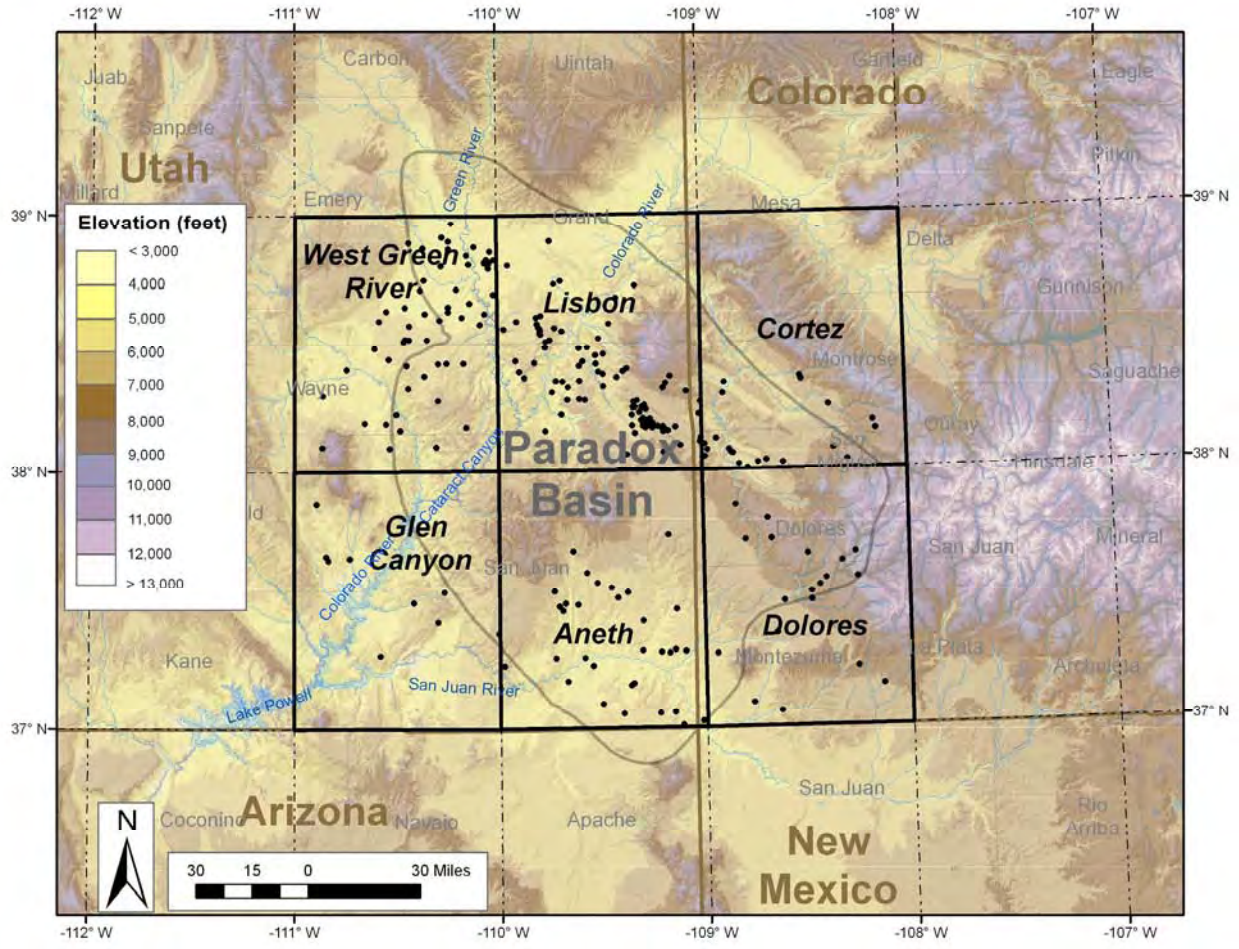

Figure 11-5. Subdivision of the Paradox Basin into six, one-degree by one-degree quadrangles, for which DST pressure data are consolidated. Dots indicate the distribution of wells which had DST measurements within the Mississippian or older formations. Names assigned to the quadrangles are for this report only, and do not correspond to U.S. Geological Survey quadrangles.

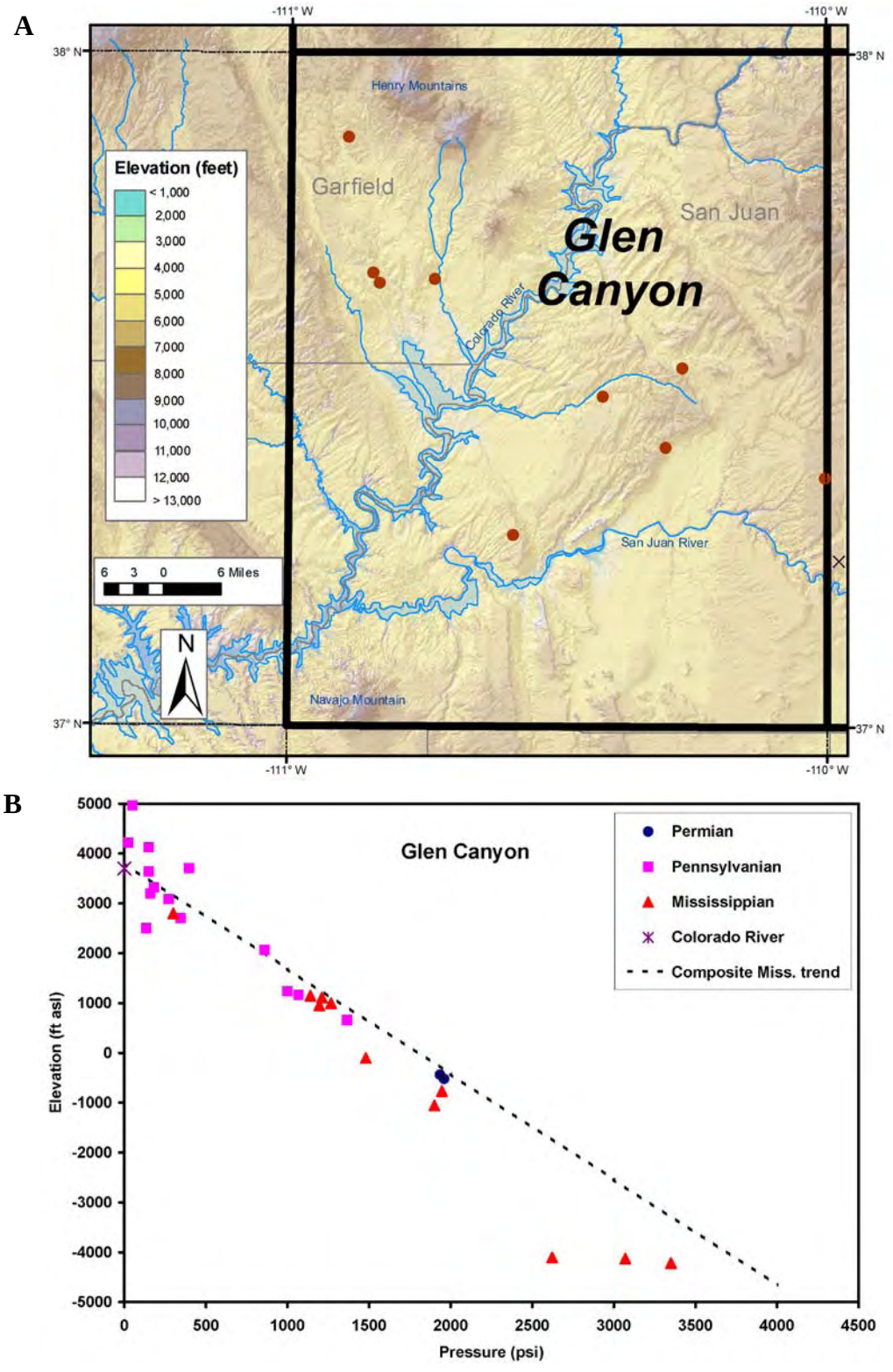

Figure 11-6. Glen Canyon quadrangle. A – Location of wells within the quadrangle for which DST measurements from the Mississippian (and older) strata have been used in the pressure trend graph in (B). Sometimes more than one DST is available from a well. B – Trend of DST shut-in pressures in the quadrangle. The dashed line is derived from a composite pressure plot discussed in a later figure. Note that the pressures from DSTs tend to be minimums because of possible lack of full equilibrium at the end of the test.

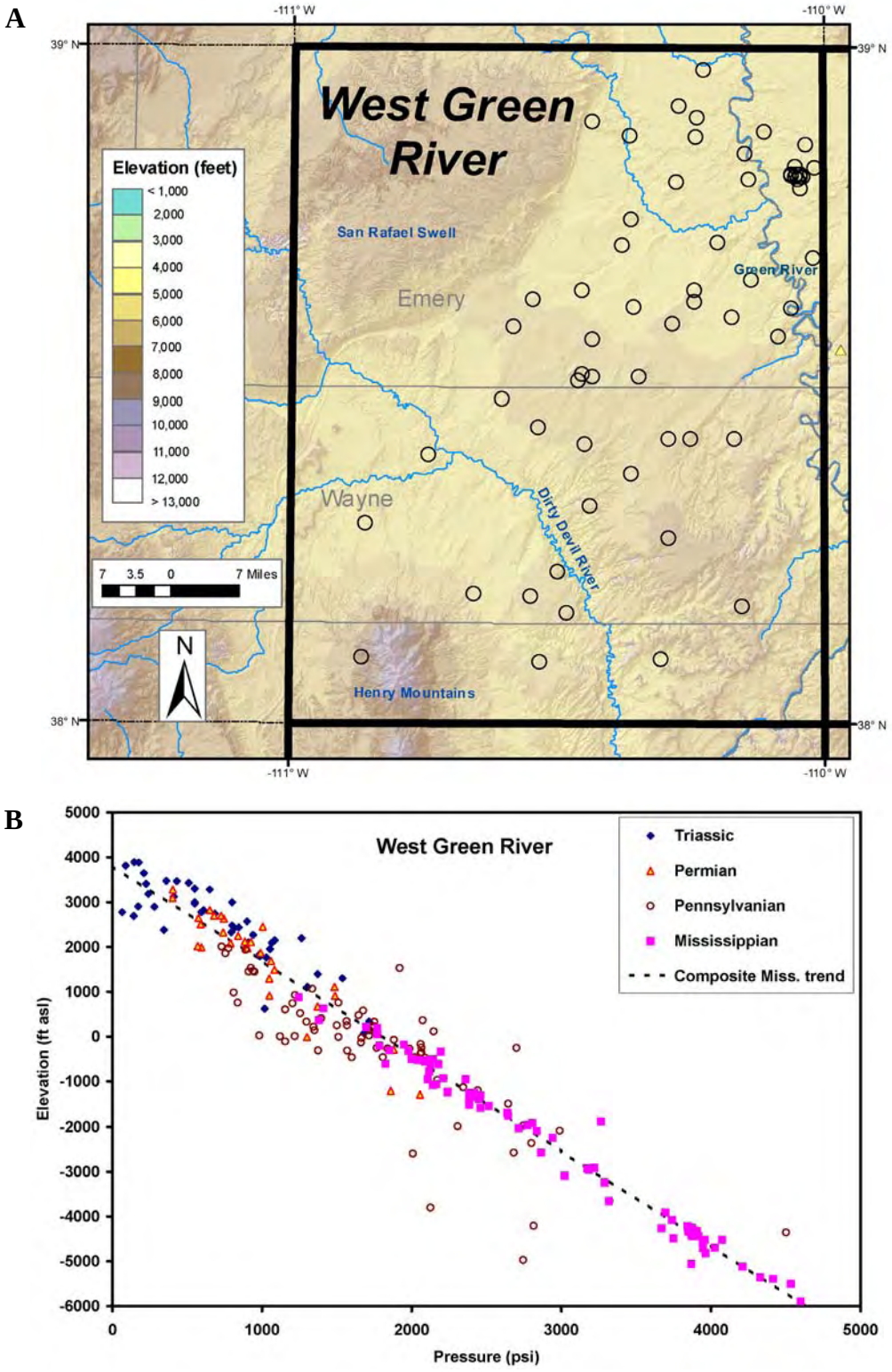

Figure 11-7. West Green River quadrangle. A – Location of wells within the quadrangle for which DST measurements from the Mississippian (and older) strata have been used in the pressure trend graph in (B). Sometimes more than one DST is available from a well. B – Trend of DST shut-in pressures in the quadrangle. The dashed line is derived from a composite pressure plot discussed in a later figure. Note that the pressures from DSTs tend to be minimums because of possible lack of full equilibrium at the end of the test.

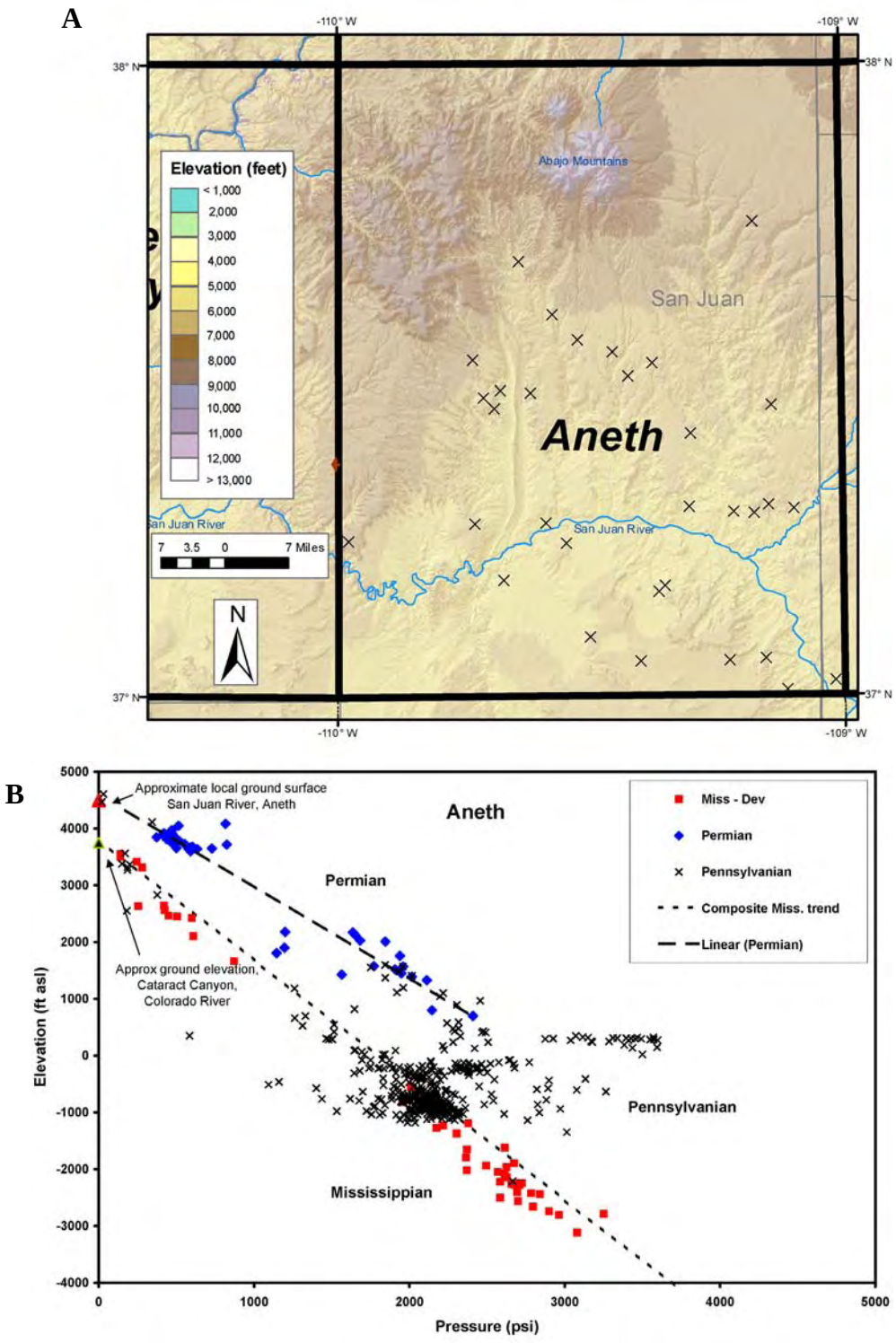

Figure 11-8. Aneth quadrangle. A – Location of wells within the quadrangle for which DST measurements from the Mississippian (and older) strata have been used in the pressure trend graph in (B). Sometimes more than one DST is available from a well. B – Trend of DST shut-in pressures in the quadrangle. The dashed line is derived from a composite pressure plot discussed in a later figure. Note that the pressures from DSTs tend to be minimums because of possible lack of full equilibrium at the end of the test.

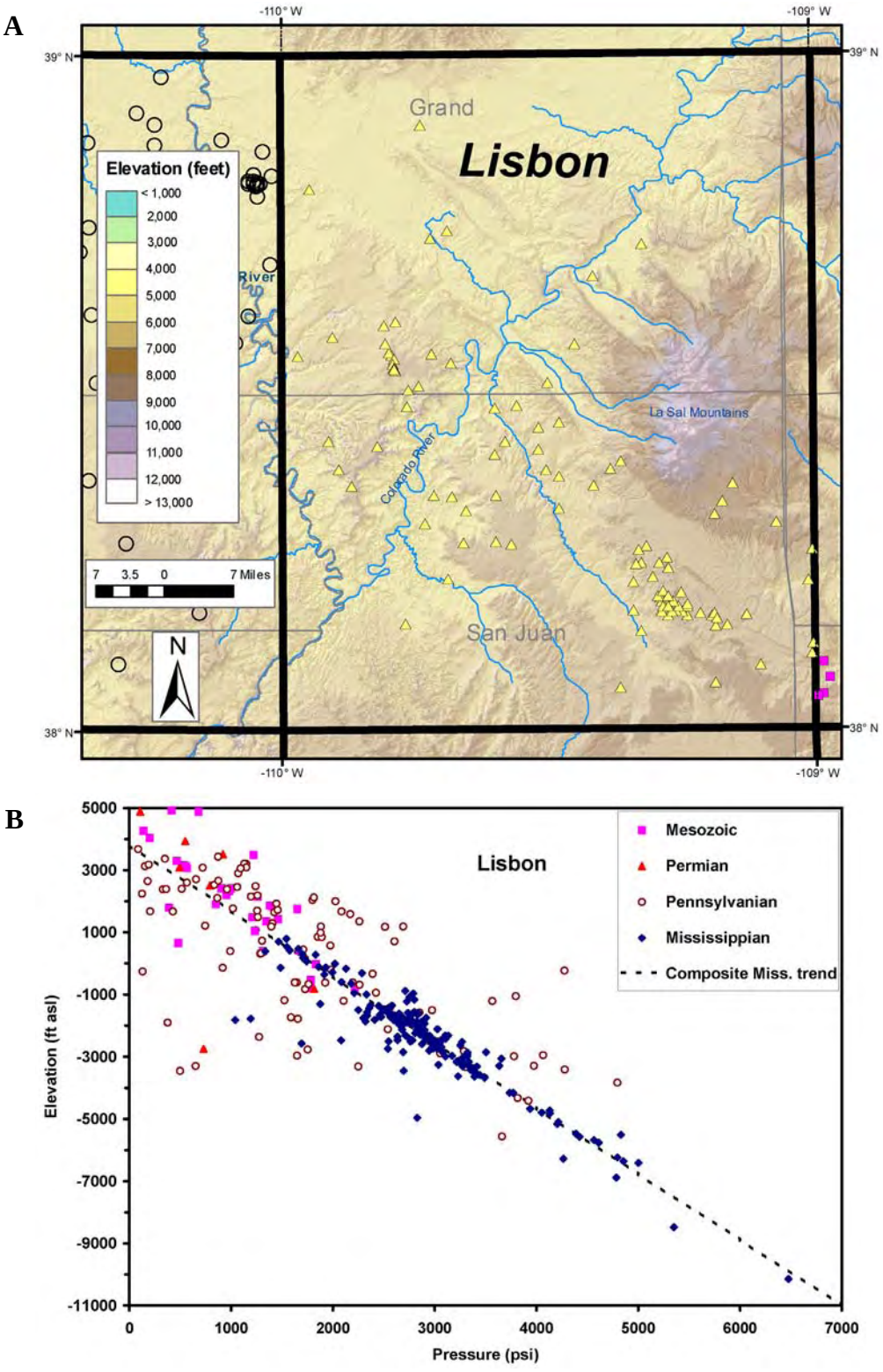

Figure 11-9. Lisbon quadrangle. A – Location of wells within the quadrangle for which DST measurements from the Mississippian (and older) strata have been used in the pressure trend graph in (B). Sometimes more than one DST is available from a well. B – Trend of DST shut-in pressures in the quadrangle. The dashed line is derived from a composite pressure plot discussed in a later figure. Note that the pressures from DSTs tend to be minimums because of possible lack of full equilibrium at the end of the test.

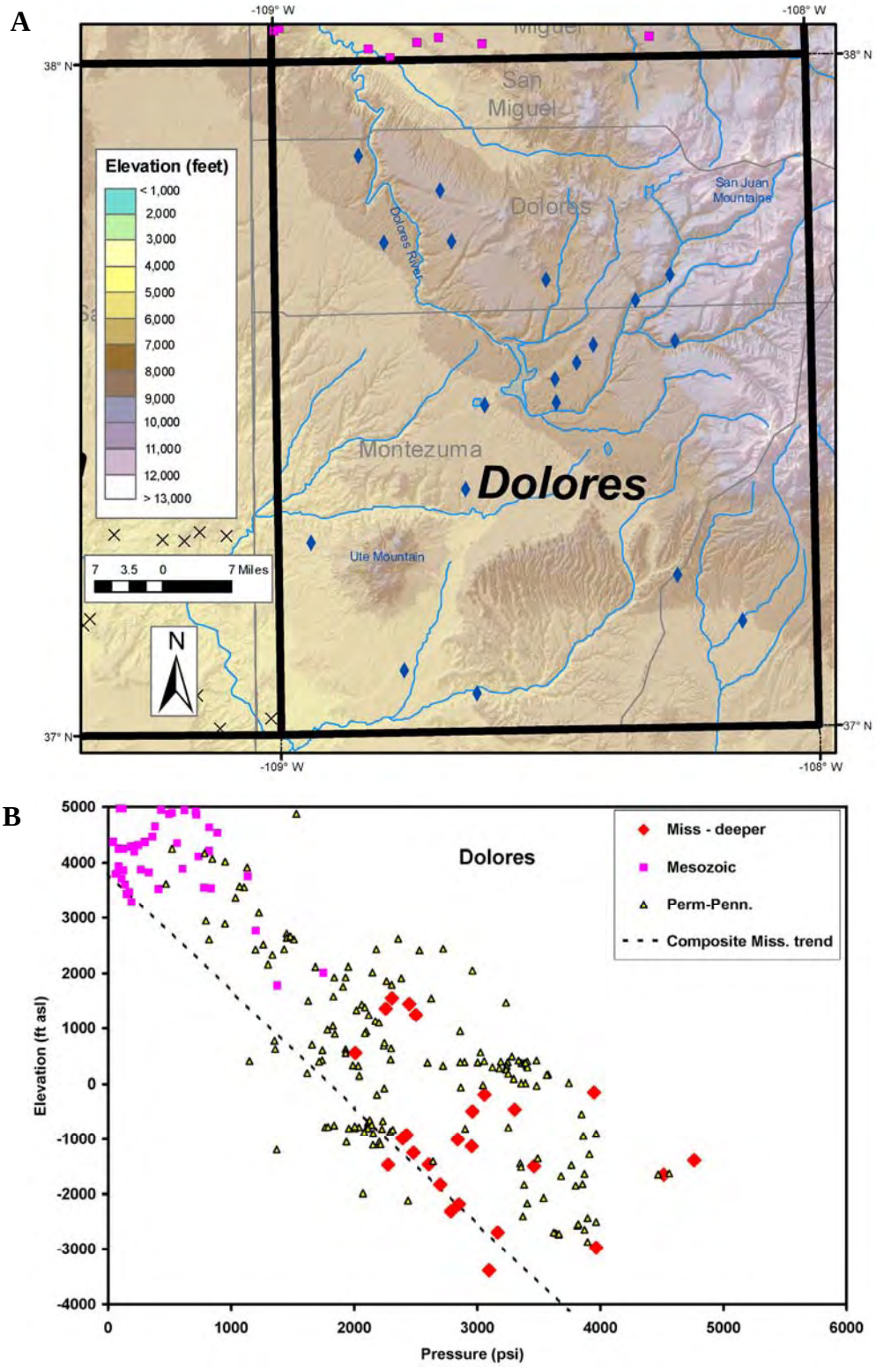

Figure 11-10. Dolores quadrangle. A – Location of wells within the quadrangle for which DST measurements from the Mississippian (and older) strata have been used in the pressure trend graph in (B). Sometimes more than one DST is available from a well. B – Trend of DST shut-in pressures in the quadrangle. The dashed line is derived from a composite pressure plot discussed in a later figure. Note that the pressures from DSTs tend to be minimums because of possible lack of full equilibrium at the end of the test.

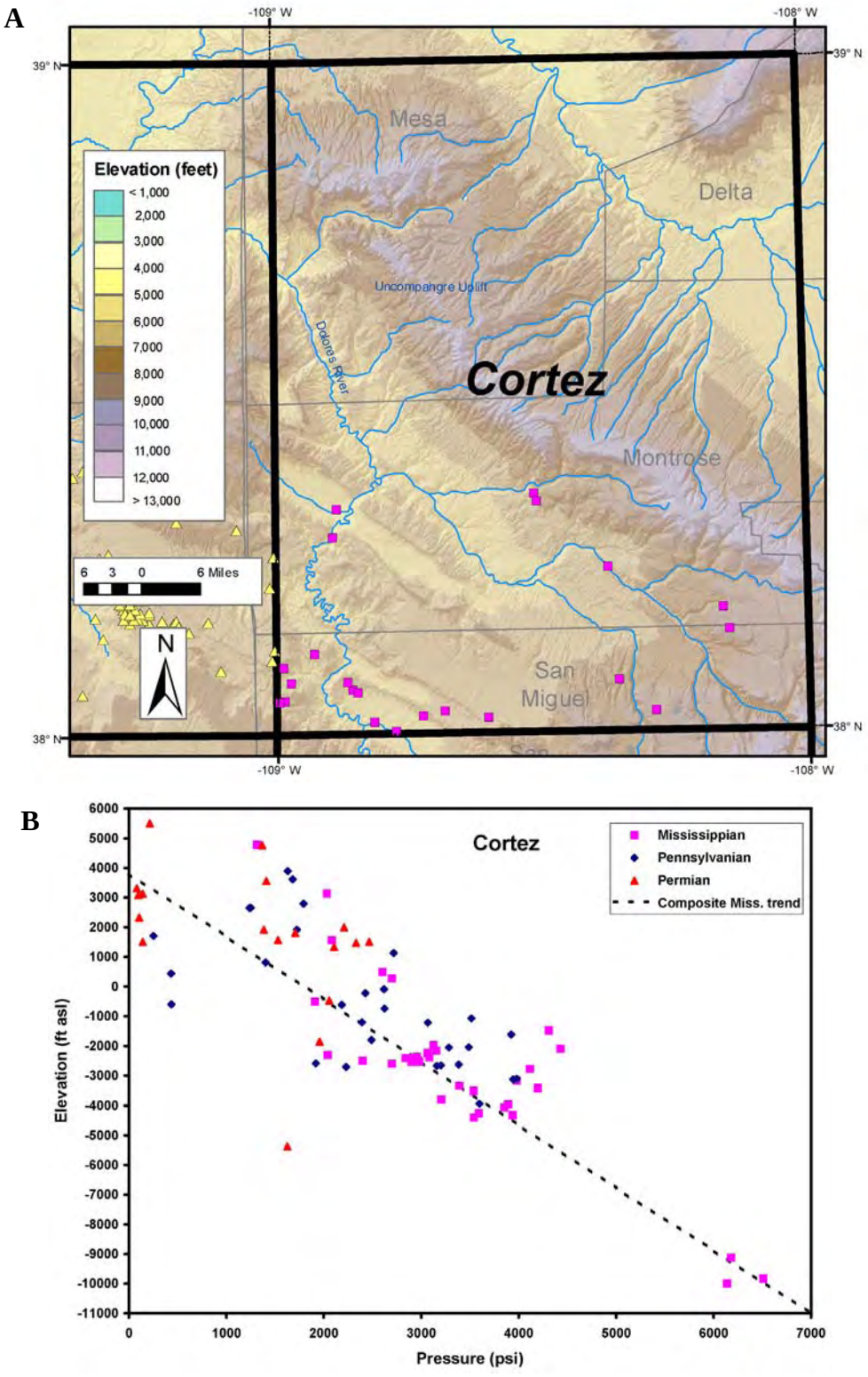

Figure 11-11. Cortez quadrangle. A – Location of wells within the quadrangle for which DST measurements from the Mississippian (and older) strata have been used in the pressure trend graph in (B). Sometimes more than one DST is available from a well. B – Trend of DST shut-in pressures in the quadrangle. The dashed line is derived from a composite pressure plot discussed in a later figure. Note that the pressures from DSTs tend to be minimums because of possible lack of full equilibrium at the end of the test.

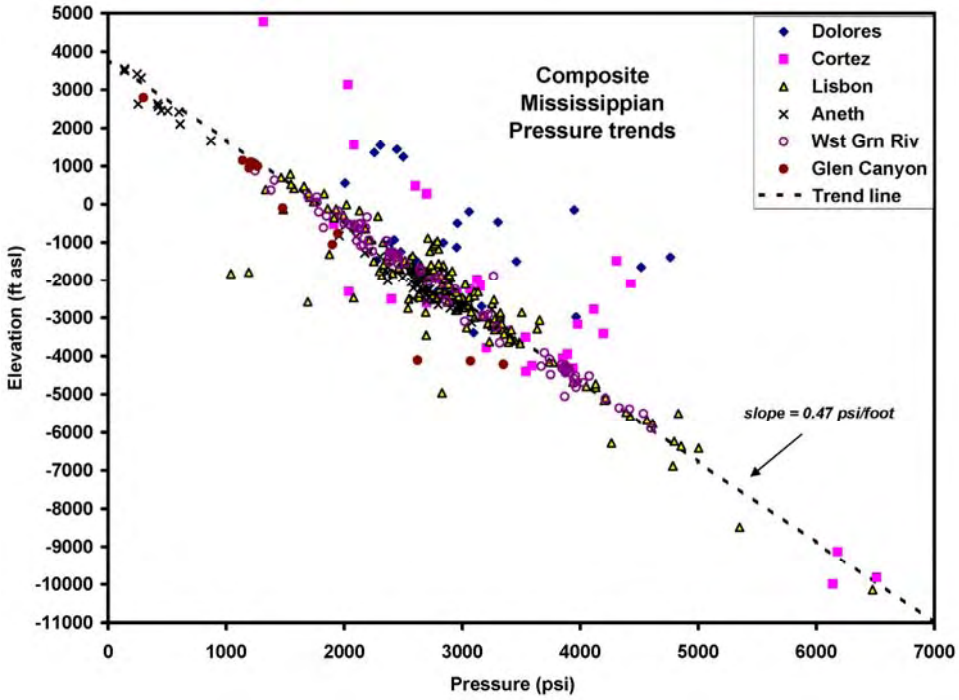

Figure 11-12. Compilation of DST pressure measurements from all six quadrangles for the Mississippian and older formations. Dashed line is referred to in the text as the "composite pressure trend."

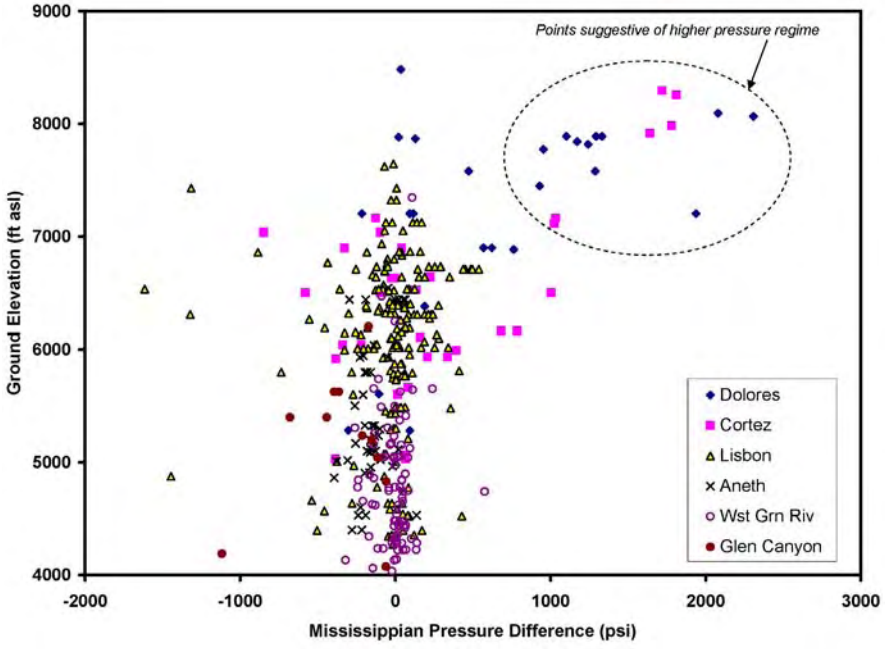

Figure 11-13. Distribution of pressure differences between the actual DST pressure measurement and the pressure inferred from the composite line for that elevation. The pressure differences are plotted against the ground elevation for the well with the DST. This shows that most of the DSTs in the Dolores and Cortez quadrangles that appear in figure 11-12 to be at systematically higher pressures, are also at higher ground elevations. They also are in the eastern portions of the two quadrangles, as shown in figure 11-14.

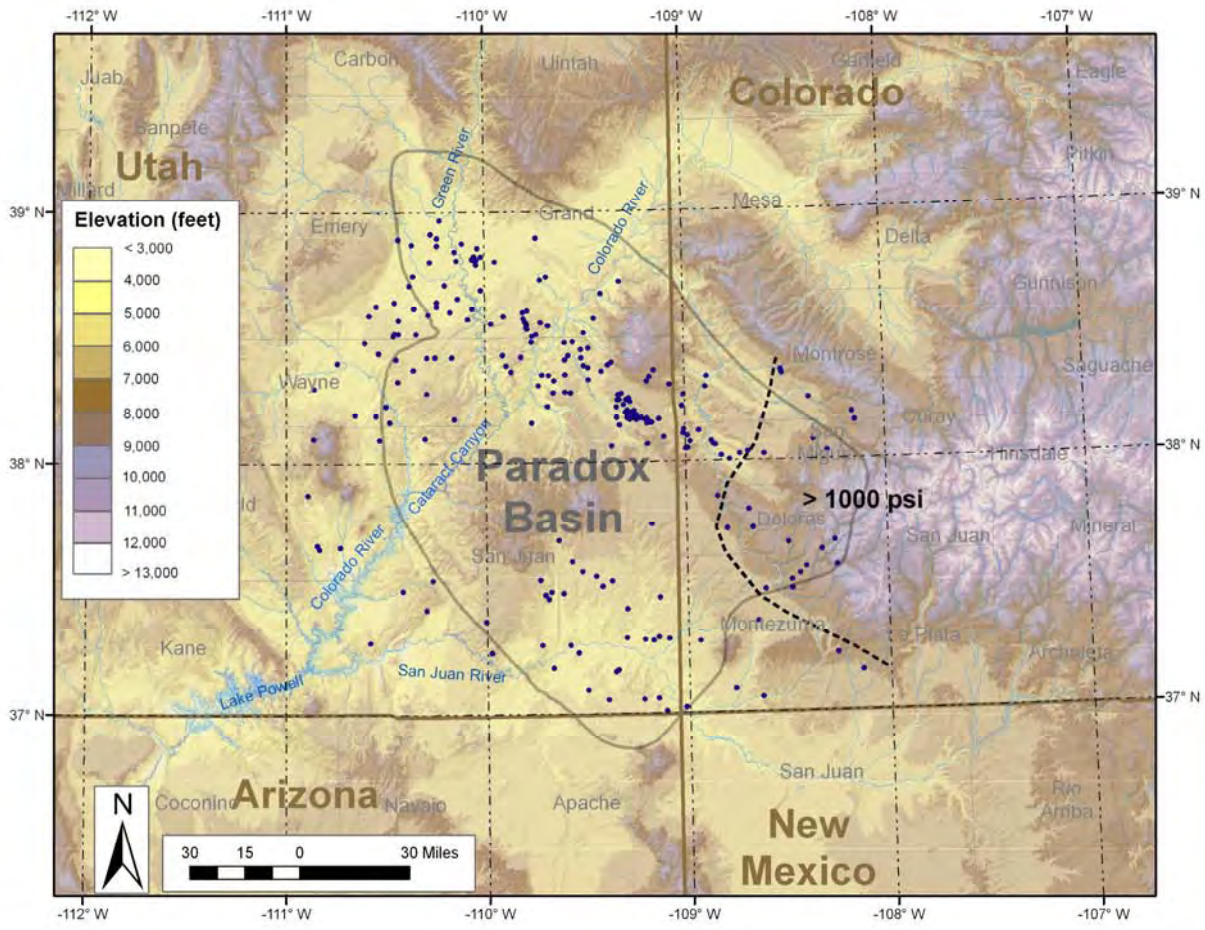

Figure 11-14. Summary of the region of anomalous pressures identified in figures 11-12 and 11-13 for the Mississippian and older rocks of the Paradox Basin. Elsewhere, pressures are close to hydrostatic with a zero-pressure intercept of 3800 to 4000 ft asl.

CHAPTER 12
SUMMARY AND CONCLUSIONS

Thomas C. Chidsey, Jr., Utah Geological Survey

The Mississippian (late Kinderhookian to early Meramecian) Leadville Limestone is a shallow, open-marine, carbonate-shelf deposit. The Leadville has produced over 53 million barrels (8.4 million m^3) of oil/condensate from seven fields in the Paradox fold and fault belt of the Paradox Basin, Utah and Colorado. Most Leadville oil and gas production is from basement-involved structural traps. All of these fields are currently operated by independent producers. This environmentally sensitive, 7500-square-mile (19,400 km^2) area is relatively unexplored with only about 100 exploratory wells that penetrated the Leadville (less than one well per township), and thus the potential for new discoveries remains great. There have been no significant new oil discoveries since the early 1960s, and only independent producers continue to explore for Leadville oil targets in the region, 85% of which is under the stewardship of the federal government.

The overall goals of this report are to (1) develop and demonstrate techniques and exploration methods never tried on the Leadville Limestone, (2) target areas for exploration, (3) increase deliverability from new and old Leadville fields through detailed reservoir characterization, (4) reduce exploration costs and risk especially in environmentally sensitive areas, and (5) add new oil discoveries and reserves. The final results, summarized below, will hopefully reduce exploration costs and risk, especially in environmentally sensitive areas of the Paradox Basin, and add new oil discoveries and reserves.

Lisbon Field, San Juan County, Utah: A Case Study of Leadville Limestone Lithofacies and Diagenetic History

Prior to this study, reservoir characterization of the Leadville Limestone was not complete and little pertinent information (core descriptions, permeability data, and diagenetic analysis) had been published. Lisbon field, San Juan County, Utah, accounts for most of the Leadville oil production in the Paradox Basin. Its reservoir characteristics, particularly diagenetic overprinting and history, and Leadville lithofacies can be applied regionally to other fields and exploration trends in the basin. The UGS had a wealth of undescribed core and other raw data at the Survey's Core Research Center. Initial investigations indicated the possible presence of hydrothermal dolomite, a key component in the development of diagenetic hydrocarbon traps, which would imply a new potential for the Leadville in the Paradox Basin. Therefore, Lisbon was selected as the case-study field for this Leadville Limestone project. The following sections summarize the lithofacies, diagenesis (including scanning electron microscopy, epifluorescence, cathodoluminescence), fluid inclusion, isotopic, and burial history studies of Lisbon field, and provides conclusions and recommendations for independents exploring for Leadville targets.

Lithofacies

1. Leadville lithofacies include open marine (crinoidal banks or shoals and Waulsortian-type buildups), oolitic and peloid shoals, and middle shelf.

2. Rock units with open-marine and restricted-marine lithofacies constitute a significant reservoir potential, having both effective porosity and permeability when dissolution of skeletal grains followed by dolomitization has occurred.

Diagenetic History

1. Leadville reservoir quality at Lisbon is greatly enhanced by dolomitization and dissolution of shallow water limestone. There are two basic types of dolomite: (1) very fine, early dolomite, and (2) coarse, late dolomite. Early dolomitization preserves depositional fabrics and has limited porosity development, except for limited dissolution of fossils, and has very low permeabilities. Late dolomitization has two morphologies: rhombic dolomites and saddle dolomites. Most reservoir rocks within Lisbon field appear to be associated with the second, late type of dolomitization and associated leaching events.

2. Pyrobitumen coats most intercrystalline dolomite as well as dissolution pores associated with the second type of dolomite. Fracturing and brecciation caused by hydrofracturing are widespread within Lisbon field. Sediment-filled cavities, related to karstification of the previously exposed Leadville, are relatively common throughout the upper third of the formation in the field. Other diagenetic products include syntaxial cement, sulfide minerals, anhydrite cement and replacement, and late macrocalcite.

3. Late dolomitization, saddle dolomite, and dolomite cement precipitation, as well as sulfides and brecciation, may have developed from hydrothermal events that can greatly improve reservoir quality. The result can be the formation of large, diagenetic-type hydrocarbon traps.

Scanning electron microscopy (SEM): Scanning electron microscopy demonstrates how Leadville reservoir quality at Lisbon is greatly enhanced by dolomitization and dissolution of shallow water limestone.

- Pyrobitumen coats most intercrystalline dolomite in the Leadville as well as dissolution pores associated with the second type of dolomite. Fractures enhance the permeability in several intervals.

- Minor euhedral quartz is present in several samples. Anhydrite and sulfide mineral(s) are also present in moderate abundance.

- The general diagenetic sequence for these samples, based on SEM analysis, is (1) dolomitization, (2) dissolution, (3) dolomite cementation, (4) fracturing, (5) quartz cementation, (6) calcite cementation, (7) clay precipitation, (8) anhydrite cementation, (9) pyrobitumen emplacement, and (10) sulfide precipitation.

Epifluorescence (EF): Epifluorescence petrography makes it possible to clearly identify grain types and shapes, within both limestone and dolomite reservoir intervals in Leadville thin sections from cores in the study. In particular, identification of peloids, skeletal grain types, and

coated grains is easy in rocks where these grains have been poorly preserved, partially leached, or completely dolomitized. Depositional textures that are frequently occult or poorly preserved can often be clearly distinguished using blue-light EF microscopy.

- In many limestones and finely crystalline dolomites of the Leadville reservoir at Lisbon field, the differences between muddy and calcarenitic fabrics can only be clearly appreciated with fluorescence lighting.

- Epifluorescence petrography clearly and rapidly images pore spaces that cannot otherwise be seen in standard viewing under transmitted polarized lighting. In addition, the cross-sectional size and shape of pores are easy to determine.

- Much of the Leadville porosity is very heterogeneous and poorly connected as viewed under EF. In particular, intercrystalline porosity within some of the reservoir in Lisbon field can be resolved much more clearly than with transmitted polarized lighting. The EF examination helps see the origin of most types of porosity. Transmitted polarized lighting does not image intercrystalline porosity in carbonate samples very well, even though blue-dyed epoxy can be impregnated into even very small pores. In addition, opaque bitumen linings prevent light from passing through some of the pores to the observer. Without the aid of the EF view, the amount of visible open pore space would be underestimated in the plane-light image.

- Where dolomitization has occurred, EF petrography often shows the crystal size, shape, and zonation far better than transmitted plane or polarized lighting. This information is often very useful when considering the origin and timing of dolomitization as well as evaluating the quality of the pore system within the dolomite.

- Permeability differences within these dolomite and limestone samples are also easy to image because of the differential oil saturations between the tighter areas and the more permeable lithologies. Low-permeability carbonates from this study area show bright yellow fluorescence due to trapped live oil that is retained within tighter parts of the reservoir system. More permeable rocks show red fluorescence due to the epoxy fluorescence where oil has almost completely drained from the better quality portions of the reservoir.

Cathodoluminescence (CL): Cathodoluminescence imaging of samples nicely complements the types of information derived from EF of carbonate thin sections. Cathodoluminescence also displays original depositional textures and the outlines of original carbonate grains and distinctly images pore spaces. This information is often very useful when considering the origin and timing of dolomitization as well as evaluating the quality of the pore system within the dolomite.

- Cathodoluminescence shows a wide range of Leadville crystal size and growth habits within the dull red luminescing, matrix-replacing dolomite. The vast majority of the dolomite within areas of fabric-selective dolomitization is a deep or intense red color. Between many of the grains, there is a lighter red luminescence where early cements

have been dolomitized. Some of the coarser dolomite crystals appear to have an overgrowth of brighter red luminescent material.

- The amount of open porosity under CL is considerably greater than that visible under plane-light microscopy. Between other grains are interparticle pores that are still open. In a few areas, these early pores have been solution-enlarged and lined with a later generation of coarse, rhombic dolomite.

- Examination of saddle dolomites in the Leadville can provide more information about these late, elevated-temperature (often hydrothermal) mineral phases. For instance, saddle dolomites show nice growth banding. These saddle dolomites display dull, red luminescence in their core areas and slightly bright, orange-red luminescence toward their rim areas. In addition, CL makes it possible to see the growth bands in these coarse dolomite crystals due to slight luminescence differences between each growth zone.

- Cathodoluminescence imaging shows that the contact between the transported material related to karstification and the limestone country rock can be sharp, irregular, and corroded.

Fluid inclusions: During crystal growth, imperfections may trap fluids present in the environment at that time. Later mineral precipitation and deformation, such as development of fractures, can create additional crystal imperfections that may also trap fluids. Fluid inclusions provide pressure, volume, and temperature information about the conditions when the crystal precipitated. The fluids in the inclusion may be connate water, oil, or a sample of the mineralizing fluid.

- The fluid inclusion and mineral relationships suggest the following diagenetic sequence of events for the Lisbon Leadville reservoir: (1) dolomite precipitation, (2) anhydrite deposition, (3) anhydrite dissolution and quartz precipitation, (4) dolomite dissolution and late calcite precipitation, (5) trapping of a mobile oil phase, and (6) formation of bitumen.

- Aqueous fluid inclusions in early calcite, which typically forms coarse-grained crystals, display a range of liquid to vapor ratios suggesting they have necked. Primary oil inclusions studied in one calcite crystal from the Lisbon No. D-616 well, however, display consistent liquid to vapor ratios. These oil inclusions yielded homogenization temperatures ranging from 48 to 70^{o}C (118-158^{o}F). These temperatures represent the minimum temperature of oil formation, not of calcite deposition. The oil was generated in place by maturation of organic material. Both the oil inclusions and the common presence of two-phase, necked aqueous inclusions imply trapping at elevated temperatures. It is suggested trapping occurred when the original calcite recrystallized during burial.

- Fluid inclusions in dolomite have reequilibrated (stretched, necked, refilled) since trapping. The common presence of single-phase aqueous inclusions suggests that the

fine-grained dolomite and cores of saddle dolomite were deposited at temperatures less than about 50°C (<~122 °F).

- Coarse-grained quartz crystals containing solid inclusions of anhydrite are found at a depth of 8356 feet in the Lisbon No. D-616 well. Homogenization temperatures of primary inclusions range from 120 to 130°C (~248-266°F). The presence of gas-rich inclusions in the quartz suggests these temperatures are close to the true trapping temperatures and possibly maximum burial temperatures.

- The low ice-melting temperatures of quartz and calcite-hosted inclusions from the Lisbon No. D-616 well, suggest chemically complex Ca-Mg-bearing brines associated with evaporite deposits were responsible for mineral deposition. Calcite from the Lisbon NW USA No. B-63 well trapped fluids with lower salinities.

- Oil trapped in early calcite as primary inclusions, as secondary inclusions in calcite of undetermined age, and as "primary" inclusions in recrystallized portions of saddle dolomite fluoresces with a bluish green color, suggesting an API gravity of 35 to 40 °. Homogenization temperatures of primary inclusions in early calcite and saddle dolomite are similar and range from 48 to 70°C (118-158 °F). The oil inclusions trapped in the white, recrystallized and inclusion-poor saddle dolomite indicate the temperature was at least 70°C (158 °F) during oil deposition and recrystallization. Oil trapped in the saddle dolomite must represent oil that was mobile at this time.

- Oil deposited in healed fractures within late, pore-filling calcite has similar fluorescence as the primary inclusions but lower homogenization temperatures of about 40°C (~104 °F). The lower temperatures of the secondary oil inclusions allow the possibility that the temperatures were decreasing, perhaps due to unroofing, prior to bitumen formation.

- It is possible live oil was preserved in the calcite and dolomite, but not in the main fractures, which now contain bitumen because the oil was not degassed.

Isotopic analysis: Stable isotope geochemistry has been used in recent years to provide insights into the chemical differences between preserved remnants of depositional components and the various diagenetic events in carbonate rocks, as recognized from core examination and thin section petrography. There are broad fields of carbon and oxygen isotope compositions for various carbonate rock settings. Strontium isotope analysis is used most frequently as an age-dating tool in marine carbonates.

- Stable carbon and oxygen isotope data indicate that all Lisbon Leadville dolomites were likely associated with brines whose composition was enriched in ^{18}O compared with late Mississippian seawater (several per mil heavier than normal seawater).

- Stable oxygen isotope analyses of the Leadville replacement dolomites indicate that temperatures of precipitation ranged from about 60 to 90°C (~140-194 °F). Saddle dolomite cements were precipitated at temperatures greater that 90°C (>194 °F).

- High Sr isotopic ratios for late burial diagenetic mineral phases at Lisbon field indicate contributions by waters enriched in ^{87}Sr that were derived from either granitic Precambrian basement rocks or the Devonian McCracken Sandstone.

Burial history and possible heat sources: We propose a model with thermal convection cells bounded by basement-rooted faults to transfer heat and fluids from possible crystalline basement, Pennsylvanian evaporites, and Oligocene igneous complexes.

- Early Tertiary reactivation of basement-involved, high-angle normal faults associated with Precambrian tectonics may have allowed hot, deep-seated fluids from the granitic basement or the McCracken Sandstone to communicate upwards with the Leadville carbonate section. Brines from evaporites in the Pennsylvanian Paradox Formation may have also entered the Leadville along the large fault bounding the northeast flank of the field.

- Burial history and temperature profiles for the Leadville at Lisbon field provide some guidance as to when important diagenetic and porosity-forming events occurred. Porous replacement dolomites probably formed during the early and middle portions of the burial history at Lisbon field.

- Inferred elevated temperature spikes during maximum burial, late Laramide faulting/uplift, and Oligocene igneous activity may account for the high temperatures responsible for quartz precipitation, sulfide mineralization, pyrobitumen formation, late dissolution of carbonates, and late saddle dolomite cements.

- We recommend that any future evaluation of a Leadville Limestone prospect include stable carbon and oxygen isotope analysis of diagenetic components, strontium isotope analysis for tracing the origin of fluids responsible for different diagenetic events, and production of burial history and temperature profiles to help determine when the diagenetic events occurred.

Exploration Techniques for the Mississippian Leadville Limestone Play

Exploring the Leadville Limestone has been high risk, with less than a 10% chance of success based on the drilling history of the region. New prospect definition often requires expensive, 3D seismic acquisition, at times in environmentally sensitive areas. These facts make exploring difficult for independents that have limited funds available to try new, unproven techniques that might increase the chance of successfully discovering oil. Using surface geochemical surveys and regional oil-show data to identify potential oil-prone areas first, will reduce the risk taken by an independent producer in looking for Leadville oil. These techniques will help independents to recognize or eliminate areas and exploration targets prior to spending significant financial resources on seismic data acquisition and potential environmental litigation, and therefore increase the chance of successfully finding new economic accumulations of Leadville oil.

Surface Geochemical Surveys in the Lisbon and Lightning Draw Southeast Field Areas

Surface geochemical surveys help identify areas of poorly drained or by-passed oil in other basins. Lisbon field was ideal for a surface geochemical survey because proven hydrocarbons underlie the area, sample sites are relatively easily accessible, and the surface geology is similar to the structure of the field. To the southwest, the recently discovered Lightning Draw Southeast (LDSE) field has similar geology to Lisbon field, both in terms of Leadville reservoir lithology, structure, and gas composition. It consists of two wells, producing primarily gas and condensate, along with barren dry wells off structure. However, the field is still near original reservoir pressure and therefore hydrocarbon microseepage to the surface may be more significant than at Lisbon field. Proving the success of relatively low-cost geochemical surveys at Lisbon and LDSE field allows independent operators to reduce risks and minimize impacts on environmentally sensitive areas while exploring for Leadville targets.

The geochemical survey consisted of collecting shallow soil samples at 1500-foot intervals (500 m) on a 16-square-mile (42 km^2) rectangular grid over and around the Lisbon field to map the spatial distribution of surface hydrocarbon anomalies. The sampling grid extends beyond the proven limits of Lisbon field to establish background readings. The area chosen sufficiently covers the oil leg, gas cap, and water leg/background barren areas. In addition, samples were collected over gas, oil, and dry wells for analogue matching purposes and to refine the discriminant model for Lisbon field. Samples were collected LDSE field along northwest-southeast and northeast-southwest grid lines and around both the producing wells and barren dry wells. Free-gas samples were also collected over LDSE field and known non-productive areas off the structure. Finally, joints in the Jurassic Navajo and Entrada Sandstones may provide pathways for hydrocarbon microseepage to the surface. Therefore, soil, sand, bryophytes, and lichen samples were collected along joints for geochemical analyses.

The soil, sand, bryophytes, and lichen samples were placed and stored in airtight, Teflon-sealed glass soil jars to prevent hydrocarbon contamination during transport. Samples were dried and sieved, and aliquots weighed out for geochemical analyses for 40 hydrocarbon compounds in the C_1 to C_{12} range, 53 major and trace elements, seven anion species, and for synchronous scanned fluorescence analyses. Free-gas samples were stored in 1-liter Tedlar bags for hydrocarbon and fixed gas analyses and/or in lead-lined CO_2 cartridges for helium analysis.

The conclusion drawn from this evaluation of surface geochemical methods over the Lisbon and LDSE fields is that certain methods are effective as non-invasive, pre-screening and follow-up tools in the exploration for Leadville hydrocarbon reservoirs. More specific conclusions are as follows:

1. Light alkane (C_1 to C_6) and heavy (C_{24} to C_{36}) aromatic hydrocarbons are the most important variables in surface soils and outcrop fracture-fill lichen and soils for distinguishing the surface expression of productive and non-productive areas over Mississippian Leadville reservoirs.

2. Discriminant functions developed for Lisbon and LDSE fields predict and cross-validate each other adding confidence to the models.

3. Microseepage over the Lisbon gas cap is better distinguished from the water leg than is the oil leg, probably because of the better production from the gas cap and therefore more intense microseepage.

4. Linear combinations of thermally desorbed hydrocarbons from outcrop fracture-fill lichen and soils better discriminate between the Lisbon gas cap, oil leg, and water leg.

5. Free-gas hydrocarbons, carbon dioxide, and hydrogen from Pennsylvannian Ismay and/or Mississippian Leadville Limestone reservoirs are anomalous over the LDSE field. Helium and carbon dioxide anomalies at the margin of the reservoir are probably sourced from Leadville.

6. Heavy metals (Hg, Pb, Cd, U, Mo, V, and Mn) are indirect indicators of hydrocarbon seepage over Lisbon and LDSE fields. The mercury and lead in anomalies over the fields are probably derived from oil that ascends faults and joints. Uranium anomalies over Lisbon, however, are derived from exposed mineralization in the Chinle Formation and old mine workings. Fluoride anomalies over LDSE field could reflect the ascent of brines with oil along an alluvium-covered northwest-trending fault. The origin of the widely dispersed arsenic anomalies at LDSE, which do not spatially correlate with the oil seep over the southeast part of the field is unknown.

Recommendations for future surface geochemical surveys for Leadville exploration in the Paradox Basin are:

1. Reconnaissance exploration should include the collection of surface soils (outcrop fracture-fill lichen and soils where applicable) for thermally desorbed and solvent-extractable hydrocarbons.

2. Discriminant functions and factors derived in this study should be used as a guideline for detecting microseepage related to Leadville reservoirs elsewhere in the Paradox Basin.

Anomalous areas identified in reconnaissance soil surveys should be followed up with the collection of deep free-gas samples for hydrocarbon, hydrogen, carbon dioxide, and helium analysis. Helium and carbon dioxide anomalies may be found at the margins of Leadville Limestone reservoirs.

Potential Oil-Prone Areas in the Paradox Fold and Fault Belt Based on Shows in Drill Cuttings Using Epifluorescence Microscopy Techniques

1. Epifluorescence petrography makes it possible to clearly identify hydrocarbon shows in Leadville cuttings selected for study. It is a non-destructive procedure that can be done using a petrographic microscope equipped with reflected light capabilities, mercury-vapor light, and appropriate filtering. Sample preparation is inexpensive and rapid.

2. Cuttings from 32 productive or dry exploratory wells penetrating the Leadville Limestone in the Utah part of the Paradox fold and fault belt were examined under a binocular microscope.

Over 900 samples of porous dolomite and some limestone were selected from various zones over the Leadville section for EF evaluation.

3. Epifluorescence allows one to observe the presence or absence of any soluble hydrocarbons, especially in high porosity dolomite. Samples displaying fluorescence represent areas where hydrocarbons may have migrated or accumulated. If no fluorescence is observed in porous dolomites, the samples are also good representatives of areas where hydrocarbons have not migrated or accumulated.

4. A qualitative visual "rating" scale (a range and average) based on EF evaluation was applied to the group of cuttings from each depth in each well. The highest maximum and highest average EF reading from each well were plotted and mapped.

5. The maps show a regional southeast-northwest trend of relatively high EF for Leadville cuttings parallels the southwestern part of the Paradox fold and fault belt from Lisbon field northwest to west of the town of Green River. The northeastern part of the fold and fault belt shows a regional trend of low EF including a large area of essentially no EF centered around the town of Moab. As expected, productive Leadville wells have cuttings distinguished by generally higher EF ratings.

6. Hydrocarbon migration and alteration dolomitization was associated with regional northwest-trending faults and fracture zones, which created potential oil-prone areas along the southwest part of the fold and fault belt. Hydrocarbons may have migrated from organic-rich shales in the Pennsylvanian Paradox Formation where they are in contact with the Leadville Limestone along faults. Fluid inclusions indicate some hydrocarbons were generated in-place. Hydrothermal alteration associated with these faults and related fracture zones may have generated late, porous dolomite and thus produced diagenetic traps. Hydrocarbons flushed to the southwest by hydrodynamic processes may also account for the lack of significant EF in the northeast parts of the fold and fault belt. In addition, these EF trends could be related to facies or karst development in the Leadville.

7. Exploration efforts should be concentrated in suggested oil-prone areas along the southwest part of the Paradox fold and fault belt.

Regional Studies of the Mississippian Leadville Limestone

Regional facies were determined by evaluating cores and correlating geophysical well logs throughout the Paradox Basin to target areas for Leadville exploration. These facies were compared to both outcrop and modern analogs. The regional brine chemistries and hydrodynamic pressure regimes for the Paleozoic formations of the Paradox Basin provide clues to potential Leadville oil migration directions; very little had been published previously on these topics for the Paradox Basin. These studies will further assist independent producers and explorers who have limited financial and personnel resources to conduct such studies on their own.

Regional Correlation and Facies of the Leadville Limestone in the Paradox Basin and Neighboring Area

1. Leadville facies include open marine (crinoidal banks or oolitic shoals and Waulsortian-type buildups), middle shelf, and restricted marine (peloidal muds).

2. The Leadville Limestone is more than 700 feet (200 m) to less than 200 feet (60 m) thick, and thins to the southeast across the Paradox Basin due to both depositional onlap and erosional wedging. It is bounded above and below by unconformities within the basin.

3. The Leadville is mostly pure limestone with some reflux dolomitization implying arid conditions on a shallow shelf.

4. Subaerial erosion resulted in lateritic regolith formed over most of the Leadville Limestone in the Paradox Basin. Brecciation and sediment-filled cavities, related to karstification of the exposed Leadville, are relatively common throughout the upper third of the formation.

5. Regionally, an intraformational disconformity divides the Leadville Limestone into informal upper and lower members.

6. Early movement on northwest-trending faults may have affected deposition of the Leadville Limestone.

7. Hydrocarbon production and shows are primarily along the northwest-trending faults in the Paradox fold and fault belt. Stratigraphic traps developed by the erosional regolith and Waulsortian mounds, or other carbonate buildups, may exist in the Leadville southwest of the fold and fault belt. Diagenetic traps resulting primarily from late (hydrothermal) dolomitization, represent untapped but difficult to identify drilling targets in the fold and fault belt.

Outcrop Reservoir Analogs for the Mississippian Leadville Limestone: South Flank of the Uinta Mountains, Utah

1. Utah is fortunate that representative outcrop analogs (depositional or diagenetic) for the Leadville Limestone play are present near the Paradox Basin. Production-scale analogs provide an excellent view, often in 3D, of reservoir-facies characteristics, geometry, distribution, diagenetic characteristics, and nature of boundaries, all of which contribute to the overall heterogeneity of reservoir rocks.

2. Although not exposed in southeastern Utah, Mississippian rocks equivalent to the Leadville Limestone outcrop in the northern and western parts of the state. These formations include the Madison, Gardison, Deseret, Humbug Formations, and have generally the same characteristics as the Leadville.

3. The Madison and equivalent formations were deposited in a shallow, warm-water, relatively high-energy, epeiric sea that extensively covered a large part of the craton. Depositional

environments include tidal-flat mud; deeper subtidal burrowed pellet muds; shallow subtidal bay; beach/foreshore; oolitic shoal; storm-dominated, outer-shelf, crinoid shoals; low-energy, open-marine, muddy intershoal; low-energy, open-marine, outer shelf above storm wave base. All of the Madison Limestone depositional environments are also observed in Leadville cores from Lisbon field.

4. The Madison Limestone contains local zones of breccia due to either collapse or natural hydrofracturing. Breccia associated with sediment-filled collapsed cavities is relatively common. These cavities are related to paleokarstification of the Madison when exposed during Late Mississippian time. Brecciation caused by explosive natural hydrofracturing, created the same shattered-looking, pulverized rock identified in Lisbon cores. Possible breccia pipes may be related to past hydrothermal activity.

5. The basal Cambrian Tintic Quartzite or Lodore Sandstone were important contributors to the hydrothermal story. They served as aquifers supplying hot water to the hydrothermal system. Through the central part of the south flank of the Uinta Mountains, porous Cambrian sandstone is missing and the Mississippian lies unconformably on middle Neoproterozoic Red Pine Shale. No Madison hydrothermal breccia zones or pipes are found in the central part of the south flank leading credence to the concept that aquifers below in the Tintic and Lodore may be a required condition for past hydrothermal activity to have occurred. Thus, targeting Leadville Limestone areas for potential hydrothermal dolomite and enhanced reservoir quality due to hydrofracturing, may require an aquifer below as a necessary ingredient.

Modern Reservoir Analogs for the Mississippian Leadville Limestone: Southern Florida and the Bahamas

1. Environments of the Leadville Limestone have modern analogs in southern Florida-Bahamas region – a world class natural laboratory to study "tropical" carbonate depositional systems. This region represents a time horizon where one can observe carbonate deposition, the conditions (physical, biological, and chemical) which create various carbonate sediments, and the processes by which the deposits change.

2. The southern Florida-Bahamas region is a warm-water carbonate factory. The Leadville Limestone was most likely deposited in a warm-water carbonate factory during Mississippian time on an epeiric attached platform, that is, an extensive cratonic area covered by a shallow sea.

3. Although the organisms in warm-water carbonate settings today are different from those of the past due to organic evolution, the roles of sediment producer and modifier have remained largely unchanged through time. Warm marine water is also often supersaturated with respect to calcium carbonate which can be precipitated to form carbonate grains such as ooids, peloids, grapestone, and carbonate mud.

4. Southern Florida is an attached, rimmed carbonate platform. From northwest to southeast, the platform consists of mangrove swamps and supratidal flats (Everglades), an inner shelf (Florida Bay), inner and outer shelf margins, and a shallow slope into the Straits of Florida.

5. Florida Bay is triangular shaped due to barriers that restrict circulation. A variety of sedimentary environments are represented in Florida Bay as part of a transgressive record: (1) fresh-water pond, (2) coastal mangrove swamp, (3) broad, shallow bay basins ("lake"), (4) mud mounds, and (5) island. From our work on the Leadville Limestone, we recognize the shallow bay basins and mud mounds as modern analogs.

6. The southern Florida attached platform has a rimmed margin formed by the arcuate reef track band. Sedimentary environments include the seaward forereef, discontinuous outer barrier reef, and back reef consisting of a sand apron and lagoon (containing patch reefs and sand shoals). There are no barrier reefs known in the Leadville Limestone. However, from our work, we recognize the marine mud mounds, patch reefs, and sand shoals in the reef tract as modern analogs.

7. The Great Bahama Bank is an unattached, isolated, rimmed carbonate platform. From east to west, the Great Bahama Bank consists of Earth's third longest barrier reef, a narrow lagoon, Andros Island (exposed Pleistocene limestone) with modern carbonate tidal flats on the western side, the shelf lagoon, and oolitic shoals. The carbonate tidal flats are laterally extensive along strike and represent part of a shallowing upward cycle. From our work on the Leadville Limestone, we recognize ooid shoals and shelf lagoonal sedimentation as modern analogs. Paleocarbonate tidal flats are productive in Williston Basin fields and other carbonate reservoirs. Recognizing the modern characteristics of carbonate tidal flats in the Leadville Limestone may provide additional target areas for drilling.

Mississippian/Devonian and Pennsylvanian Brine Chemistry and Trends within the Paradox Basin, Utah

1. There is a systematic change in the chemistry of both the Mississippian/Devonian and Pennsylvanian brine systems from north to south through the Paradox Basin, and the associated counties.

2. The Pennsylvanian-system brines are more saline than the Mississippian/Devonian-system brines. Piper and Stiff diagrams show that the brines from both systems are predominantly sodium-rich in nature, with some samples containing greater percentages of calcium and to a lesser extent magnesium. The Piper and Stiff diagrams also show that both brine systems are high in chloride with some samples being high in sulfate content. Bicarbonate is very low in both brine systems.

3. Based on brine chemistry the direction of ground-water movement in the Mississippian/Devonian and Pennsylvanian systems is generally southwestward toward the topographically low outcrop areas along the Colorado River in Arizona.

Regional Middle Paleozoic Hydrodynamic Pressure Regime of the Paradox Basin, Utah and Colorado

1. Shut-in DST pressure data from petroleum exploration and development wells in the Paradox Basin were used to establish the major hydrodynamic trends, especially within the Mississippian (395 DSTs).

2. With the exception of the eastern edge of the basin (western flanks of the San Juan Mountains), there is a single pressure regime for the Mississippian, having a composite pressure gradient of 0.47 pounds per square inch/foot (10.6 kPa/m) over an elevation range of +4000 to -10,000 ft asl (1200 to -3000 m asl). This remarkably uniform pressure regime over an area of at least 100 by 100 miles (260 by 260 km) indicates relatively high permeability within the Mississippian.

3. The pressure gradient is about 10% above hydrostatic for fresh water, but is consistent with the density of relatively saline water having a total dissolved solids concentration of 100,000 to 150,000 mg/kg. The head is between 3800 and 4000 ft asl (1160 and 1200 m asl), and coincides with the elevation of the lower Green River and Cataract Canyon section of the Colorado River where they traverse the basin.

4. It appears that the Mississippian and older reservoirs across most of the Paradox Basin are in good hydrological communication with the Colorado River system, perhaps because they are within about 1000 feet (300 m) of the surface beneath Cataract Canyon. This large-scale hydrological connection between the surface and the Mississippian maybe a geologically recent occurrence.

5. Consideration of the rate of incision by the Colorado River system suggests that the Mississippian could have been hydrologically isolated and fully saturated several million years ago, and could have held significantly greater quantities of oil and gas. Some of this greater volume of oil could be preserved as the tar sand deposits (Tar Sand Triangle, White Canyon, and Ten Mile Wash), found along the western margin of the Paradox Basin, that may have been a larger pool trapped in what is now partially breached Monument upwarp.

REFERENCES

Ahr, W.M., 1989, Mississippian reef facies in the Southwest—a spectrum of variations in depositional style and reservoir characteristics: Ft. Worth Geological Society and Texas Christian University, Symposium on the Petroleum Geology of Mississippian Carbonates in North Central Texas, p. 1-19 (Ch-3, Ch-7).

Ake, J., Mahrer, K., O'Connell, D., and Block, L., 2005, Deep-injection and closely monitored induced seismicity at Paradox Valley, Colorado: Bulletin of the Seismological Society of America, v. 95, no. 2, p. 664-683 (Ch-11).

Al-Aasm, I.S., and White, T., 1995, Mississippian hydrothermal dolomitization of the upper Debolt Formation, Sikanni gas field, northeastern British Columbia [abs.]: Geological Association of Canada, Mineralogical Association of Canada, and Canadian Geophysical Union Joint Meeting, Program with Abstracts, v. 20, p. 1 (Ch-4).

Allan, J.R., and Wiggins, W.D., 1993, Dolomite reservoirs - geochemical techniques for evaluating origin and distribution: American Association of Petroleum Geologists, Continuing Education Course Note Series 36, 129 p. (Ch-4).

Allis, R.G., Bergfield, D., Moore, J.N., McClure, K., Morgan, C., Chidsey, T.C., Jr., Heath, J., and McPherson, B., 2005, Implications of results from CO_2 systems for long-term monitoring: Proceedings Volume, Fourth Annual Conference on Carbon Capture and Sequestration, May 2-5, 2005, Alexandria, VA, p. 1367-1388 (Ch-11).

Anderson, J.H., 1985, Depositional facies and carbonate diagenesis of the downslope reefs in the Nisku Formation (Upper Devonian) central Alberta, Canada: Austin, University of Texas, Ph.D. dissertation, 393 p. (Ch-4).

Anderson, J.H., and Machel, H.G., 1988, The Upper Devonian Niski reef trend in central Alberta, *in* Geldsetzer, H.H.J., James, N.P., Tebbutt, G.E., editors, Reefs, Canada and adjacent areas: Canadian Society of Petroleum Geologists Memoir 13, p. 391-398 (Ch-4).

Baars, D.L., 1966, Pre-Pennsylvanian paleotectonics—key to basin evolution and petroleum occurrences in the Paradox Basin, Utah and Colorado: American Association of Petroleum Geologists Bulletin, v. 50, no. 10, p. 2082-2111 (Ch-3, Ch-7).

Baer, J.L., and Rigby, J.K., 1978, Geology of the Crystal Geyser and environmental implications of its effluent, Grand County, Utah: Utah Geological and Mineral Survey, Utah Geology, v. 5, no. 2, p. 125-130 (Ch-11).

Ball, M.M., 1967, Carbonate sand bodies of Florida and the Bahamas: Journal of Sedimentary Petrology, v. 37, p. 556-591 (Ch-9).

Bammel, B.H., Chamberlain, C.P., and Birnie, R.W., 1994, Stable isotope evidence of vertical hydrocarbon microseepage, Little Buffalo Basin oil field: Association of Petroleum Geochemical Explorationists Bulletin, v. 10, p. 1-23 (Ch-5).

Barker, C.E., and Kopp, O.C., editors, 1991, Luminescence microscopy - quantitative and qualitative aspects: Society for Sedimentary Geology (SEPM) Short Course 25 Notes, p. 1-7 (Ch-4).

Bebout, D.G., and Loucks, R.G., 1984, Handbook for logging carbonate rocks: Bureau of Economic Geology, University of Texas at Austin, Handbook 5, 43 p. (Ch-3).

Blakey, R., and Ranney, W., 2008, Ancient landscapes of the Colorado Plateau: Grand Canyon, Grand Canyon Association, p. 21-27 (Ch-7).

Bodnar, R.J., 1993, Revised equation and table for determining the freezing-point depression of H_2O-NaCl solutions: Geochimica Cosmochimica Acta, v. 57, p. 683-684 (Ch-4).

Bosence, D.W.J., 1985, The morphology and ecology of a mound-building coralline alga (*Neogoniolithon strictum*) from the Florida Keys: Paleontology, v. 28, p. 189-206 (Ch-9).

Bosence, D.W.J., 1995, Anatomy of a Recent biodetrital mud-mound, Florida Bay, USA, *in* Monty, C.L.V., Bosence, D.W.J., Bridges, P.H., and Pratt, B.R., editors, Carbonate mud-mounds: their origin and evolution: International Association of Sedimentologists Special Publication 23, p. 475-493 (Ch-9).

Bosence, D.W.J., and Wilson, R.C.L., 2005, Carbonate depositional systems, *in* Coe, A.L., editor, The sedimentary record of sea-level change: New York, Cambridge University Press, p. 209-227 (Ch-9).

Brass, G.W., 1976, The variation of the marine $^{87}Sr/^{86}Sr$ ratio during Phanerozoic time - interpretation using a flux model: Geochimica et Cosmochimica Acta, v. 40, p. 721-730 (Ch-4).

Bredehoeft, J.D., 1965, The drill-stem test – the petroleum industry's deep-well pumping test: Ground Water, v. 3, p. 31-36 (Ch-11).

Breit, G.N. (compiler), no date, Produced waters database: U.S. Geological Survey: Online, <http://energy.cr.usgs.gov/prov/prodwat/>, accessed May 2003 (Ch 10).

Bruckschen, P., Onesmann, S. and Viezer, J., 1999, Isotope stratigraphy of the European Carboniferous - proxy signals for ocean chemistry, climate and tectonics: Chemical Geology, v. 161, p. 127-163 (Ch-4).

Budd, D.A., Hammes, U., and Ward, W.B., 2000, Cathodoluminescence in calcite cements - new insights on Pb and Zn sensitizing, Mn activation, and Fe quenching at low trace-element concentrations: Journal of Sedimentary Petrology, v. 70, p. 217-226 (Ch-4).

Burke, W.H., Denison, R.E., Heatherington, E.A., Koepnick, R.B., Nelson, H.F., and Otto, J.B., 1982, Variation of seawater $^{87}Sr/^{86}Sr$ throughout Phanerozoic time: Geology, v. 10, p. 516-519 (Ch-4).

Burruss, R.C., 1981, Hydrocarbon fluid inclusions in studies of sedimentary diagenesis, *in* Hollister, L.S., and Crawford, M.L., editors, Fluid inclusions - applications in petrology: Mineralogical Association of Canada Short Course Notes, v. 6, p. 138-156 (Ch-4).

Burruss, R.C., 1991, Practical aspects of fluorescent microscopy of petroleum fluid inclusions, *in* Barker, C.E., and Kopp, O.C., editors, Luminescence microscopy - quantitative and qualitative aspects: Society for Sedimentary Geology (SEPM) Short Course 25 Notes, p. 1-7 (Ch-4).

Burruss, R.C., Cercone, K.R., and Harris, P.M., 1986, Timing of hydrocarbon migration - evidenced from fluid inclusions in calcite cements, tectonics and burial history, *in* Schneidermann, Nahum, and Harris, P.M., editors, Carbonate cements: Society for Sedimentary Geology (SEPM) Special Publication 36, p. 277-289 (Ch-4)

Burtner, R.L., 1987, Origin and evolution of Weber and Tensleep Formation waters in the greater Green and Uinta-Piceance Basins, northern Rocky Mountains area, USA: Chemical Geology, v. 65, p. 255-282 (Ch-4).

Cander, H.S., Kauffman, J., Daniels, L.D., and Meyers, W.J., 1988, Regional dolomitization in the Burlington-Keokuk Formation (Mississippian), Illinois and Missouri - constraints from cathodoluminescent zonal stratigraphy, *in* Shukla, V., and Baker, P.A., editors, Sedimentology and geochemistry of dolostones: Society for Sedimentary Geology (SEPM) Special Publication No. 43, p. 129-144 (Ch-4).

Cather, M.E., Morrow, N.R., Brower, K.R., and Buckley, J.S., 1989a, Uses of epi-fluorescent microscopy in evaluation of Mesaverde tight gas sands [abs.]: American Association of Petroleum Geologists Bulletin, v. 73, p. 1150-1151 (Ch-4).

Cather, M.E., Morrow, N.R., and Klich, I., 1989b, Applications of fluorescent dye staining techniques to reservoir studies of tight gas sands, Mesaverde Group, southwestern Colorado [abs.]: American Association of Petroleum Geologists Bulletin, v. 73, p. 342 (Ch-4).

Cercone, K.R., and Pedone, V.A., 1987, Fluorescence (photoluminescence) of carbonate rocks - instrumental and analytical sources of observational error: Journal of Sedimentary Petrology, v. 57, p. 780-782 (Ch-4).

Chafin, D.T., 2002, Effect of the Paradox Valley Unit on the dissolved-solids load of the Dolores River near Bedrock, Colorado, 1988-2001: U.S. Geological Survey Water-Resources Investigations Report 02-4275, 6 p. (Ch-11).

Chenoweth, W.L., 1990, Lisbon Valley, Utah's premier uranium area, a summary of exploration and ore production: Utah Geological and Mineral Survey Open-File Report 188, 45 p. (Ch-5).

Chenoweth, W.L., 1996, The uranium industry in the Paradox Basin, *in* Huffman, A.C., Jr., Lund, W.R., and Godwin, L.H., editors, Geology and resources of the Paradox Basin: Utah Geological Association Publication 25, p. 95-108 (Ch-5).

Choquette, P.W., and Pray, L.C., 1970, Geologic nomenclature and classification of porosity in sedimentary carbonates: American Association of Petroleum Geologists Bulletin, v. 54, no. 2, p. 207-250 (Ch-4).

Clark, C.R., 1978, Lisbon, San Juan County, Utah, *in* Fassett, J.E., editor, Oil and gas fields of the Four Corners area: Four Corners Geological Society, v. II, p. 662-665 (Ch-2).

Coleman, D.D., Meents, W.F., Liu, Chao-Li, and Keough, R.A., 1977, Isotopic identification of leakage gas from underground storage reservoirs – a progress report: Illinois State Geological Survey, Illinois Petroleum No. 111, 10 p. (Ch-5).

Colorado Oil and Gas Conservation Commission, 2008, Colorado oil and gas information system (COGIS) - production data inquiry: Online, <oil-gas.state.co.us/cogis/ProductionSearch2.asp>, accessed May 25, 2008 (Ch-1).

Conel, J.E., and Alley, R.E., 1985, Lisbon Valley, Utah uranium test site report, *in* Abrams, M.J., Conel, J.E., Lang, H.R., and Paley, H.N., editors, The joint NASA Geosat test case project – final report: American Association of Petroleum Geologists Special Publication, pt. 2, v. 1, p. 8-1-8-158 (Ch-5).

Coniglio, M., Zheng, Q., and Carter, T.R., 2003, Dolomitization and recrystallization of Middle Silurian reefs and platformal carbonates of the Guelph Formation, Michigan Basin, southwestern Ontario: Bulletin of Canadian Petroleum Geology, v. 51, p. 177-199 (Ch-4).

Coumou, D., Driesner, T., Heinrich, A., 2008, The structure and dynamics of mid-ocean ridge hydrothermal system: Science Magazine, v. 321, p. 1825-1828 (Ch-8).

Dansereau, P., and Bourque, P.A., 2001, The Neigette breccia - remnant of the West Point reef tract in the Matapedia Valley area, and witness to Late Silurian synsedimentary faulting, Gaspe Belt, Northern Appalachians, Quebec: Bulletin of Canadian Petroleum Geology, v. 49, p. 327-345 (Ch-4).

Davies, G.R., 2004, Hydrothermal (thermobaric) dolomite and leached limestone reservoirs – general principles, genetic connections, and economic significance in Canada [abs]: American Association of Petroleum Geologists Annual Convention, Official Program with Abstracts, v. 13, p. A32 (Ch-4).

Davies, G.R., and Smith, L.B., Jr., 2006, Structurally controlled hydrothermal alteration of

carbonate reservoirs – an overview: American Association of Petroleum Geologists Bulletin (Special Issue: Hydrothermally altered carbonate reservoirs), v. 90, no. 11, p. 1641-1690 (Ch-4).

Davis, S.W., Davis, M.E., Lucchitta, I., Hanks, T.C., Finkel, R.C., and Caffee, M., 2001, Erosional history of the Colorado River through Glen and Grand Canyons, *in* Young, R.A., and Spamer, E.E., editors, Colorado River origin and evolution—proceedings of a symposium held at Grand Canyon National Park in June, 2000: Grand Canyon Association, p. 135-139 (Ch-11).

Denison, R.E., Koepnick, R.B., Burke, W.H., Heatherington, E.A., and Fletcher, A., 1994, Construction of the Mississippian, Pennsylvanian and Permian seawater $^{87}Sr/^{86}Sr$ curve: Chemical Geology, v. 112, p. 145-167 (Ch-4).

DePaolo, D.J., 1986, Detailed record of the Neogene strontium isotopic evolution of seawater from DSDP site 5908: Geology, v. 14, p. 103-106 (Ch-4).

DePaolo, D.J., and Finger, K.L., 1991, High-resolution strontium-isotope stratigraphy and biostratigraphy of the Miocene Monterey Formation, central California: Geological Society of America Bulletin, v. 103, p. 112-124 (Ch-4).

DePaolo, D.J., and Ingram, B., 1985, High-resolution stratigraphy with strontium isotopes: Science, v. 227, p. 938-941 (Ch-4).

Dockal, J.A., 1980, Petrology and sedimentary facies of Redwall Limestone (Mississippian) of Uinta Mountains, Utah and Colorado: Iowa City, Iowa State University, Ph.D. dissertation, 423 p. (Ch-8).

Doelling, H.H., 2000, Geology of Arches National Park, Grand County, Utah, *in* Sprinkel, D.A., Chidsey, T.C., Jr., and Anderson, P.B., editors, Geology of Utah's parks and monuments: Utah Geological Association Publication 28, p. 11-36 (Ch-1).

Doelling, H.H., 2005, Geologic map of the La Sal 30' x 60' quadrangle, San Juan, Wayne, and Garfield Counties, Utah, and Montrose and San Miguel Counties, Colorado: Utah Geological Survey Map M-205DM, 2 plates, scale 1:100,000 (Ch-5).

Dorobek, S.L., Read, J.F., Niemann, J.M., Pong, T.C., and Haralick, R.M., 1987, Image analysis of cathodoluminescence-zoned calcite cements: Journal of Sedimentary Petrology, v. 57, p. 766-770 (Ch-4).

Dravis, J.J., 1988, Deep-burial microporosity in Upper Jurassic Haynesville oolitic grainstones, East Texas: Sedimentary Geology, v. 63, p. 325-341 (Ch-4).

Dravis, J.J., 1991, Carbonate petrography – update on new techniques and applications: Journal of Sedimentary Petrology, v. 61, p. 626-628 (Ch-4).

Dravis, J.J., 1992, Burial dissolution in limestones and dolomites – criteria for recognition and discussion of controls - a case study approach (Pt. 1: Upper Jurassic Haynesville limestones, East Texas; Pt. 2: Devonian Upper Elk Point dolomites, western Canada): American Association of Petroleum Geologists Bulletin/Canadian Society of Petroleum Geologists Short Course Notes, Subsurface Dissolution Porosity in Carbonates (Ch-4).

Dravis, J.J., and Yurewicz, D.A., 1985, Enhanced carbonate petrography using fluorescence microscopy: Journal of Sedimentary Petrology, v. 55, p. 795-804 (Ch-4).

Duchscherer, W., 1984, Geochemical hydrocarbon prospecting, with case histories: Tulsa, Oklahoma, PennWell Publishing, 196 p. (Ch-5).

Duchscherer, W., 1986, Delta carbonate hydrocarbon prospecting, *in* Davidson, M.J., editor, Unconventional methods in exploration for petroleum and natural gas, symposium IV: Dallas, Southern Methodist University Press, p. 173-182 (Ch-5).

Dunham, R.J., 1962, Classification of carbonate rocks according to depositional texture, *in* Ham, W.E., editor, Classification of carbonate rocks: American Association of Petroleum Geologists Memoir 1, p. 108-121 (Ch-3, Ch-4).

Eby, D.E., and Hager, R.C., 1986, Fluorescence petrology of San Andres dolomites – H.O. Mahoney lease, Wasson field, Yoakum County, Texas: Permian Basin Section, Society for Sedimentary Geology (SEPM) Publication 86-26, p. 37-38 (Ch-4).

Elderfield, H., 1986, Strontium isotope stratigraphy, *in* Shackleton, N.J., editor, Boundaries and events in the Paleogene: Paleogeography, Paleoclimatology, Paleoecology, v. 57, p. 71-90 (Ch-4).

Embry, A.R., and Klovan, J.E., 1971, A Late Devonian reef tract on northeastern Banks Island, Northwest Territories: Canadian Petroleum Geologists Bulletin, v. 19, p. 730-781 (Ch-3, Ch-4).

Enos, P., 1977, Holocene sediment accumulations of the south Florida shelf margin, *in* Enos, P, and Perkins, R.D., editors, Quaternary sedimentation of South Florida: Geological Society of America Memoir 147, p. 1-130 (Ch-9).

Enos, P., and Perkins, R.D., 1979, Evolution of Florida Bay from island stratigraphy: Geological Society of America Bulletin, Part I, v. 90, p. 59-83 (Ch-9).

Fairchild, I.J., 1983, Chemical studies of cathodoluminescence of natural dolomites and calcites: Sedimentology, v. 30, p. 572-583 (Ch-4).

Faure, G., 1977, Principles of isotope geology: New York, John Wiley and Sons, 464 p. (Ch-4).

Faure, G., and Powell, J.L., 1972, Strontium isotope geology: Berlin, Springer Verlag, 188 p. (Ch-4).

Filippelli, G.M., and DeLaney, M.L., 1992, Quantifying cathodoluminescent intensity with an on-line camera and exposure meter: Journal of Sedimentary Petrology, v. 62, p. 724-725 (Ch-4).

Folk, R.L., 1987, Detection of organic matter in thin sections of carbonate rocks using a white card: Sedimentary Geology, v. 54, p. 193-200 (Ch-4).

Fouret, K.L., 1982, Depositional and diagnetic environment of the Mississippian Leadville Formation at Lisbon field, Utah: College Station, Texas A&M University, M.S. thesis, 119 p. (Ch-3).

Fouret, K.L., 1996, Depositional and diagnetic environment of the Mississippian Leadville Limestone at Lisbon field, Utah, *in* Huffman, A.C., Jr., Lund, W.R., and Godwin, L.H., editors, Geology and resources of the Paradox Basin: Utah Geological Association Publication 25, p. 129-138 (Ch-3, Ch-7).

Frahme, C.W., and Vaughn, E.B., 1983, Paleozoic geology and seismic stratigraphy of the northern Uncompahgre front, Grand County, Utah, *in* Lowell, J.D., editor, Rocky Mountain foreland basins and uplifts: Rocky Mountain Association of Geologists Guidebook, p. 201-211 (Ch-1).

Frank, J.R., Carpenter, A.B., and Oglesby, T.W., 1982, Cathodoluminescence and composition of calcite cement in Taum Sauk Limestone (Upper Cambrian), southeast Missouri: Journal of Sedimentary Petrology, v. 52, p. 631-638 (Ch-4).

Frank, T.D., Lohmann, K.C., and Meyers, W.J., 1996, Chemostratigraphic significance of cathodoluminescence zoning in syntaxial cement - Mississippian Lake Valley Formation, New Mexico: Sedimentary Geology, v. 105, p. 29-50 (Ch-4).

Gardner, K.L., 1980, Impregnation technique using colored epoxy to define porosity in petrographic thin sections: Canadian Journal of Earth Sciences, v. 17, p. 1104-1107 (Ch-4).

Gerling, C.R., 1983, McElmo Dome Leadville carbon dioxide field, Colorado, *in* Fassett, J.E., editor, Oil and gas fields of the Four Corners area: Four Corners Geological Society, v. III, p. 735-739 (Ch-11).

Gies, R.M., 1987, An improved method for viewing micropore systems in rocks with the polarizing microscope: Society of Petroleum Engineers Formation Evaluation, v. 2, p. 209-214 (Ch-4).

Ginsburg, R.N., 1956, Environmental relationships of grain size and constituent particles in some south Florida carbonate sediments: American Association of Petroleum Geologists Bulletin, v. 40, p. 2384-2427 (Ch-9).

Goldstein, R.H., and Reynolds, T.J., 1994, Systematics of fluid inclusions in diagenetic minerals: Society for Sedimentary Geology (SEPM) Short Course 31, 199 p. (Ch-4).

Grammer, M.G., Harris, P.M., and Eberli, G.P., 2001, Carbonate platforms – exploration- and production-scale insight from modern analogs in the Bahamas: The Leading Edge, March 2001, p. 252-261 (Ch-9).

Gregg, J.M., and Karakus, M., 1991, A technique for successive cathodoluminescence and reflected light microscopy: Journal of Sedimentary Petrology, v. 61, p. 613-635 (Ch-4).

Guihaumou, N., Szydlowskii, N., and Padier, B., 1990, Characterization of hydrocarbon fluid inclusions by infra-red and fluorescence microspectrometry: Mineralogical Magazine, v. 54, p. 311-324 (Ch-4).

Gwynn, J.W., 1995, Resistivities and chemical analyses of selected oil and gas field, water well, and spring waters, Utah: Utah Geological Survey Circular 87, 142 p. (Ch 10).

Hahn, G.A., and Thorson, J.P., 2006, Geology of the Lisbon Valley sandstone-hosted disseminated copper deposits, San Juan County, Utah, *in* Bon, R.L., Gloyn, R.W, and Park, G.M., editors, Mining districts of Utah: Utah Geological Association Publication 32, p. 511-533 (Ch-4).

Hamblin, W.K., and Rigby, J.K., 1968, Guidebook to the Colorado River, Part 1 – Lee's Ferry to Phantom Ranch in Grand Canyon National Park (Studies for Students No. 4): Brigham Young University Geology Studies, v. 15, pt. 5, 84 p. (Ch-8).

Hanks, T.C., Lucchitta, I., Davis, S.W., Davis, M.E., Finkel, R.C., Lefton, S.A., and Garvin, C.D., 2001, The Colorado River and the age of Glen Canyon, *in* Young, R.A., and Spamer, E.E., editors, Colorado River origin and evolution—proceedings of a symposium held at Grand Canyon National Park in June, 2000: Grand Canyon Association, p. 129-133 (Ch-11).

Hanshaw, B.B., and Hill, G.A., 1969, Geochemistry and hydrodynamics of the Paradox Basin region, Utah, Colorado, and New Mexico, *in* Angino, E.E., and Billings, G.K., editors, Geochemistry of subsurface brines: Chemical Geology, v. 4, no. 1/2, p. 263-294 (Ch 10, Ch-11).

Hardie, L.A. and Shinn, E.A., 1986, Carbonate Depositional Environments, part 3 – tidal flats: Colorado School of Mines Quarterly, v. 81, p. 1-74 Ch-9.

Harr, C.L., 1996, Paradox oil and gas potential of the Ute Mountain Ute Indian Reservation, *in* Huffman, A.C., Jr., Lund, W.R., and Godwin, L.H., editors, Geology of the Paradox Basin: Utah Geological Association Publication 25, p. 13-28 (Ch-1).

Harry, D.L., and Mickus, K.L., 1998, Gravity constraints on lithospheric flexure and the structure of the late Paleozoic Ouachita orogen in Arkansas and Oklahoma, south-central North America: Tectonics, v. 17, no. 2, p. 187-202 (Ch-1).

Heath, J.E., 2004, Hydrogeochemical characterization of leaking carbon dioxide-charged fault zones in east-central Utah: Logan, Utah State University, M.S. thesis, 175 p. (Ch-11).

Hemming, N.G., Meyers, W.J., and Grams, J.C., 1989, Cathodoluminescence in diagenetic calcites - the roles of Fe and Mn as deduced from electron probe and spectrophotometric measurements: Journal of Sedimentary Petrology, v. 59, p. 404-411 (Ch-4).

Herbert, C.F., 1984, Geochemical prospecting for oil and gas using hydrocarbon fluorescence techniques, *in* Davidson, M.J., Gottlieb, B.M., and Price, E., editors., Unconventional methods in exploration for petroleum and natural gas, symposium III: Dallas, Southern Methodist University Press, p. 40-58 (Ch-5).

Hintze, L.F., 1993, Geologic history of Utah: Brigham Young University Geology Studies Special Publication 7, 202 p. (Ch-1, Ch-8, Ch-11).

Hintze, L.F., Willis, G.C., Laes, D.Y.M., Sprinkel, D.A., and Brown, K.D., 2000, Digital geologic map of Utah: Utah Geological Survey Map 179DM, scale 1:500,000 (Ch-1, Ch-5, Ch-8).

Horvitz, L., 1985, Geochemical exploration for petroleum: Science, v. 229, p. 821-827 (Ch-5).

Howells, Lewis, 1990, Base of moderately saline ground water in San Juan County, Utah: Utah Department of Natural Resources Technical Publication 94, 35 p. (Ch 10).

Huntoon, P.W., 1979, The occurrence of ground water in the Canyonlands area of Utah, with emphasis on water in the Permian section, *in* Baars, D.L., editor, Permianland: Four Corners Geological Society Guidebook, 9th Annual Field Conference, p. 39-46 (Ch 10).

James, N.P., and Ginsburg, R.N., 1979, The seaward margin of Belize barrier and atoll reefs: International Association of Sedimentologists Special Publication 3, 191 p. (Ch-4).

Johnson, C.F., 1970, Top of structure of the Leadville Limestone, Lisbon field: unpublished map, Union Oil Company of California files (Ch-2, Ch-4, Ch-5).

Kinney, D.M., 1955, Geology of the Uinta River-Brush Creek area, Duchesne and Uintah Counties, Utah: U.S. Geological Survey Bulletin 1007, 185 p. (Ch-8).

Kirby, K.C., and Tinker, S.W., 1992, The Keg River/Winnipegosis petroleum system in northeast Alberta [abs.]: American Association of Petroleum Geologists Annual Convention, Official Program with Abstracts, v. 1, p. A66 (Ch-4).

Kirby, S., 2008, Geologic and hydrologic characterization of the Dakota-Burro Canyon aquifer near Blanding, San Juan County, Utah: Utah Geological Survey Special Study 123, 53 p. (Ch-11).

Kitcho, C.H., 1981, Characteristics of surface faults in the Paradox Basin, *in* Wiegnand, D.L., editor, Geology of the Paradox Basin: Rocky Mountain Association of Geologists Guidebook, p. 1-21 (Ch-1).

Klusman, R.W., 1993, Soil gas and related methods for natural resource exploration: Chichester, John Wiley & Sons, 483 p. (Ch-5).

Klusman, R.W., Mahyoub, A., and Abu-Ali, M.A., 1992, The potential use of biogeochemistry in the detection of petroleum microseepage: American Association of Petroleum Geologists Bulletin, v. 76, p. 851-863 (Ch-5).

Kluth, C.F., 1986, Plate tectonics of the Ancestral Rocky Mountains, *in* Peterson, J.A., editor, Paleotectonics and sedimentation in the Rocky Mountain region, United States: American Association of Petroleum Geologists Memoir 41, p. 353-369 (Ch-1).

Kluth, C.F., and Coney, P.J., 1981, Plate tectonics of the Ancestral Rocky Mountains: Geology, v. 9, p. 10-15 (Ch-1).

LaFlamme, A.K., 1992, Replacement dolomitization in the Upper Devonian Leduc and Swan Hills Formations, Caroline area, Alberta, Canada [abs.]: American Association of Petroleum Geologists Annual Convention, Official Program with Abstracts, v. 1, p. A70 (Ch-4).

Lammers, D.A., 1991, Soil survey of Canyonlands area, Utah, parts of Grand and San Juan Counties: U.S. Department of Agriculture, Soil Conservation Service, 293 p., 57 sheets, general soil map, scale 1:443,520 (Ch-5).

Land, L.S., 1980, The isotopic and trace element geochemistry of dolomite - the state of the art, *in* Zenger, D.H., Dunham, J.B., and Ethington, R.L., editors, Concepts and models of dolomitization: Society for Sedimentary Geology (SEPM) Special Publication 28, p. 87-110 (Ch-4).

LaVoie, D., Chi G., and Fowler, M.G., 2001, The Lower Devonian Upper Gaspe Limestones in eastern Gaspe - carbonate diagenesis and reservoir potential: Bulletin of Canadian Petroleum Geology, v. 49, p. 346-365 (Ch-4).

LaVoie, D., and Morin, C., 2004, Hydrothermal dolomitization in the Lower Silurian Sayabee Formation in northern Gaspe – Matapedia (Quebec) - constraint on timing of porosity and regional significance for hydrothermal reservoirs: Bulletin of Canadian Petroleum Geology, v. 52, p. 256-269 (Ch-4).

Lees, A., and Miller, J., 1995, Waulsortian banks, *in* Monty, C.L.V., Bosencce, D.W.J., Bridges, P.H., and Pratt, B.R., editors, Carbonate mud-mounds – their origin and evolution: International Association of Sedimentologists Special Publication No. 23, p. 191-271 (Ch-3).

Lewis, R.Q., Sr., and Campbell, R.H., 1965, Geology and uranium deposits of Elk Ridge and vicinity, San Juan County, Utah: U.S. Geological Survey Professional Paper 474-B, 69 p., 2 plates, scale 1:62,500 (Ch-11).

MacDonald, R.W., and Davies, G.R., 1997, Revised Livingstone/Turner Valley to Mount Head stratigraphy; Mississippian of southwestern Alberta Foothills: Canadian Society of Petroleum Geologists/Society for Sedimentary Geology (SEPM) Convention Publication, p. 169-199 (Ch-4).

Machel, H.G., 2000, Application of cathodoluminescence to carbonate diagenesis, *in* Pagel, M., Barbin, V., Blanc, P., and Ohnenstetter, D., editors, Cathodoluminescence in geosciences: New York, Springer, p. 271-301 (Ch-4).

Machel, H.G., and Burton, E.A., 1991, Factors governing cathodoluminescence in calcite and dolomites and their implications for studies of carbonate diagenesis, *in* Barker, C.E., and Kopp, O.C., editors, Luminescence microscopy - quantitative and qualitative aspects: Society for Sedimentary Geology (SEPM) Short Course 25 Notes, p. 37-57 (Ch-4).

Marchetti, D.W., and Cerling, T.E., 2001, Bedrock incision rates for the Fremont River tributary of the Colorado River, 2001, *in* Young, R.A., and Spamer, E.E., editors, Colorado River origin and evolution—Proceedings of a symposium held at Grand Canyon National Park in June, 2000: Grand Canyon Association, p. 125-127 (Ch-11).

Marshall, D.J., 1988, Cathodoluminescence of geological materials: Winchester, Massachusetts, Allen and Unwin, 128 p. (Ch-4).

Marshall, D.J., 1991, Combined cathodoluminescence and energy dispersive spectroscopy, *in* Barker, C.E., and Kopp, O.C., editors, Luminescence microscopy - quantitative and qualitative aspects: Society for Sedimentary Geology (SEPM) Short Course 25 Notes, p. 27-36 (Ch-4).

McArthur, J.M., and Howarth, R.J., 2004, Strontium isotope stratigraphy, *in* Gradstein, F.M., Ogg, J.G., and Smith, A.G., editors, A geologic time scale 2004: Cambridge, Cambridge University Press, p. 96-105 (Ch-4).

McKee, E.D., 1969, Paleozoic rocks of the Grand Canyon, *in* Baars, D.L., editor, Geology and natural history of the Grand Canyon region: Four Corners Geological Society, 5th Field Conference, Powell Centennial River Expedition, p. 78-90 (Ch-8).

Merin, I.S., and Segal, D.B., 1989, Diagenetic alteration of Wingate Formation – possible indicators of hydrocarbon microseepage, Lisbon Valley, Utah: Journal of Geology, v. 97, p. 719-734 (Ch-5).

Meyers, W.J., 1974, Carbonate cement stratigraphy of the Lake Valley Formation (Mississippian), Sacramento Mountains, New Mexico: Journal of Sedimentary Petrology, v. 44, p. 837-861 (Ch-4).

Meyers, W.J., 1978, Carbonate cements - their regional distribution and interpretation in Mississippian limestones of southwestern New Mexico: Sedimentology, v. 25, p. 371-400 (Ch-4).

Meyers, W.J., 1991, Cement stratigraphy - an overview, *in* Barker, C.E., and Kopp, O.C., editors, Luminescence microscopy - quantitative and qualitative aspects: Society for Sedimentary Geology (SEPM) Short Course 25 Notes, p. 133-148 (Ch-4).

Miller, J., 1988, Cathodoluminescence microscopy, *in* Tucker, M., editor, Techniques in sedimentology: Oxford, Blackwell Publications, p. 174-190 (Ch-4).

Milliman, J.D., Freile, D., Steinen R.P., and Wilber, R.J., 1993, Great Bahama Bank aragonitic muds – mostly inorganically precipitated, mostly exported: Journal of Sedimentary Petrology, v. 63, p. 589-595 (Ch-9).

Mitchell, J.G. 1961, A detailed lithologic zonation of the Mississippian at Northwest Lisbon field, San Juan County, Utah, *in* Symposium on lower and middle Paleozoic rocks of Colorado: Rocky Mountain association of Geologists, 12th Field Conference, p. 175-184 (Ch-3, Ch-7).

Morgan, C.D., 1993, Mississippian Leadville Limestone, *in* Hjellming, C.A., editor, Atlas of major Rocky Mountain gas reservoirs: New Mexico Bureau of Mines and Mineral Resources, p. 94 (Ch-2, Ch-3).

Morrow, D.W., Cumming, G.L., and Aulstead, K.L., 1990, The gas-bearing Devonian Manetoe facies, Yukon and Northwest Territories: Geological Survey of Canada Bulletin, v. 400, 40 p. (Ch-4).

Nelson, P.H., 2002, Subsurface fluid pressures from drill-stem test, Uinta Basin, Utah: The Mountain Geologist, v. 39, no. 1, p. 17-26 (Ch-11).

Newell, N.D., Imbrie, J., Purdy, E.G., and Thurber, D.L., 1959, Organism communities and bottom facies, Great Bahama Bank: American Museum of Natural History Bulletin, v. 117, p. 183-228 (Ch-9).

Packard, J.J., Pellegrin, G.J., Al-Aasm, I.S., Samsson, I.M., and Gagnon, J., 1990, Diagenesis and dolomitization associated with hydrothermal karst in Famennian upper Wabamun ramp sediments, northwestern Alberta, *in* Bloy, G.R., and Hadley, M.G., editors, The

development of porosity in carbonate reservoirs: Canadian Society of Petroleum Geologists Short Course Notes, p. 9.1-9.27 (Ch-4).

Parker, J.W., and Roberts, J.W., 1963, Devonian and Mississippian stratigraphy of the central part of the Colorado Plateau: Four Corners Geological Society, 4th Field Conference Guidebook, p. 31-60 (Ch-1, Ch-7).

Pederson, J., Karlstrom, K., Sharp, W., and McIntosh, W., 2002, Differential incision of the Grand Canyon related to Quaternary faulting—constraints from U-series and Ar/Ar dating: Geology, v. 30, p. 739-742 (Ch-11).

Petroleum Information, 1984, Paradox Basin–unravelling the mystery: Petroleum Frontiers, v. 1, no. 4, p. 22 (Ch-1).

PI/Dwights Plus, 2008, IHS Energy/Welldata, v. 18, issue 5 (Ch-11).

Pogorski, L.A., and Quirt, S.G., 1981, Helium enanometry in exploring for hydrocarbons— part 1, *in* Gottlieb, B.M., editor, Unconventional methods in exploration for petroleum and natural gas, symposium II: Dallas, Southern Methodist University Press, p. 124-135 (Ch-5).

Potter, R.W. II, Harington, P.A., Silliman, A.H., and Villenave, J.H., 1996, Significance of geochemical anomalies in hydrocarbon exploration, *in* Schumacher, D., and Abrams, M.A., editors, Hydrocarbon migration and its near-surface expression: American Association of Petroleum Geologists Memoir 66, p. 431-439 (Ch-5).

Price, L.C., 1986, A critical review and proposed working model of surface geochemical exploration, *in* Davidson, M.J., editor, Unconventional methods in exploration for petroleum and natural gas IV: Dallas, Southern Methodist University Press, p. 245-304 (Ch-5).

Price, L.C., 1993, Microbial-soil surveying— preliminary results and implications for surface geochemical exploration: Association of Petroleum Geochemical Explorationists Bulletin, v. 9, p. 81-129 (Ch-5).

Purdy, E.G., 1963, Recent calcium carbonate facies of the Great Bahama Bank: Journal of Geology, v. 72, p. 334-355; 479-497 (Ch-9).

Qing, H., and Mountjoy, E.W., 1994, Origin of dissolution vugs, caverns, and breccias in the Middle Devonian Presqu'ile barrier, host of Pine Point Mississippi Valley-type deposits: Economic Gelogy, v. 89, no. 4, p. 858-876 (Ch-4).

Radke, B.M., and Mathis, R.L., 1980, On the formation and occurrence of saddle dolomite: Journal of Sedimentary Petrology, v. 50, p. 1149-1168 (Ch-4).

Rankey, E.C., 2002, Spatial patterns of sediment accumulation on a Holocene carbonate tidal

flat, northwest Andros Island, Bahamas: Journal of Sedimentary Research, v. 72, p. 591-601 (Ch-9).

Rankey, E.C., and Morgan, J., 2002, Quantified rates of geomorphic change on a modern carbonate tidal flat, Bahamas: Geology, v. 30, no. 7, p. 583-586 (Ch-9).

Rankey, E.C., Enos, S., Steffen, K., and Druke, D., 2004, Lack of impact of Hurricane Michelle on tidal flats, Andros Island, Bahamas – integrated remote sensing and field observations: Journal of Sedimentary Research, v. 74, p. 654-661 (Ch-9).

Reid, R.P., and Browne, K.M., 1991, Intertidal stromatolites in a fringing Holocene reef complex, Bahamas: Geology, v. 19, p. 15-18 (Ch-9).

Roberts, A.A., Dalziel, M., Pogorski, L.A., and Quirt, S.G., 1976, A possible petroleum related helium anomaly in the soil gas, Boulder and Weld Counties, Colorado: U.S. Geological Survey Open-File Report No. 76-544, 7 leaves, 3 maps (Ch-5).

Roehl, P.O, 1967, Stony Mountain (Ordovician) and Interlake (Silurian) facies analogs of recent low-energy marine and subaerial carbonates, Bahamas: American Association of Petroleum Geologists Bulletin, v. 51, no. 10, p. 1979-2032 (Ch-9).

Rost, F.W.D., 1992, Fluorescence microscopy, v. 1: New York, Cambridge University Press, 253 p. (Ch-4).

Rowley, P.D., and Hansen, W.R., 1979, Geologic map of the Split Mountain quadrangle, Uintah County, Utah: U.S. Geological Survey Map GQ-1515, scale 1:24,000 (Ch-8).

Roylance, M.H., 1984, Depositional and diagenetic control of petroleum entrapment in the Desert Creek interval, Paradox Formation, southeastern Utah and southwestern Colorado: Lawrence, University of Kansas, M.S. thesis, 178 p. (Ch-4).

Roylance, M.H., 1990, Depositional and diagenetic history of a Pennsylvanian algal-mound complex - Bug and Papoose Canyon fields, Utah and Colorado: American Association of Petroleum Geologists Bulletin, v. 74, p. 1087-1099 (Ch-4).

Saunders, D.F., Burson, K.R., and Thompson, C.K., 1999, Model for hydrocarbon microseepage and related near-surface alterations: American Association of Petroleum Geologists Bulletin, v. 83, no. 1, p. 170-185 (Ch-5).

Schlager, W., 1992, Sedimentology and sequence stratigraphy of reefs and carbonate platforms: American Association of Petroleum Geologists Continuing Education Course Note Series no. 34, 71 p. (Ch-9).

Scholle, P.A., and Ulmer-Scholle, D.S., 2003, A color guide to the petrography of carbonate rocks: American Association of Petroleum Geologists Bulletin Memoir 77, p. 427-440 (Ch-4).

Schultz, J.L., Boles, J.R., and Tilton, G.R., 1989, Tracking calcium in the San Joaquin Basin, California - a strontium isotope study of carbonate cements at North Coles Levee: Geochimica et Cosmochimica Acta, v. 53, p. 1991-1999 (Ch-4).

Schumacher, D., 1996, Hydrocarbon-induced alteration of soils and sediments, *in* Schumacher, D., and Abrams, M.A., editors, Hydrocarbon migration and its near-surface expression: American Association of Petroleum Geologists Memoir 66, p. 71-89 (Ch-5).

Schumacher, D., and LeSchack, L.A. (editors), 2002, Surface exploration case histories – applications of geochemistry, magnetics, and remote sensing: American Association of Petroleum Geologists Studies in Geology 48, 500 p. (Ch-5).

Segal, D.B., and Merin, I.S., 1989, Successful use of Landsat Thematic Mapper Data for mapping hydrocarbon microseepage-induced mineralogic alteration, Lisbon Valley, Utah: Photogrammetric Engineering and Remote Sensing, v. 55, no. 8, p. 1137-1145 (Ch-5).

Segal, D.B., Ruth, M.D., and Merin, I.S., 1986, Remote detection of anomalous mineralogy associated with hydrocarbon production, Lisbon Valley, Utah: The Mountain Geologist, v. 23, no. 2, p. 51-62 (Ch-5).

Seneshen, D.M., Viellenave, J.H., and Fontana, J.V., 2006, The surface geochemical expression of carbonate-hosted hydrocarbon reservoirs and faults in New York, Ohio, Nevada, and Utah [abs.]: American Association of Petroleum Geologists Annual Convention Abstracts, v. 15, p. 98 (Ch-5).

Shinn, E.A., 1968, Burrowing in recent lime sediments of Florida and the Bahamas: Journal of Paleontology, v. 42, p. 879-894 (Ch-9).

Shinn, E.A., and Lloyd, R.M., 1969, Anatomy of a modern carbonate tidal-flat, Andros Island, Bahamas: Journal of Sedimentary Petrology, v. 39, no. 3, p. 1202-1228 (Ch-9).

Shipton, Z.K., Evans, J.P., Kirschner, D., Kolesar, P.T., Williams, A.P., and Heath, J., 2004, Analysis of CO_2 leakage through 'low permeability' faults from natural reservoirs in the Colorado Plateau, east-central Utah, *in* Baines, S.J., and Worden, R.H., editors, Geological storage of carbon dioxide: London, Geological Society Special Publication 233, p. 43-58 (Ch-11).

Sipple, R.F., and Glover, E.D., 1965, Structures in carbonate rocks made visible by luminescence petrography: Science, v. 150, p. 1283-1287 (Ch-4).

Smith, L.B., 2004, Hydrothermal alteration of carbonate reservoirs – how common is it? [abs.]: American Association of Petroleum Geologists Annual Convention, Official Program with Abstracts, v. 13, p. A130 (Ch-4).

Smith, L.B. Jr., 2006, Origin and reservoir characterisitics of Upper Ordovician Trenton – Black River hydrothermal dolomite reservoirs in New York: American Association of Petroleum Geologists Bulletin (Special Issue: Hydrothermally altered carbonate reservoirs), v. 90, no. 11, p. 1691-1718 (Ch-4).

Smith, L.B., Jr. and Davies, G.R., 2006, Structurally controlled hydrothermal alteration of carbonate reservoirs – introduction: American Association of Petroleum Geologists Bulletin (Special Issue: Hydrothermally altered carbonate reservoirs), v. 90, no. 11, p. 1635-1640 (Ch-4).

Smith, K.T., and Prather, O.E., 1981, Lisbon field – lessons in exploration, *in* Wiegand, D.L., editor, Geology of the Paradox Basin: Rocky Mountain Association of Geologists Guidebook, p. 55-59 (Ch-2).

Smouse, DeForrest, 1993, Lisbon, *in* Hill, B.G., and Bereskin, S.R., editors, Oil and gas fields of Utah: Utah Geological Association Publication 22, non-paginated (Ch-2).

Soeder, D.J., 1990, Applications of fluorescent microscopy to study of pores in tight rocks: American Association of Petroleum Geologists Bulletin, v. 74, p. 30-40 (Ch-4).

Spangler, L.E., Naftz, D.L., and Peterman, Z.E., 1996, Hydrology, chemical quality, and characterization of salinity in the Navajo aquifer and near the Greater Aneth oil field, San Juan County, Utah: U.S. Geological Survey Water-Resources Investigations Report 96-4155, 90 p. (Ch 10).

Stevenson, G.M., and Baars, D.L., 1986, The Paradox—a pull-apart basin of Pennsylvanian age, *in* Peterson, J.A., editor, Paleotectonics and sedimentation in the Rocky Mountain region, United States: American Association of Petroleum Geologists Memoir 41, p. 513-539 (Ch-1).

Stevenson, G.M., and Baars, D.L., 1987, The Paradox—a pull-apart basin of Pennsylvanian age, *in* Campbell, J.A., editor, Geology of Cataract Canyon and vicinity: Four Corners Geological Society, 10th Field Conference, p. 31-55 (Ch-1).

Stockman, K.W., Ginsburg, R.N., and Shinn, E.A., 1967, The production of lime mud by algae in south Florida: Journal of Sedimentary Petrology, v. 37, no. 2, p. 633-648 (Ch-9).

Stowe, Carlton, 1972, Oil and gas production in Utah to 1970: Utah Geological and Mineral Survey Bulletin 94, p. 41 (Ch-2).

Teichmuller, M., and Wolf, M., 1977, Application of fluorescence microscopy in coal petrology and oil exploration: Journal of Microscopy, v. 109, p. 49-73 (Ch-4).

Tremain, C.M., 1993, Low-BTU gas in Colorado, *in* Hjellming, C.A., editor, Atlas of major Rocky Mountain gas reservoirs: New Mexico Bureau of Mines and Mineral Resources, p. 172 (Ch-11).

Turmel, R.J., and Swanson, R.G., 1976, The development of Rodriguez Bank, a Holocene mudbank in the Florida reef tract: Journal of Sedimentary Petrology, v. 46, no. 3, p. 497-518 (Ch-9).

Utah Division of Oil, Gas and Mining, 2008, Oil and gas production report, December: Online, <http://www.ogm.utah.gov/oilgas/PUBLICATIONS/Reports/PROD_book_list.htm>, accessed December 10, 2008 (Ch-1, Ch-2).

Utah Division of Oil, Gas and Mining, 2008, Oil and gas production report, August: Online, <http://www.ogm.utah.gov/oilgas/PUBLICATIONS/Reports/PROD_book_list.htm>, accessed January 12, 2009 (Ch-5).

van Gijzel, P., 1967, Palynology and fluorescence microscopy: Reviews of Paleobotany and Palynology, v. 1, p. 49-79 (Ch-4).

Veizer, J., 1989, Strontium isotopes in seawater through time: Ann. Rev. Earth Planetary Scientific Letters, v. 17, p. 141-167 (Ch-4).

Veizer, J., Ala, D., Azmy, K., Bruckschen, P., Buhl, D., Bruhn, F., Carden, G.A.F., Diener, A., Ebneth, S., Godderis, Y., Jasper, T., Korte, C., Pawellek, F., Podlaha, O.G., and Strauss, H., 1999, $^{87}Sr/^{86}Sr$, delta ^{13}C and delta ^{18}O evolution of Phanerozoic seawater: Chemical Geology, v. 161, no. 1-3, p. 59-88 (Ch-4).

Walker, G., and Burley, S., 1991, Luminescence petrography and spectroscopic studies of diagenetic minerals, *in* Barker, C.E., and Kopp, O.C., editors, Luminescence microscopy - quantitative and qualitative aspects: Society for Sedimentary Geology (SEPM) Short Course 25 Notes, p. 83-96 (Ch-4).

Welsh, J.E., and Bissell, H.J., 1979, The Mississippian and Pennsylvanian (Carboniferous) Systems in the United States—Utah: U.S. Geological Survey Professional Paper 1110-Y, 35 p. (Ch-3, Ch-7).

White, W.B., 1979, Karst landforms in the Wasatch and Uinta Mountains, Utah; National Speleological Society Bulletin 41, p. 80-88. (Ch-8).

Wilson, J.L., 1975, Carbonate facies in geologic history: New York, Springer-Verlag, 471 p. (Ch-3, Ch-7).

Wood, J.R., Bornhorst, T.J., Chittick, S.D., Harrison, W.B., Quinlan, W., and Taylor, E., 2001, Using recent advances in 2D seismic technology and surface geochemistry to economically redevelop a shallow shelf carbonate reservoir – Vernon field, Isabella County, MI - annual report, March 20, 2000-March 20, 2001: U.S. Department of Energy, DOE/BC/15122-1, 25 p. (Ch-5).

Wood, J.R., Bornhorst, T.J., Harrison, W.B., and Quinlan, W., 2002, Using recent advances in 2D seismic technology and surface geochemistry to economically redevelop a shallow shelf carbonate reservoir – Vernon field, Isabella County, MI - annual report, March 21, 2001-March 20, 2002: U.S. Department of Energy, DOE/BC/15122-2, 20 p. (Ch-5).

Wood, H.B., 1968, Geology and exploration of uranium deposits in the Lisbon Valley area, Utah, *in* Ridge, J.D., editor, Ore deposits of the United States, 1933-1967: New York, American Institute Mining, Metallurgical, and Petroleum Engineers, Inc., v. 1, p. 770-789 (Ch-5).

Wood, W.W., Sanford, W.E., and Al Habshi, A.R.S., 2002, Source of solutes to the coastal sabkha of Abu Dhabi: Geological Society of America Bulletin, v. 114, no. 3, p. 259-268 (Ch-4).

Yanatieva, O.K., 1946, Polythermal solubilities in the systems $CaCl_2$-$MgCl_2$-H_2O and $CaCl_2$-NaCl-H_2O: Zhurnal Prikladnox Khimii, v. 19, p. 709-722 (Ch-4).

Yanguas, J.E., and Dravis, J.J., 1985, Blue fluorescent dye technique for recognition of microporosity in sedimentary rocks: Journal of Sedimentary Petrology, v. 55, p. 600-602 (Ch-4).

Zinger, A.S., 1962, Molecular hydrogen in gas dissolved in waters of oil-gas fields, lower Volga region: Geochemistry, no. 10, p. 1015-1023 (Ch-5).

APPENDIX A - TECHNOLOGY TRANSFER

Project Presentations

"The Mississippian Leadville Limestone Exploration Play, Grand County, Utah" by Thomas C. Chidsey, Jr., Moab, Utah, May 4, 2004, to the Grand County Council, members of the press, and general public. The petroleum geology of the Paradox Basin and an overview of project goals, activities, and results were part of the presentation.

"The Mississippian Leadville Limestone Exploration Play, Utah and Colorado" by Thomas C. Chidsey, Jr., and David E. Eby, American Association of Petroleum Geologists (AAPG) Rocky Mountain Section Meeting/Rocky Mountain Natural Gas Strategy Conference and Investment Forum (hosted by the Colorado Oil & Gas Association), August 10, 2004, in Denver, Colorado. The talk presented a general overview of the Leadville Limestone, and facies, petrography, and diagenesis of the Lisbon case-study field.

"Current Oil and Gas Program of the Utah Geological Survey" by Thomas C. Chidsey, Jr., at the Society of Petroleum Engineers, Salt Lake Petroleum Section, "Gas and Oil Developments in Utah: 2005 Update" symposium in Salt Lake City, Utah, May 20, 2005. The presentation reviewed DOE-funded UGS projects including the PUMPII, Class II Oil Revisit Paradox Basin horizontal drilling, and the Advanced and Key Oilfield Technologies for Independents (Area 2 – Exploration) Leadville Limestone studies.

"Dolomitization of the Mississippian Leadville Reservoir at Lisbon Field, Paradox Basin, Utah" by David E. Eby, Thomas C. Chidsey, Jr., Craig D. Morgan, Kevin McClure, John D. Humphrey, Joseph N. Moore, Louis H. Taylor, and Virginia H. Weyland, at the AAPG Annual Convention in Calgary, Canada, June 20, 2005. The presentation included a poster display of the general petroleum geology of the Leadville Limestone, and facies, petrography, and diagenesis, especially dolomite, of the Lisbon case-study field in Utah.

"Dolomitization of the Mississippian Leadville Reservoirs (with emphasis on Lisbon Field), Northern Paradox Basin, Utah and Colorado" by David E. Eby, at the Fort Worth Geological Society monthly meeting in Fort Worth, Texas, October 10, 2005. The presentation included a poster display of the general petroleum geology of the Leadville Limestone, and facies, petrography, and diagenesis, especially dolomite, of the Lisbon case-study field in Utah.

"Dolomitization of the Mississippian Leadville Limestone, Paradox Basin, Utah" by Thomas C. Chidsey, Jr., David E. Eby, Craig D. Morgan, Kevin McClure, Joseph N. Moore, and John D. Humphrey, at the Geological Society of America Annual Meeting in Salt Lake City, Utah, October 19, 2005. The presentation included a poster display of the general petroleum geology of the Leadville Limestone, and facies, petrography, and diagenesis, especially dolomite, of the Lisbon case-study field in Utah.

"Major Oil Plays in San Juan County" by Roger L. Bon, May 15, 2006, to the San Juan County Commissioners and general public, Monticello, Utah. The petroleum geology of the Paradox

Basin, play potentials, land-use issues, and the economic impact on the county were the focus of the discussion.

"Utah's Petroleum Systems, Enhanced Oil Recovery, and Opportunities for CO_2 Sequestration" by Rick Allis, May 23, 2006, at the Interstate Oil & Gas Compact Commission Midyear Issues Summit, Billings, Montana. Utah's exploration history and an overview of the petroleum geology of the major plays and their potential were part of the presentation.

"Gas and Oil in Utah: Potential, New Discoveries, and Hot Plays" by T.C. Chidsey, November 9, 2006, presented at the fall Utah Alumni Meeting sponsored by BP America Producing Company and Brigham Young University, Houston, Texas. An overview of major Utah oil plays including the Mississippian Leadville Limestone play and the surface geochemical survey program were included in the presentation.

"Current Highlights and Major Oil and Gas Plays of Utah" by T.C. Chidsey, March 1, 2007, presented at the monthly meeting of the Utah Association of Professional Landmen, Salt Lake City, Utah. An overview of major Utah oil plays including the Mississippian Leadville Limestone play and the surface geochemical survey program were included in the presentation.

"The Surface Geochemical Expression of Carbonate-Hosted Hydrocarbon Reservoirs" by David Seneshen and Jim Viellenave, March 22, 2007, at the Petroleum Technology Transfer Council workshop "Michigan Field Experiences - Focus on Hydrothermal Dolomites," Mount Pleasant, Michigan. The presentation included an overview of the Leadville project and the surface geochemical survey.

"New Techniques for New Discoveries – Results from the Lisbon Field Area, Paradox Basin, Utah" by David Seneshen, T.C. Chidsey, C.D. Morgan, and M.D. Vanden Berg, presented at the AAPG Annual Convention, in Long Beach, California, April 2, 2007. The presentation included an overview of the Leadville project and the surface geochemical survey.

"Gas and Oil in Utah: Potential, New Discoveries, and Hot Plays" by Thomas C. Chidsey, Jr., presented at the annual meeting of the International Oil Scouts Association in Park City, Utah, June 19, 2007. An overview of major Utah oil plays including the Mississippian Leadville Limestone play and the surface geochemical survey program were included in the presentation.

"New Techniques for New Discoveries – Results from the Lisbon Field Area, Paradox Basin, Utah" by David Seneshen, T.C. Chidsey, C.D. Morgan, and M.D. Vanden Berg, presented at the AAPG Eastern Section meeting, in Lexington, Kentucky, September 17, 2007. The presentation included an overview of the Leadville project and the surface geochemical survey.

"New Techniques for New Discoveries – Results from the Lisbon Field Area, Paradox Basin, Utah" by David Seneshen, T.C. Chidsey, C.D. Morgan, and M.D. Vanden Berg, presented at the AAPG Rocky Mountain Section meeting in Snowbird, Utah, October 8, 2007. This presentation included an overview of the Leadville project and the results of the Lisbon-area surface geochemical survey.

"The Use of Epifluorescence Techniques to Determine Potential Oil-Prone Areas in the Mississippian Leadville Limestone, Northern Paradox Basin, Utah" by D.E. Eby, T.C. Chidsey, Jr., and C.D. Morgan, presented at the AAPG Rocky Mountain Section meeting in Denver, Colorado, July 9-10, 2008. This poster presentation identified potential oil-prone areas in the Paradox fold and fault belt based on hydrocarbon shows using epifluorescence techniques.

"New Techniques for New Discoveries – Results from the Lisbon Field Area, Paradox Basin, Utah" by David Seneshen, T.C. Chidsey, C.D. Morgan, and M.D. Vanden Berg, presented during the Rocky Mountain Association of Geologists (RMAG) 2008 Paradox Basin field trip, September 19, 2008. This presentation included an overview of the Leadville project and the results of the Lisbon-area surface geochemical survey.

Project Publications

Abstracts

Chidsey, T.C., Jr., Morgan, C.D., McClure, K., and Eby, D.E., 2004, The Mississippian Leadville Limestone exploration play, Utah and Colorado [abs.]: American Association of Petroleum Geologists, Rocky Mountain Section Meeting Official Program Book, p. 94.

Eby, D.E., Chidsey, T.C., Jr., Humphrey, J.D., and Taylor, L.H., 2004, Dolomitization of the Mississippian Leadville reservoir at Lisbon field, Paradox Basin, Utah [abs.]: Rocky Mountain Association of Geologists Hydrothermal Dolomite Symposium and Core Workshop Program, p. 31-32.

Eby, D.E., Chidsey, T.C., Jr., Morgan, C.D., McClure, K., Humphrey, J.D., Moore, J.N., Taylor, L.H., and Weyland, V.H., 2005, Dolomitization of the Mississippian Leadville reservoir at Lisbon field, Utah [abs.]: American Association of Petroleum Geologists Annual Convention, Official Program with Abstracts, v. 14, p. A40.

Chidsey, T.C., Jr., Eby, D.E., Morgan, C.D., McClure, K., Moore, J.N., and Humphrey, J.D., 2005, Dolomitization of the Mississippian Leadville Limestone, Paradox Basin, southeastern Utah [abs.]: Abstracts with Programs, Geological Society of America, v. 37, no. 7, paper 4-12.

Seneshen, D.M., Chidsey, T.C., Jr., Morgan, C.D., and Vanden Berg, M.D., 2007, New techniques for new discoveries – results from the Lisbon field area, Paradox Basin, Utah [abs.]: American Association of Petroleum Geologists Annual Convention Abstracts, v. 16, p. 126.

Seneshen, D.M., Chidsey, T.C., Jr., Morgan, C.D., and Vanden Berg, M.D., 2007, New techniques for new discoveries – results from the Lisbon field area, Paradox Basin, Utah [abs.]: American Association of Petroleum Geologists, Eastern Section Meeting Official Program.

Seneshen, D.M., Chidsey, T.C., Jr., Morgan, C.D., and Vanden Berg, M.D., 2007, New techniques for new discoveries – results from the Lisbon field area, Paradox Basin, Utah [abs]: American Association of Petroleum Geologists, Rocky Mountain Section Meeting Official Program, p. 55-56.

Eby, D.E., Chidsey, T.C., Jr., and Morgan, C.D., 2008, The use of epifluorescence techniques to determine potential oil-prone areas in the Mississippian Leadville Limestone, northern Paradox Basin, Utah [abs.]: Rocky Mountain Natural Gas Geology and Resource Conference, Rocky Mountain Section of the American Association of Petroleum Geologists and Colorado Oil & Gas Association Official Program with Abstracts, p. 88-89.

Eby, D.E., Chidsey, T.C., Jr., Morgan, C.D., Sprinkel. D.A., and Laine, M.D., 2009, A tale of two breccia types in the Mississippian Leadville Limestone, Lisbon field, Paradox Basin, southeastern Utah [abs.]: American Association of Petroleum Geologists Annual Convention Abstracts, v. 18, in press.

Technical Papers

Seneshen, D.M., Chidsey, T.C. Jr, Morgan, C.D., and Vanden Berg, M.D., 2009, New techniques for new discoveries – surface geochemical results from the Lisbon field area, Paradox Basin, Utah, *in* Houston, W., Moreland, P., and Wray, L., editors, Petroleum geology of the Paradox Basin: Rocky Mountain Association of Geologists Guidebook, in press.

Non-Technical Papers and Articles

Chidsey, T.C., Jr., 2004, The UGS awarded DOE grant to study the Mississippian Leadville Limestone oil exploration play in Utah and Colorado: Utah Geological Survey, Survey Notes, v. 36, no. 1, p. 5-6.

PI/Dwights Plus Drilling Wire, 2004, UGS carrying out study of Leadville in Paradox Basin: PI/Dwights Rocky Mountain Region, Four Corners Edition, Section I, February, p 3.

Chidsey, T.C., Jr., 2004, The Mississippian Leadville Limestone exploration play, Utah and Colorado: Rocky Mountain Association of Geologists, The Outcrop, v. 53, no. 10, p. 1 and 6.

Durham, L.S., 2007, Geochem offers Paradox option – lichens, free gas yield clues: American Association of Petroleum Geologists Explorer (August), v. 28, no. 8, p. 8-12.

Semi-Annual Technical Progress Reports

Chidsey, T.C., Jr., Morgan, C.D., and McClure, Kevin, 2004, The Mississippian Leadville Limestone exploration play, Utah and Colorado: exploration techniques and studies for independents – semi-annual technical progress report for the period October 1, 2004 to

March 31, 2004: U.S. Department of Energy, DOE/BC15424-1, 26 p.

Chidsey, T.C., Jr., Morgan, C.D., McClure, Kevin, Bon, R.L., and Eby, D.E., 2005, The Mississippian Leadville Limestone exploration play, Utah and Colorado: exploration techniques and studies for independents – semi-annual technical progress report for the period April 1 to September 31, 2004: U.S. Department of Energy, DOE/BC15424-2, 42 p.

Chidsey, T.C., Jr., Morgan, C.D., Eby, D.E., Moore, J., and Taylor, L. 2005, The Mississippian Leadville Limestone exploration play, Utah and Colorado: exploration techniques and studies for independents – semi-annual technical progress report for the period October 1, 2004 to March 31, 2005: U.S. Department of Energy, DOE/BC15424-3, 69 p.

Chidsey, T.C., Jr., Eby, D.E., and Humphrey, J.D., 2005, The Mississippian Leadville Limestone exploration play, Utah and Colorado: exploration techniques and studies for independents – semi-annual technical progress report for the period April 1, 2005 to September 30, 2005: U.S. Department of Energy, DOE/BC15424-4, 34 p.

Chidsey, T.C., Jr., Gwynn, J.W., Morgan, C.D., Vanden Berg, M.D., and Seneshen, D.M., 2006, The Mississippian Leadville Limestone exploration play, Utah and Colorado: exploration techniques and studies for independents – semi-annual technical progress report for the period October 1, 2005 to March 31, 2006: U.S. Department of Energy, DOE/BC15424-5, 43 p.

Chidsey, T.C., Jr., Morgan, C.D., Vanden Berg, M.D., and Seneshen, D.M., 2006, The Mississippian Leadville Limestone exploration play, Utah and Colorado: exploration techniques and studies for independents – semi-annual technical progress report for the period April 1, 2006 to September 30, 2006: U.S. Department of Energy, DOE/BC15424-6, 39 p.

Chidsey, T.C., Jr., Morgan, C.D., Vanden Berg, M.D., and Seneshen, D.M., 2007, The Mississippian Leadville Limestone exploration play, Utah and Colorado: exploration techniques and studies for independents – semi-annual technical progress report for the period October 1, 2006 to March 31, 2007: U.S. Department of Energy, DOE/BC15424-7, 75 p.

Chidsey, T.C., Jr., Morgan, C.D., and Eby, D.E., 2007, The Mississippian Leadville Limestone exploration play, Utah and Colorado: exploration techniques and studies for independents – semi-annual technical progress report for the period April 1, 2007 to September 30, 2007: U.S. Department of Energy, DOE/BC15424-8, 28 p.

Allis, R.G., Chidsey, T.C., Jr., Morgan, C.D., Heuscher, Sonja, and McDonald, Ammon, 2008, The Mississippian Leadville Limestone exploration play, Utah and Colorado: exploration techniques and studies for independents – semi-annual technical progress report for the period October 1, 2007 to March 31, 2008: U.S. Department of Energy, DOE/BC15424-9, 34 p.

Morgan, C.D., and Chidsey, T.C., Jr., 2008, The Mississippian Leadville Limestone exploration play, Utah and Colorado: exploration techniques and studies for independents – semi-annual technical progress report for the period April 1, 2008 to September 30, 2008: U.S. Department of Energy, DOE/BC15424-10, 23 p.

Project Deliverables

Deliverable 1-1 – Core Descriptions, Core Photographs, and Core Analysis: Lisbon Field, San Juan County, Utah

Deliverable 1-2 – Geophysical Well Logs Tied to Core Descriptions: Lisbon Field, San Juan County, Utah

Deliverable 1-3A – Catalog of Leadville Porosity Types and Diagenesis: Lisbon Field, San Juan County, Utah

Deliverable 1-3B – Scanning Electron Microscopy, Epifluorescence, Cathodoluminescence, Fluid Inclusions, and Isotopic Studies: Lisbon Field, San Juan County, Utah

Deliverable 1-4 – Field Maps and Cross Sections: Lisbon Field, San Juan County, Utah

Core Workshops

"Dolomitization of the Mississippian Leadville Reservoir at Lisbon Field, Paradox Basin, Utah" by David E. Eby, Thomas C. Chidsey, Jr., John D. Humphrey, and Louis H. Taylor, Rocky Mountain Association of Geologists Hydrothermal Dolomite Symposium and Core Workshop, November 15, 2004, Colorado School of Mines, Golden, Colorado. The presentation included a technical talk, poster, and core display of the general petroleum geology of the Leadville Limestone, and facies, petrography, and diagenesis, especially dolomite, of the Lisbon case-study field in Utah.

"Depositional Environments, Diagenesis, and Hydrothermal Alteration of the Mississippian Leadville Limestone Reservoir, Paradox Basin, Utah: A Core Workshop," was presented by Dave Eby and Tom Chidsey on October 6, 2007, at the AAPG Rocky Mountain Section meeting and was sponsored by Utah Geological Survey and U.S. Department of Energy. This workshop was for geoscientists with interests in exploration and development of shallow-shelf carbonate reservoirs. It was designed for geoscientists who wished to examine a large collection of carbonate core (both limestone and dolomite) presented within lithofacies, diagenetic, and petrophysical context. Representative core from Utah's Lisbon field was examined. The core workshop was organized into two topical sessions: Leadville Facies/Fabrics and Leadville Burial Overprint. Participants performed a series of group exercises using core, geophysical well logs, and photomicrographs from thin sections. These sessions included describing reservoir versus non-reservoir lithofacies; determining diagenesis, hydrothermal alteration, and porosity from core; recognizing barriers and baffles to fluid flow; correlating core to geophysical well logs; and identifying potential completion zones. Following the core sessions, we presented a summary

lecture on our Leadville diagenetic/alteration interpretation based on geochemical analysis and petrographic techniques. Twenty-two geologists attended the course.

This workshop was presented again on May 23, 2008, at the U.S. Geological Survey's Denver Core Research Center and was sponsored by the Petroleum Technology Transfer Council and the RMAG. Forty geologists attended the course.

Project Displays at American Association of Petroleum Geologists Annual Meetings

Project materials, plans, objectives, and results were displayed at the UGS booth during the following meetings of the AAPG:

AAPG Annual Convention, April 18-24, 2004, Dallas, Texas
AAPG Rocky Mountain Section Meeting/Rocky Mountain Natural Gas Strategy Conference and Investment Forum (hosted by the Colorado Oil & Gas Association), August 9-11, 2004, in Denver, Colorado
AAPG Annual Convention, June 19-22, 2005, Calgary, Canada
AAPG Rocky Mountain Section Meeting, September 23-24, 2005, Jackson, Wyoming
AAPG Annual Convention, April 9-12, 2006, Houston, Texas
AAPG Rocky Mountain Section Meeting, June 10-13, 2006, Billings, Montana
AAPG Annual Convention, April 1-4, 2007, Long Beach, California
AAPG Rocky Mountain Section Meeting, October 7-9, 2007, Snowbird, Utah
AAPG Annual Convention, April 20-23, 2008, San Antonio, Texas
AAPG Rocky Mountain Section Meeting, July 9-11, 2008, Denver, Colorado

Utah Geological Survey Web Site

The UGS maintains a Web site on the Internet, http://geology.utah.gov. The UGS site includes a page under the heading *Oil, Gas, Coal, & CO_2*, which describes the UGS/DOE cooperative studies past and present (PUMPII, Paradox Basin [two projects evaluating the Pennsylvanian Paradox Formation], Ferron Sandstone, Bluebell field, Green River Formation), and has a link to the DOE Web site. Each UGS/DOE cooperative study also has its own separate page on the UGS Web site. The Leadville Limestone project page, http://geology.utah.gov/emp/leadville/index.htm, contains (1) a project location map, (2) a description of the project, (3) a reference list of all publications that are a direct result of the project, (4) poster presentations, and (5) semi-annual technical progress reports.

Technical Advisory Board

Titan Energy Resources, Park City, Utah
EnCana Oil & Gas (USA) Inc., Denver, Colorado
Legacy Energy Corp., Denver, Colorado
Bill Barrett Corporation, Denver, Colorado
ST Oil Company, Denver, Colorado
Ken Grove, Geologic Consultant, Lafayette, Colorado
Navajo Nation Oil and Gas Company, Inc., Window Rock, Arizona

GLNA, LLC, Golden, Colorado
Red Willow Production Co., Southern Ute Indian Tribe, Ignacio, Colorado
Scott Geological Consultants, Evergreen, Colorado
Resolute Natural Resources, Denver, Colorado
Williams Production Company, Denver, Colorado
Tidewater Oil & Gas LLC, Denver, Colorado
ExplorTech LLC, Littleton, Colorado
Bob Grundy, Geological Consultant, Morrison, Colorado
Coleman Oil & Gas, Inc., Denver, Colorado
Integrated Resource Technology, Littleton, Colorado
Waseem A., Sayed, China Hills, California

Stake Holders Board

Utah Division of Oil, Gas and Mining, Salt Lake City, Utah
Colorado Oil and Gas Conservation Commission, Denver, Colorado
U.S. Bureau of Land Management, Moab Field Office, Moab, Utah
Utah Petroleum Association, Bountiful, Utah
Utah School and Institutional Trust Lands Administration, Salt Lake City, Utah

APPENDIX B
STRATIGRAPHIC SECTIONS

(1) Moab-Arches-La Sal area

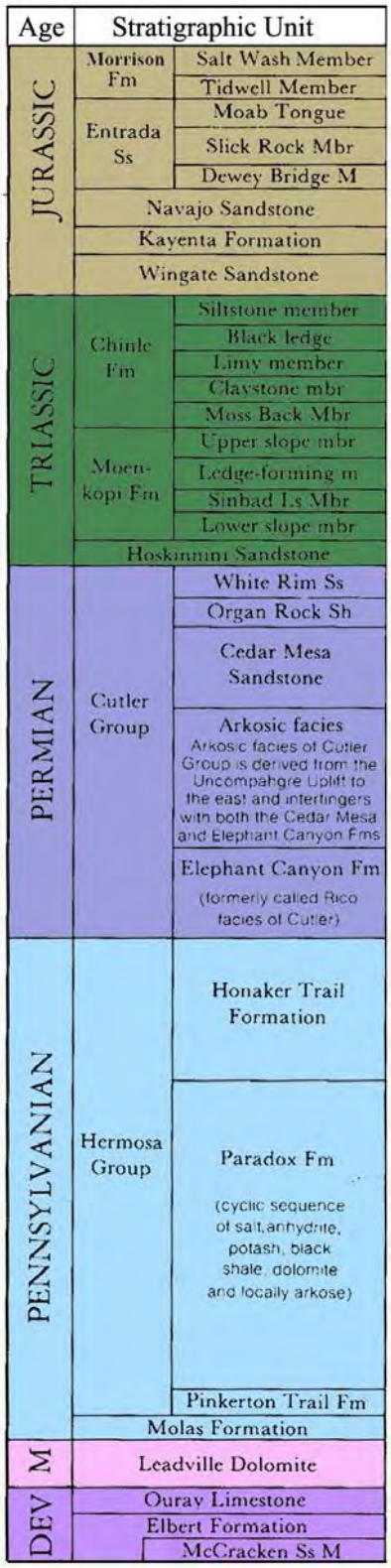

(2) Canyonlands Park area

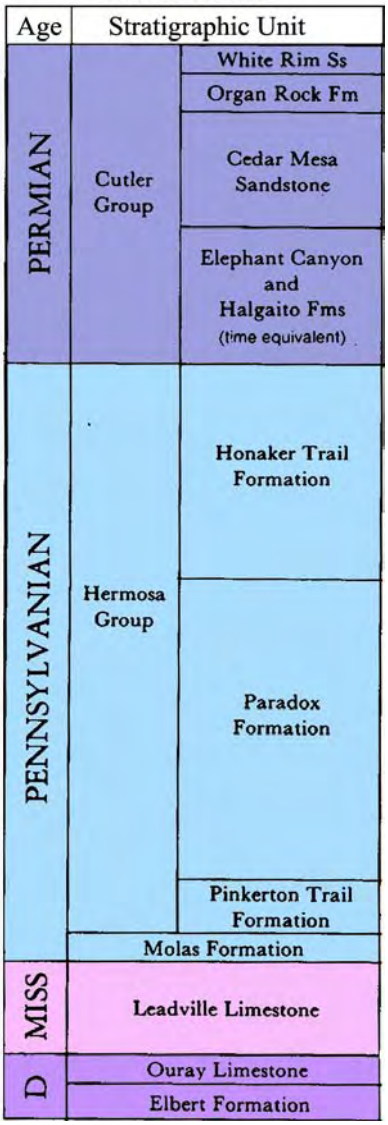

(3) Monticello-Bluff-Aneth area

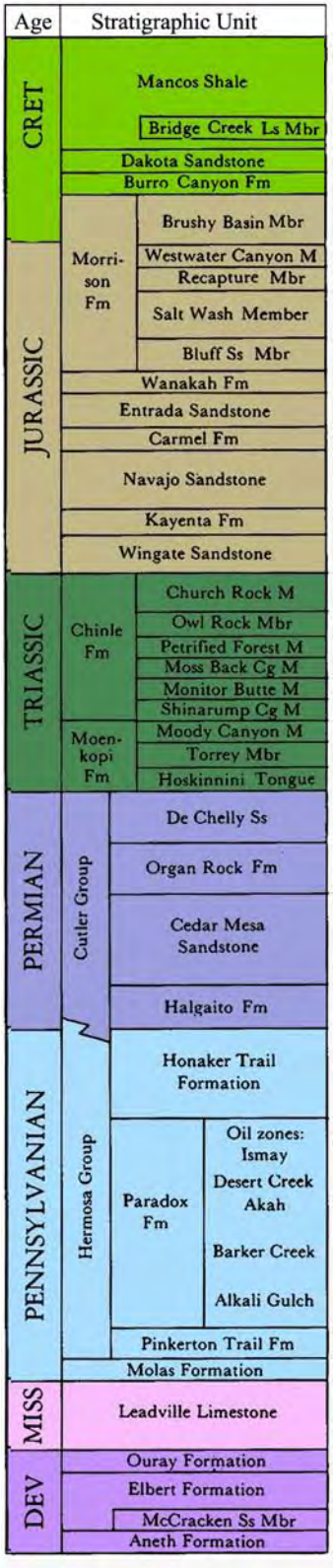

Modified from Hintze, 1993

APPENDIX C – LISBON-LIGHTNING DRAW SURFACE GEOCHEMICAL DATA (compact disc)

APPENDIX D - EPIFLUORESCENCE ANALYSES AND DESCRIPTIONS OF WELL CUTTINGS FROM THE PARADOX FOLD AND FAULT BELT AREA, UTAH

Table D-1. Epifluorescence analyses and descriptions of well cuttings from the Paradox fold and fault belt area, Utah.

Map #	Well Name	Location	County	Interval	N	Rating*		Sample Type	Comments	Photomicrographs	Binocular Microscope Image
						Range	Ave				
1	Humble Woodside 1	SESE 12 19S 13E	Emery	6580-90	7	0.0-patches of 1.5	1.2	cuttings	medium to coarsely crystalline dolomite, fair to good intercrystalline porosity with abundant bitumen, drillstem test flowed water	x	
1	Humble Woodside 1	SESE 12 19S 13E	Emery	6590-6600	5	0.0-1.0	0.3	cuttings	fine to medium crystalline dolomite, none to minor intercrystalline porosity, trace to common bitumen		
1	Humble Woodside 1	SESE 12 19S 13E	Emery	6735-40	4	0.0-0.5	0.2	cuttings	finely crystalline dolomite and limestone (?), very low visible porosity, no bitumen, drillstem test flowed water		
1	Humble Woodside 1	SESE 12 19S 13E	Emery	6740-50	7	0.0-0.5, with small patches up to 1.5	0.5	cuttings	finely crystalline dolomite and limestone (?), very low visible porosity, no bitumen, drillstem test flowed water		
2	Carter Oil Hatch Sphinx Unit 1-A	SWNW 35 19S 14E	Emery	8670-75	5	0.2-0.5	0.3	cuttings	medium to coarse crystalline dolomite, minor visible intercrystalline porosity, traces of bitumen		
2	Carter Oil Hatch Sphinx Unit 1-A	SWNW 35 19S 14E	Emery	8675-80	7	0.2-1.0	0.5	cuttings	medium to coarse crystalline dolomite, minor visible intercrystalline porosity, traces of bitumen		
2	Carter Oil Hatch Sphinx Unit 1-A	SWNW 35 19S 14E	Emery	8680-85	8	0.0-1.0	0.5	cuttings	fine to coarse crystalline dolomite, low visible porosity, minor amounts of bitumen, some orange and red (iron-rich?) epifluorescence		
2	Carter Oil Hatch Sphinx Unit 1-A	SWNW 35 19S 14E	Emery	8690-95	8	0.2-1.0	0.6	cuttings	coarse crystalline dolomite, fair to good intercrystalline porosity, traces of bitumen, possible fracture-filling coarse dolomite		
2	Carter Oil Hatch Sphinx Unit 1-A	SWNW 35 19S 14E	Emery	8700-05	8	0.4-1.0	0.8	cuttings	coarse crystalline dolomite, very low visible porosity, no visible bitumen		
2	Carter Oil Hatch Sphinx Unit 1-A	SWNW 35 19S 14E	Emery	8710-15	9	0.4-1.0	0.7	cuttings	coarse crystalline dolomite, very low visible porosity, no visible bitumen		
3	Denison Mines 5-1	SENE 5 21S 14E	Emery	5830-40	4	0.0-0.5	0.2	cuttings	microcrystalline dolomite, trace of bitumen possibly along fractures, very low visible porosity		
3	Denison Mines 5-1	SENE 5 21S 14E	Emery	5840-50	7	0-0	0.0	cuttings	microcrystalline dolomite, no visible bitumen, very low porosity		
3	Denison Mines 5-1	SENE 5 21S 14E	Emery	5850-60	6	0.5-2.5	1.5	cuttings	microcrystalline dolomite, fair to good visible micro-intercrystalline porosity, no visible bitumen	x	
3	Denison Mines 5-1	SENE 5 21S 14E	Emery	5860-70	6	0.0-2.0	1.5	cuttings	microcrystalline dolomite, fair to good micro-intercrystalline porosity, no bitumen	x	
4	Superior Salt Wash 22-34	SENW 34 22S 17E	Grand	10,070-75	6	0.0-0.3	0.1	cuttings	microcrystalline dolomite, very low visible porosity, no visible bitumen		

Map #	Well Name	Location	County	Interval	N	Rating*		Sample Type	Comments	Photomicrographs	Binocular Microscope Image
						Range	Ave				
4	Superior Salt Wash 22-34	SENW 34 22S 17E	Grand	10,075-80	5	0.0-0.3	0.1	cuttings	microcrystalline dolomite and possible limestone, no visible porosity, no bitumen		
4	Superior Salt Wash 22-34	SENW 34 22S 17E	Grand	10,080-85	5	0.0-0.3	0.1	cuttings	microcrystalline dolomite and possible limestone, no visible porosity, no bitumen		
5	Texaco Government Smoot 1	CSENE 17 23S 17E	Grand	8732-33	4	1.5-2.5	2.0	core chip	medium to coarsely crystalline dolomite with fair intercrystalline porosity, trace of bitumen	x	
5	Texaco Government Smoot 1	CSENE 17 23S 17E	Grand	8733-34	4	0.5-2.5	1.8	core chip	medium to coarsely crystalline dolomite with good intercrystalline porosity completely lined with bitumen	x	
5	Texaco Government Smoot 1	CSENE 17 23S 17E	Grand	8734-35	4	0.5-2.5	1.8	core chip	medium to coarsely crystalline dolomite with good intercrystalline porosity completely lined with bitumen	x	
5	Texaco Government Smoot 1	CSENE 17 23S 17E	Grand	8736-37	4	0.5-1.5	1.0 with patches up to 2.0	core chip	medium to coarsely crystalline dolomite with good intercrystalline porosity and vugs lined with bitumen	x	
6	Shell Chaffin 1	NENW 21 23S 15E	Emery	7460-70	4	0.0-0.0	0.0	cuttings	finely crystalline dolomite and limestone (?), none to minor visible porosity, trace of bitumen		
6	Shell Chaffin 1	NENW 21 23S 15E	Emery	7500-10	7	0.0-0.5	0.4	cuttings	medium to coarsely crystalline dolomite, no visible bitumen, minor to fair intercrystalline porosity		
6	Shell Chaffin 1	NENW 21 23S 15E	Emery	7510-20	3	0.0-0.0	0.0	cuttings	finely crystalline dolomite and limestone, very low visible porosity, no bitumen		
6	Shell Chaffin 1	NENW 21 23S 15E	Emery	7520-30	5	0.0-1.5	1.0	cuttings	fine to medium crystalline dolomite, minor to fair intercrystalline porosity, no visible bitumen, patchy good epifluorescence	x	
6	Shell Chaffin 1	NENW 21 23S 15E	Emery	7530-40	7	0.5-1.5	1.2	cuttings	very finely crystalline dolomite, high porosity, low permeability, no bitumen	x	
7	Federal Hatt 1	SESE 19 23S 14 E	Emery	5905-15	5	0.0-0.0	0.0	cuttings	microcrystalline limestone/dolomite, no visible porosity, no visible bitumen		
7	Federal Hatt 1	SESE 19 23S 14 E	Emery	5935-45	7	0.5-3.0, continuous to patchy	2.3	cuttings	dolomite, fine to medium crystalline with fair to good intercrystalline porosity, bimodal distribution of shows	x (see figure 6-4A)	
7	Federal Hatt 1	SESE 19 23S 14 E	Emery	5970-80	9	1.5-2.5	2.3	cuttings	medium to coarse crystalline dolomite, low to fair porosity, no bitumen	x	
7	Federal Hatt 1	SESE 19 23S 14 E	Emery	6005-10	5	0.2-1.0	0.3	cuttings	fine to medium dolomite, low to good intercrystalline porosity, no visible bitumen, appears wet	x	
7	Federal Hatt 1	SESE 19 23S 14 E	Emery	6015-20	7	0.5-1.0	0.8	cuttings	fine to medium crystalline dolomite, low to fair intercrystalline porosity, trace of bitumen		
8	General Petroleum Gov 45-5	NESW 5 24S 15E	Emery	6899-07	1	none	0.2	core chip	minor intercrystalline porosity, trace of bitumen		

Map #	Well Name	Location	County	Interval	N	Rating*		Sample Type	Comments	Photomicrographs	Binocular Microscope Image
						Range	Ave				
8	General Petroleum Gov 45-5	NESW 5 24S 15E	Emery	6907-32	2	0.2-0.5	see comment	core chip	chip 1 = 0.2, chip 2 = 0.5, minor to fair intercrystalline porosity, none to trace of bitumen		
8	General Petroleum Gov 45-5	NESW 5 24S 15E	Emery	6932-35	2	0.0-0.3	see comment	core chip	chip 1 = 0.0, chip 2 = 0.3, minor intercrystalline porosity, no bitumen		
9	Tiger Oil State 12-11	SWNW 11 24S 20E	Grand	11,810-20	7	0.5-1.0	0.7	cuttings	medium to coarse crystalline dolomite, fair to well-connected intercrystalline porosity with some fractures, fractures and pores completely lined with bitumen, some large saddle dolomites		
9	Tiger Oil State 12-11	SWNW 11 24S 20E	Grand	11,825 (circulation sample)	8	0.0-0.5	0.2	cuttings	medium to coarse crystalline dolomite, poor to fair intercrystalline porosity, some stylolites, trace of bitumen		
9	Tiger Oil State 12-11	SWNW 11 24S 20E	Grand	11,820-30	8	0.0-0.5	0.3	cuttings	fine to medium crystalline dolomite and possible limestone, poor to fair intercrystalline porosity with bitumen lining		
9	Tiger Oil State 12-11	SWNW 11 24S 20E	Grand	11,836 (45-minute circulation sample)	7	0.0-0.5	0.2	cuttings	fine to medium crystalline dolomite, generally poor porosity lined with bitumen		
9	Tiger Oil State 12-11	SWNW 11 24S 20E	Grand	11,830-40	10	0.0-0.5	0.3	cuttings	fine to medium crystalline dolomite, very poor intercrystalline porosity lined with bitumen		
9	Tiger Oil State 12-11	SWNW 11 24S 20E	Grand	11,840-50	10	0.0-0.5	0.3	cuttings	fine to medium crystalline dolomite, very poor intercrystalline porosity lined with bitumen		
10	Conoco Federal 31	NWSE 31 24S 23E	Grand	10,450-60	4	0.0-0.5	0.2	cuttings	finely crystalline dolomite and possible limestone, trace of intercrystalline porosity with bitumen		
10	Conoco Federal 31	NWSE 31 24S 23E	Grand	10,460-70	6	0.0-0.5	0.2	cuttings	finely crystalline dolomite and possible limestone, trace of intercrystalline porosity with bitumen		
10	Conoco Federal 31	NWSE 31 24S 23E	Grand	10,470-80	4	0.0-patchy 1.5	0.3	cuttings	fine to medium crystalline dolomite, possible limestone, modest intercrystalline porosity, small vugs, fracture porosity, trace of bitumen	x	
10	Conoco Federal 31	NWSE 31 24S 23E	Grand	10,740-50	7	0.0-0.2	0.1	cuttings	fine to coarse crystalline dolomite with large intercrystalline pores, significant bitumen, drillstem test flowed non-flammable gas	x	
10	Conoco Federal 31	NWSE 31 24S 23E	Grand	10,750-60	6	0.0-0.2	0.1	cuttings	fine to coarse crystalline dolomite with large intercrystalline pores, significant bitumen, drillstem test flowed non-flammable gas	x	
11	Shell Gruvers Mesa 2	NENW 10 25S 16E	Emery	6750-55	5	0.0-1.2	1.0	cuttings	fine to medium crystalline limestone and dolomite, low visible porosity, trace of bitumen, possible open fractures		

Map #	Well Name	Location	County	Interval	N	Rating*		Sample Type	Comments	Photomicrographs	Binocular Microscope Image
						Range	Ave				
11	Shell Gruvers Mesa 2	NENW 10 25S 16E	Emery	6755-60	4	0.1-0.5	0.3	cuttings	fine to medium crystalline limestone and dolomite, low visible porosity but possible open fractures, no bitumen		
11	Shell Gruvers Mesa 2	NENW 10 25S 16E	Emery	6785-90	7	0.0 - limestone, 1.0-2.0 - dolomite	1.5	cuttings	very finely crystalline limestone and dolomite, dolomite has high micro-intercrystalline porosity, no permeability, no bitumen		
11	Shell Gruvers Mesa 2	NENW 10 25S 16E	Emery	6790-95	5	1.0-2.2	1.8	cuttings	finely crystalline dolomite, high micro-intercrystalline porosity, low permeability, stylolites, no bitumen		
11	Shell Gruvers Mesa 2	NENW 10 25S 16E	Emery	6900-05	5	0.0-0.3	0.1	cuttings	microcrystalline limestone and dolomite, no visible porosity, trace of bitumen		
11	Shell Gruvers Mesa 2	NENW 10 25S 16E	Emery	6905-10	6	0.0-0.3	0.1	cuttings	fine to medium crystalline limestone and dolomite, traces to fair intercrystalline porosity, no bitumen		
12	McRae Fed 1	SWSW 10 25S 18E	Grand	8485-95	6	0-2.5	0.8	cuttings	no visible porosity to minor porosity, no significant bitumen	x	
12	McRae Fed 1	SWSW 10 25S 18E	Grand	8547-50	2	none	0.3	cuttings	low to no visible porosity, no bitumen		
13	Superior Bow Knot Unit 1	NESE 20 25S 17.5E	Grand	6075-80	6	0.0-2.5	2.0	cuttings	fine to medium crystalline dolomite, poor to fair intercrystalline porosity with abundant bitumen	x	
13	Superior Bow Knot Unit 1	NESE 20 25S 17.5E	Grand	6080-85	6	0.0-2.5, patchy and continuous	2.0	cuttings	fine to medium crystalline dolomite, high micro-intercrystalline porosity, low permeability, trace to common bitumen	x	
13	Superior Bow Knot Unit 1	NESE 20 25S 17.5E	Grand	6362-67	4	1.0-1.5	1.2	core chip	fine to medium crystalline dolomite, very low visible porosity, no bitumen		
13	Superior Bow Knot Unit 1	NESE 20 25S 17.5E	Grand	6367-73	4	1.0-1.5	1.2	core chip	fine to medium crystalline dolomite, very low visible porosity, no bitumen		
13	Superior Bow Knot Unit 1	NESE 20 25S 17.5E	Grand	6373-79	3	1.5-2.5	2.0	core chip	fine to medium crystalline limestone and dolomite, low matrix porosity, no bitumen, doesn't look like moveable oil is present		
13	Superior Bow Knot Unit 1	NESE 20 25S 17.5E	Grand	6390-95	4	0.0-0.8	0.5	cuttings	fine to medium crystalline dolomite, fair to moderate intercrystalline porosity, no bitumen		
13	Superior Bow Knot Unit 1	NESE 20 25S 17.5E	Grand	6395-6400	4	0.3-0.6	0.4	cuttings	medium crystalline dolomite, fair to good intercrystalline porosity, common bitumen, probably wet	x	
14	Big Flat/Bartlett Flat 1	NENE 26 25S 19 E	Grand	8560-70	2	0.0-1.3	0.5	cuttings	drillstem test top, microcrystalline dolomite with stylolites, no visible bitumen, patchy epifluorescence	x	
14	Big Flat/Bartlett Flat 1	NENE 26 25S 19 E	Grand	8570-80	7	0.0-1.5	0.5	cuttings	fine to medium crystalline dolomite, trace of bitumen, micro-stylolites, low visible porosity, intercrystalline porosity, patchy fluorscence	x	
14	Big Flat/Bartlett Flat 1	NENE 26 25S 19 E	Grand	8630-40	4	0.0-2.0	1.5	cuttings	microcrystalline dolomite, high porosity, low permeability, no visible bitumen	x	

Map #	Well Name	Location	County	Interval	N	Rating*		Sample Type	Comments	Photomicrographs	Binocular Microscope Image
						Range	Ave				
14	Big Flat/Bartlett Flat 1	NENE 26 25S 19 E	Grand	8640-50	4	0.5 to patchy 1.5	0.8	cuttings	fine to medium crystalline dolomite with low to medium visible porosity, minor bitumen and possible sulfide mineralization	x	
15	Standard Lookout Point 1	SWSW 29 25S 16E	Emery	6380-90	6	0.0-0.5	0.4	cuttings	no visible porosity, no bitumen		
15	Standard Lookout Point 1	SWSW 29 25S 16E	Emery	6394-95	3	2.0-3.0	2.5	core chip	microcrystalline dolomite with high micro-intercrystalline porosity, low permeability, minor anhydrite	x	
15	Standard Lookout Point 1	SWSW 29 25S 16E	Emery	6500-10	9	0.0-2.0	0.4	cuttings	no to poor visible intercrystalline porosity, no significant bitumen	x	
15	Standard Lookout Point 1	SWSW 29 25S 16E	Emery	6510-20	4	0.0-0.0	0.0	cuttings	no visible porosity, no bitumen, fine microcrystalline dolomite		
16	Fed Oil Fed Bowknoll 1	NESE 30 25S 18 E	Grand	7375-80	4	0.5-2.5	1.8	cuttings	fair intercrystalline porosity, possible fractures, abundant bitumen	x	
16	Fed Oil Fed Bowknoll 1	NESE 30 25S 18 E	Grand	7380-85	4	0.0-0.5	0.3	cuttings	perforated zone, low visible porosity, none to trace of bitumen		
16	Fed Oil Fed Bowknoll 1	NESE 30 25S 18 E	Grand	7385-90	4	0.5-2.5	1.0	cuttings	minor to fair porosity, none to minor bitumen	x	
17	Southern Natural Long Canyon 1	NENW 9 26S 20E	Grand	7560-71	7	0.0-0.8	0.4	cuttings	fine-medium crystalline dolomite and limestone, trace of intercrystalline porosity, trace of bitumen		
17	Southern Natural Long Canyon 1	NENW 9 26S 20E	Grand	7580-85	6	0.0-patches of 1.4	0.4	cuttings	medium to coarse dolomite, poor to fair intercrystalline porosity, fairly abundant bitumen, pale-green epifluorescence	x	
17	Southern Natural Long Canyon 1	NENW 9 26S 20E	Grand	7585-90	10	0.0-patches of 1.5	0.4	cuttings	fine-medium crystalline dolomite with fair to good intercrystalline porosity, traces of bitumen and probable sulfides	x	
17	Southern Natural Long Canyon 1	NENW 9 26S 20E	Grand	7610-20	11	0.0-0.5	0.2	cuttings	fine-medium crystalline dolomite with traces of intercrystalline porosity, traces to abundant bitumen		
17	Southern Natural Long Canyon 1	NENW 9 26S 20E	Grand	7620-30	10	0.0-0.3	0.1	cuttings	fine to medium crystalline dolomite, fair to good intercrystalline porosity with abundant bitumen		
18	Pure Mineral Point 1	NESE 7 26S 18E	Grand	6875-80	5	0-0.5	0.1	cuttings	minor amount of intercrystalline porosity with abundant bitumen		
18	Pure Mineral Point 1	NESE 7 26S 18E	Grand	6880-85	7	0-0.5	0.1	cuttings	minor amount of intercrystalline porosity with abundant bitumen		
18	Pure Mineral Point 1	NESE 7 26S 18E	Grand	6885-90	4	0-1.0	0.5	cuttings	very low to minor intercrystalline porosity, scattered bitumen		
18	Pure Mineral Point 1	NESE 7 26S 18E	Grand	7040-45	9	0-1.0	0.2	cuttings			
18	Pure Mineral Point 1	NESE 7 26S 18E	Grand	7045-50	6	0-0.5	0.1	cuttings	no to very minor, intercrystalline porosity		
18	Pure Mineral Point 1	NESE 7 26S 18E	Grand	7050-55	7	0-0.5	0.3	cuttings	no visible porosity to minor intercrystalline porosity, none to minor bitumen		

Map #	Well Name	Location	County	Interval	N	Rating*		Sample Type	Comments	Photomicrographs	Binocular Microscope Image
						Range	Ave				
18	Pure Mineral Point 1	NESE 7 26S 18E	Grand	7055-60	10	0.5-1.5 with a few small patches of 2.0	1.2	cuttings	minor to good intercrystalline porosity, scattered bitumen		
18	Pure Mineral Point 1	NESE 7 26S 18E	Grand	7060-65	7	0.5-2.5	2.0	cuttings	porosity fair to good; pore types include moldic, intercrystalline, small vugs; moderate bitumen	x	
18	Pure Mineral Point 1	NESE 7 26S 18E	Grand	7065-70	6	0-0.5	0.2	cuttings	no visible porosity, no bitumen		
18	Pure Mineral Point 1	NESE 7 26S 18E	Grand	7070-75	4	0-0.5	0.2	cuttings	low to minor intercrystalline porosity, traces of bitumen		
19	Pure Big Flat 3	NENE 23 26S 19E	Grand	7714-15	6	0.0-0.5	0.3	core chip	medium to coarse crystalline dolomite, good intercrystalline porosity, plus moldic and vuggy porosity, bitumen-lined pores, small isolated patches of epifluorescence up to 1.5 in several samples	x	x
19	Pure Big Flat 3	NENE 23 26S 19E	Grand	7715-16	8	0.0-1.0	0.5	core chip	medium to coarse crystalline dolomite, good intercrystalline porosity, plus moldic and vuggy porosity, bitumen-lined pores, small isolated patches of epifluorescence up to 1.5 in several samples	x	x
19	Pure Big Flat 3	NENE 23 26S 19E	Grand	7716-17	4	0.0-0.5	0.3	core chip	fine to medium crystalline dolomite, generally poor intercrystalline porosity lined with bitumen	x	x
19	Pure Big Flat 3	NENE 23 26S 19E	Grand	7717-18	4	0.0-0.5	0.2	core chip	fine to medium crystalline dolomite, poor to fair intercrystalline porosity with some bitumen lined pores, occasional speckles of epifluorescence in pores up to 1.2	x	
19	Pure Big Flat 3	NENE 23 26S 19E	Grand	7718-19	5	0.0-0.3	0.1	core chip	medium crystalline dolomite, poor to fair porosity with some microfractures lined with bitumen	x	
19	Pure Big Flat 3	NENE 23 26S 19E	Grand	7719-20	5	0.0-0.5	0.2	core chip	fine to medium crystalline dolomite, fair to good visible porosity but low permeability, trace of bitumen	x	x
19	Pure Big Flat 3	NENE 23 26S 19E	Grand	7720-21	5	0.0-1.0	0.8 with isolated patches up to 1.5	core chip	medium to coarsely crystalline dolomite, fairly good porosity with bitumen lining, microfractures lined with bitumen	x	x
19	Pure Big Flat 3	NENE 23 26S 19E	Grand	7721-22	3	0.0-0.5	0.4 with isolated patches and speckles up to 1.5	core chip	medium to coarsely crystalline dolomite with fair to poor intercrystalline porosity, lined with bitumen	x	x
19	Pure Big Flat 3	NENE 23 26S 19E	Grand	7723-24	5	0.0-0.5	0.3	core chip	very fine to medium crystalline dolomite, poor to fair visible porosity lined with bitumen	x	x
19	Pure Big Flat 3	NENE 23 26S 19E	Grand	7724-25	6	0.3-1.0	0.7	core chip	fine to medium crystalline dolomite with fair to good intercrystalline porosity and small vugs lined with bitumen		x

Map #	Well Name	Location	County	Interval	N	Rating*		Sample Type	Comments	Photomicrographs	Binocular Microscope Image
						Range	Ave				
20	British America Federal Ornsby 1	NWNE 3 27S 19E	Wayne	7740-50	5	0.0-2.0, bimodal	1.0	cuttings	poor sample quality/unwashed, very fine to medium crystalline dolomite, some samples no porosity and permeability, some samples high porosity and no permeability, no bitumen	x	
20	British America Federal Ornsby 1	NWNE 3 27S 19E	Wayne	7750-60	6	0.0-0.5	0.3	cuttings	fine to medium crystalline dolomite and fossilferous limestone, very low visible porosity, no bitumen		
20	British America Federal Ornsby 1	NWNE 3 27S 19E	Wayne	7760-70	2	0.3-1.5	1.0	cuttings	finely crystalline dolomite, medium to high intercrystalline porosity, low permeability		
20	British America Federal Ornsby 1	NWNE 3 27S 19E	Wayne	7790-7800	6	0.0-0.5	0.3	cuttings	microcrystalline dolomite and probable limestone, no visible porosity, no bitumen		
20	British America Federal Ornsby 1	NWNE 3 27S 19E	Wayne	7800-10	6	0.5-2.0	1.5	cuttings	fine to medium crystalline dolomite, no visible porosity to high porosity, low permeability	x	
21	Exxon Gold Basin 1	NWNW 15 27S 24E	San Juan	14,300-10	8	0.0-0.1	0.0	cuttings	microcrystalline dolomite and limestone, no visible porosity, no bitumen		
21	Exxon Gold Basin 1	NWNW 15 27S 24E	San Juan	14,310-20	5	0.0-0.5	0.3	cuttings	microcrystalline dolomite and limestone (?), no visible porosity, healed fractures, no bitumen		
21	Exxon Gold Basin 1	NWNW 15 27S 24E	San Juan	14,350-60	7	0.0-1.8	0.5	cuttings	microcrystalline dolomite and limestone (?), no visible porosity, healed fractures, possible traces of bitumen along fractures		
21	Exxon Gold Basin 1	NWNW 15 27S 24E	San Juan	14,360-70	8	0.0-1.8	0.5	cuttings	microcrystalline dolomite and limestone (?), no visible porosity, healed fractures, one sample with bitumen filled fractures containing small patches up to 1.8 epifluorescence		
21	Exxon Gold Basin 1	NWNW 15 27S 24E	San Juan	14,390-14,400	2	0	0.0	cuttings	microcrystalline limestone and dolomite, no visible porosity or bitumen, minor patches of sulfide minerals (opaque)		
21	Exxon Gold Basin 1	NWNW 15 27S 24E	San Juan	14,400-10	7	0.0-2.0	0.8	cuttings	microcrystalline limestone and dolomite, some dolomite with micro-intercrystalline porosity, very low visible porosity, low permeability, traces of bitumen		
22	Putnam 1	SENE 15 27S 22 E	San Juan	7410-20	6	0.0-0.5	0.2	cuttings	fine-grained dolomite and siltstone, micro-intercrystalline porosity with no visible porosity or bitumen		
22	Putnam 1	SENE 15 27S 22 E	San Juan	7420-30	6	0.0-0.4	0.1	cuttings	microcrystalline dolomite, no visible bitumen or porosity		
22	Putnam 1	SENE 15 27S 22 E	San Juan	7440-50	8	0.0-0.8	0.2	cuttings	microcrystalline dolomite, no visible bitumen or porosity		
22	Putnam 1	SENE 15 27S 22 E	San Juan	7480-90	10	0.0-0.5	0.3	cuttings	fine to coarse crystalline dolomite with fair intercrystalline porosity, no bitumen		
23	Humble Unit 1 Bridger Sack Mesa	SESE 17 27S 22 E	San Juan	7030-40	5	0.3-0.5	0.4	cuttings	medium to coarsely crystalline dolomite (hydrothermal ?), fairly good intercrystalline porosity, trace of bitumen		

Map #	Well Name	Location	County	Interval	N	Rating*		Sample Type	Comments	Photomicrographs	Binocular Microscope Image
						Range	Ave				
23	Humble Unit 1 Bridger Sack Mesa	SESE 17 27S 22 E	San Juan	7040-50	8	0.2-0.5	0.3	cuttings	fine to medium crystalline limestone and dolomite, low to moderate amount of intercrystalline porosity, no significant bitumen		
23	Humble Unit 1 Bridger Sack Mesa	SESE 17 27S 22 E	San Juan	7050 (2 hr cirulation sample)	10	0.2-0.5	0.3	cuttings	medium crystalline dolomite, fair to good intercrystalline porosity, some pores lined with bitumen		
23	Humble Unit 1 Bridger Sack Mesa	SESE 17 27S 22 E	San Juan	7050-55	10	0.2-0.5	0.5	cuttings	fine-grained limestone and medium-crystalline dolomite with small patches up to 1.0 epifluorescence, trace to heavy amounts of bitumen, low to intermediate intercrystalline porosity		
23	Humble Unit 1 Bridger Sack Mesa	SESE 17 27S 22 E	San Juan	7055-60	6	0.5-1.0	0.8	cuttings	fine to medium crystalline dolomite with some patches of very coarse saddle dolomite, trace of bitumen, fair to good intercrystalline porosity		
23	Humble Unit 1 Bridger Sack Mesa	SESE 17 27S 22 E	San Juan	7060-65	3	0.1-0.4	0.2	cuttings	finely crystalline limestone and dolomite with possible small fractures lined with fine dolomite, some bitumen		
23	Humble Unit 1 Bridger Sack Mesa	SESE 17 27S 22 E	San Juan	7065-70	11	0.0-0.5	0.2	cuttings	fine to medium crystalline dolomite and limestone, trace of intercrystalline porosity, trace of bitumen		
24	California Oil Muleshoe 1	SWNW 2 28S 23E	San Juan	10,240-50	3	0.0-2.0	0.2 with one bright patch of 2.0	cuttings	fine to medium crystalline dolomite	x (see figure 6-4B)	
24	California Oil Muleshoe 1	SWNW 2 28S 23E		10,270-80	6	0		cuttings	no visible porosity to minor intercrystalline porosity, some bitumen		
25	Gulf Lockhard Fed 1	SW1/2 22 28S 20E	San Juan	5130-35	11	0.5-1.5	1.0	cuttings	abundant pyrobitumen in every sample, intercrystalline porosity in most samples		
25	Gulf Lockhard Fed 1	SW1/2 22 28S 20E	San Juan	5135-40	11	0.5-2.0	1.5	cuttings	better intercrystalline porosity, vugs with scattered bitumen, spotty shows		
25	Gulf Lockhard Fed 1	SW1/2 22 28S 20E	San Juan	5140-45	7	0.5-2.5	1.8	cuttings	fair-to-good intercrystalline porosity with abundant bitumen		
25	Gulf Lockhard Fed 1	SW1/2 22 28S 20E	San Juan	5145-50	8	1.0-2.5	2.0	cuttings	coarsely crystalline dolomite with good intercrystalline porosity, some bitumen	x	
26	Richfield Hatch Mesa 1	SESW 22 28S 21E	San Juan	7780-90	7	0.5-2.5	1.0	cuttings	medium to coarse crystalline dolomite, some bitumen linings, minor intercrystalline porosity, speckled epifluorescence to 2.5		x (see figure 6-3A)
26	Richfield Hatch Mesa 1	SESW 22 28S 21E	San Juan	7790-7800	5	0.0-1.5	1.0	cuttings	medium to coarse crystalline dolomite, minor bitumen linings, very minor visible intercrystalline porosity		x (see figure 6-1D and 6-3B)
26	Richfield Hatch Mesa 1	SESW 22 28S 21E	San Juan	7800-10	5	0.0-1.5	0.3	cuttings	medium to coarse crystalline dolomite, no visible bitumen or porosity, patches of orange fluorescence		x (see figure 6-1B and 6-3C)
26	Richfield Hatch Mesa 1	SESW 22 28S 21E	San Juan	7810-20	6	0.0-0.5	0.3	cuttings	medium to coarse crystalline dolomite, no visible bitumen or porosity, patches of orange fluorescence		x

Map #	Well Name	Location	County	Interval	N	Rating*		Sample Type	Comments	Photomicrographs	Binocular Microscope Image
						Range	Ave				
27	Pure USA Big Indian 1	NWSESE 33 29S 24E	San Juan	9960-70	3	0.0-0.0	0.0	cuttings	fine to medium crystalline dolomite, abundant intercrystalline pores completely lined with bitumen, very small patches of 0.5 epifluorescence speckles		
27	Pure USA Big Indian 1	NWSESE 33 29S 24E	San Juan	10,020-23	10	0.0-0.3	0.2	cuttings	medium to coarse crystalline dolomite with fair to good intercrystalline porosity and small vugs completely lined with bitumen, isolated patches and speckles up to 1.5 epifluorescence	x (see figure 6-4D)	x (see figure 6-1C and 6-3D)
27	Pure USA Big Indian 1	NWSESE 33 29S 24E	San Juan	10,024-29	10	0.0-0.1	0.1	cuttings	medium to coarse dolomite with abundant intercrystalline porosity completely lined with bitumen, very small speckles of 0.5 epifluorescence	x	x
27	Pure USA Big Indian 1	NWSESE 33 29S 24E	San Juan	10,029-32	8	0.0-0.1	0.1	cuttings	fine to coarse crystalline dolomite, poor to fair intercrystalline porosity lined with bitumen		
27	Pure USA Big Indian 1	NWSESE 33 29S 24E	San Juan	10,074-77	10	0.0-0.4	0.2	cuttings	fine to medium crystalline dolomite with fair to good intercrystalline porosity, completely lined with bitumen, rare speckles up to 0.5 epifluorescence		
27	Pure USA Big Indian 1	NWSESE 33 29S 24E	San Juan	10,080-86	8	0.0-1.0	0.8	cuttings	medium to coarsely crystalline dolomite, generally good intercrystalline porosity and small vugs lined with bitumen, probable gas/oil transition at 10,080-85		
27	Pure USA Big Indian 1	NWSESE 33 29S 24E	San Juan	10,086-90	6	0.5-1.5	1.0	cuttings	medium to coarsely crystalline dolomite, good to excellent intercrystalline porosity and small vugs lined with bitumen	x	
28	Belco State 1	NENE 32 29.5S 24E	San Juan	9835-36	4	2.0-3.0	2.5	core chip	medium to coarsely crystalline dolomite (probable hydrothermal), fair to good intercrystalline porosity and fractured porosity, trace of bitumen, patchy to continuous epifluorescence, possible oil film	x	
28	Belco State 1	NENE 32 29.5S 24E	San Juan	9836-37	2	0.0-0.3	0.2	core chip	medium to coarsely crystalline dolomite, poor to fair intercrystalline porosity, trace of bitumen around pores		
28	Belco State 1	NENE 32 29.5S 24E	San Juan	9837-38	3	0.0-0.5	0.4	core chip	medium to coarsely crystalline dolomite, poor to fair intercrystalline porosity, epifluorescence is patchy surrounding coarser dolomite crystals, trace of bitumen		
28	Belco State 1	NENE 32 29.5S 24E	San Juan	9838-39	2	0.0-0.2	0.1	core chip	coarsely crystalline dolomite matrix consists of isolated patches of 0.2-0.8 epifluorescence along fractures and intercrystalline spaces, looks wet with trace of oil, fairly good intercrystalline porosity and vuggy porosity, trace of bitumen		

Map #	Well Name	Location	County	Interval	N	Rating*		Sample Type	Comments	Photomicrographs	Binocular Microscope Image
						Range	Ave				
28	Belco State 1	NENE 32 29.5S 24E	San Juan	9850-51	3	0.0-0.2	0.1	core chip	medium to coarse crystalline dolomite with fair intercrystalline porosity, trace of bitumen, matrix contains small patches of remnant epifluorescence 1.0-1.5 around isolated crystals and fractures	x	
28	Belco State 1	NENE 32 29.5S 24E	San Juan	9851-52	2	0.0-0.0	0.0	core chip	medium to coarse dolomite with very low porosity, no bitumen, samples are "dead"		
29	Pure NW Lisbon St. A-1	SWSE 2 30S 24E	San Juan	9710-15	2	0.5-2.0, spotty	1.0	cuttings	minor intercrystalline porosity, significant amount of bitumen, two possible types of epifluorescence - pale-green yellow and bright yellow, indicating two oils or partially degraded oil	x	
29	Pure NW Lisbon St. A-1	SWSE 2 30S 24E	San Juan	9715-20	5	0.5-2.0, in patches	1.0	cuttings	poor to fair intercrystalline porosity, abundant bitumen, possible microfractures	x	
29	Pure NW Lisbon St. A-1	SWSE 2 30S 24E	San Juan	9720-25	5	0.0-1.5, along microfractures only		cuttings	no visible porosity except microfractures, no visible bitumen	x	
30	Elliot Inc. Lisbon Valley C-1 (Lisbon)	NENW 9 30S 24E	San Juan	8765-70	20	0.0-1.5	1.0, small specks in patches that range up to 1.5	cuttings	fine to medium crystalline dolomite with fair to good intercrystalline porosity and small vugs completely lined with bitumen		
31	Pure Lisbon 814-A	CNWSW 14 30S 24E	San Juan	8870-75	8	0.5-2.5	1.8	cuttings	medium to coarse crystalline dolomite, abundant bitumen linings, some large patches of intercrystalline porosity, speckled epifluorescence to 2.5	x	x
31	Pure Lisbon 814-A	CNWSW 14 30S 24E	San Juan	8875-80	6	1.0-3.0	2.0	cuttings	medium to coarse crystalline dolomite, good intercrystalline porosity and abundant bitumen linings, good pale-yellow to greenish yellow epifluorescence	x	
31	Pure Lisbon 814-A	CNWSW 14 30S 24E	San Juan	8890-95	14	0.0-1.8	0.8	cuttings	fine to medium crystalline dolomite, abundant bitumen linings, low amounts of visible porosity, speckled yellow epifluorescence	x	x
31	Pure Lisbon 814-A	CNWSW 14 30S 24E	San Juan	8895-8900	11	0.0-0.5	0.2	cuttings	fine crystalline dolomite, low amounts of visible porosity, traces of bitumen only		x
31	Pure Lisbon 814-A	CNWSW 14 30S 24E	San Juan	8900-05	9	0.0-2.5	1	cuttings	generally fine to medium crystalline dolomite, no visible bitumen		x
31	Pure Lisbon 814-A	CNWSW 14 30S 24E	San Juan	8905-10	7	0.2-2.2	1.5	cuttings	fine to medium crystalline dolomite, minor to fair visible bitumen coatings and porosity, pale-yellow epifluorescence		
31	Pure Lisbon 814-A	CNWSW 14 30S 24E	San Juan	8910-15	8	0.0-2.0	1.3	cuttings	medium to coarse crystalline dolomite, minor visible intercrystalline porosity, some bitumen coatings		x
31	Pure Lisbon 814-A	CNWSW 14 30S 24E	San Juan	8915-20	5	0.0-1.2	0.8	cuttings	fine to coarse crystalline dolomite, patches of good visible intercrystalline porosity, traces of bitumen coatings		

Map #	Well Name	Location	County	Interval	N	Rating*		Sample Type	Comments	Photomicrographs	Binocular Microscope Image
						Range	Ave				
31	Pure Lisbon 814-A	CNWSW 14 30S 24E	San Juan	8920-25	5	0.1-2.2	1.8	cuttings	fine to coarse crystalline dolomite, some visible intercrystalline porosity, no visible bitumen		
31	Pure Lisbon 814-A	CNWSW 14 30S 24E	San Juan	8925-30	7	0.3-0.8	0.8	cuttings	medium to coarse crystalline dolomite, low visible porosity, no visible bitumen		x
32	Pure Oil Spiller Canyon State 1	SWSW 16 30S 25E	San Juan	9080-90	5	0	0.0	cuttings	finely crystalline dolomite and limestone (?), low visible porosity with some bitumen		
32	Pure Oil Spiller Canyon State 1	SWSW 16 30S 25E	San Juan	9090-9100	6	0.0-0.2 with rare patches up to 0.5	0.1	cuttings	fine to medium crystalline dolomite with fair intercrystalline porosity lined with abundant bitumen	x	
32	Pure Oil Spiller Canyon State 1	SWSW 16 30S 25E	San Juan	9100-10	8	0.0-0.5	0.4	cuttings	medium to coarsely crystalline dolomite with poor to fair porosity, lined with bitumen	x	x
32	Pure Oil Spiller Canyon State 1	SWSW 16 30S 25E	San Juan	9150-60	7	0.1-1.0	0.6	cuttings	medium to coarsely crystalline dolomite with fairly good intercrystalline porosity completely lined with bitumen, microfractures also lined with bitumen	x (see figure 6-4C)	x
32	Pure Oil Spiller Canyon State 1	SWSW 16 30S 25E	San Juan	9180-90	4	0.3-1.0	0.7	cuttings	fine to medium crystalline dolomite with poor to fair porosity lined with bitumen, some microfractures lined with bitumen		
32	Pure Oil Spiller Canyon State 1	SWSW 16 30S 25E	San Juan	9190-9200	10	0.3-1.0	0.7 with small patches up to 2.0	cuttings	fine to medium crystalline dolomite and limestone with poor to fair intercrystalline porosity lined with bitumen	x	
32	Pure Oil Spiller Canyon State 1	SWSW 16 30S 25E	San Juan	9330-40	10	0.5-1.0	0.7 small speckled areas up to 2.0	cuttings	medium to coarsely crystalline dolomite (saddle dolomite), fair to good intercrystalline porosity lined with bitumen	x	x
32	Pure Oil Spiller Canyon State 1	SWSW 16 30S 25E	San Juan	9360-70	10	0.3-1.0	0.7	cuttings	finely to coarsely crystalline dolomite with poor to fair intercrystalline porosity, lined with bitumen, speckled areas up to 1.5 epifluorescence	x	
32	Pure Oil Spiller Canyon State 1	SWSW 16 30S 25E	San Juan	9380-90	7	0.5-1.5	1.0	cuttings	finely to coarsely crystalline dolomite, fair to good porosity lined with bitumen, some microfractures also lined with bitumen	x	
32	Pure Oil Spiller Canyon State 1	SWSW 16 30S 25E	San Juan	9410-20	8	0.3-1.0	0.7	cuttings	medium to coarsely crystalline dolomite, poor to fair intercrystalline porosity lined with bitumen, isolated patches of epifluorescence up to 1.5	x	x (see figure 6-1A)

- evaluated at 100X
- highlighted epifluorescence rating represents the highest maximum value for the well

Epifluorescence Photomicrographs and Binocular Microscope Images

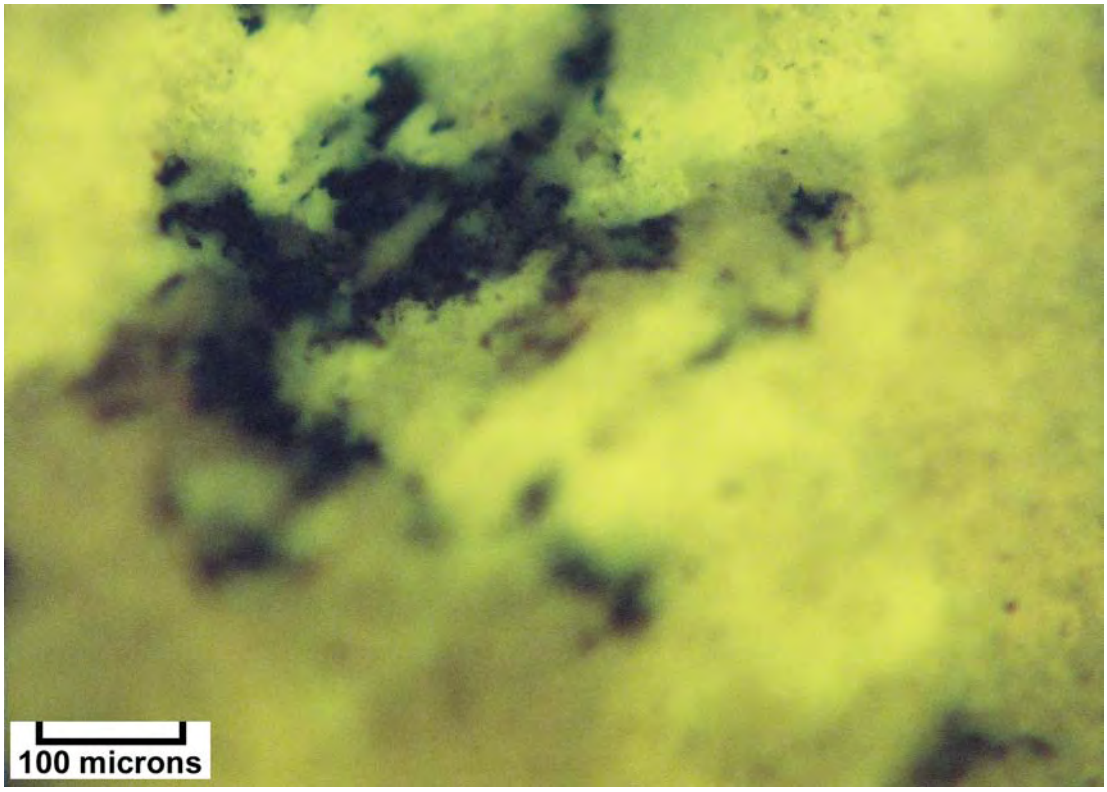

Photomicrograph – Humble Woodside 1 (Map #1), 6580-90 feet, patches of 1.5 epifluorescence in porous, bitumen-bearing dolomite.

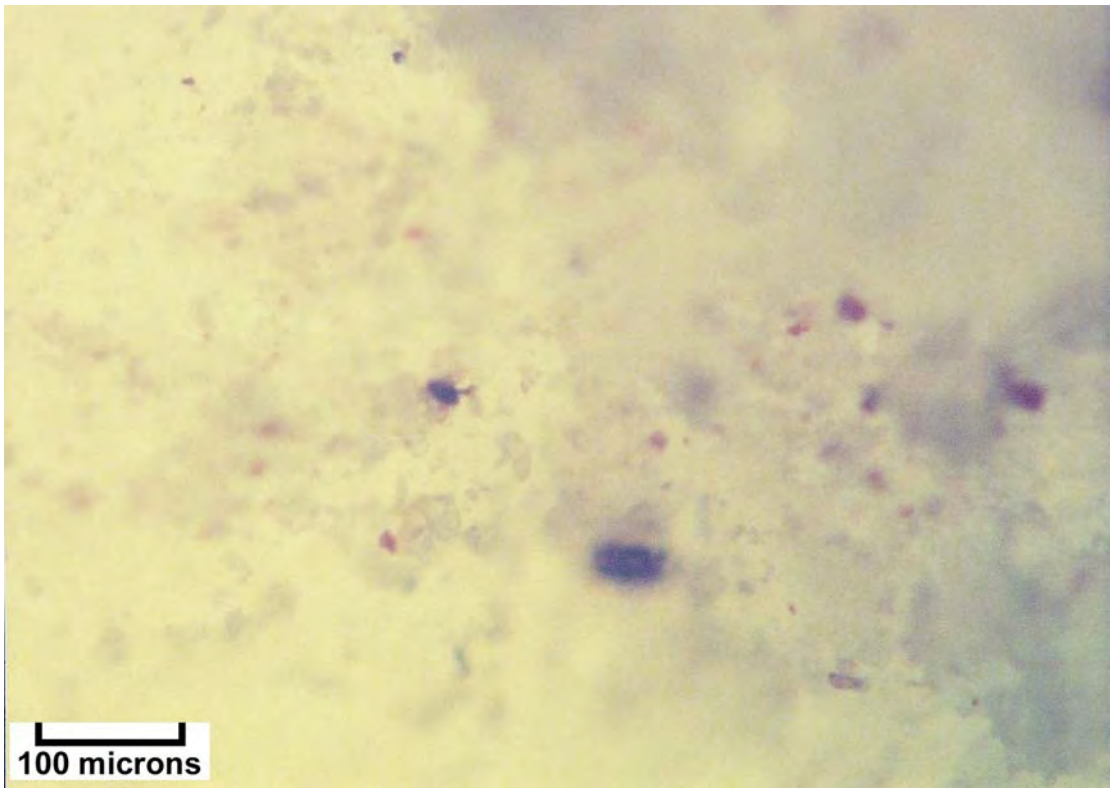

Photomicrograph – Denison Mines 5-1 (Map #3), 5850-60 feet, 2.5 epifluorescence in microcrystalline dolomite with no bitumen.

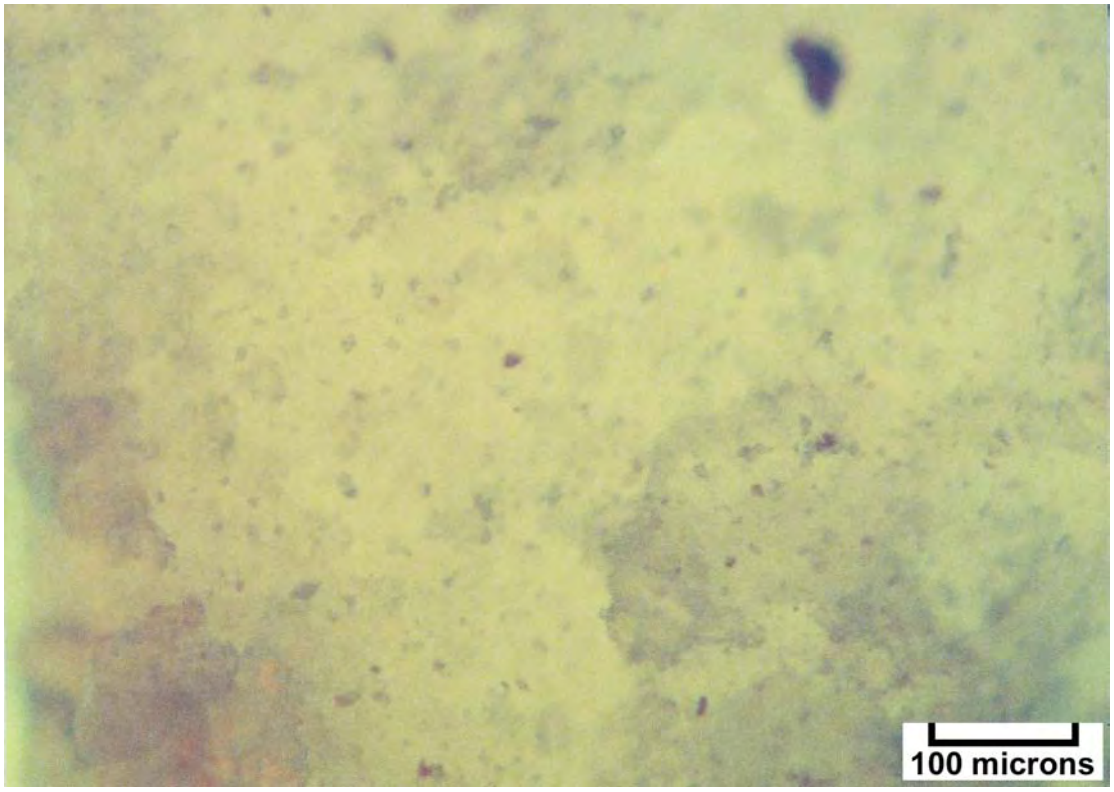

Photomicrograph – Denison Mines 5-1 (Map #3), 5860-70 feet, 2.0 epifluorescence in microcrystalline dolomite with no bitumen, high porosity and low permeability.

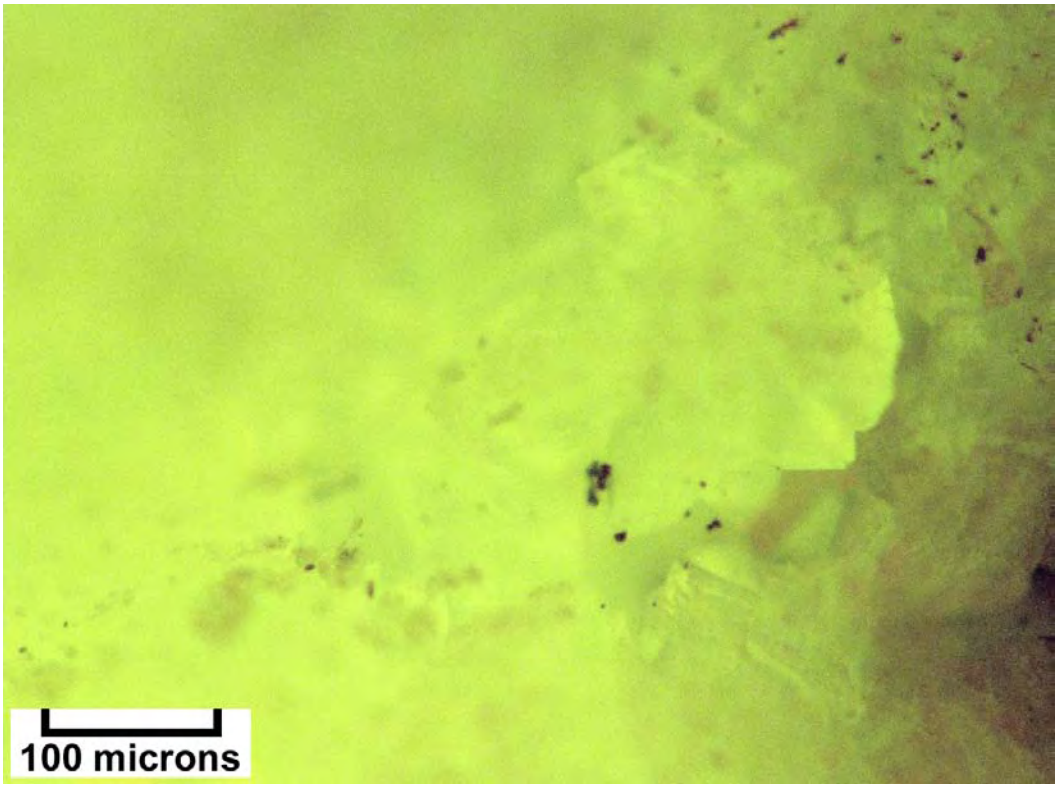

Photomicrograph – Texaco Government Smoot 1 (Map #5), 8732-33 feet, 2.0 epifluorescence, pale yellow, possible high gravity oil in medium crystalline dolomite.

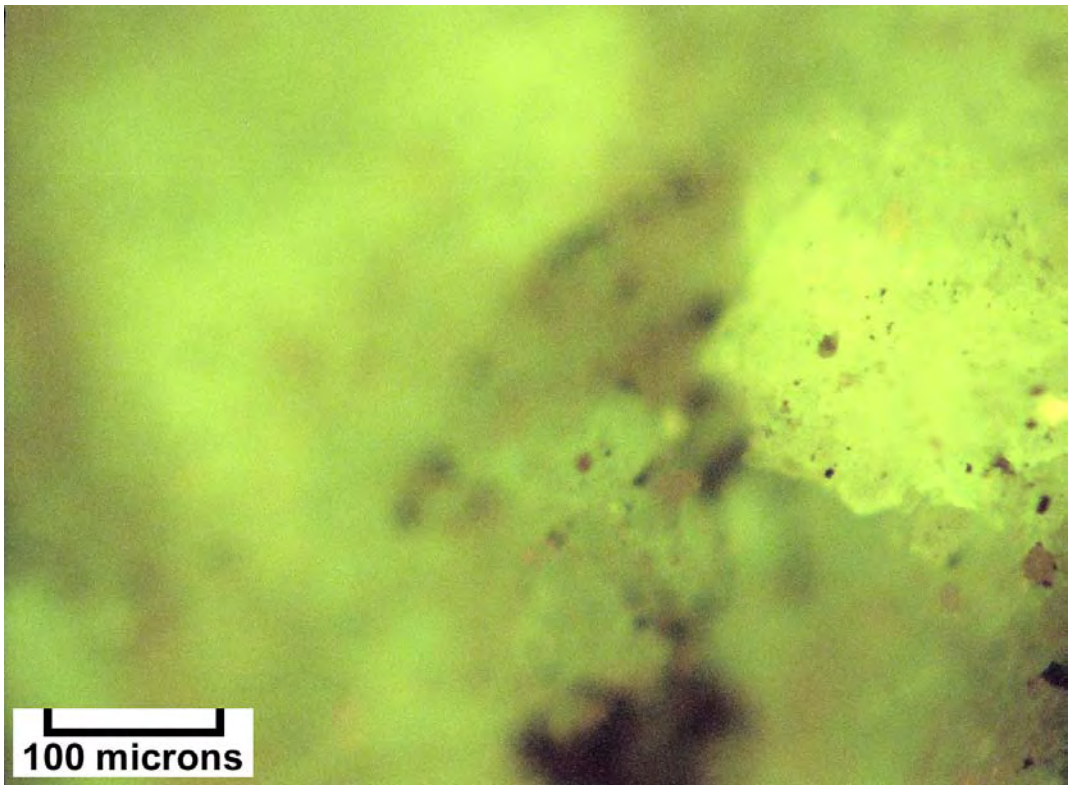

Photomicrograph – Texaco Government Smoot 1 (Map #5), 8733-34 feet, 1.8 epifluorescence in medium crystalline dolomite with good intercrystalline porosity lined with bitumen.

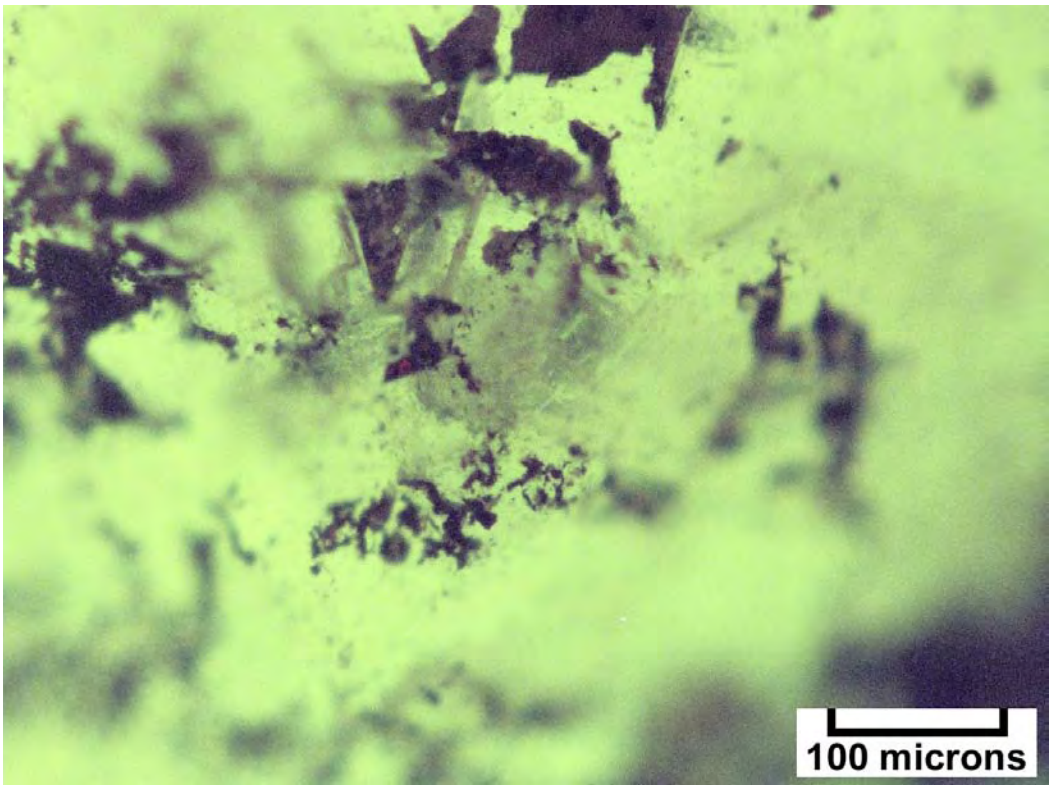

Photomicrograph – Texaco Government Smoot 1 (Map #5), 8734-35 feet, 1.8 epifluorescence in coarsely crystalline dolomite with good intercrystalline pores completely lined with bitumen.

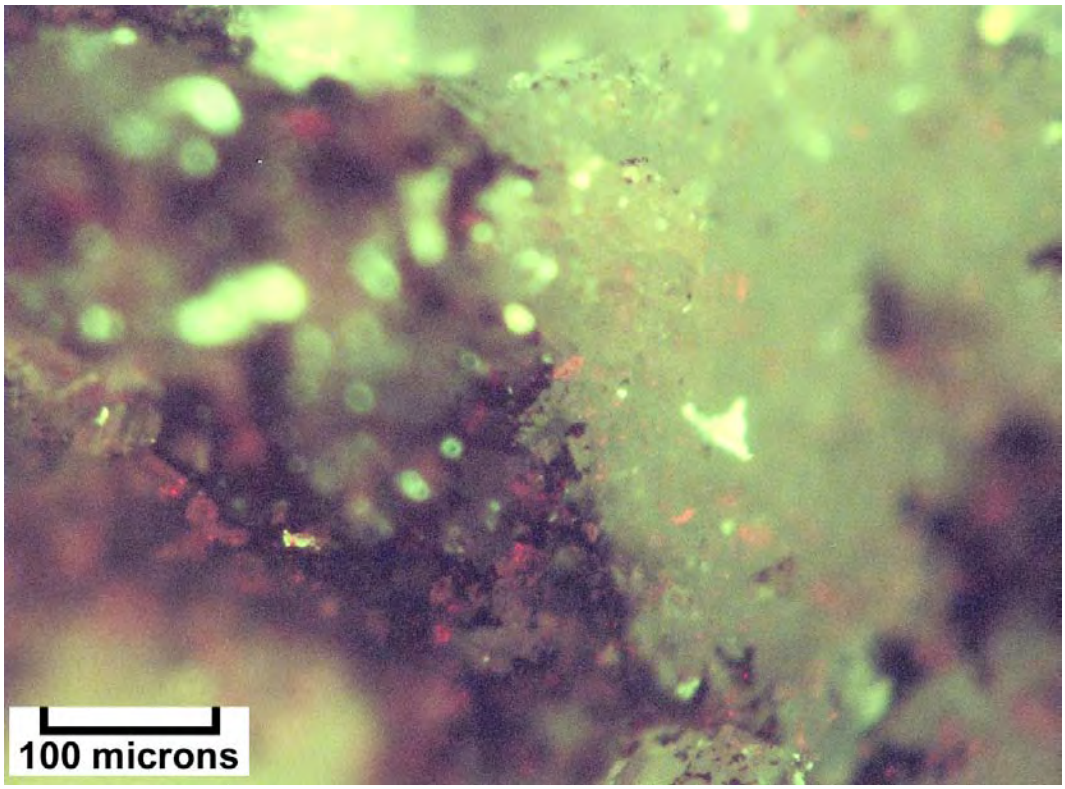

Photomicrograph – Texaco Government Smoot 2 (Map #5), 8736-37 feet, small "speckles" of live epifluorescence up to 2.0 in coarsely crystalline dolomite with good intercrystalline porosity lined with bitumen.

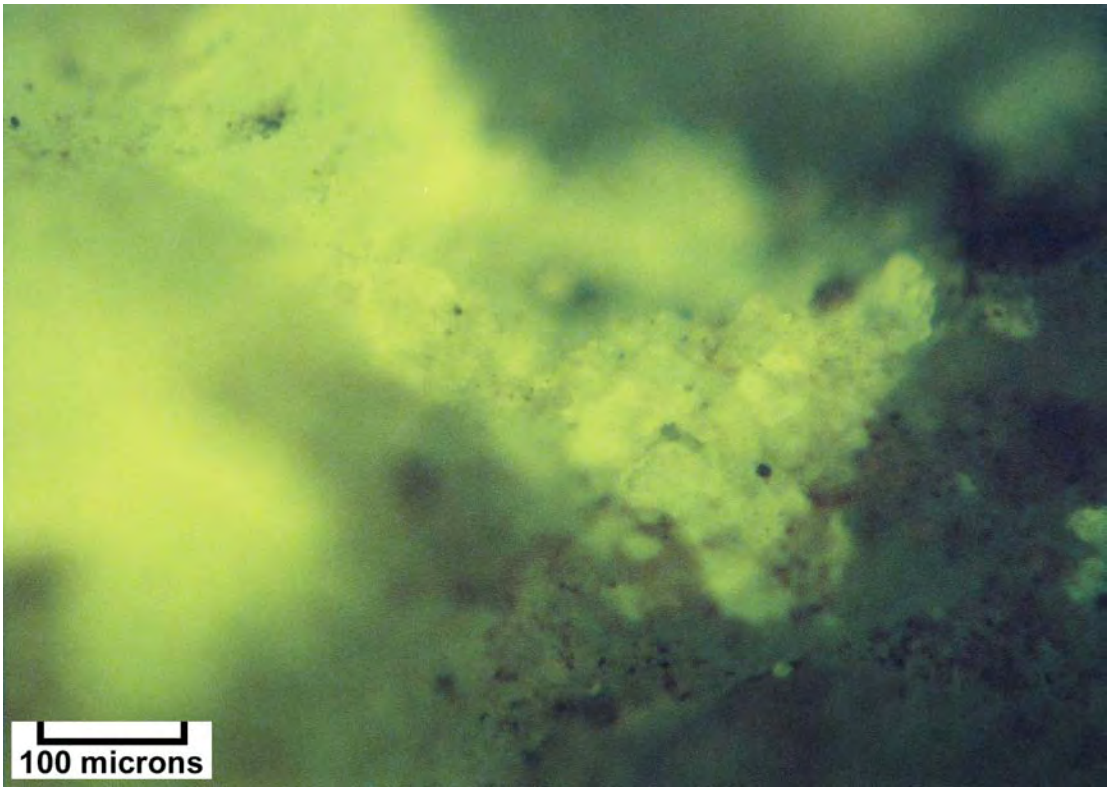

Photomicrograph – Shell Chaffin 1 (Map #6), 7520-30 feet, 1.5 epifluorescence patches surrounded by a "dead" matrix medium crystalline dolomite with minor intercrystalline porosity.

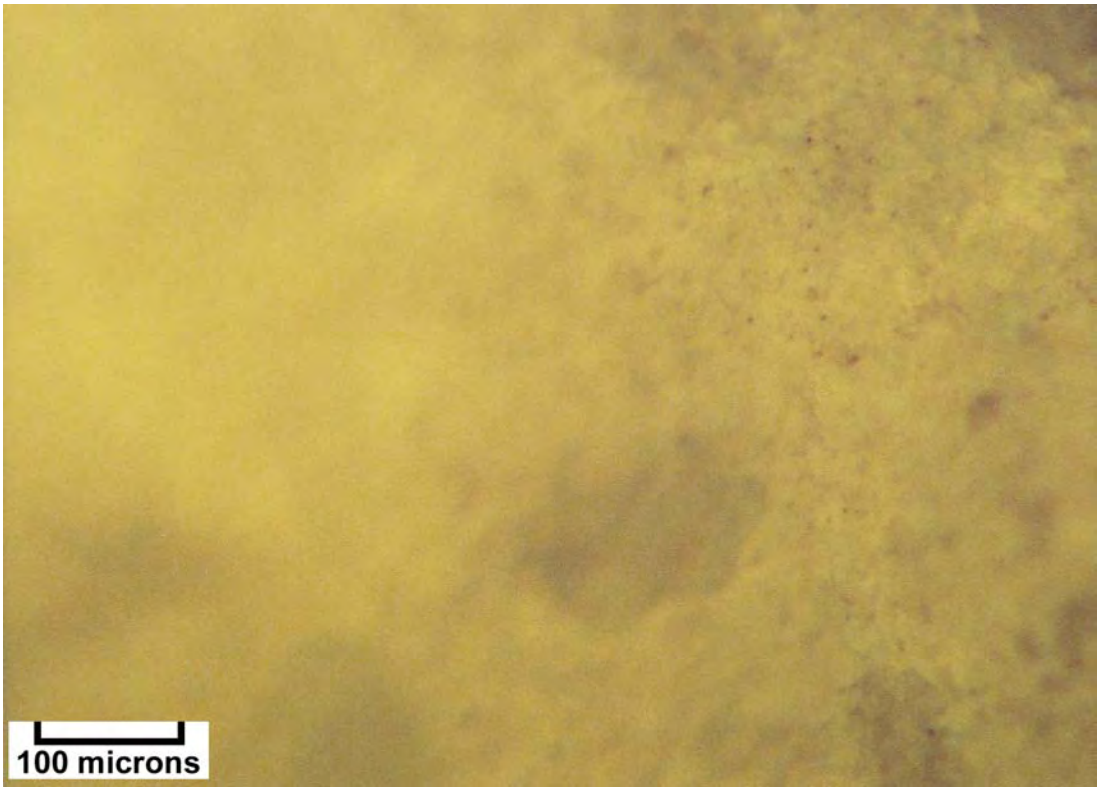

Photomicrograph – Shell Chaffin 1 (Map #6), 7530-40 feet, 1.5 epifluorescence in finely crystalline dolomite containing high porosity and low permeability, no bitumen.

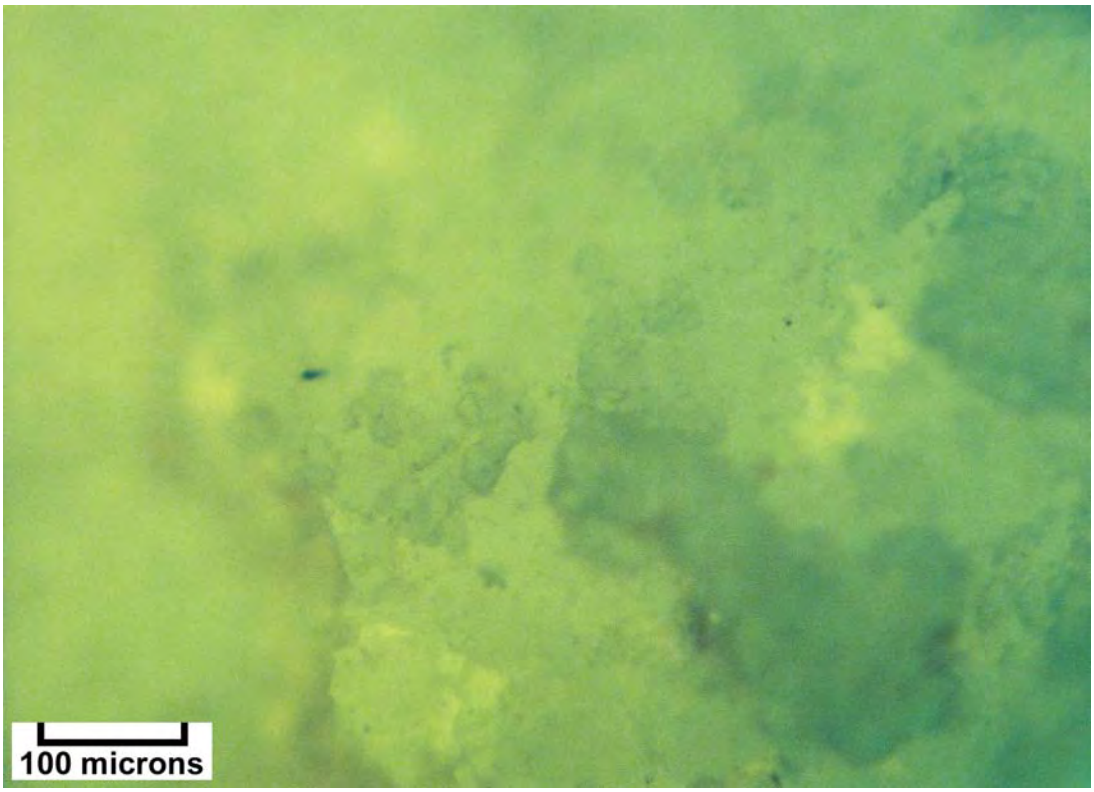

Photomicrograph – Federal Hatt 1 (Map #7), 5970-80 feet, 2.5 epifluorescence in medium crystalline dolomite, no bitumen.

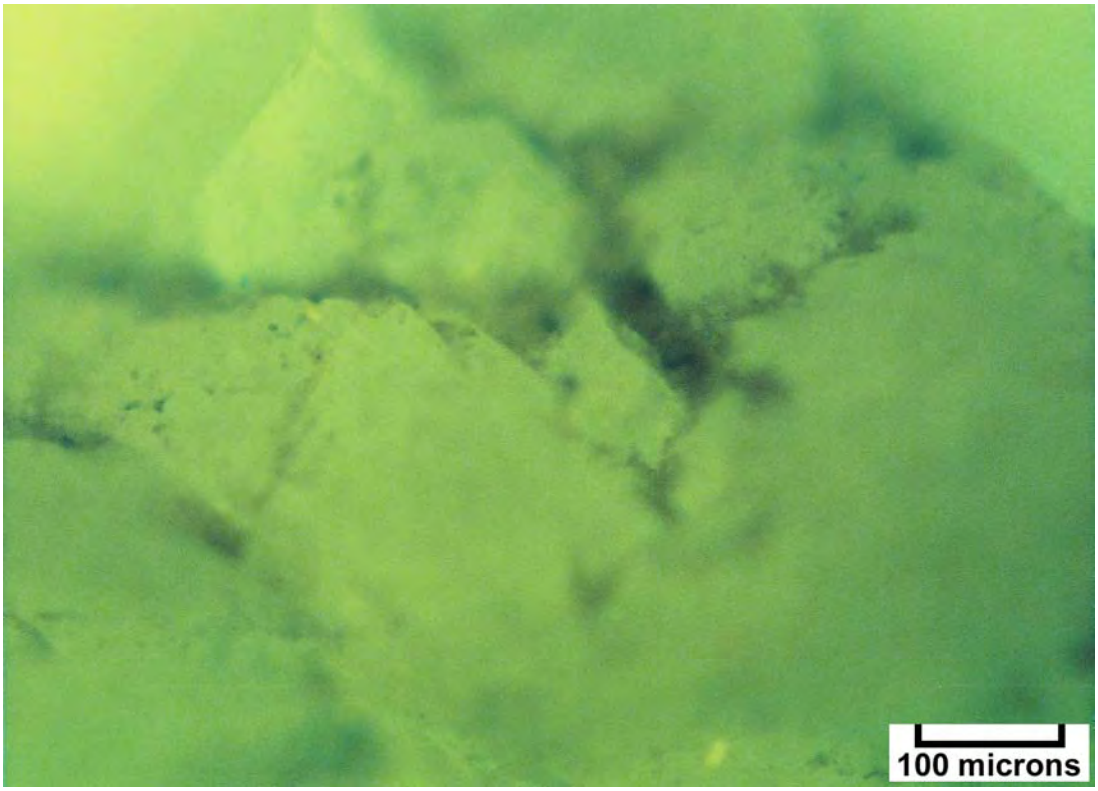

Photomicrograph – Federal Hatt 1 (Map #7), 6005-10 feet, 0.5 epifluorescence in coarsely crystalline dolomite, very good intercrystalline porosity and no bitumen.

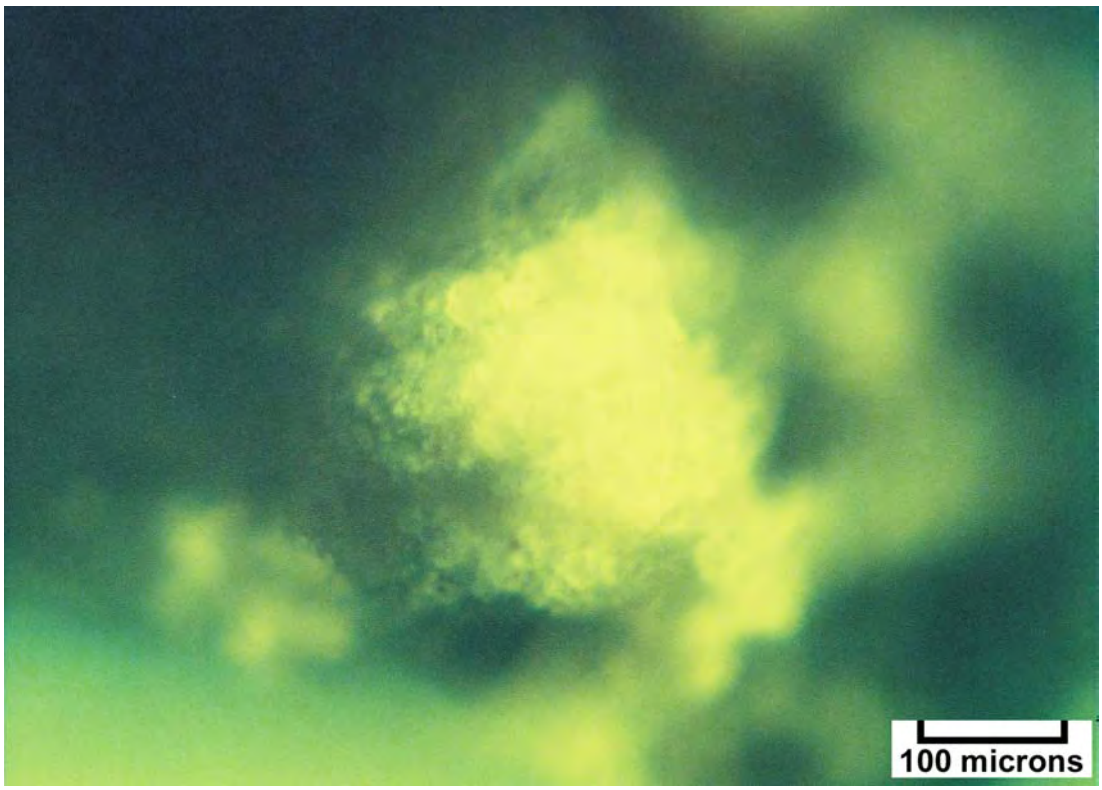

Photomicrograph – Conoco Federal 31 (Map #10), 10,470-80 feet, patchy 1.5 epifluorescence surrounded by zero epifluorescence in finely crystalline dolomite with minor intercrystalline porosity.

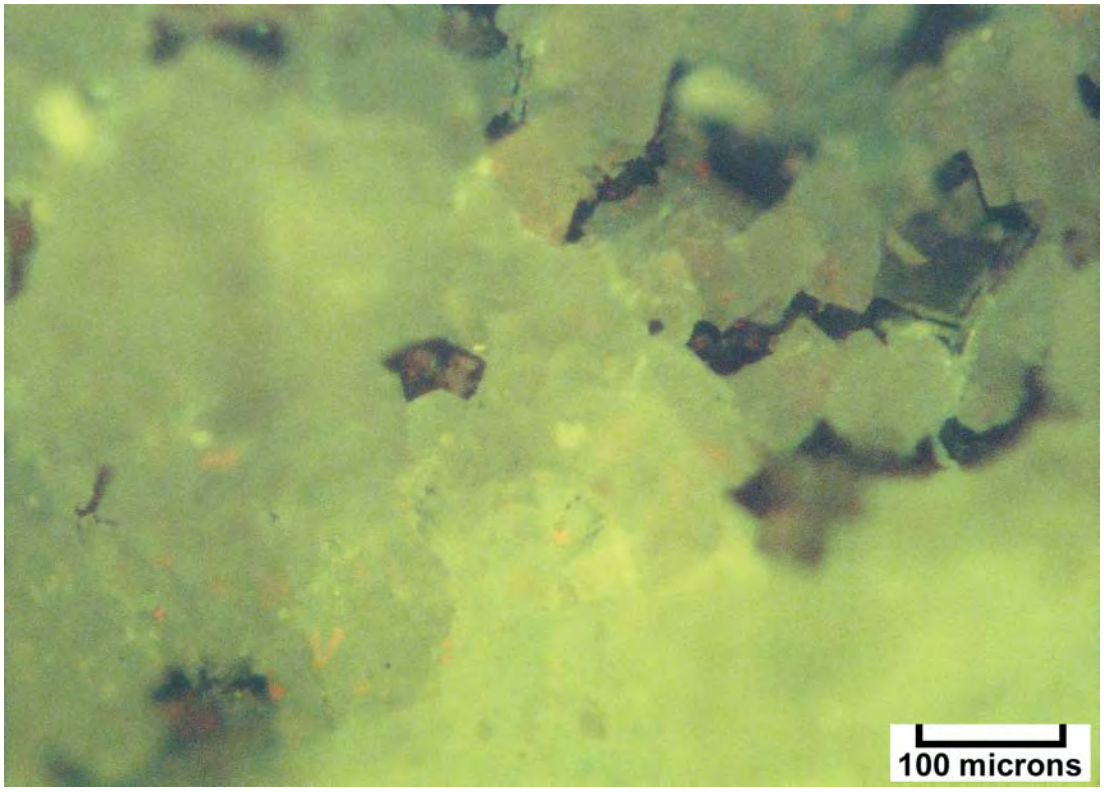

Photomicrograph – Conoco Federal 31 (Map #10), 10740-50 feet, essentially no epifluorescence in coarsely crystalline dolomite with good intercrystalline pores containing bitumen.

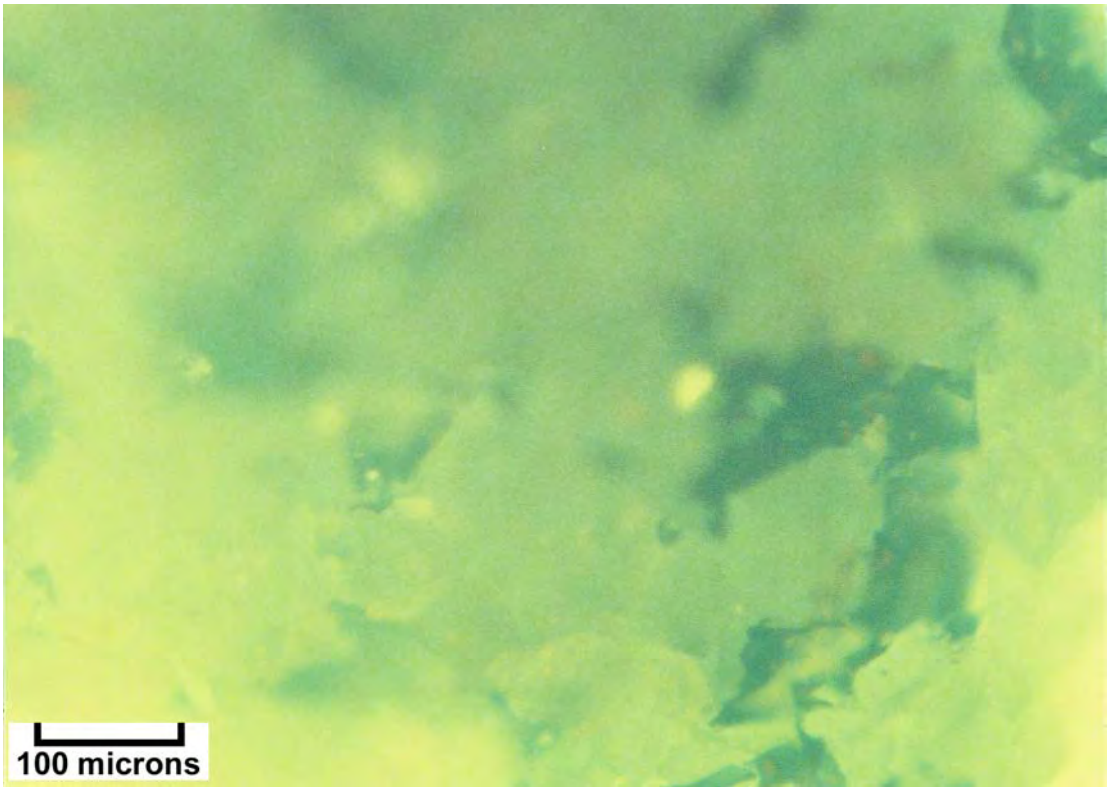

Photomicrograph – Conoco Federal 31 (Map #10), 10,750-60 feet, no epifluorescence in coarsely crystalline dolomite containing good intercrystalline porosity and significant amounts of bitumen.

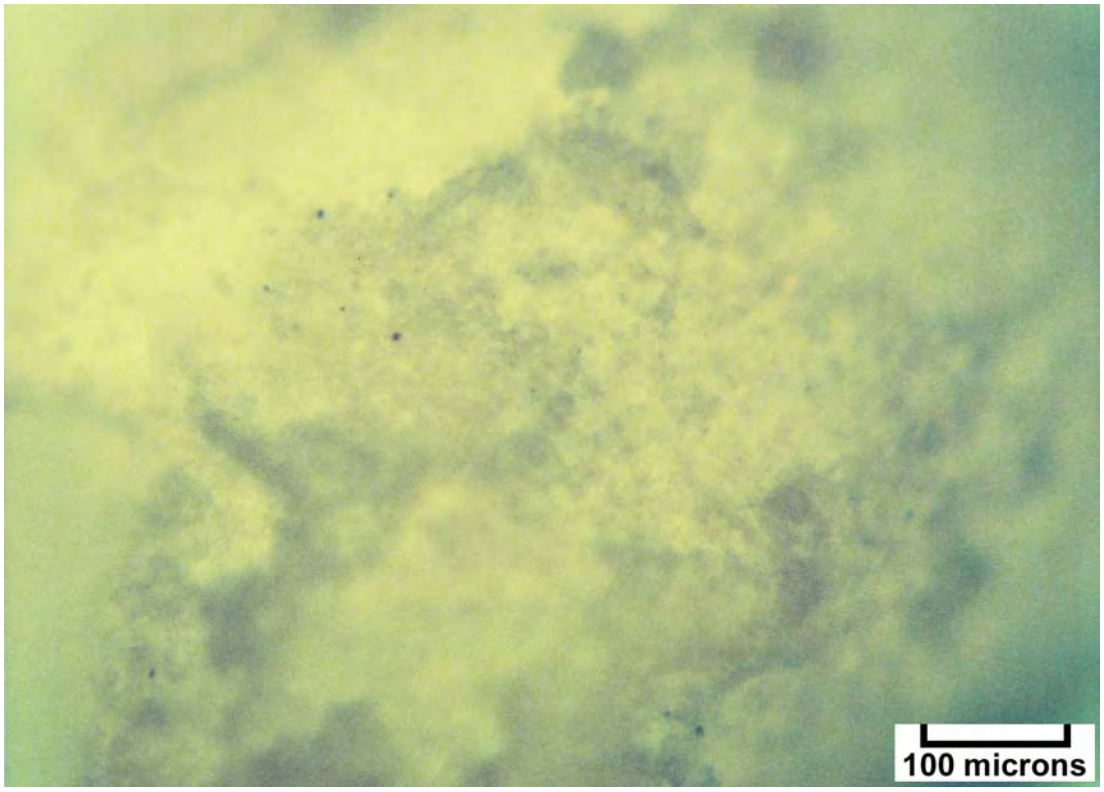

Photomicrograph – McRae Federal 1 (Map #12), 8485-95 feet, 2.5 epifluorescence in medium crystalline dolomite containing no porosity or bitumen.

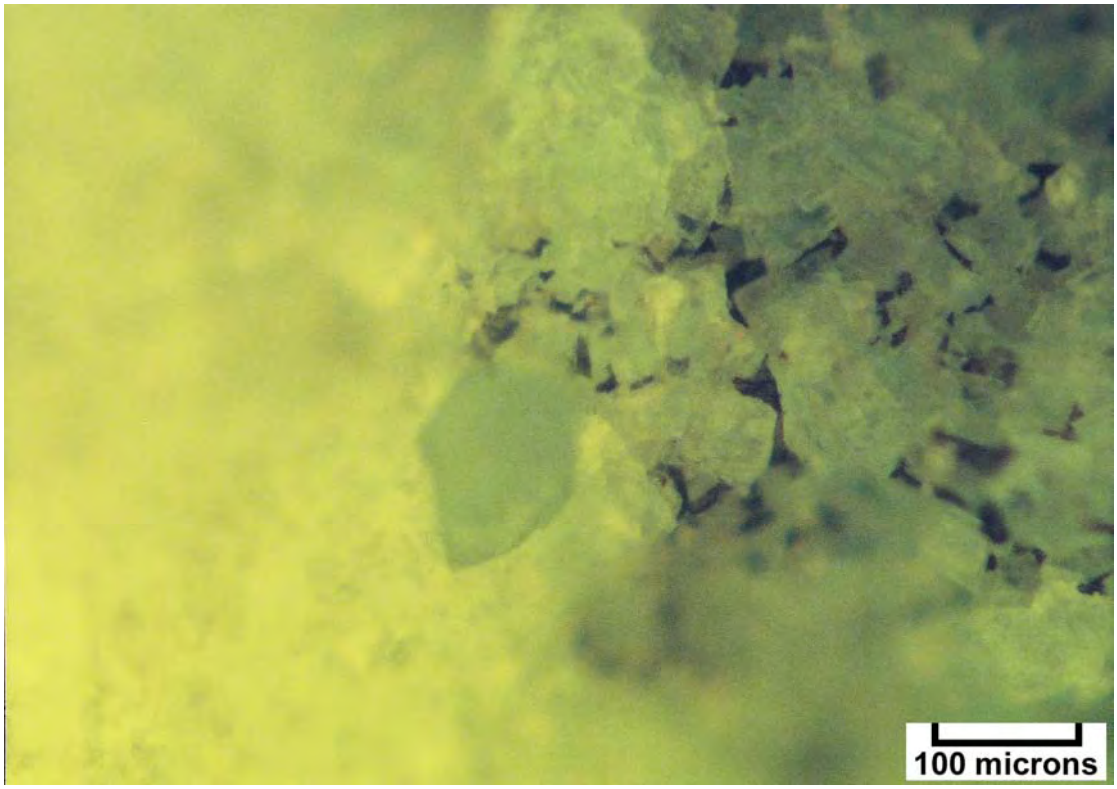

Photomicrograph – Superior Bow Knot Unit 1 (Map #13), 6075-80 feet, patchy 2.0 epifluorescence in medium crystalline dolomite with abundant intercrystalline pores and bitumen.

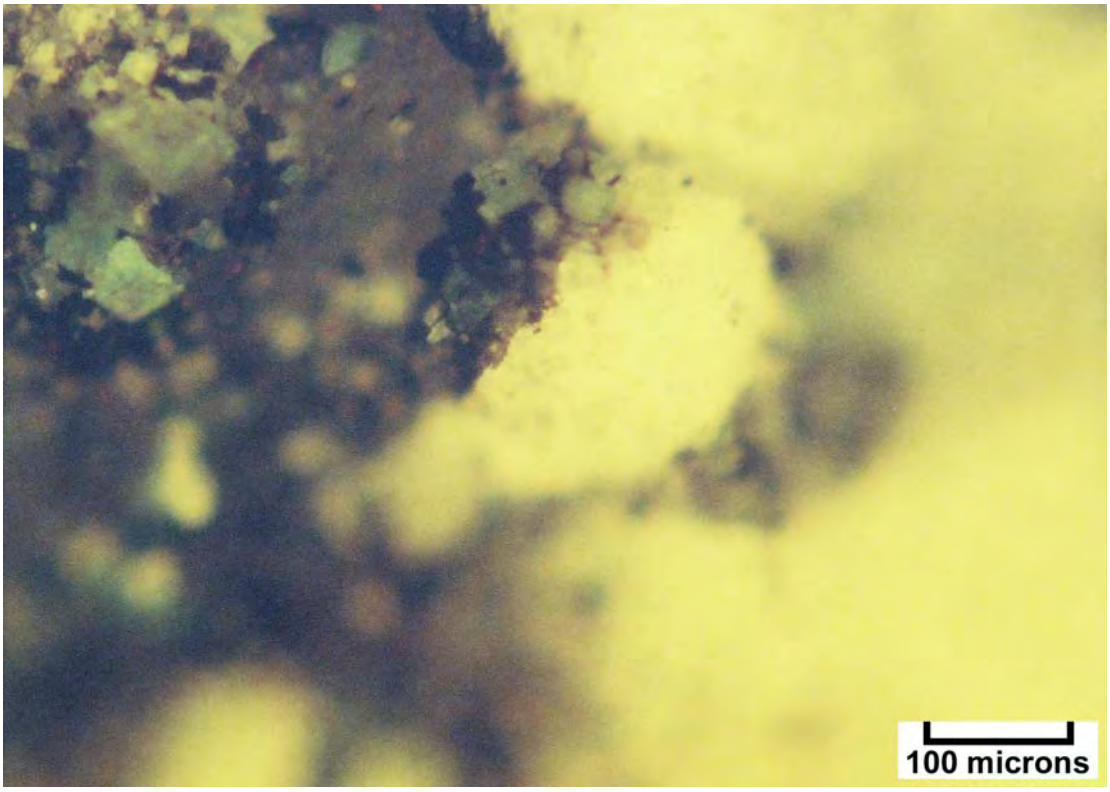

Photomicrograph – Superior Bow Know Unit 1 (Map #13), 6080-85 feet, patchy 2.5 epifluorescence in areas of good intercrystalline porosity and abundant bitumen in medium crystalline dolomite.

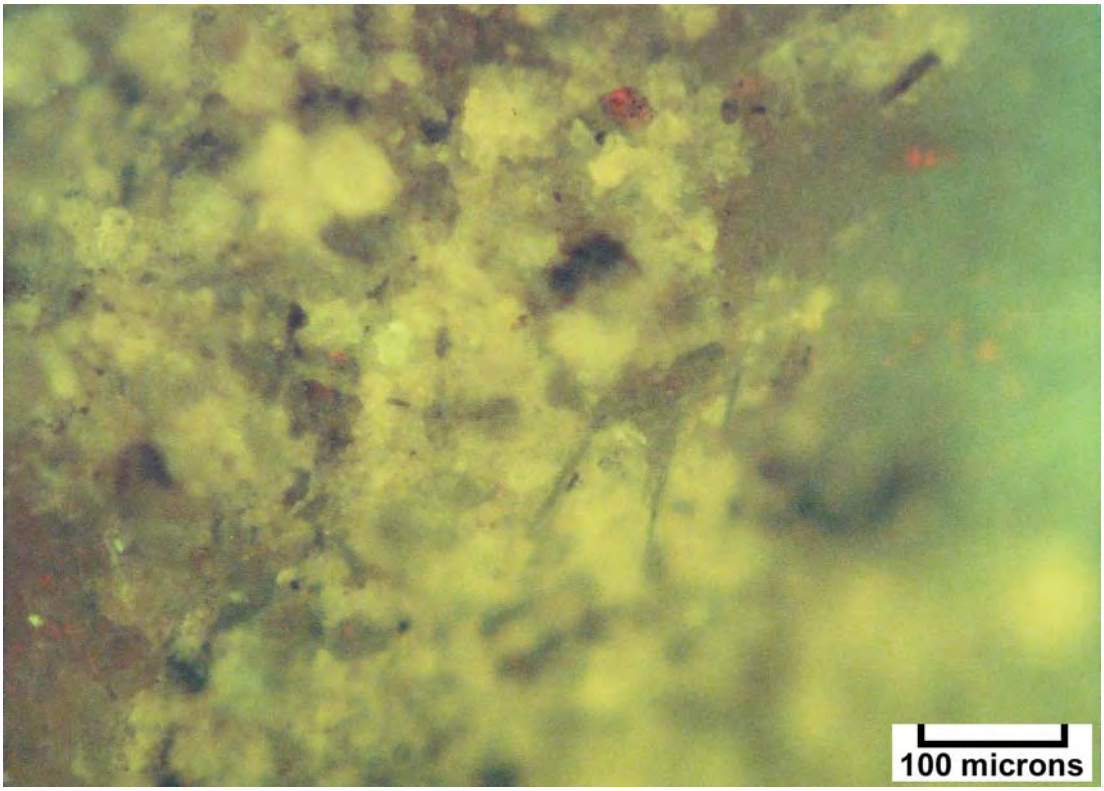

Photomicrograph – Superior Bow Know Unit 1 (Map #13), 6395-6400 feet, 0.5 epifluorescence in medium crystalline dolomite with good intercrystalline porosity and a trace of bitumen.

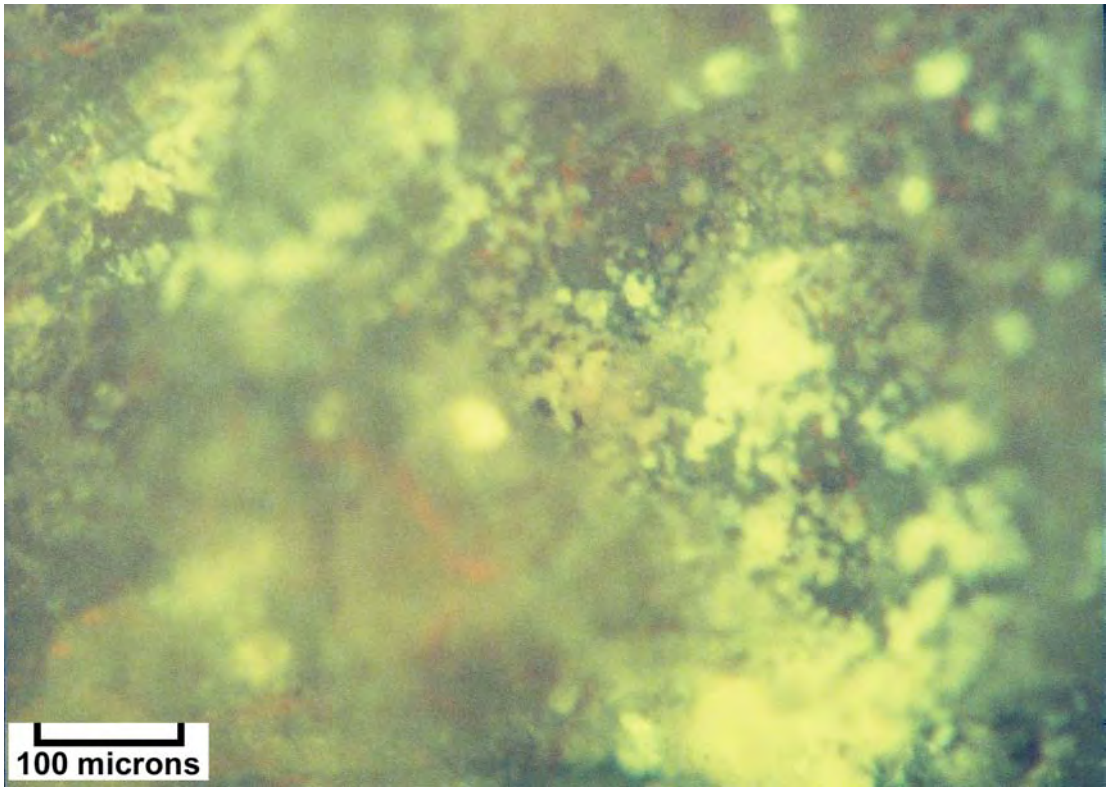

Photomicrograph – Big Flat/Bartlett Flat 1 (Map #14), 8560-70 feet, patchy 1.5 epifluorescence in microcrystalline dolomite.

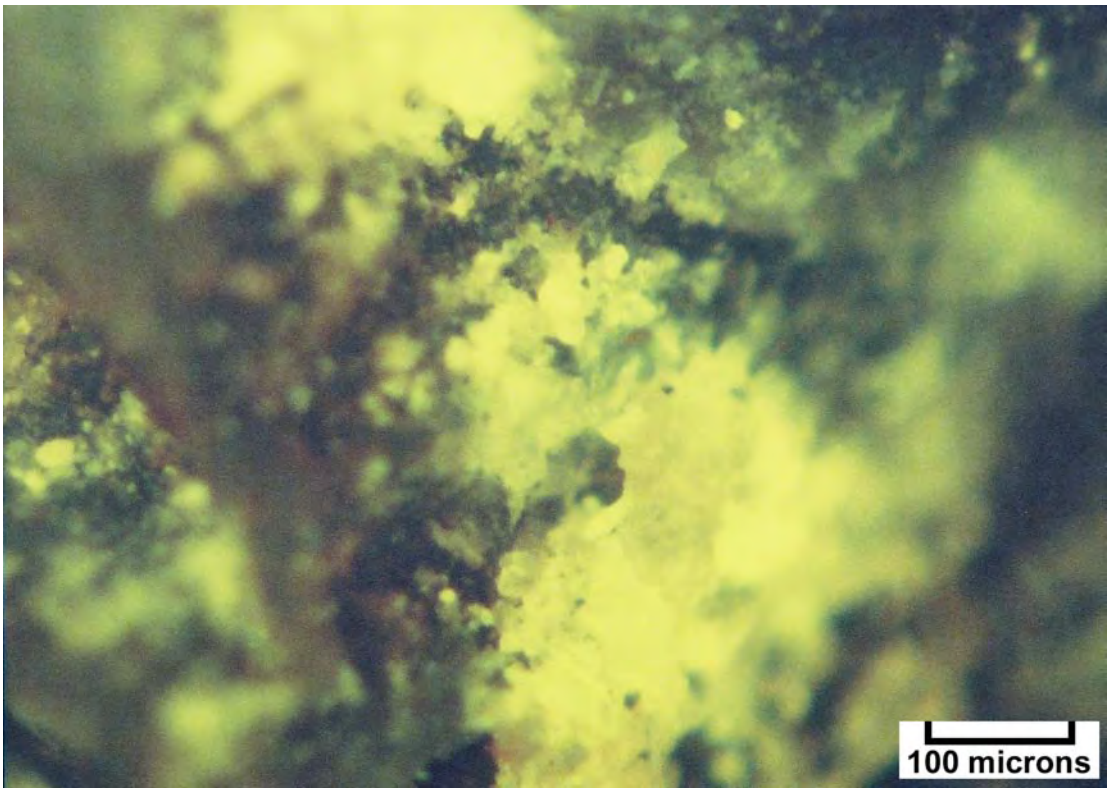

Photomicrograph – Big Flat/Bartlett Flat 1 (Map #14), 8570-80 feet, patchy 1.5 epifluorescence in microcrystalline dolomite with intercrystalline porosity.

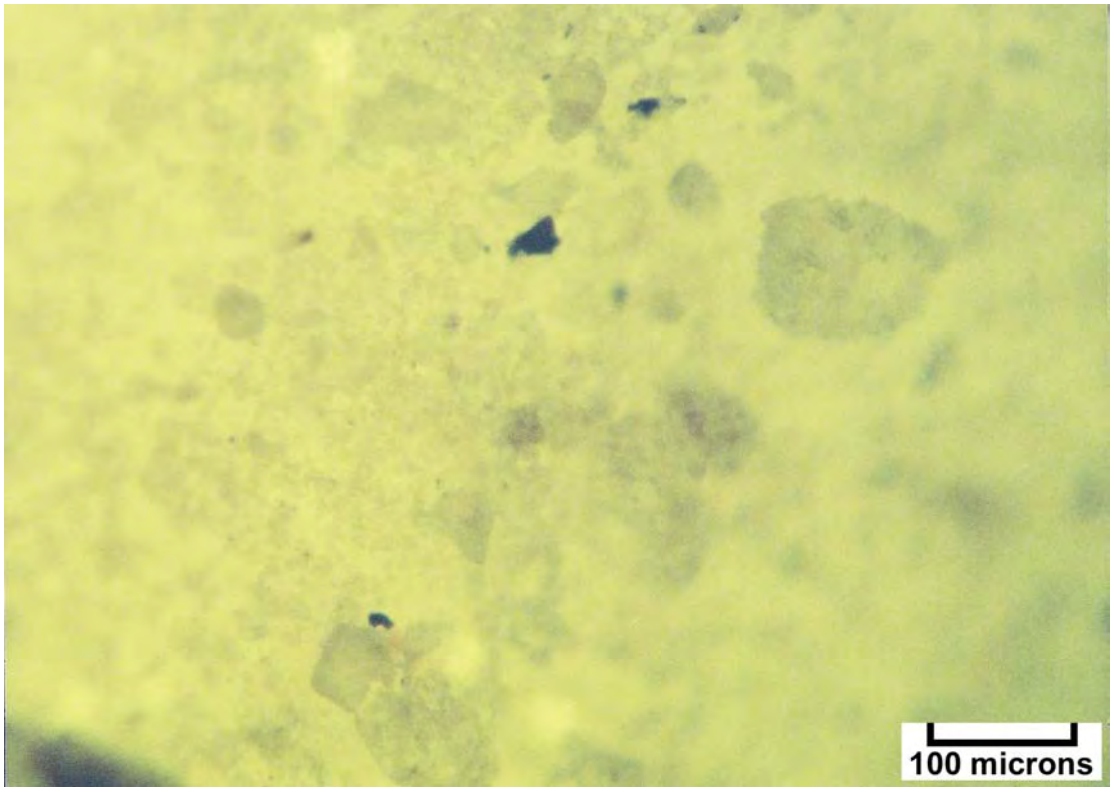

Photomicrograph – Big Flat/Bartlett Flat 1 (Map #14), 8630-40 feet, 2.0 epifluorescence in microcrystalline dolomite with high microcrystalline porosity and low permeability.

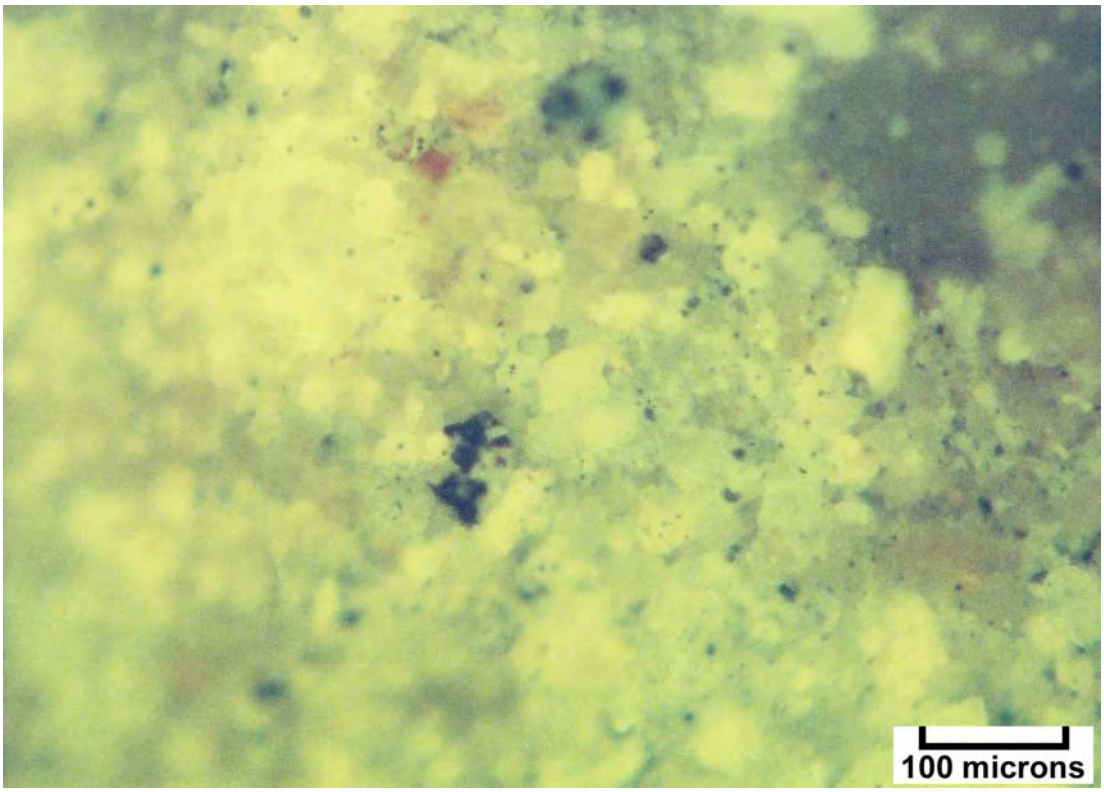

Photomicrograph – Big Flat/Bartlett Flat 1 (Map #14), 8640-50 feet, patches of 1.5 epifluorescence in medium crystalline dolomite with low intercrystalline porosity, minor bitumen, and possible sulfide mineralization.

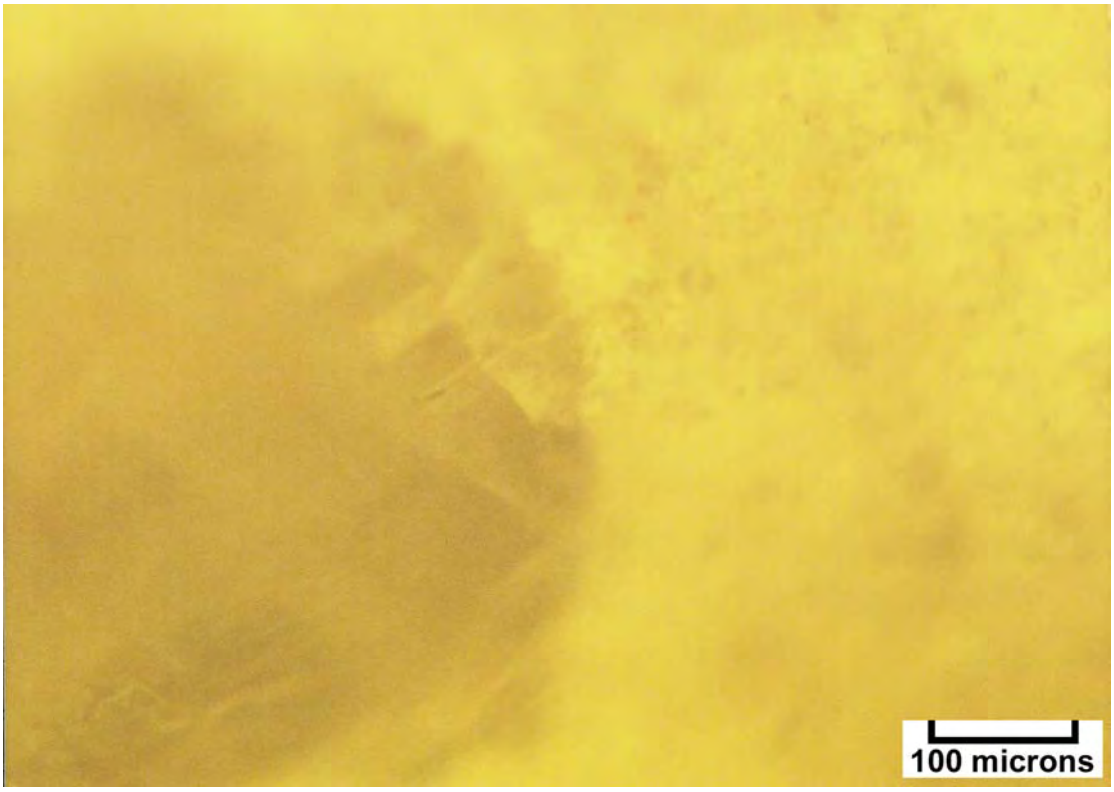

Photomicrograph – Standard Lookout Point 1 (Map #15), 6394-95 feet, 2.5 epifluorescence in microcrystalline dolomite with "dead" patch of anhydrite.

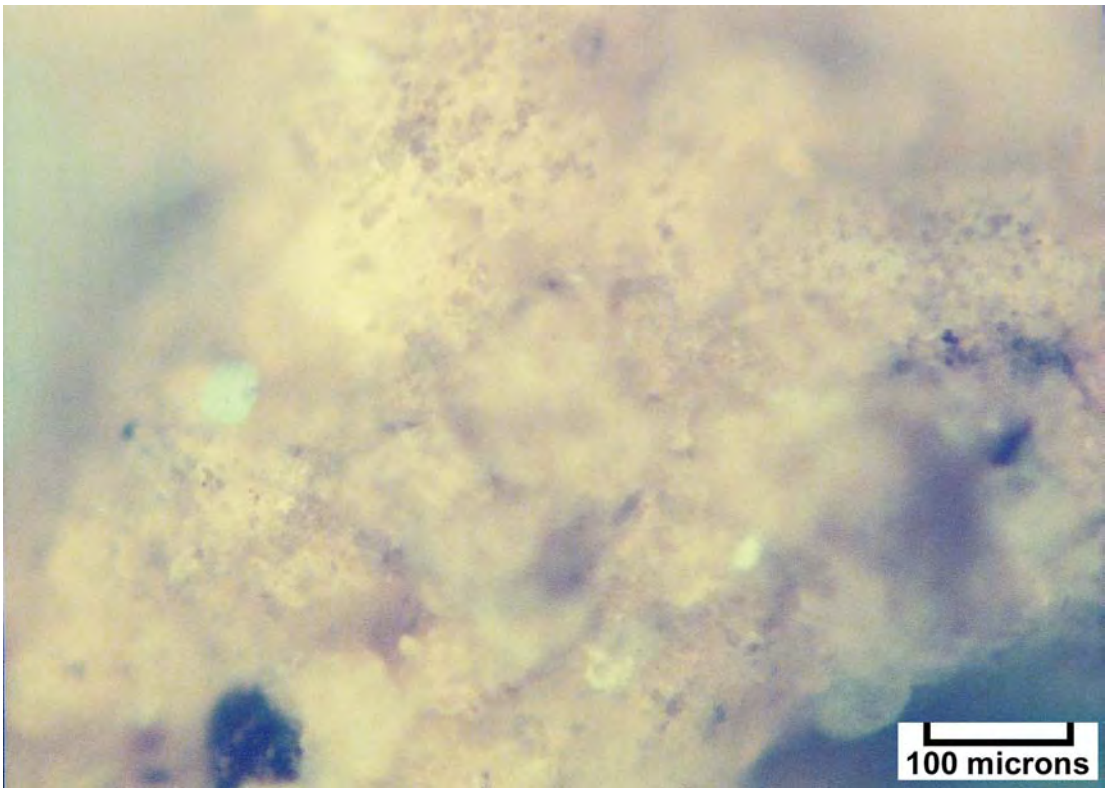

Photomicrograph – Standard Lookout Point 1 (Map #15), 6500-10 feet, 2.0 epifluorescence in coarsely crystalline dolomite containing modest intercrystalline porosity.

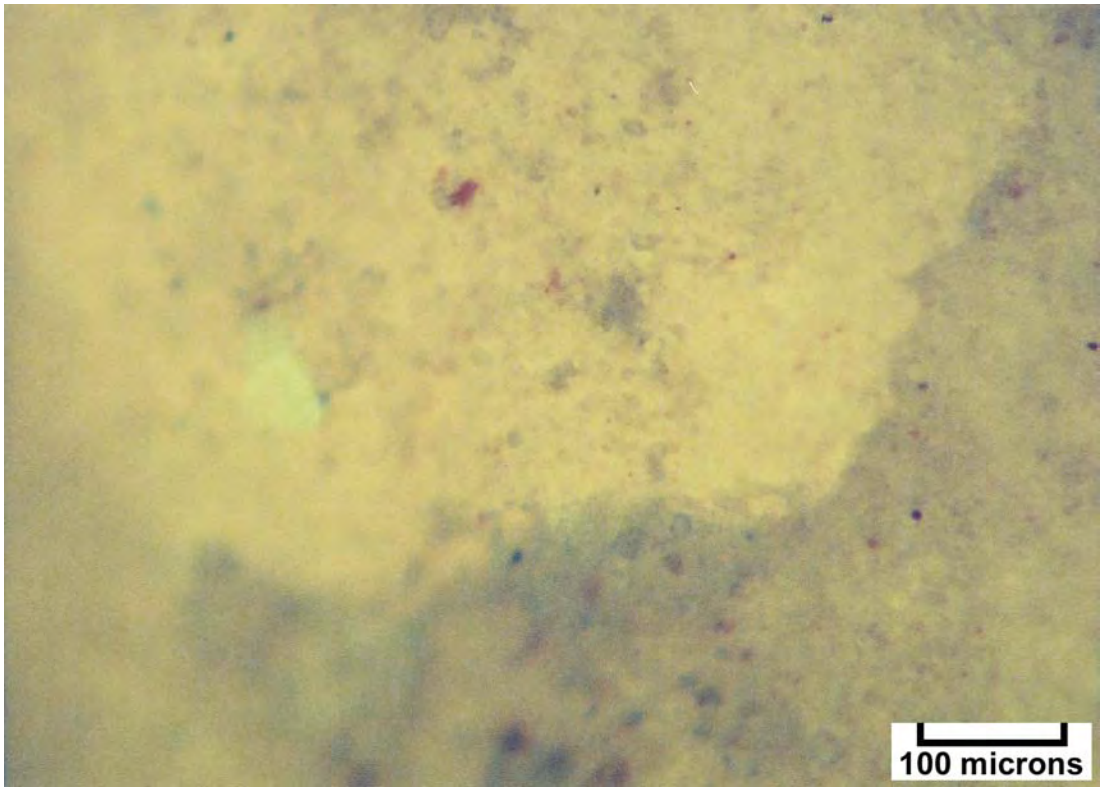

Photomicrograph – Federal Oil Bowknoll 1 (Map #16) 7375-80 feet, 2.5 epifluorescence in finely crystalline dolomite with fair intercrystalline porosity.

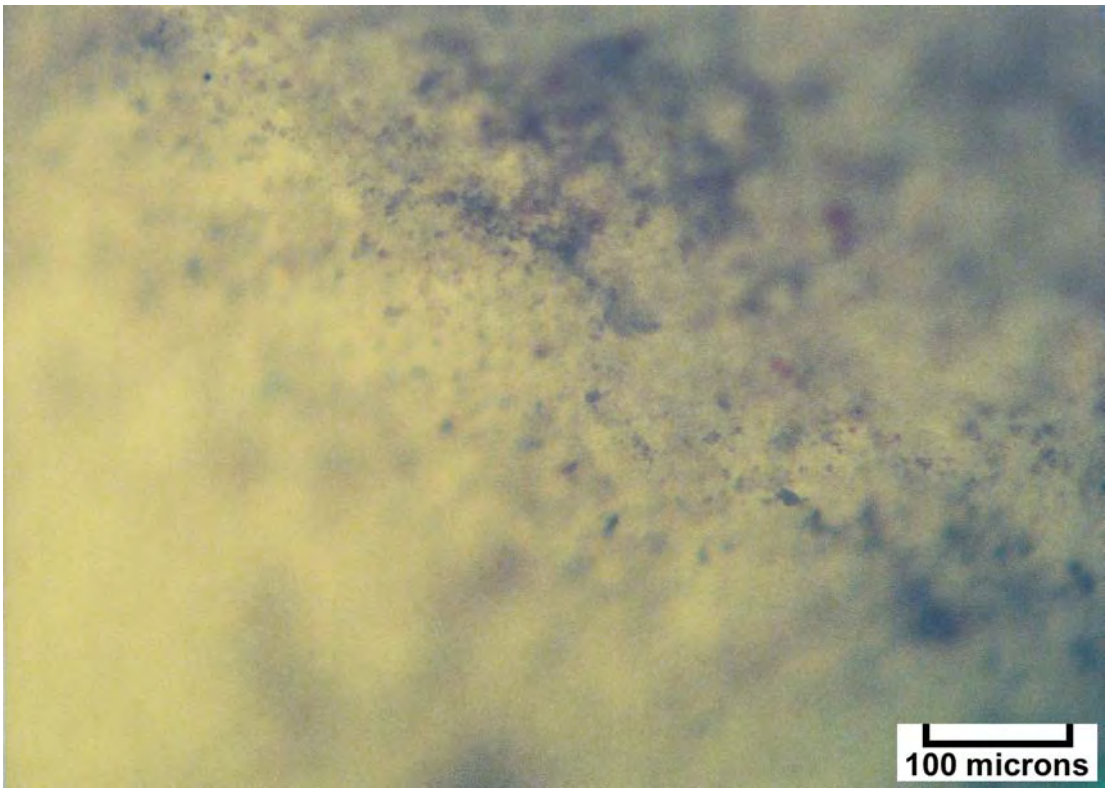

Photomicrograph – Federal Oil Bowknoll 1 (Map #16), 7385-90 feet, 2.5 epifluorescence in finely crystalline dolomite with minor intercrystalline porosity.

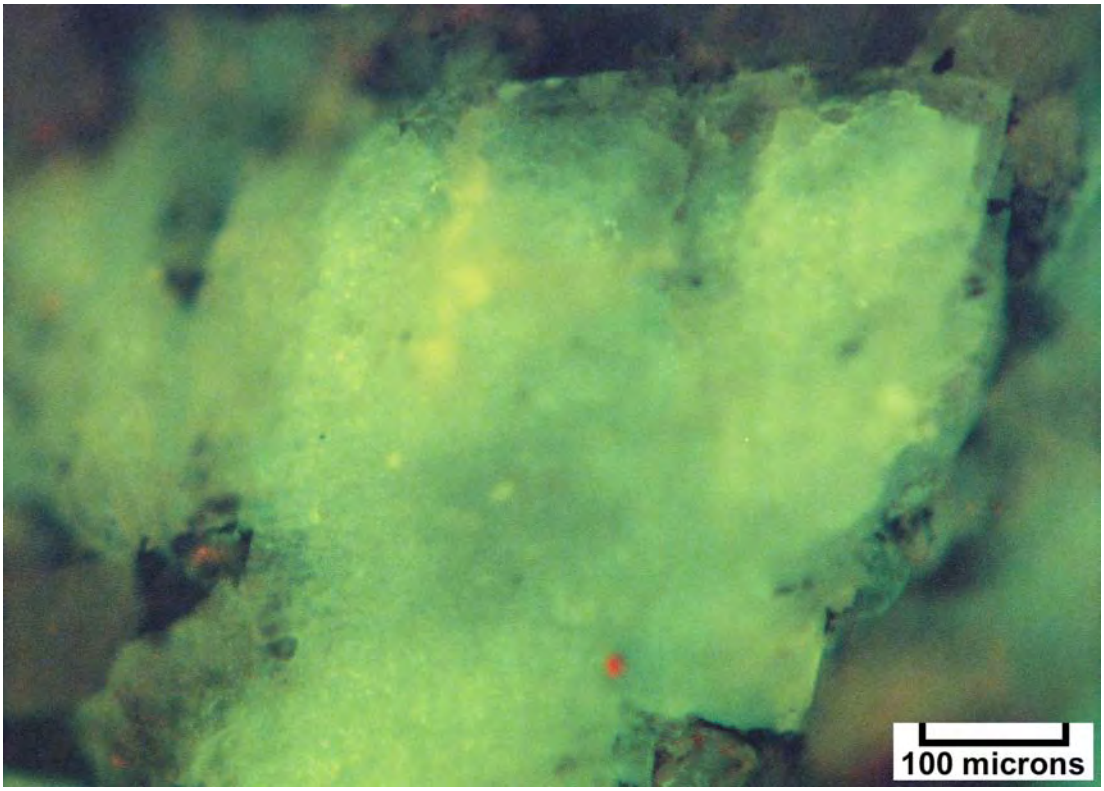

Photomicrograph – Southern Natural Long Canyon 1 (Map #17), 7580-85 feet, pale green 1.4 epifluorescence in coarse dolomite with good intercrystalline porosity and bitumen.

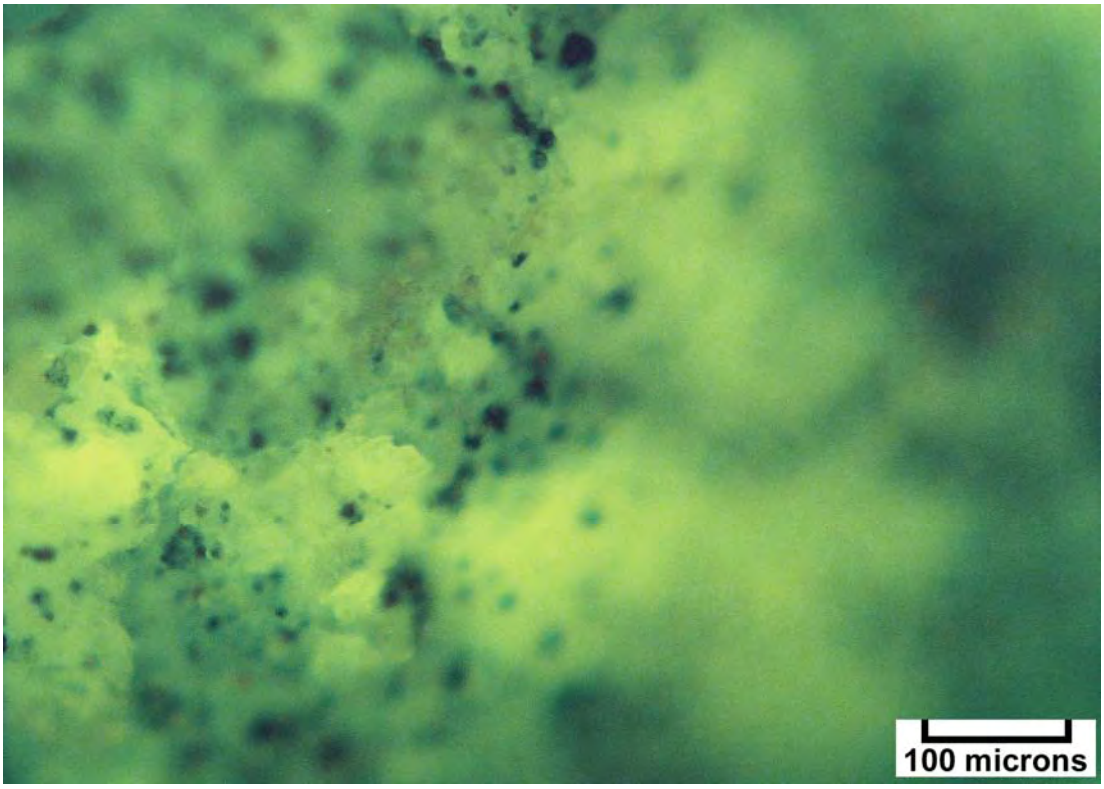

Photomicrograph – Southern Natural Long Canyon 1 (Map #17), 7585-90 feet, patches of 1.0 epifluorescence in medium crystalline dolomite containing good intercrystalline porosity and bitumen.

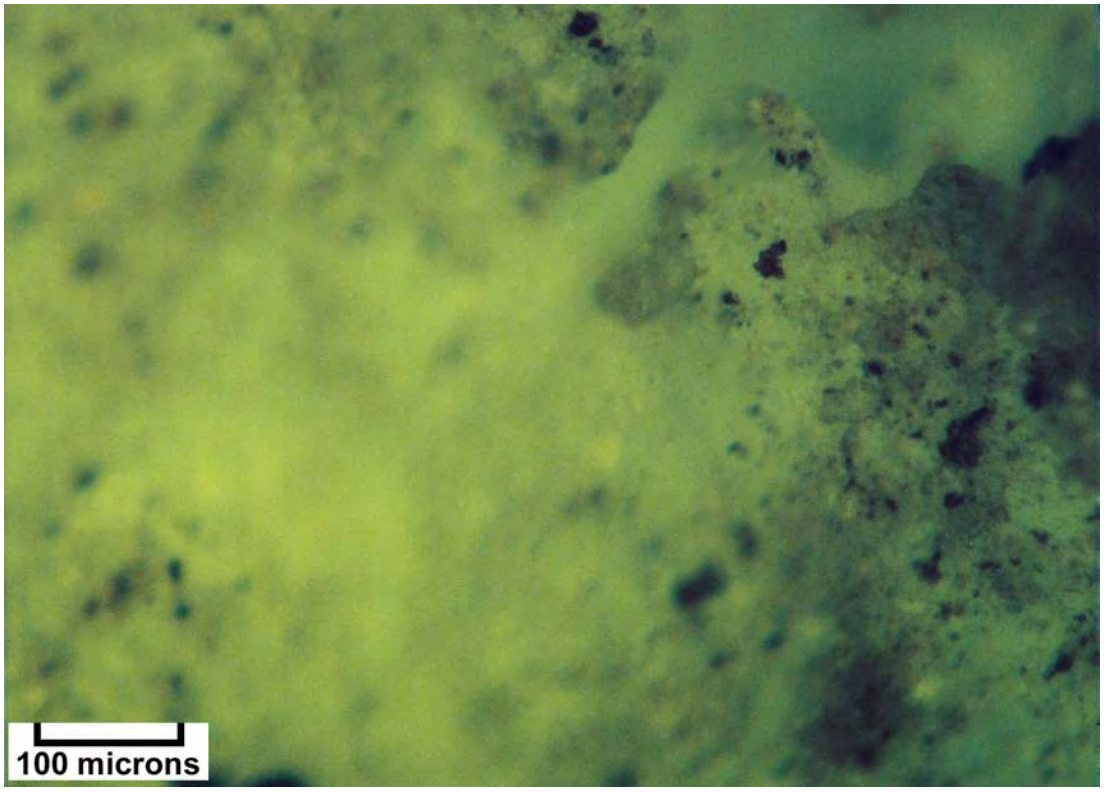

Photomicrograph – Pure Mineral Point 1 (Map #18), 7060-65 feet, 2.5 epifluorescence in medium crystalline dolomite with fair intercrystalline porosity and some bitumen.

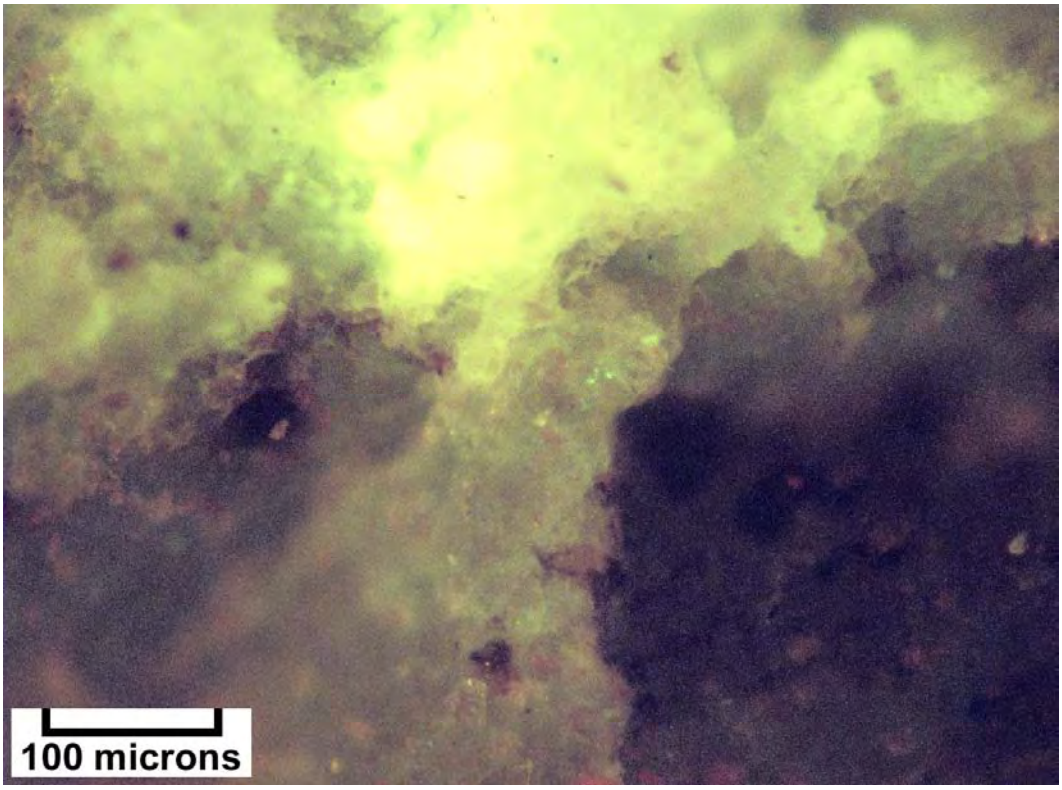

Photomicrograph – Pure Big Flat 3 (Map #19), 7714-15 feet, patchy 1.5 epifluorescence of a darker yellow color in coarsely crystalline dolomite containing good intercrystalline and vuggy porosity lined with bitumen.

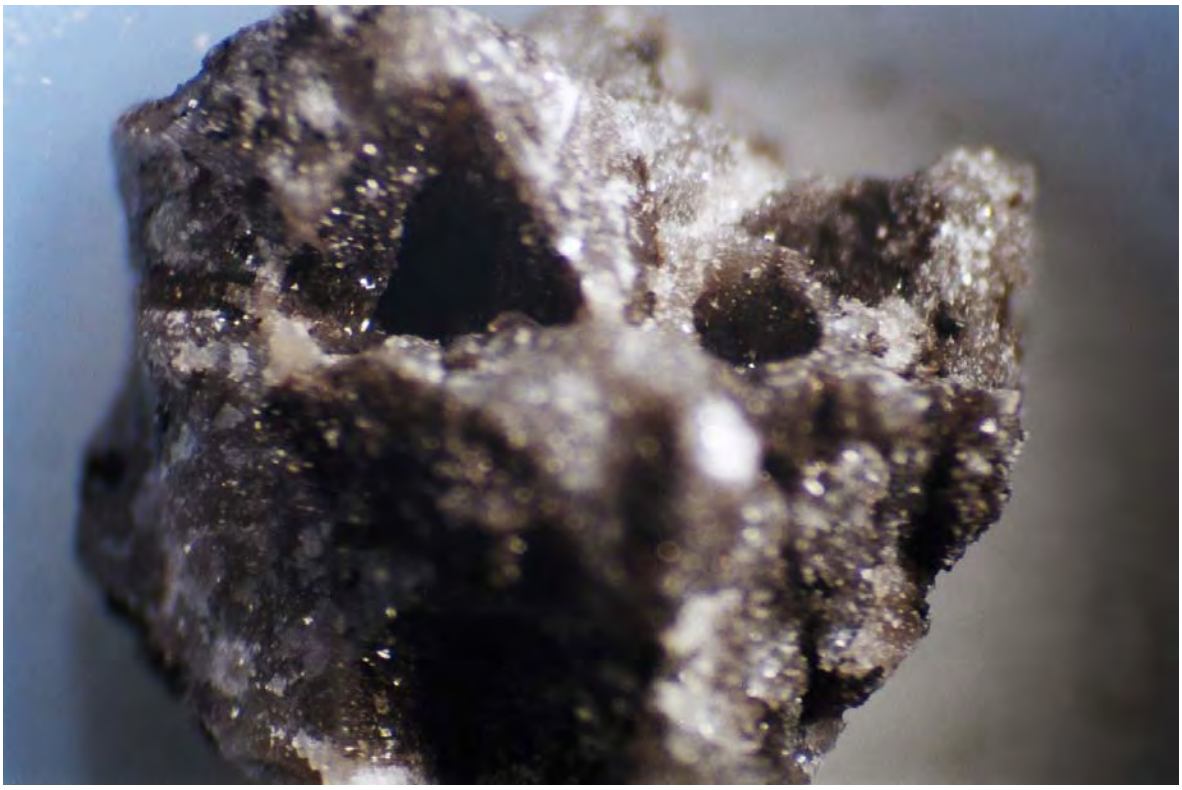

Binocular microscope image (2400x) – Pure Big Flat 3 (Map #19), 7714-15 feet, large cutting with rounded vugs and molds (?), dolomite crystals lining large pores. Note probable oil staining and bitumen.

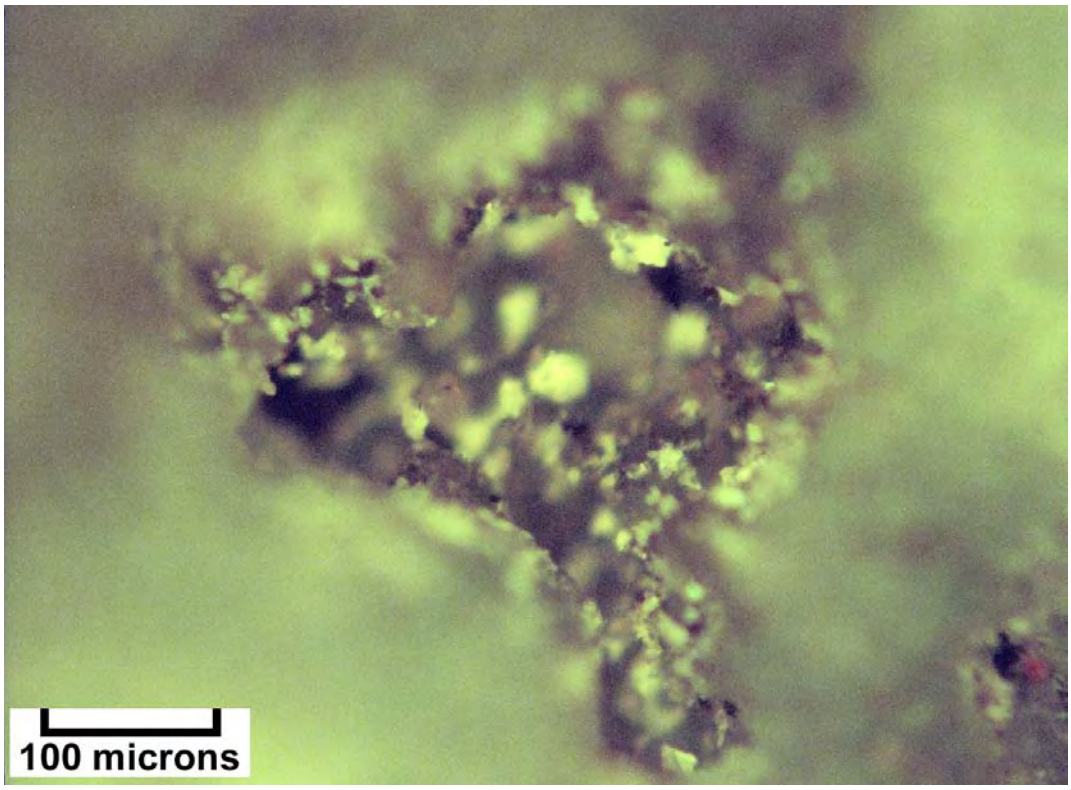

Photomicrograph – Pure Big Flat 3 (Map #19), 7715-16 feet, patches or speckles of dark yellow 1.5 epifluorescence in medium crystalline dolomite containing moldic and vuggy porosity lined with bitumen.

Binocular microscope image (3000x) – Pure Big Flat 3 (Map #19), 7715-16 feet, representative core chip with moldic/microvuggy porosity and bitumen (plus drilling mud).

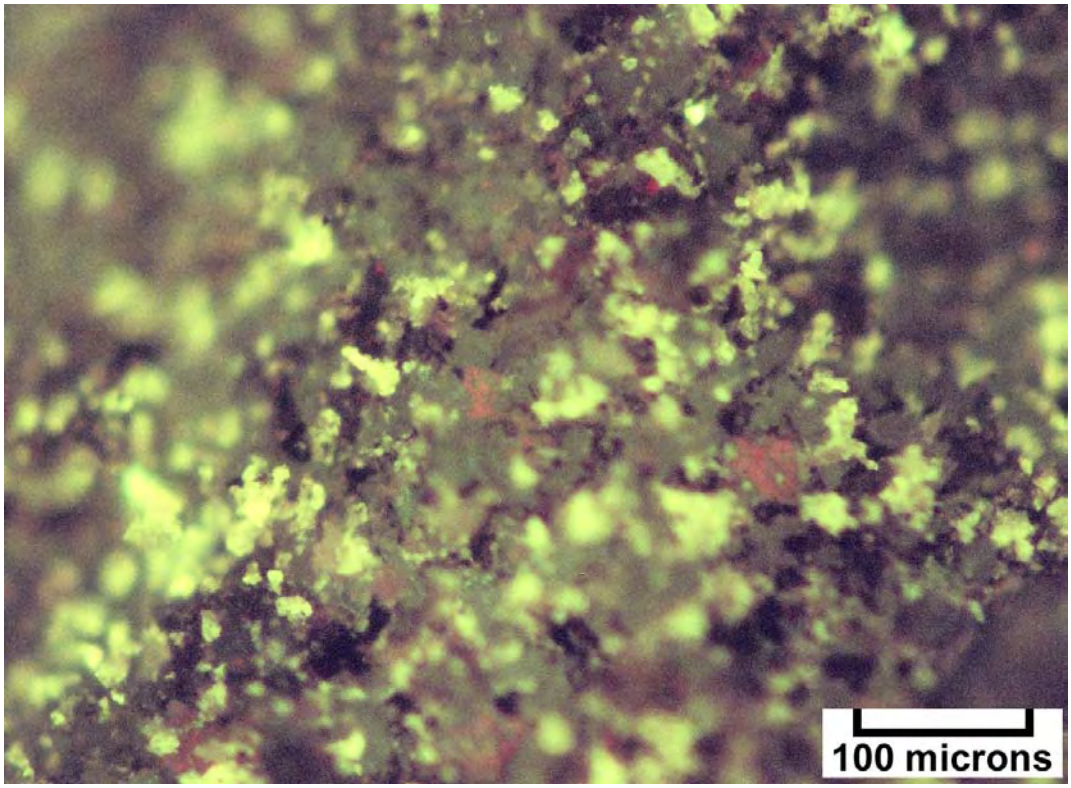

Photomicrograph – Pure Big Flat 3 (Map #19), 7716-17 feet, speckled dark yellow 0.5 epifluorescence in open pore with bitumen from a medium crystalline dolomite.

Binocular microscope image (1400x) – Pure Big Flat 3 (Map #19), 7716-17 feet, four representative samples used for grading showing tight white dolomite.

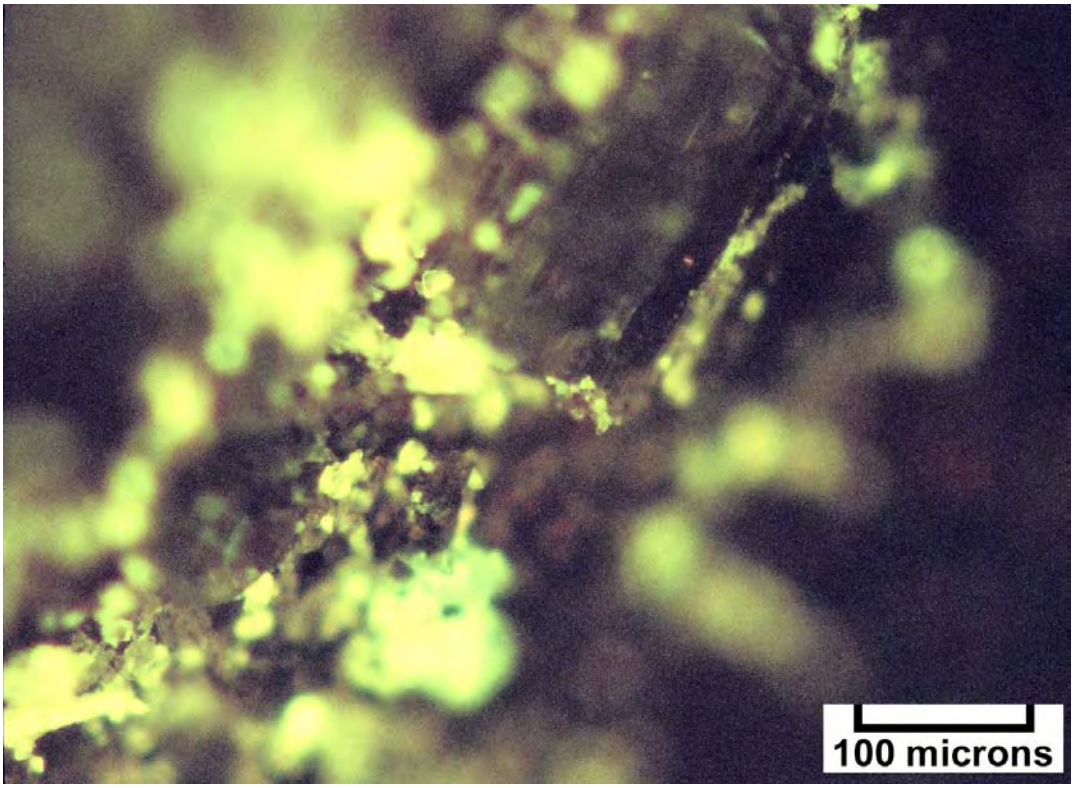

Photomicrograph – Pure Big Flat 3 (Map #19), 7717-18 feet, very speckled 1.2 epifluorescence on a bitumen surface and finely crystalline dolomite.

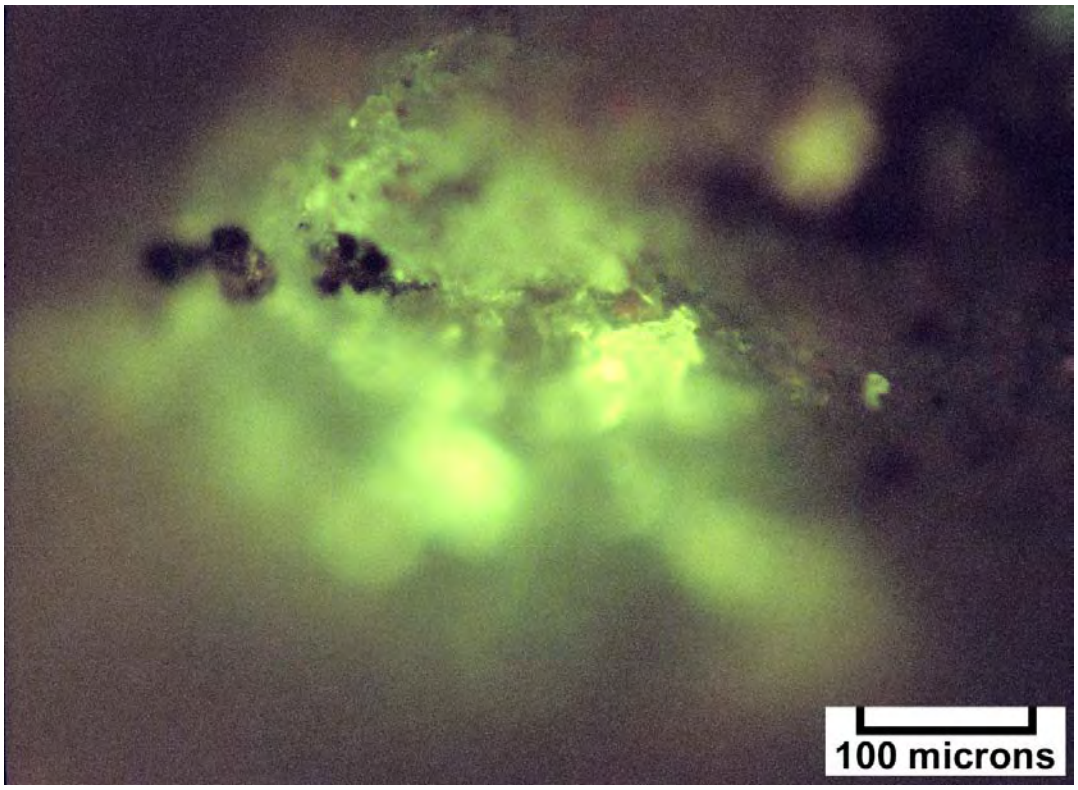

Photomicrograph – Pure Big Flat 3 (Map #19), 7718-19 feet, one bright patch of 0.3 epifluorescence with films around medium-sized dolomite crystals.

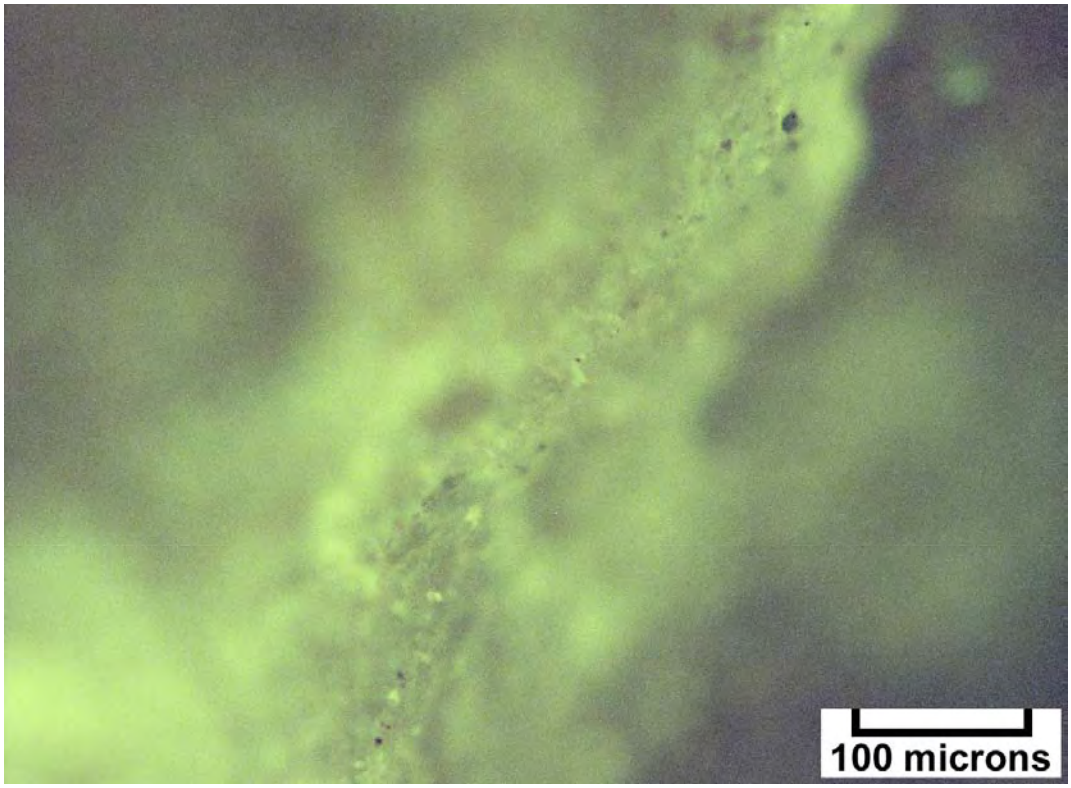

Photomicrograph – Pure Big Flat 3 (Map #19), 7719-20 feet, possible fracture showing good continuous 0.5 epifluorescence in a finely crystalline dolomite.

Binocular microscope image (1200x) – Pure Big Flat 3 (Map #19), 7719-20 feet, low porosity dolomite samples selected for epifluorescence grading.

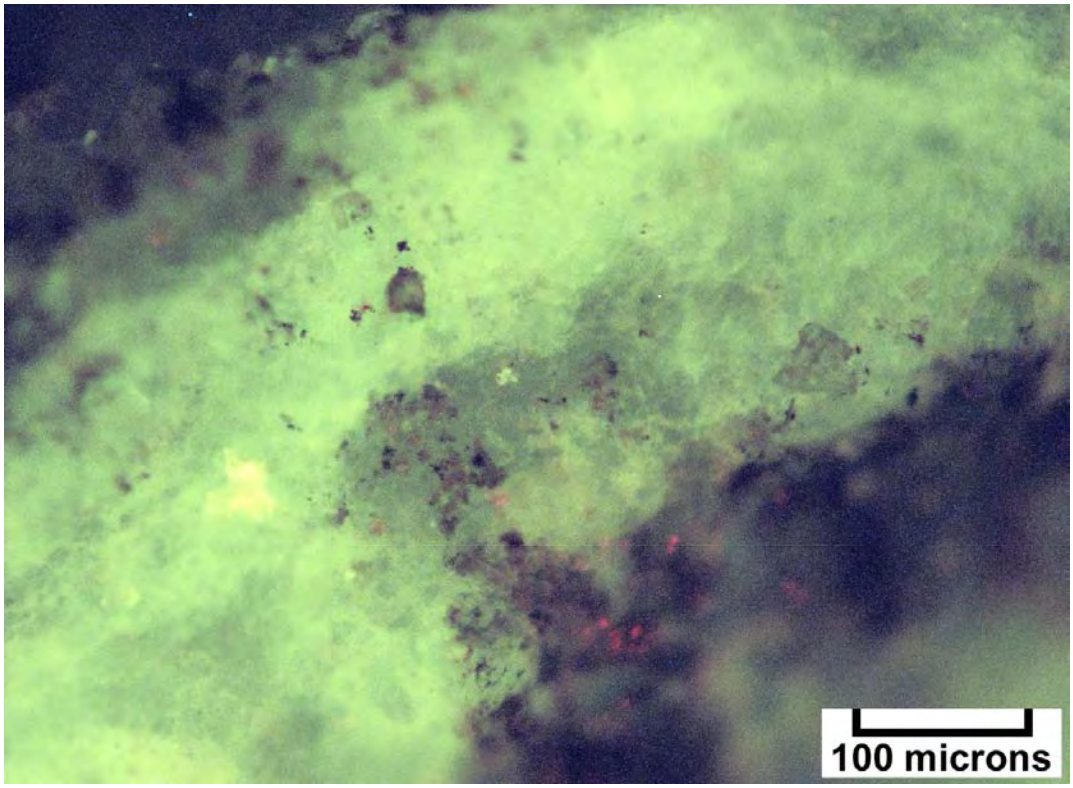

Photomicrograph – Pure Big Flat 3 (Map #19), 7720-21 feet, good bright continuous medium yellow 1.5 epifluorescence in medium crystalline dolomite.

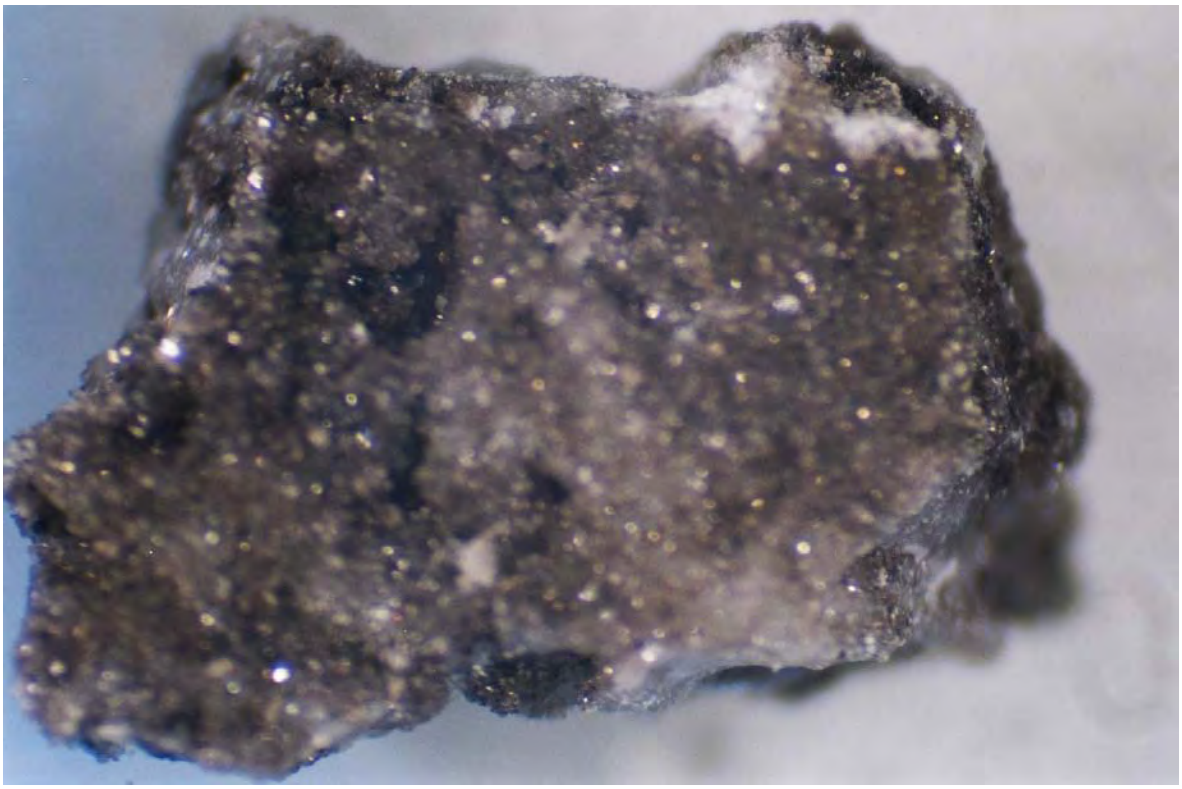

Binocular microscope image (2800x) – Pure Big Flat 3 (Map #19), 7720-21 feet, representative cutting showing porosity and bitumen in medium crystalline dolomite.

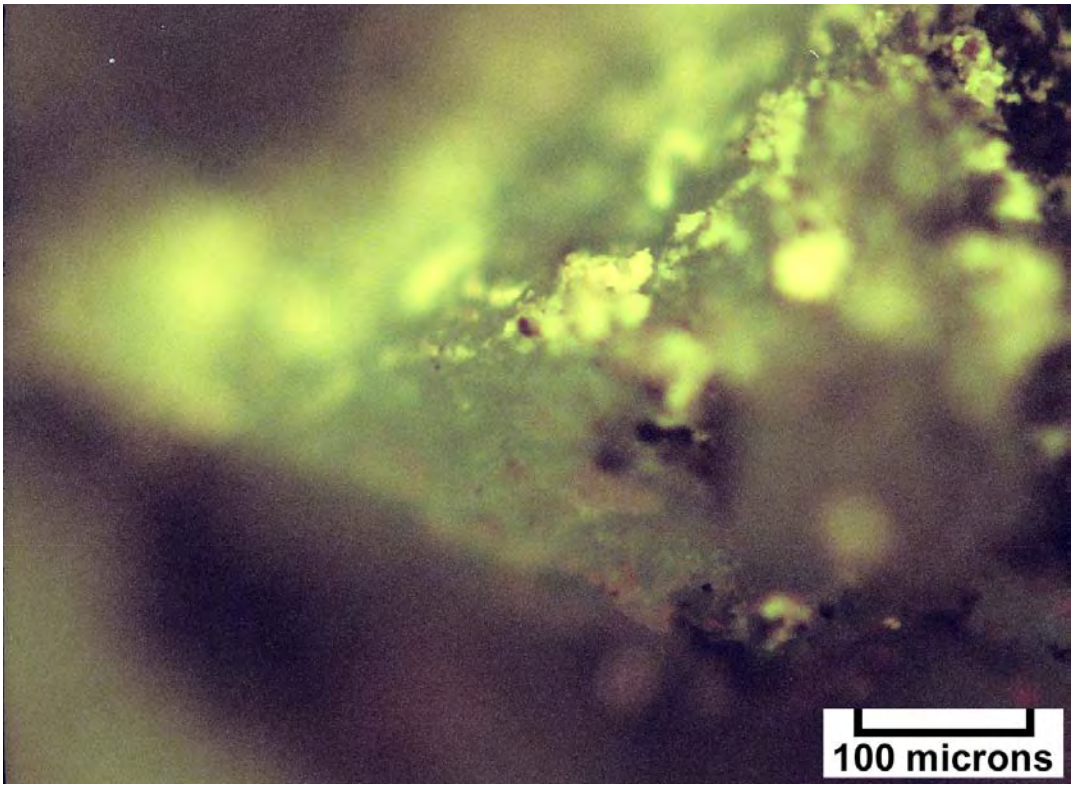

Photomicrograph – Pure Big Flat 3 (Map #19), 7721-22 feet, bitumen-lined pore with speckles of medium yellow 1.5 epifluorescence in medium crystalline dolomite.

Binocular microscope image (1500x) – Pure Big Flat 3 (Map #19), 7721-22 feet, representative samples showing oil-stained porosity and bitumen (bladed) in medium crystalline dolomite.

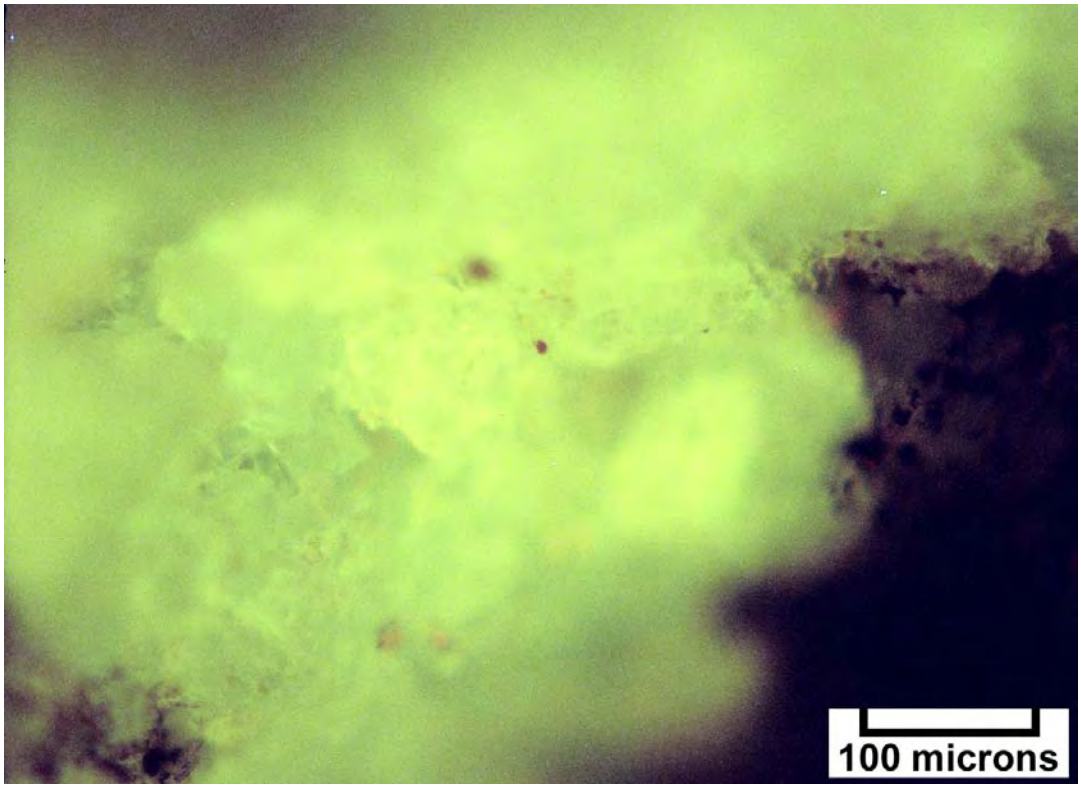

Photomicrograph – Pure Big Flat 3 (Map #19), 7723-24 feet, dim 0.3 epifluorescence with "dead" and "live" areas in medium crystalline dolomite.

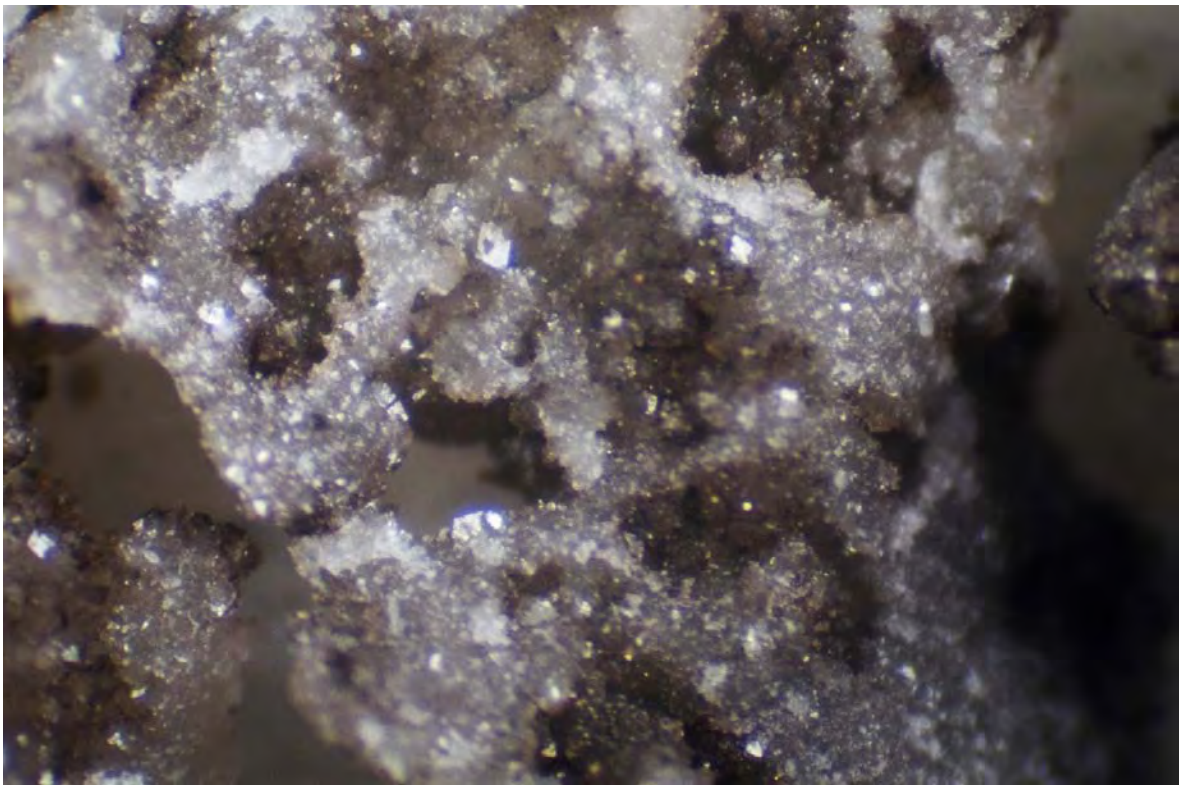

Binocular microscope image (4500x) – Pure Big Flat 3 (Map #19), 7724-25 feet, close-up of open dolomite-lined and oil-stained vugs and bitumen in medium crystal dolomite matrix.

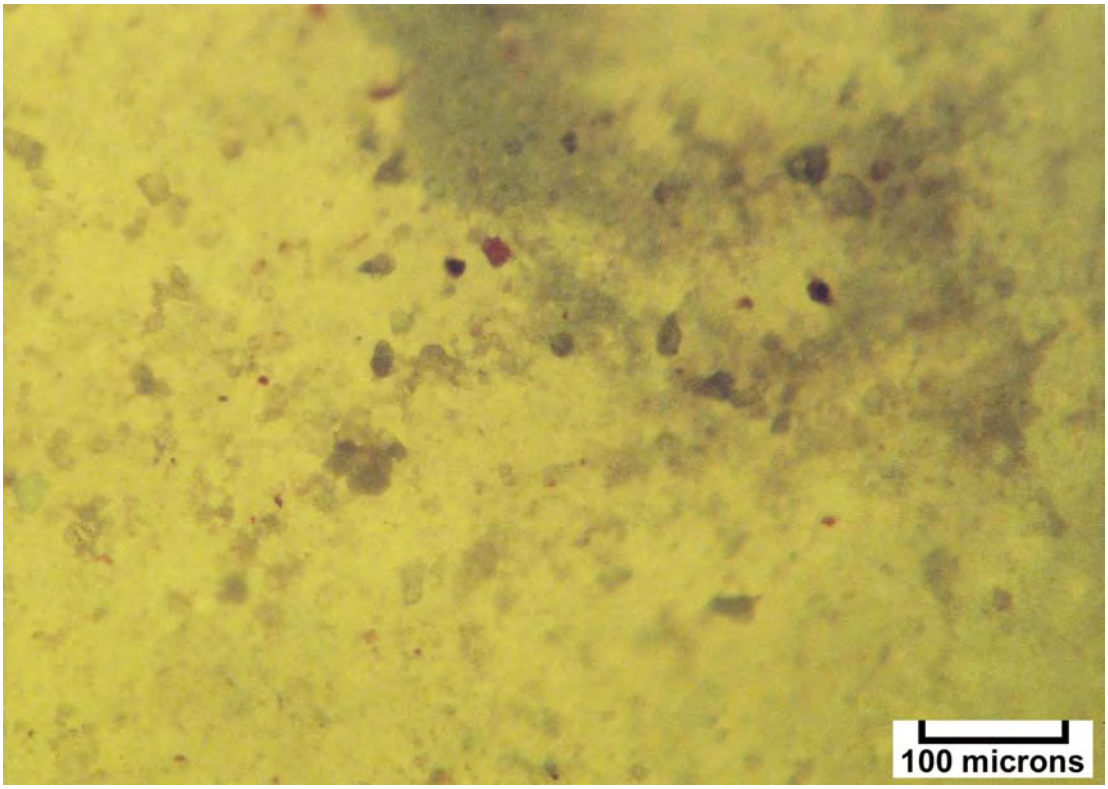

Photomicrograph – British America Federal Ornsby 1 (Map #20), 7740-50 feet, 2.0 epifluorescence in high porosity and low permeability very finely crystalline dolomite containing no bitumen.

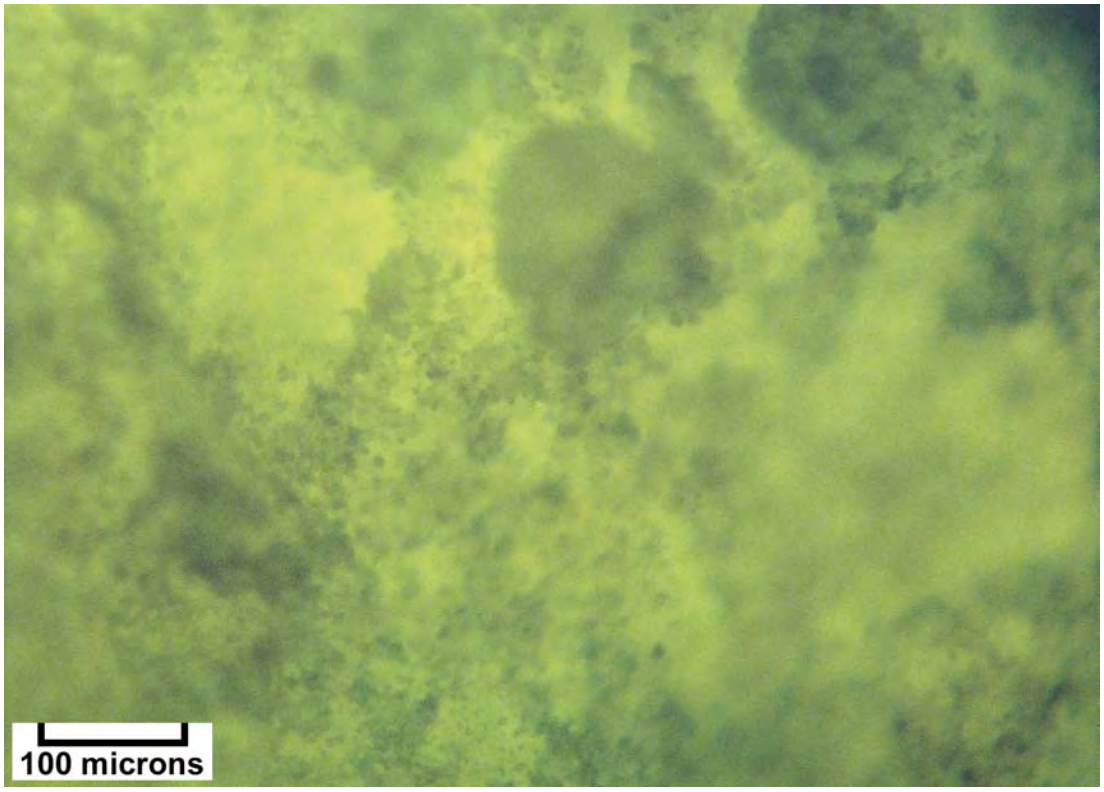

Photomicrograph – British America Federal Ornsby 1 (Map #20), 7800-10 feet, 1.5 epifluorescence in moderately high porosity and low permeability finely crystalline dolomite containing no bitumen.

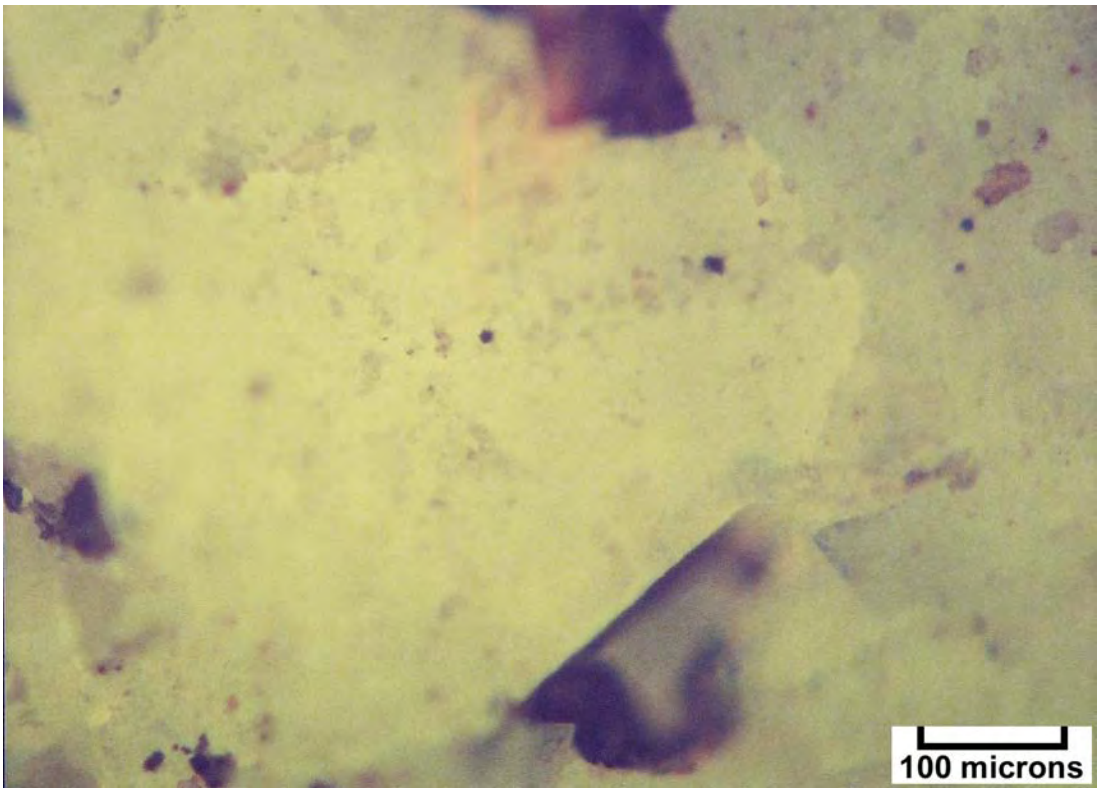

Photomicrograph – Gulf Lockhard Federal 1 (Map #25), 5145-50 feet, 1.8 epifluorescence in coarsely crystalline dolomite with good intercrystalline porosity.

Binocular microscope image (1400x) – Richfield Hatch Mesa 1 (Map #26), 7810-20 feet, representative samples with crinoid moldic porosity and mini-vugs in medium crystalline dolomite.

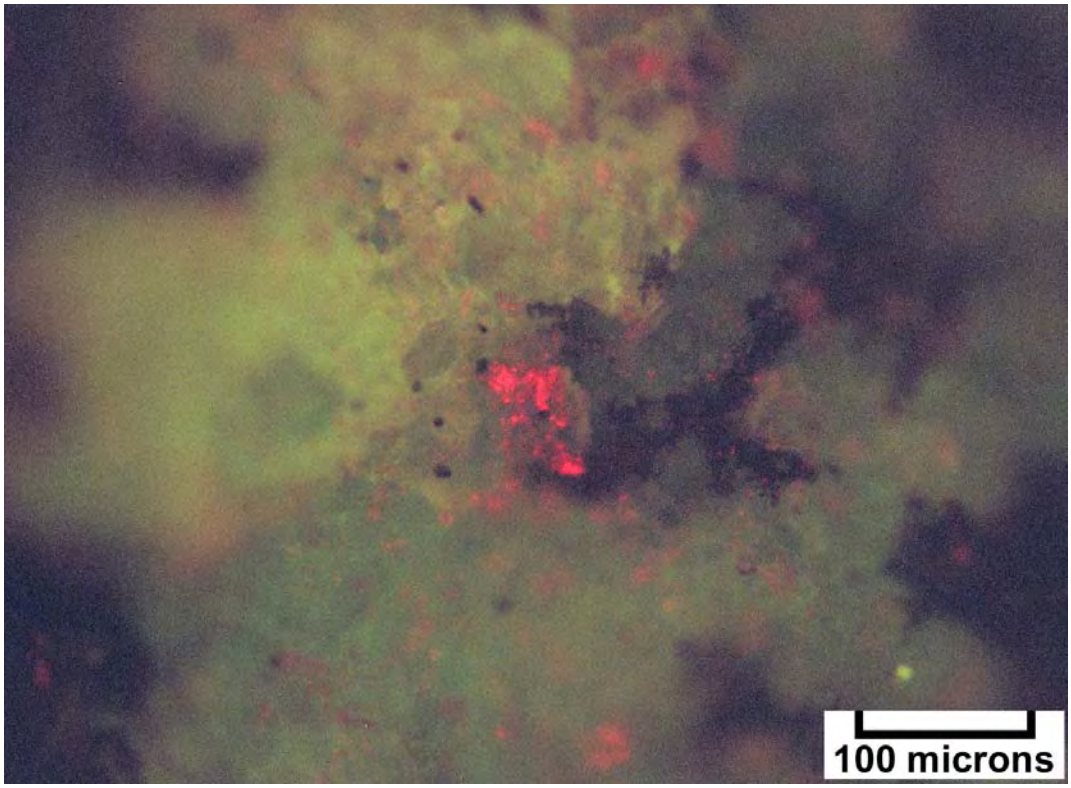

Photomicrograph – Pure USA Big Indian 1 (Map #27), 10,024-29 feet, speckles of 0.5 epifluorescence in coarse crystalline dolomite surrounding dead bitumen-lined pores.

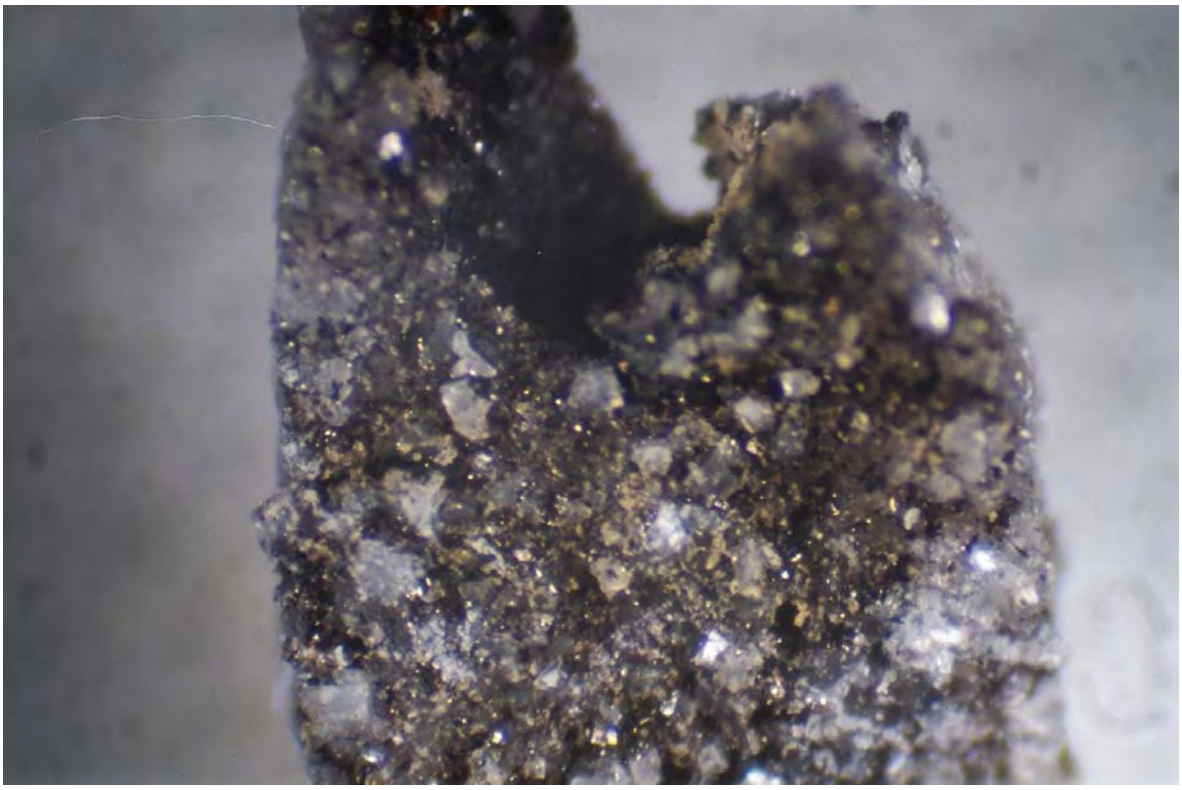

Binocular microscope image (4500x) – Pure USA Big Indian 1 (Map #27), 10,024-29 feet, closeup of a single vug lined with dolomite crystals and bitumen.

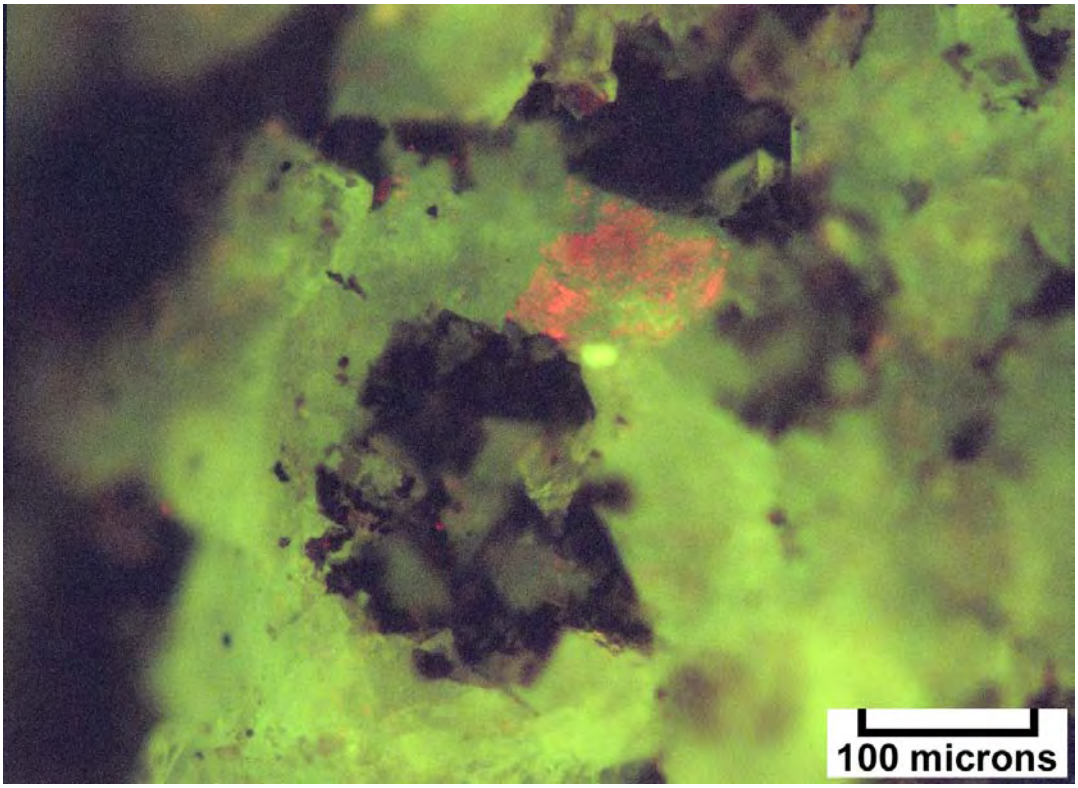

Photomicrograph – Pure USA Big Indian 1 (Map #27), 10,086-90 feet, 1.5 epifluorescence in coarsely crystalline dolomite containing good intercrystalline dolomite and bitumen.

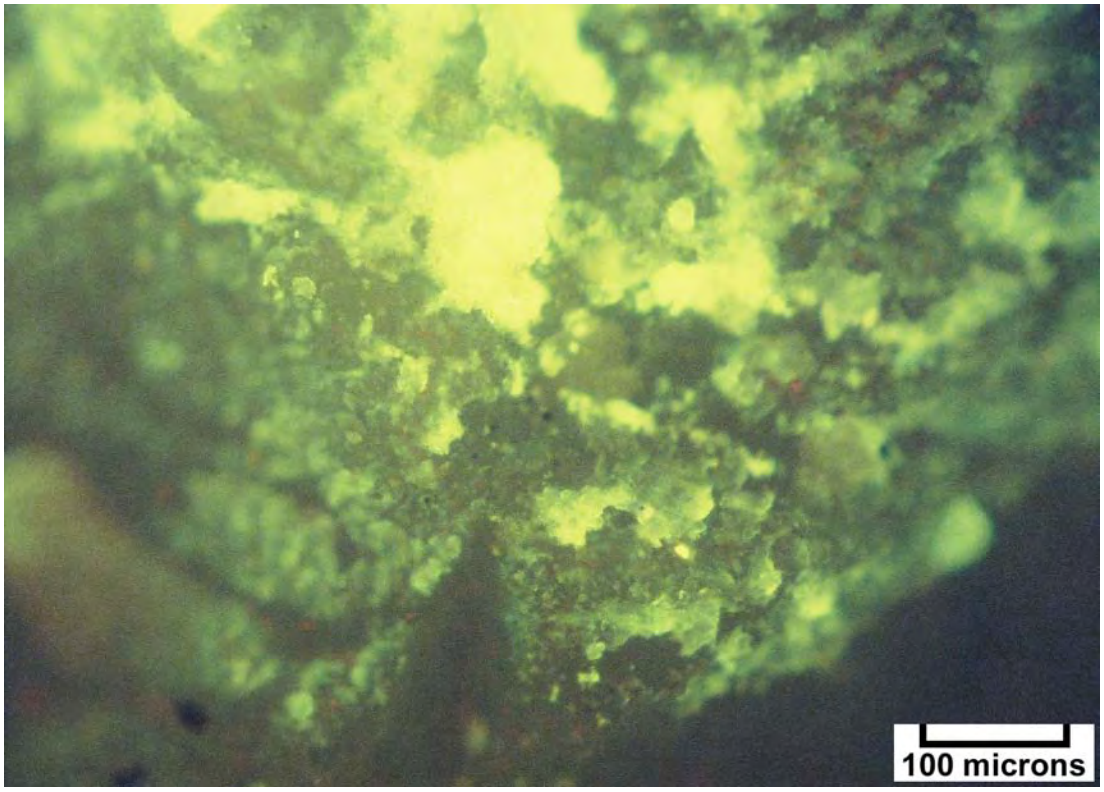

Photomicrograph – Belco State 1 (Map #28), 9835-36 feet, bright yellow 2.5 epifluorescence in medium to coarse dolomite with a trace of bitumen.

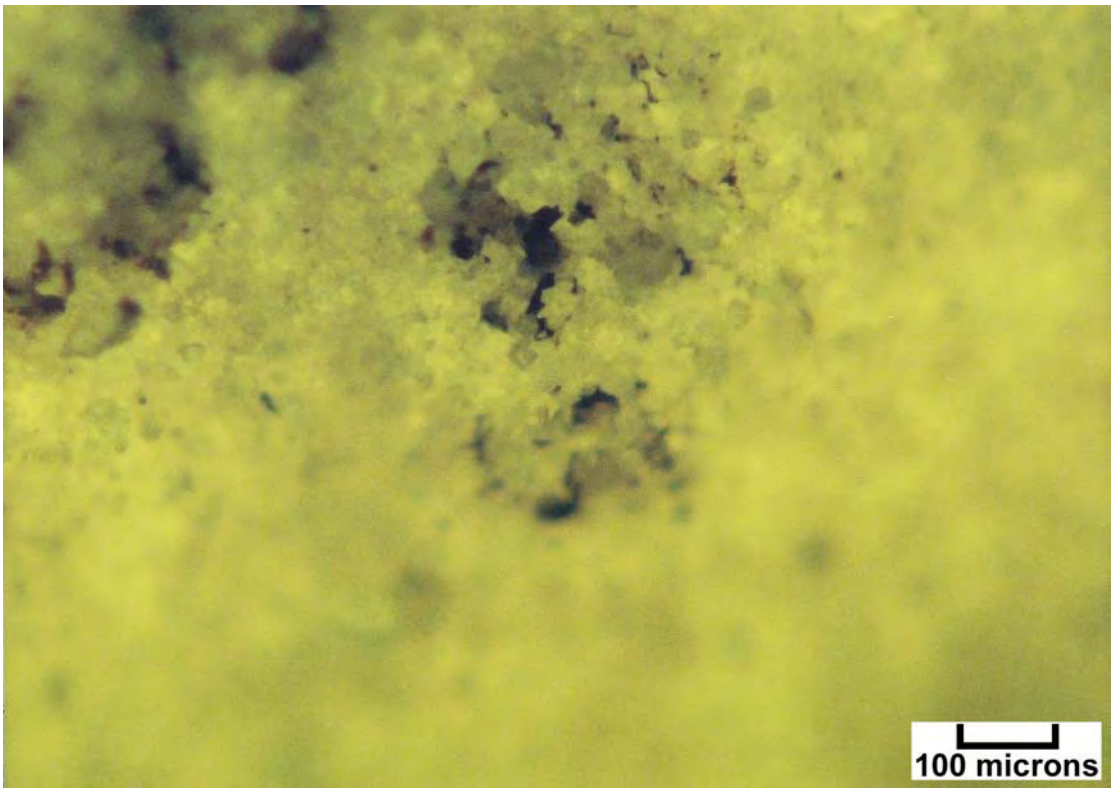

Photomicrograph – Belco State 1 (Map #28), 9850-51 feet, 1.5 epifluorescence with a good oil show in a 0.0 epifluorescence matrix of medium crystalline dolomite.

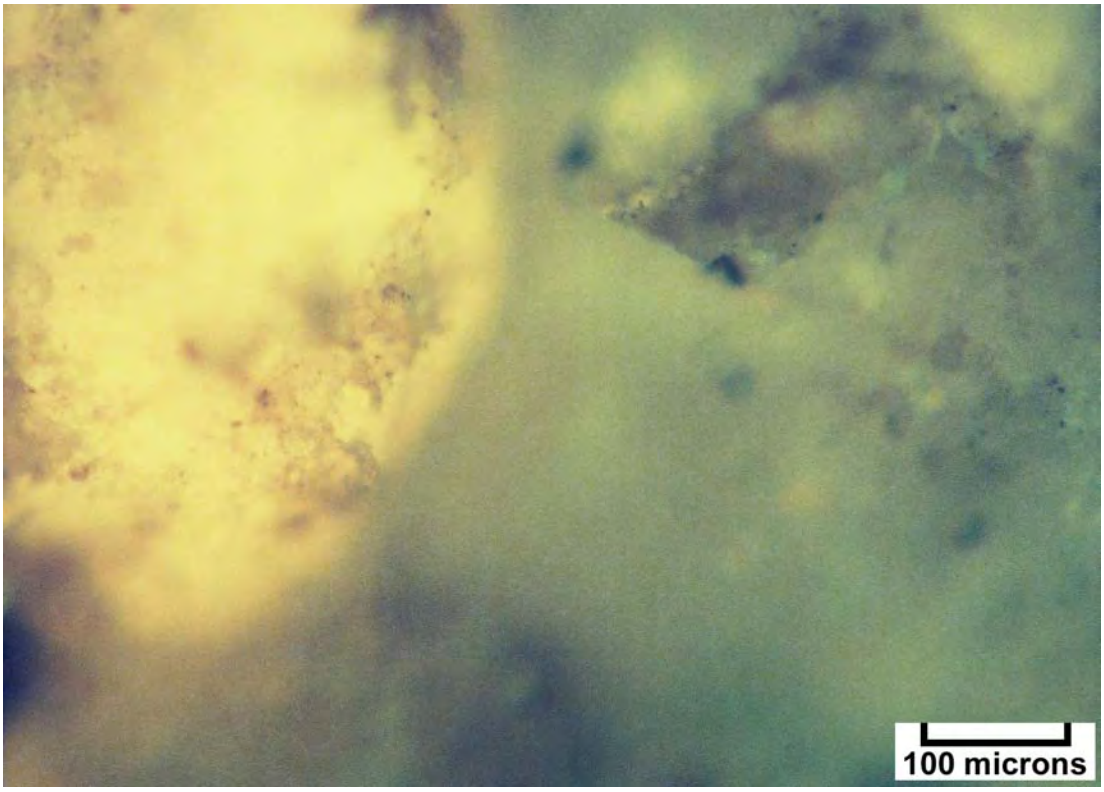

Photomicrograph – Pure NW Lisbon State A-1 (Map #29), 9710-15 feet, two types of epifluorescence: pale-green yellow at 0.5 and bright yellow at 2.0, indicating two oils or partially degraded oil.

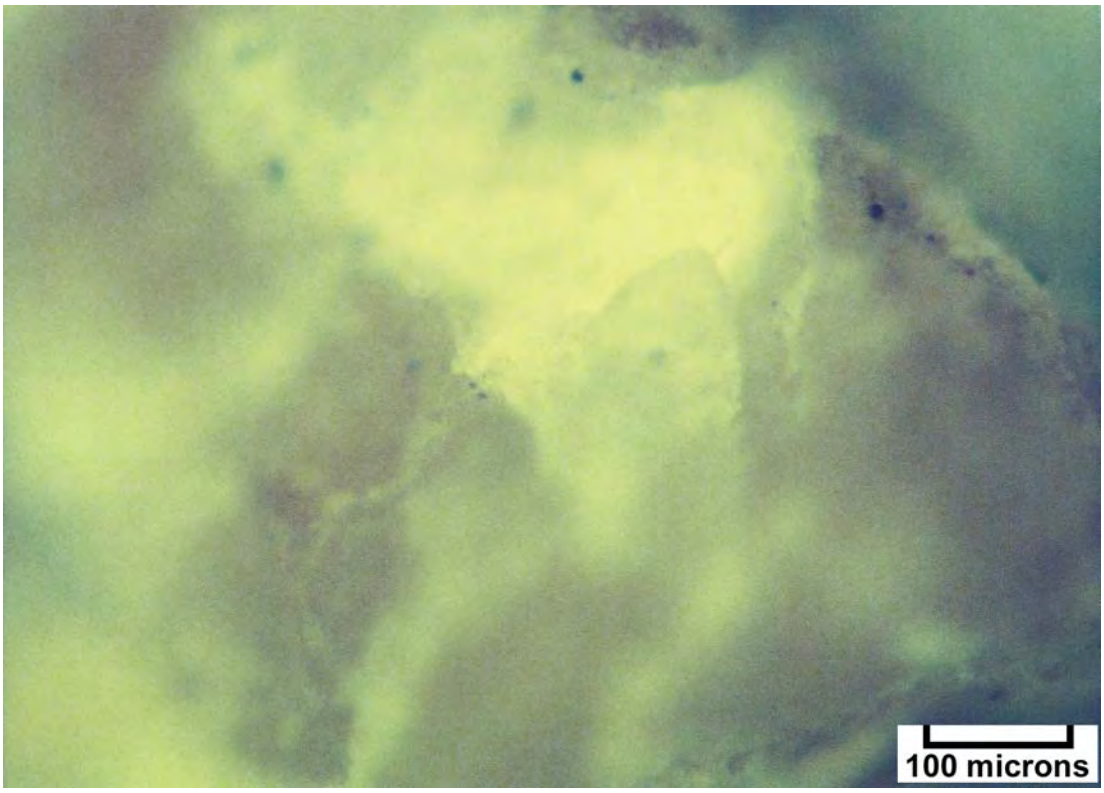

Photomicrograph – Pure NW Lisbon State A-1 (Map #29), 9715-20 feet, patch of 2.0 epifluorescence in coarse grained dolomite.

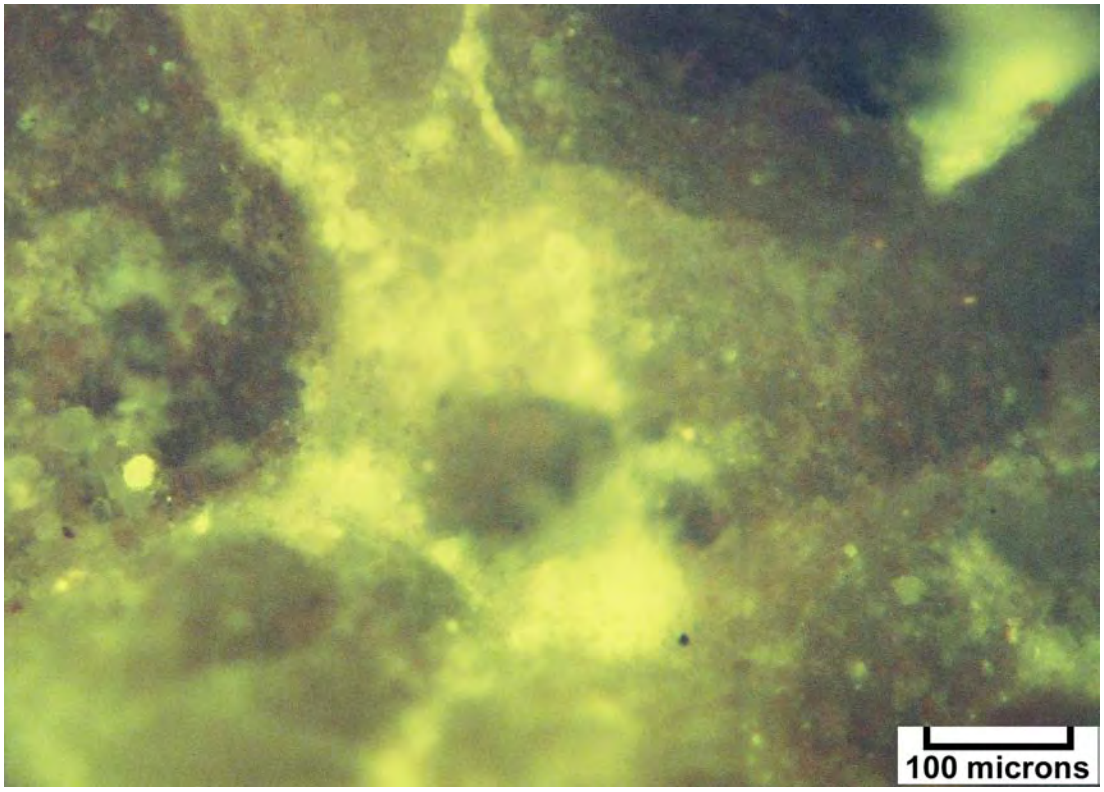

Photomicrograph – Pure NW Lisbon State A-1 (Map #29), 9720-25 feet, 1.5 epifluorescence along a microfracture.

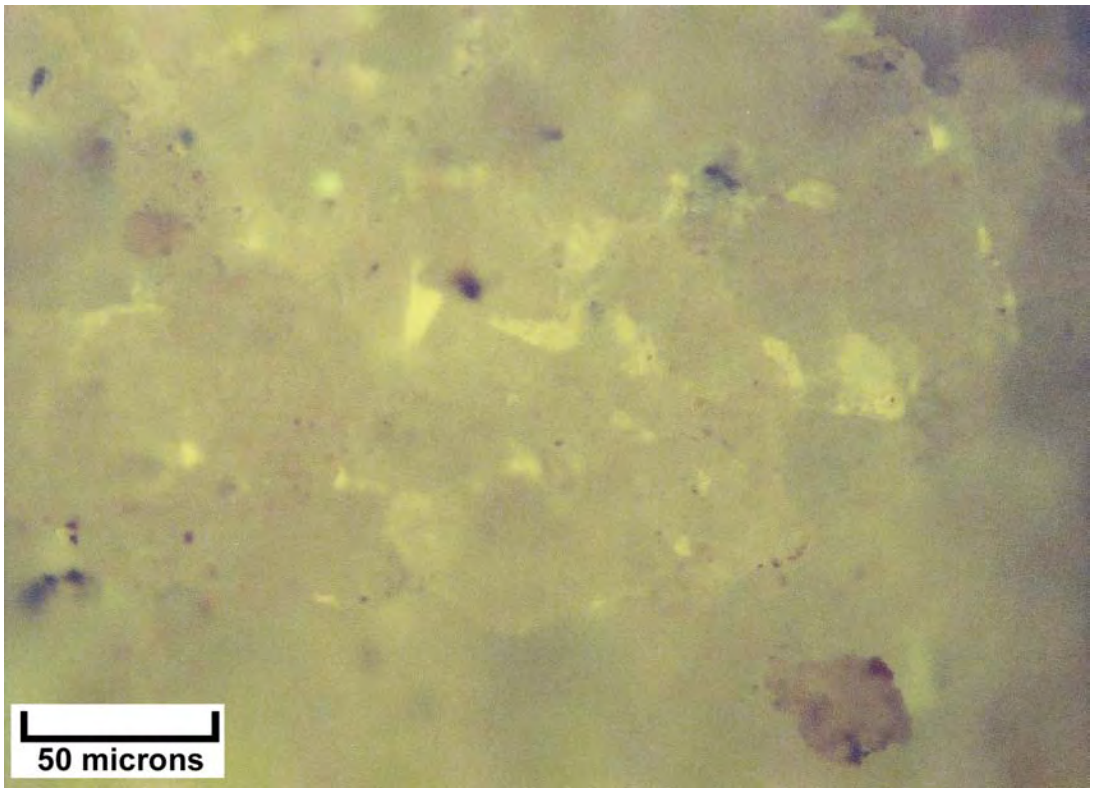

Photomicrograph – Pure NW Lisbon State 814-A (Map #31), 8870-75 feet, closeup of possible oil films and 2.5 epifluorescence in coarsely crystalline dolomite.

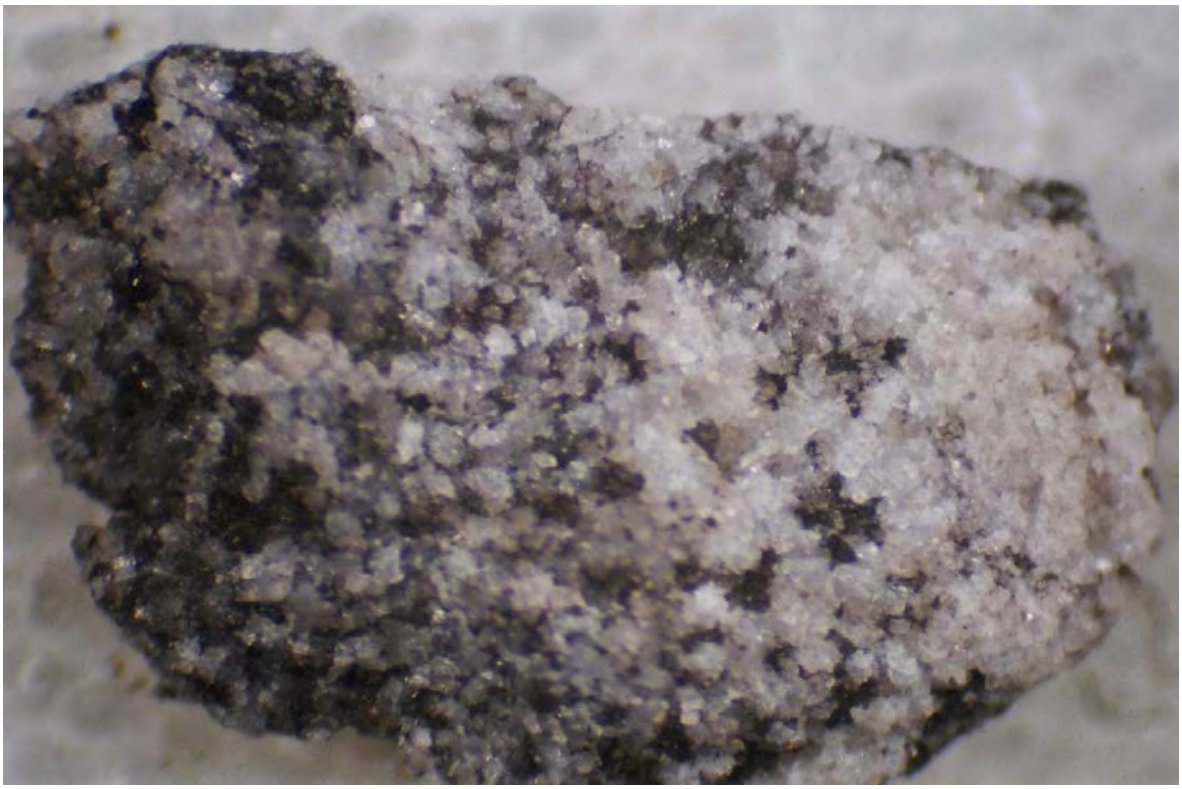

Binocular microscope image (3700x) – Pure Lisbon 814-A (Map #31), 8870-75 feet, dolomite with fair intercrystalline porosity and bitumen from a producing oil well at Lisbon field.

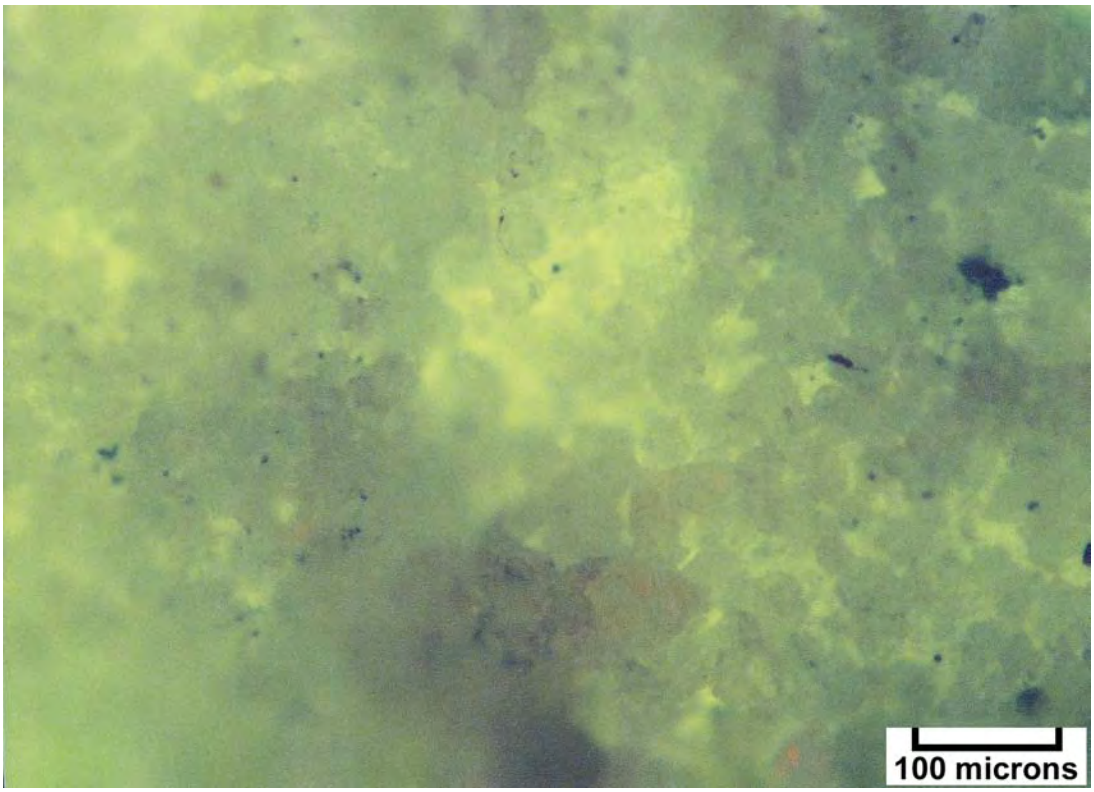

Photomicrograph – Pure Lisbon 814-A (Map #31), 8875-80 feet, 3.0 epifluorescence in medium crystalline dolomite with good oil saturation throughout.

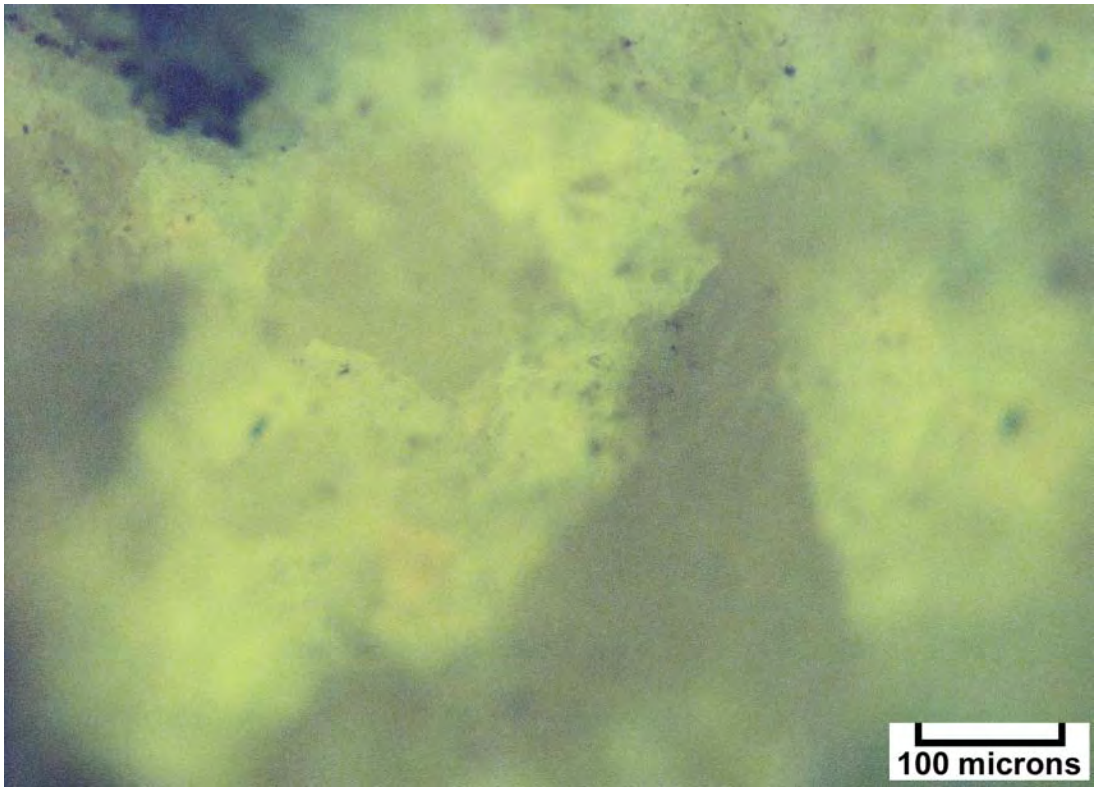

Photomicrograph – Pure Lisbon 814-A (Map #31), 8890-95 feet, representative sample with good bright 1.8 epifluorescence in a medium crystalline dolomite containing bitumen.

Binocular microscope image (2500x) – Pure Lisbon 814-A (Map #31), 8890-95 feet, three samples with modest porosity, bitumen, and sulfides. Note possible oil stain in the left hand sample.

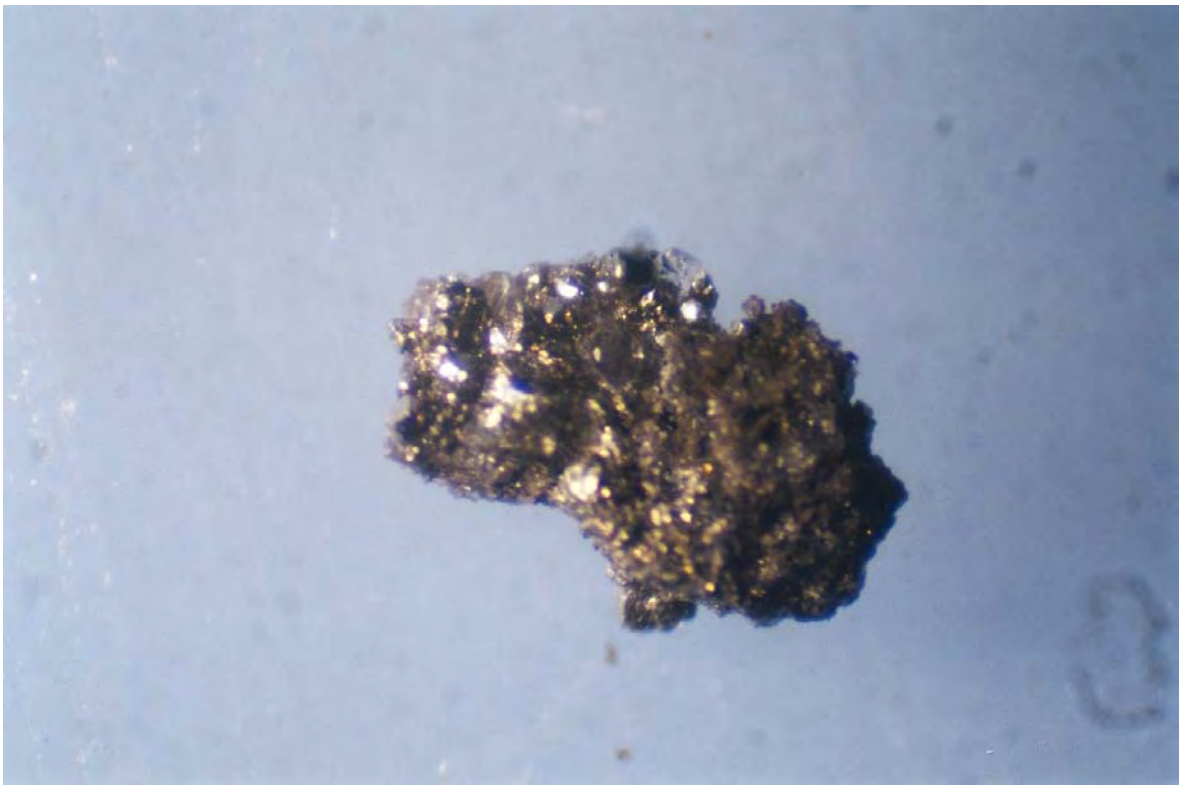

Binocular microscope image (4500x) – Pure Lisbon 814-A (Map #31), 8895-8900 feet, cluster of sulfides, probably pyrite.

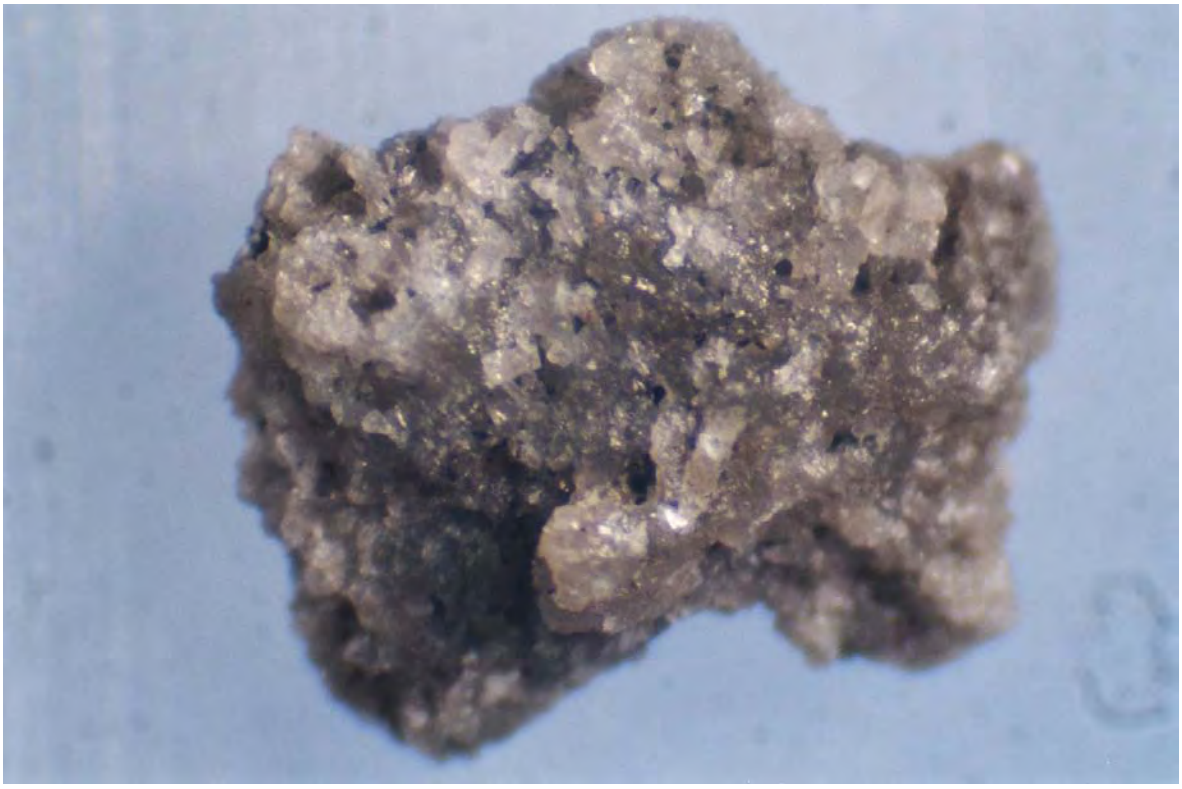

Binocular microscope image (4500x) – Pure Lisbon 814-A (Map #31), 8900-05 feet, single dolomite cutting with intercrystalline porosity and traces of bitumen.

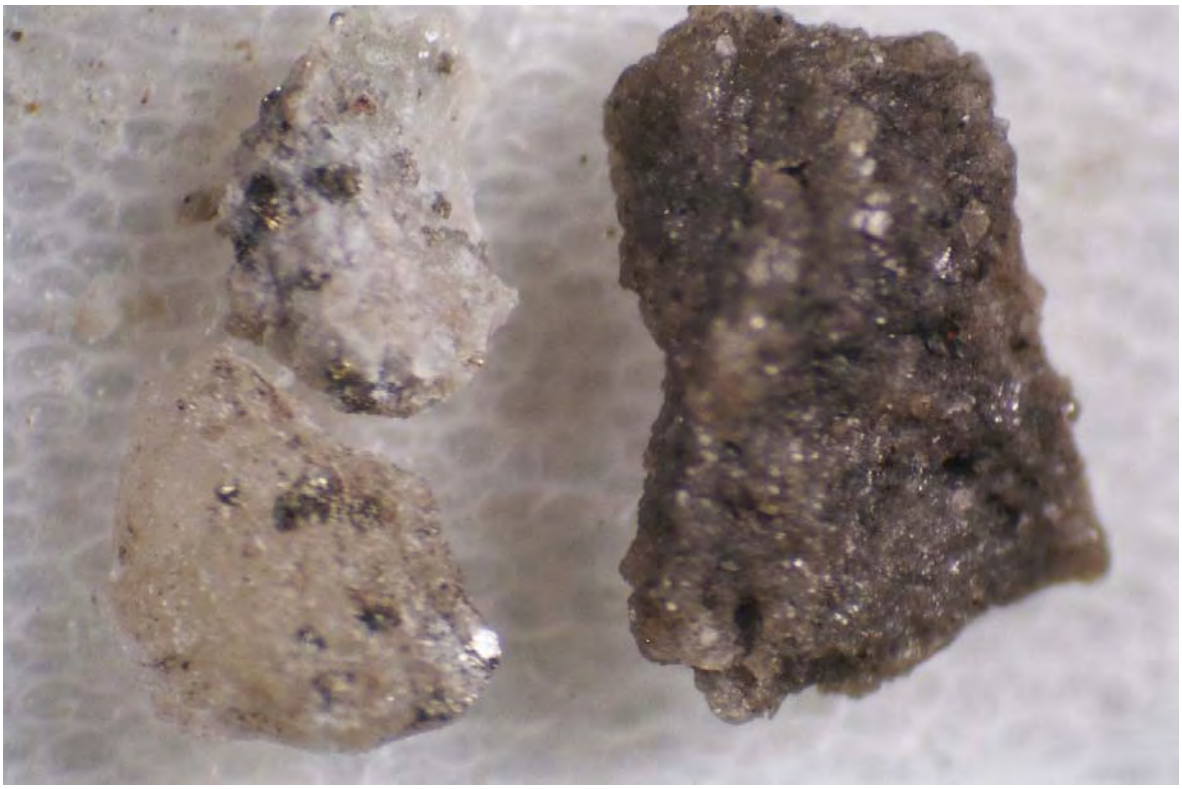

Binocular microscope image (2500x) – Pure Lisbon 814-A (Map #31), 8910-15 feet, dolomite cuttings, the large sample containing intercrystalline porosity, the two small samples showing sulfides.

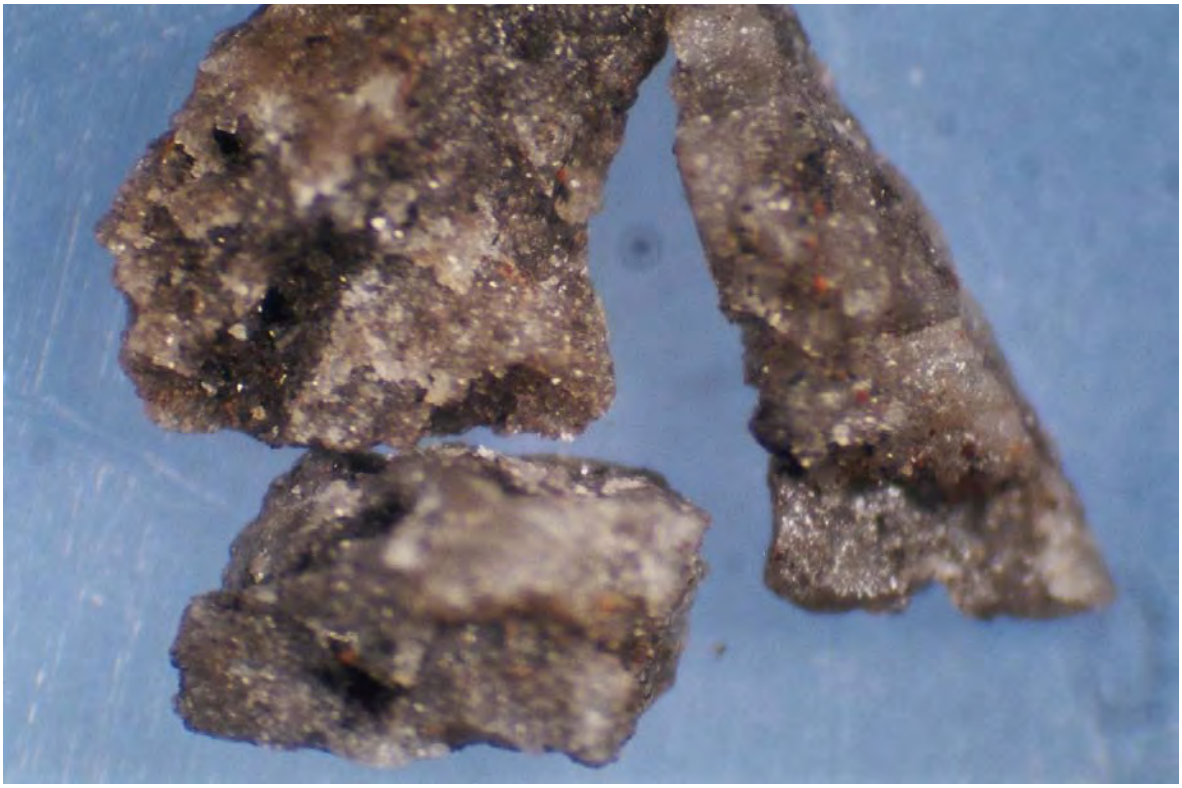

Binocular microscope image (3100x) – Pure Lisbon 814-A (Map #31), 8925-30 feet, dolomite cuttings containing intercrystalline and microvuggy porosity.

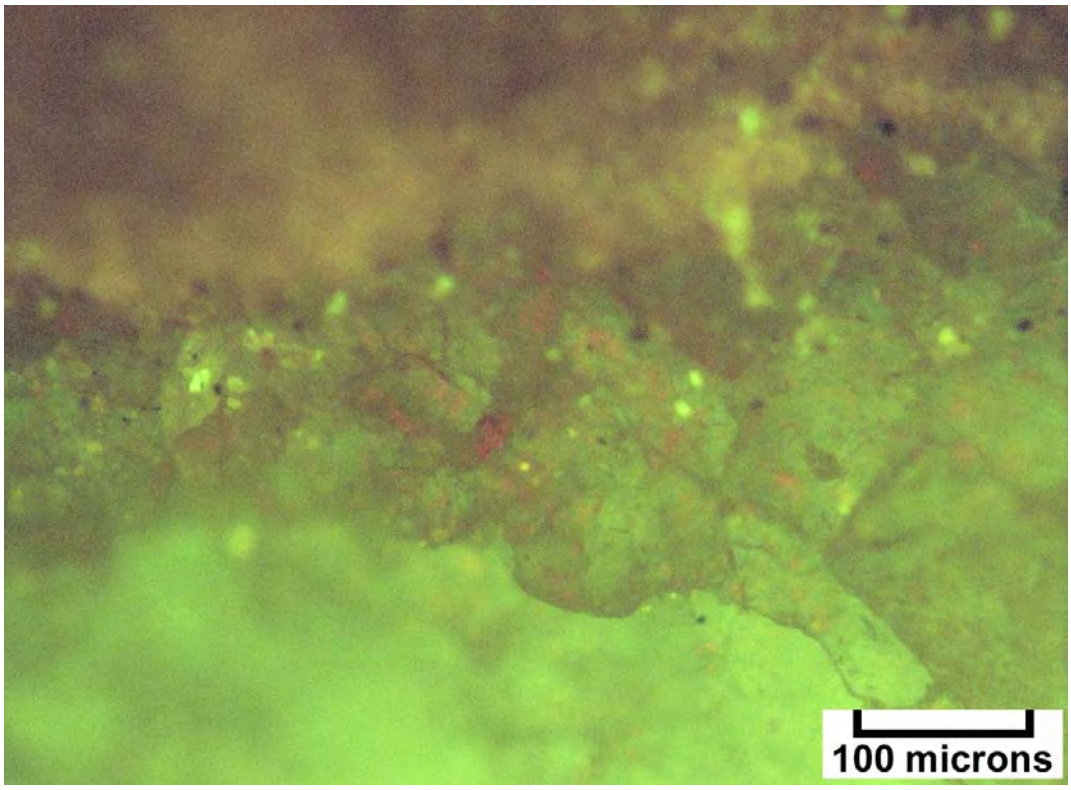

Photomicrograph – Pure Spiller Canyon State 1 (Map #32), 9090-9100 feet, dull pale yellow 0.2 epifluorescence in medium crystalline dolomite.

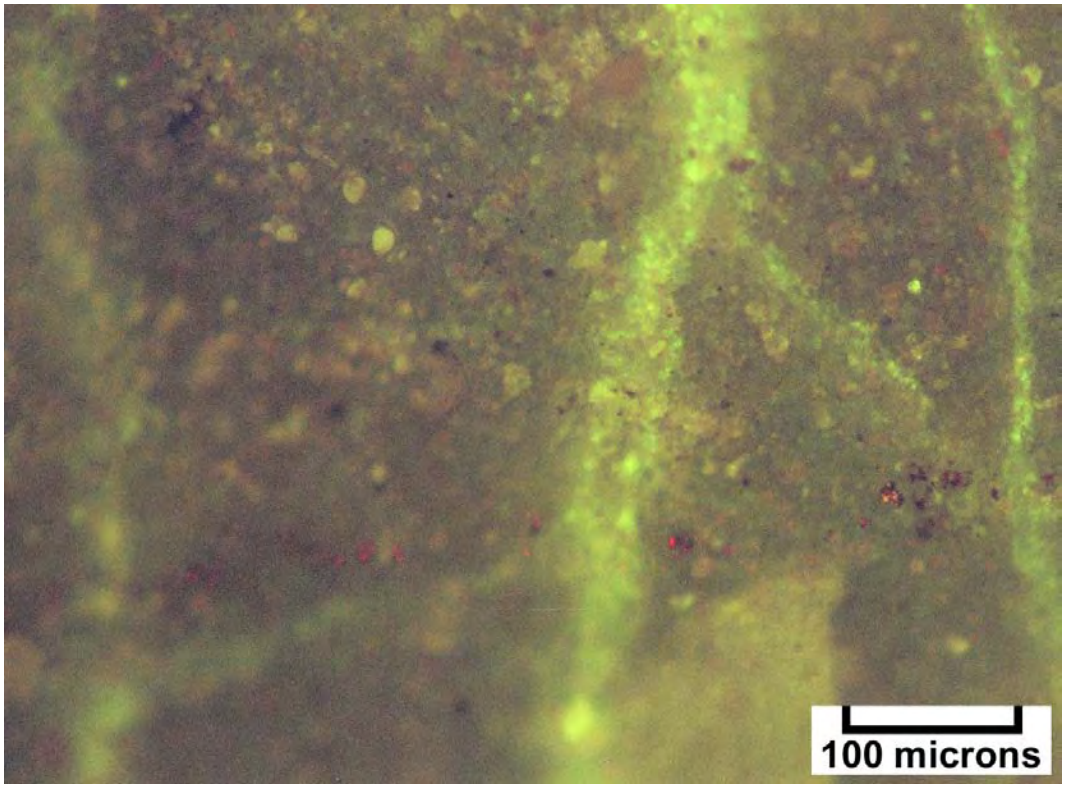

Photomicrograph – Pure Spiller Canyon State 1 (Map #32), 9100-10 feet, 0.5 epifluorescence along swarms of fractures in medium crystalline dolomite.

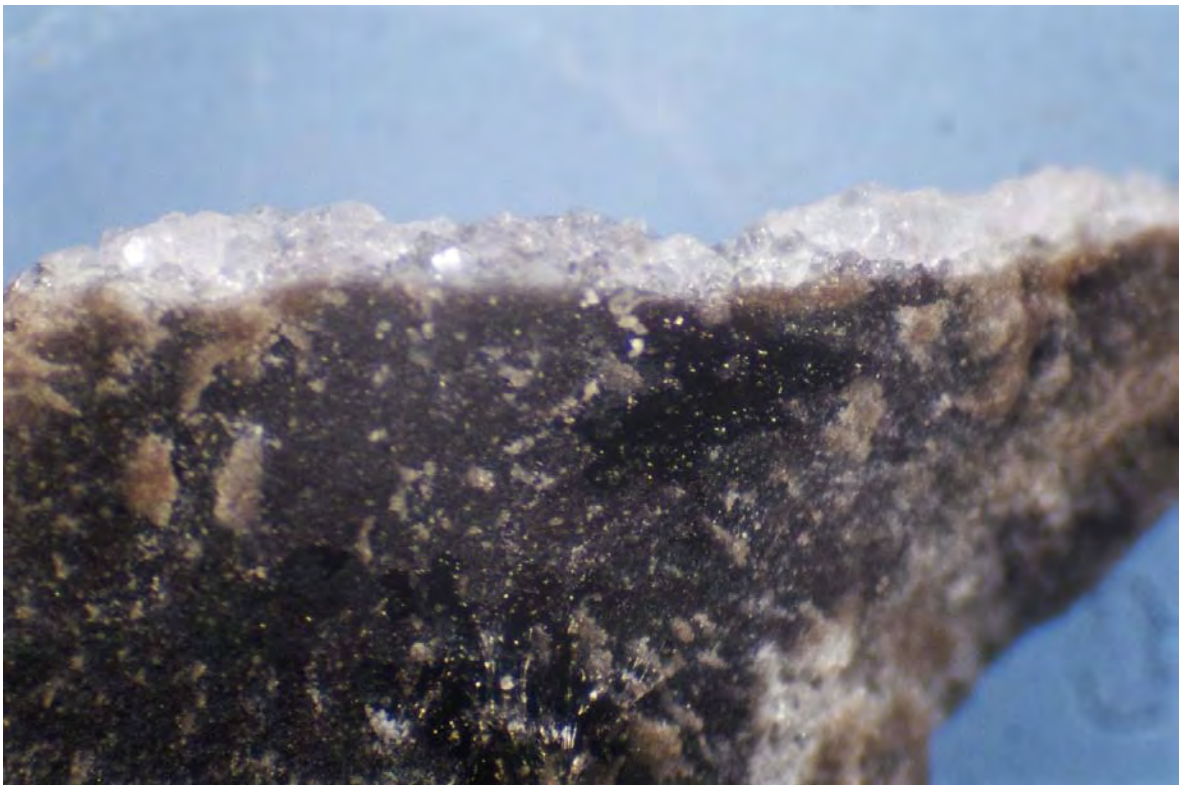

Binocular microscope image (3700x) –Pure Spiller Canyon State 1 (Map #32), 9100-10 feet, dense dolomite cutting with white dolomite crystals lining fracture.

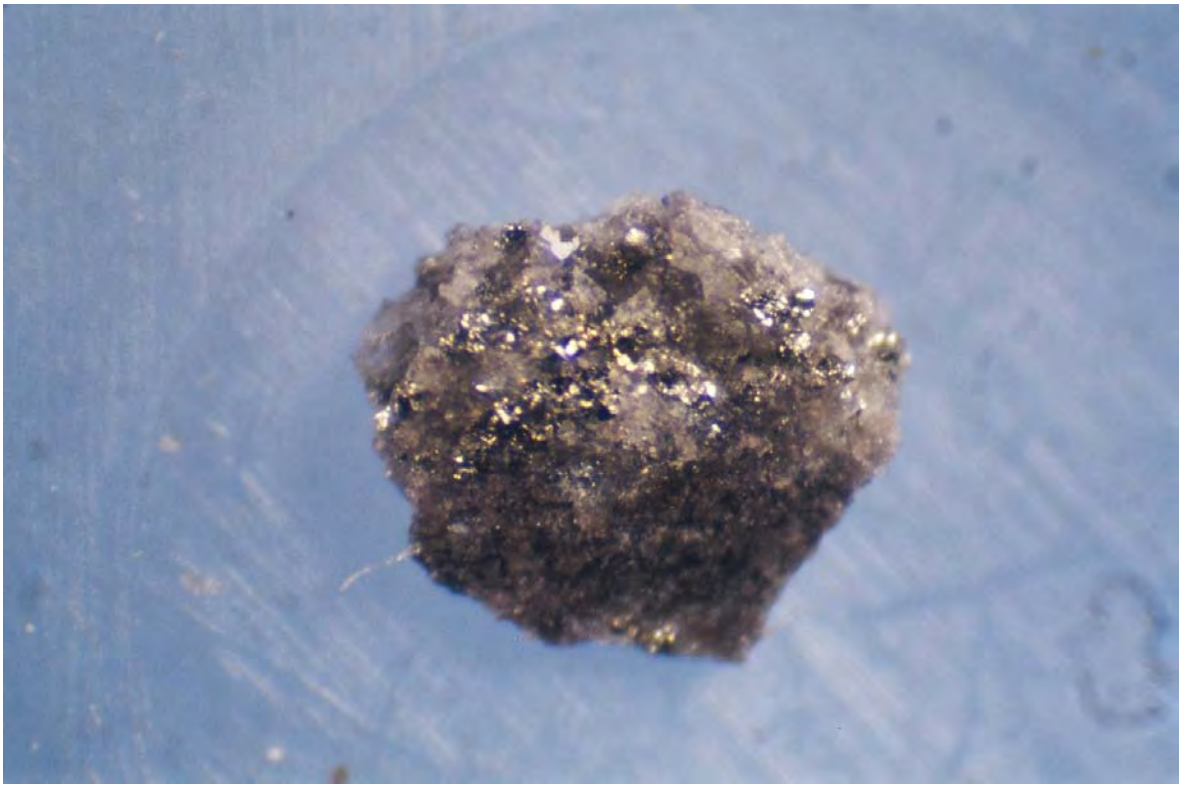

Binocular microscope image (4500x) – Pure Spiller Canyon State 1 (Map #32), 9150-60 feet, sulfides replacing dolomite.

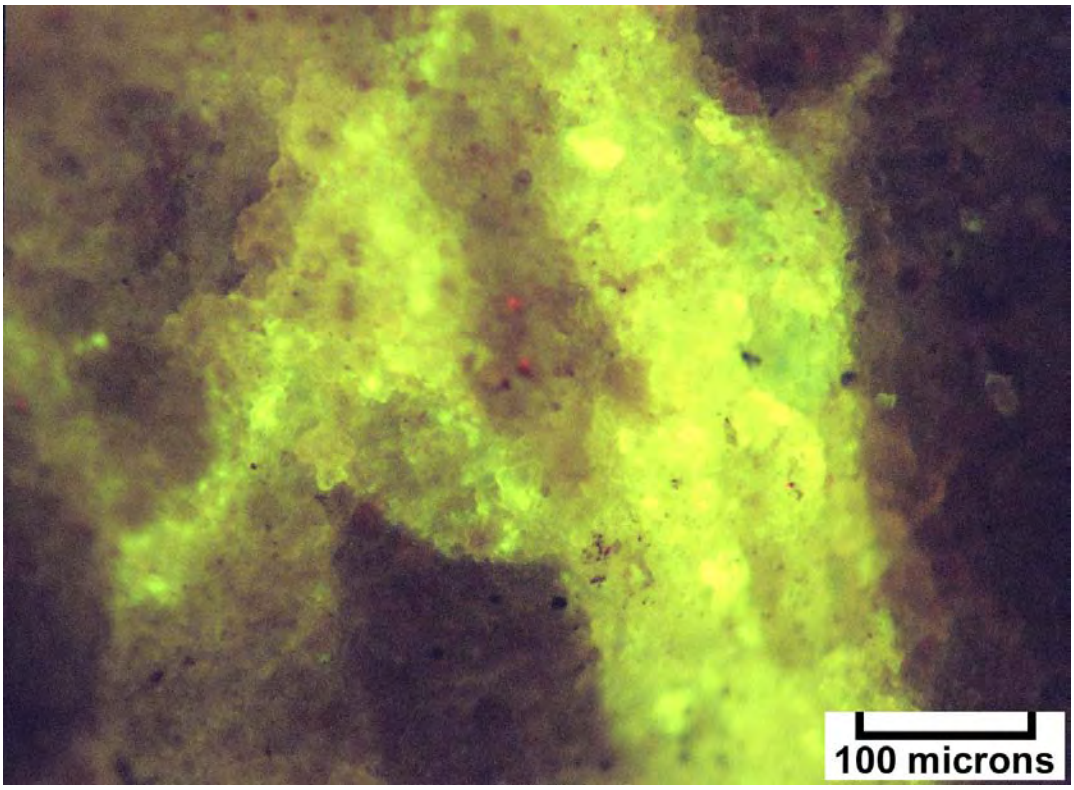

Photomicrograph – Pure Spiller Canyon State 1 (Map #32), 9190-9200 feet, fracture swarm lined with dolomite displaying pale yellow 1.0 epifluorescence.

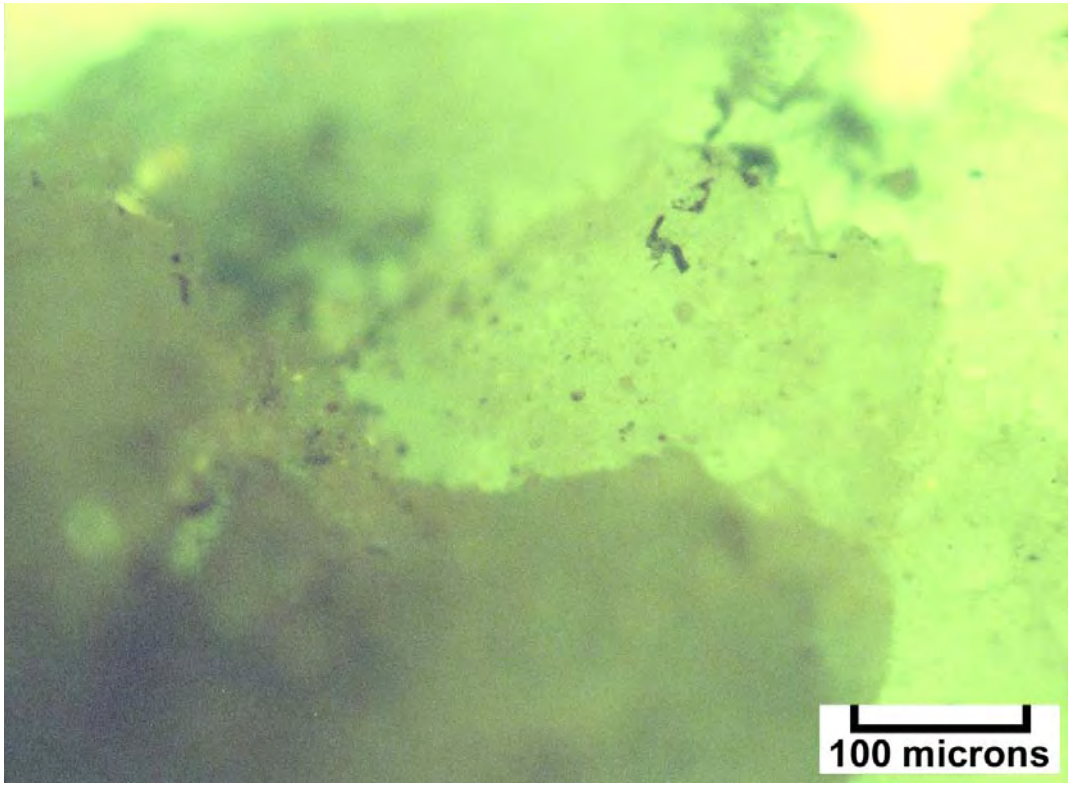

Photomicrograph – Pure Spiller Canyon State 1 (Map #32), 9330-40 feet, 0.7 epifluorescence in "dead" matrix with minor bitumen.

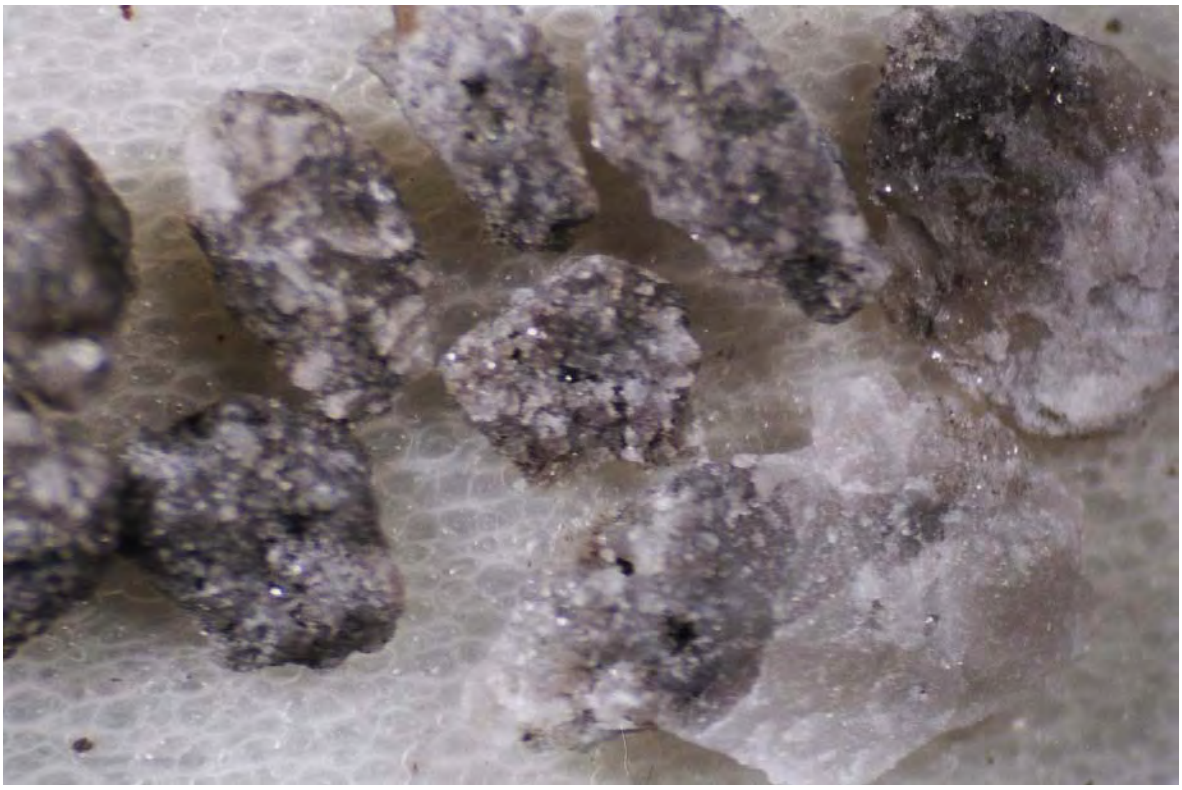

Binocular microscope image (1700x) – Pure Spiller Canyon State 1 (Map #32), 9330-40 feet, samples of dolomite with good intercrystalline porosity and bitumen.

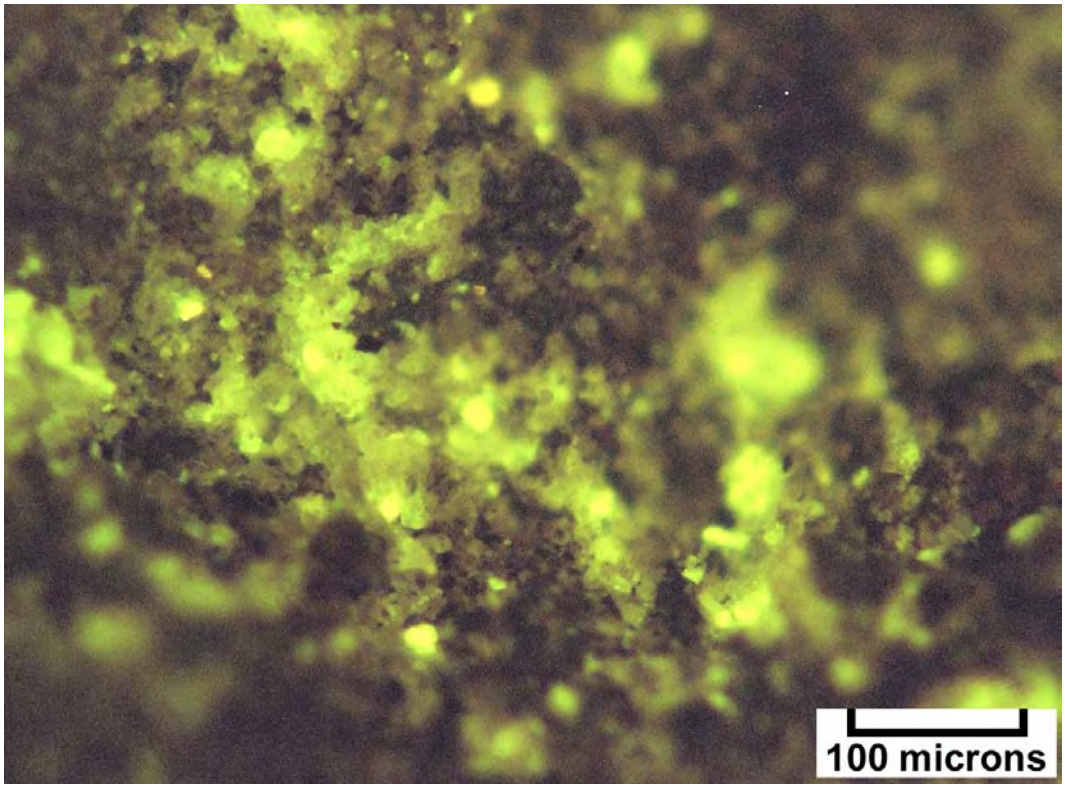

Photomicrograph – Pure Spiller Canyon State 1 (Map #32), 9360-70 feet, speckled 1.5 epifluorescence around small dolomite crystals.

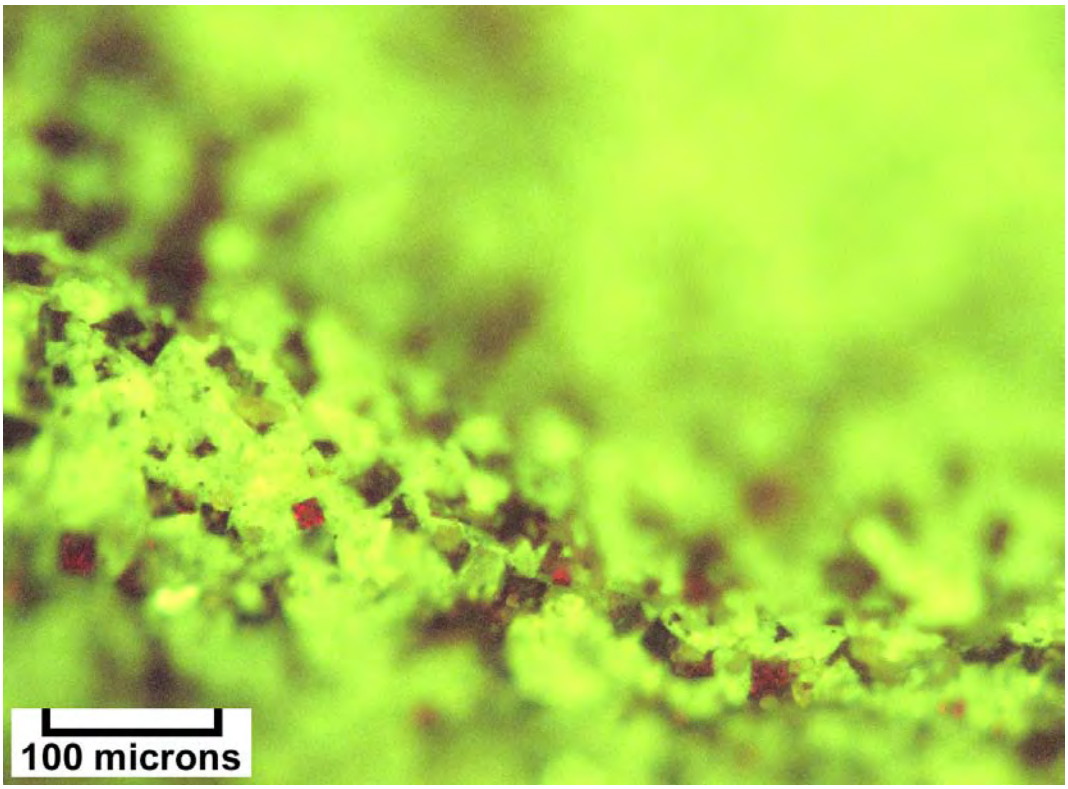

Photomicrograph – Pure Spiller Canyon State 1 (Map #32), 9380-90 feet, speckled 1.5 epifluorescence showing bitumen and small crystals with pale yellow epifluorescence.

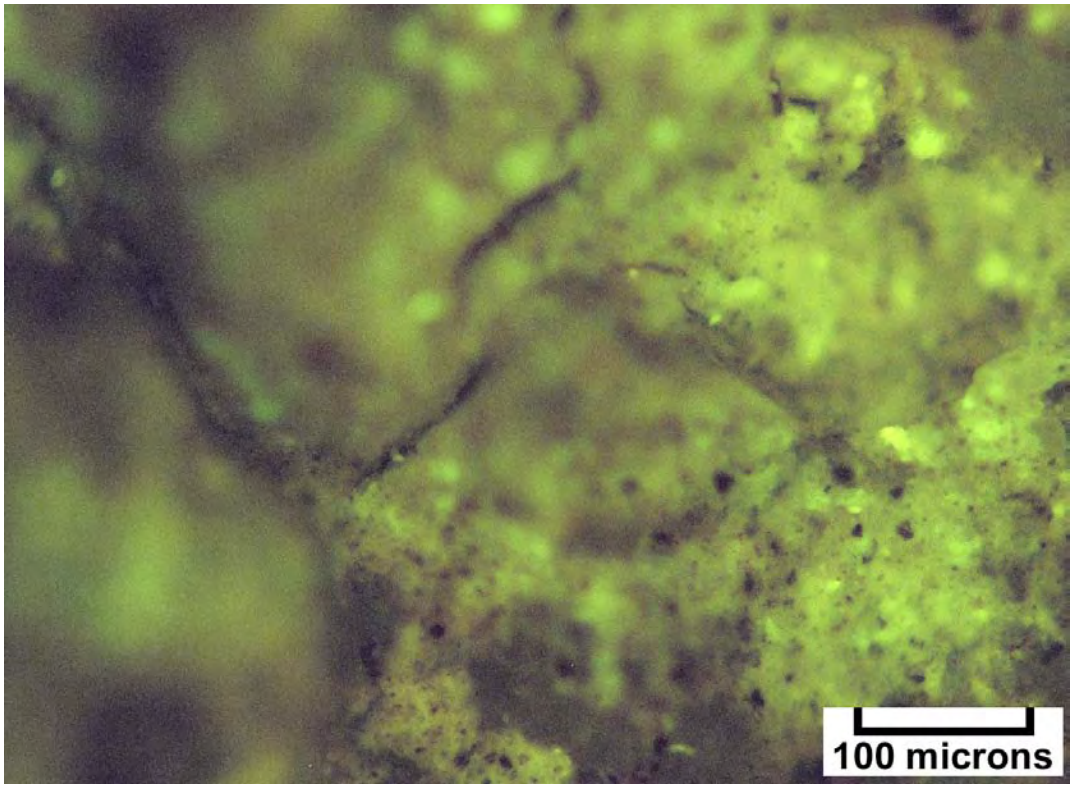

Photomicrograph – Pure Spiller Canyon State 1 (Map #32), 9410-20 feet, very dull 1.0 epifluorescence in medium crystalline dolomite with minor speckles of 1.5 epifluorescence.

APPENDIX E – MEASURED STRATIGRAPHIC SECTIONS, MISSISSIPPIAN MADISON LIMESTONE, SOUTH FLANK OF THE UINTA MOUNTAINS

Study Site 2 – Madison Limestone, Dry Fork Canyon (Red Cloud Loop/North Fork Intersection), Section 26, T. 2 S., R. 19 E., Uintah County, Utah

Unit	Unit (feet)	Total (feet)	Description
8	2	41.5	Dolomite; light brown to buff, mudstone, with continuous mm scale cryptalgal laminates, possible desiccation cracks and rip-up clasts, no fossils, probable pellets, dolomite is microcrystalline, low porosity and probably low permeability, depositional environment – tidal-flat mud.
7	13	39.5	Dolomite; light to medium brown, oolitic grainstone, fine to medium crystalline, low to medium angle cross-stratification, upper surface appears to be rippled to channelized with “cookie chip-like” mud clasts and fossil fragments in the troughs, local nodular calcite masses may be relic evaporite structures, very good porosity and permeability, depositional environment - oolitic shoal.
6	5	26.5	Limestone; light blue gray, pelloidal/skeletal/packstone/grainstone with endothyrid forams and other microfossils, thin bedded to bioturbated, no visible matrix porosity, depositional environment - stable shallow subtidal bay.
5	4	21.5	Dolomite; medium brown, slightly calcareous, soft pellet mudstone, no visible fossils, massive to heavily bioturbated, strong petroliferous odor, micro-intercrystalline dolomite with moderately high porosity and probably low permeability, may contain significant organic matter, sharp base, high-order cycle boundary (shoaling up), depositional environment – deeper subtidal burrowed pellet muds.
4	2	17.5	Dolomite; light to medium brown, soft pellet mudstone with crinkly continuous cryptalgal laminates, minor amounts of skeletal microfossils including ostracods and benthic forams, probable rip-up intraclasts, finely crystalline, low porosity and probably low permeability, recessively weathered, depositional environment - tidal flat mud.
3	7.5	15.5	Dolomite; light to medium gray, oolitic/hard pellet grainstone, well-defined bedding, small- to medium-scale cross-bedded, closely spaced swarms of vertical fractures, no visible fossils, fine to medium crystalline, moderate porosity, probably low permeability, depositional environment - oolitic shoal.
2	2.5	8	Dolomite; calcareous, medium brown and gray, pelloidal/skeletal packstone/grainstone with hard pellets, benthic forams, and other microfossils, wavy bedded to bioturbated, top may be channelized, no visible porosity, probably low permeability, depositional environment - stable shallow subtidal bay.
1	5.5	5.5	Dolomite; calcareous, light brown to brown gray, oolitic/hard pellet grainstone, distinctive pocked marked weathering, well laminated at the centimeter scale probably due to grain size and early cementation differences, well-defined planar to low-angle cross-stratification, upper 6 inches may contain beach rock and semi-lithified rip-up clasts, no visible porosity, probably low permeability, contact with unit 2 above is sharp, thickness to base (covered), depositional environment - beach/foreshore.

Study Site 3 – Madison Limestone, Crouse Reservoir/Diamond Mountain Plateau, S1/2 Section 34, T. 1 S., R. 24 E., Uintah County, Utah

Unit	Unit (feet)	Total (feet)	Description
11	7	116.5	Limestone; light gray, grainstone (encrinite), well sorted coarse sand to granule size crinoid fragments, wavy-thin to medium bedding, upper contact not exposed, depositional environment - storm-dominated outer shelf crinoid shoals.
10	12	109.5	Limestone; light medium gray, skeletal wackestone/packstone with tubular tempestites, within muds are well-preserved articulated crinoid columnals, fenestrate bryozoans, depositional environment – low-energy open marine outer shelf above storm wave base.
9	9	97.5	Limestone; interbedded light to medium gray, soft peloid/crinoid wackestone/packstone and grainstone (encrinite), medium- to large-scale cross-stratification including bimodal or herringbone cross bedding, locally well-sorted medium- to coarse-grained crinoid fragments, local concentrations of partially silicified burrows, includes several 6-inch to 2-foot tidally dominated, bimodally well sorted, cross-bedded skeletal grainstone beds, ledge former across the landscape, depositional environment - storm-dominated outer shelf crinoid shoals to low-energy, open marine, muddy intershoal.
8	28	88.5	Limestone; light medium gray, skeletal wackestone/packstone with tubular tempestites, within muds are well-preserved articulated crinoid columnals, fenestrate bryozoans, locally abundant nodular cherts, biogenic graded with increasing mud content and decreasing crinoids upward, depositional environment – low-energy open marine outer shelf above storm wave base.
7	9	60.5	Limestone; light gray, grainstone (encrinite), well sorted, very coarse grained crinoid fragments and large crinoid columnals, wavy bedding and possible medium-scale cross-bedding, locally burrowed with some chert replacement, depositional environment - storm-dominated outer shelf crinoid shoals.
6	5.5	51.5	Limestone; light medium gray, skeletal wackestone/packstone with tubular tempestites, within muds are well-preserved articulated crinoid columnals, fenestrate bryozoans, depositional environment – low-energy open marine outer shelf above storm wave base.
5	8	46	Limestone; light gray, grainstone (encrinite), well sorted coarse sand to granule size crinoid fragments, wavy-thin to medium bedding, depositional environment - storm-dominated outer shelf crinoid shoals.
4	10	38	Limestone; light medium gray, skeletal wackestone/packstone with grainstone burrow infills, contains biogenetically skeletal burrow fillings at several scales, the larger burrow networks appear to be open burrows filled with coarse storm-pumped shells (tubular tempestites), within muds are well-preserved articulated crinoid columnals, also present are fenestrate bryozoans, locally abundant nodular cherts probably following burrow systems, depositional environment – low-energy open marine outer shelf above storm wave base.
3	9	28	Limestone; white to very light gray, skeletal grainstone, coarse grained, consists of crinoid and other skeletal fragments, well-developed syntaxial calcite cements, wavy medium-scale bedding; depositional environment - storm-dominated outer shelf crinoid shoals.
2	12	19	Limestone; light to medium gray, soft peloid/crinoid wackestone/packstone, appears to be burrowed, some well-preserved fenestrate bryozoans, mostly covered so poorly exposed, depositional environment – low-energy, open marine, muddy intershoal.
1	7	7	Limestone; light gray, grainstone (encrinite), well sorted coarse sand to granule size crinoid fragments, wavy-thin to medium bedding, upper contact is sharp with undulatory topography, possible small-scale interference ripples and small rugose corals on top, base not exposed, depositional environment - storm-dominated outer shelf crinoid shoals.

National Energy Technology Laboratory

626 Cochrans Mill Road
P.O. Box 10940
Pittsburgh, PA 15236-0940

3610 Collins Ferry Road
P.O. Box 880
Morgantown, WV 26507-0880

One West Third Street, Suite 1400
Tulsa, OK 74103-3519

1450 Queen Avenue SW
Albany, OR 97321-2198

2175 University Ave. South
Suite 201
Fairbanks, AK 99709

Visit the NETL website at:
www.netl.doe.gov

Customer Service:
1-800-553-7681